THE UNIVERSITY OF OKLAHOMA

GRADUATE COLLEGE

A STUDY OF THE DYNAMIC ADSORPTION BEHAVIOR OF METHANE - N-PENTANE - N-HEXANE - N-HEPTANE BINARY AND MULTICOMPONENT MIXTURES ON 03 GRADE SILICA GEL

A DISSERTATION

SUBMITTED TO THE GRADUATE FACULTY

in partial fulfillment of the requirements for the

degree of

DOCTOR OF PHILOSOPHY

BY

FRANK EDMUND ASHFORD

Norman, Oklahoma

1970

A STUDY OF THE DYNAMIC ADSORPTION BEHAVIOR OF METHANE - N-PENTANE - N-HEXANE - N-HEPTANE BINARY AND MULTICOMPONENT MIXTURES ON 03 GRADE SILICA GEL

APPROVED BY

Paul J. Root

D E Mcnzie

J M Townsend

J Campbell

Chairman

DISSERTATION COMMITTEE

ACKNOWLEDGMENT

With sincere appreciation, the author wishes to gratefully acknowledge the assistance of the following individuals and company for their contributions to this dissertation:

Dr. John M. Campbell, director of this work, for his assistance, criticism, enthusiasm, and invaluable support throughout the entire research period.

Davison Chemical Company of Baltimore, Maryland, for their financial support of the natural gas research project of the University of Oklahoma, where this work was conducted.

To my wife, Sisti, for her patience and encouragement.

DEDICATION

To Charlie

TABLE OF CONTENTS

Page

F. Example Calculations for Binary and Multi-component Mixtures

LIST OF TABLES

LIST OF ILLUSTRATIONS

A STUDY OF THE DYNAMIC ADSORPTION BEHAVIOR OF METHANE N-PENTANE N-HEXANE N-HEPTANE BINARY AND MULTICOMPONENT MIXTURES ON 03 GRADE SILICA GEL

CHAPTER I

INTRODUCTION TO AND STATEMENT OF THE PROBLEM

The application of static as well as dynamic adsorption concepts have been extensively analyzed and investigated in the past. Numerous authors, (T1), (G3), (R1), (H3), (M1), (A1) have given detailed and complete mathematical presentations of the adsorption phenomenon, and its application to industrial processes.

Although explicit mathematical solutions involving adsorption mechanics have been derived for some time, a major portion of former research efforts have not been successfully applied to commercial operations. The lack of application of readily available analytical solutions to the dynamic adsorption process results, perhaps, from the complex nature of these modeling procedures. The lack of laboratory information necessary to convert mathematically stated concepts into practical engineering design criteria, has also impeded actual application of dynamic adsorption theory.

In the area of natural gas adsorption, attempts have been made to apply various theoretical solutions to hydrocarbon recovery by the dynamic adsorption process. The solutions of Klinkenburg (K1), Rosen (R1), Thomas (T2), Vermeulen and Hiester (V4), and Gleukauf and Coates (G2), among others, have been successfully applied to the recovery of

the paraffin hydrocarbon family on granulated solids such as activated carbon, and silica gel. These applications are limited to binary adsorbates.

The data presented by McLeod (M2) and Needham (N1), as well as Day (D1) indicated that recoveries of binary mixtures of methane with n-butanes through n-hexanes could be predicted by direct application of various existing analytical solutions. These data are invaluable because they established a premise with which the academic mathematically oriented approach to the adsorption mechanics could be supported and applied to actual operations.

The efforts of McLeod (M2) and Needham (N1) were especially useful in that they pointed out the particular techniques and solutions especially applicable to binary gas mixtures of n-pentane/methane and n-hexane/methane dynamically adsorbed on a granulated solid. The data presented previously, however, was but the first step towards a usable design criteria that could realistically predict the dynamic adsorption behavior of the numerous multicomponent mixtures of hydrocarbons found in actual field operations.

The purpose of this dissertation is to attempt to achieve a practical solution to the dynamic adsorption of multicomponent mixtures of: 1) methane - n-pentane - n-hexane, and 2) methane - n-pentane - n-hexane - n-heptane at 800 psig and 90°F on 03 grade Silica Gel. The dynamic studies were all conducted at the natural gas research laboratory located on the north campus of the University of Oklahoma.

CHAPTER II

THE ADSORPTION PROCESS

Static Adsorption

The phenomenon exhibited by a solid in its affinity for fluid particles brought into contact with its surface area can be generalized as the adsorption process. Although the mechanics of adsorption apply to both liquid-solid as well as gas-solid mass transfer, this presentation will deal strictly with gaseous mixtures of adsorbates and solid adsorbents.

The accepted terminology in the area of adsorption relates the level of any adsorbate concentration, c_o, in the gaseous phase to the concentration of the adsorbate on the adsorbent, q_∞, utilizing an appropriate isotherm. The isotherm, in effect, is the most applicable mathematical model best suited to relate constant temperature adsorbate concentrations in both solid and gaseous phases.

There are, perhaps, three main isotherms whose characteristic shapes govern virtually all natural gas to solid adsorption processes.

1) The Linear Isotherm - occurring when the adsorbate concentration of the adsorbent continues to increase linearly with the adsorbate gaseous concentration.

2) The Favorable Isotherm or the Langmuir or Freundlich Relationships - occurring when relatively high concentrations of the adsorbate

are achieved on the adsorbent for low adsorbate gas concentrations. This isotherm tends to achieve a maximum asymptotic component adsorbent concentration.

3) The Unfavorable Isotherm - occurring when the adsorbate solid concentration is very low for a wide range of gaseous compositions resulting in poor recovery on the solid adsorbent.

Illustration II-1 indicates the importance of the linear isotherm in the determination of the ability of any solid to adsorb a particular component. This relationship has gained wide acceptance in the prediction of adsorbent concentrations because of its simplicity, yet overall applicability. This general trend can be classified as a Type I isotherm.

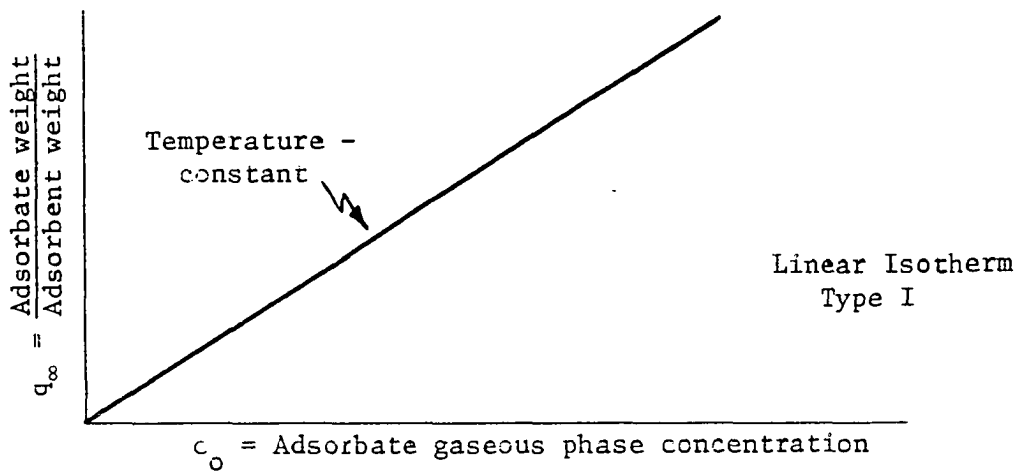

Illustration II-1

Although the representation in Illustration II-1 is linear, i.e., the slope of the adsorbent-adsorbate concentration line is constant, this condition has historically been proven strictly true only in very dilute gaseous mixtures. Freundlich presented an empirical isotherm for static

adsorption equilibrium that related the adsorbate-adsorbent component concentrations with a correlating exponent, n, characteristic of the component in question:

$$q_\infty = A\, c_o^{\,n} \quad . \qquad \text{II-1}$$

The value of n is very important in determining the nature of the Freundlich theory. For natural gas application, the isotherm seems well suited for general prediction of recovery concentrations, with a value of n less than but very close to 1.0. Illustration II-2 shows a graph of the Freundlich isotherm. In essence this isotherm can be considered a favorable isotherm, especially with $n < 1.0$ because of the increased adsorbent recovery for any equivalent adsorbate concentration.

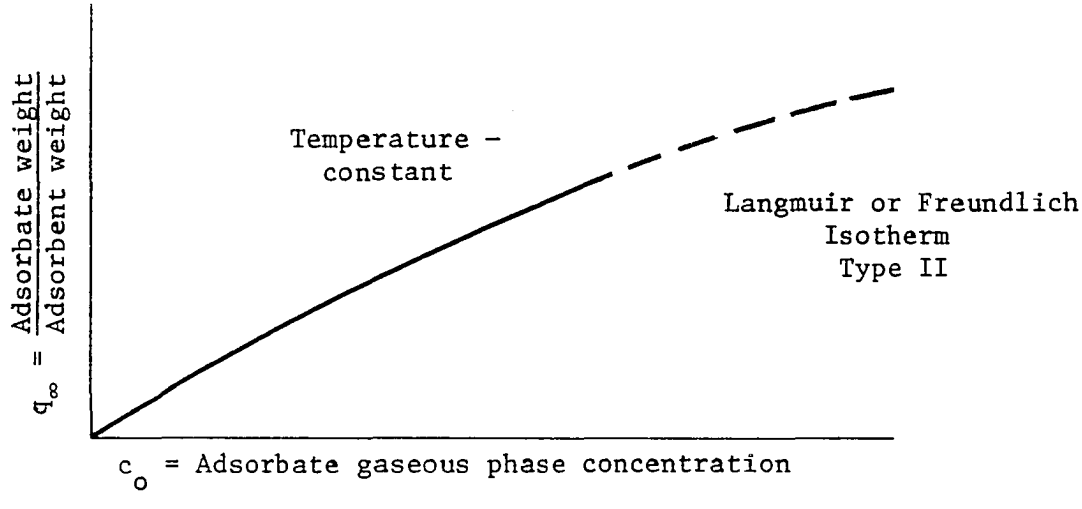

Illustration II-2

The Freundlich theory can be classified as the Type II isotherm in its application to natural gas adsorption.

The Langmuir isotherm is another favorable Type II isotherm that has found recent acceptance in the area of natural gas adsorption. This isotherm will be discussed in more detail in this chapter. Mathemati-

cally, the Langmuir theory states:

$$q_\infty = \frac{k_{AD}^{\,o}\, c_o\, q_\infty^{\,o}}{1 + k_{AD}^{\,o}\, c_o} \qquad \text{II-2}$$

where: $k_{AD}^{\,o}$ = the component adsorption equilibrium constant

$q_\infty^{\,o}$ the theoretical ultimate adsorbent capacity for the adsorbate.

The efforts in this dissertation are directed towards the application of this isotherm to natural gas mixtures.

A third type of isotherm, Type III, which falls into the category of a non-favorable class is depicted in Illustration II-3. In this case the adsorbate concentration of the adsorbing solid is very low for any corresponding gaseous phase adsorbate concentration. In simple terminology, to recover the same amount of any component from a gas mixture, a Type III isotherm would require more solid in contact with the gas than would Type II or Type I.

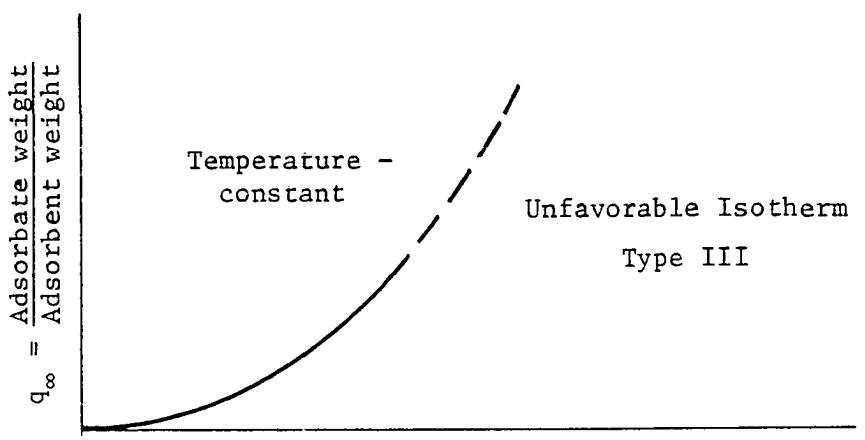

Illustration II-3

Dynamic Adsorption

The dynamic adsorption process is unlike the static only in that the adsorbate is present in a carrier gas that is in motion over a granular solid. As with the static case, the dynamic adsorption process usually occurs at constant system pressure and temperature. It is intuitively reasonable to assume that the motion of the carrier gas should not affect the equilibrium between the gaseous and adsorbed component on the solid. Day (D1) has presented data in support of this conclusion. The difference between the two procedures, i.e., static-dynamic lies in the following criteria:

1) The formation of a mass transfer zone in the dynamic case causes the adsorbate to distribute itself on the adsorbent in a 'transient' fashion. A position on the solid where the adsorbate concentration is zero is termed the leading edge of the zone. Where the solid concentration has reached its equilibrium level is denoted as the trailing edge. That portion of the adsorbent below the leading edge is virgin solid, whereas behind the trailing edge the bed or adsorbent is exhausted. See Illustration II-4.

2) The adsorbate concentration in the gas phase remains constant in the dynamic process whereas in the static case, the gas phase concentration continually decreases while the solid phase increases until equilibrium is achieved.

The overall equilibrium achieved on the solid adsorbent by either the static or dynamic system is the same, depending only on the pressure, temperature, and final adsorbate gas phase composition.

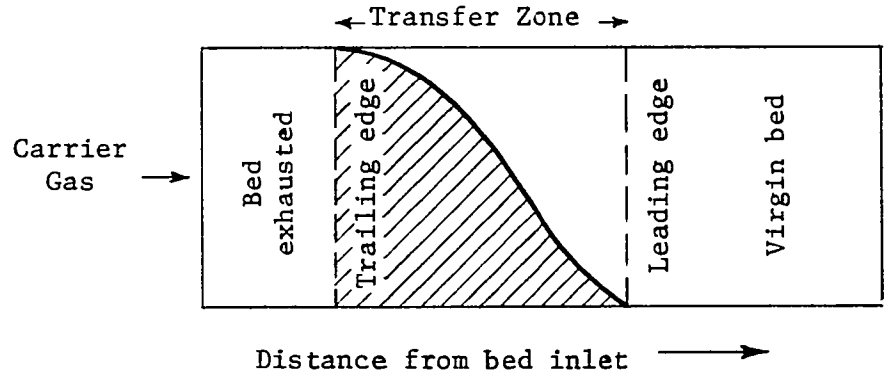

Illustration II-4

The important parameters that need to be considered in describing a dynamic system can be enumerated as follows:

1) The carrier gas composition.

2) The adsorbent equilibrium capacity for the adsorbate.

3) The system pressure and temperature.

4) The velocity of the carrier gas.

5) The length and cross sectional area of the adsorbing bed.

The carrier gas composition and resulting equilibrium concentration on the adsorbent are perhaps the most important of all the defining parameters influencing the mechanics of dynamic adsorption. Many relationships involving both the Langmuir and Freundlich isotherms have been presented for various gases in a binary mixture. More recently, the work of McLeod (M2), Needham (N1), Ashford (A2), and Ennecking (E1) have related binary equilibrium concentrations of hydrocarbons on activated carbon and silica gel. As yet, however, there is no general relationship relating multicomponent hydrocarbon mixtures to their equilibrium dynamic adsorption capacity. This study will seek to relate such hydrocarbon mixtures to their corresponding solid adsorption capacities.

The pressure and temperature are, of course, critical in determining the behavior of fixed bed dynamic adsorption. In order to minimize the inter-relationships between parameters, however, the studies that were conducted in support of this dissertation were all made at 90°F and 800 psig. These values of temperature and pressure were felt to be the best representative values of field operations involving the adsorption process.

Gas velocities and bed characteristics were varied in order to include the affects on the transient behavior of the adsorption mechanism.

The Langmuir Theory and Its Application to Binary and Multicomponent Mixtures

Basically, the Langmuir isotherm describes the relationship between the adsorption of any component on a solid adsorbent, and the desorption of this component from the solid to the gas. At such a time when the two mechanisms are equal, equilibrium will have been achieved for the particular system. Stated mathematically:

$$k_{ADS} (\delta^{o} - \delta)P_{pi} = k_{DES} (\delta) \qquad \text{II-3}$$

where: δ = that portion of the total possible solid surface area covered by the adsorbate - L^2

δ^{o} = the total area available - L^2

P_{pi} = the partial pressure of the component in question in the gas phase - FL^{-2}

k_{ADS} = the adsorption proportionality factor

k_{DES} = the desorption factor.

In application of the isotherm to natural gas adsorption, it has been

customary to redefine Equation II-3 into a more useful form by writing:

$$c_a = k_{ADS_1} P_{pi} \qquad \text{II-4}$$

$$\frac{\delta}{\delta^o} = \frac{q_a}{q_\infty^{\,o}} \qquad \text{II-5}$$

where: k_{ADS_1} = proportionality factor relating the partial pressure of the gas to its composition - L^2F^{-1}

$q_a/q_\infty^{\,o}$ = the ratio of the instantaneous component solid concentration to the absolute maximum concentration.

Rewriting II-3 gives:

$$c_a \left(1 - \frac{q_a}{q_\infty^{\,o}}\right) = \frac{k_{DES}\, k_{ADS}}{k_{ADS_1}} \frac{q_a}{q_\infty^{\,o}} \quad . \qquad \text{II-6}$$

Now, at such a time that the solid is fully saturated for any corresponding gas composition, c_o, the value of q_a will become q_∞, the equilibrium concentration. Thus:

$$c_o k_{AD}^{\,o} \left(1 - \frac{q_\infty}{q_\infty^{\,o}}\right) = \frac{q_\infty}{q_\infty^{\,o}} \quad . \qquad \text{II-7}$$

Where now the group of terms: $k_{ADS_1}/(k_{DES}k_{ADS})$ is redefined as $k_{AD}^{\,o}$, the Adsorption Equilibrium Constant for the component at any pressure and temperature.

Solving II-7 for q_∞ gives:

$$q_\infty = \frac{k_{AD}^{\,o}\, c_o\, q_\infty^{\,o}}{1 + k_{AD}^{\,o}\, c_o} \quad . \qquad \text{II-8}$$

When written in terms of the Langmuir Isothen, the c_o and c_a values are written in mole percents.

or:

$$\frac{1}{q_\infty} = \frac{1}{q_\infty^{\,o}} + \left[\frac{1}{k_{AD}^{\,o}\, q_\infty^{\,o}}\right] \frac{1}{c_o} \quad . \qquad \text{II-9}$$

Equation II-9 is extremely useful for two reasons: first, it affords a way in which to graphically represent adsorption data in order to obtain a "fit" for subsequent predictions, and second, the important parameters $k_{AD}^{\,o}$ and $q_\infty^{\,o}$, the adsorption equilibrium constant, and the ultimate solid capacity can be obtained from the plot. This particular isotherm is discussed by Vermeulen (V2), Thomas (T2), and Heister and Vermeulen (H2), in theoretical adsorption rate equation developments. No data has yet been presented for dynamic natural gas adsorption to support the validity of II-9 for this particular application. Later chapters will discuss the determination and application of the values $k_{AD}^{\,o}$ and $q_\infty^{\,o}$ and their relationship to dynamic adsorption.

Equation II-9 in its given form is good only for a binary mixture of an adsorbate and the carrier gas stream. In other terms, the parameters q_∞, c_o, and $k_{AD}^{\,o}$ are <u>binary</u> data values, and if the Langmuir isotherm is to be used to predict multicomponent mixtures, provisions must be made to redefine q_∞ as well as $k_{AD}^{\,o}$ for the multicomponent cases. These provisions will be discussed in subsequent chapters.

Adsorption Mechanics

In order to formulate the physical adsorption phenomenon into meaningful mathematical relationships the following criteria must be available:

1) A dynamic differential material balance, describing individual component behavior as a function of the rate and time of adsorption must

be written to incorporate governing variables.

2) An expression must be written, that governs the transient equilibrium achieved by the gaseous or solid adsorbate concentration in contact with the opposite phase.

3) A basic assumption must be made concerning the mechanics involved in the adsorption process.

4) Conditions must be set which govern whether the solutions to the equations arising from conditions 1) and 2) are transient solutions (i.e., a non-stable mass transfer zone, or steady state solutions, i.e., solutions that are independent of the distance covered by the adsorption front).

Illustration II-5 shows a differential element that represents the physical adsorption phenomenon. The rigorous derivation of the problem is given in Appendix C. The solution is similar to the energy exchange in heat transfer first treated by Schuuman (S1), and later by Furnas (F1).

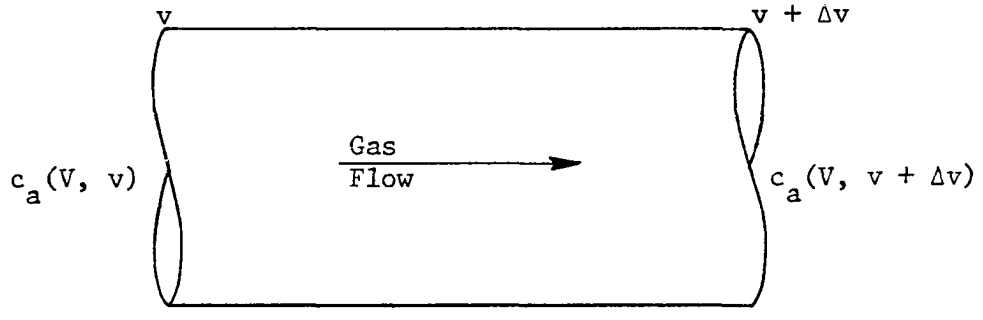

Illustration II-5

The units of $c_a(V, v)$ are now written as M/L^3.

Expressed analytically the material balance (for a given time differential, $\Delta\theta$) is:

$$-\left(\frac{\partial c_a}{\partial v}\right)_V = \Phi\left(\frac{\partial c_a}{\partial V}\right) + \rho_B\left(\frac{\partial q_a}{\partial V}\right)_v \qquad \text{II-10}$$

where: V = Total volume of soute or carrier gas passed through the element during a given time - L^3

v = Differential element volume - L^3

Φ = Packed bed porosity

ρ_B = Packed bed density - M/L^3

Equation II-10 is sometimes written in terms of the bed length, h, and the time of adsorption, θ, as given by Klinkenburg (K1) and discussed by Klotz (K3), and Needham (N1). This transformation is done by noting simply that:

$$A_B \frac{G}{\rho_g} \Delta\theta = \Delta V \qquad \text{II-11A}$$

and

$$(A_B \Delta h) = \Delta v \quad . \qquad \text{II-11B}$$

Thus, II-10 becomes:

$$-\left(\frac{\partial c_a}{\partial h}\right)_\theta \frac{1}{A_B} = \Phi\left(\frac{\partial c_a}{\partial \theta}\right) \frac{\rho_g}{A_B G} + \rho_B\left(\frac{\partial q_a}{\partial \theta}\right) \frac{\rho_g}{A_B G} \qquad \text{II-11C}$$

II-11C then becomes:

$$-v_g\left(\frac{\partial c_a}{\partial h}\right)_\theta = \Phi\left(\frac{\partial c_a}{\partial \theta}\right)_h + \rho_B\left(\frac{\partial q_a}{\partial \theta}\right)_h . \qquad \text{II-12}$$

Equations II-12 or II-10, with an appropriate rate equation, will define the solution for $c_a = c_a(\theta, h)$, or $c_a = c_a(V, v)$ as the conditions describe. Appendix C gives the complete derivations for the various rate equations assumed along with II-12 and II-10 for both transient and steady state phenomenon.

The Langmuir isotherm is again well suited to describe the instantaneous equilibrium achieved when the adsorbate concentration is increas-

ing on the adsorbent during the transient phenomena of the adsorption cycle. The ensuing relationship is perhaps the most important factor in the determination of realistic solutions involving all variables.

Returning to Equation II-8, and rewriting the relationship for any concentration q_a^* in equilibrium with a transient c_a:

$$q_a^* = \frac{k_{AD}^{\,o}\, c_a\, q_\infty^{\,o}}{1 + k_{AD}^{\,o}\, c_a} \quad . \qquad \text{II-13}$$

Thus, dividing II-13 by II-8 gives:

$$\frac{q_a^*}{q_\infty} = (c_a/c_o)\, \frac{(1 + k_{AD}^{\,o}\, c_o)}{(1 + k_{AD}^{\,o}\, c_a)} \quad . \qquad \text{II-14}$$

The factor: $\dfrac{1}{1 + k_{AD}^{\,o}\, c_o}$ is defined as the Equilibrium Parameter, r.

From this relationship:

$$k_{AD}^{\,o} = \frac{1 - r}{r\, c_o} \quad . \qquad \text{II-14A}$$

Equation II-14 then becomes:

$$\frac{q_a^*}{q_\infty} = \frac{c_a/c_o}{r + (1-r)\, c_a/c_o} \quad . \qquad \text{II-15}$$

Equation II-15 relates the transient instantaneous equilibrium in the solid with the gas phase concentration. Further, the equation relates the relative gaseous concentration to the equilibrium concentration at the corresponding c_o, q_∞, rather than the ultimate value, $q_\infty^{\,o}$, as in the isotherm relationship, II-9.

Hiester and Vermeulen (H2) have shown that another expression for r is:

$$r = 1 - \frac{q_\infty}{q_\infty^o} . \qquad \text{II-16}$$

The development of this expression is given in Appendix B. This equation, along with II-15, formulate the basic analytical expressions involving important adsorption parameters.

It is obvious from II-16 that adsorption values of r must range between zero, (0), for very high concentrations of the adsorbate in the carrier gas, to one (1.0) for very dilute systems that correspond to the trace chromatograms. The value of r is critical to the solution of the analytical problem, and special solutions arise for values of r between zero and one, as well as at the end points (i.e., 1.0 and 0).

In actuality, the values of r can be greater than 1.0. This case, however, corresponds to that of elution kinetics discussed by Vermeulen (V4), and Thomas (T1). This presentation will not deal with the elution equations involved in the desorption process.

For multicomponent applications, Equation II-15, along with Equation II-16 and the appropriate rate and material balance equation will serve as the necessary relationships to achieve a practical solution to the transient adsorption phenomena required before a system can be adequately defined.

CHAPTER III

ADSORPTION MECHANICS AND RATE EQUATIONS FOR BINARY AND MULTICOMPONENT MIXTURES

Basic Definitions

In any dynamic process, the assumption made concerning the adsorption mechanics drastically affects the solution of the basic mathematical relationships. Regardless of the rate equations incorporated into the solution, one of the following mechanisms controls the transient mass transfer:

1) Internal Solid Phase Diffusion
   a) Occurring when the controlling resistance to the energy or mass transfer process is present on the solid phase at the solid-gas interface.
2) External Phase Diffusion
   a) Occurring when the controlling resistance occurs at an imaginary gas "film" at the gas-solid interface.
3) External Reaction Kinetics
   a) Occurring when the governing mass transfer mechanism is a net kinetic reaction between adsorption and desorption rates.
4) Combined Phases Diffusion
   a) Occurring when the appropriate kinetic relationships are

a linear combination of the reaction mechanics of 1) through 3)

5) Steady State Adsorption - Incorporating the Michaels (M3) type of mass transfer as in the analagous ion exchange described also by Vermeulen (V3).

The terminology utilized in adsorption relationships is common to virtually all equations, regardless of the assumptions involved. These terms are all defined in the nomenclature.

General Mathematical Models - The Material Balance Equation

As described in Chapter II the material balance, or continuity equation expressed in differential form is:

$$-\left(\frac{\partial c_a}{\partial v}\right)_V = \left(\frac{\partial c_a}{\partial V}\right)_v \Phi + \rho_B \left(\frac{\partial q_a}{\partial V}\right)_v \cdot \qquad \text{III-1}$$

Many authors, including Klinkenburg (K1), Rosen (R1), Klotz (K1), Thomas (T2), and others discuss the transformation of variables in Equation III-1. This transformation follows in an analagous form to the work done originally by Schuuman (S1) in the heat transfer area, and later extended by Furnas (F1). These relationships are discussed in Appendix C. Vermeulen and Hiester, however, outline the general material balance as:

$$-\left(\frac{\partial x}{\partial \Sigma}\right)_{ZN} = \left(\frac{\partial y}{\partial (ZN)}\right)_{\Sigma} \cdot \qquad \text{III-2}$$

As discussed by Thomas (T2), and Goldstein (G3), Equation III-2 is of the generalized hyperbolic type of partial differential equations wherein a particular function f (Σ, ZN) is assured such that:

$$df\ (\Sigma, ZN) = \left(\frac{\partial f}{\partial \Sigma}\right)_{ZN} d\Sigma + \left(\frac{\partial f}{\partial ZN}\right)_{\Sigma} d(ZN) \qquad \text{III-3}$$

where: $$x = \left(\frac{\partial f}{\partial ZN}\right)_{\Sigma} \qquad \text{III-3A}$$

$$y = \left(\frac{\partial f}{\partial \Sigma}\right)_{ZN}. \qquad \text{III-3B}$$

In addition:

$$df(\Sigma, ZN) = 0. \qquad \text{III-3C}$$

Equation III-2 is the nucleus of the mathematical model that yields a particular solution depending on the rate equation incorporated into the analysis.

Proportionate Pattern Results

In cases where large adsorbent bed volumes are involved, i.e., $N >> 1.0$ the results of Devault (D2) and Wilson (W1), yield:

$$x = \frac{(r/Z)^{1/2} - r}{1 - r} . \qquad \text{III-4}$$

Equation III-4 relates x to Z at a constant r. This equation holds true, however, only for the proportionate pattern case, i.e.:

$$\frac{dy}{d\theta} \simeq \frac{dx}{d\theta} \qquad \text{III-4A}$$

or

$$\frac{dt}{ds} \simeq \frac{dy}{dx} .$$

Unfortunately, this condition does not apply to most cases of hydrocarbon dynamic adsorption, especially when N is moderately low.

Constant Pattern Diffusion: Binary Equations

As pointed out by Michaels (M2), and discussed by Vermeulen (V2), the constant pattern diffusion process presents a very powerful and useful tool in predicting adsorbate recoveries in dynamic systems.

McLeod (M2) has utilized this approach in predicting binary methane - n-pentane and methane - n-hexane system.

At such a time that a bed is fully saturated at a volume, $v\Phi$, a macroscopic material balance around the volume will yield:

$$c_o V = c_o v\Phi + q_\infty \rho_B v. \quad (c_o \text{ is in proper units}). \qquad \text{III-5}$$

This equation demands that the ratio of the dimensionless parameters be unity. Thus:

$$\left(\frac{\partial \Sigma}{\partial (ZN)}\right)_x = 1.0. \qquad \text{III-6}$$

When III-6 is incorporated into the material balance, there results:

$$x = y. \qquad \text{III-7}$$

External Phase Diffusion

Previous discussions concerning the external phase diffusion case have dealt with the general aspects of the particular solution. The rate equation for this assumption is as follows:

$$\frac{dq_a}{d\theta} = k_f a_p{}^o \frac{\phi}{\rho_B} [c_a - c_a{}^*]. \qquad \text{III-8}$$

The transient equilibrium established between $c_a{}^*$ and q_a is represented by:

$$\frac{c_a{}^*}{c_o} = \frac{r\, q_a/q_\infty}{1-(1-r)q_a/q_\infty}. \qquad \text{III-9}$$

Now for the case of a constant, r, and for constant pattern diffusion, i.e., y=x, Michaels (M2) first solved Equation III-8 with III-9 to give:

$$\left(\frac{1}{1-r}\right) \ln \frac{x_2(1-x_1)}{x_1(1-x_2)} + \ln \frac{(1-x_2)}{(1-x_1)} = N_f(Z_2 - Z_1). \qquad \text{III-10}$$

The solution III-10 is now a function of the column throughput parameter, θ, only.

Solid Phase Diffusion

This equation is both the general solution to the internal phase case, but represents the "steady state" solution that reflects the initial assumptions. McLeod (M2) has shown that the solid phase relationships is perhaps the best suited mechanism available to describe steady-state hydrocarbon dynamic adsorption behavior. The rate equation for this case is:

$$\frac{d\, q_a}{d\, \theta} = k_p a_p^{\,o} \, (q_a^{\,*} - q_a) \qquad \text{III-11}$$

while the transient isotherm is:

$$\frac{q_a^{\,*}}{q_\infty} = \frac{c_a/c_o}{r + (1-r)\, c_a/c_o} \,. \qquad \text{III-12}$$

Along with the constant pattern assumption ($y = x$), these expressions integrate to give:

$$\left(\frac{r}{1-r}\right) \ln \frac{x_2\,(1-x_1)}{x_1\,(1-x_2)} - \ln \frac{(1-x_2)}{(1-x_1)} = N_p\,(Z_2 - Z_1)\,. \qquad \text{III-13}$$

This equation was found by McLeod (M2) to be the most representative of methane - n-pentane and methane - n-hexane systems. It is, in fact, the primary relationship used in this work. Previous work has, however, limited this relationship to binary systems.

The effluent concentration, x, is again a function of the column throughput parameter, Θ, and is defined from a reference point Z_1. The asymptotic nature of x with increasing ΔZ as $\Delta Z \to \infty$, has histor-

ically named the solution the Solid Phase Asymptotic Solution.

Kinetic Reaction - Classical Solutions

This solution follows more closely with the Langmuir theory in the definition of the rate equation. For this case, the relationship is:

$$\frac{dq_a}{d\theta} = k_{kin}\left[c_a(q_\infty{}^o - q_a) - \frac{q_a}{k_{AD}{}^o}\right]. \qquad \text{III-14}$$

It is this equation that serves as a basis for defining the dimensionless variables t, s, Θ and Σ as pointed out by Vermeulen (V1). In addition, Equation III-14 reduces to: (see Appendix B)

$$\frac{dy}{dt} = [x(1 - y) - ry(1-x)]. \qquad \text{III-15}$$

This general expression along with the material balance yields the general solution presented in its most complete form by H. C. Thomas (T2) as:

$$x = \frac{1 - \int_0^{rs} e^{-t-\xi} I_o(2\sqrt{t\xi})\, d\xi}{1 - \int_0^{rs} e^{t-\xi} I_o(2\sqrt{t\xi})\, d\xi + e^{(r-1)(t-s)}\left[\int_0^{s} e^{-rt-\xi} I_o(2\sqrt{rt\xi}\, d\xi\right]} \qquad \text{III-16}$$

In terms of N and NZ III-16 becomes:

$$x = \frac{J(rN, ZN)}{J(rN, ZN) + e^{(r-1)N(Z-1)}[1-J(N,rZN)]}. \qquad \text{III-17}$$

These equations hold for any value of N, r, or ZN, and are not governed by the limiting assumption of constant pattern mass transfer within the packed bed.

The "J" function corresponds to the general case of:

$$J(x,y) = 1 - \int_0^x e^{-y-\xi} I_o \left(2\sqrt{y\xi}\right) d\xi. \qquad \text{III-18}$$

These solutions are very rigorous and complete. By their very nature, however, they do not easily lend themselves to workable design equations that would be readily usable in practical operations. In addition, the pertinent parameters in the equations, i.e., s, t, r cannot be defined unless previous laboratory data has predescribed the limits, nature, and application of the relationships. Since the historical application of III-16 and III-17 has been with binary mixtures, the applications are limited to that type of data. The next chapter will discuss the laboratory measurements involved in determining the proportionality factors required for use of the equations.

An interesting case of Equation III-17 occurs when the equilibrium parameter, r, is equal to 1.0. This corresponds to the linear isotherm, i.e.,

$$\frac{q_a^*}{q_\infty} = \frac{c_a}{c_o} \quad (r = 1.0). \qquad \text{III-19}$$

This case was used by Needham (N1) in his application of the Rosen (R1) and Klinkenburg (K2) solutions of analagous heat transfer problems to binary mixtures of methane and n-pentane. The general solution to Equation III-14 with r = 1.0 is the general case solved

first by Schuuman (S1) and later extended by Furnas (F1):

$$x = 1 - \int_0^s e^{-t-\xi} I_o(2\sqrt{t\xi})\, d\xi \ . \qquad \text{III-20}$$

This case is very limited, however, since r = 1.0 is approximated only by very dilute solute concentrations. In addition, the assumption of a linear isotherm is somewhat of a limitation. This hindrance is not as severe in binary adsorption, as shown by Needham (N1), but is more pronounced for multicomponent processes.

Combined Phases Reaction

In many instances, it is advantageous to obtain a knowledge of the overall behavior of an adsorption system as an average between the solid and external cases. This particular solution is especially useful when the 'film' resistances expressed by Equations III-8 and III-17 are approximately the same order of magnitude. For this case Vermeulen (V1) has shown that adding the internal and external rate equations yields an expression for the resistance equivalent to:

$$R(\text{combined}) = \frac{\rho_B q_\infty}{k_f a_p{}^o \Phi c_o} + \frac{1}{k_p a_p{}^o} \ . \qquad \text{III-21}$$

The equation has been redefined as:

$$\frac{D}{k_f a_p{}^o} + \frac{1}{k_p a_p{}^o} = \frac{q_\infty\, b}{q_\infty{}^o\, k_{kin}\, c_o} \qquad \text{III-22}$$

where:

$$b = \frac{(q_a{}^* - q_a)\, c_o + q_\infty (c_a - c_a{}^*)}{c_a (q_\infty - q_a) - r q_a (c_o - c_a)} \ . \qquad \text{III-23}$$

Vermeulen (V1) discusses the technique required to calculate values of b, by defining a mechanism parameter, i.e.:

$$\xi = \frac{q_\infty (c_a - c_a^*)}{c_o (q_a^* - q_a)} \quad . \qquad \text{III-24}$$

The author presents a graphical relationship for the calculation of b. For the mechanisms present in hydrocarbon adsorption, however, b is very nearly constant and between values of 2.0 and 1.0. McLeod reports a value of 1.20 for n-pentane methane mixtures at 90°F and 800 psig while the corresponding n-hexane methane value is 1.43. These numbers were based on a constant value for the equilibrium parameter, r. This assumption is not true, and is only an average representation of the mechanics of the adsorption process.

Applications of the Rate Equations

Fortunately much has been done in the area of natural gas dynamic adsorption towards the application of previously derived solutions. Needham (N1), has 'fit' the Rosen (R1) and Klinkenburg (K2) solutions to n-pentane-methane binary mixtures, and McLeod has applied the constant pattern solutions of Michaels (M3) and Gluekauf and Coates (G2) to methane-n-pentane and methane-n-hexane systems. Their work is most valuable, because they established the following criteria:

1) Solid phase particle diffusion was the controlling mechanism for both n-pentane and n-hexane as the adsorbate. Values reported by both Needham (N1) and McLeod (M2) indicate that the term $k_p a_p^o$ is much smaller than the corresponding $k_f a_p^o$ values for virtually all component concentrations and gas flow rate ranges. The following table

illustrates an example of the values for the correlating parameters taken from their work.

N-PENTANE-METHANE

McLeod 3-8 mesh gel				Needham 3-4 mesh gel		
$k_p a_p^o$	$k_f a_p^o$	c_o	Q(SCF/hr)	$k_{kin} c_o$	c_o	v_g
.397	338	1.46	1583	.44	1.4	All
.576	338	2.04	1562	.70	2.0	Velocities
.272	680	.55	6688	.26	.55	

2) The steady state solutions (i.e., constant pattern diffusion) can be utilized to adequately represent adsorption phenomena for hydrocarbon binary mixtures at 800 psig and 90°F.

3) In Needham's (N1) work the more rigorous solution was very close to the constant pattern case applied by McLeod, lending support to stipulation (2).

The purpose of the remainder of this work, therefore, will be to apply the solid phase diffusion equation to multicomponent systems. In order to accomplish an adequate solution, however, the following re-evaluations are noted:

1) In the solution to binary mixtures the solid phase Equation III-17 applies in its present form. However, multicomponent mixtures require that provisions be included in the calculation of the relative effluent concentration, x, in order to account for the increased instantaneous equilibrium reached while one mass transfer is being displaced by another.

2) Previous work done by McLeod (M2), considered only a constant value for r, the equilibrium parameter for methane - n-pentane and methane - n-hexane mixtures. These values were respectively: .667 for n-pentane and .4 for n-hexane. While a constant value of r, indeed, simplifies the approach taken in "fitting" effluent curves to Equation III-13 the results are only an average representation of actual adsorption parameters. The existing binary analysis reported by McLeod was re-evaluated for both the n-pentane and n-hexane cases in order to arrive at more meaningful values for the pertinent parameters.

3) The work done by Needham, (N1), considered only the linear isotherm i.e., $d\, q_\infty / d\, c_o$ = const. with r = 1.0. The slope of the dynamic adsorption isotherm, however, can be more nearly represented by:

$$\left(\frac{d\, q_\infty}{d\, c_o}\right) = \frac{q_\infty}{c_o r} \,, \qquad \text{III-25}$$

where r is defined by the adsorbate in question. Subsequent chapters will show, however, that the value $q_\infty / c_o r$ is a very slowly varying number over a good portion of the applicable range of c_o. In fact, for multicomponent mixtures a simplifying assumption is made on the basis of III-25 in order to achieve a practical multicomponent solid phase asymptotic solution.

4) Previous authors have not reported a general isotherm that is applicable to dynamic systems. McLeod reports limits over which the Freundlich isotherm gives reasonable agreement with measured binary data. Moreover, a method of defining adsorbent component concentrations for multicomponent data is essential to the solution

of multicomponent adsorption using the constant pattern approach. Subsequent chapters will discuss such an application.

5) Cases arise where the constant pattern diffusion case for any rate mechanism is indeed a non-applicable assumption. For predictions, therefore, employing the asymptotic solution, care must be taken to ascertain the nature of "current" adsorption parameters in relation to their 'steady-state' values. Provisions are also made in this study to derive transient data from constant pattern diffusion values.

Limitations

It is beyond the scope of this work to consider defining pertinent parameters for the components lighter than n-pentane, or heavier than n-hexanes.

The effect of n-heptane concentrations on the adsorptive phenomenon relating to n-pentane and n-hexane, was studied in the three adsorbate runs made. However, no single n-heptane runs were made to define binary parameters for this component. It is felt that a description of the n-pentane and n-hexane results should represent an adequate start to aid in the application of laboratory information to field installations and design.

Likewise, the application of this data will be of an approximate nature when sizeable quantities of butanes are in process gases. For moderate to low butane concentrations, however, the effect of that component on the adsorptive behavior of heavier components is minimal.

CHAPTER IV

BINARY AND MULTICOMPONENT ADSORPTION ISOTHERMS AND EQUATIONS FOR THE SOLID PHASE DIFFUSION CASE

Requirements for Defining the Problem Analytically

The general requirements for binary data applications of Equation III-13, i.e.:

$$\frac{r}{1-r} \ln \frac{x_2 (1-x_1)}{x_1 (1-x_2)} - \ln \frac{(1 - x_2)}{(1 - x_1)} = N_p \Delta Z \qquad \text{III-13}$$

can be summarized as the following:

1) An available isotherm relating the known parameter, c_o to the resulting q_∞. This isotherm, in turn, defines r for the specific case,

$$r = 1 - \frac{q_\infty}{q_\infty^o} \quad .$$

2) Measured binary steady state data that can be related to III-13 as outlined by McLeod (M2). The resulting parameters, i.e., $k_p a_p^o$ and N_p should serve as a basis for predicting further multicomponent values.

Hydrocarbon Adsorption Applications - The Langmuir Isotherm: Present and Previous Work

The Langmuir isotherm has been used to correlate dynamic adsorption values of c_o and q_∞ for both binary and multicomponent mixtures. The data reported by McLeod and Needham have been represented in the graphical format demanded by the isotherm (see Appendix A) i.e.:

$$\frac{1}{q_\infty} = \frac{1}{q_\infty^{o}} + \frac{1}{k_{AD}\, q_\infty^{o}} \frac{1}{c_o} \quad . \qquad \text{IV-1}$$

Figures A-1 and A-2 represent the results of the plot for both n-pentane and n-hexane on 03 grade silica gel at 90°F and 800 psig.

As denoted by IV-1, the "apparent" intercept of the plot, i.e., $1/q_\infty^{o}$ occurs when $1/c_o = 0$. This condition is, of course, impossible, since the maximum value n-pentane could achieve in any binary system of methane n-pentane must be less than 100.0%. However, at $c_o \approx 100\%$ the value of the term:

$$\frac{1}{k_{AD}^{o}\, c_o\, q_\infty^{o}} \quad ,$$

is seen to be quite small in comparison with the intercept q_∞^{o-1}. In addition, the absolute values of $1/q_\infty$ for concentrations of either n-pentane or n-hexane above 99%, do not vary appreciably. The results of the plot therefore, can be taken as directly representative values for both q_∞^{o} and k_{AD}^{o}.

The following parameters were found to be the most representative values for both q_∞^{o} and k_{AD}^{o} for the binary n-pentane and n-hexane isotherms:

Component	k_{AD}^{o}	q_∞^{o}
N-Pentane	.444	.333
N-Hexane	.959	.408

It can be seen, therefore, that for any binary system defined by the Langmuir isotherm r varies as:

$$r = \frac{1}{1 + .444\ c_o} \quad , \text{ or}$$

$$r = 1 - \frac{q_\infty}{.333}$$

for n-pentane, while for n-hexane:

$$r = \frac{1}{1 + .959\ c_o} \quad , \text{ or}$$

$$r = 1 - \frac{q_\infty}{.408}$$

are seen to apply.

Day (D1) and Needham (N1) have reported maximum "monolayer" adsorption capacities wherein physical constants reported by Hirshfelder (H3) for n-pentane and n-hexane were used to compute the maximum equilibrium adsorption concentration achieved when the surface area available in a 21A° pore size gel was completely covered with the adsorbate. This condition is denoted in Illustration IV-1.

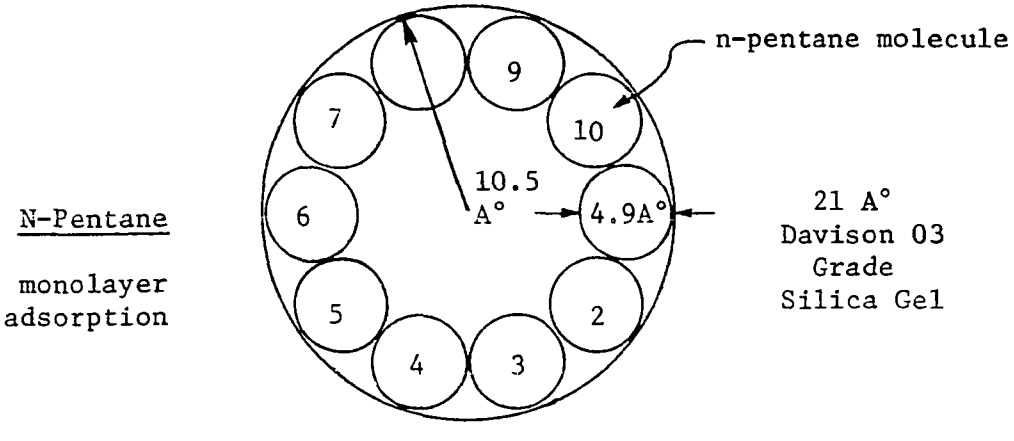

Illustration IV-1

The values reported by both Day (D2) and Needham (N1) for the pertinent adsorbates are reported as:

Day		Needham	
Adsorbate	q_∞ (Monolayer)	Adsorbate	q_∞ (Monolayer)
N-Butane	.134	N-Pentane	.136 - .145

These numbers are presented to point out an interesting fact. If, indeed, the monolayer calculations are correct, and the 'extensions' of the corresponding Langmuir isotherms to $1/K_{AD}^{o}\ q_\infty^{o}\ c_o \simeq 0$ are correct, then it follows that the monolayer capacity is not the 'ultimate' gel capacity. It seems, therefore, that at high concentrations of the adsorbates, n-pentane and n-hexane, multiple layers of the adsorbed phase are formed within the pore structure of the adsorbent. Brunaer (B3), points out that localized 'cylindrical' orientation of the adsorbate molecules is not inherently assumed by a particular isotherm. Conversely, monolayer adsorption, as discussed by Day (D1), results in the following stipulations:

1) No molecular interaction of the adsorbate

2) Constant heat of adsorption within each adsorption site.

On the basis of the presently calculated values of .333 lb/lb n-pentane and .408 lb/lb n-hexane the number of molecules needed within the internal surface area of a $21A^{o}$ gel can be summarized as follows:

N-Pentane

$\pi DL = 800\ \frac{m^2}{gm}$ (maximum surface area)

$L = 11.38 \times 10^{20}\ A^{o}$ length of single capillary of uniform size.

Now with an absolute maximum adsorption capacity of .333 for n-pentane

$$\frac{.333}{72} = 4.62 \times 10^{-3}\ \text{gm-moles/gm-gel}$$

the number of molecules per gram of gel would be:

$$4.62 \times 10^{-3} \times 6.02 \times 10^{23} = 27.85 \times 10^{20} \text{ molecules/gm-gel}$$

Using the values reported by Hirshfelder for n-pentane, i.e., molecular diameter 4.9A°, molecular length 10A°, gives:

$$\frac{11.38 \times 10^{20}}{10} = 11.38 \times 10^{19} \text{ units of n-pentane/gm-gel}$$

The number, N, of molecules per n-pentane unit is:

$$N = \frac{27.85 \times 10^{20}}{11.38 \times 10^{19}} = 24 \text{ molecules/unit}$$

Needham (N1) has shown that two-layer perfectly oriented adsorption in the surface area of a 3-4 mesh gel would yield 13 molecules. The above reasoning, therefore, suggests that in dynamic equilibrium, a strong molecular deformation or interaction occurs.

Needham (N1) points out, that monolayer, highly oriented molecular arrangement seems to predominate in dynamic adsorption. However, his dynamic data for n-pentane in methane was fit to an empirical Freundlich type isotherm for an adsorbate concentration range of .075-3.0 mole % n-pentane. Perhaps at higher adsorbate concentrations molecular interaction could predominate in the adsorption mechanics, causing a greater than the ideal packing density. In addition, Needham's data was reported for a 21A° silica gel, whereas the present data was measured for a 22-23 A° gel.

McLeod (M1), moreover, reports equilibrium parameters values of .667 and .4 for n-pentane and n-hexane in methane. According to the definition of r:

$$r = 1 - \frac{q_\infty}{q_\infty^o}, \quad \text{(for n-pentane)},$$

$$\frac{q_\infty}{q_\infty^o} = .333.$$

For an 'average' value of q_∞, say .1, which corresponds to a 1.0 mole % pentane (in methane) gives a value of:

$$q_\infty^o = \frac{.1}{.333} = .30.$$

For MeLeod's data, taken under the same conditions as this work the value for the ultimate capacity, q_∞^o, seems more in agreement with the present number, .333.

Day (D1) has reported static binary equilibrium data for both n-pentane and n-hexane in methane at pressures ranging from 100 psig to 1000 psig. Beyond 1000 psig the adsorption capacity decreases for both adsorbates. His findings indicate that at pressures greater than 650 psig and less than or equal to 1000 psig, the adsorption isotherms are virtually identical. This phenomenon suggests that silica gel pore volume 'fill-up' occurs at pressures slightly less than 600 psig for all concentration levels, remain at that equilibrium level and then desorption occurs when molecular interaction or deformation forces the adsorbate into the gas phase in order to compensate for the increased partial molar volumes of the component in that phase. The n-pentane and n-hexane data presented by Day has been replotted in the present units as $1/c_o$ vs. $1/q_\infty$ and the results are shown in Appendix A. For the case of the n-pentane data, there is good agreement between equilibrium values at 685, and 1000 psig and 100°F and the present dynamic isotherm; expressed in Figure (A-3) as:

$$\frac{1}{q_\infty} = 3.00 + 67.6\,\frac{1}{c_o}\,. \qquad \text{(N-Pentane-Methane)}$$

The 'intercept' of the static data, however, indicate a somewhat higher value than the reported monolayer capacity for n-pentane, i.e., .136 lb/lb. For n-hexane, Day's data are reported along with the present n-hexane dynamic isotherm, i.e.:

$$\frac{1}{q_\infty} = 2.45 + 25.5 \frac{1}{c_o} . \qquad \text{(N-Hexane-Methane)}$$

Again, the data show remarkably good agreement taking into consideration the fact that these values cover a range of ±300 psig and 10°F (i.e., 700 to 1000 psig and 90 to 100°F).

All indications are, therefore, that at higher n-pentane and n-hexane concentrations than normally encountered in naturally occurring hydrocarbon mixtures (i.e., >5.0 mole %), the adsorption is not necessarily limited to that of the (highly oriented) monolayer. Indeed, the practicality in the reported relationships for n-pentane and n-hexane lies in the ability of the isotherm to reproduce (by calculation) previously measured data.

The Multicomponent Isotherm

The Langmuir approach has now been established as perhaps the best suited isotherm for binary hydrocarbon mixtures as it has correlated well with experimental data. A re-evaluation of the parameters of the isotherm are necessary, however, to predict multicomponent behavior from binary data. Expressed in its usual fashion, the Langmuir isotherm is again written parametrically:

$$\frac{q_\infty}{q_\infty^{\,o}} = \frac{k_{AD}^{\,o} c_o}{1 + k_{AD}^{\,o} c_o} . \quad (c_o \text{ is in mole \%}). \qquad \text{IV-2}$$

Now the effect of more than one adsorbate (excluding methane, whose equilibrium capacity is assumed to be negligible) in an adsorbing system can be described by Illustration IV-2.

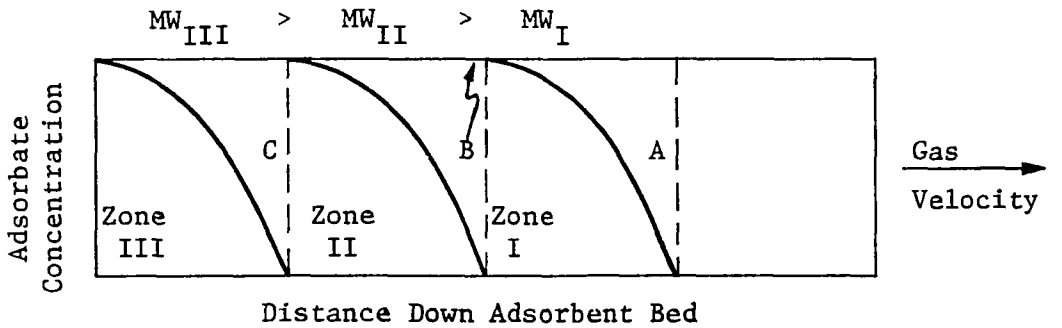

Illustration IV-2

The phenomenon of chromatographic separation demands that the adsorbate of highest molecular weight be predominantly attracted to the adsorbing media, while the lightest molecular weight component is least attracted to the adsorbent. The physical result of this mechanism, is that hydrocarbons of highest molecular weight emerge last from the outlet of the adsorbent bed while the most volatile emerges first. During the adsorption process, however, an overall 'equilibrium' is achieved in the adsorbent medium between all adsorbate solid concentrations and the corresponding gas phase concentrations. This adsorbent concentration must be lower than the corresponding binary level, because the particular adsorbate must share the adsorption area with the other "n" components.

This overall equilibrium is not achieved uniformly, however, while the adsorption process is in progress. In the leading edge of the lightest components' mass transfer zone, (Point A in Illustration IV-2), the adsorbate concentration is increasing normally in a transient fashion to its binary level, q_∞. This level is represented

by Point B where the gas phase adsorbate concentration has reached c_o. The adsorbate in Zone II, however, cannot experience such binary equilibrium concentrations because of the residual concentration of adsorbate I in the zone. In fact, when adsorbate I first occupied the gel at the inlet to the adsorbent bed, adsorbate II began physically "displacing" or "desorbing" I while the former progressed over the gel already laden with adsorbate I. Component II continually displaces the binary levels of I until equilibrium is achieved as the conditions demand. In a similar manner, component III or any "n" component likewise will displace II and I from the available adsorption sites until an overall dynamic equilibrium is achieved between "n" components for any concentration levels, and a particular pressure and temperature. The displacement of one component by the correspondingly higher molecular weight components is termed the "differential desorption" or simply the "desorption" of one component by another.

An interesting facet of the desorption mechanism is that the trailing edges of all but the heaviest components in a mixture of "n" adsorbates will have locally higher equilibrium adsorbate and adsorbent concentrations. This phenomenon arises because while the desorption mechanics are in progress, the adsorbate I, for example, desorbed by II, will enter the gas phase at a point B where the transient gas phase component concentration is already c_o. Thus, the localized levels of c_o increase as a function of the concentration level of adsorbate II, as well as the length of the bed. Illustration IV-3 denotes this point.

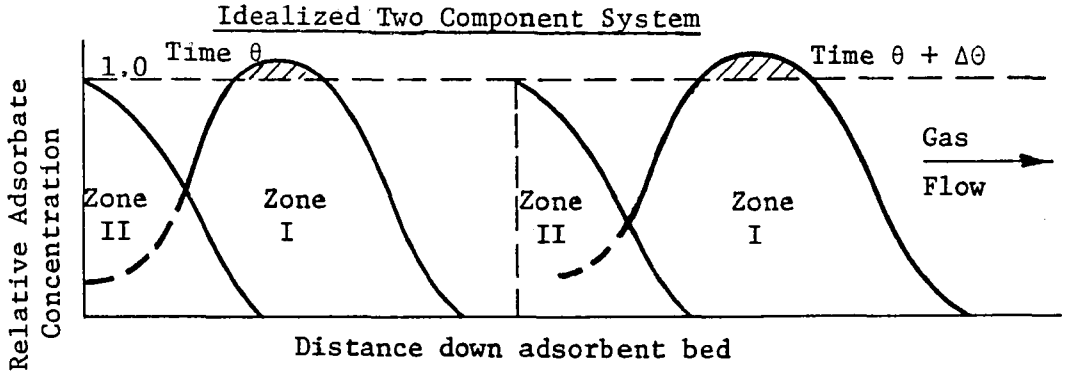

Illustration IV-3

The cross-hatched areas illustrate the desorbed portion of the I adsorbate, that is present in Zone I for a localized increase in c_o and q_∞ respectively. For three component mixtures, Illustration IV-4 indicates the corresponding description:

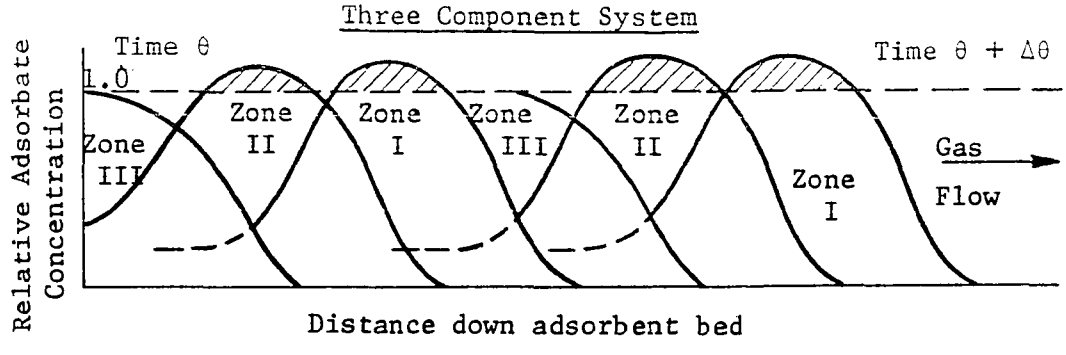

Illustration IV-4

Thus the procedure follows until the final equilibrium values are reached for all three components at the trailing edge of the last zone. These values of q_∞', however, are less than the binary values of q_∞ by an amount equal to the desorption:

$$q_{\infty i}' = q_{\infty i} - \Delta q_{\infty i,\ i+1} \qquad \text{IV-3}$$

$$q_{\infty i}'' = q_{\infty i} - \sum \Delta q_{\infty i,\ i+1,\ i+2} \qquad \text{IV-4}$$

or in general terms

$$q_{\infty i}^{n\prime} = q_{\infty i} - \sum_{j=1}^{n} \Delta q_{\infty i,\ i+j}$$

Returning to IV-2 and rewriting the isotherm for any multicomponent mixture involving the i^{th} component:

$$\frac{q'_{\infty i}}{q^{o}_{\infty}} = \frac{k'_{ADi}\, c_{oi}}{1 + k'_{ADi}\, c_{oi}}\,, \qquad \text{IV-5}$$

where the singly "primed" parameters indicate ternary or two adsorbate systems.

Likewise, the $i^{th} + 1$ component has an isotherm:

$$\frac{q'_{\infty i+1}}{q^{o}_{\infty i+1}} = \frac{k'_{ADi+1}\, c_{oi+1}}{1 + k'_{ADi+1}\, c_{oi+1}}\,. \qquad \text{IV-6}$$

Now, it can be seen that a plot of either IV-5 or IV-6 would yield a figure such as one shown by Illustration IV-5.

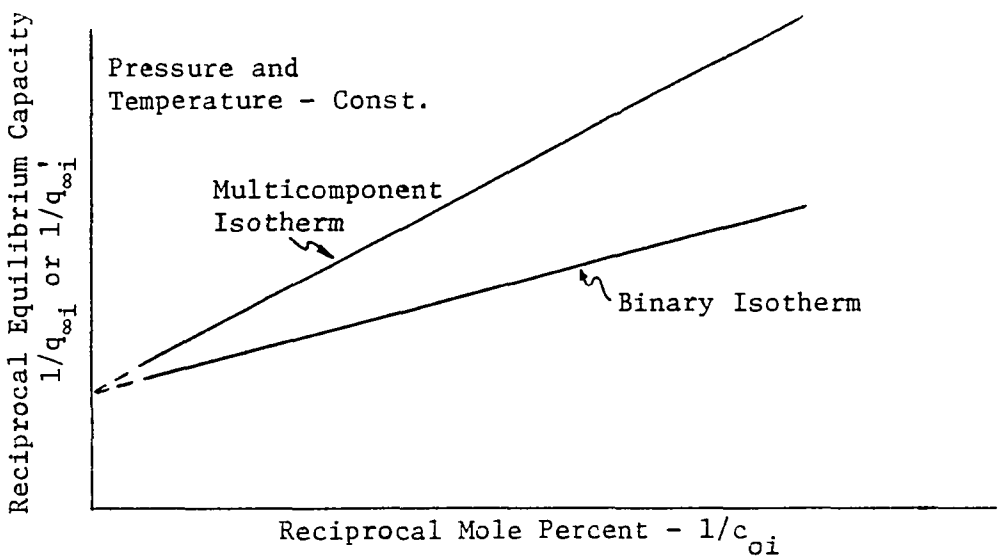

Illustration IV-5

It is reasonable to assume that the value of k'_{ADi} or k'_{ADi+1} can be characterized as a constant depending on the concentration level of the "i" or "i+1" component, whichever happens to be the "key" component.

As before, the pressure and temperature are assumed constant. Thus, for a system of n-pentane - methane to which n-hexane has been added, the value of $k_{AD}^{o} = .444$ for n-pentane will decrease because of the decreased value of $q_{\infty i}'$. The slope of the new isotherm will be:

$$\frac{1}{k_{ADi}' \, q_{\infty}^{o}} .$$

For moderate composition levels of the second adsorbate, the value of the intercept, q_{∞}^{o}, should be very nearly constant, as the mole percents of the gaseous components are plotted as "reciprocal" values. Thus, for, say an "i+1" concentration of 50%, the absolute maximum "i" concentration must be less than 50% (in a methane carrier). The reciprocals, however, i.e., 1/50 are sufficiently close to zero to give virtually the value of q_{∞}^{c}, for the adsorbate corresponding to the binary case.

Thus, returning to IV-5 and IV-6 and solving each by its corresponding value of k_{ADi}':

$$\frac{1}{q_{\infty i}} - \frac{1}{q_{\infty i}^{o}} = \left(\frac{1}{k_{ADi}' \, q_{\infty i}^{o}}\right) \left(\frac{1}{c_{oi}}\right) \qquad \text{IV-7}$$

$$k_{ADi}' = \left(\frac{1}{q_{\infty i}^{o} \, c_{oi}}\right) \left(\frac{q_{\infty i}^{o} \, q_{\infty i}'}{q_{\infty}^{o} - q_{\infty i}'}\right) \qquad \text{IV-7A}$$

$$k_{ADi}' = \left(\frac{1}{c_{oi}}\right) \left(\frac{q_{\infty i}}{q_{\infty}^{o} - q_{\infty i}'}\right) . \qquad \text{IV-7B}$$

Likewise:

$$k_{ADi+1}' = \frac{1}{c_{oi+1}} \left(\frac{q_{\infty i+1}'}{q_{\infty i+1}^{o} - q_{\infty i+1}'}\right) .$$

Dividing IV-7A and IV-7B by the corresponding binary values for k_{AD}^{o} gives:

$$\frac{k_{ADi}'}{k_{ADi}^{o}} = \frac{q_{\infty i}'}{k_{ADi}^{o}\, c_{oi}(q_{\infty i}^{o} - q_{\infty i}')} = \alpha_i \ , \qquad \text{IV-8}$$

and

$$\frac{k_{ADi+1}'}{k_{ADi+1}^{o}} = \frac{q_{\infty i+1}'}{k_{ADi+1}^{o}\, c_{oi+1}\, (q_{\infty i+1}^{o} - q_{\infty i+1}')} = \alpha_{i+1}. \qquad \text{IV-8A}$$

The value of α_i or α_{i+1} denotes the relative increase in slope of the dynamic isotherm at any concentration of the alternate adsorbate. α_i and α_{i+1} have been calculated for n-pentane - n-hexane mixtures in methane. The results are discussed more thoroughly in a subsequent chapter. However, the various levels of α_i or k_{ADi}' correlate very readily with the mole percent of the alternate adsorbate concentration.

For a multicomponent system of say methane, n-pentane, and n-hexane the level of n-pentane determines the value of k_{ADhx}' (n-hexane) and the concentration of n-hexane sets the value of k_{ADp}' (n-pentane). The multicomponent isotherm for any <u>one</u> component is defined <u>only</u> at the level of the other adsorbate. A system therefore, of two or more adsorbates is defined by any one point on each adsorbate isotherm.

The foregoing analysis works also very well for mixtures of three adsorbates with methane as the carrier gas. For this particular multicomponent case, (i.e., mixtures beyond ternary levels) the Equations IV-8 and IV-8A for α_i and α_{i+n} become:

$$\alpha_i' = \frac{q_{\infty i}''}{k_{ADi}''\, c_{oi}(q_{\infty i}^{o} - q_{\infty i}'')} \ , \qquad \text{IV-9}$$

$$i \leq n$$

where now:

α_i' = ratio of the adsorption equilibrium constants

$q_{\infty i}''$ = the equilibrium level of the adsorbate on the adsorbent in multicomponent mixtures lb/lb

n = number of adsorbates

Values of α_i' have been correlated successfully for a "pseudoternary" system of the particular component "i" and the sum of the mole percent of the remainder of the adsorbates. This procedure is again discussed in a subsequent chapter.

The value of $q_{\infty i}^{o}$, as mentioned previously, is assumed to be constant at the measured binary level, i.e., where

$$\frac{1}{k_{ADi}^{o}\, q_{\infty i}^{o}\, c_{oi}} \simeq 0 \,. \qquad \text{IV-10}$$

The Solid Phase Constant Pattern Diffusion Equation for Multicomponent Mixtures

As already shown, the transient equilibrium achieved instantaneously between the solid-gas interface is expressed by the Langmuir type isotherm:

$$\frac{q_a^{*}}{q_\infty} = \frac{c_a/c_o}{r + (1-r)\, c_a/c_o} \,. \qquad \text{IV-11}$$

This equation, however, is valid for the range $0 \leq c_a/c_o \leq 1.0$ where the corresponding q_a^{*}/q_∞ for the solid phase is a function of α only. For multicomponent simultaneous mass transfer, equilibrium values for c_o (and q_a^{*}) can reach levels greater than the input c_o level for the gas phase. This phenomenon arises from the zone desorption of one component by another of higher molecular weight as previously shown. Consequently,

values of q_a^*/q_∞ are likewise greater than 1.0, as the solid phase adsorbate concentration strives to reach a dynamic equilibrium during mass exchange with the gas phase. This phenomenon is indicated in the multicomponent effluent concentrations in the laboratory collected data shown graphically in Appendix A.

It is convenient, to define a Relative Concentration Enhancement Factor, λ, or an Equilibrium Enhancement Factor, that describes the final value of the effluent gas adsorbate concentration achieved as the mass transfer zones progress the length of the adsorbent bed, h. For any adsorbate in question, "i", this factor (λ) can readily be seen to be a direct function of the following parameters:

1) The concentration of the displaced zone - c_{oi}
2) The concentration of the displacing zone - c_{oi+1}
3) The adsorption pressure and temperature, psig - °F
4) The length of the adsorbent bed - H_T.

Of these parameters (1), (2), and (4) are, of course, the ones pertinent to this work and will be considered in the development of the solid phase diffusion model.

For a given equilibrium condition, at $h = H_T$ the adsorbent bed length:

$$c_a\ (q_\infty^{\ o} - q_{am}^*) = \frac{q_{am}^*}{k_{ADm}'}\ , \qquad \text{IV-12}$$

where the subscript "m" denotes the respective multicomponent values for any adsorbate, replacing the "i" subscript for generalization.

Now, by the hypothesis made concerning λ, at $h = H_t$ and $c_a = f(c_o)$, the actual value of c_a at its maximum level will be

$$\lambda(c_o,\ H_T)\ c_o\ , \qquad \text{IV-13}$$

where now $\lambda(c_o, H_T)$ is the unknown enhancement factor for the equilibrium concentration increase.

Previous analysis has shown that the slope of the dynamic isotherm is:

$$\frac{dq_{\infty m}}{dc_o} = \frac{q_{\infty m}}{c_o r} = f(D,r). \qquad \text{IV-14}$$

In addition, the values of q_∞/c_{or} are seen to be approximately constant, as indicated by Figure A-6 in Appendix A.

In view of the above criteria, it is reasonable to assume, as an estimate, that λ for the gas phase applies also to the solid phase concentration. The approach is obviously not exactly true since:

$$\frac{q_\infty}{c_o r} = f(r), \qquad \text{IV-14A}$$

and values of q_a beyond q_∞ would have to be found by:

$$dq_a = \frac{q_\infty}{c_o r} \int_0^{\lambda c_o} dc_o. \qquad \text{IV-14B}$$

However, in order to simplify the ensuing relationships, a linear isotherm is applied at the higher concentrations, i.e., $> c_o$: $> q_\infty$. Needham (N1) has indeed shown the applicability of such an approach.

Thus, with simplified terminology:

$$\lambda = \lambda(c_o, H_T)$$

$$\frac{q_{\infty m}}{q_\infty} = \frac{f(D,r)\ \lambda c_o}{f(D,r)\ c_o} = \lambda. \qquad \text{IV-15}$$

Where now the value of $q_{\infty m}/c_{om}$ for any adsorbate in a multicomponent mixture is equivalent to:

$$\frac{q_{\infty m}}{c_{om}} = \frac{(q_\infty - \Sigma\Delta q_\infty)}{c_{om}} = \frac{q_\infty^{\,o}\, k_{ADm}'}{1 + k_{ADm}'\, c_{om}} \qquad \text{IV-16}$$

and again the "m" subscript has replaced the "i" of previous developments and denotes $c_a/c_o > 1.0$.

Returning to IV-12 and simplifying:

$$\frac{q_a^*}{q_\infty^{\,o}} = \frac{k_{ADm}'\, c_a}{1 + k_{ADm}'\, c_a} . \qquad \text{IV-17}$$

Dividing IV-17 by IV-16:

$$\frac{q_a^*}{q_{\infty m}} = \left[\frac{k_{ADm}'\, c_a}{1 + k_{ADm}'\, c_a}\right] \left[\frac{1 + k_{ADm}'\, c_{om}}{k_{ADm}'\, c_{om}}\right] \qquad \text{IV-18}$$

$$\frac{q_a^*}{q_{\infty m}} = \frac{c_a/c_{om}}{r_m + (1-r_m)\, c_a/c_{om}} , \qquad \text{IV-19}$$

where now the multicomponent equilibrium parameter is given by:

$$r_m = 1.0 - \frac{(q_\infty - \Sigma\Delta q_\infty)}{q_\infty^{\,o}} . \qquad \text{IV-20}$$

Where the values of $q_\infty - \Sigma\Delta q_\infty$ are calculated from the multicomponent isotherm as discussed.

Equation IV-19 is identical with the binary development, except for the values of c_{om} and $q_{\infty m}$.

In the case where solid phase diffusion is controlling the adsorption process:

$$\frac{dq_a}{d\theta} = k_p a_p^{\,o}[q_a^* - q_a]. \qquad \text{IV-21}$$

The value of q_a^* now is replaced by IV-19. The resulting expression as given in Appendix C results in:

$$\frac{dy}{d\Theta} = \frac{(\lambda-x)\ x\ (1-r_m)}{\lambda r_m + (1-r_m)\ x} \quad . \qquad \text{IV-22}$$

This equation integrates to:

$$\left(\frac{r_m}{1-r_m}\right)\ \left[\ln\left\{\left(\frac{x_2}{x_1}\right)\ \left(\frac{\lambda-x_1}{\lambda-x_2}\right)\right\}\right] - \ln\left\{\frac{\lambda-x_2}{\lambda-x_1}\right\} = \Delta\Theta \ , \qquad \text{IV-23}$$

which is identical to the one derived by Gleukauf and Coates (G2) except for the value of λ, which allows the instantaneous relative concentration levels of x to be greater than 1.0.

Equation IV-23 has been successfully applied to multicomponent mixtures of n-pentane, n-hexane - methane, and n-pentane, n-hexane, n-heptane - methane. The results are discussed in a subsequent chapter. Values of the throughput parameter $\Delta\Theta$ are also discussed as the multicomponent nature of the system requires a re-evaluation of the parameters defining $\Delta\Theta$. Even for the binary case, Equation IV-23, which reduces to III-13 is not completely rigorous.

As values of x_2 approach λ, (or 1.0), values of $\Delta\Theta$ become increasingly large. In fact, x_2 never achieves a value of λ and becomes asymptotic with the x axis for infinitely large values of $\Delta\Theta$. For this reason, values of x_2 = .95 for the binary case usually denote the <u>zone exhaustion</u> while the value of x_1 = .05 will correspond to $\Delta\Theta$ = 0.

In addition, IV-23 does not account for reductions in the value of x once x_2 has achieved a stabilized value of λ in multicomponent mixtures. A value of $x_2 = \lambda - .05$ will sufficiently define the multicomponent zone exhaustion, but no provisions are made in this work to allow for decreasing values of c_o beyond $\Delta\theta$ for $x_2 > (\lambda - .05)$.

The fact remains, however, that IV-23 or III-13 are extremely use-

ful in predicting zone emergence times for particular tower and adsorption conditions, as well as effluent behavior for those values of time during which the zone is emerging from the tower (i.e., $x_1 \leq x \leq \lambda - .05$). As will be shown in a subsequent chapter, IV-23 can be used to calculate values of λ from input adsorption parameters.

CHAPTER V

APPLICATION OF THE CONSTANT PATTERN SOLID PHASE DIFFUSION THEORY AND EQUATIONS TO BINARY AND MULTICOMPONENT MIXTURES

The Michaels Approach - Steady State Adsorption

Before the development of any relationships pertaining to dynamic adsorption can be meaningful, a set of parameters must be defined for the steady state case.

Michaels (M3), has perhaps the most direct approach to the problem in his treatment of ion exchange theory. The ion-exchange theory is identical with constant pattern mass transfer phenomenon, and the terminology used is most useful in describing dynamic performance characteristics.

Michaels, likewise, described a mass transfer zone, wherein the solute adsorbate concentration was:

$$0 \leq c_a/c_o \leq 1.0 .$$

As the zone progressed through the resin, at a constant velocity, V_Z, with height, H_Z, the time at which the zone emerged from a bed of volume $v\Phi$, was θ_B. Likewise, the time required for the zone to travel the length of the bed and emerge, was θ_E. Illustrations V-1 graphically represent the Michaels system for the dynamic process, and during the zone emergence times at the bed outlet. ($\theta_E \geq \theta \geq \theta_B$).

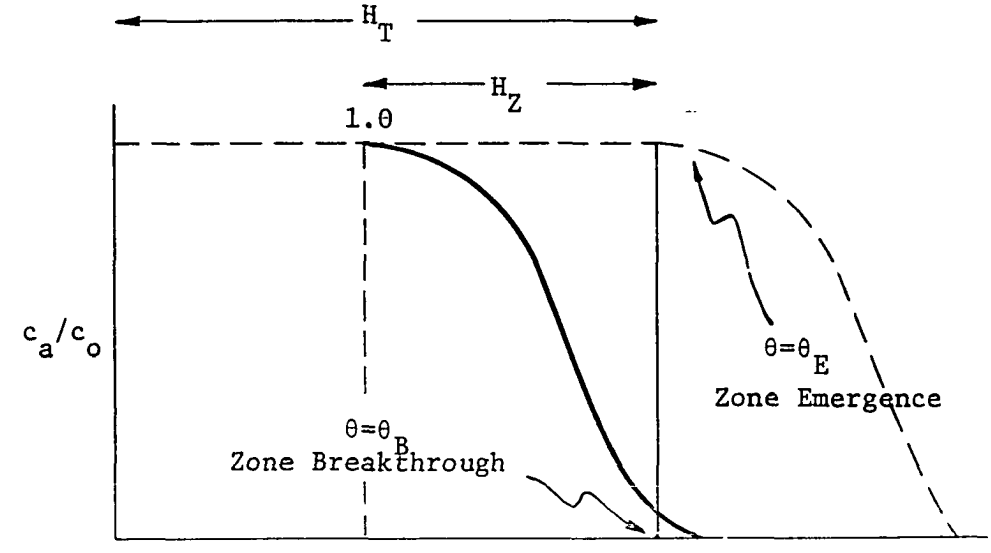

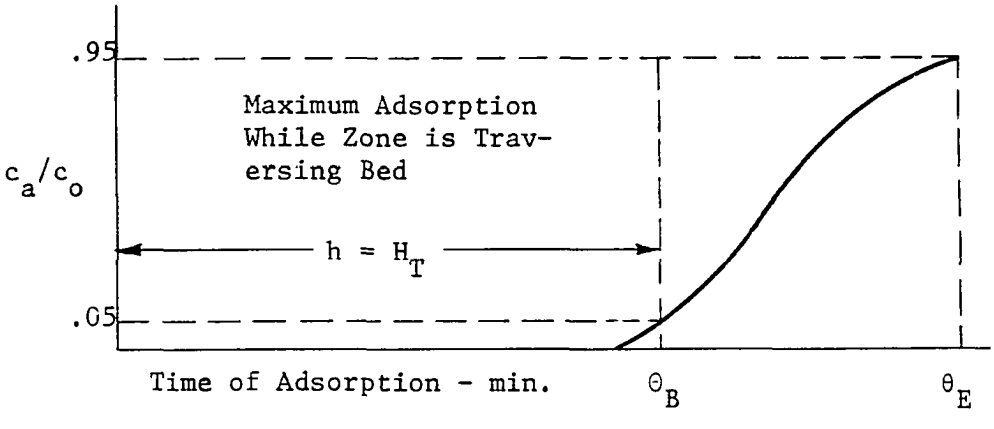

Illustrations V-1

From this analysis Michaels defined various terms that are redefined herein for the mass transfer case:

θ_B = The effective zone breakthrough at bed outlet - min. defined as the time at which x = .05

θ_E = The effective zone exhaustion time at bed outlet at which x = .95 - min.

θ_F = The time required for the zone to form - min.

H_Z = The length of the mass transfer zone - ft.

H_T = The length of the adsorbent bed - ft.

Q_B = The amount of adsorbate on the bed at $\theta = \theta_B$ - lb.

Q_T = The amount of adsorbate on the bed at $\theta = \theta_E$ - lb.

F = The fractional capacity of the bed at $\theta_B \leq \theta \leq \theta_E$, also defined as:

$$F = \frac{\int_{\theta_B}^{\theta_E} (1 - c_a/c_o)\, d\theta}{\theta_E - \theta_B} .$$

V_{Zm}^{o} = The constant macroscopic rate of advance of the Michael's type zone while in the tower - ft/min.

From these definitions, it is possible to derive important relationships that are useful in calculating steady state data from laboratory measured values. These equations are derived in Appendix E and are discussed in a subsequent chapter.

Before the Michaels type approach can be applied to the solid phase diffusion equation, in order to describe effluent behavior, a knowledge

of the limiting conditions for the constant pattern mechanics must be achieved. For this reason, existing binary adsorption models were re-evaluated in order to extend the adsorption theory to multicomponent behavior.

Criteria for the Constant Pattern

A critical part in the role of the constant pattern diffusion equation is the successful application of representative laboratory data for subsequent parametric analysis of the relationships. Thomas (T1), Rosen (R1) and others have, indeed, shown that certain criteria must be met before a dynamic system has achieved constant pattern mass exchange.

The general stipulations and mathematical requirements involved in the correct application of the diffusion equation apply in context to both binary and multicomponent mixtures as well. The ensuing review, therefore, is intended for both systems, while later sections of this chapter will deal with particular aspects of the separate dynamic systems.

As pointed out by Vermeulen (V1), the constant pattern diffusion case implies:

$$y = x \qquad \text{V-1}$$

or states that the rate of advance of the zone does not affect the shape of the zone on the adsorbent bed.

Illustration V-2 illustrates a mass transfer zone for binary adsorption during transient conditions at $\theta = \theta_1$, and later at constant pattern conditions $\theta = \theta_2$.

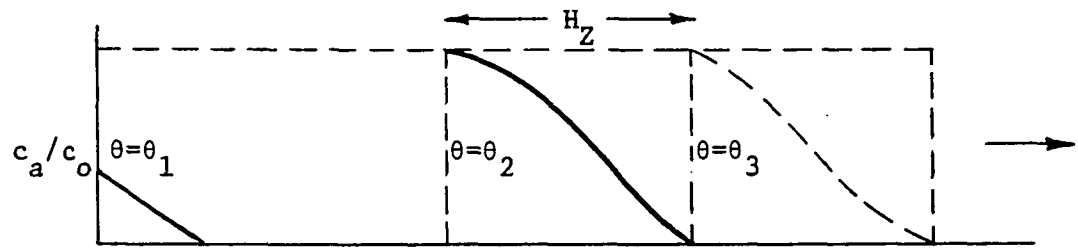

Distance Down Adsorbent Bed - Ft.
Illustration V-2

While the zone is growing, i.e., $dq_a/d\Theta \neq 0$ @ h = o, the length of the mass transfer unit is variable with time. At such a time, however, when the zone is stable, a material balance around a differential bed element (i.e., H_Z in Illustration V-2) gives:

$$\frac{Q\Delta\theta - H_Z A_B \Phi}{D\ A_B\ H_Z \Phi} = 1.0. \qquad \text{V-2}$$

The conditions that must be met in satisfying stabilization of the zone can be summarized analytically as:

$$\left(\frac{\partial y}{\partial v}\right)_\theta = 0 \quad , \quad v = V_Z\theta\ A_B\Phi\ . \qquad \text{V-3}$$

Where V_Z = velocity of the advancing zone - ft/min.

In addition, while the zone traverses a distance say, H_Z, (its own length) to a position denoted by the dashed line of Illustration V-2 @ $\theta=\theta_3$

$$-\left(\frac{\partial x}{\partial \theta}\right)_h \Big/ \left(\frac{\partial x}{\partial h}\right)_\theta = V_Z \text{ (const.)} \qquad \text{V-4}$$

Returning to the definitions of the throughput parameter, θ, and the column capacity parameter, Σ: (for binary applications)

$$\Theta = k_p a_p{}^o \left[\frac{V - v\Phi}{Q}\right] \qquad \text{V-5}$$

$$\Sigma = k_p a_p^{\circ} D \frac{v\Phi}{Q} \quad . \qquad \text{V-6}$$

V-2 can be seen as the result of dividing V-5 by V-6:

$$Z = \frac{\Theta}{\Sigma} = \frac{V - v\Phi}{D\ v\Phi} \quad . \qquad \text{V-7}$$

Where: $V = Q\ \Delta\theta$

$v\Phi = A_B\ H_Z^{\Phi}$.

The condition for Z = 1 in Equation V-7 is very important to the dynamic system in that at this particular arrangement of the pertinent parameters the material balance is satisfied. Thus, any particular tower volume $v\Phi$, defined by a corresponding h value, distribution coefficient, D, and the volume flow rate Q, will define the time at which the amount of adsorbate contained by the carrier gas is <u>stoichimetrically</u> equal to the component adsorbed by the solid dessicant at its equilibrium capacity:

$$Z_m = 1 = \left(\frac{Q\theta_m - v\Phi}{D\ v\Phi}\right) . \qquad \text{V-8}$$

Equation V-8 is extremely useful in describing and predicting real adsorption times from dimensionless parameters as it is a function of known tower and dynamic conditions. The parameters, of course, pertain to binary systems of one adsorbate in a carrier stream. V-8 holds true for any tower volume $v\Phi$ and says nothing of the actual mechanics of the adsorption procedure.

There is a further criteria, however, that describes the conditions for stabilization. These conditions can be described by returning to Equation V-7 in terms of the parameters Θ and Σ.

$$\Theta = \Sigma\left[\frac{V - v\Phi}{D\ v\Phi}\right] . \qquad \text{V-7}$$

Thus:

$$d\,\Theta = \frac{k_p a_p^{o}}{Q}\,[Q\,d\theta - A_B\Phi\,dh], \qquad \text{V-9}$$

and

$$d\Sigma = \frac{k_p a_p^{o} D}{Q}\,A_B\Phi\,dh. \qquad \text{V-10}$$

Replacing V-10 in V-9 gives:

$$d\Theta = \frac{d\Sigma Q}{D\,A_B\,\Phi dh\,Q}\,[Q\,d\theta - A_B\Phi dh]. \qquad \text{V-11}$$

Now V-11 is defined at a constant value of x (or c_a) so that the partial derivative would be:

$$\left(\frac{\partial\Theta}{\partial\Sigma}\right)_x = \frac{1}{D\,A_B\,\Phi}\,\left[Q\,\frac{d\theta}{dh} - A_B\Phi\right] \qquad \text{V-12}$$

$$\left(\frac{\partial\Theta}{\partial\Sigma}\right)_x = \frac{v_g}{D\Phi}\,\frac{d\theta}{dh} - \frac{1}{D}\,. \qquad \text{V-13}$$

Now the term $\frac{d\theta}{dh}$ can be described as the rate of change of the absolute real time, θ, with the adsorbent bed distance, h, at constant c_a:

$$d\,c_a = 0 = \left(\frac{\partial\,c_a}{\partial\,\theta}\right)_h d\theta + \left(\frac{\partial\,c_a}{\partial\,h}\right)_\theta dh \qquad \text{V-14}$$

or:

$$\frac{d\theta}{dh} = -\,(\partial c_a/\partial h)\theta\;/\;(\partial c_a/\partial\theta)\;h \qquad \text{V-15}$$

$$\frac{d\theta}{dh} = \frac{1}{V_Z}\,. \qquad \text{V-16}$$

This value is therefore the reciprocal of the "zone velocity" or the rate of advance of the mass transfer mechanism, along c_a = const. Returning to V-13:

$$\left(\frac{\partial\theta}{\partial\Sigma}\right)_x = \frac{v_g}{D\Phi}\,\frac{1}{V_Z} - \frac{1}{D}\,, \qquad \text{V-17}$$

or solving for V_Z:

$$V_Z = \frac{v_g}{\phi[D\ (\frac{\partial\theta}{\partial\Sigma})_x + 1]} \quad . \qquad \text{V-18}$$

Thus, V_Z is an inverse function of the partial derivative of the dimensionless parameters Θ and Σ. V_Z as defined by V-18 is called the constant-pattern zone velocity V_{Zcp}.

McLeod (M2) has outlined a procedure by which the solid phase diffusion equation may be applied to corrected laboratory data. The corrections involve comparison of the generalized Thomas solution slopes of:

$$(\frac{dx}{dZ})_\theta \quad \text{(Thomas)} \quad (\theta >> 1.0)$$

to slopes calculated from effluent plots of x vs. ΔZ. The transient laboratory measured slopes, are thereby corrected to "steady-state" slopes by the appropriate conversion factor.

A procedure that accomplishes the same objective arises by establishing the conditions for a constant zone velocity, i.e.:

$$(\frac{\partial\Theta}{\partial\Sigma})_x = 1.0 \qquad \text{V-19}$$

in Equation V-18. When this condition is met, constant pattern diffusion requirements are not in the tower, and the mass transfer zone proceeds at velocity, V_Z, until it has traversed the remaining adsorbent bed. When V-19 is viewed in the light of the material balance in the tower for Z = 1.0, it can be surmized the values of Σ are at first <u>higher</u> than corresponding values of Θ (for a constant x) until such a time that $\Sigma = \Theta$ and then both Z = 1 and $(\partial\Sigma/\partial\Theta) = 1.0$. Equation V-19 can be visualized by the following criteria:

The material balance in differential form gives:

$$\left(\frac{\partial x}{\partial \Sigma}\right)_{\theta} = - \left(\frac{\partial y}{\partial \theta}\right)_{\Sigma}. \qquad \text{V-20}$$

Equation V-14, rewritten in terms of θ and Σ gives:

$$dx = 0 = \left(\frac{\partial x}{\partial \theta}\right)_{\Sigma} d\theta + \left(\frac{\partial x}{\partial \Sigma}\right)_{\theta} d\Sigma \ . \qquad \text{V-21}$$

Now:

$$\left(\frac{\partial \Sigma}{\partial \theta}\right)_{x} = - \left(\frac{\partial x}{\partial \theta}\right)_{\Sigma} / \left(\frac{\partial x}{\partial \Sigma}\right)_{\theta} = 1.0. \qquad \text{V-22}$$

By the hypothesis of V-19, and V-20:

$$\left(\frac{\partial x}{\partial \theta}\right)_{\Sigma} = \left(\frac{\partial y}{\partial \theta}\right)_{\Sigma}, \qquad \text{V-23}$$

or simply:

$$x = y.$$

Since the criteria for constant pattern diffusion, i.e., $x = y$, is satisfied, it follows that V-19 is, indeed, the correct analogy for V_Z = const. Likewise, justification for the application of constant pattern mechanics arises from a constant zone velocity.

The generalized Thomas solution will yield the corresponding conditions at which V-19 is satisfied. Analytically, the Thomas solution must be differentiated at a constant x, and solved for a value of $(\partial\Sigma/\partial\theta) = 1.0$. As the mathematical differentiation of this equation is quite involved, a much more direct approach can be achieved by graphical differentiation of the variables. Values of the variable $(\theta/\Sigma - 1)$ reported by Hiester (H1) have been plotted vs. the equilibrium parameter, r, for a constant x. From these plots, the values of θ, Σ, and r that satisfy constant pattern criteria can be readily determined.

This criteria has been carried out by a cross plot of the Thomas solution for the solid diffusion case. The relationships involving the parameters Θ and Σ supplied by Hiester were represented at a constant x for a variable equilibrium parameter, r (see Figures A-20 and A-21). A subsequent chapter will discuss the results of the plot and the limits at which constant pattern diffusion actually occurs. In summary, however, the stabilized condition of the zone for a constant Σ(Np) was found to be dependent on r only. It was observed that abnormally large values of Σ and Θ were required for the condition $\Sigma = \Theta$ and likewise $(\partial\Theta/\partial\Sigma) = 1.0$. Although large Σ were required for complete stabilization, the slopes of the parametric plot were found to approach 1.0 quite rapidly, achieving values of approximately 1.05 at values of Σ less than half those required for complete stabilization. This criteria is very important in dynamic adsorption, as for all practical purposes the mass transfer zones can be considered stabilized for $\partial\Theta/\partial\Sigma = 1.05$. These values of Σ at which the partial derivative is 1.05 is noted below:

$$(\partial\Theta/\partial\Sigma)_{x=.01} = 1.05$$

Σ	r
13	.4
20	.6
67	.8
160	.9
209	.95
269	.99

Under the conditions described, then the zone velocity equation results in:

$$V_Z^{\circ} \simeq \frac{v_g/\Phi}{1+D} \; ; \; \left(\left(\frac{\partial\Theta}{\partial\Sigma}\right)_x \leq 1.05\right) \qquad \text{V-23A}$$

which is the steady state zone velocity for any component adsorbing under conditions described by v_g and D.

From V-9 it can be noted that when the mass transfer coefficient, $k_p a'_p$ is not the binary, steady state value, the derivation for V_Z is altered. For this condition:

$$d\Theta = k_p a'_p \, d\theta - \frac{k_p a'_p \Phi}{v_g} dh + [\theta - \frac{h\Phi}{v_g}] d\,(k_p a'_p) \qquad \text{V-23B}$$

and,

$$d\Sigma = k_p a'_p \frac{D\Phi}{v_g} dh + \frac{D\Phi h}{v_g} d(k_p a'_p) \qquad \text{V-23C}$$

Denoting, as before, $(d\theta/dh) = 1/V'_Z$, and $\theta' = \theta - h\Phi/v_g$:

$$(\frac{\partial\Theta}{\partial h})_x = \frac{k_p a'_p}{V'_Z} - \frac{k_p a'_p \Phi}{v_g} + \theta' \frac{d(k_p a'_p)}{dh} \, . \qquad \text{V-23D}$$

Also:

$$(\frac{\partial\Sigma}{\partial h})_x = k_p a'_p \frac{D\Phi}{v_g} + \frac{D\, h\Phi}{v_g} \frac{d(k_p a'_p)}{dh} \, . \qquad \text{V-23E}$$

So that the term $(\partial\Theta/\partial\Sigma)_x$ becomes:

$$(\frac{\partial\Theta}{\partial\Sigma})_x = \frac{\frac{1}{V'_Z} - \frac{\Phi}{v_g} + \theta' \frac{d(\ln k_p a'_p)}{dh}}{\frac{D\Phi}{v_g} + \frac{Dh\Phi}{v_g} \frac{d(\ln k_p a'_p)}{dh}} \, . \qquad \text{V-23F}$$

This expression may be solved for V'_Z in terms of the remaining variables. This solution represents the transient case for variable $k_p a'_p$ as well as the derivative $(\partial\theta/\partial\Sigma)_x$ itself. Rewriting V-23F gives:

$$\frac{1}{V'_Z} = \frac{\Phi}{v_g} [(\frac{\partial\Theta}{\partial\Sigma})_x D[1 + \frac{d(\ln k_p a'_p)}{d\ln h}] + 1 - \frac{v_g}{\Phi} \theta' \frac{d\ln(k_p a'_p)}{dh}] . \qquad \text{V-23G}$$

Finally,

$$V'_Z = \frac{v_g/\Phi}{\left(\frac{\partial\Theta}{\partial\Sigma}\right)_x D + 1 + \frac{d\ln(k_p a'_p)}{d\ln h}\left[\left(\frac{\partial\Theta}{\partial\Sigma}\right)_x D + 1 - \frac{v_g\theta}{\Phi h}\right]} \qquad \text{V-23H}$$

Equation V-23H will reduce to the constant pattern equation when $k_p a'_p = k_p a^o_p$ and the derivative of the dimensionless parameters is identical with one. In cases, however, the value of $k_p a'_p$ is very transient, and is a function of the absolute tower length, h. This phenomenon will be presented in more detail in Chapter VII in the discussion of the laboratory data.

It is of interest in this chapter to define, nevertheless, V'_Z for cases when $k_p a'_p$ is not constant. For this condition, the derivative of the logarithm of $k_p a'_p$ with the logarithm of the tower length is negative, while the bracketed term in the denominator of V-23H is also negative for moderate ranges of the gas velocity, as used in this study. The product:

$$\frac{d\ln k_p a'_p}{d\ln h}\left[\left(\frac{\partial\Theta}{\partial\Sigma}\right)_x D + 1 - \frac{v_g\theta}{\Phi h}\right]$$

is therefore positive and greater than one. Resulting values of V'_Z are therefore generally less than V'_{Zcp}. No attempt has been made in this work to calculate the reduced V'_Z values, as a function of the above product; however, the theory was verified by calculation of the Michael's zone velocities for the three adsorbate runs under strongly transient conditions. These cases, as well as the criteria employed to utilize the constant pattern results, will be discussed in a subsequent chapter.

Real Time Evaluation - Binary Mixtures

As with the case of Z = 1, the time required for the zone to emerge and proceed to a time corresponding with Z = 1.0 can be computed by observing V-8 and the general Equation IV-23 with $\lambda = 1.0$.

$$\theta_M = \frac{1}{Q} [Dv\Phi + v\Phi] . \qquad \text{V-24}$$

The physical significance of this time is very important in helping define breakthrough times, θ_B, as well as exhaustion times, θ_E.

Illustration V-3 indicates the time, θ_M, corresponding to Z = 1. As can be seen by the plot, the corresponding value of x_m (i.e., c_a/c_o @ Z = 1.0) occurs when the amount of effluent emerging from the tower at times greater than θ_B is numerically equal to the amount that will be adsorbed between that time and $\theta = \theta_E$.

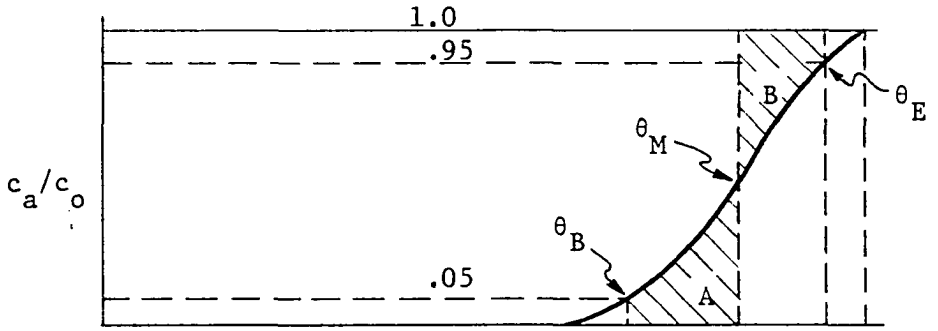

Illustration V-3

Thus at θ_M, the 'areas' A and B are equivalent, as the total adsorbate in the effluent up to time θ_M is equal to the amount adsorbed by the dessicant. Expressed mathematically:

$$\int_{\theta_B}^{\theta'} c_a/c_o \, d\theta = \int_{\theta'}^{\theta_E} (1 - c_a/c_o) \, d\theta \qquad \text{V-24A}$$

$(\theta' = \theta_M)$.

Another chapter will discuss the values of x for various adsorption conditions. The value, x_m, is an important parameter as it serves as a key relative concentration level effluent on which design criteria may be based.

In a similar manner, the zone breakthrough time can be represented by:

$$\theta_B = \theta_M - \Delta\theta_B(r,N_p). \qquad \text{V-25}$$

Where $\Delta\theta_B$ = The time required for the zone to reach θ_M from breakthrough. $\Delta\theta_B$, however, is equivalent to:

$$\Delta\theta_B(r,N_p) = \frac{1}{Q}\left\{\frac{Dv\Phi}{N_p}\left[\left(\frac{r}{1-r}\right)\ln\left(\frac{x_m\,(1-x_1)}{x_1\,(1-x_m)}\right) - \ln\frac{(1-x_m)}{(1-x_1)}\right]\right\} \qquad \text{V-26}$$

where x_m = The effluent concentration at Z = 1.0

x_1 = The appropriate adsorbate effluent concentration at zone emergence.

In order to avoid meaningless solutions to V-26 (or any arrangement of the diffusion model) at x = 0 a limiting value is generally chosen as the zone breakthrough concentration. This limiting value of x_1 is usually set at .05 while the analagous zone exhaustion time value of x_2 is usually accepted as .95. With x_1 = .05, V-26 simplifies to:

$$\Delta\theta_B = \frac{1}{Q}\left[Dv\Phi\ \Delta Z_{\theta_B}(r,N_p)\right]. \qquad \text{V-27}$$

Replacing in V-25 gives:

$$\theta_B = \theta_M - \frac{1}{Q}\left[Dv\Phi\ \Delta Z_{\theta_B}(r,N_p)\right]. \qquad \text{V-28}$$

Now:

$$\theta_M = \frac{Dv\Phi + v\Phi}{Q} .$$

So that θ_B results in:

$$\theta_B = \frac{Dv\Phi}{Q} [1 - \Delta Z_{\theta_B} (r,N_p) + \frac{1}{D}]. \qquad V\text{-}29$$

By a similar analysis, the value for θ_E, the zone exhaustion time for a binary mixture is:

$$\theta_E = \theta_M + \Delta\theta_E (r,N_p). \qquad V\text{-}30$$

For this condition, $\Delta\theta_E$ is:

$$\Delta\theta_E = \frac{1}{Q} \left\{\frac{Dv\Phi}{N_p} [\frac{r}{1-r} \ln \frac{x_2 (1-x_m)}{x_m (1-x_2)} - \ln \frac{(1-x_2)}{(1-x_m)}]\right\} . \qquad V\text{-}31$$

Where:

$$x_2 = .95.$$

Replacing this relationship in V-30 gives:

$$\theta_E = \frac{Dv\Phi + v\Phi}{Q} + \frac{1}{Q} [Dv\Phi \Delta Z_{\theta_E} (r,N_p)], \qquad V\text{-}32$$

$$\theta_E = \frac{v\Phi}{Q}\{D[1 + \Delta Z_{\theta_E} (r,N_p)] + 1\}. \qquad V\text{-}33$$

Equations V-33, V-29, and V-8, therefore describe the Michaels (M3) parameters required for determining the three important times involved during the effluent period of the adsorption process.

Values of ΔZ_{θ_B} and ΔZ_{θ_E} have been calculated for various r and N_p values. A subsequent chapter will describe the correlations and their application to binary adsorption more fully.

Real Time Evaluations - Multicomponent Mixtures

The material balance around the tower at the stoichimetric constant value for Z, i.e., Z = 1 for binary mixtures is not true in the case of multicomponent systems. For this case, the material balance yields:

$$V_m c_o = q_\infty' \rho_B A_B H_T + c_o \Phi v + \Delta Q_D \qquad \text{V-34}$$

Where: c_o = The appropriate units required to uphold the equality

ΔQ_D = The amount of adsorbate contained in the portion of the component mass transfer zone where $c_a/c_o > 1.0$.

Equation V-34 is written so as to recognize the fact that not all the tower is experiencing q_∞' as the equilibrium value of the adsorbate on the adsorbent. ΔQ_D is the amount of that adsorbate, therefore, that one zone will displace from the zone immediately in front of it in the adsorbent bed. For the case of more than two adsorbates, q_∞' will become q_∞'' and ΔQ_D then represents the amount of <u>total</u> adsorbate desorbed from the effluent bed by the <u>remaining</u> adsorbates.

Defining a multicomponent throughput parameter, Z_m as with the binary case:

$$Z_m = \frac{V - v\Phi}{D' v\Phi} \qquad \text{V-35}$$

Where:

D' = The multicomponent column distribution coefficient.

V-35 indicates values of V that are less than or greater than V_m.

The term $\Delta Q_D/\rho_B q_\infty' A_B H_T$ resulting from V-34 can be simplified and written as the <u>desorption of any component per unit weight of adsorbate on the adsorbent bed</u>.

$$\frac{\Delta Q_D}{\rho_B q_\infty' A_B H_T} = \Delta q_{\infty D}'. \qquad \text{V-35A}$$

Thus: $$Z_{mc} = 1 + \Delta q_{\infty D}' \qquad \text{V-35B}$$

is the stoichiometric constant for multicomponent mixtures. Z_{mc}, of course, is greater than 1.0 by the amount given in V-35A, the desorption concentration. V-35B can be related to its corresponding real time by:

$$\theta_{Mm} = \frac{1}{Q}\left[D'v\Phi\ [1 + q_{\infty D}'] + v\Phi\right]. \qquad \text{V-36}$$

As before, the multicomponent breakthrough time θ_{Bm} is equivalent to:

$$\theta_{Bm} = \theta_{Mm} - \Delta\theta_{Bm}\ (r_m, \lambda, N_p). \qquad \text{V-37}$$

Including the expression for $\Delta\theta_{Bm}(r, \lambda, N_p)$

$$\Delta\theta_{Bm} = \frac{1}{Q}\left\{\frac{D'v\Phi}{N_p}\left[\left(\frac{r_m}{1-r_m}\right) \ln \left(\frac{x_{mm}(\lambda - x_1)}{x_1(\lambda - x_{mm})}\right) - \ln\left(\frac{\lambda - x_{mm}}{\lambda - x_1}\right)\right]\right\} \qquad \text{V-38}$$

or:

$$\theta_{Bm} = \frac{1}{Q}\left\{D'v\Phi[1 + \Delta q_{\infty D}'] + v\Phi\right\} - \frac{1}{Q}\left\{D'v\Phi\Delta Z_{\theta_{Bm}}\ (r_m, \lambda, N_p)\right\}. \qquad \text{V-39}$$

Simplifying the expression gives:

$$\theta_{Bm} = \frac{D'v\Phi}{Q}\left[1 + \Delta q_{\infty D}' - \Delta Z_{\theta_{Bm}}\ (r_m, \lambda, N_p) + \frac{1}{\tau_D}\right]. \qquad \text{V-40}$$

Where:

$\Delta Z_{\theta_{Bm}}(r_m, \lambda, N_p)$ = Denotes the differential throughput parameter to zone breakthrough for the multicomponent case, i.e., $\lambda > 1.0$.

Likewise, exhaustion times for any system involving multicomponent mixtures is expressed by:

$$\theta_{Em} = \theta_{Mm} + \Delta\theta_{Em}\ (r_m, \lambda, N_p). \qquad \text{V-41}$$

Where:

$$\Delta\theta_{Em} = \frac{1}{Q}\left\{\frac{D'v\Phi}{N_p}\left[\left(\frac{r_m}{1-r_m}\right)\ln\left(\frac{x_2(\lambda - x_{mm})}{x_{mm}(\lambda - x_2)}\right) - \ln\left(\frac{\lambda - x_2}{\lambda - x_{mm}}\right)\right]\right\}. \quad V\text{-}42$$

For the case of multicomponent systems the value of x_2 can be 1.0. This value is permissible only because the increased zone instantaneous equilibrium, at $\theta > \theta_E$, reflected by λ, is greater than 1.0. In actual fitting of the multicomponent data, it was discovered that the times between values of $x_2 = 1.0$ and $x_2 = .95$ were very close, due to the 'steep' effluent curve during these times. For consistency, however, the data were analyzed for $x_2 = .95$, as was done for the binary case:

$$\theta_{Em} = \frac{1}{Q}\left\{D'v\Phi[1 + \Delta q_{\infty D}']\right\} + v\Phi\} + \frac{1}{Q}\left\{D'v\Phi\ \Delta Z_{\theta Em}(r_m, \lambda, N_p)\right\} \quad V\text{-}43$$

Further simplification of V-43 yields:

$$\theta_{Em} = \frac{v\Phi}{Q}\left\{D'[1 + \Delta q_{\infty D}' + \Delta Z_{\theta Em}(r_m, \lambda, N_p)] + 1\right\}. \quad V\text{-}44$$

Equations V-40, V-36, and V-44 are the relationships desired that define the respective times and relative concentration ratios for multicomponent mixtures in the following manner:

Time	x_m
θ_{Mm}	$f(r, \lambda, N_p)$
θ_{Bm}	.05
θ_{Em}	.95

The parameters that are still undefined at this time for the multicomponent case are values $\Delta q_{\infty D}'$, λ, and x_{mm}. In order to evaluate these terms it is necessary to resort to further dynamic adsorption relationships.

Evaluation of the Desorption Concentration - $\Delta q'_{\infty D}$

The value of $\Delta q'_{\infty D}$, as previously defined applies only to a system of two or more components simultaneously adsorbing in a dynamic system. For this case the amount of each adsorbate adsorbed on the bed is given by $q'_{\infty i}$, where each component's particular isotherm yields the respective value of $q'_{\infty i}$, as defined previously.

The difference in the amount adsorbed in the multicomponent case and the 'ideal' binary case, for any component is then:

$$\Delta Q_T = (q_{\infty i} - q'_{\infty i})\, A_B \rho_B\, H_T \quad . \qquad \text{V-45}$$

Now, Equation V-45 gives the total difference in the adsorbate adherred to the solid, but does not indicate what fraction of the decreased capacity is actually contained in that portion of the zone where $q_{ai} > q_{\infty i}$. Illustration V-4 indicates the manner in which the effluent concentration appears in a multicomponent system, as compared to a theoretical binary system.

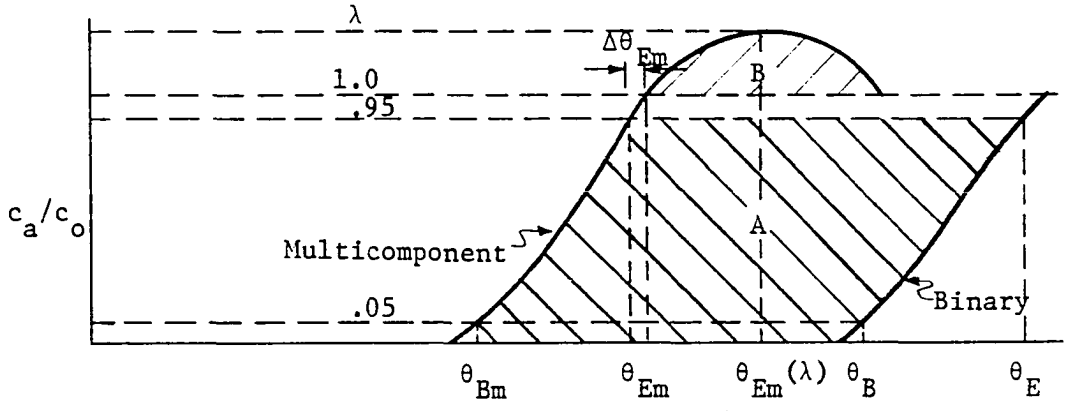

Illustration V-4

Due to the decreased adsorption sites available for any given component, the value of θ_{Bm} is less than the corresponding θ_B. Likewise, θ_{Em} will be less than θ_E. The area "A" in Illustration V-4 denotes the difference

in equilibrium capacity up to zone exhaustion, while the area "B" indicates the additional adsorbate in the mass transfer zone due to increased gas phase concentrations ($c_{ai} > c_{oi}$) in the desorption of zone "i" by zone "i + 1". The value of λ is noted in the Illustration as the maximum concentration achieved, i.e.:

$$\lambda = \frac{c_{ai}}{c_{oi}} \quad (\max) \quad ,$$

by the gas phase at the corresponding time $\theta_{Em}(\lambda)$. The value of "λ", therefore, is proportional to "B".

Now the amount of binary adsorption can be denoted by:

$$(\theta_B)\ (\text{I.R.}) + (\theta_E - \theta_B)\ F\ (\text{I.R.}) = q_\infty\ A_B \rho_B\ H_T = Q_T. \qquad \text{V-46}$$

Where:

I.R. = The component mass injection rate into the tower - lb/min.

θ_B for the binary case can be found in the following manner. Referring to Illustration V-1:

$$\theta_B = \theta_F + \frac{H_T - H_Z}{V_Z^o} \qquad \text{V-47}$$

$$\theta_B = (1 - F)\ \theta_Z + \frac{H_T - H_Z}{V_Z^o} \qquad \text{V-47A}$$

$$\theta_B = (1 - F)\ \frac{H_Z}{V_Z^o} + \frac{H_T - H_Z}{V_Z^o} \qquad \text{V-48}$$

$$\theta_B = \frac{H_T - FH_Z}{V_Z^o} \quad . \qquad \text{V-49}$$

Likewise, θ_E is:

$$\theta_E = \theta_B + \frac{H_Z}{V_Z^o} \qquad \text{V-50}$$

$$\theta_E = \frac{H_T + (1-F)H_Z}{V_Z} . \qquad \text{V-51}$$

The corresponding multicomponent terms are similarly:

$$\theta_{Bm} = \frac{H_T - F_m H_{Zm}}{V_Z'} \qquad \text{V-52}$$

$$\theta_{Em} = \frac{H_T + (1-F_m) H_{Zm}}{V_Z'} . \qquad \text{V-53}$$

Writing V-46 for both the binary and the multicomponent cases:

$$\left[\frac{H_T - FH_Z}{V_Z^o}\right] (I.R.) + \left[\left(\frac{H_T + (1-F) H_Z}{V_Z^o}\right) - \left(\frac{H_T - FH_Z}{V_Z^o}\right)\right] F(I.R.) = Q_T \qquad \text{V-54}$$

$$\left[\frac{H_T - F_m H_Z}{V_Z'}\right] I.R. + \left[\frac{(H_T + (1-F_m) H_Z)}{V_Z'} - \frac{(H_T - F_m H_Z)}{V_Z'}\right] F_m (I.R.) = Q_{Tm} \qquad \text{V-55}$$

simplification and subtraction of V-55 from V-54 gives:

$$\left[\frac{H_T}{V_Z^o} - \frac{H_T}{V_Z'}\right] I.R. = \Delta Q_{Tm} . \qquad \text{V-56}$$

Where ΔQ_{Tm} is not the actual difference denoted by V-45 because of ΔQ_D still within the bed at $\theta = \theta_{Em}$.

Since:

$$\Delta Q_T = \Delta Q_{Tm} + \Delta Q_D \qquad \text{V-57}$$

Equation V-56 gives:

$$(q_{\infty i} - q_{\infty i}') A_B \rho_B H_T - \left(\frac{H_T}{V_Z^o} - \frac{H_T}{V_Z'}\right) (I.R.) = \Delta Q_D \qquad \text{V-58}$$

Since all the parameters in V-58 are defined, ΔQ_D, can be solved for directly in terms of the equilibrium concentrations, the component mass injection rate, and the zone velocities. $\Delta q_{\infty D}'$ readily follows from V-58 for any component:

$$\Delta q_{\infty D}' = \frac{\Delta Q_D}{q_\infty' A_B \rho_B H_T}. \qquad \text{V-59}$$

Evaluation of V-58 and V-59 will be discussed in a subsequent chapter covering the applications of the data.

Evaluation of the Equilibrium Enhancement Factor - λ

The solid phase diffusion Equation is defined by the parameters λ and N_p for any particular r. Even at values of x greater than 1.0, the shape of the effluent curve is governed by the number of transfer units contained in the bed, N_p, and the equilibrium enhancement factor, λ.

Equation V-59 defines the amount of any adsorbate contained within the desorbed portion of the effluent curve. This relationship gives no indication, however, of the shape of the effluent curve.

In order to achieve an expression for λ, using the results of V-59 it is necessary to make the following assumptions:

1) The desorbed portion of the effluent curve, i.e., $1.0 \leq x_m \leq \lambda$ is symmetrical about a value, $Z_E(\lambda)$, defined as the Z occurring when $x = \lambda$.

2) Desorption commences at a value of Z_{Em} equivalent to:

$$Z_{Em} = Z_{x=.95} + \left(\frac{\partial Z}{\partial x}\right)_{x=.95} (.05). \qquad \text{V-60}$$

Assumption (1) is depicted in Illustration V-5.

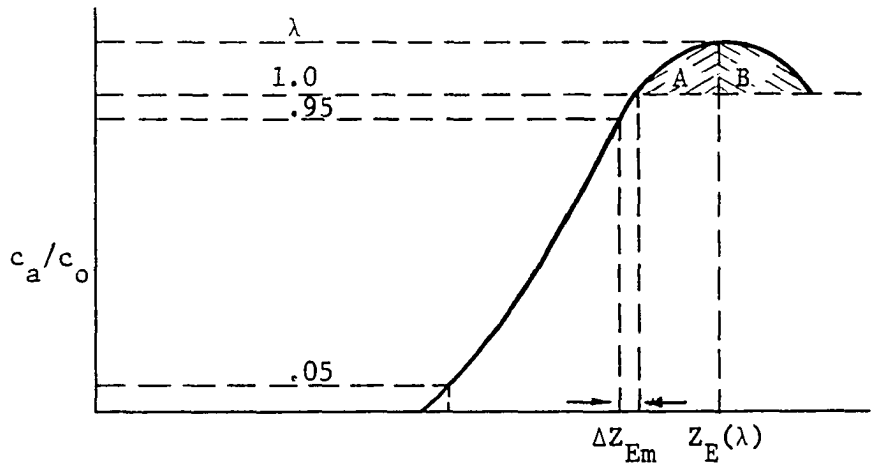

Throughput Parameter-Z

Illustration V-5

As with the binary asymptotic solution, the practical zone exhaustion time for any λ in the multicomponent case was taken as λ - .05. The theoretical solution was therefore defined only to that particular value. Area "A" in the Illustration is defined by the curve, while area "B" is assumed symmetrical about point $Z_E(\lambda)$. This assumption is a reasonable one, since the maximum effluent concentration has been achieved and must decrease to its normal "inlet" level (1.0). This criteria is not strictly true, however, as numerous laboratory studies have shown that the trailing edge of the desorption effluent is sometimes skewed with respect to its maximum effluent value, λ. For the purpose of achieving a practical solution to this specific portion of the adsorption cycle, however, the above assumption is justified. Data presented in a subsequent chapter will substantiate the preceding stipulations.

Since V-59 defines the total adsorbate physically contained in areas "A" and "B" of Illustration V-5, the amount of the adsorbate contained in area "A" is simply one half that of Equation V-58.

$$\Delta Q_D(\lambda) = \frac{\Delta Q_D}{2} . \qquad \text{V-61}$$

The average concentration over the interval Z_{Em} to $Z_E(\lambda)$ is:

$$\bar{x}_{mD} = \frac{\int_{Z_{Em}}^{Z_E(\lambda)} x \, dZ}{Z_E(\lambda) - Z_{Em}} \quad . \qquad \text{V-62}$$

It has been found, however, that the value of $\bar{x}_{mD}$ is very close to a linear average of λ and 1:

$$\bar{x}_{mD} \simeq \left(\frac{\lambda + 1}{2}\right). \qquad \text{V-62A}$$

This condition arises, because of the linearity of the effluent concentration curve at values of x around 1.0.

The value of ΔZ_D equal to:

$\Delta Z_D = Z(\lambda) - Z_{Em}$, is:

$$\Delta Z_D = \frac{1}{N_p} \left\{ \left(\frac{r_m}{1-r_m}\right) \ln\left(x_2 \frac{(\lambda - 1)}{2(\lambda - x_2)}\right) - \ln\left(\frac{\lambda - x_2}{\lambda - 1}\right) \right\}. \qquad \text{V-63}$$

Where:

$$1.0 \leq x_2 \leq (\lambda - .05).$$

In particular, the amount $\Delta Q_D(\lambda)$ can be defined as:

$$\Delta Q_D(\lambda) = (\text{I.R.}) \, (\bar{x}_{mD} - 1) \, \Delta\theta_D. \qquad \text{V-64}$$

Where:

$\Delta\theta_D$ = The real time associated with ΔZ_D.

The value of $\Delta\theta_D$ is calculated by:

$$\Delta\theta_D = \Delta Z_D \frac{D' v \Phi}{Q} \qquad \text{V-65}$$

$$\Delta\theta_D = \Delta Z_D \frac{N_p}{k_p a'_p} \quad . \qquad \text{V-65A}$$

Replacing V-65A, V-62A in V-64 gives:

$$\Delta Q_D(\lambda) = (I.R.)\ (\frac{\lambda-1}{2})\ \Delta Z_D\ \frac{N_p}{k_p a'_p}. \qquad V\text{-}66$$

Equation V-66 contains the unknown parameter, λ, as well as ΔZ_D, which is itself a function of λ. The solution of V-66 is therefore accomplished by a trial-and-error routine. Values of ΔZ_D have been calculated for a range of input parameters, as will be discussed in a subsequent chapter. However, by assuming a value of λ, finding ΔZ_D, and then recalculating λ by:

$$\lambda = (\frac{2}{I.R.})\ (\frac{\Delta Q_D(\lambda)}{\Delta Z_D})\ (\frac{k_p a'_p}{N_p}) + 1. \qquad V\text{-}67$$

λ (calculated) must, of course, be equal to λ (assumed) or the trial-and-error process repeated until a 'match' is attained. Rewriting V-67 in terms of V-59 and an expression for the mass injection rate, I.R.:

$$I.R. = 2.62 \times 10^{-7}\ \frac{c_{oi} MW_i G_m}{G} = \text{lb/min.} \qquad V\text{-}68$$

or,

$$I.R. = .0181\ MW_i\ c_{oi}\ Q = \text{lb/min.}\ (G = .6) \qquad V\text{-}68A$$

Where:

MW_i = The molecular weight of the adsorbate lb/lb mole

G_m = The inlet gas mass flow rate - lb/hr ft^2

G = The specific gravity of the inlet gas (Air = 1.0)

Q = Gas flow rate -MMCFD

$$\lambda = 2.62 \times 10^{-7}\ (\frac{G\ \Delta q'_{\infty D}\ q'_{\infty}\ A_B \rho_B\ H_T}{c_{oi} MW_i G_m})\ (\frac{k_p a'_p}{N_p})(\frac{1}{\Delta Z_D})\ + 1. \qquad V\text{-}69$$

Equation V-69 is, of course, an approximation to the actual value of λ,

whose precise calculation is more complex, and will not be developed here. In light of the assumptions simplifying the mechanics of the desorption portion of the effluent curve, V-69 has proved to be a useful and valuable relationship in this work.

The actual time at which λ occurs, (i.e. $\theta_E(\lambda)$) is defined by:

$$\theta_E(\lambda) = \theta_{Em} + \Delta Z_{Em} \frac{D'v\Phi}{Q} + \Delta Z_D \frac{D'v\Phi}{Q} . \qquad \text{V-70}$$

Where θ_{Em} is the zone exhaustion times at x = .95. As denoted by V-60:

$$\Delta Z_{Em} \simeq \left(\frac{\partial Z}{\partial x}\right)_{x=.95} (.05). \qquad \text{V-71}$$

The partial derivative in V-71 can be found by differentiating the original solid diffusion equation: assuming the binary case applies.

$$\frac{dZ}{dx} \simeq \frac{1}{N_p} \left[\frac{(r_m + (1-r_m)\, x)}{x(1-x)(1-r_m)}\right]. \qquad \text{V-72}$$

At x = .95 the total derivative in V-72 becomes the partial in V-71. The slope given by V-72 is <u>assumed</u> to be constant at x = .95.

$$\left(\frac{\partial Z}{\partial x}\right)_{x=.95} \simeq \frac{1}{N_p} \left[\frac{r_m + .95(1-r_m)}{.0475(1-r_m)}\right] \qquad \text{V-73}$$

At values of N_p say of 50, and r_m of .75 (taken as example values) V-73 becomes:

$$\Delta Z_{Em} = \frac{.05 \times .9875}{50 \times .0475 \times .25} = .0832.$$

With $\frac{Dv\Phi}{Q}$ taken as 20.0, $\Delta\theta_{Em}$ is equal to:

$$\Delta\theta_{Em} = .0832 \times 20 = 1.664 \text{ min.}$$

This procedure has served only to indicate that for correct <u>orders</u> of

magnitude for N_p, r, and $\frac{Dv\Phi}{Q}$, the value of $\Delta\theta_{Em}$ is usually small in comparison to $\Delta\theta_D$ in Equation V-70. Thus, V-70 can be rewritten as:

$$\theta_E(\lambda) \simeq \theta_{Em} + \Delta Z_D \frac{Dv\Phi}{Q} . \qquad \text{V-74}$$

With:

$$\Delta Z_{Em} \frac{Dv\Phi}{Q} << \Delta Z_D \frac{Dv\Phi}{Q} .$$

For cases in which the stipulations of V-74 are not true, as in multicomponent mixtures where $r_m > .95$, the proper relationship is:

$$\theta_E(\lambda) = \theta_{Em} + \frac{D'v\Phi}{Q} [\Delta Z_{Em} + \Delta Z_D], \qquad \text{V-75}$$

where again the "Z" terms are defined by a particular value of λ, r_m and N_p.

Evaluation of the Stoichimetric Constant Effluent Concentration - x_{mm}

As denoted by Illustration V-3, showing a typical binary case effluent plot, the binary value of the effluent concentration at Z = 1 is x_m. For the multicomponent case, however, Equation V-35B yields the value for Z_m at such a time, θ_{Mm}, when the total adsorbate contained in the carrier gas to that time is equal to the amount in the adsorbent bed. The only difference, in Z_c and Z_{mc} (multicomponent) is the term $\Delta q_{\infty D}'$. Appendix A gives a plot indicating that x_{mm} is a function of λ and r_m but not of N_p. Thus, for $Z_{mc} = 1 + \Delta q_{\infty D}'$, and λ and $q_{\infty D}'$ defined, the actual effluent relative concentration is defined. Values of x_{mm} are summarized as follows for λ and r_m.

λ = 1.4		1.3		1.2		1.1	
x_{mm}	r_m	x_{mm}	r_m	x_{mm}	r_m	x_{mm}	r_m
.457	.4	.469	.4	.484	.4	.508	.4
.447	.6	.457	.6	.471	.6	.494	.6
.441	.8	.449	.8	.462	.8	.481	.8
.438	.9	.446	.9	.458	.9	.476	.9

The definition, therefore, of the real times: θ_{Bm}, θ_{mm}, θ_{Em}, $\theta_{Em} + \Delta\theta_{Em}$, $\theta_E(\lambda)$, define the following effluent relative concentration values, that are useful in establishing the effluent curve:

x	θ
.05	θ_{Bm}
$f(\lambda, r_m)$	θ_{Mm}
.95	θ_{Em}
1.00	$\simeq\theta_{Em}$ or $(\theta_{Em} + \Delta\theta_{Em})$
λ	$\theta_E(\lambda)$

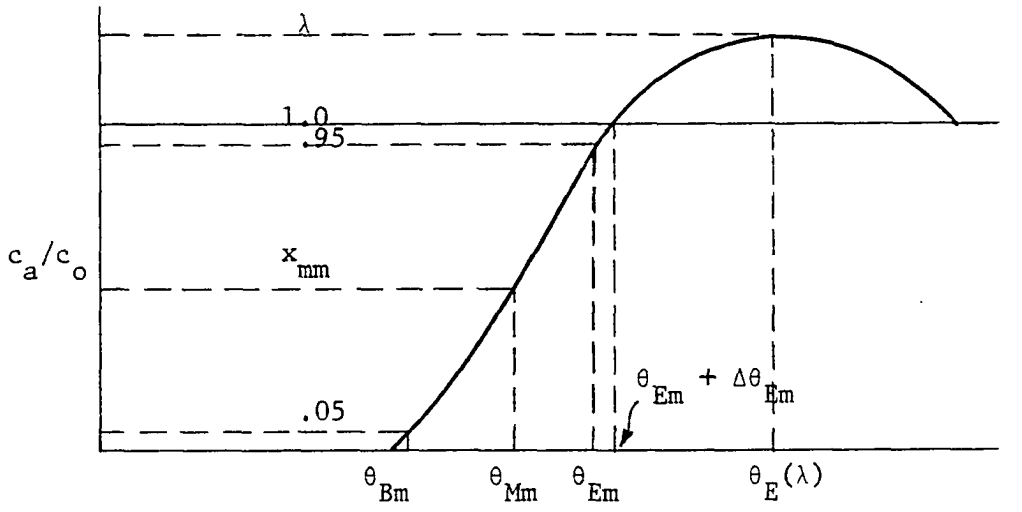

Illustration V-6

CHAPTER VI

LABORATORY EQUIPMENT AND EXPERIMENTAL PROCEDURE

Description of the System - Adsorption Cycle

This study was conducted at the Natural Gas Research Laboratory of the School of Petroleum and Geological Engineering of the University of Oklahoma. The installation was located at the North Campus of the university.

The experimental equipment employed in the dynamic studies is shown schematically in Illustration VI-1.

Dry gas supplied by the Oklahoma Natural Gas Company through a 2" entry line (P1) at 100 psig was compressed to 800 psig (I), (see Illustration VI-1), by a two stage 60 HP Chicago Pneumatic interccoled compressor. An inlet low pressure surge and discharge high pressure surge combination (J) were installed to minimize pressure fluctuations in the lines, as well as to control gas flow rates by cycling high pressure gas back to the low pressure side. Power to the compressor was supplied by a 220 volt 3 phase electrical motor. After compression to a constant system pressure of 800 psig a portion of the intercooled gas was routed through a 'fin-fan' happy air cooler (K) and a water counter flow heat exchange (L) in a sufficient quantity to give an overall adsorption column (D) temperature of 90°F. The intercooled and

after-cooled gas were joined at point (L1), and routed through an activated carbon "pre-adsorber" (O), in order to remove any substantial quantities of the adsorbate (n-C_5, n-C_6, or n-C_7) contained in the carrier gas. The carrier gas analysis varied slightly as shown by Table VI-1; although the system was generally between 85-90% methane. The lines connecting various components of the laboratory apparatus were 1/2" 2000 psi test lines, insulated and wrapped with 1/2" magnesium fiber insulation.

The carrier stream emerged from the carbon beds practically void of any adsorbate quantities. Prior to tower inlet a small scrubber (D1) containing steel mesh screen, was placed in the flow line to trap suspended contaminants as well as any liquid accumulations.

The gas was then routed from the scrubber to the adsorbent bed (D). This bed was actually two 8' towers constructed of 2.9" ID (3" nominal) 3000 psi test pipe fitted with 3" flange connections at the top and 3" - 1/2" swedge connections at the tower bases. The towers were covered with 3" magnesium fiber insulation connected by a 1/2" insulated line approximately 8' long. Thermocouple installations made of 1/8" x 1 1/2" stainless steel wells were installed every 2 1/2' for a total of 8 units. Bed temperatures (D2), were thus monitored by a Honeywell temperature recorder (C). The sensing devices were wrapped iron-constantan probes inserted in the tower wells for continuous recording.

Gas exiting from the bed was routed to a Kimray downstream pressure regulator (G) that was located close enough to the tower to maintain the pressure at approximately 800 psig. Friction losses in the tower were neglected, as they were of no consequence within the pressure range of

the studies.

A 2" meter run was installed downstream from the pressure controller (G1), where 1/4" pressure taps sensed pressure differential recorded by a 1.75 specific gravity merriam fluid. A high pressure differential manometer was installed (G2), for conventional flow rate control.

While the system was being brought to the constant run conditions of 800 psig and 90°F, the carrier gas was received by the inlet spherical surge tank (P), and recycled to the compressor. During the actual adsorption cycle, when the carrier was laden with adsorbate concentrations, (as with during the regeneration cycle) the gas was blown to the atmosphere via a 12', 1/2" venting column.

Liquid adsorbates, n-pentane, n-hexane, n-heptane, contained in 55 gallon commercial grade liquid drums, were the principle adsorbate supply. Multi-component adsorbate mixtures for given "pre-set" concentrations, were mixed in a high pressure liquid feed tank (E) in weight fractions corresponding to equivalent mole percents. The liquid feed tank was then pressured to 100 psig to insure complete liquefaction of the adsorbate mixtures prior to injection into the carrier gas. Subsequent phase interchange between the adsorbates and the carrier gas was neglected. A Wallace and Tiernan triplex hydrocarbon injection pump (E) was used to inject the liquid feed to the carrier gas. The injection point was at the carbon bed exit (01). The liquid feed injection line was 1/4" 2000 psig copper tubing, inserted in a 5/8" copper tubing line. The annular space 5/8" - 1/4" served as a "steam-jacket" to insure evaporation of the adsorbates once they entered the carrier gas. A steam generator (N), supplied the necessary energy to the line.

Gas gravities were continuously recorded by a Kimray gas gravitometer. This monitoring was installed, in order to obtain a representative specific gravity during the entire adsorption cycle. The gravity of the gas was instrumental in overall flow rate calculations.

Sampling and analysis of the gas was accomplished with a CEC (Consolidated Electrodynamics Corporation) 26-212 Process Chromatograph (A). The chromatograph analyzer (F) unit was located as close as possible to the tower outlet in order to minimize time lags in obtaining effluent samples. The detector in the analyzer unit was a twin wire thermal-conductivity 'block' type with a helium cooled reference wire on the side and the gas sample wire on the remaining side. Helium (F1), was also used to 'sweep' the effluent sample into the detector on the sample side. Nitrogen pressure (F2), was used to operate the pneumatic valves in the analyzer. The recording unit of the chromatograph (A), was remotely located and connected to a Honeywell .5-1.5 mv stripchart recorder (B). Automatic 3 minute cycle sampling cams operated a 12 channel recording system from the recorder to analyzer. Differences in detector potentials, induced by dissimilar hydrocarbon thermal conductivities were transmitted as voltage peaks to the Honeywell recorder. A voltage vs. time history was thus recorded. As the voltages were proportional to the component concentration levels the recorded data represented the effluent concentration-time histograms.

Calibration of the peak 'heights' on the recorder for a particular component was achieved by analyzing a sample gas of known composition and recording relative pen deflections. Subsequent data were compared to the known sample 'peak' for composition determination.

Regeneration and Cooling Cycle

Upon completion of an adsorption cycle, the adsorbate laden gel was stripped of its hydrocarbon components by passing the same carrier gas, free of any adsorbate, over the gel. Prior to entering the tower, however, the gas was heated to 600°F in a salt bath heater (M). The hot regeneration gas then flowed over the bed at 800 psig. Sampling was continued during the regeneration process in order to substantiate the adsorption mass accumulations by a tower material balance. The gas was cooled by the happy fin-fan cooler, and liquid condensate recovered in a high pressure separator. The cooled regeneration gas was vented to the atmosphere, to avoid any possible contamination of the supply gas contained in the spherical surge tank. The Honeywell temperature recorder monitored the regeneration temperatures at all 8 thermocouple locations. At such a time that the sample monitoring indicated that the bed was void of any adsorbates, the regeneration gas was routed around the tower, and "cool" supply gas introduced to the bed. Subsequent cooling brought the bed temperature down to the adsorption level of 90°F for future runs.

Any residual concentrations of components lighter than n-pentane on the bed were ignored after the cooling gas had come to thermal as well as adsorption equilibrium with the gel. In view of the high concentration of methane and ethane in the supply gas, and the negligible adsorption equilibrium concentrations of these components, the assumption seemed well justified.

Adsorbent

The adsorbent employed for all the dynamic studies was supplied by the Davison Chemical Company, a division of the Grace Company of Balti-

more, Maryland. The adsorbent was a 22A^{o} 03 grade silica gel. Table VI-2 summarizes the physical properties of the gel.

The two 8' towers employed in the runs held approximately 30-35 lbs. of the gel. This corresponded to approximately 47-54 lb/ft^3 packing density for a 14' bed, which was higher than the 45 lb/ft^3 reported by Davison. For all practical purposes 45 lb/ft^3 is a reasonable number for overall application in future design procedures.

TABLE VI-1

CARRIER GAS ANALYSIS VARIATION

Component	Mole %	Component	Mole %
O_2	.415	O_2	.114
N_2	5.348	N_2	4.416
CO_2	.180	CO_2	.229
C_1	83.135	C_1	83.545
C_2	9.379	C_2	9.886
C_3	1.399	C_3	1.653
iC_4	.012	iC_4	.013
nC_4	.023	nC_4	.020
iC_5	.005	iC_5	.004
nC_5	.008	nC_5	.006
C_6	.030	C_6	.008
C_{7+}	.066	C_{7+}	.106
	100.000		100.000

TABLE VI -2

PHYSICAL AND CHEMICAL PROPERTIES OF

03 GRADE SILICA GEL

Typical Analysis - Dry Basis

Component	Weight Percent
Silica as SiO_2	99.71
Iron as Fe_2O_3	.03
Aluminum as Al_2O_3	.10
Titanium as TiO_2	.09
Calcium as CaO	.01
Sodium as Na_2O	.02
Zirconium as Zr_2O	.01
Trace Elements	.03
	100.00
Total Volatile at 1750°F	5.0 to 6.5%
Specific Heat	0.22 BTU/lb/°F
True Density of Silica (no porosity)	137 lbs/cu. ft.
Thermal Conductivity	1 BTU/sq.ft./hr/°F/in.
Reactivation Temperature Range	250 - 600°F

(350°F bed temperature is adequate for most uses)

TABLE VI - 2

PROPERTIES OF SILICA GEL, GRADE 03

Sieve Analysis

Mesh Size	Weight Fraction
3-4	.189
4-6	.454
6-8	.318
Fines (through 8 mesh)	.037
	.998

Packed Bed Density - lbs/cu. ft.	45.0
Solid Density - lbs/cu. ft.	75.0
Total Volatile Percent at 1750°F (max.)	6.0
Surface Area (sq. meters/gm) (precision $\pm$ 25 m^2/gm at 95% basis)	750-800
Pore Volume - cc/gm (precision $\pm$ .02 cc/gm)	0.43
Calculated Average Pore Size	22 Angstrom Units
Theoretical Porosity - %	40; $(1 - \frac{45}{75})$

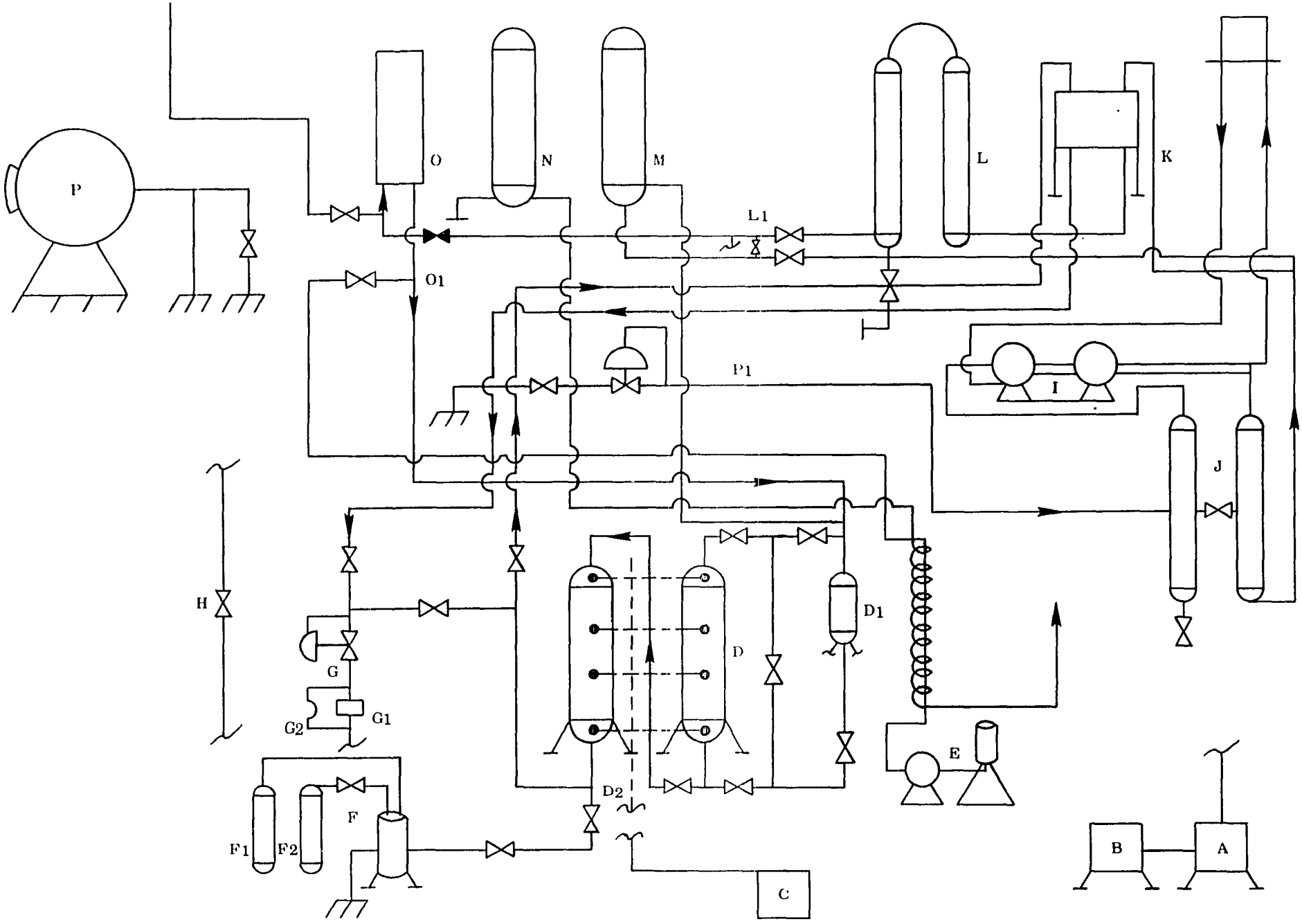

DYNAMIC ADSORPTION LABORATORY FLOW CHART
ILLUSTRATION VI-1

CHAPTER VII

DISCUSSION OF DATA - RESULTS FOR BINARY AND MULTICOMPONENT SYSTEMS

Binary Data - Results

Dynamic Isotherms

The initial endeavor of this work was to establish workable dynamic isotherms for the two principle adsorbates in a methane carrier. The assumption that the carrier was 100% methane was, of course, invalidated by the fact that the supply gas to the laboratory was not of constant composition. Nevertheless, the carrier analysis was sufficiently close to a pure methane source to give practical binary isotherms.

Figures A-1 and A-2 show the results of plotting $1/c_o$ vs. $1/q_\infty$ for all binary measurements. These runs represent the data reported by McLeod (M2), but reflect the Langmuir theoretical approach, i.e.:

$$\frac{1}{q_\infty} = \frac{1}{q_\infty^o} + \frac{1}{k_{AD}^o q_\infty^o}\left(\frac{1}{c_o}\right) \cdot \qquad \text{VII-1}$$

The data represent a good correlation for the majority of the experimental runs. In addition, high pressure runs for both adsorbates are shown with the 800 psig 90°F data for comparison. These data are too limited, however, to draw any conclusions as to the validity of their application.

The data of Day (D2) is represented in Figures A-3 and A-4. These values, representing 685 - 1000 psig and 100°F static measurements, support the validity of the 800 psig 90°F dynamic isotherm over the pressure range reported by that author. The two dynamic isotherms herein presented were used for the data comparison.

Laboratory Evaluation of the Constant Solid Pattern Phase Diffusion Equation

In his treatment of the dynamic binary data, McLeod (M2) was able to establish important criteria leading to substantial proof that the solid phase diffusion process was, indeed, the controlling mechanism in the adsorption process. In support of McLeod's contention of the solid phase diffusion being the dominant mechanism in dynamic adsorption, Figure A-5 presents the dynamic column adsorption efficiency calculated in the laboratory by:

$$F = \frac{\int_{\theta_B}^{\theta_E} (1-x)\, d\theta}{\theta_E - \theta_B} \qquad \text{VII-2}$$

compared against purely theoretical results computed from the solid phase diffusion equation, i.e.:

$$F\ (\text{Solid}) = \frac{N_p \int_{0}^{\Delta Z_{\theta_B} + \Delta Z_{\theta_E}} (1-x)\, d\, Z}{\left(\frac{r}{1-r}\right) \ln\left(\frac{.95}{.05}\right)^2 - \ln\left(\frac{.05}{.95}\right)} \quad . \qquad \text{VII-2A}$$

The measured data correlate fairly well with theoretical constant pattern data, taking into consideration the variation of the carrier gas analysis, as well as the narrow range of deviation for F itself. Most values of F were grouped between .4 to .5. Figure A-32 is included in Appendix A to show the variation of F with r for both binary and multicomponent mixtures. The data reported by McLeod, however, were evaluated using a constant r for n-pentane and n-hexane an assumption substantially invalidated due to the basic definition for r. Application of the previously reported binary data would, consequently, hinder the possible functional relationships between binary data and subsequent multicomponent analyses.

It was decided, therefore, to analyze the previously collected binary data on the basis of a variable value for r, as defined by:

$$r = 1 - \frac{q_\infty}{q_\infty^o} .$$

Following the procedure outlined by McLeod, a series of master curves were calculated using the solid phase constant pattern diffusion equation for values of r ranging between .4 and .99. The third parameter of the plots was the number of transfer units, N_p. Thus, for a constant r value determined by the appropriate isotherm, the number of transfer units that best matched the laboratory test data would be the one that most closely reproduced the measured data curves. Figures A-57 through A-62 in Appendix A show the results of the theoretical effluent plots for the binary case. Each plot is defined by a constant equilibrium parameter, while N_p varies from 50 to 5.

The laboratory data used by McLeod were collected by a joint effort at the Natural Gas Laboratory at the University of Oklahoma. These effluent curves for n-pentane and n-hexane are shown in Figures A-97 through A-145 in Appendix A. As shown by the plots, the gas velocities and inlet adsorbate concentrations were chosen in the following ranges for both adsorbates:

Gas Velocity	Adsorbate Concentration
10-45 ft/min	.1 - 2.0 mole %

These values were chosen since they were most representative of actual values encountered in the field.

In order to calculate the number of transfer units, N_p, for each run, the relative effluent vs. time plots were replotted on a relative effluent concentration throughput parameter scale. For the purpose of calculating the throughput parameters, the column distribution coefficient, D, the flow rate, Q, and the effective tower volume $v\Phi$, were computed from laboratory data. These values are summarized in Tables A-1 and A-4 for n-pentane and Tables A-5 and A-8 for n-hexane. Values of ΔZ, the throughput parameter, were computed by dividing the differential times, $\Delta\theta$, commencing from x = .05, by the factor:

$$\frac{Dv\Phi}{Q} . \qquad \text{VII-3}$$

Since $\Delta Z = 0$, x = .05, the plots were defined only for the effluent portion of each run.

When the overall adsorption equilibrium adsorbent concentration was obtained, i.e.:

$$q_{\infty} = \frac{\text{I.R.} \left[\int_{0}^{\theta_E} (1-x)\, d\theta \right]}{A_B \rho_B H_T} , \qquad \text{VII-4}$$

the corresponding value of r was calculated and the correct master curve chosen for the fitting procedure. Figures A-166 through A-216 Appendix A show the resulting plots for both adsorbates. The closest fitting values of "N_p" are noted for each plot.

Once the number of transfer units was obtained for each run, the values of N_p were used to determine the overall mass transfer coefficients, $k_p a_p^o$. These values were calculated by application of the defining equation for N_p:

$$N_p = k_p a_p^o \frac{Dv\Phi}{Q} . \qquad \text{VII-5}$$

Figures A-17 and A-18 show the results of the calculations for $k_p a_p^o$ for both n-pentane and n-hexane. These values were seen to be a function of the inlet adsorbate concentration, with the gas velocity as a third parameter. Although McLeod's (M2) values for N_p are of the same order of magnitude, he did not obtain a well-defined correlation for $k_p a_p^o$ for either n-pentane nor n-hexane with c_o. The reason, perhaps, for this limited correlation was the application of the data with the assumption that r was constant. In addition, McLeod reports an increasing value for r for increasing adsorbate mole percents, whereas this report indicates the opposite. The disagreement again arises because of the assumption of constant equilibrium parameters. In view of the limiting rate at which the adsorbate may be physically adsorbed onto the surface of the gel, and subsequently into the pore network, it seems rea-

sonable that at larger c_o values (for a given gas velocity) the mass transfer zone will be longer in order to accommodate more adsorbate. A longer zone, indicates a shorter number of transfer units contained within the bed and thus a smaller $k_p a_p^o$ for the same value of $Dv\Phi/Q$.

Since the value of $Dv\Phi/Q$ is very dependent on the gas velocity, (i.e. $v_g = Q/A_B$), the values for $k_p a_p^o$ at a constant adsorbate mole percent, and varying v_g should be dissimilar. This phenomenon was not reported in McLeod's correlation. For example, with decreased values for ΔZ, incurred by increased Q, values for $k_p a_p^o$ likewise rise. This increase accounts for the fact that N_p varies inversely with the gas velocity; however, the changes in N_p are not of the same order of magnitude as changes in the group, $Dv\Phi/Q$.

Further relationships involving N_p can be seen by analyzing the individual transfer height, HTU^o, for each adsorbate. As shown by Heister and Vermeulen (H2), this parameter is:

$$HTU^o = \frac{v_g/\Phi}{k_p a_p^o D} . \qquad \text{VII-6}$$

Thus, relating VII-6 to N_p gives:

$$N_p = k_p a_p^o \frac{Dv\Phi}{Q} \qquad \text{VII-6A}$$

$$= \frac{H_T}{HTU^o} . \qquad \text{VII-6B}$$

The column is therefore "factored" into a series of available mass transfer areas according to VII-6.

Figures A-25 and A-26 show the variation of the n-pentane and n-hexane (HTU^o) values. As shown by the plots, the heights vary inversely

with r (directly with c_o) and directly with v_g, the gas velocity. The variation with v_g, however, is not as pronounced as it is with r. This phenomenon accounts for the instances that occur when an increase in adsorption gas velocity is accompanied by a decrease in the value of N_p, or an increase in $k_p a_p^o$ due to the reduction of r.

Zone Stabilization

Any application of the foregoing analysis, assumes steady state (i.e., constant pattern) diffusion, as previously described in Chapter V. The necessary and sufficient criteria for constant pattern diffusion is such that:

$$\left(\frac{\partial \Sigma}{\partial \Theta}\right)_x = 1.0 \qquad \text{VII-7}$$

For the purpose of determining which runs were, indeed, constant pattern runs, and which were still experiencing transfer height "growth" with time, a plot of the Thomas Solution, Figure A-19, was employed to aid in determining the region of stability. As discussed in a previous chapter, the explicit differentiation of the Thomas Solution is quite involved. However, cross plot of the parameters Σ vs. Θ can be obtained readily from Figure A-19. These values are represented in Figures A-20 and A-21, covering a range of equilibrium parameters from .4 to .99. From a graphical differentiation of these plots, the value of Σ (or Θ) at which $(\partial\Sigma/\partial\Theta)$ was precisely 1.0 could be found. It was discovered that the values of Σ were initially somewhat higher than corresponding values of Θ. The derivative $(\partial\Sigma/\partial\Theta)$, was therefore greater than 1.0. Since Θ increases, as Σ increases, the slope of the plot approaches unity, as demanded by the theory, at $\Sigma=\Theta$. The figures show, however,

that for the mass transfer zones to completely stabilize, extremely large values for the dimensionless variables are required. This phenomenon was especially true for high values of r (low adsorbate concentrations).

Conversely, at moderate values of r, (shown by the figures), the zones stabilize much more rapidly with respect to the dimensionless parameters. In fact, the derivative, $(\partial\Sigma/\partial\Theta)$, approaches a value close to 1.0 very rapidly for all values of r. The corresponding N_p values for "pseudo-stabilized" conditions are vastly less than the completely stabilized parameters. This criteria is shown in the plots by a dashed line indicating a slope $(\partial\Sigma/\partial\Theta)$ of 1.05. At this condition the zone is 95% stabilized but continues to "grow", although the rate of growth has diminished. The large difference in the actual value of Σ, at which $\Theta = \Sigma$, and the value at which $\partial\Sigma/\partial\Theta = 1.05$ indicates that the zone would probably never completely stabilize in most commercial towers. However, for application of collected experimental data, the point at which the zone is 95% stabilized seems a minimum practical condition at which "steady-state" can be assumed to occur. These values have been incorporated into this work and are again summarized herein:

$$\partial\Sigma/\partial\Theta = 1.05$$

r	Σ
.4	13
.6	20
.8	67
.9	160
.95	209
.99	269

These data reflect an effluent relative concentration of 0.01. From these values it is possible to construct a curve of the minimum column capacity parameter, Σ (or N_p) vs. r. Figure A-22 indicates such a plot in which lines representing 90 and 85% stabilization are also shown. After fitting of the laboratory measurements determined corresponding values for N_p, these were plotted on the figure to determine the region of stabilization of the zones.

As shown by the plot of the n-hexane and n-pentane data, most of the n-hexane data was "stabilized", whereas a major portion of the n-pentane data fell within the 85% limits. In view of the good correlations obtained for the mass transfer coefficients for both adsorbates, however, the data was accepted as "stabilized" data. The scattering of the points in Figure A-17 for $k_p a_p^o$, indicates runs where N_p was not its precise stabilized value.

Another important feature of the stabilization limits is in the direct application to column design. Equation VII-5 may be rewritten to show:

$$N_p(r) = k_p a_p^o D \frac{H_T^o \phi}{v_g} \quad , \qquad \text{VII-7}$$

thus

$$H_T^o = \left(\frac{1}{k_p a_p^o D}\right)\left(\frac{v_g}{\phi}\right) N_p(r) . \qquad \text{VII-8}$$

Where H_T^o is the minimum distance, in feet, required for application of VII-7 in a constant pattern system. Values of H_T^o have been plotted in Figures A-49 through A-56 for values of r between .4 and .99. These plots are useful in that values of H_T^o actually "demanded" by the adsorp-

tion parameters can be compared to the length of the adsorbent bed available, H_T, and the applicability of the steady state data established. In cases where:

$$H_T < H_T^o,$$

the zone can be expected to behave as a non-constant pattern zone. For this particular case, design values of $k_p a_p^o$, and likewise N_p would not be applicable. This particular occurrence applicable mainly to multicomponent systems, will be discussed later in the chapter. For cases where:

$$H_T \geq H_T^o$$

the zone can be expected to behave normally and steady-state data applied.

To further substantiate the contention that the n-pentane and n-hexane zones had been essentially stabilized for the experimental procedure, the zone velocities as calculated by:

$$\frac{H_T}{\theta_B + F\theta_Z} = V_{Zm}^o \quad , \qquad \text{VII-9}$$

and by

$$\frac{v_g/\Phi}{1 + D} = V_{Zcp}^o \qquad \text{VII-10}$$

were plotted in Figures A-11 and A-13. Tables A-3 and A-7 summarize the calculations. As Equation VII-10 is a special case of the general zone velocity equation for $\partial\Sigma/\partial\Theta = 1.0$, agreement of the two steady state approaches should indicate near-stabilization. The figures show a good

correlation between measured data and Equation VII-10 represented as:

$$\underline{\text{Steady State Equation}} \qquad \frac{1}{V_Z^{\,o}} = \frac{\Phi}{v_g} + \frac{\Phi}{v_g}\frac{1}{D} \cdot \qquad \text{VII-11}$$

In addition to Figures A-11 and A-13, an independent expression for the zone velocity has been derived from purely mathematical concepts. The derivation is shown in Appendix D and is summarized herein:

$$\underline{\text{Zone Velocity Model}} \qquad \frac{1}{V_Z^{\,o}} = \frac{\Phi}{v_g} + \frac{400\rho_B MW_g}{v_g \rho_g MW_i}\left[\frac{q_\infty q_\infty^{\,o}}{c_o}\frac{(q_\infty^{\,o} - q_\infty)}{(2q_\infty^{\,o} - q_\infty)^2}\right] \qquad \text{VII-12}$$

Figures A-12 and A-14 show the plot of Equation VII-1 whose slope is:

$$\frac{400\ \rho_B\ MW_g}{v_g\ \rho_g\ MW_i} \qquad \text{VII-12A}$$

and whose intercept is:

$$\frac{\Phi}{v_g} \cdot \qquad \text{VII-12B}$$

Again the results are very good for the two adsorbates in question.

On the basis of the foregoing arguments, the binary data reported by McLeod, and herein re-evaluated, represent a good estimate of stabilized conditions for the respective dynamic binary systems. These parameters are most useful in developing criteria for the design of multicomponent mixture parameters.

Design Parameters

For the binary case, i.e., $\lambda = 1.0$, values of ΔZ_{θ_B} and ΔZ_{θ_E} have been calculated and represented graphically. These differential through-

put parameters represent the incremental values of:

$$\Delta Z = \frac{1}{N_p} \left\{ \left(\frac{r}{1-r}\right) \ln \frac{x_2(1-x_1)}{x_1(1-x_2)} - \ln \frac{(1-x_2)}{(1-x_1)} \right\} \qquad \text{VII-13}$$

determined from a real time corresponding to:

$$\theta_M = \frac{Dv\Phi}{Q} + \frac{v\Phi}{Q} \cdot \qquad \text{VII-14}$$

Figures A-33 and A-34 show the results for various r and N_p values. The relationships corresponding to values for θ_B and θ_E have been developed in Chapter V and are:

$$\theta_B = \frac{Dv\Phi}{Q} \left[1 - \Delta Z_{\theta_B} + \frac{1}{D}\right] \qquad \text{VII-15}$$

$$\theta_E = \frac{v\Phi}{Q} \left[D\left[1 + \Delta Z_{\theta_E}\right] + 1\right]. \qquad \text{VII-16}$$

In addition to these relationships, values for x_m, the binary relative effluent concentration, have been calculated and plotted in Figure A-31. Multicomponent values are also shown in the figure, and will be discussed later in the chapter. Determination of N_p, by calculating $k_p a_p{}^o \frac{Dv\Phi}{Q}$, therefore, determines the values for the three times θ_B, θ_M, θ_E.

Multicomponent Data - Results for Two Adsorbate Analysis N-Pentane, and N-Hexane in Methane

The Multicomponent Isotherm for the Two Adsorbate Case

As the binary data served to establish the basic criteria for dynamic adsorption design employing the solid phase diffusion equation, additional two adsorbate runs were made covering the same input conditions. These runs are shown in Figures A-146 through A-157, where the relative effluent concentration, x, for n-pentane and n-hexane is shown

on the same scale. The time, θ, of adsorption is the independent variable. Pertinent parameters for the runs are summarized on each sheet.

The primary step in the analysis, was to determine the shape of the isotherm for both n-pentane and n-hexane in methane, while both adsorbates progressed simultaneously in the mechanics of the adsorption process. The equations discussed in Chapter IV present the necessary empirical criteria for establishing the effect of one component on another:

$$\alpha_i = \frac{q_{\infty i}'}{k_{ADi}^{o} c_{oi} (q_{\infty i}^{o} - q_{\infty i}')} . \qquad \text{VII-17}$$

Table A-9 summarizes the adsorption conditions for the two component runs, while Table A-10 indicates the calculated equilibrium adsorption constant k_{ADi}^{o} for each component. Figures A-7 and A-8 show a graphical relationship between:

$$\alpha_i k_{ADi}^{o} = k_{ADi}' , \qquad \text{VII-18}$$

and the corresponding <u>alternate</u> adsorbate level that caused the k_{ADi}'. In both plots, the indicated relationships agree well with the initial "binary" values of k_{ADi}^{o} for both adsorbates, (i.e., .444 for n-pentane and .959 for n-hexane). This condition occurs when the alternate adsorbate concentration is precisely zero. The apparent scatter in the relationships, can be partially explained by the fact that the carrier gas was not of the same total composition for each run.

An interesting point to consider is that the multicomponent isotherm for any adsorbate can be written in a similar fashion as the binary

isotherm only for a constant concentration level of one of the adsorbates. For example, if a particular n-pentane concentration were "c_{op}" then the n-hexane adsorption equilibrium factor α_i would define $k'_{AD_{hx}}$. The isotherm for n-hexane, could then be described:

$$\frac{1}{q'_{\infty_{hx}}} = \frac{1}{q^{o}_{\infty_{hx}}} + \frac{1}{k'_{AD_{hx}} q^{o}_{\infty_{hx}}} \left(\frac{1}{c_{o_{hx}}}\right) . \qquad \text{VII-19}$$

Likewise, the n-pentane corresponding equation for a constant n-hexane level would be:

$$\frac{1}{q'_{\infty_{p}}} = \frac{1}{q^{o}_{\infty_{p}}} + \frac{1}{k'_{AD_{p}} q^{o}_{\infty_{p}}} \left(\frac{1}{c_{o_{p}}}\right) . \qquad \text{VII-20}$$

When both n-pentane and n-hexane concentrations are fixed, Equations VII-19 and VII-20 are valid only at one point on each isotherm. The concentration of one adsorbate thus defines the 'slope' of the isotherm for the alternate adsorbate.

The procedure outlined above is admittedly not completely rigorous. The data supporting the multicomponent isotherm is an empirical correlation between pertinent variables. Application of the presented relationships, however, will yield relatively good mixture adsorbent concentrations within the range of the data.

Laboratory Evaluation of the Multicomponent Solid Phase Diffusion Equation

Definition of the n-pentane and n-hexane isotherms for the multicomponent equilibrium parameter for each adsorbate, i.e.:

$$r_{mi} = 1 - \frac{q'_{\infty i}}{q^{o}_{\infty i}} \qquad \text{VII-21}$$

where i represents either component. The newly obtained equilibrium parameter along with the equilibrium enhancement factor, λ, and the column capability parameter for each component, are the parameters needed to define the multicomponent equation

$$\left(\frac{r_{mi}}{1-r_{mi}}\right) \ln\left\{\frac{x_2}{x_1}\frac{(\lambda_i - x_1)}{(\lambda_i - x_2)}\right\} - \ln\left\{\frac{(\lambda_i - x_2)}{(\lambda_i - x_1)}\right\} = N_p \Delta Z . \qquad \text{VII-22}$$

General master curves, calculated from VII-22 with values of r_m from .4 to .99, and values of λ from 1.4 to 1.05 were prepared graphically and are shown in Figures A-63 through A-96. These figures serve as a basis for "fitting" of the multicomponent effluent data.

In addition to the general master curves, values of $\Delta Z_{\theta B}(r_m, \lambda, N_p)$ $\Delta Z_{\theta E}(r_m, \lambda, N_p)$, ΔZ_D (as outlined in Chapter IV) were calculated and plotted vs. N_p for a constant r_m. These curves are intended for breakthrough time and zone exhaustion time calculations. They should be useful in future tower design for multicomponent systems. These curves are presented in Figures A-35 through A-48.

The values of $q'_{\infty i}$ for each run in the two adsorbate case are summarized in Table A-10 along with other important parameters. These equilibrium values were calculated by:

$$q'_{\infty i} = \frac{\left[\int_0^{\theta_{EM} + \Delta\theta_{EM}} (1-x)\, d\theta - \int_{\theta_{EM} + \Delta\theta_{EM}}^{\theta'_{EM}(\lambda)} x\, d\theta\right]}{A_B \rho_B H_T} , \qquad \text{VII-23}$$

where the second term of Equation VII-23 is negative since the additional adsorbate in the mass transfer zone represented by $x > 1.0$ is actually the

desorbed amount of the adsorbate, $\theta'_{EM}(\lambda)$ is the actual total exhaustion time of each run.

Values of N_p were calculated in a manner similar to the binary case. The corresponding values of $\Delta\theta$ (from $\theta = \theta_B$) were divided by:

$$\frac{D'v\Phi}{Q} \quad , \qquad \text{VII-24}$$

where:

$$D' = \frac{q'_{\infty i}\ \rho_B\ T\ R}{c_o\ MW_i\ \Phi\ P} \ . \qquad \text{VII-25}$$

The resulting values of ΔZ were plotted versus the corresponding effluent levels.

A current master curve, for the measured values of λ and r_m, was compared against the plotted "run" curve, and the best value of N_p chosen for that run. The resulting x_m vs. ΔZ plots are shown in Figures A-214 through A-225.

For n-pentane, or the adsorbate emerging first from the adsorbent bed, the effluent concentration ranged from $x = 0$ to $x_m = \lambda$. For the displacing adsorbate, n-hexane, however, the value of x_m ranged only from 0 to 1.0, as in the binary case. Since n-hexane was the "heaviest" adsorbate present, there was no displacing component behind it to increase the zone and corresponding gaseous effluent concentrations greater than 1.0. For n-hexane the binary master curves (Figures A-57 through A-62) were used for the N_p evaluation.

Table A-13 shows the overall results obtained for the two adsorbate fitting of the solid phase equation, and subsequent mass transfer ($k_p a_p'$) determination. In addition, Table A-14 shows the evaluation of λ as

calculated from the iterative procedure outlined in Chapter V.

As indicated in Table A-13, the values of $k_p a_p'$ for the two adsorbate system do not necessarily agree with the correlation for the binary values for $k_p a_p^o$. The dissimilarity occurs because the length of the transient transfer unit, HTU_T as defined by:

$$HTU_T = HTU = \frac{v_g/\Phi}{k_p a_p {}^oD}, \qquad \text{VII-25A}$$

is still experiencing growth within the bed. Corresponding values of N_p will be large in order to account for the "apparent" number of transfer units contained in the bed during the transient adsorption.

The interim transfer unit height, HTU_T, has been correlated with a parametric group. This correlation will be discussed in this chapter after the presentation of the three adsorbate data.

Zone Stabilization for the Two Adsorbate System - Zone Velocities

The overall number of transfer units for n-pentane and n-hexane were compared to the zone stabilization plot, as with the binary case. Figure A-23 shows the results of the procedure, and indicates the increase in the transient nature of the two adsorbate runs. While most of the data fall within the 80% limits, a good portion of the data fall outside the area of stabilization. It was decided, nevertheless, to attempt to describe the multicomponent zone velocities, V_Z', as a function of v_g, Φ, and D'. As with the binary data, the two adsorbate zone velocity data were plotted versus the multicomponent column distribution coefficient, D'. Figure A-15 shows the results of computing V_{Zm}' from the Michaels type approach, i.e.:

$$V_{Z_m}' = \frac{H_T}{\theta_B + F\theta_Z}, \qquad \text{VII-26}$$

and by the constant pattern equation:

$$V_{Z_{cp}}' = \frac{v_g/\phi}{1 + D'}. \qquad \text{VII-27}$$

The solid lines in Figure A-15 show the graphical plot of Equation VII-27, while the plotted data result from Equation VII-26. The data show a remarkable agreement, even though the partial derivative, $(\partial\Sigma/\partial\Theta)$, is greater than 1.0, for a portion of the data. These data indicate an insensitivity of the zone velocities to the column throughout parameter, once the zone is fairly well defined. Figure A-21A is included to show that for a value of x = .01, the column capacity parameter to column throughput parameter ratio, Σ/Θ, is 1.0 at Σ = 1000.0. The figure corresponds to a value of r of 0.5 and was calculated from a plot of the Thomas solution presented by Hiester and Vermeulen (H2). This discussion indicates that while the zone will not completely stabilize until large values of N_p are attained, the growth of the zone beyond moderate values of N_p is very slow. For this reason, the constant pattern mechanics, i.e., x = y, can readily apply to certain multicomponent adsorption cases with a good degree of reliability.

Design Parameters - Two Adsorbate System

Definition of the zone velocities for the two adsorbate case, allows the evaluation of ΔQ_D:

$$\Delta Q_D = (q_{\infty i} - q_{\infty i}')(A_B \rho_B H_T) - \left(\frac{H_T}{V_{Z_o}} - \frac{H_T}{V_Z'}\right)(\text{I.R.}). \qquad \text{VII-28}$$

The value of $\Delta q_{\infty D}'$ is then defined:

$$\Delta q_{\infty D}' = \frac{\Delta Q_D}{A_B \rho_B H_T q_{\infty i}'} . \qquad \text{VII-29}$$

Likewise, the value of λ can be evaluated from:

$$\lambda = \left(\frac{2}{I.R.}\right)\left(\frac{\Delta Q_D(\lambda)}{\Delta Z_D}\right)\left(\frac{k_p a_p'}{N_p}\right) + 1, \qquad \text{VII-30}$$

where all terms have been previously defined. Evaluation of λ defines the master curves to be used in defining the effluent times:

$$\theta_{Bm} = \frac{D'v\Phi}{Q}\left[1 + \Delta q_{\infty D}' - \Delta Z_{\theta B}\left(r_m, \lambda, N_p\right) + \frac{1}{D'}\right] \qquad \text{VII-31}$$

$$\theta_{Mm} = \frac{v\Phi}{Q}\left[D'\left[1 + \Delta q_{\infty D}'\right] + 1\right] \qquad \text{VII-32}$$

$$\theta_{Em} = \frac{v\Phi}{Q}\left[D'\left[1 + \Delta q_{\infty D}' + \Delta Z_{\theta E}\left(r_m, \lambda, N_p\right)\right] + 1\right] \qquad \text{VII-33}$$

$$\theta_{Em} + \Delta\theta_{Em} = \theta_{Em} + \frac{D'v\Phi}{Q}\Delta Z_{Em} \qquad \text{VII-34}$$

$$\theta_E(\lambda) = \theta_{Em} + \frac{D'v\Phi}{Q}\left[\Delta Z_D\left(r_m, \lambda, N_p\right) + \Delta Z_{Em}\right] \qquad \text{VII-35}$$

The corresponding values of x_m are defined by:

x_m	θ
.05	θ_{Bm}
$f(r_m, \lambda)$	θ_{Mm}
.95	θ_{Em}
λ	$\theta_E(\lambda)$

The value of x_{mm} is given as a function of λ and r_m in Figure A-31.

In "constructing" the effluent curve, a convenient way to determine the shape of the relationship, is to require that the second derivative of the effluent time plot be equal to zero at $x_m = x_{mm}$:

$$\left(\frac{\partial^2 x}{\partial \theta^2}\right)_{\theta_{Mm}} = 0 \ @ \ x_m = x_{mm} \ . \qquad \text{VII-36}$$

With this procedure, the curve will have an "inflection" point at θ_{Mm} and x_{mm} that is characteristic of virtually all dynamic adsorption data. The presentation of an example calculation will illustrate this curve plotting.

Multicomponent Data - Results for the Three Adsorbate Analysis - N-Pentane, N-Hexane, N-Heptane in Methane

The Multicomponent Isotherm for the Three Adsorbate Case

The effect of the component heavier than n-hexane on the binary Langmuir Isotherm, is much the same as with the two adsorbate case. For the three component analysis, the component factor:

$$\alpha_i' = \frac{k_{ADi}''}{k_{ADi}^o} \ , \qquad \text{VII-37}$$

is correlated with the sum of the remaining adsorbate concentrations. The three adsorbate runs performed in the laboratory are summarized in Table A-16. Pertinent adsorption parameters are also shown. Table A-17 shows the calculation of the adsorption equilibrium constant k_{AD_p}'' for n-pentane and $k_{AD_{hx}}''$ for n-hexane. Figures A-9 and A-10 show the plot of the constants for each adsorbate.

Again the data correlate well within the limits of the laboratory procedure. The binary constants for each adsorbate are shown, (at zero for the "alternate" adsorbate concentration) and these values fit well with the correlations.

The inherent assumption in the re-evaluation of the adsorption equilibrium constant is that the system is a "pseudobinary" mixture of the adsorbates in question, and the carrier, methane.

Laboratory Evaluation of the Multicomponent Solid Phase Diffusion Equation for the Three Adsorbate Case

Definition of the equilibrium adsorbent concentration, $q''_{\infty i}$ via the appropriate isotherm is the necessary parameter needed in evaluating r_m. The procedure is the same as with the two component case. The assumption is that the asymptotic solution is defined as long as its parameters are themselves independently defined, regardless of the number of adsorbable components in the carrier gas.

Thus, calculations of $q''_{\infty i}$, λ_i, and $\Delta q''_{\infty Di}$ represent the variables needed to define the effluent parameters. The real time and effluent concentrations follow exactly as with the two adsorbate system.

Table A-20 shows the data used in calculating the three component values for N_p. Again, the three component effluents were plotted on a time scale (Figures A-158 through A-165), and the subsequent $\Delta\theta$ values related to their corresponding ΔZ values by dividing each $\Delta\theta$ by:

$$\frac{D''v\Phi}{Q} . \qquad \text{VII-38}$$

The D" value is the three adsorbate column distribution coefficient. The resulting x vs. ΔZ plots are shown in Figures 371 through 378 , with

pertinent data for each run noted on each graph. The "master" curves used for the fitting procedure were Figures A-226 through A-233, as with the two adsorbate system.

Calculations for the values for ΔQ_D, from which $\Delta q''_{\infty Di}$ was obtained are shown in Table A-21. Subsequent calculations for λ for each run are also shown in Table A-21.

The agreement between the calculated $\Delta q''_{\infty Di}$ and λ parameters with measured laboratory data are shown in the tables. While the comparisons are not exact, the calculated values are reasonably close to the measured data.

In the actual calculation of the effluent times, i.e.: θ_{Bm}, θ_{Em}, etc. the values of $q_{\infty i}$, $\Delta q''_{\infty Di}$, are essential, but a change in the value of $\Delta Q''_{\infty Di}$ from .05 to, say, .075 will not affect the calculated value of θ_{Bm} or θ_{Em} by the same magnitude. For example, assuming a value of $\Delta q''_{\infty Di}$ .05 with the following parameters:

$r_m = .85$

$\lambda = 1.1$ $\qquad \Delta Z_{\theta B}(r_m, \lambda, N_p) = .36$ (Figure A-37)

$N_p = 50$

$D'' = 75$

$\frac{v\Phi}{Q} = .25$ $\qquad \Delta Z_{\theta E}(r_m, \lambda, N_p) = .36$ (Figure A-38)

yield the indicated values for $\Delta Z_{\theta B}(r_m, \lambda, N_p)$ and $\Delta Z_{\theta E}(r_m, \lambda, N_p)$. Thus, calculations for the corresponding times give:

$$\theta_{Bm} = \frac{D''v\Phi}{Q}\left[1 + \Delta q''_{\infty Di} - \Delta Z_{\theta B}(r_m, \lambda, N_p) + \frac{1}{D''}\right]$$

$$= 18.75\ [1 + .063 - .36] = \underline{13.18 \text{ minutes}}$$

$$\theta_{Em} = \frac{v\Phi}{Q} [D'' [1 + \Delta q''_{\infty Di} + \Delta Z_{\theta E} (r_m, \lambda, N_p)] + 1]$$

$$= .25 [75 [1 + .05 + .36] + 1]$$

$$= \underline{26.70 \text{ minutes}}$$

with $\Delta q''_{\infty Di}$ equal to .075:

$$\theta_{Bm} = 18.75 \times .728 = \underline{13.65 \text{ minutes}}$$

and,

$$\theta_{Em} = .25 \times 108.8 = \underline{27.1 \text{ minutes}}.$$

The preceding example shows the importance in the determination of the respective ΔZ terms as opposed to the corresponding $\Delta q''_{\infty Di}$ terms. Generally, therefore, a good estimate of the value of $\Delta q''_{\infty Di}$ is sufficient to satisfy the material balance requirements.

Likewise, an evaluation of the λ term does not affect the determination of a corresponding ΔZ to a marked degree, as long as a good estimate of λ is achievable. An observation of Figures A-37 through A-42 will show that for $\lambda = 1.3$, $N_p = 50$, and $r_m = .85$; $\Delta Z_{\theta B} = .33$. Similarly for $\lambda = 1.1$, $\Delta Z_{\theta B} = .36$. The binary value ($\lambda = 1.0$) is $\Delta Z_{\theta B} = .40$. Evaluation of the adsorption terms, therefore, are more dependent on a reliable determination of $q''_{\infty i}$ rather than the subsequent desorption and multicomponent material balance parameters. This discussion shows the importance of the multicomponent isotherm in any real dynamic adsorption design.

Zone Stabilization for the Three Adsorbate System - Zone Velocities

As with the two adsorbate system, values of N_p were plotted against their corresponding values of r_m, in an effort to determine the region of

stabilization for each run. Figure A-24 shows the results in graphical form. While most of the n-hexane runs showed good stabilization, a good number of the n-pentane runs were "outside" the 85% limits determined from the slope of the Thomas solution. This criteria is also shown in the calculation of the Michaels zone velocities shown in Table A-19. The n-hexane values as calculated by:

$$\text{(Michaels) } V_{Zm}'' = \frac{H_T}{\theta_{Bm} + F_M \theta_{Zm}} \qquad \text{VII-39}$$

compare well with those calculated by the constant pattern equation:

$$\text{(Constant Pattern) } V_{Zcp}'' = \frac{v_g/\Phi}{D''+1} \cdot \qquad \text{VII-40}$$

The values for n-pentane, however, show considerable deviation in some instances. Figure A-16 points out this deviation graphically, showing the displacement of the measured data from the lines representing:

$$\frac{1}{V_{Zcp}''} = \frac{\Phi}{v_g} + \frac{\Phi}{v_g} D'' \cdot \qquad \text{VII-41}$$

In Chapter V, an expression was developed relating the transient zone velocity, V_Z' (or V_Z'') to the variables present in Equation VII-41, as well as those not shown:

$$V_Z'' = \frac{v_g/\Phi}{\left(\frac{\partial\Theta}{\partial\Sigma}\right) D'' + 1 + \frac{d \ln k_p a_p''}{d \ln h} \left[\left(\frac{\partial\Theta}{\partial\Sigma}\right) D'' + 1 - \frac{v_g \theta}{\Phi h}\right]} \cdot \qquad \text{VII-42}$$

This equation indicates that, although $(\partial\Theta/\partial\Sigma)$ is <u>less</u> than 1.0, the overall change in the denominator of VII-42 is such that it is somewhat larger than $(D'' + 1)$.

This fact is borne out by Figure A-30, which shows the constant pattern zone velocity calculated by VII-41, divided by the Michaels zone velocity, i.e., Equation VII-39. The abcissa of Figure A-30 is the term: H_T°/H_T, which is determined from known laboratory data and Figures A-49 through A-56.

The curves represented by Figures A-49 through A-56, have been defined as denoting the minimum bed length required to establish a 95% stabilized zone for the equilibrium parameter in question. Thus, the multicomponent value of the column distribution coefficient, D' or D" multiplied by the <u>stabilized</u> mass transfer coefficient, $k_p a_p^{\circ}$, i.e.:

$$k_p a_p^{\circ} D' \text{ or } k_p a_p^{\circ} D'' \quad ,$$

gives an indication of the bed length, H_T°, required for stabilization as calculated by:

$$\Sigma = k_p a_p^{\circ} D \frac{H_T^{\circ} \phi}{v_g} . \qquad \text{VII-43}$$

Where, as before, $(\partial\Sigma/\partial\Theta) \simeq 1.0$ at Σ. D is either the two or three adsorbate column distribution coefficient. The value of H_T°, divided by the <u>available</u> length, H_T, is an indication of the stabilization of the transient mass transfer coefficients as well as the zone velocity. Thus for H_T°/H_T less than or equal to 1.0, V_{Zm}' (Michaels) = V_{Zcp}' (constant pattern), while for H_T°/H_T greater than 1.0, the ratio V_{Zcp}'/V_{Zm}' is greater than 1.0. Figure A-30 shows the close agreement mentioned for the n-hexane data in both two and three adsorbate measurements. While the n-pentane velocity ratios were very close to one in the two adsorbate case, the data show values greater than one in the three adsorbate case. Figure A-30 is an attempt to correct the constant pattern velocity back

to its "laboratory" value for subsequent parametric calculations.

Transient Mass Transfer Coefficients

The variation of the transfer unit height, HTU^o, has been discussed in relation to constant pattern conditions. In effect, values of the HTU's are given in Figures A-25 and A-26 for n-pentane and n-hexane, as calculated by:

$$HTU^o = \frac{v_g/\Phi}{k_p a_p{}^o D} \quad . \qquad \text{VII-44}$$

If the effluents are measured at an interim value of $v\Phi$ corresponding to a non stable Σ, then the overall value of $k_p a_p{}'$ will be greater than $k_p a_p{}^o$ by an amount inversely proportional to the height of the mass transfer unit. Tables A-13 and A-20 indicate the rather large values of $k_p a_p{}'$ (two adsorbate) and $k_p a_p{}''$ (three adsorbate) obtained. The reduced values of the column distribution coefficients, D' and D'' explain in part the increase in $k_p a_p$ as lowering these parameters increases r_m, and subsequently shortens the length of the ultimate HTU' length.

Since values of $k_p a_p{}^o$ are calculated by VII-44, transient values likewise are calculated by:

$$k_p a_p{}' = \frac{v_g/\Phi}{HTU'D'} \quad . \qquad \text{VII-45}$$

Dividing $k_p a_p{}'$ by $k_p a_p{}^o$:

$$k_p a_p{}' = \left(\frac{HTU^o}{HTU'}\right) \left(\frac{D}{D'}\right) k_p a_p{}^o \, . \qquad \text{VII-46}$$

where each HTU' can now be generalized as the Transient Transfer Unit Height, HTU_T, corresponding to the two or three adsorbate system.

Unfortunately, values of HTU_T cannot be directly calculated as they are dependent on values of $k_p a_p'$ themselves. In considering that the transient zone heights are related to a possible parametric group, the important variables to consider can be summarized as:

1) The velocity of the gas, v_g/Φ
2) The adsorbate concentration, c_o
3) The relative column height, H_T^o/H_T.

Thus, HTU_T can be written as:

$$HTU_T = f(v_g/\Phi,\ c_o,\ H_T^o/H_T,\ D'). \qquad \text{VII-47}$$

Removing the functional proportionality:

$$HTU_T = \alpha_T \frac{v_g\ c_o\ H_T}{\Phi\ D'\ H_T^o} \qquad \text{VII-47A}$$

where:

α_T = Dimensional constant relating HTU_T to the variables - min.

The ratio $H_T^o/\ H_T$ has been discussed, and applies in Equation VII-47A only for the limits:

$$H_T^o/H_T \geq 1.0.$$

When $H_T^o/H_T = 1.0$, the transfer run height should be equivalent to its multicomponent constant pattern level as given by VII-45. For this case, the value of $k_p a_p'$ is given by VII-46.

Figures A-28 and A-29 show the group contained in VII-47A named the Transient Column Parameter, plotted vs. calculated transient transfer zone heights. The values are summarized in Tables A-15 and A-22 for both two and three adsorbate runs. Figure A-27, shows the computed constant pattern

values of HTU^{O} as a function of the equilibrium parameter, r (or r_m), and the gas velocity.

Within the limits of the recorded data, this correlation should adequately represent the transient growth of the zone. No attempt has been made to express VII-47A in equational form, although the coordinates of Figures A-28 or A-29 indicate a logarithmic correlation for the data.

Further applications of the data, as supplied to practical calculations for binary and multicomponent adsorption will be presented in an example calculation involving all parameters herein discussed.

CHAPTER VIII

CONCLUSIONS

Application of the binary and multicomponent dynamic hydrocarbon adsorption design criteria, as presented in the preceding chapters, leads to a series of important conclusions pertaining to the application of the theory.

1) The Langmuir Isotherm is well suited to represent dynamic adsorption data. Although the binary data re-evaluated in this work were collected at 90°F and 800 psig, these data are essentially identical with static equilibrium data collected by Day (D2) at pressures of 685 to 1000 psig. The adsorption process, therefore, is relatively insensitive to pressure in the range: $650 \leq P \leq 1000$ (psia). The 800 psig, 90°F. binary isotherms proposed in this work for n-pentane and n-hexane should be applicable for conditions falling within these pressure limits. For most binary applications n-pentane and n-hexane obey the mechanics of the constant pattern process. These conditions are generally met by normal parameters encountered in the field, i.e.: gas velocities of 20-40 ft/min. and tower lengths of 15-25 ft.

2) As established by McLeod's work on binary mixtures, the solid phase asymptotic solution first derived by Gleukauf and Coates (G2) best represents the dynamic mechanics for steady state hydrocarbon adsorption.

The re-evaluation of the binary mixtures in this work further confirms McLeod's findings.

3) The solid phase asymptotic solution can be extended to the multicomponent case, where relative effluent concentrations of the displaced components reach equilibrium levels greater than '1.0'. Constant pattern mechanics are not necessarily obeyed, but transient parameters can be obtained that render the theory applicable to non-stable conditions.

4) The rate of advance of the mass transfer zone is relatively insensitive to column lengths, although the length of the transfer unit is directly proportional to the length of the adsorbent bed only while transient conditions are prevalent.

NOMENCLATURE

Definitions

A_B = Cross sectional area of adsorbing bed - $ft.^2$

a_p = Surface area of the adsorbent available for adsorption per unit volume of bed - $ft.^2/ft.^3$

c_a = Transient concentration in the gas phase in equilibrium with q_a^* - mole% ; or M/L^3 units when used in the material balance.

c_o = Final equilibrium concentration of the adsorbate in the gas phase in equilibrium with q_∞ - mole%

c_a^* = Instantaneous concentration of the adsorbate in the gas phase in equilibrium with the transient adsorbent concentration - mole%

$(\frac{D}{Z})$ = Column distribution coefficient, equivalent to:

$$(\frac{D}{Z}) = (100)\frac{q_\infty \rho_B T R}{c_o MW_i P\Phi} = D \text{ (for } Z = 1)$$

G = Mass flow rate of the gas based on the absolute tower area - $lb/hr.\ ft.^2$

h = Distance down the adsorbing bed - ft.

k_m = Proportionality factor, dependent on the adsorption mechanics assumed

k_f = Rate coefficient for the external phase diffusion case - ft./min.

k_p = Rate coefficient for the solid phase diffusion case - ft./min.

$k_p a_p^o$ = Overall mass transfer coefficient for the binary solid phase diffusion case - $min.^{-1}$

$k_p a_p'$ = Multicomponent mass transfer coefficient - dependent on total adsorbates - $min.^{-1}$

$k_f a_p^o$ = Overall mass transfer coefficient for the external phase diffusion case - $min.^{-1}$

$k_f a_p'$ = Multicomponent equivalent of $k_f a_p^o$ - $min.^{-1}$

k_{kin} = Rate coefficient for the kinetic reaction case - ft/min.

$k_{kin} c_o$ = Mass transfer coefficient for the kinetic reaction case - ft/min.

k_{AD}^o = Binary adsorption equilibrium constant as defined by the Langmuir Isotherm - $(mole\%)^{-1}$

k_{AD}' = Adsorption equilibrium constant for multicomponent mixtures; dependent on the number and character of the components.

MW_i = Molecular weight of component in question - lb/mole

N_E = Dimensionless column capacity parameter for the external phase diffusion case; number of transfer units

N_p = Dimensionless column capacity parameter for the solid phase diffusion case. Also equivalent to the number of transfer units contained within tower volume, v

N_R = Dimensionless column capacity parameter for the kinetic reaction case. Also, number of transfer units for this case

P = System pressure - psia

q_a = Transient concentration of the adsorbate on the adsorbent in equilibrium with c_a^* - lb/lb, or lb/ft^3.

q_a^* = Equilibrium concentration of the adsorbate on the adsorbent directly opposite the corresponding gas phase - lb/lb; lb/ft^3.

q_∞ = Final binary equilibrium concentration on the adsorbent as a function of the adsorbate gas phase concentration level - lb/lb

q_∞' = Equilibrium adsorbent concentration for the two adsorbate multicomponent case - lb/lb

q_∞'' = Equilibrium adsorbent concentration for the three adsorbate case

q_∞^o = Ultimate theoretical capacity of the adsorbent for the adsorbate at 100% concentration of the adsorbate in the gas phase - lb/lb

Q = Gas flow rate, dependent on the system pressure and temperature, and given by:

$$Q = .00974\ A_B \frac{GT}{P} - ft^3/min$$

r = Binary equilibrium parameter

r_m = Multicomponent equilibrium parameter

R = Ideal gas law constant - 10.72 lb. $ft.^3/in.^2$ mole °F

s = Dimensionless distance defined by:

$$s = k_m \frac{v\Phi}{Q}$$

or

$$s = k_m \frac{h\Phi}{v_g}$$

t = Dimensionless time as defined by:

$$t = \frac{k_m}{D} \left(\frac{V - v\Phi}{Q}\right)$$

T = System temperature - (°F + 460)

v = Column absolute volume - $ft.^3$

v_g = Superficial velocity of the gas, based on the tower or adsorbing bed area - ft./min.

V = Total volume of solute or carrier gas that has passed at a point,

h, in the tower - $Q\Delta\theta$ - $ft.^3$

V_Z^o = Binary steady state zone velocity - ft./min.

V_{Zcp} = Constant pattern zone velocity - ft./min.

V_{Zm} = Michaels type zone velocity - ft./min.

V_Z' = Two adsorbate zone velocity - ft./min.

V_Z'' = Three adsorbate zone velocity - ft./min.

x = Ratio of the transient adsorbate gas phase concentration c_a, to the equilibrium concentration $c_o - c_a/c_o$

y = Ratio of the transient component adsorbent concentration q_a, to the equilibrium adsorbent capacity, $q_\infty - q_a/q_\infty$

Z = Throughput parameter, equivalent to

$$Z = \frac{V - v\Phi}{D\ v\ \Phi}$$

Symbols

Φ = Adsorbent packed bed porosity - $ft.^3/ft.^3$

ρ_B = Adsorbent packed bed density - $lb/ft.^3$

$\Sigma_p = N_p$

$\Sigma_E = N_E$

$\Sigma_R = N_R$

θ = Absolute time of adsorption at any point, h - min.

Θ_p = Column throughput parameters for the solid phase diffusion case

$\Theta_p = N_p Z$

Θ_E = Column throughput parameter for the external phase diffusion case

$\Theta_E = N_E Z$

α = Ratio of component adsorption equilibrium constants.

BIBLIOGRAPHY

A1. Anzelius, A. Z. "Uber Erwarmung Vemittels Durchstromender Medien," Angen Math and Mech. (1926).

A2. Ashford, F. E. Dynamic Adsorption of N-Pentane and N-Hexane on Silica Gel. M. P. E. Thesis, University of Oklahoma, Norman, Oklahoma (1963).

B1. Barry, H. M. "Fixed Bed Adsorption," Chem. Engr. (Feb. 8, 1960).

B2. Brunauer, S., Emmett, P. H., and Teller. "Adsorption of Gases in Multimolecular Layers," J. Am. Chem. Soc. (1938) 60, 309.

B3. Brunauer, S. Advances in Chemistry Series No. 33. R. F. Gould Ed. (1961).

C1. Campbell, J. M., Ashford, F. E., Needham, R. B., and Reid, L. S. "More Insight into Adsorption Design," Hydrocarbon Processing and Petroleum Refiner. (1963) Vol. 42, No. 12.

D1. Dale, G. H., Haskel, D. M., Keeling, H. E. and Worael, L. A. "Dynamic Adsorption of Isobutane and Isopentane on Silica Gel," Chemical Engineering Progress Symposium Series Vol. 57 No. 34, 1961, pp. 42-49.

D2. Day, J. J. Equilibrium Adsorption of Hydrocarbon Gas Mixtures on 03 Silica Gel. Ph. D. Thesis, University of Oklahoma, Norman, Oklahoma (1965).

D3. Devault, D. "The Theory of Chromatography", J. Am. Chem. Soc. (1943) 65, 532.

E1. Ennecking, J. C. "Hydrocarbon Recovery with Activated Carbon," Proceedings of the Gas Conditioning Conference; University of Oklahoma, Norman, Oklahoma, April, 1966.

F1. Furnas, C. C. "Heat Transfer from Gas to Broken Solids," U. S. Dept. of Commerce Bulletin, (1930) 362, 17.

F2. Furnas, C. C. Trans. Am. Inst. Chem. Engr. (1930) 24, 142.

G1. Gleukauf, E. "The Theory of Chromatography, Part II", J. Chem. Soc. (1947) 1302.

G2. Gleukauf, E., and Coates, J. I. "The Theory of Chromatography, Part IV," J. Chem. Soc. (1947) 1315.

G3. Goldstein, S. "On the Mathematics of Exchange Processes in Fixed Columns," Proc. Roy. Soc. (1953) A219, 151.

H1. Hiester, N. K. Personal Communication.

H2. Hiester, N. K., and Vermeulen, T. "Saturation and Performance of Ion Exchange and Adsorption Columns," Chem. Engr. Progr. (1952) Vol. 48, No. 10, 505.

H3. Hirshfelder, J. O., Curtis, C. F., Bird, R. B. Molecular Theory of Gases and Liquids, New York: John Wiley and Sons, Inc. (1954), p. 195.

H4. Hougan, O. A., and Marshall, W. R. Jr. "Adsorption from a Fluid Stream Flowing through a Stationary Granular Bed," Chem. Engr. Prog. (1947) Vol. 43, No. 4, 197.

K1. Klinkenburg, A. "Heat Transfer in Cross-Flow Heat Exchanges and Packed Beds," Ind. and Engr. Chem. (1954) Vol. 48, No. 11, 2285.

K2. Klinkenburg, A. "Numerical Evaluation of Equations Describing Transient Heat and Mass Transfer in Packed Solids," Ind. and Engr. Chem. (1948) 40, 1992.

K3. Klotz, I. M. "The Adsorption Wave," Chem. Reviews (1946) 39, 241.

M1. Masamune, Shinobu, and Smith, J. M. "Adsorption Rate Studies - Significance of Pore Diffusion," A. I. Ch. E. J. (1964) Vol. 10 No. 2, 246.

M2. McLeod, H. O. A Study of the Mechanisms by Which Pentane and Hexane Are Adsorbed on Silica Gel. Ph. D. Thesis, University of Oklahoma, Norman, Oklahoma (1965).

M3. Michaels, A. S. "Simplified Method of Interpreting Kinetic Data in Fixed-Bed Ion Exchange," Ind. and Engr. Chem. (1952) Vol. 44, No. 8, 1922.

N1. Needham, R. B. Characterization of Dynamic Adsorption of Pentane on Silica Gel. Ph. D. Thesis, University of Oklahoma, Norman, Oklahoma (1965).

R1. Rosen, T. B. "General Numerical Solution for Solid Diffusion in Fixed Beds," Ind. and Engr. Chem. (1954) Vol. 46, No. 8, 1590.

S1. Schuman, T. E. W. "Heat Transfer: A Liquid Flowing Through a Prism," J. Franklin Inst. (1929) 208, 509.

T1. Thomas, H. C. "Chromatography: A Problem in Kinetics," Ann. N. Y. Acad. Sci. (1948) 49, 161.

T2. Thomas, H. C. "Heterogenious Ion Exchange in a Flowing System," J. Am. Chem. Soc. (1944) 66, 1664.

V1. Vermeulen, T. "Separation by Adsorption Methods," Advances in Chemical Engineering, Vol. II New York: Academy Press, Inc. (1958) 147-208

V2. Vermeulen, T. "Theory for Irreversible and Constant Pattern Diffusion," Ind. and Engr. Chem. (1953) 45, 1664.

V3. Vermeulen, T., and Hiester, N. K. "Ion Exchange Chromatography of Trace Components," Ind. and Engr. Chem. (1952) 44, 636.

V4. Vermeulen, T., and Hiester, N. K. "Ion Exchange and Adsorption Column Kinetics with Uniform Partial Presaturation", J. Chem. Phys. (1954) 22, 96.

APPENDIX A

TABLES AND FIGURES

TABLE A-1

ADSORPTION PARAMETERS
N-PENTANE

RUN	v_g ft/min	Q ft^3/min	H_T ft	θ_B min	θ_E min	H_Z ft
56	22.5	1.059	14.6	16.6	46.5	14.50
57	21.7	1.021	14.6	24.5	52.2	10.80
58	10.8	.511	14.6	42.5	72.8	7.69
59	11.2	.532	14.6	42.4	74.9	8.24
60	10.5	.494	14.6	53.0	93.0	8.14
61	10.8	.511	14.6	41.0	68.0	7.44
62	10.7	.509	14.6	47.8	85.0	8.40
63	11.1	.524	14.6	48.5	90.6	8.89
64	23.0	1.109	14.6	16.4	42.4	14.40
65	23.0	1.150	14.6	18.5	48.3	14.40
66	23.0	1.097	14.6	16.4	40.0	12.72
68	23.4	1.090	14.6	23.5	52.0	11.00
84	45.8	2.135	14.6	10.0	31.7	16.69
86	45.1	2.080	14.6	12.4	33.2	13.80
87	44.5	2.105	14.6	9.0	28.7	16.70
88	45.7	2.150	14.6	11.2	34.7	15.85
89	44.9	2.120	14.6	11.5	34.4	16.30
90	46.4	2.190	14.6	10.0	29.5	16.10
119	10.3	.484	7.5	32.7	59.8	4.48
120	10.4	.486	7.5	29.0	63.9	5.50
121	10.8	.508	7.5	35.2	70.0	5.04
122	18.9	.890	7.5	11.0	32.0	8.65
125	41.0	1.930	7.5	3.3	21.3	12.80
126	35.7	1.676	15.0	16.7	35.7	11.30
131	10.0	.476	15.0	59.7	97	7.20
132	20.2	.954	15.0	29.7	58.7	10.20
135	10.0	.466	13.8	60.0	113.6	8.84
193	47.2	2.125	14.1	1.5	35.0	-
194	46.9	2.210	14.1	1.0	17.5	-

TABLE A-2

EQUILIBRIUM CAPACITY - EQUILIBRIUM PARAMETER
N-PENTANE

RUN	P psig	T °F	c_o mole %	q_∞ lb/lb	r
56	800	91.5	1.021	.101	.723
57	813	89.5	.511	.057	.830
58	813	91.5	1.459	.124	.630
59	800	93.0	1.693	.146	.564
60	835	90.7	.660	.069	.792
61	811	97.0	2.040	.158	.527
62	810	91.0	1.489	.140	.581
63	800	88.8	.561	.058	.833
64	800	95.8	1.519	.125	.638
65	800	92.0	1.143	.111	.664
66	810	92.0	1.550	.132	.603
68	805	91.0	.538	.064	.807
84	805	89.2	1.226	.138	.586
86	808	90.0	.378	.049	.855
87	803	90.5	1.622	.161	.519
88	810	89.0	.467	.060	.819
89	800	91.0	.990	.117	.648
90	795	90.0	1.603	.169	.885
119	805	90.0	1.113	.130	.610
120	800	87.0	.642	.579	.762
121	800	91.0	.937	.130	.609
122	800	90.0	1.022	.092	.713
125	800	90.0	1.031	.110	.670
126	800	92.0	.973	.110	.670
131	805	91.0	1.314	.131	.608
132	800	91.0	.874	.095	.715
133	400	92.0	.906	.128	-
134	400	92.2	.942	.128	-
153	398	90.0	1.444	.127	-
154	1200	90.5	1.092	1.061	-
155	1210	90.7	.947	.059	-
156	1210	91.8	.889	.049	-
193	800	91.4	.428	.036	.898
194	800	91.0	1.950	.098	.706

TABLE A-3

COMPARISON OF MEASURED AND CALCULATED PARAMETERS
N-PENTANE

	MEASURED				CALCULATED			CONSTANT PATTERN	ZONE VELOCITY
RUN	θ_B min	θ_E min	F	V_Z ft/min	θ_B min	θ_E min	F	V_{Zcp} ft/min	V_Z ft/min
56	16.6	46.5	.455	.484	20.2	46.9	.470	.441	.446
57	24.5	52.2	.467	.390	24.8	52.1	.483	.383	.408
58	42.5	72.8	.457	.254	41.1	75.8	.457	.250	.241
59	42.4	74.9	.468	.254	42.1	73.0	.445	.252	.246
60	53.0	93.0	.465	.204	52.4	96.4	.478	.195	.194
61	41.0	68.0	.441	.275	39.0	68.5	.441	.272	.275
62	47.8	85.0	.450	.226	48.7	82.5	.449	.224	.248
63	48.5	90.6	.494	.210	46.4	91.1	.482	.210	.198
64	16.4	42.4	.406	.540	15 5	40.6	.458	.535	.542
65	18.5	48.3	.416	.474	18.4	43.6	.461	.467	.475
66	16.4	40.0	.452	.540	16.7	54.5	.452	.531	.533
68	23.5	52.0	.504	.386	21.7	54.5	.480	.382	.350
84	10.0	31.7	.414	.770	9.9	30.1	.586	.761	.780
86	12.4	33.2	.460	.664	11.0	33.3	.485	.681	.664
87	9.0	28.7	.419	.846	9.5	24.4	.437	.890	.890
88	11.2	34.7	.445	.674	9.9	31.1	.482	.716	.661
89	11.5	34.4	.493	.712	11.8	28.0	.459	.759	.751
90	10.0	29.5	.396	.823	11.4	25.5	.435	.819	.876
119	32.7	59.8	.445	.166	33.1	58.9	.452	.164	.178
120	29.0	63.9	.500	.157	31.8	63.9	.474	.157	.164
121	35.2	70.0	.462	.144	36.0	69.0	.453	.145	.150
122	11.0	32.0	.466	.389	10.6	32.8	.467	.355	.392
125	3.3	21.3	.462	.712	3.4	18.8	.478	.710	.700
126	16.7	35.7	.462	.595	17.2	34.7	.478	.591	.620
131	59.7	97.0	.472	.193	59.0	97.4	.452	.193	.208
132	29.7	58.7	.439	.352	29.3	56.2	.468	.350	.385
135	60.0	113.6	.502	.164	57.0	114.0	.485	.162	.180

TABLE A-4

MASS TRANSFER COEFFICIENT CALCULATIONS
N-PENTANE

RUN	(D/Z)	v_ϕ ft^3	$\frac{Dv_\phi}{Q}$ min	N_p	HTU° ft	$k_p a_p$° min^{-1}
56	126.9	.2685	32.1	20.0	.730	.624
57	141.0	.2685	37.0	40.0	.365	1.080
58	107.0	.2685	56.1	21.0	.696	.374
59	110.0	.2685	55.5	18.0	.810	.561
60	134.0	.2685	72.9	41.0	.356	.561
61	98.1	.2685	51.4	16.0	.911	.311
62	118.5	.2685	62.4	21.0	.695	.337
63	131.5	.2685	67.4	41.0	.356	.609
64	106.5	.2685	25.8	13.0	1.120	.504
65	125.0	.2685	29.2	17.0	.859	.581
66	107.0	.2685	26.1	14.0	1.042	.536
68	152.1	.2685	37.5	34.0	.430	1.080
84	148.9	.2685	18.7	14.0	1.042	.774
86	164.0	.2685	20.3	40.0	.365	1.960
87	123.8	.2685	15.8	10.0	1.460	.633
88	158.1	.2685	19.7	29.0	.504	1.470
89	147.0	.2685	18.7	16.5	.884	.881
90	140.6	.2685	17.2	10.5	1.390	.610
119	156.0	.1368	44.0	22.0	.340	.500
120	164.5	.1368	46.2	33.0	.226	.715
121	186.0	.1368	50.0	19.0	.394	.380
122	132.1	.1368	20.3	15	.497	.740
125	143.0	.1368	10.1	10	.748	.990
126	149.5	.2750	24.5	21	.710	.885
131	130.1	.2750	75.2	26	.575	.345
132	143.1	.2750	41.3	29	.515	.700
135	151.5	.2535	82.6	47	.294	.566

TABLE A-5

ADSORPTION PARAMETERS
N-HEXANE

RUN	$\dot{v}_g$ ft/min	Q ft^3/min	H_T ft	θ_B min	θ_E min	H_Z ft
52	24.6	.494	5.39	10.8	34	5.11
55	23.0	.463	5.39	9.2	34	8.00
69	24.4	1.130	14.60	55.7	83.3	5.96
70	24.5	1.110	14.60	43.5	67.3	6.64
71	10.5	.495	14.60	132.4	165.0	4.12
72	10.7	.519	14.60	86.2	106.5	3.07
73	11.2	.530	14.60	133.0	183.0	4.64
74	11.3	.543	14.60	100.6	130.6	3.78
76	21.2	1.021	14.60	34.2	58.6	8.30
77	19.9	.958	14.60	48.0	72.4	6.10
78	20.0	1.000	14.60	59.4	96.5	7.04
79	42.8	1.925	14.60	26.7	49.3	9.06
80	44.2	2.080	14.60	28.4	52.6	12.18
81	39.1	1.835	14.60	20.9	50.0	13.20
83	45.8	2.175	14.60	18.4	31.1	8.25
117	11.5	.539	3.58	20.5	37.8	2.14
118	10.5	.494	7.48	53.9	70.5	2.00
123	19.9	.936	7.48	52.8	32.0	3.68
124	43.7	2.020	7.48	12.5	28.0	6.10
129	41.0	1.935	14.95	34.6	51.8	5.98
130	10.8	.506	14.95	108.2	124.3	2.08
143	40.5	1.910	13.80	19.5	38.0	13.80

TABLE A-6

EQUILIBRIUM CAPACITIES AND EQUILIBRIUM PARAMETERS
N-HEXANE

RUN	P psig	T °F	c_o mole %	q_∞ lb/lb	r
52	801	90.0	.509	.127	.69
55	790	90.0	1.162	.222	.46
69	810	91.3	.495	.132	.68
70	808	89.0	.930	.188	.55
71	806	91.0	.610	.156	.63
72	805	90.2	1.200	.199	.51
73	802	91.0	.467	.131	.68
74	785	92.0	.996	.204	.50
76	815	93.0	1.357	.200	.51
77	820	88.0	.939	.179	.56
78	800	91.0	.479	.123	.70
79	800	91.0	.424	.105	.74
80	808	91.0	.367	.105	.74
81	800	88.0	.755	.152	.63
83	802	91.3	1.310	.208	.49
117	800	94.0	.853	.173	.57
118	805	93.0	.884	.171	.58
123	800	91.0	.589	.146	.64
124	805	90.0	.684	.171	.58
129	800	93.0	.676	.180	.56
130	800	90.8	.925	.175	.57
143	800	91.2	.994	.184	.55

TABLE A-7

COMPARISON OF MEASURED AND CALCULATED PARAMETERS
N-HEXANE

	MEASURED				CALCULATED			CONSTANT PATTERN	ZONE VELOCITY
RUN	θ_B min	θ_E min	F	V_Z ft/min	θ_B min	θ_E min	F	V_{Zcp} ft/min	V_Z ft/min
52	10.8	34.0	.502	.261	10.4	33.9	.463	.259	.210
55	9.2	34.0	.310	.311	8.8	28.0	.427	.313	.322
69	55.7	83.3	.435	.215	55.6	81.6	.465	.214	.185
70	43.5	67.3	.367	.279	23.8	63.0	.444	.278	.260
71	132.4	165.0	.431	.099	127.0	160.0	.457	.101	.100
72	86.2	106.5	.505	.151	80.0	107.1	.437	.150	.155
73	133.0	183.0	.493	.093	134.5	174.0	.465	.093	.086
74	100.6	130.6	.513	.126	99.0	126.5	.437	.125	.126
76	34.2	58.6	.353	.341	33.0	53.4	.438	.335	.357
77	48.0	72.4	.432	.249	46.0	69.5	.445	.249	.264
78	59.4	96.5	.478	.190	59.0	96.0	.466	.188	.190
79	26.7	49.3	.429	.405	26.8	49.6	.473	.395	.405
80	28.4	52.6	.423	.361	28.4	52.6	.473	.359	.333
81	20.9	50.0	.384	.456	19.8	43.1	.457	.452	.477
83	18.4	31.1	.331	.646	17.5	34.2	.435	.638	.646
117	20.5	37.8	.486	.124	20.4	39.8	.445	.121	.124
118	53.9	70.5	.454	.121	52.1	71.5	.450	.120	.130
123	52.8	32.0	.470	.177	32.0	53.4	.458	.176	.200
124	12.5	28.0	.425	.388	13.4	27.7	.451	.385	.388
129	34.6	51.8	.487	.348	35.4	51.1	.446	.345	.378
130	108.2	124.3	.492	.129	101.5	129.0	.447	.128	.129
143	19.5	38.0	.329		-	-	-		

TABLE A-8

MASS TRANSFER COEFFICIENT CALCULATIONS
N-HEXANE

RUN	(D/Z) -	$v\Phi$ ft^3	$\frac{Dv\Phi}{Q}$ min	N_p -	HTU° ft	$k_p a_p$° min^{-1}
52	237.0	.0421	21.6	13.0	.414	.600
55	183.1	.0421	16.6	7.0	.770	.421
69	283.0	.2680	67.0	40.0	.365	.596
70	210.0	.2680	50.0	25.0	.584	.495
71	260.0	.2680	141.0	55.0	.266	.395
72	177.0	.2680	91.0	31.0	.472	.342
73	300.0	.2680	151.0	60.0	.244	.398
74	223.3	.2680	110.5	36.0	.415	.326
76	151.1	.2680	41.1	19.0	.769	.462
77	198.5	.2680	55.4	25.0	.584	.452
78	277.0	.2680	72.4	40.0	.365	.553
79	267.0	.2680	37.2	35.0	.417	.941
80	306.0	.2680	39.4	35.0	.417	.890
81	215.0	.2680	31.4	21.0	.695	.670
83	178.0	.2680	21.9	16.0	.914	.730
117	235.0	.0658	28.7	15.0	.239	.524
118	218.0	.1365	60.0	35.0	.214	.584
123	282.0	.1365	41.1	26.0	.287	.633
124	282.5	.1365	19.1	15.5	.492	.811
129	295.0	.2750	41.8	29.0	.515	.695
130	208.0	.2750	113.1	42.0	.570	.372
143	-	-	-			

TABLE A-9

ADSORPTION PARAMETERS
N-PENTANE - N-HEXANE

RUN	v_g ft/min	Q ft^3/min	H_T ft	θ_B min	θ_E min	H_T ft	Component -
1	35.7	.715	5.39	3.5	12.0	5.75	n-C_5
1				9.8	23.1	4.71	n-C_6
4	34.7	.695	5.39	3.0	11.8	7.00	n-C_5
4				8.0	20.0	4.86	n-C_6
46	24.3	.476	5.39	5.0	14.8	5.39	n-C_5
46				11.7	31.3	5.16	n-C_6
49	24.8	.506	5.39	3.0	12.0	6.21	n-C_5
49				9.0	25.0	5.78	n-C_6
51	24.3	.483	5.39	2.8	13.5	7.34	n-C_5
51				7.5	25.9	6.29	n-C_6
103	11.3	.534	14.95	56.5	99.1	8.29	n-C_5
103				106.0	140.6	4.21	n-C_6
105	11.8	.555	14.95	44.2	59.9	4.41	n-C_5
105				66.9	110.2	7.59	n-C_6
106	22.4	1.058	14.95	24.6	45.2	8.55	n-C_5
106				54.1	95.1	8.54	n-C_6
108	21.3	1.000	14.95	27.9	56.0	9.95	n-C_5
108				62.5	103.0	7.34	n-C_6
110	44.1	2.080	14.95	9.0	20.0	10.82	n-C_5
110				19.0	36.0	9.84	n-C_6
112	23.1	1.090	14.95	15.7	25.1	6.86	n-C_5
112				25.0	48.8	10.65	n-C_6
113	45.2	2.150	14.95	10.0	28.0	13.81	n-C_5
113				27.2	60.2	12.01	n-C_6

TABLE A-10

MULTICOMPONENT ADSORPTION EQUILIBRIUM CONSTANTS
N-PENTANE - N-HEXANE

RUN	c_o mole %	q_∞' lb/lb	q_∞ lb/lb	α_i -	k'_{AD} $(\text{mole \%})^{-1}$
1	.45	.0509	.0550	.902	.400
1	.42	.1122	.1175	.976	.935
4	1.01	.0933	.1042	.866	.385
4	.45	.0964	.1220	.716	.687
46	.57	.0531	.0661	.751	.334
46	.50	.1230	.1334	.904	.864
49	1.05	.0821	.1051	.702	.312
49	.48	.0885	.1300	.600	.575
51	.87	.0755	.0926	.702	.311
51	.40	.0755	.1110	.606	.580
103	.50	.0545	.0950	.880	.390
103	.74	.1595	.1665	.906	.868
105	1.17	.0800	.1150	.608	.270
105	1.03	.1611	.2040	.690	.660
106	.61	.0561	.0715	.748	.332
106	.54	.1331	.1390	.973	.931
108	.45	.0482	.0555	.846	.376
108	.40	.1121	.1145	.984	.945
110	.81	.0680	.0877	.714	.316
110	.80	.1444	.1670	.745	.714
112	1.61	.0840	.1335	.472	.209
112	1.42	.1803	.2445	.611	.585
113	.34	.0390	.0435	.876	.389
113	.30	.0867	.0910	.941	.900

TABLE A-11

EQUILIBRIUM CAPACITIES AND EQUILIBRIUM PARAMETERS
N-PENTANE - N-HEXANE

RUN	P psig	T °F	c_o mole %	q_∞' lb/lb	r_m -
1	810	89	.45	.0550	.847
1			.42	.1122	.725
4	785	93	1.01	.0933	.720
4			.45	.0964	.764
46	803	92	.57	.0531	.840
46			.50	.1230	.700
49	806	90	1.05	.0821	.753
49			.48	.0885	.795
51	807	91	.87	.0755	.773
51			.40	.0755	.816
103	805	98	.50	.0545	.815
103			.74	.1595	.609
105	800	92	1.17	.0800	.760
105			1.03	.1611	.605
106	790	94	.61	.0564	.831
106			.54	.1331	.674
108	805	91	.45	.0482	.855
108			.40	.1121	.725
110	800	93	.81	.0680	.796
110			.80	.1444	.646
112	815	92	1.61	.0840	.748
112			1.42	.1803	.559
113	800	94	.34	.0390	.883
113			.30	.0867	.788

TABLE A-12

COMPARISON OF MEASURED AND CALCULATED RESULTS
N-PENTANE - N-HEXANE

	MEASURED				CALCULATED			CONSTANT PATTERN
RUN	θ_B min	θ_E min	F_m	V_Z' ft/min	θ_B min	θ_E min	F_m	V_{Zcp}' ft/min
1	3.5	12.0	.524	.678	3.5	13.8	.492	.678
1	9.8	23.1	.413	.355	9.4	22.7	.470	.345
4	3.0	11.8	.431	.794	2.9	11.4	.470	782
4	8.0	20.0	.442	.406	7.3	19.8	.475	.405
46	5.0	14.8	.489	.550	4.2	17.6	.492	.561
46	11.7	31.3	.447	.262	12.5	31.5	.466	.260
49	3.0	12.0	.536	.688	3.6	12.7	.482	.698
49	9.0	25.0	.368	.361	8.0	21.4	.478	.357
51	2.8	13.5	.474	.685	4.1	14.5	.479	.624
51	7.5	25.9	.447	.342	7.3	25.2	.480	.332
103	56.5	99.1	.458	.195	51.5	97.0	.497	.200
103	106.0	140.6	.493	.122	104.2	140.5	.452	.121
105	44.2	59.9	.580	.281	43.9	63.9	.573	.332
105	66.9	110.2	.426	.176	69.0	112.0	.452	.173
106	24.6	45.2	.552	.416	23.4	45.0	.525	.456
106	54.1	95.1	.434	.208	55.6	89.0	.462	.207
108	27.9	56.0	.518	.353	26.6	54.0	.529	.384
108	62.5	103.0	.541	.177	64.5	104.8	.470	.177
110	9.0	20.0	.564	.985	10.5	20.5	.535	1.01
110	19.0	36.0	.412	.576	18.5	35.3	.470	.564
112	15.7	25.1	.511	.731	26.0	45.4	.545	.865
112	25.0	48.8	.355	.448	15.4	23.4	.444	.426
113	10.0	28.0	.526	.770	10.2	29.3	.525	.760
113	27.2	60.2	.422	.363	27.0	56.0	.478	.358

TABLE A-13

MASS TRANSFER COEFFICIENT CALCULATIONS
N-PENTANE - N-HEXANE

RUN	(D'/Z) -	vΦ ft^3	$\frac{Dv\Phi}{Q}$ min	N_p -	HTU' ft	$k_p a_p'$ min^{-1}
1	132.9	.0421	7.82	27	.195	3.450
1	258.0		15.19	22	.245	1.450
4	110.0	.0421	6.66	14	.384	2.120
4	214.0		13.00	22	.245	1.690
46	107.5	.0421	9.52	25	.215	2.620
46	235.0		20.80	18	.300	.866
49	87.6	.0421	7.29	17	.317	2.320
49	172.1		14.28	29	.185	2.030
51	96.6	.0421	8.42	19	.284	2.260
51	182.5		15.95	26	.202	1.630
103	140.5	.2750	69.6	45	.332	.644
103	232.0		120.08	40	.374	.321
105	87.5	.2750	43.4	38	.394	.876
105	108.5		83.4	40	.374	.479
106	121.2	.2750	31.6	38	.394	1.200
106	271.0		70.6	31	.482	.501
108	137.0	.2750	37.7	44	.340	1.169
108	301.0		82.6	40	.374	.544
110	108.0	.2750	14.26	29	.516	2.040
110	195.0		25.90	22	.680	.856
112	65.6	.2750	16.50	35	.426	2.120
112	134.2		33.90	19	.786	.560
113	148.2	.2750	18.95	40	.374	2.110
113	314.0		40.20	36	.415	.895

TABLE A-14

MULTICOMPONENT EQUILIBRIUM ENHANCEMENT FACTOR
N-PENTANE - N-HEXANE

RUN	r_m -	$k_p a_p'$ min^{-1}	N_p -	$\Delta Q_D/2$ lb	I.R. lb/min	ΔZ_D -	λ CALCULATED	λ MEASURED
1	.847	3.450	27	.00095	.0382	.10	1.0634	1.050
1	-	-	-	-	-	-	-	-
4	.720	2.120	14	0	.0798	-	1.000	1.000
4	-	-	-	-	-	-	-	-
46	.840	2.620	25	.00300	.0322	.21	1.090	1.060
46	-	-	-	-	-	-	-	-
49	.750	2.320	17	.00402	.0614	.13	1.092	1.050
49	-	-	-	-	-	-	-	-
51	.773	2.260	19	0	.0499	-	1.000	1.020
51	-	-	-	-	-	-	-	-
103	.836	.644	45	.02710	.0263	.18	1.160	1.100
103	-	-	-	-	-	-	-	-
105	.760	.876	38	.25400	.0628	.30	1.55	1.39
105	-	-	-	-	-	-	-	-
106	.831	1.200	38	.1136	.0616	.35	1.30	1.160
106	-	-	-	-	-	-	-	-
108	.855	1.169	44	.0843	.0436	.26	1.20	1.16
108	-	-	-	-	-	-	-	-
110	.796	2.040	29	.0325	.1625	.18	1.15	1.19
110	-	-	-	-	-	-	-	-
112	.750	2.120	35	.2770	.1725	.35	1.50	1.25
112	-	-	-	-	-	-	-	-
113	.88	2.110	40	0	.0720	-	1.00	1.16
113	-	-	-	-	-	-	-	-

TABLE A-15

TRANSIENT COLUMN PARAMETER
N-PENTANE - N-HEXANE

RUN	c_o mole %	D' -	D -	$k_p a_p{}^\circ$ min^{-1}	$H_T{}^\circ/H_T$ ft/ft	HTU°/HTU' ft/ft	$\frac{v_g c_o H_T}{\Phi D' H_T{}^\circ}$ min^{-1}	$k_p a_p{}'$ CALC.
1	.45	132.9	140.5	1.45	9.650	1.950	.0313	3.000
1	.42	258.0	270.0	.72	3.160	1.835	.0461	1.384
4	1.01	110.0	123.0	.85	5.560	1.770	.1431	1.685
4	.45	214.0	272	.71	5.010	1.750	.0363	1.580
46	.57	107.5	134.0	1.00	10.500	1.860	.0309	2.350
46	.50	235.0	252.5	.57	1.850	1.300	.0700	.790
49	1.05	87.6	112.2	.69	8.160	1.875	.0909	1.660
49	.48	172.1	253.0	.60	5.750	1.430	.0302	1.265
51	.87	96.6	118.8	.78	8.000	1.835	.0684	1.760
51	.40	182.5	268.0	.62	8.350	1.270	.0156	1.169
103	.50	140.5	155.0	.64	2.110	1.060	.0476	.705
103	.74	232.0	242.0	.34	.427	1.000	-	.387
105	1.17	87.5	126	.46	2.24	1.100	.1760	.729
105	1.03	168.5	213	.34	.569	1.000	-	.430
106	.61	121.2	154.5	.96	3.330	1.000	.0846	1.220
106	.54	271.0	283.0	.55	.600	1.000	-	.574
108	.45	137.0	158.0	1.14	2.900	1.010	.0592	1.312
108	.40	301.0	306.0	.58	.804	1.000	-	.590
110	.81	108.0	139.5	1.07	4.000	1.030	.2070	1.440
110	.80	195.0	225.0	.80	.836	1.000	-	.924
112	1.61	65.6	104.6	.49	5.240	1.400	.2710	1.090
112	1.42	134.2	182.0	.44	.802	1.000	-	.596
113	.34	148.2	165.5	1.70	4.080	1.010	.0634	1.92
113	.30	314.0	330.0	.94	1.540	1.00	-	.988

TABLE A-16

ADSORPTION PARAMETERS
N-PENTANE - N-HEXANE - N-HEPTANE

RUN	v_g ft/min	Q ft^3/min	H_T ft	θ_B min	θ_E min	H_Z ft	COMPONENT -
201	40.8	1.910	14.06	7.0	21.0	14.04	n-C_5
201				17.0	35.5	9.79	n-C_6
201				48.0	60.0	-	n-C_7
217	30.7	1.420	14.06	6.0	27.0	16.95	n-C_5
217				8.0	36.0	17.61	n-C_6
217				29.0	68.5	-	n-C_7
220	30.6	1.435	14.06	10.0	32.0	14.04	n-C_5
220				30.0	52.0	7.55	n-C_6
220				60.0	91.0	-	n-C_7
221	30.5	1.390	14.06	5.0	30.0	18.00	n-C_5
221				20.0	48.0	10.55	n-C_6
221						-	n-C_7
222	30.8	1.415	14.06	5.0	27.5	17.75	n-C_5
222				19.0	37.5	10.65	n-C_6
222				40.0	63.0	-	n-C_7
225	32.0	1.472	14.06	9.0	29.0	15.62	n-C_5
225				30.0	49.5	6.95	n-C_6
225				54.0	66.5	-	n-C_7
226	31.1	1.406	14.06	6.0	25.0	16.95	n-C_5
226				26.5	44.0	6.64	n-C_6
226				46.0	62.5	-	n-C_7
227	31.5	1.448	14.06	5.0	26.0	18.40	n-C_5
227				26.0	39.0	5.50	n-C_6
227				42.5	70.0	-	n-C_7

TABLE A-17

MULTICOMPONENT ADSORPTION EQUILIBRIUM CONSTANTS
N-PENTANE - N-HEXANE - N-HEPTANE

RUN	c_o mole %	q_∞'' lb/lb	q_∞ lb/lb	α_i' -	k''_{AD} $(\text{mole \%})^{-1}$
201	.1969	.01070	.0270	.380	.169
201	.2158	.03190	.0695	.411	.393
201	.2100	.05740	-	-	-
217	.2320	.01158	.0313	.349	.155
217	.0618	.00476	.0225	.199	.191
217	.3800	.08590	-	-	-
220	.1515	.01105	.0210	.508	.246
220	.1200	.02170	.0408	.490	.469
220	.2140	.08600	-	-	-
221	.1625	.00976	.0226	.421	.187
221	.1248	.01940	.0434	.417	.399
221	.2830	.08910	-	-	-
222	.1549	.00844	.0213	.378	.168
222	.1020	.01205	.0351	.312	.299
222	.3530	.09190	-	-	-
225	.0524	.00338	.00775	.444	.197
225	.2660	.04740	.0831	.515	.494
225	.1930	.06420	-	-	-
226	.0538	.00263	.00831	.334	.184
226	.2510	.04140	.0791	.470	.45
226	.2660	.07710	-	-	-
227	.0536	.00195	.0080	.248	.110
227	.2020	.03020	.0670	.414	.396
227	.3680	.1110	-	-	-

TABLE A-18

EQUILIBRIUM CAPACITIES AND EQUILIBRIUM PARAMETERS
N-PENTANE - N-HEXANE - N-HEPTANE

RUN	P psig	T °F	c_o mole %	q_∞'' lb/lb	r_m -
201	804	98.3	.1969	.01070	.968
201	-	-	.2158	.03190	.921
201	-	-	.2100	.05740	-
217	800	88.0	.2320	.01158	.965
217	-	-	.0618	.00476	.988
217	-	-	.3800	.08590	-
220	800	92.4	.1515	.01105	.967
220	-	-	.1200	.02170	.947
220	-	-	.2140	.08600	-
221	800	90.0	.1625	.00976	.971
221	-	-	.1248	.01940	.952
221	-	-	.2830	.0891	-
222	800	91.8	.1549	.00844	.975
222	-	-	.1020	.01205	.971
222	-	-	.3530	.09190	-
225	800	91.8	.0524	.00338	.989
225	-	-	.2660	.0474	.884
225	-	-	.1930	.0642	-
226	800	90.6	.0538	.00263	.992
226	-	-	.2310	.0414	.888
226	-	-	.2660	.0771	-
227	800	92.3	.0536	.00195	.994
227	-	-	.2020	.03020	.926
227	-	-	.3680	.11100	-

TABLE A-19

COMPARISON OF MEASURED AND CALCULATED RESULTS
N-PENTANE - N-HEXANE - N-HEPTANE

	MEASURED				CALCULATED			CONSTANT PATTERN
RUN	θ_B min	θ_E min	F_m	V''_Z ft/min	θ_B min	θ_E min	F_m	$V''_{Z_{cp}}$ ft/min
201	7.0	21.0	.500	1.010	5.2	20.5	.537	1.350
201	17.0	35.5	.519	.529	13.2	37.1	.510	.596
201	-	-	-	-	-	-	-	-
217	6.0	27.0	.541	.808	5.7	26.5	.555	1.110
217	8.0	36.0	.511	.626	6.3	32.8	.570	.850
217	-	-	-	-	-	-	-	-
220	10.0	32.0	.549	.639	7.3	33.7	.509	.744
220	30.0	52.0	.500	.343	25.7	54.6	.515	.353
220	-	-	-	-	-	-	-	-
221	5.0	30.0	.581	.724	5.0	31.4	.535	1.026
221	20.0	48.0	.624	.377	18.7	48.0	.550	.475
221	-	-	-	-	-	-	-	-
222	5.0	27.5	.566	.791	4.4	25.7	.552	1.005
222	19.0	37.0	.626	.576	18.4	37.2	.585	.555
222	-	-	-	-	-	-	-	-
225	9.0	29.0	.451	.781	8.9	25.4	.510	.884
225	30.0	49.5	.489	.357	26.2	49.4	.495	.387
225	-	-	-	-	-	-	-	-
226	6.0	25.0	.516	.887	7.6	28.7	.572	1.130
226	26.5	44.0	.611	.379	25.7	43.5	.540	.406
226	-	-	-	-	-	-	-	-
227	5.0	26.0	.436	.876	4.5	20.0	.565	1.540
227	26.0	39.0	.594	.424	24.4	40.0	.550	.456
227	-	-	-	-	-	-	-	-

TABLE A-20

MASS TRANSFER COEFFICIENT CALCULATIONS
N-PENTANE - N-HEXANE - N-HEPTANE

RUN	(D/Ż) -	$v\Phi$ ft^3	$\frac{Dv\Phi}{Q}$ min	N_p -	HTU' ft	$k_p a_p''$ min^{-1}
201	74.9	.2585	10.15	85	.1651	7.86
201	170.0	-	23.00	80	.1760	3.48
201	-	-	-	-	-	-
217	68.2	.2585	12.40	85	.1651	6.85
217	89.0	-	16.20	220	.0638	13.60
217	-	-	-	-	-	-
220	101.2	.2585	18.91	100	.1406	5.24
220	210.0	-	37.80	125	.1125	3.31
220	-	-	-	-	-	-
221	82.6	.2585	15.40	97	.1450	6.30
221	180.0	-	33.50	110	.1280	3.28
221	-	-	-	-	-	-
222	75.0	.2585	13.71	95	.1480	6.92
222	136.5	-	24.90	200	.0704	8.02
222	-	-	-	-	-	-
225	89.5	.2585	15.75	220	.0640	14.00
225	205.5	-	36.10	83	.1695	2.30
225	-	-	-	-	-	-
226	67.4	.2585	12.39	250	.0564	20.20
226	190.0	-	35.00	80	.1765	2.28
226	-	-	-	-	-	-
227	49.9	.2585	8.91	275	.0511	30.90
227	172.5	-	30.80	135	.1041	4.44
227	-	-	-	-	-	-

TABLE A-21

MULTICOMPONENT EQUILIBRIUM ENHANCEMENT FACTOR
N-PENTANE - N-HEXANE - N-HEPTANE

RUN	r_m -	$k_p a_p''$ min^{-1}	N_p -	$Q_D/2$ lb	I.R. lb/min	ΔZ_D -	λ CALCULATED	λ MEASURED
201	.968	7.86	85	.0624	.0365	.90	1.30	1.18
201	.921	3.48	80	.0675	.0484	.35	1.30	1.11
201	-	-	-	-	-	-	-	-
217	.965	6.85	85	.0725	.0319	1.2	1.31	1.22
217	.984	13.60	220	.0305	.0103	1.1	1.34	1.31
217	-	-	-	-	-	-	-	-
220	.967	5.24	100	.0285	.0213	.636	1.21	1.1
220	.947	3.31	125	.0175	.0201	.260	1.20	1.13
220	-	-	-	-	-	-	-	-
221	.971	6.30	97	.0470	.0223	.840	1.31	1.18
221	.952	3.28	110	.0270	.0205	.330	1.23	1.20
221	-	-	-	-	-	-	-	-
222	.975	6.92	95	.0445	.02150	1.0	1.31	1.20
222	.971	8.02	200	0	.0170	-	1.00	1.42
222	-	-	-	-	-	-	-	-
225	.989	14.00	220	0	.0076	-	1.00	1.12
225	.884	2.30	83	0	.0461	-	1.00	1.05
225	-	-	-	-	-	-	-	-
226	.992	20.2	250	.0138	.0075	.85	1.34	1.30
226	.888	2.28	80	.0650	.0415	.22	1.31	1.10
226	-	-	-	-	-	-	-	-
227	.994	30.90	275	.0275	.0026	2.03	1.40	1.29
227	.926	4.44	135	.0375	.0344	.26	1.29	1.20
227	-	-	-	-	-	-	-	-

TABLE A-22

TRANSIENT COLUMN PARAMETER
N-PENTANE - N-HEXANE - N-HEPTANE

RUN	c_o	D''	D	$k_p a_p''$	$H_T°/H_T$	HTU°/HTU'	$\frac{v_g c_o H_T}{\Phi D'' H_T°}$	$k_p a_p''$
	mole %	-	-	min^{-1}	ft/ft	ft/ft	min^{-1}	CALC.
201	.1969	74.9	189.0	7.86	8.75	1.180	.02990	7.45
201	.2158	170.0	371.0	3.48	7.69	1.380	.01690	2.95
201	.2100	-	-	-	-	-	-	-
217	.2320	68.2	184.2	6.85	11.10	1.270	.02350	6.51
217	.0618	89.0	420.0	13.60	17.89	3.260	.00296	13.20
217	.3800	-	-	-	-	-	-	-
220	.1515	101.2	192.2	5.24	5.40	1.385	.02120	5.91
220	.1200	210.0	395.0	3.31	6.16	2.000	.00710	3.13
220	.2140	-	-	-	-	-	-	-
221	.1625	82.6	191.0	6.30	6.95	1.310	.02160	6.66
221	.1248	180.0	411.0	3.28	7.11	1.750	.00741	3.31
221	.2830	-	-	-	-	-	-	-
222	.1549	75.0	189.5	6.92	7.84	1.281	.02020	7.24
222	.1020	136.5	398.0	8.02	11.12	2.980	.00516	7.26
222	.3530	-	-	-	-	-	-	-
225	.0524	89.5	205.5	14.00	5.31	2.105	.00880	14.5
225	.2660	205.5	383.0	2.30	4.89	1.590	.02120	2.28
225	.1930	-	-	-	-	-	-	-
226	.0538	67.4	213.0	20.20	7.11	2.300	.00870	21.8
226	.2510	190.0	364.0	2.28	5.46	1.520	.01880	2.24
226	.2660	-	-	-	-	-	-	-
227	.0536	49.9	205.0	30.90	9.60	2.540	.00880	31.25
227	.2020	172.5	383.0	4.44	7.18	2.350	.01285	4.10
227	.3680	-	-	-	-	-	-	-

FIGURE A 1

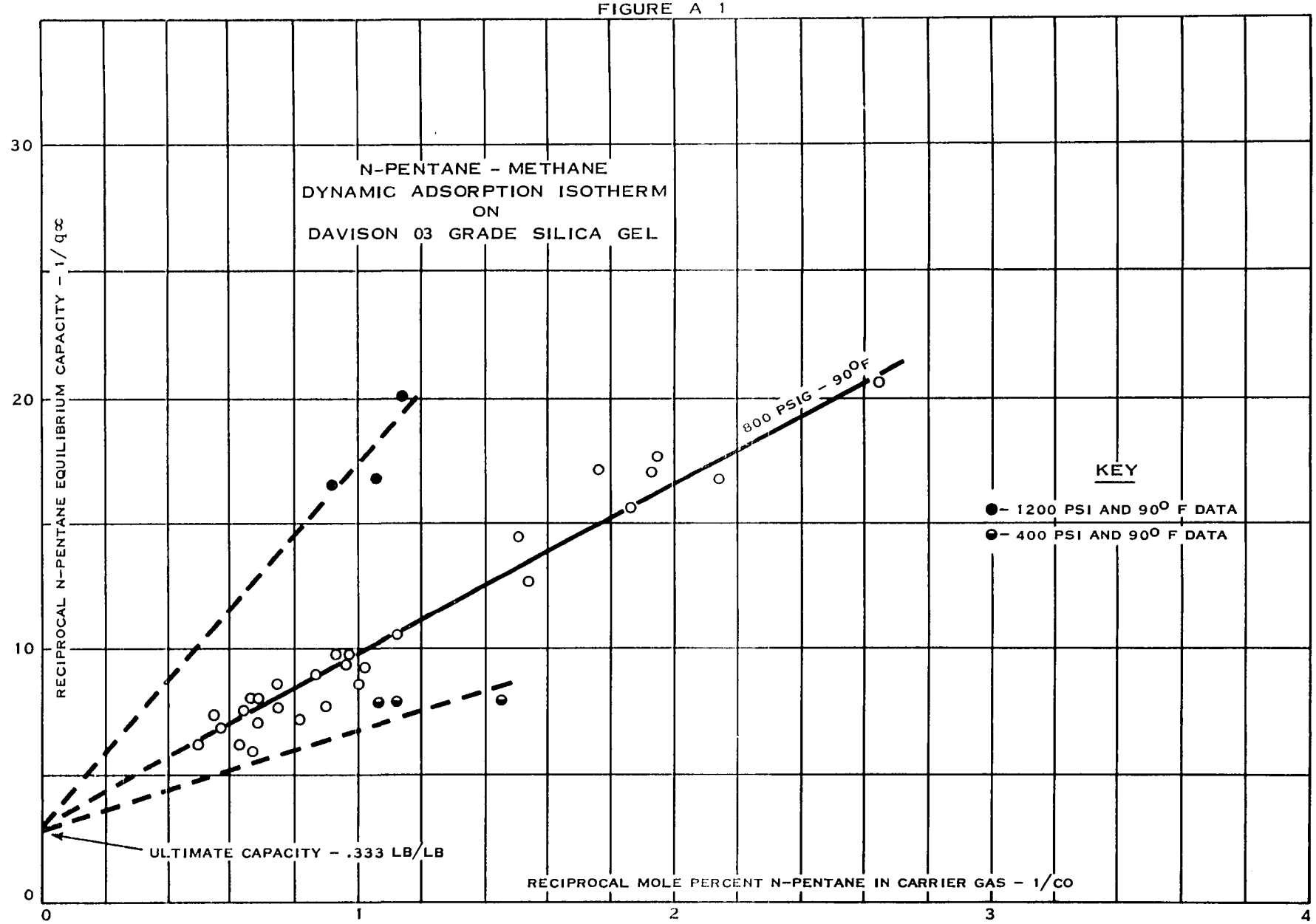
N-PENTANE - METHANE
DYNAMIC ADSORPTION ISOTHERM
ON
DAVISON 03 GRADE SILICA GEL
RECIPROCAL N-PENTANE EQUILIBRIUM CAPACITY - 1/q∞
RECIPROCAL MOLE PERCENT N-PENTANE IN CARRIER GAS - 1/CO
800 PSIG - 90°F
KEY
- 1200 PSI AND 90° F DATA
- 400 PSI AND 90° F DATA
ULTIMATE CAPACITY - .333 LB/LB
0
10
20
30
0
1
2
3
4

FIGURE A 2

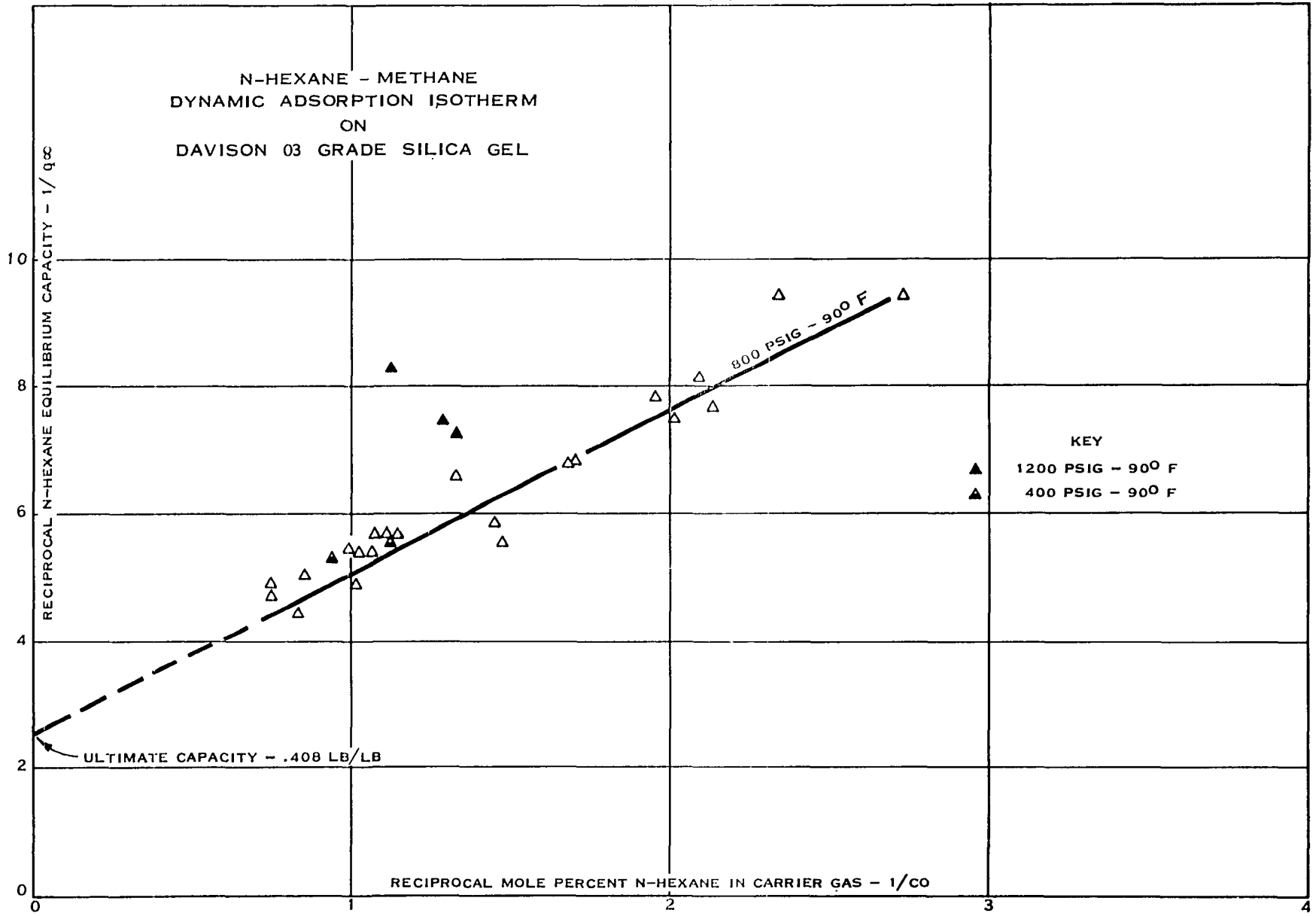
N-HEXANE - METHANE
DYNAMIC ADSORPTION ISOTHERM
ON
DAVISON 03 GRADE SILICA GEL
RECIPROCAL N-HEXANE EQUILIBRIUM CAPACITY - 1/ qe
RECIPROCAL MOLE PERCENT N-HEXANE IN CARRIER GAS - 1/CO
800 PSIG - 90° F
ULTIMATE CAPACITY - .408 LB/LB
KEY
1200 PSIG - 90° F
400 PSIG - 90° F
0
2
4
6
8
10
0
1
2
3
4

FIGURE A 3

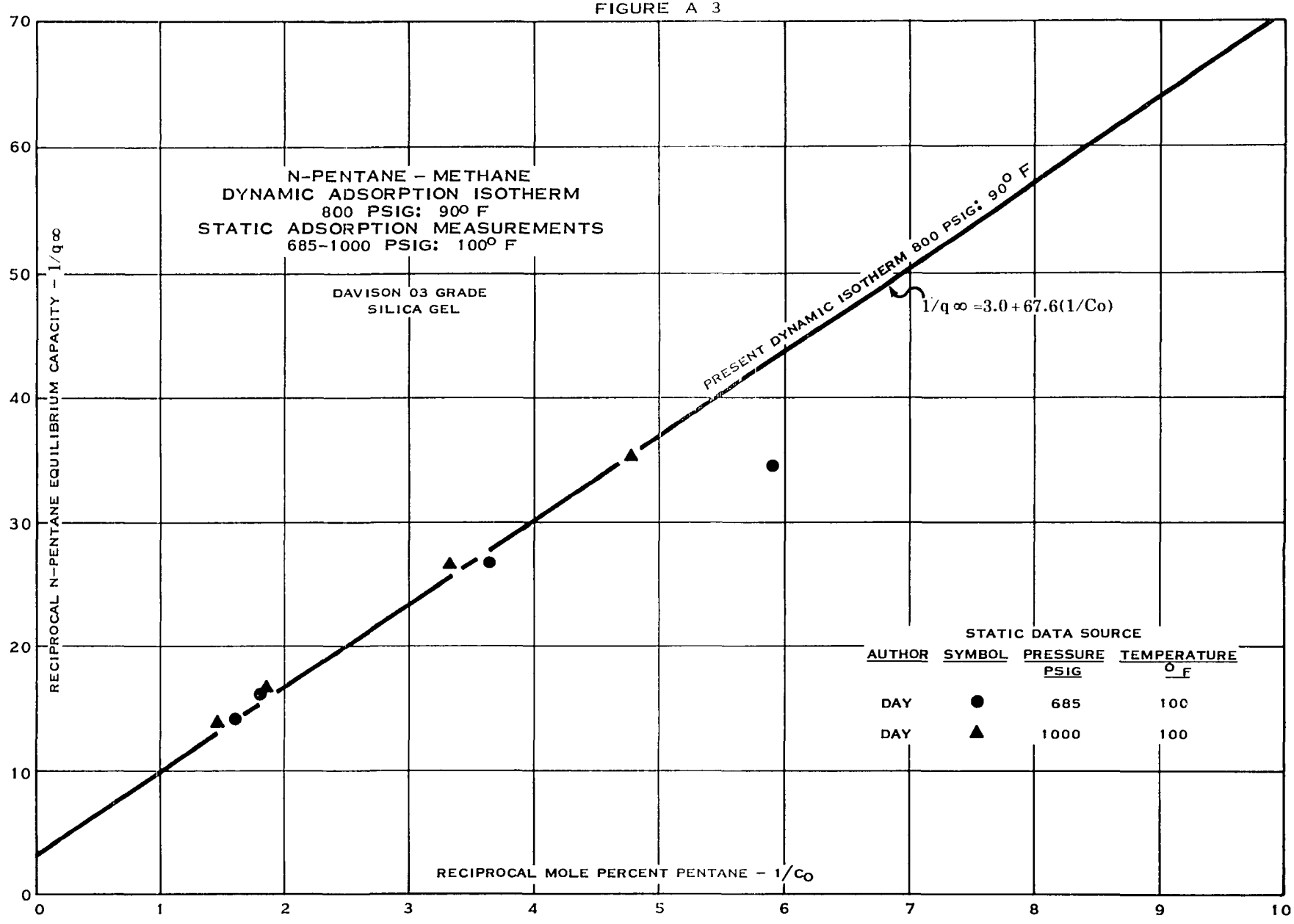
N-PENTANE – METHANE
DYNAMIC ADSORPTION ISOTHERM
800 PSIG: 90° F
STATIC ADSORPTION MEASUREMENTS
685-1000 PSIG: 100° F
DAVISON 03 GRADE
SILICA GEL
PRESENT DYNAMIC ISOTHERM 800 PSIG: 90° F
1/q∞ =3.0 + 67.6(1/Co)
RECIPROCAL N-PENTANE EQUILIBRIUM CAPACITY – 1/q∞
RECIPROCAL MOLE PERCENT PENTANE – 1/Co
0
10
20
30
40
50
60
70
0
1
2
3
4
5
6
7
8
9
10
STATIC DATA SOURCE
AUTHOR SYMBOL PRESSURE PSIG TEMPERATURE °F
DAY ● 685 100
DAY ▲ 1000 100

FIGURE A 4

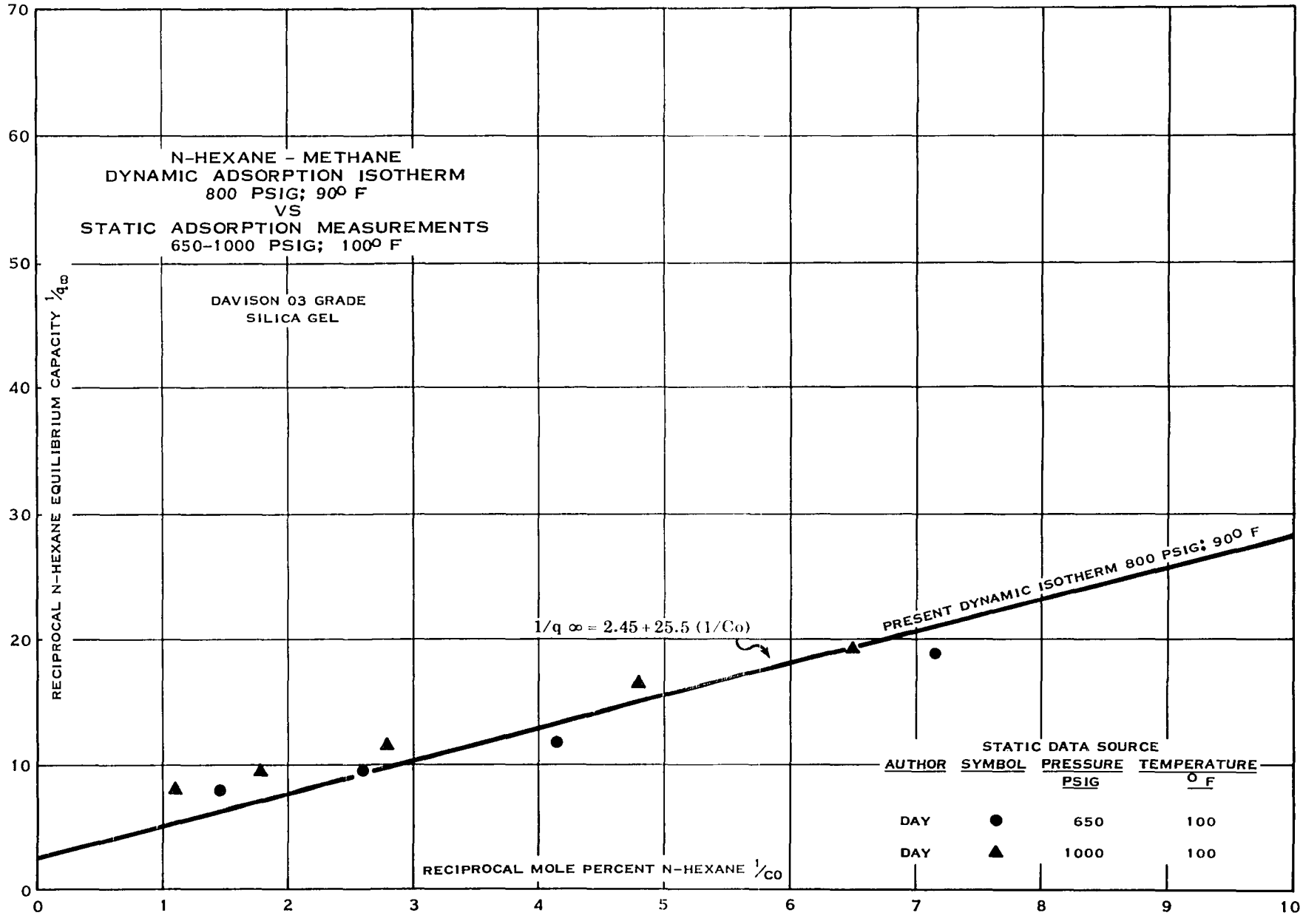
N-HEXANE - METHANE
DYNAMIC ADSORPTION ISOTHERM
800 PSIG; 90° F
VS
STATIC ADSORPTION MEASUREMENTS
650-1000 PSIG; 100° F
DAVISON 03 GRADE
SILICA GEL
RECIPROCAL N-HEXANE EQUILIBRIUM CAPACITY 1/qe
RECIPROCAL MOLE PERCENT N-HEXANE 1/Co
1/q ∞ = 2.45 + 25.5 (1/Co)
PRESENT DYNAMIC ISOTHERM 800 PSIG; 90° F
STATIC DATA SOURCE
AUTHOR SYMBOL PRESSURE PSIG TEMPERATURE °F
DAY ● 650 100
DAY ▲ 1000 100
0 10 20 30 40 50 60 70
0 1 2 3 4 5 6 7 8 9 10

FIGURE A 5

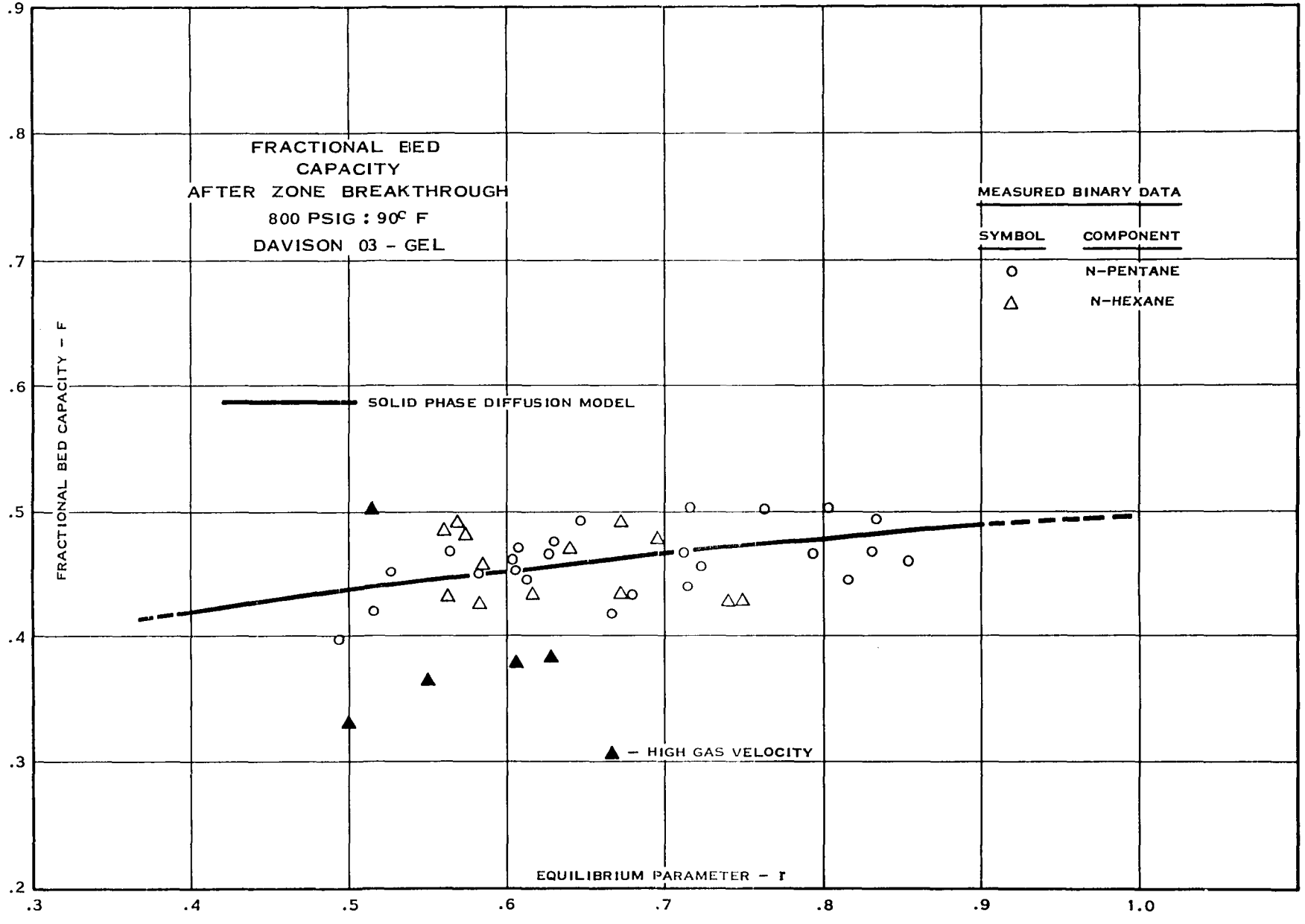
FRACTIONAL BED CAPACITY
AFTER ZONE BREAKTHROUGH
800 PSIG : 90° F
DAVISON 03 - GEL
MEASURED BINARY DATA
SYMBOL
COMPONENT
N-PENTANE
N-HEXANE
SOLID PHASE DIFFUSION MODEL
▲ – HIGH GAS VELOCITY
FRACTIONAL BED CAPACITY – F
EQUILIBRIUM PARAMETER – r
.9
.8
.7
.6
.5
.4
.3
.2
.3
.4
.5
.6
.7
.8
.9
1.0

FIGURE A 6

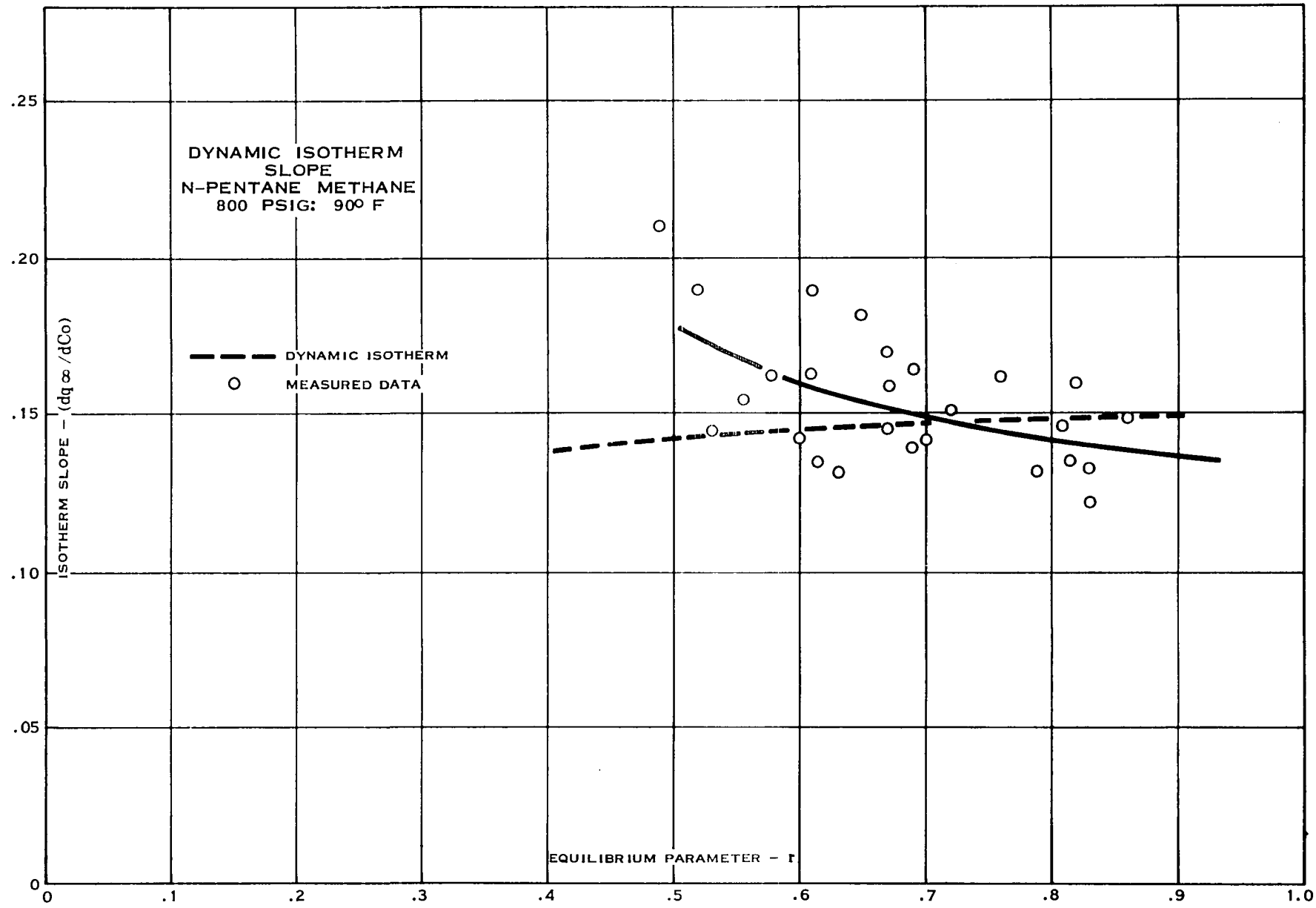
DYNAMIC ISOTHERM
SLOPE
N-PENTANE METHANE
800 PSIG: 90° F
DYNAMIC ISOTHERM
MEASURED DATA
ISOTHERM SLOPE – (dq∞/dCo)
EQUILIBRIUM PARAMETER – r
0
.05
.10
.15
.20
.25
0
.1
.2
.3
.4
.5
.6
.7
.8
.9
1.0

FIGURE A 7

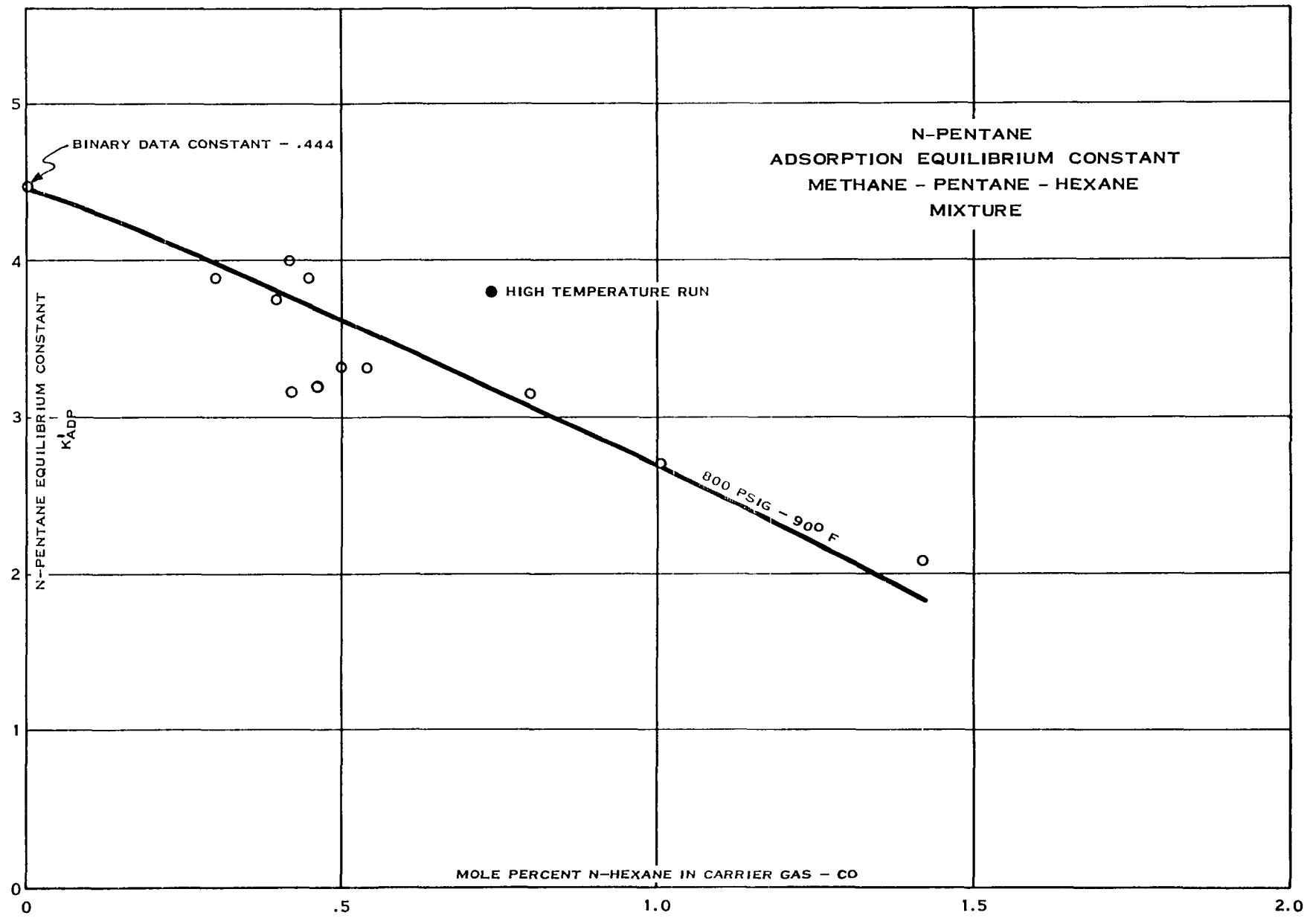
N-PENTANE
ADSORPTION EQUILIBRIUM CONSTANT
METHANE - PENTANE - HEXANE
MIXTURE
BINARY DATA CONSTANT - .444
HIGH TEMPERATURE RUN
800 PSIG - 900 F
N-PENTANE EQUILIBRIUM CONSTANT
K'_{ADP}
MOLE PERCENT N-HEXANE IN CARRIER GAS - CO
0
1
2
3
4
5
0
.5
1.0
1.5
2.0

FIGURE A 8

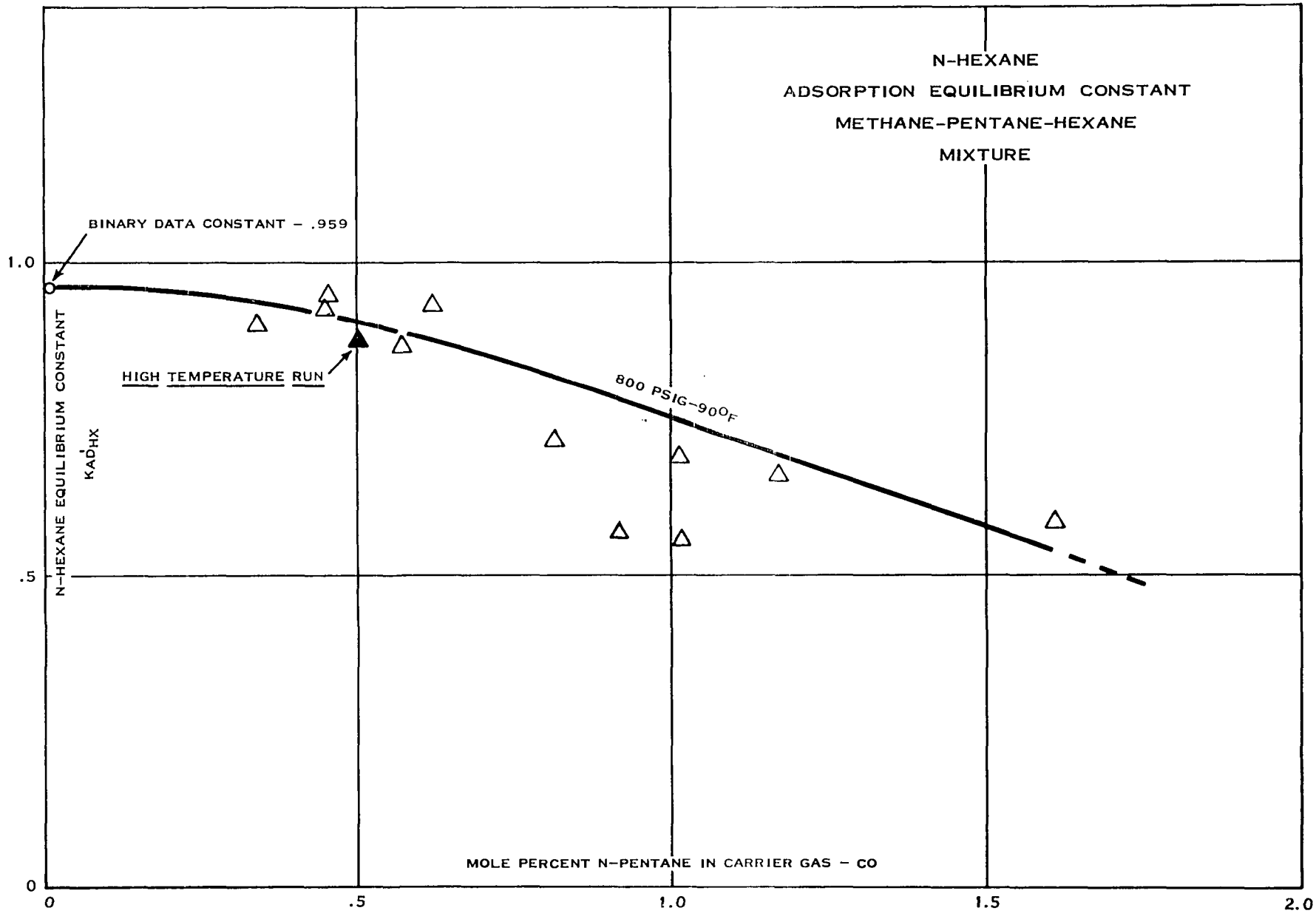
N-HEXANE
ADSORPTION EQUILIBRIUM CONSTANT
METHANE-PENTANE-HEXANE
MIXTURE
BINARY DATA CONSTANT - .959
HIGH TEMPERATURE RUN
800 PSIG-90°F
N-HEXANE EQUILIBRIUM CONSTANT
K'ADHX
1.0
.5
0
0
.5
1.0
1.5
2.0
MOLE PERCENT N-PENTANE IN CARRIER GAS - CO

FIGURE A 9

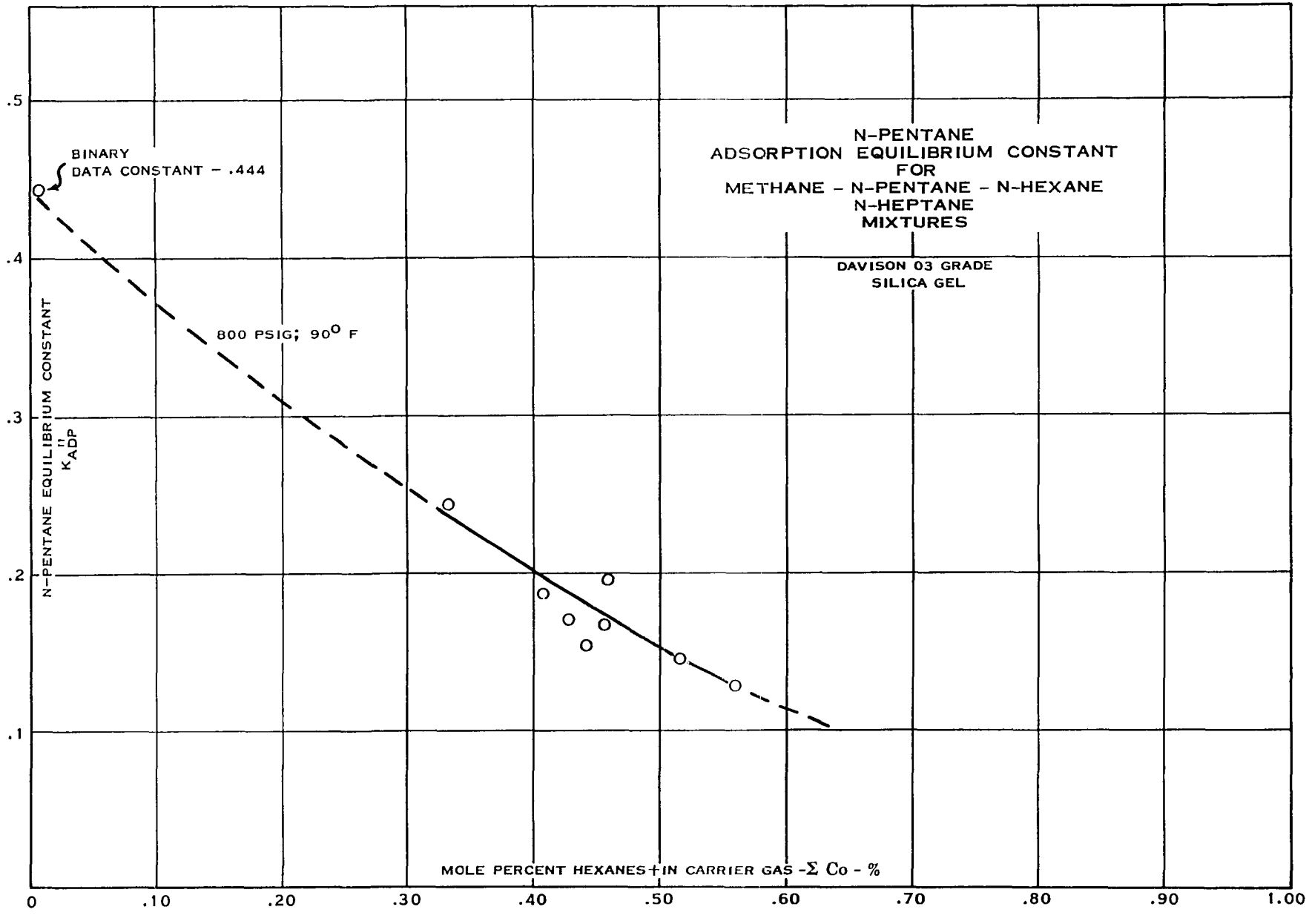
N-PENTANE
ADSORPTION EQUILIBRIUM CONSTANT
FOR
METHANE - N-PENTANE - N-HEXANE
N-HEPTANE
MIXTURES
DAVISON 03 GRADE
SILICA GEL
BINARY
DATA CONSTANT - .444
800 PSIG; 90° F
N-PENTANE EQUILIBRIUM CONSTANT
K''_{ADP}
MOLE PERCENT HEXANES+IN CARRIER GAS -Σ Co - %
.5
.4
.3
.2
.1
0
.10
.20
.30
.40
.50
.60
.70
.80
.90
1.00

FIGURE A 10

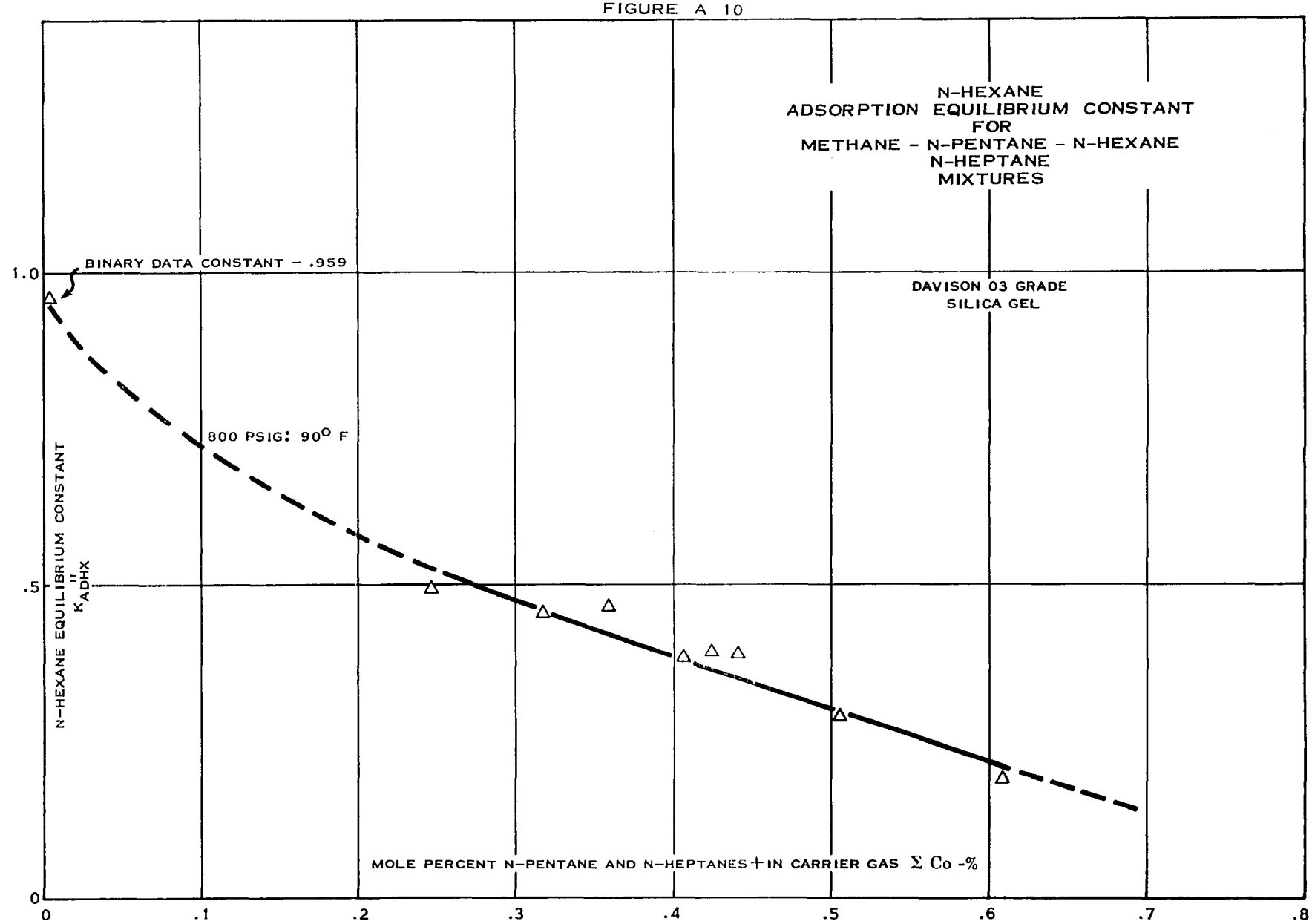
N-HEXANE
ADSORPTION EQUILIBRIUM CONSTANT
FOR
METHANE - N-PENTANE - N-HEXANE
N-HEPTANE
MIXTURES
BINARY DATA CONSTANT - .959
DAVISON 03 GRADE
SILICA GEL
800 PSIG: 90° F
N-HEXANE EQUILIBRIUM CONSTANT
K''ADHX
1.0
.5
0
0
.1
.2
.3
.4
.5
.6
.7
.8
MOLE PERCENT N-PENTANE AND N-HEPTANES + IN CARRIER GAS Σ Co -%

FIGURE A 11

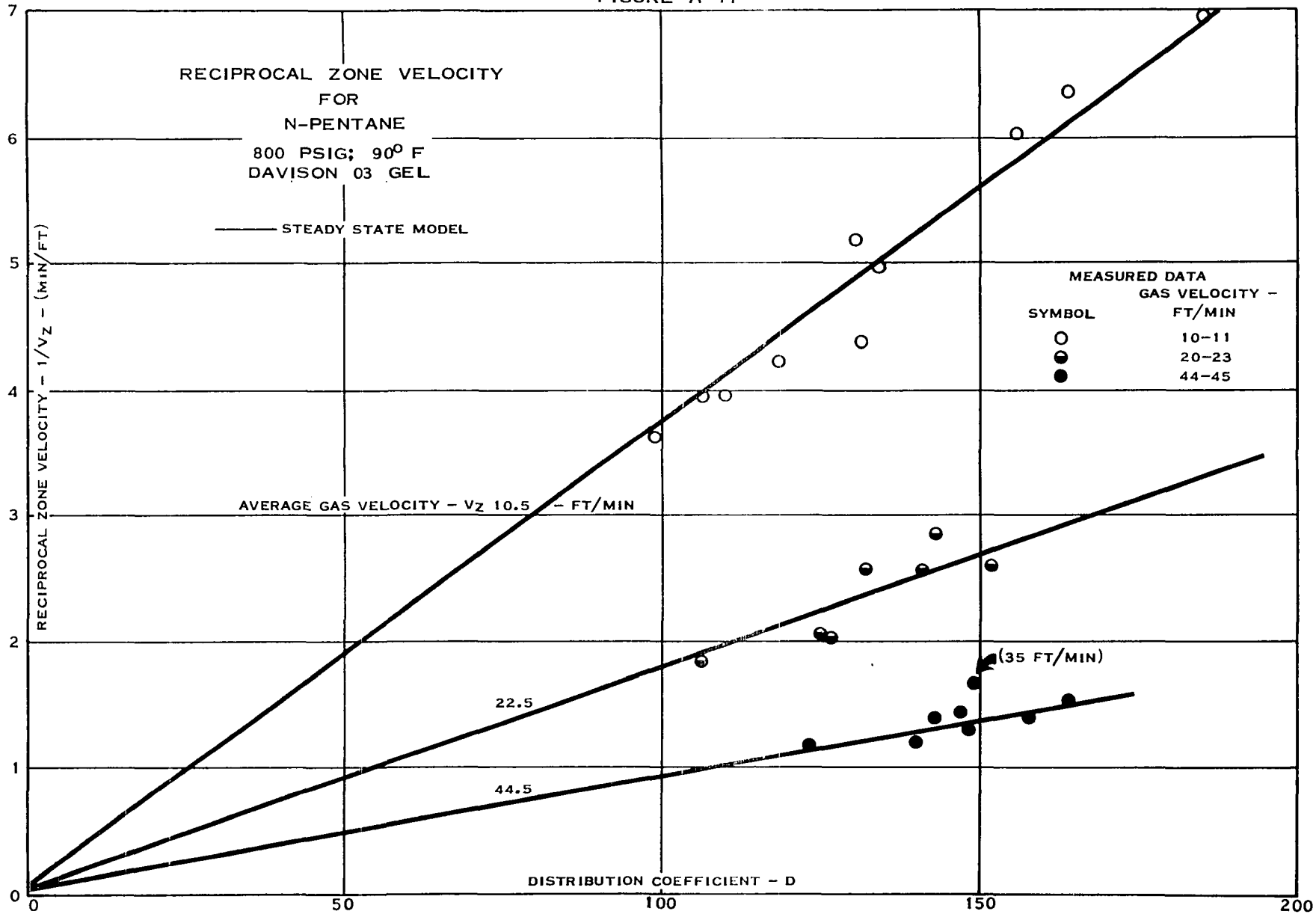
RECIPROCAL ZONE VELOCITY
FOR
N-PENTANE
800 PSIG; 90° F
DAVISON 03 GEL
STEADY STATE MODEL
MEASURED DATA
SYMBOL
GAS VELOCITY - FT/MIN
10-11
20-23
44-45
RECIPROCAL ZONE VELOCITY - 1/Vz - (MIN/FT)
AVERAGE GAS VELOCITY - Vz 10.5 - FT/MIN
22.5
44.5
(35 FT/MIN)
DISTRIBUTION COEFFICIENT - D
0
1
2
3
4
5
6
7
0
50
100
150
200

FIGURE A 12

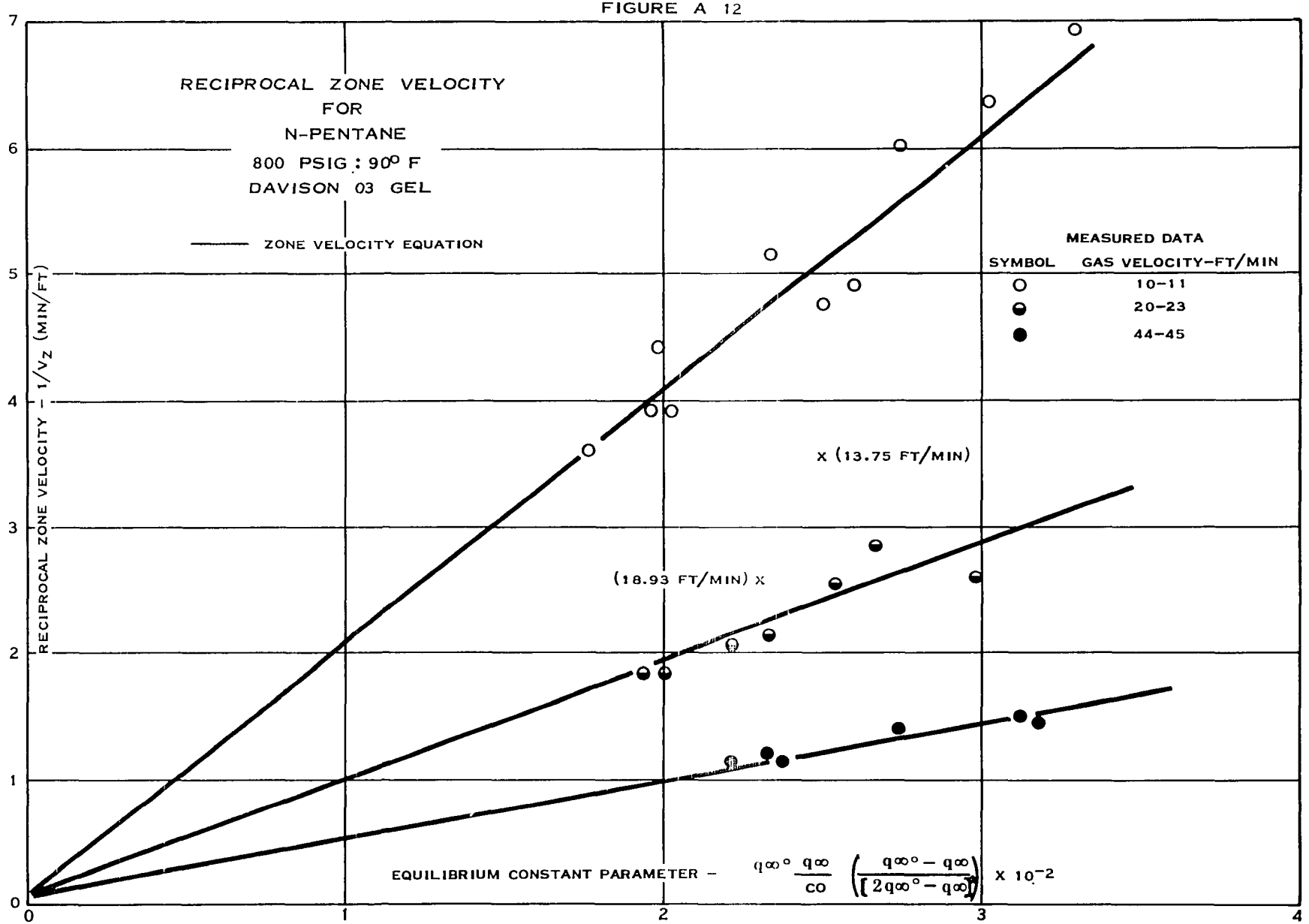
RECIPROCAL ZONE VELOCITY
FOR
N-PENTANE
800 PSIG : 90° F
DAVISON 03 GEL
ZONE VELOCITY EQUATION
MEASURED DATA
SYMBOL GAS VELOCITY-FT/MIN
10-11
20-23
44-45
X (13.75 FT/MIN)
(18.93 FT/MIN) X
RECIPROCAL ZONE VELOCITY - 1/Vz (MIN/FT)
EQUILIBRIUM CONSTANT PARAMETER - $q_{\infty}^{\circ}\frac{q_{\infty}}{co}\left(\frac{q_{\infty}^{\circ}-q_{\infty}}{[2q_{\infty}^{\circ}-q_{\infty}]}\right)^{2}$ X 10^{-2}
0
1
2
3
4
5
6
7

FIGURE A 13

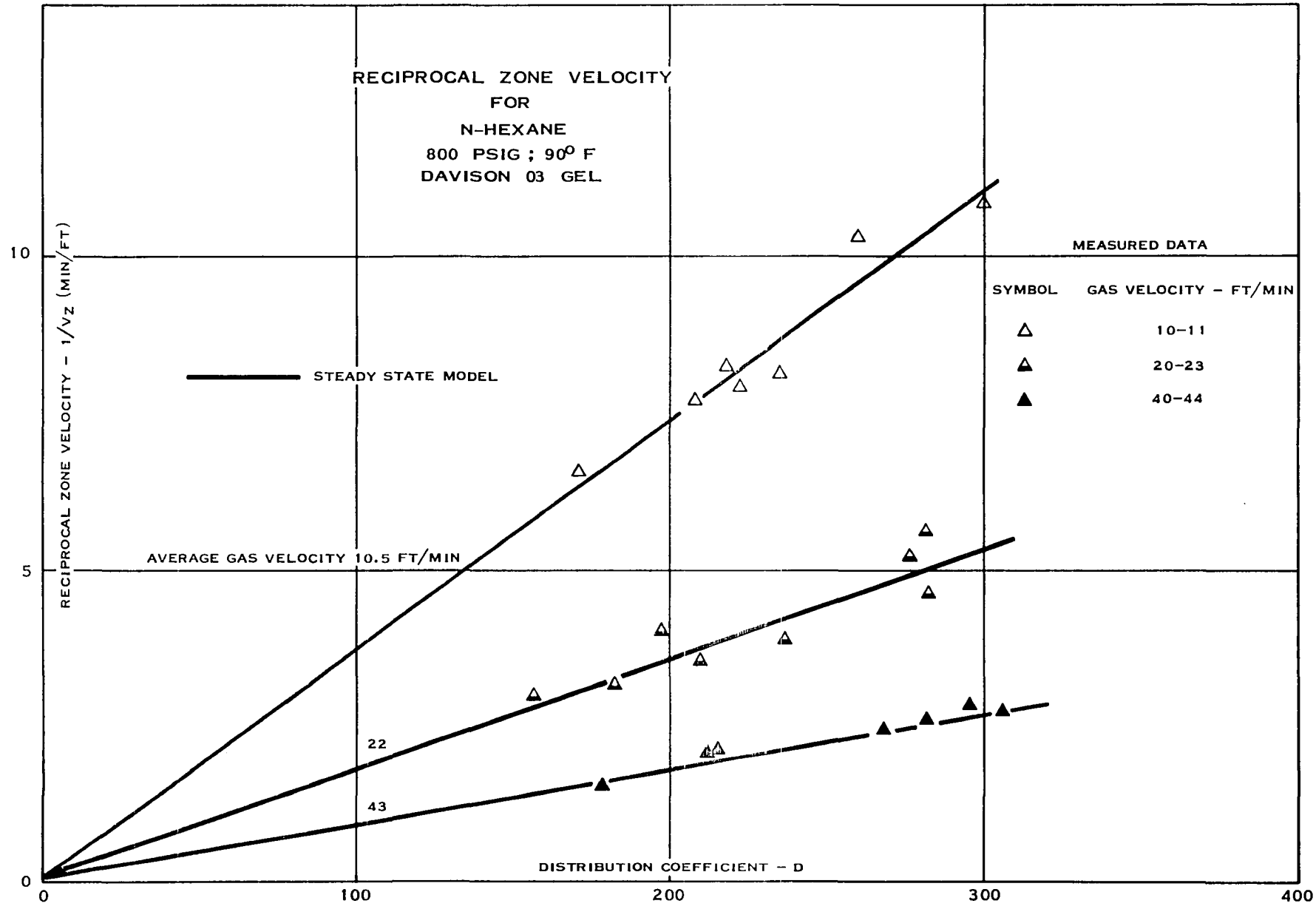
RECIPROCAL ZONE VELOCITY
FOR
N-HEXANE
800 PSIG ; 90° F
DAVISON 03 GEL
MEASURED DATA
SYMBOL
GAS VELOCITY - FT/MIN
10-11
20-23
40-44
STEADY STATE MODEL
AVERAGE GAS VELOCITY 10.5 FT/MIN
22
43
RECIPROCAL ZONE VELOCITY - 1/Vz (MIN/FT)
DISTRIBUTION COEFFICIENT - D
0
5
10
0
100
200
300
400

FIGURE A 14

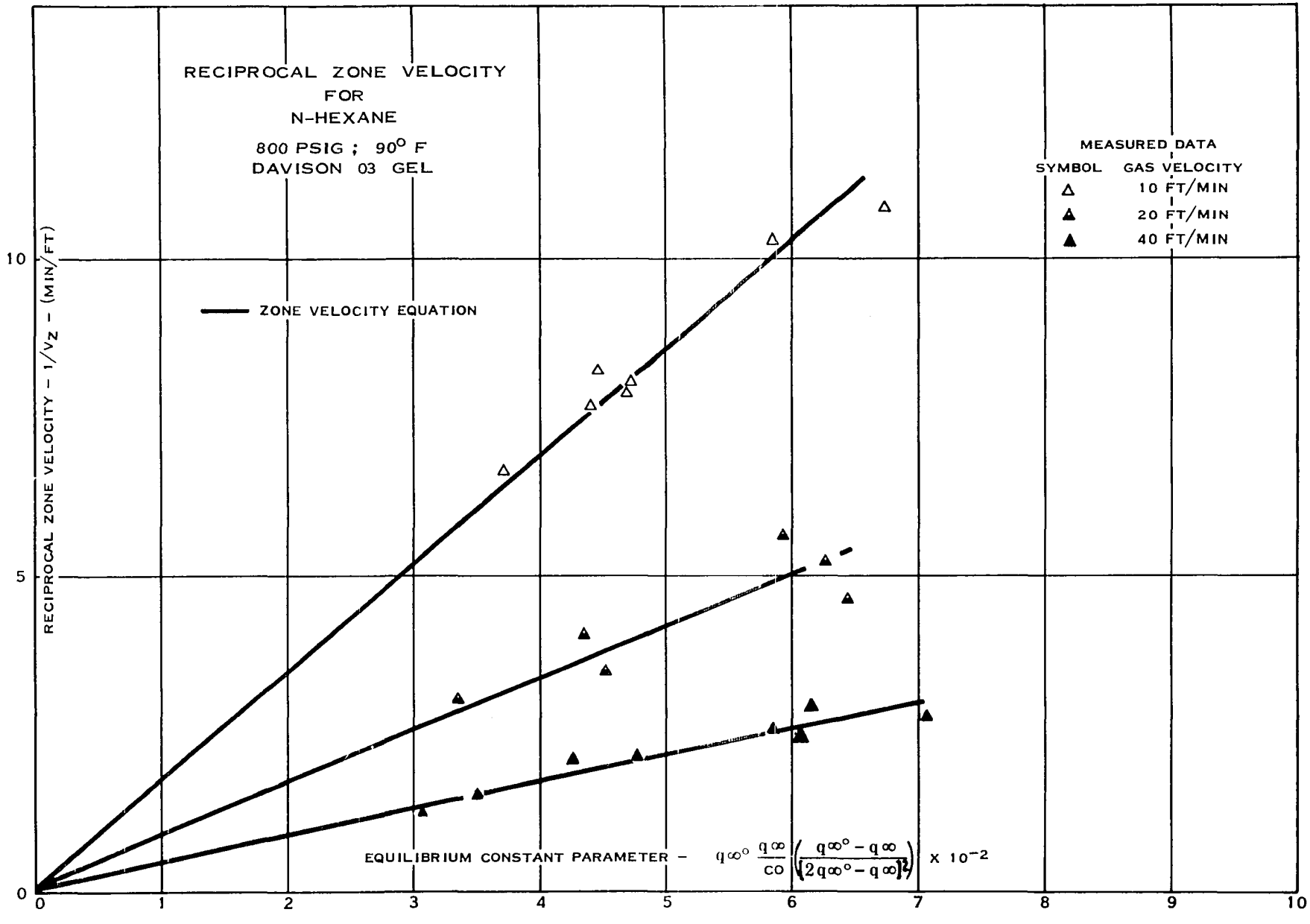
RECIPROCAL ZONE VELOCITY
FOR
N-HEXANE
800 PSIG ; 90° F
DAVISON 03 GEL
MEASURED DATA
SYMBOL GAS VELOCITY
10 FT/MIN
20 FT/MIN
40 FT/MIN
ZONE VELOCITY EQUATION
RECIPROCAL ZONE VELOCITY - 1/Vz - (MIN/FT)
EQUILIBRIUM CONSTANT PARAMETER - $q\infty^{\circ}\frac{q\infty}{CO}\left(\frac{q\infty^{\circ}-q\infty}{(2q\infty^{\circ}-q\infty)^2}\right)\times 10^{-2}$
0
5
10
0
1
2
3
4
5
6
7
8
9
10

FIGURE A 15

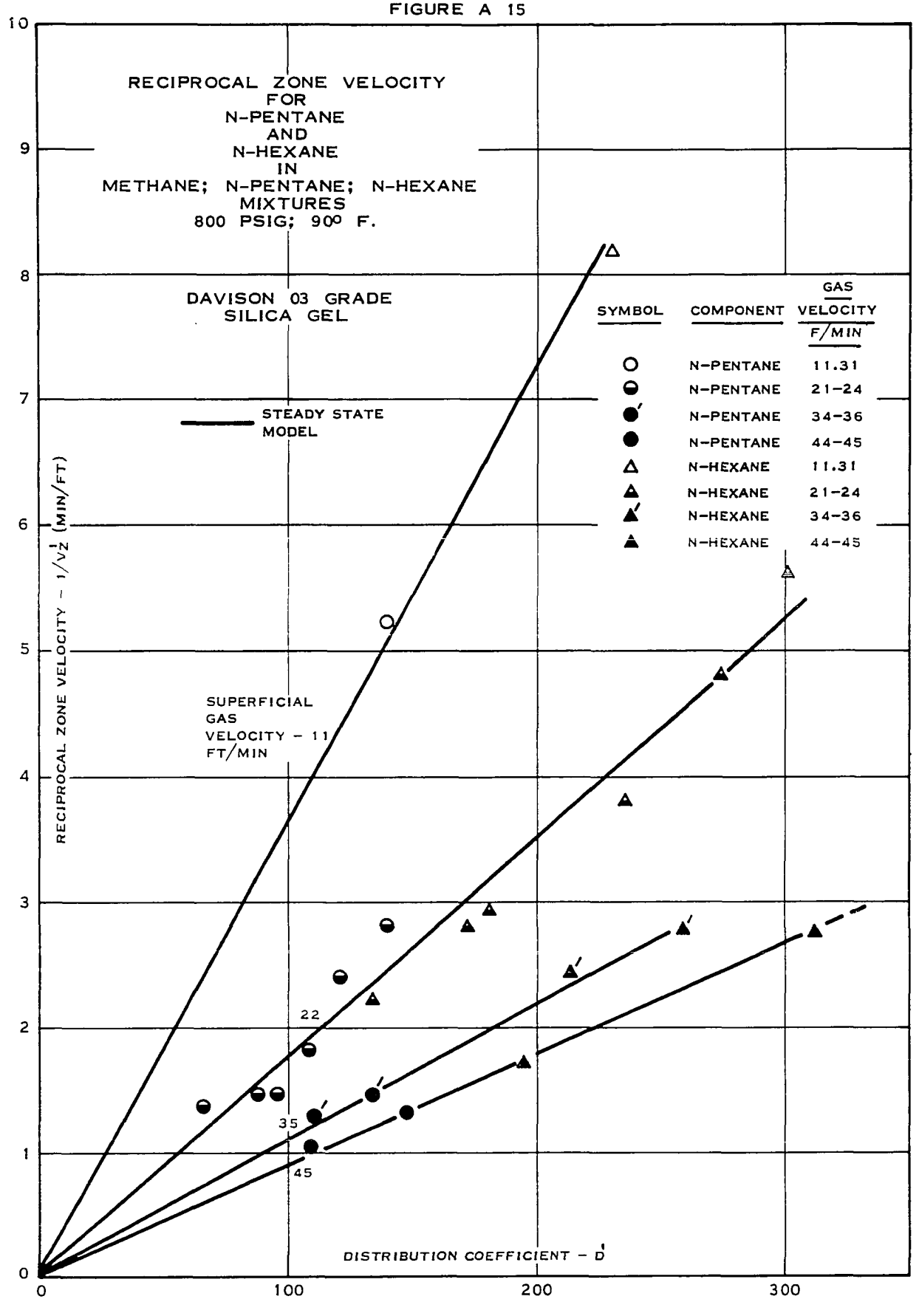
RECIPROCAL ZONE VELOCITY
FOR
N-PENTANE
AND
N-HEXANE
IN
METHANE; N-PENTANE; N-HEXANE
MIXTURES
800 PSIG; 90° F.
DAVISON 03 GRADE
SILICA GEL
STEADY STATE
MODEL
SYMBOL
COMPONENT
GAS VELOCITY F/MIN
N-PENTANE 11.31
N-PENTANE 21-24
N-PENTANE 34-36
N-PENTANE 44-45
N-HEXANE 11.31
N-HEXANE 21-24
N-HEXANE 34-36
N-HEXANE 44-45
SUPERFICIAL
GAS
VELOCITY - 11
FT/MIN
22
35
45
RECIPROCAL ZONE VELOCITY - $1/v_z^1$ (MIN/FT)
DISTRIBUTION COEFFICIENT - D^1
0
1
2
3
4
5
6
7
8
9
10
0
100
200
300

FIGURE A 16

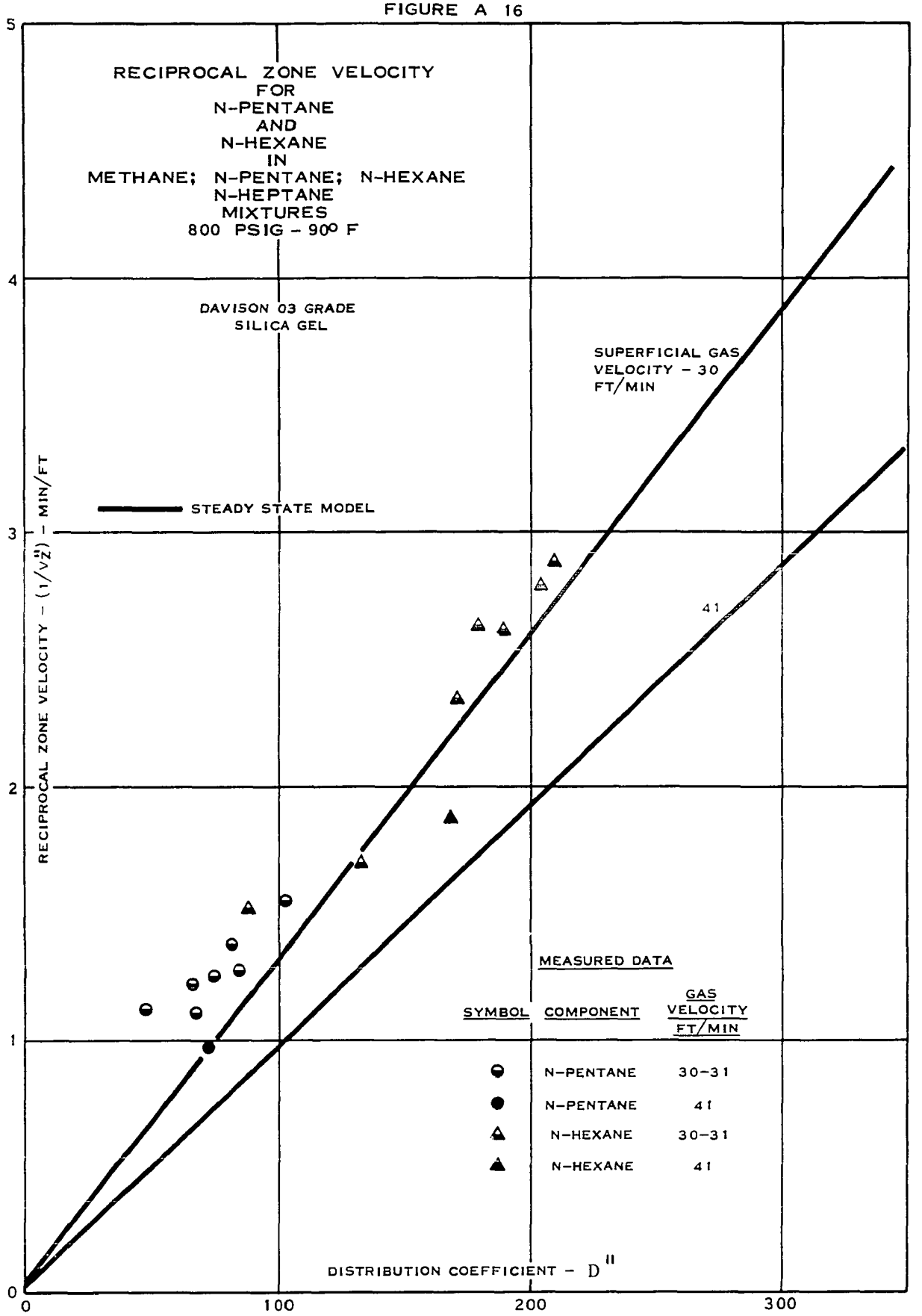
RECIPROCAL ZONE VELOCITY
FOR
N-PENTANE
AND
N-HEXANE
IN
METHANE; N-PENTANE; N-HEXANE
N-HEPTANE
MIXTURES
800 PSIG - 90° F
DAVISON 03 GRADE
SILICA GEL
SUPERFICIAL GAS
VELOCITY - 30
FT/MIN
STEADY STATE MODEL
41
RECIPROCAL ZONE VELOCITY - $(1/v_z^{II})$ - MIN/FT
MEASURED DATA
SYMBOL
COMPONENT
GAS VELOCITY FT/MIN
N-PENTANE 30-31
N-PENTANE 41
N-HEXANE 30-31
N-HEXANE 41
DISTRIBUTION COEFFICIENT - D^{II}
0
1
2
3
4
5
0
100
200
300

FIGURE A 17

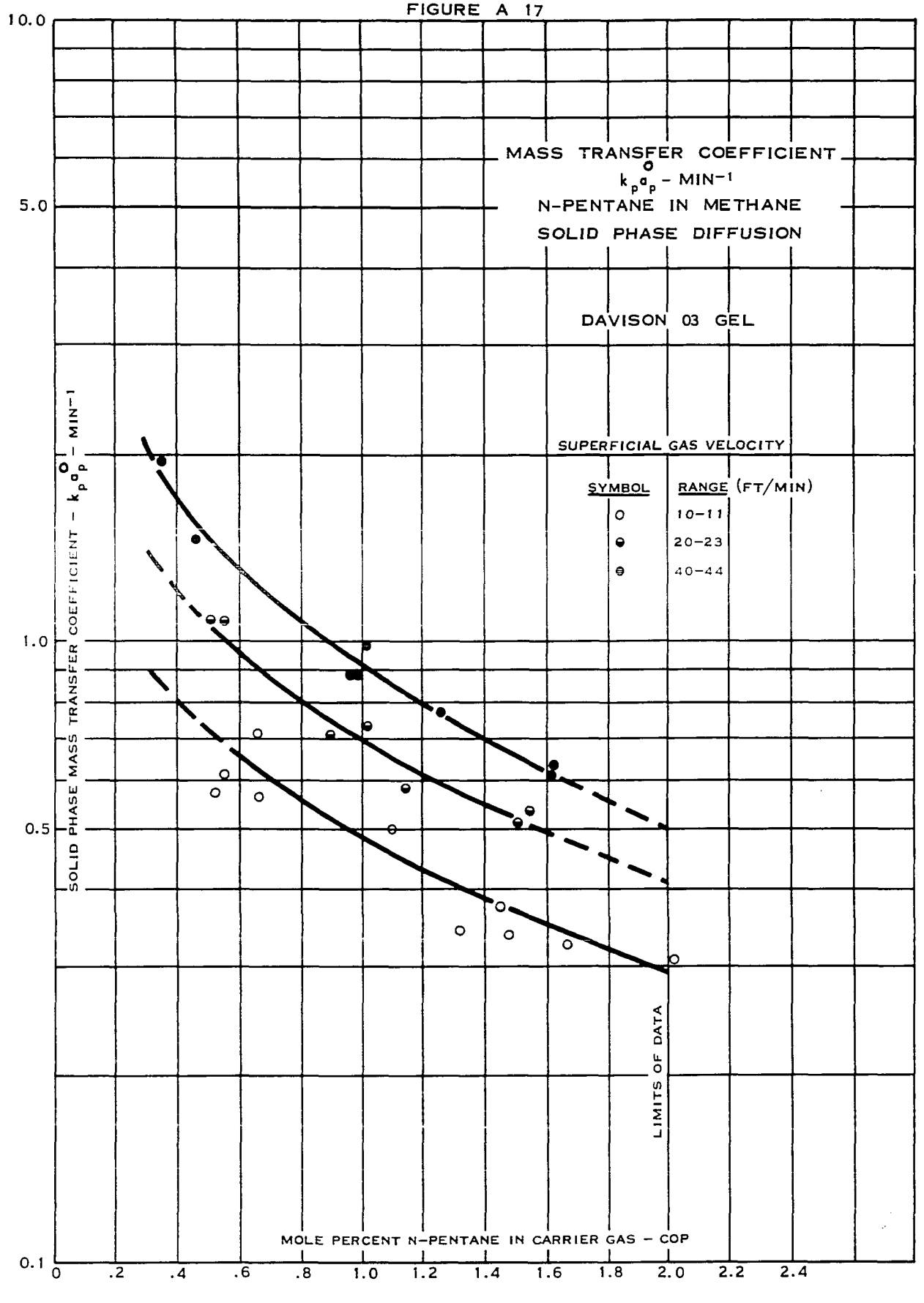
MASS TRANSFER COEFFICIENT
$k_p^o a_p$ - MIN^{-1}
N-PENTANE IN METHANE
SOLID PHASE DIFFUSION
DAVISON 03 GEL
SUPERFICIAL GAS VELOCITY
SYMBOL
RANGE (FT/MIN)
10-11
20-23
40-44
SOLID PHASE MASS TRANSFER COEFFICIENT - $k_p^o a_p$ - MIN^{-1}
LIMITS OF DATA
MOLE PERCENT N-PENTANE IN CARRIER GAS - COP
10.0
5.0
1.0
0.5
0.1
0
.2
.4
.6
.8
1.0
1.2
1.4
1.6
1.8
2.0
2.2
2.4

FIGURE A 18

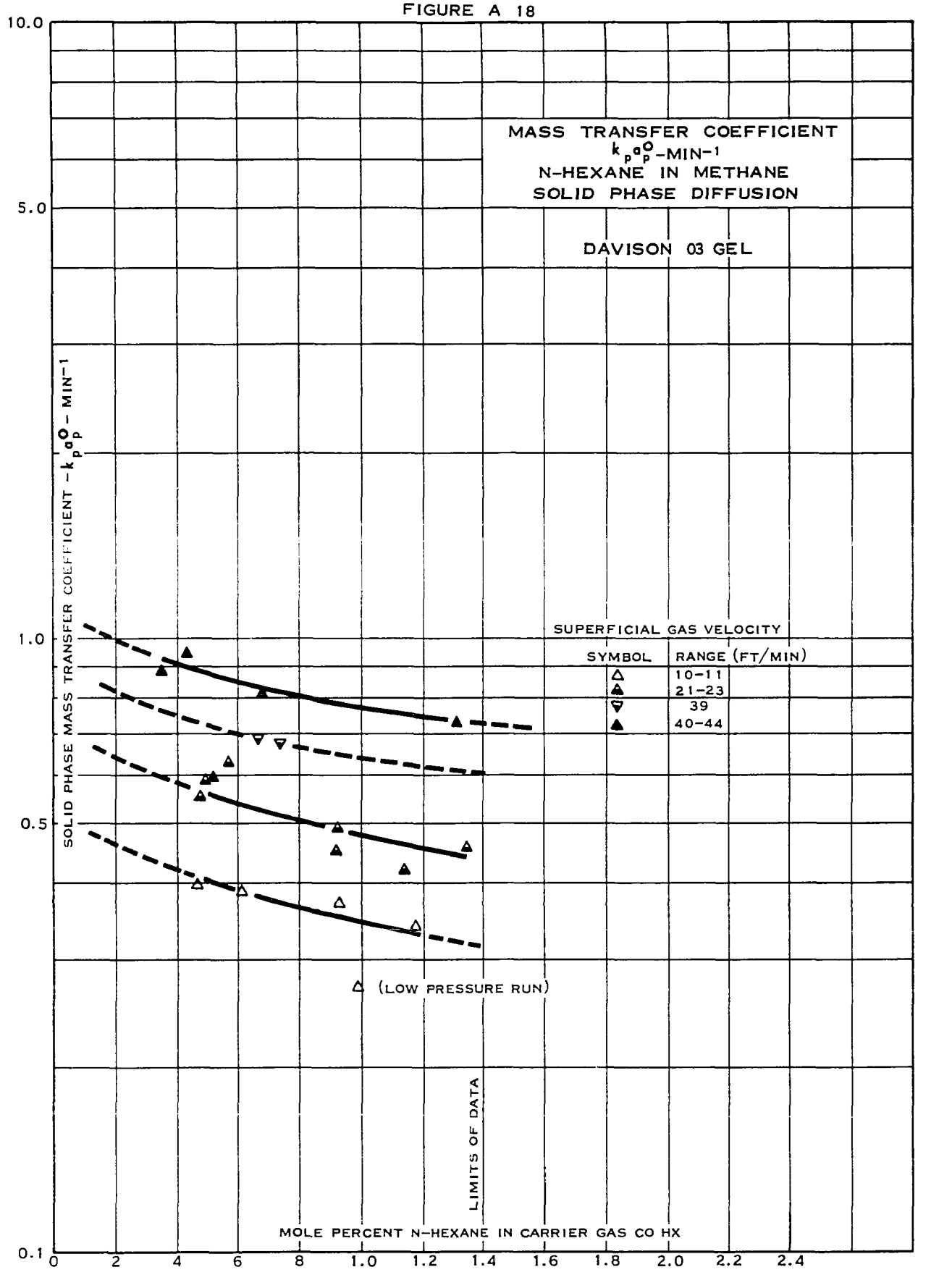
MASS TRANSFER COEFFICIENT
$k_p a_p^o$-MIN^{-1}
N-HEXANE IN METHANE
SOLID PHASE DIFFUSION
DAVISON 03 GEL
SUPERFICIAL GAS VELOCITY
SYMBOL
RANGE (FT/MIN)
10-11
21-23
39
40-44
(LOW PRESSURE RUN)
LIMITS OF DATA
SOLID PHASE MASS TRANSFER COEFFICIENT - $k_p a_p^o$ - MIN^{-1}
MOLE PERCENT N-HEXANE IN CARRIER GAS CO HX
10.0
5.0
1.0
0.5
0.1
0
2
4
6
8
1.0
1.2
1.4
1.6
1.8
2.0
2.2
2.4

FIGURE A 19

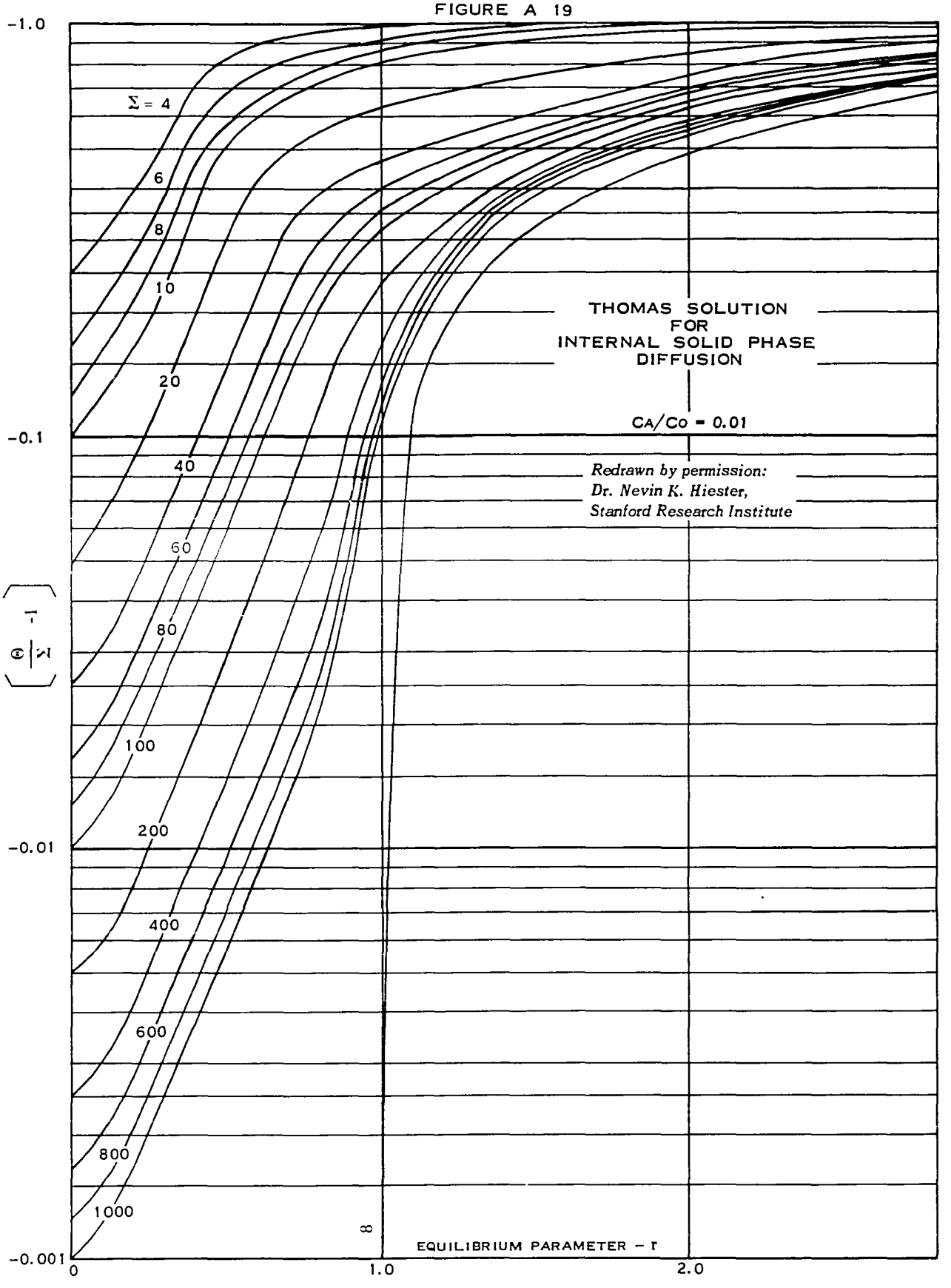
-1.0
-0.1
-0.01
-0.001
Σ = 4
6
8
10
20
40
60
80
100
200
400
600
800
1000
∞
THOMAS SOLUTION
FOR
INTERNAL SOLID PHASE
DIFFUSION
CA/Co = 0.01
Redrawn by permission:
Dr. Nevin K. Hiester,
Stanford Research Institute
EQUILIBRIUM PARAMETER - r
0
1.0
2.0

FIGURE A 20

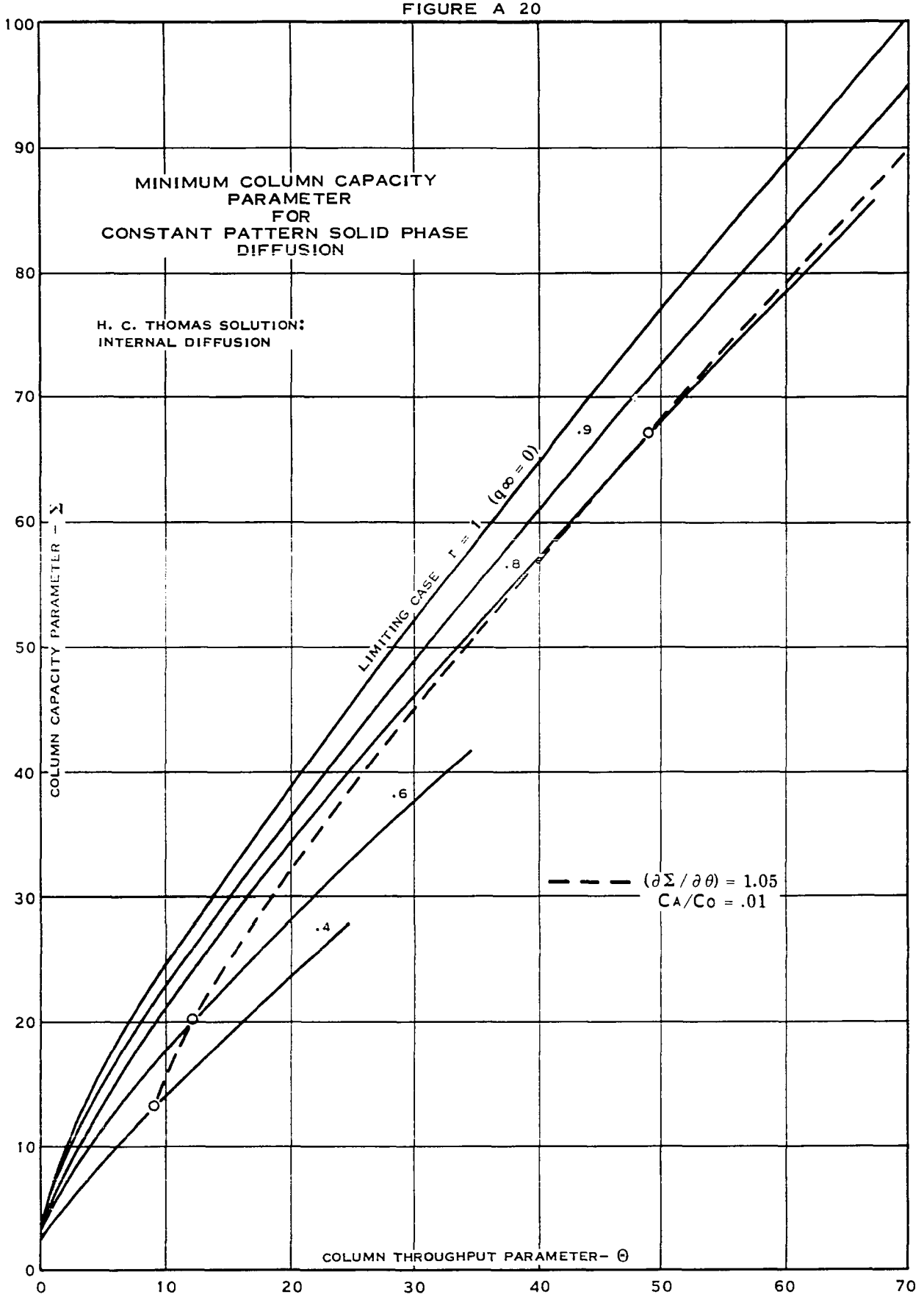
MINIMUM COLUMN CAPACITY PARAMETER FOR CONSTANT PATTERN SOLID PHASE DIFFUSION
H. C. THOMAS SOLUTION: INTERNAL DIFFUSION
LIMITING CASE r = 1, (q∞ = 0)
.9
.8
.6
.4
(∂Σ / ∂θ) = 1.05
CA/Co = .01
COLUMN CAPACITY PARAMETER - Σ
COLUMN THROUGHPUT PARAMETER- Θ
0
10
20
30
40
50
60
70
80
90
100

FIGURE A 21

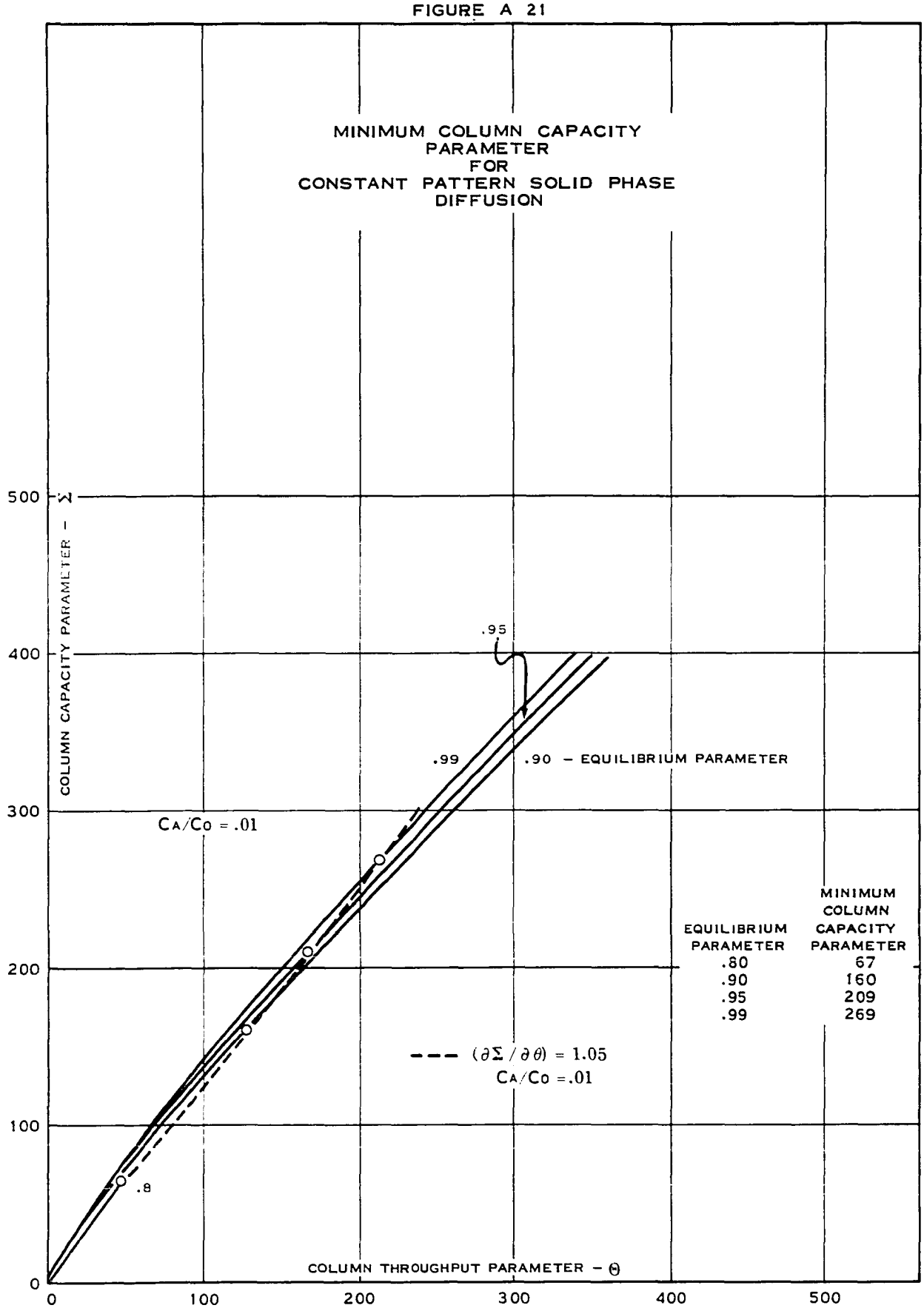
MINIMUM COLUMN CAPACITY PARAMETER FOR CONSTANT PATTERN SOLID PHASE DIFFUSION
COLUMN CAPACITY PARAMETER - Σ
COLUMN THROUGHPUT PARAMETER - Θ
0
100
200
300
400
500
.95
.99
.90 - EQUILIBRIUM PARAMETER
.8
CA/Co = .01
EQUILIBRIUM PARAMETER
MINIMUM COLUMN CAPACITY PARAMETER
.80 67
.90 160
.95 209
.99 269
(∂Σ / ∂θ) = 1.05
CA/Co = .01

FIGURE A 21-A

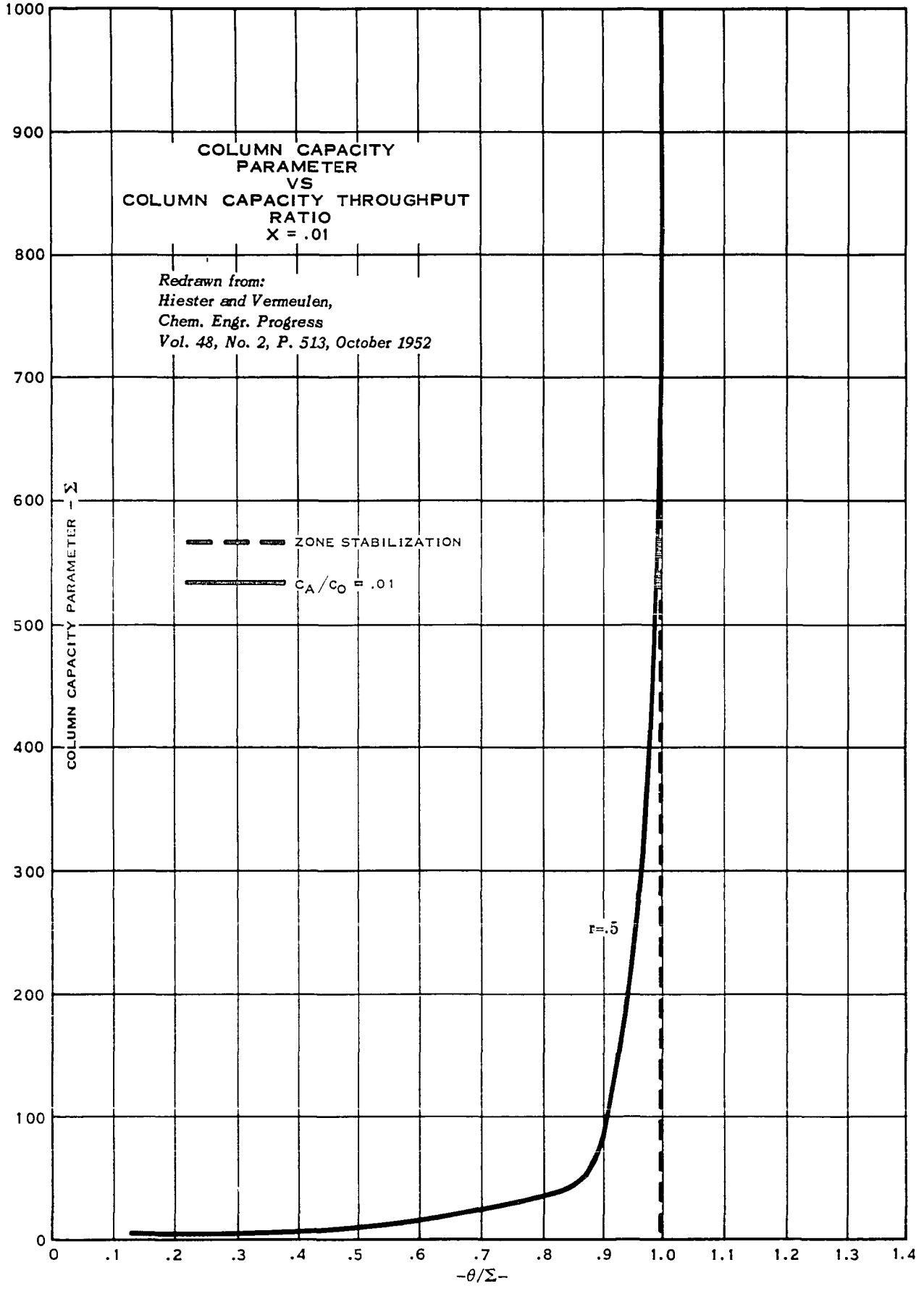
COLUMN CAPACITY
PARAMETER
VS
COLUMN CAPACITY THROUGHPUT
RATIO
X = .01
Redrawn from:
Hiester and Vermeulen,
Chem. Engr. Progress
Vol. 48, No. 2, P. 513, October 1952
ZONE STABILIZATION
C_A/C_O = .01
r=.5
COLUMN CAPACITY PARAMETER - Σ
-θ/Σ-
1000
900
800
700
600
500
400
300
200
100
0
0
.1
.2
.3
.4
.5
.6
.7
.8
.9
1.0
1.1
1.2
1.3
1.4

FIGURE A 22

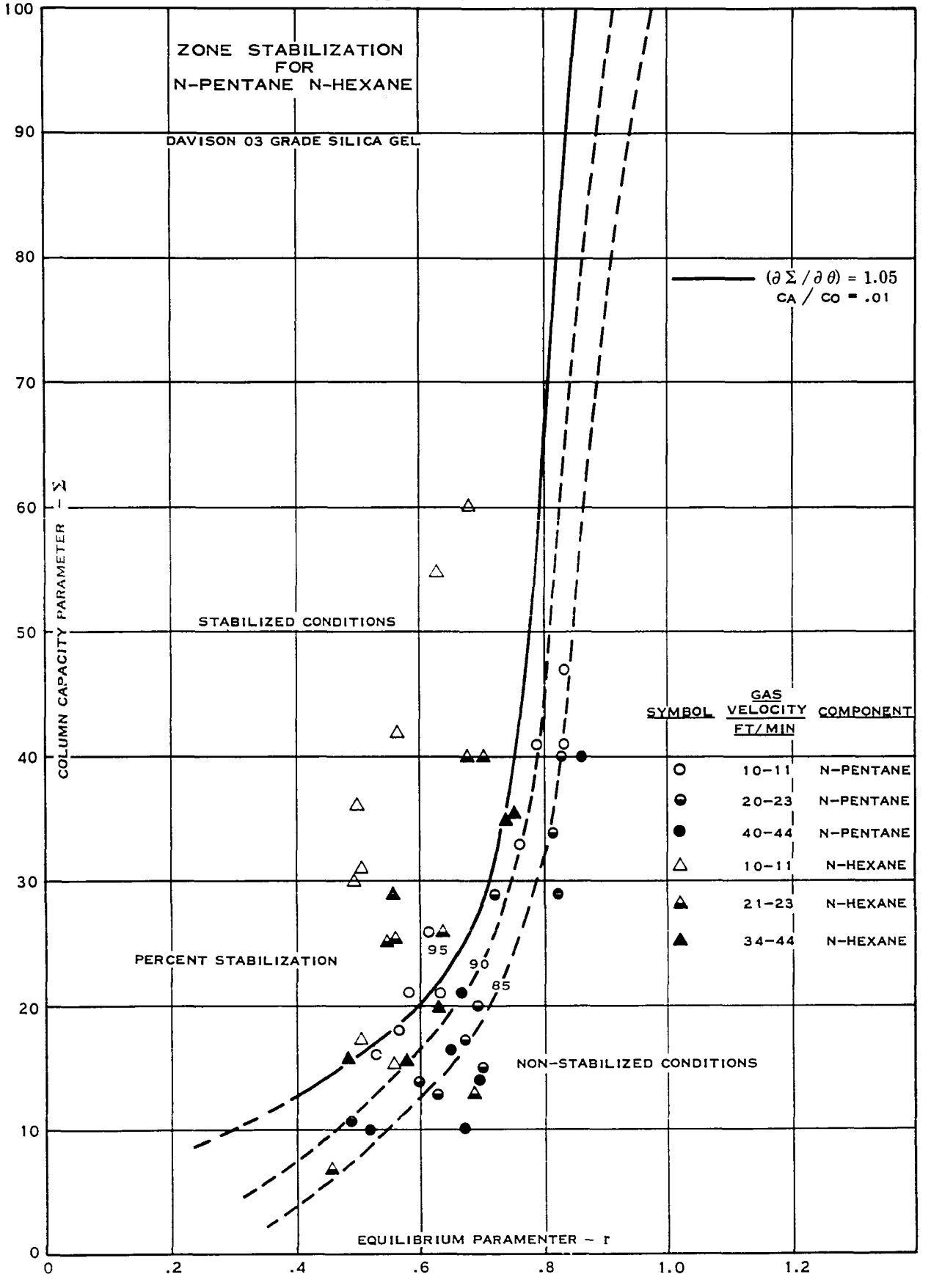
ZONE STABILIZATION
FOR
N-PENTANE N-HEXANE
DAVISON 03 GRADE SILICA GEL
$(\partial \Sigma / \partial \theta) = 1.05$
CA / CO = .01
STABILIZED CONDITIONS
NON-STABILIZED CONDITIONS
PERCENT STABILIZATION
95
90
85
SYMBOL
GAS VELOCITY FT/MIN
COMPONENT
10-11 N-PENTANE
20-23 N-PENTANE
40-44 N-PENTANE
10-11 N-HEXANE
21-23 N-HEXANE
34-44 N-HEXANE
COLUMN CAPACITY PARAMETER - Σ
EQUILIBRIUM PARAMENTER - r
0
10
20
30
40
50
60
70
80
90
100
.2
.4
.6
.8
1.0
1.2

FIGURE A 23

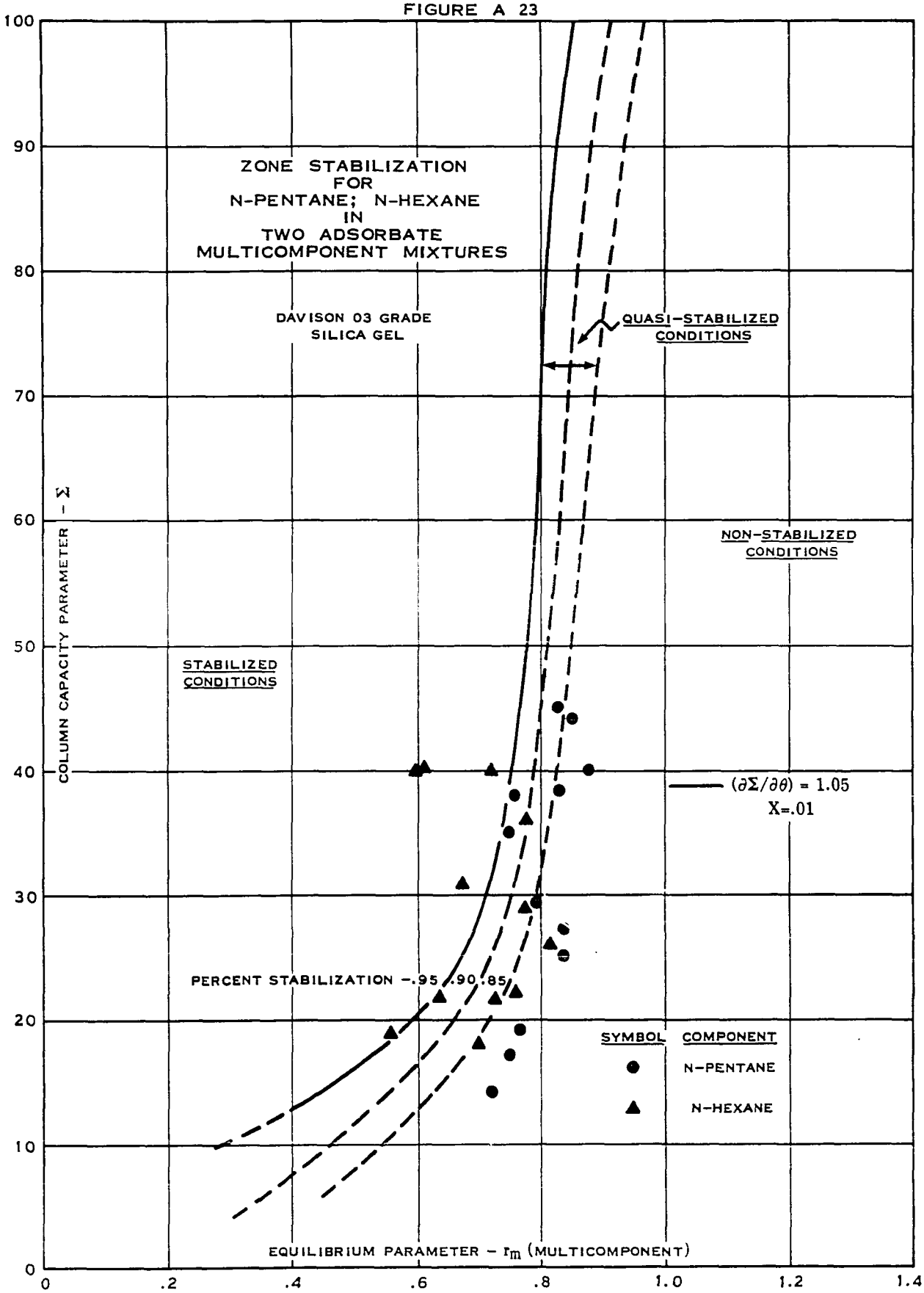
ZONE STABILIZATION
FOR
N-PENTANE; N-HEXANE
IN
TWO ADSORBATE
MULTICOMPONENT MIXTURES
DAVISON 03 GRADE
SILICA GEL
QUASI-STABILIZED
CONDITIONS
NON-STABILIZED
CONDITIONS
STABILIZED
CONDITIONS
(∂Σ/∂θ) = 1.05
X=.01
PERCENT STABILIZATION -.95 .90 .85
SYMBOL COMPONENT
N-PENTANE
N-HEXANE
COLUMN CAPACITY PARAMETER - Σ
EQUILIBRIUM PARAMETER - rm (MULTICOMPONENT)
0
10
20
30
40
50
60
70
80
90
100
0
.2
.4
.6
.8
1.0
1.2
1.4

FIGURE A 24

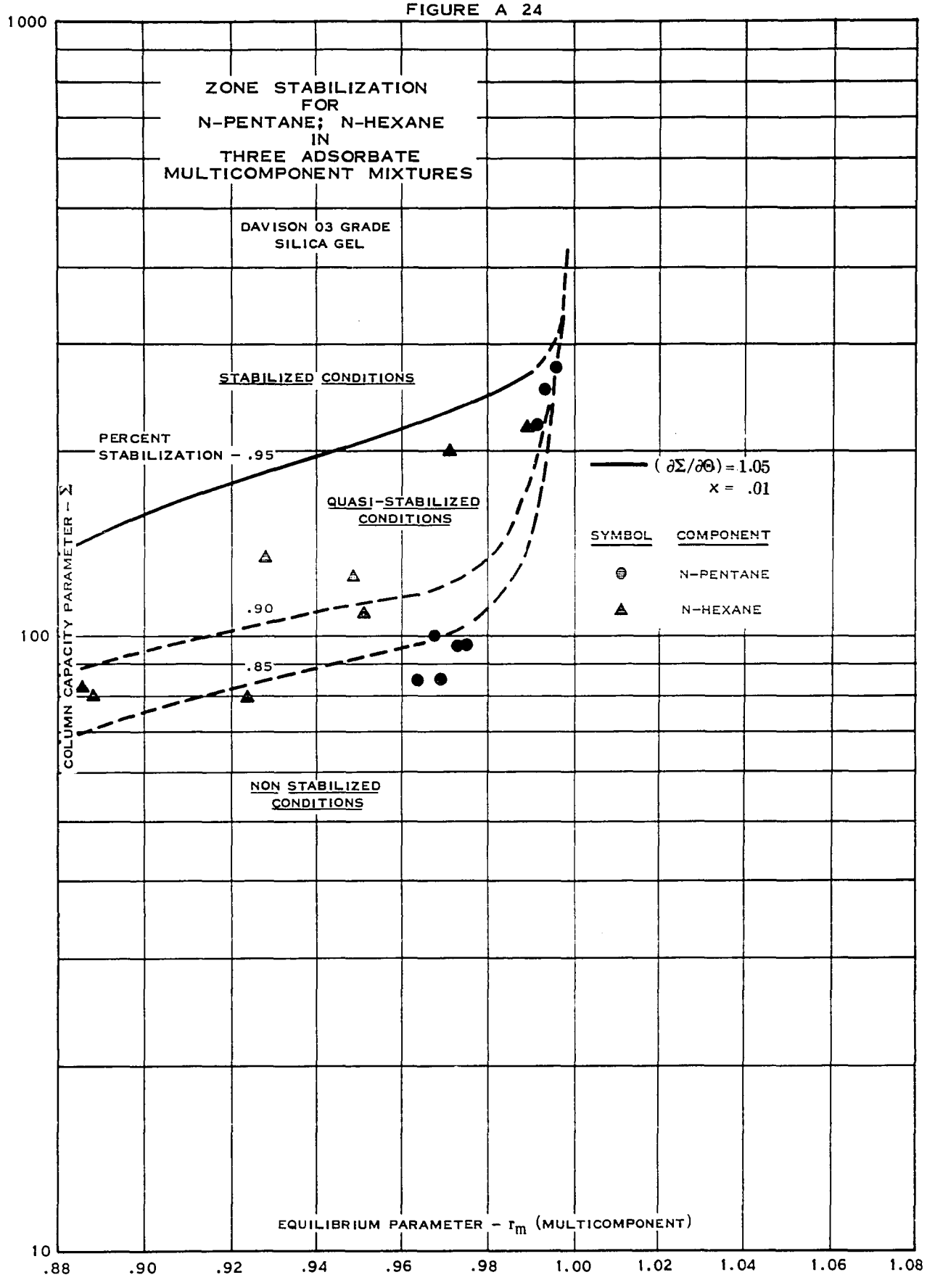
ZONE STABILIZATION
FOR
N-PENTANE; N-HEXANE
IN
THREE ADSORBATE
MULTICOMPONENT MIXTURES
DAVISON 03 GRADE
SILICA GEL
STABILIZED CONDITIONS
PERCENT
STABILIZATION - .95
QUASI-STABILIZED
CONDITIONS
.90
.85
NON STABILIZED
CONDITIONS
(∂Σ/∂Θ) = 1.05
x = .01
SYMBOL
COMPONENT
N-PENTANE
N-HEXANE
COLUMN CAPACITY PARAMETER - Σ
EQUILIBRIUM PARAMETER - r_m (MULTICOMPONENT)
1000
100
10
.88
.90
.92
.94
.96
.98
1.00
1.02
1.04
1.06
1.08

FIGURE A 25

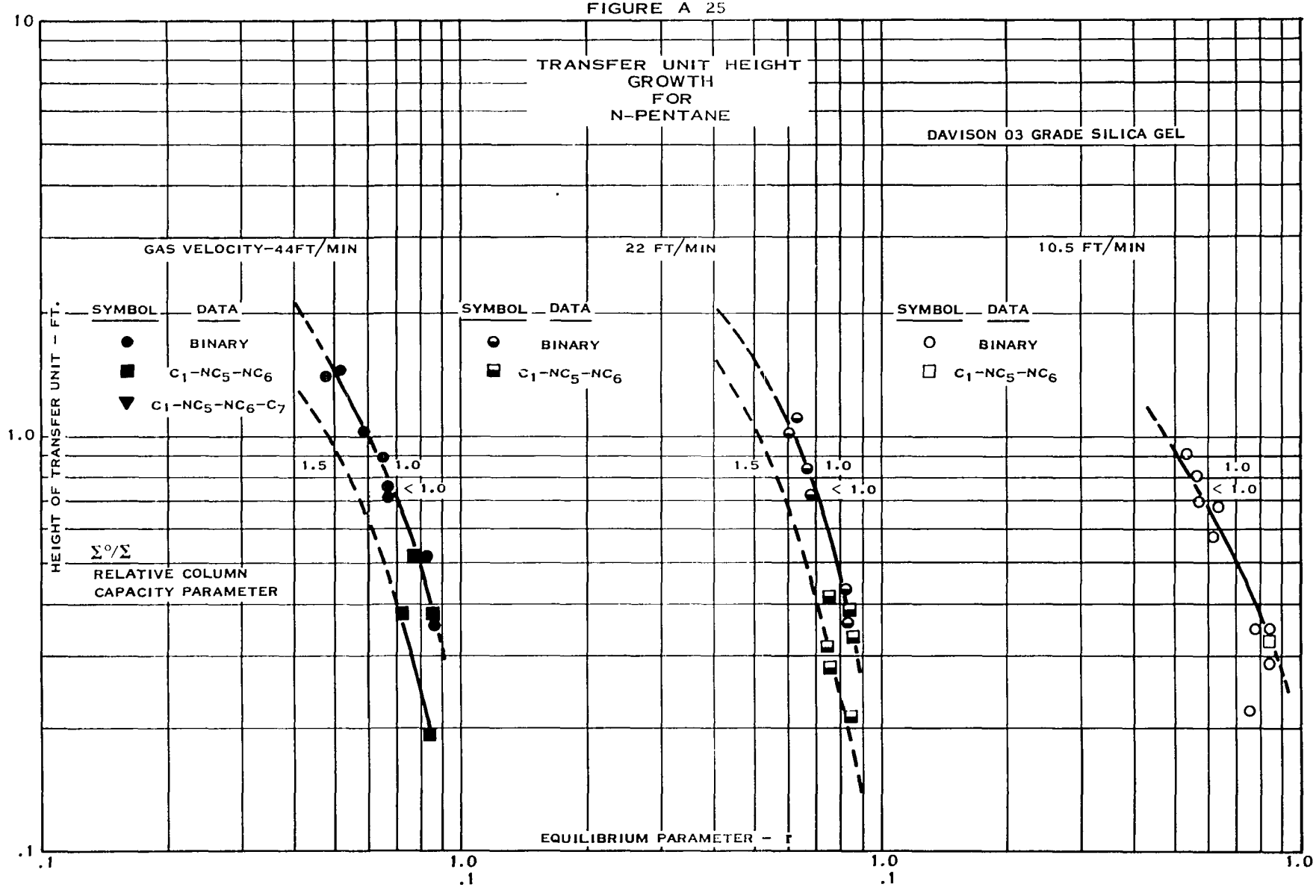
TRANSFER UNIT HEIGHT GROWTH FOR N-PENTANE
DAVISON 03 GRADE SILICA GEL
GAS VELOCITY-44FT/MIN
22 FT/MIN
10.5 FT/MIN
SYMBOL DATA
BINARY
C1-NC5-NC6
C1-NC5-NC6-C7
1.5
1.0
< 1.0
Σ°/Σ
RELATIVE COLUMN CAPACITY PARAMETER
HEIGHT OF TRANSFER UNIT - FT.
EQUILIBRIUM PARAMETER - Γ
10
1.0
.1

FIGURE A 26

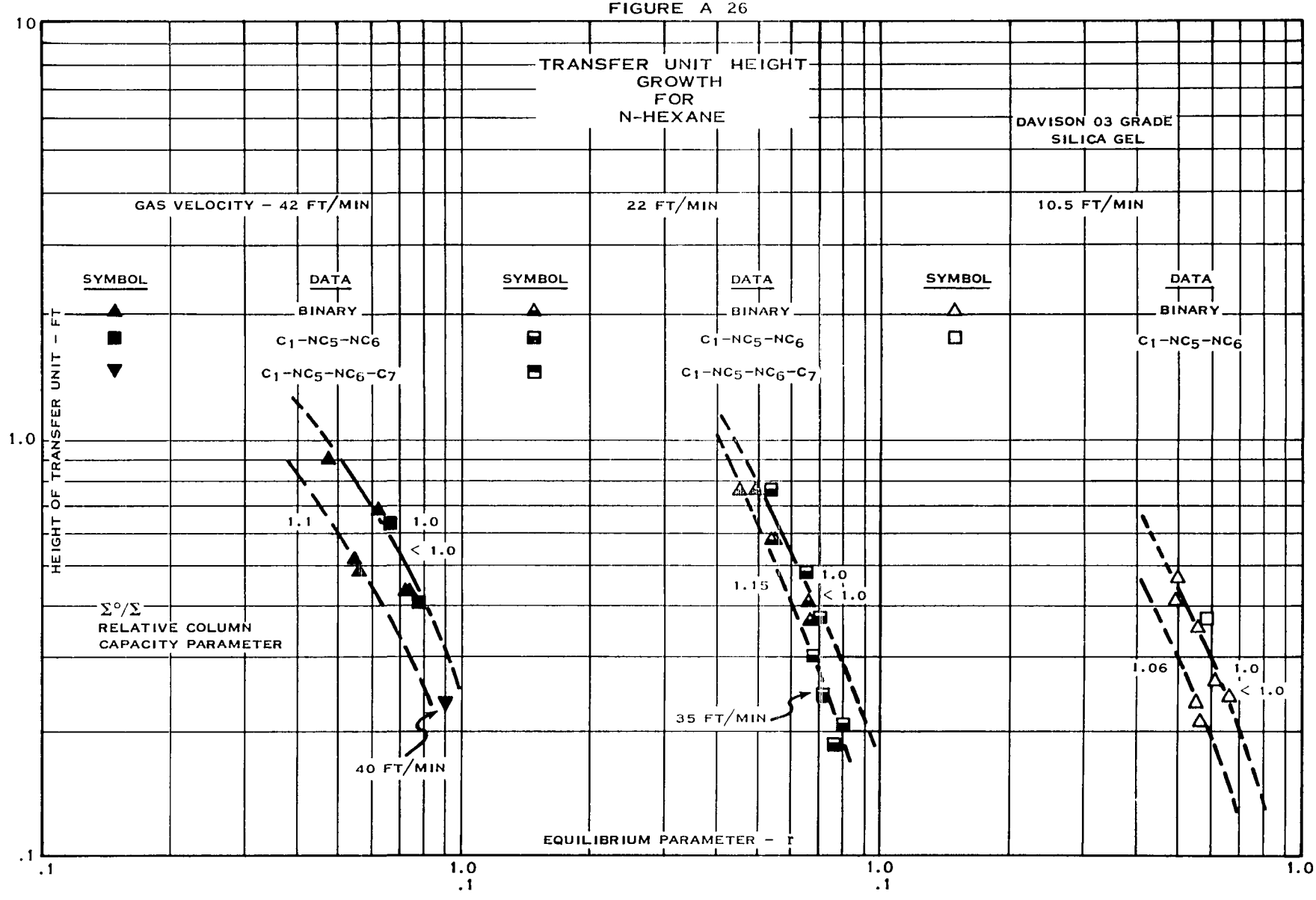
TRANSFER UNIT HEIGHT
GROWTH
FOR
N-HEXANE
DAVISON 03 GRADE
SILICA GEL
GAS VELOCITY – 42 FT/MIN
22 FT/MIN
10.5 FT/MIN
SYMBOL
DATA
BINARY
C1–NC5–NC6
C1–NC5–NC6–C7
HEIGHT OF TRANSFER UNIT – FT
Σ°/Σ
RELATIVE COLUMN
CAPACITY PARAMETER
1.1
1.0
< 1.0
1.15
1.06
40 FT/MIN
35 FT/MIN
EQUILIBRIUM PARAMETER – r
10
1.0
.1

FIGURE A 27

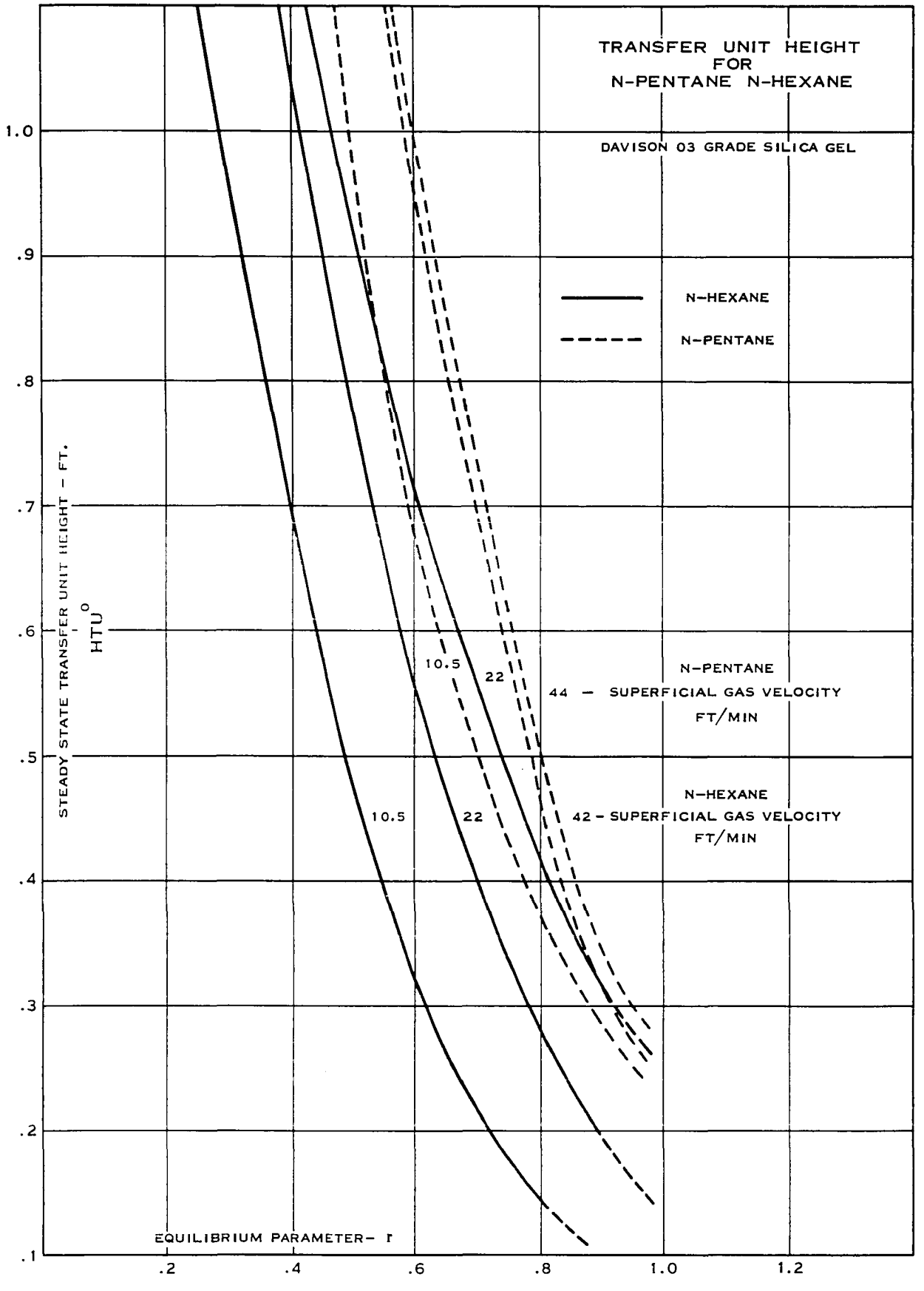
TRANSFER UNIT HEIGHT
FOR
N-PENTANE N-HEXANE
DAVISON 03 GRADE SILICA GEL
N-HEXANE
N-PENTANE
N-PENTANE
44 – SUPERFICIAL GAS VELOCITY
FT/MIN
N-HEXANE
42 – SUPERFICIAL GAS VELOCITY
FT/MIN
10.5
22
10.5
22
STEADY STATE TRANSFER UNIT HEIGHT – FT.
HTU°
EQUILIBRIUM PARAMETER– r
1.0
.9
.8
.7
.6
.5
.4
.3
.2
.1
.2
.4
.6
.8
1.0
1.2

FIGURE A 28

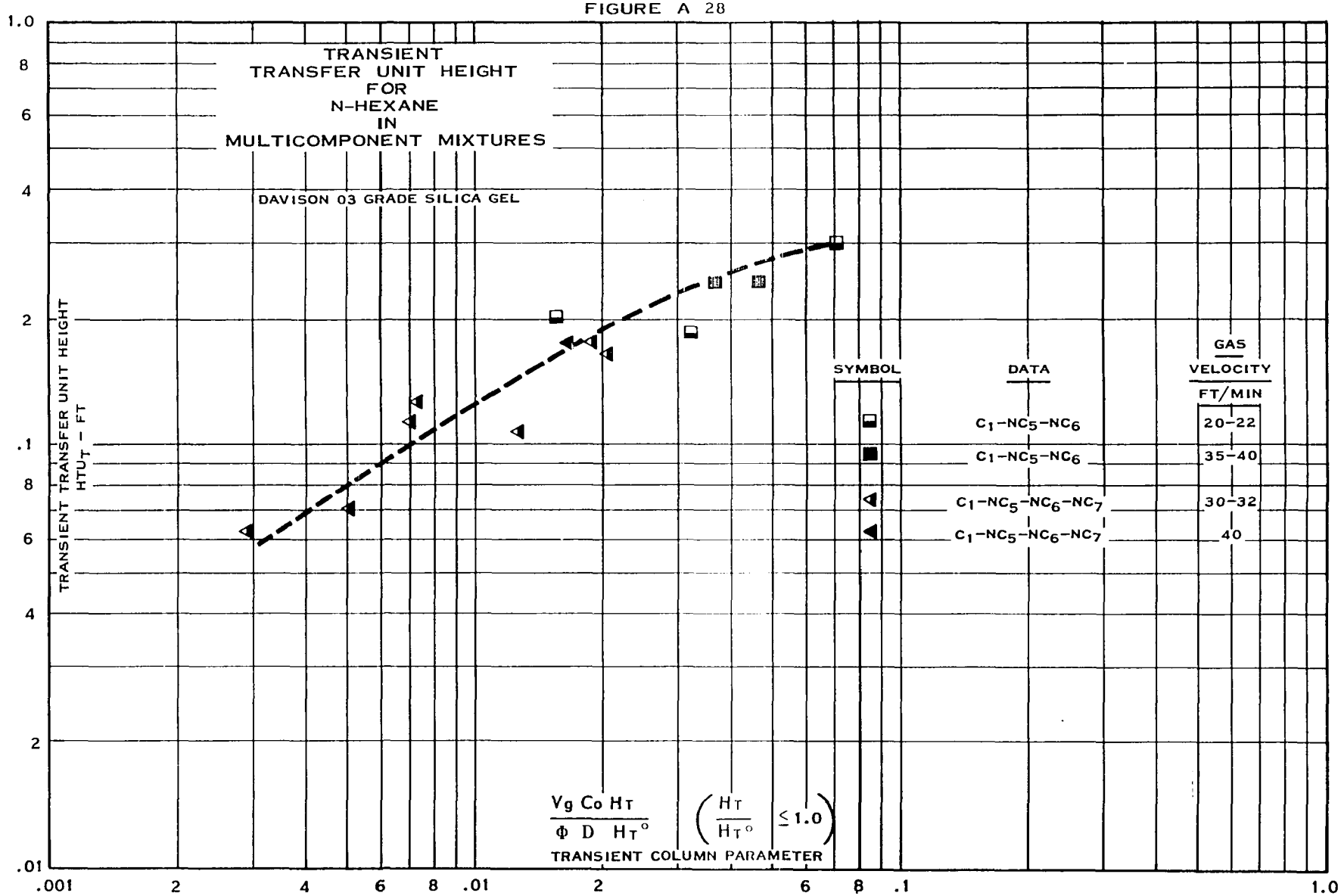
TRANSIENT
TRANSFER UNIT HEIGHT
FOR
N-HEXANE
IN
MULTICOMPONENT MIXTURES
DAVISON 03 GRADE SILICA GEL
TRANSIENT TRANSFER UNIT HEIGHT
HTU$_T$ – FT
1.0
8
6
4
2
.1
8
6
4
2
.01
.001
2
4
6
8
.01
2
6
8
.1
1.0
SYMBOL
DATA
GAS VELOCITY FT/MIN
C1–NC5–NC6
20–22
C1–NC5–NC6
35–40
C1–NC5–NC6–NC7
30–32
C1–NC5–NC6–NC7
40
$\frac{Vg\ Co\ H_T}{\Phi\ D\ H_T^\circ}$ $\left(\frac{H_T}{H_T^\circ} \leq 1.0\right)$
TRANSIENT COLUMN PARAMETER

FIGURE A 29

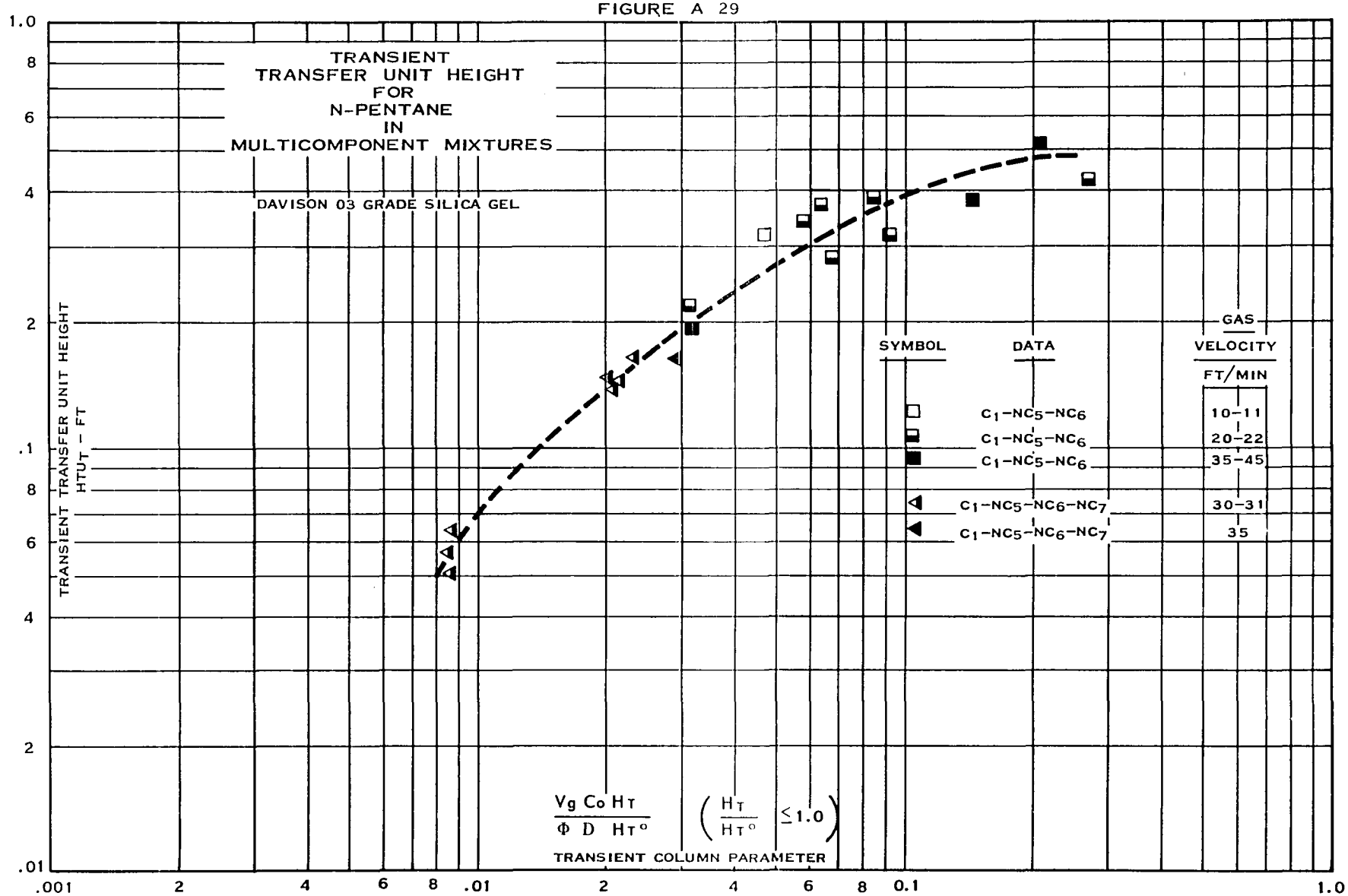
TRANSIENT
TRANSFER UNIT HEIGHT
FOR
N-PENTANE
IN
MULTICOMPONENT MIXTURES
DAVISON 03 GRADE SILICA GEL
TRANSIENT TRANSFER UNIT HEIGHT
HTU_T - FT
SYMBOL
DATA
GAS VELOCITY FT/MIN
C_1-NC_5-NC_6 10-11
C_1-NC_5-NC_6 20-22
C_1-NC_5-NC_6 35-45
C_1-NC_5-NC_6-NC_7 30-31
C_1-NC_5-NC_6-NC_7 35
$\frac{V_g C_o H_T}{\Phi D H_T^o}$ $\left(\frac{H_T}{H_T^o} \leq 1.0\right)$
TRANSIENT COLUMN PARAMETER
1.0
8
6
4
2
.1
8
6
4
2
.01
.001
2
4
6
8
.01
2
4
6
8
0.1
1.0

FIGURE A 30

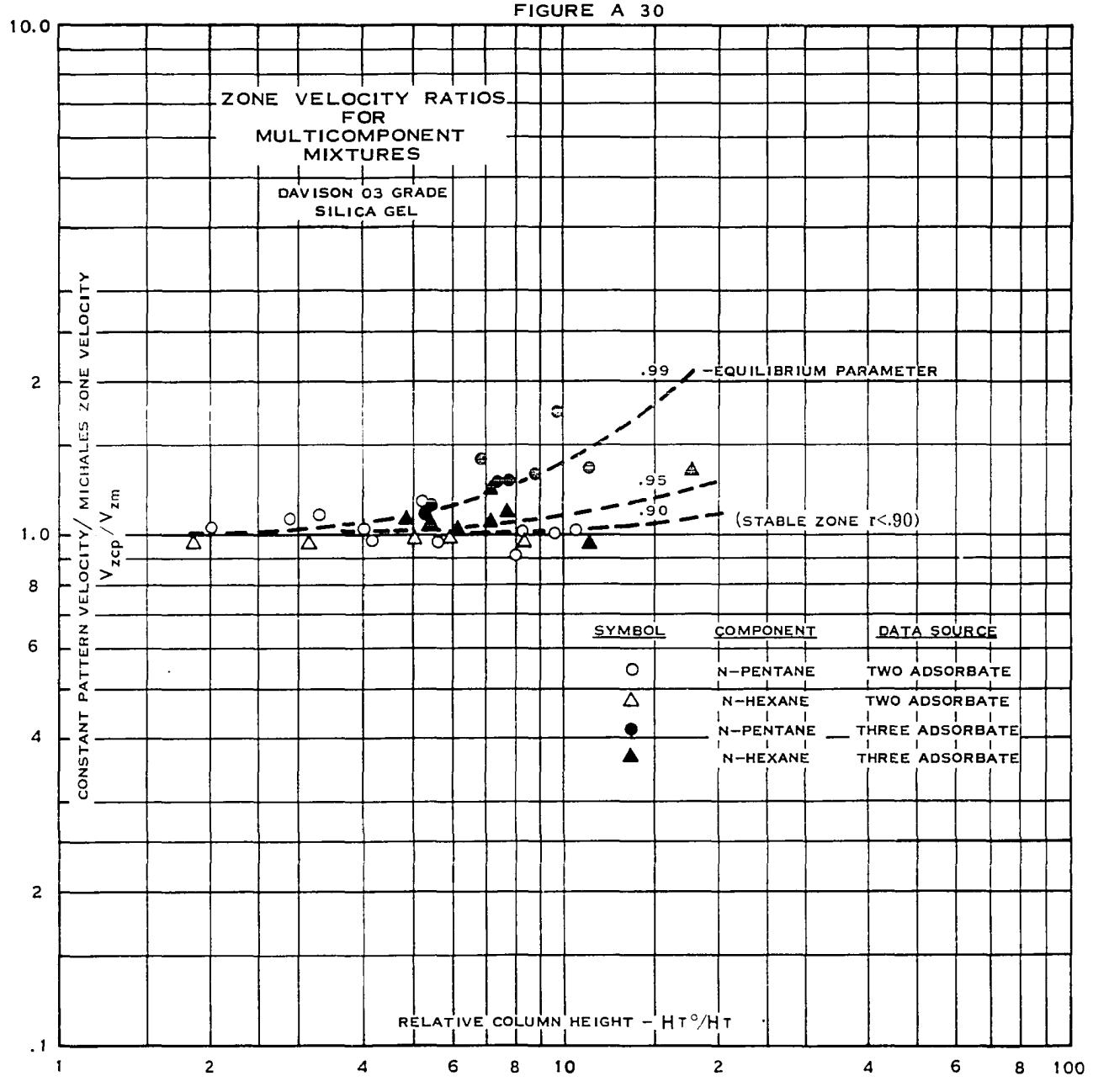
ZONE VELOCITY RATIOS FOR MULTICOMPONENT MIXTURES
DAVISON 03 GRADE SILICA GEL
CONSTANT PATTERN VELOCITY/ MICHALES ZONE VELOCITY
V_{zcp}/V_{zm}
.99 -EQUILIBRIUM PARAMETER
.95
.90
(STABLE ZONE r<.90)
SYMBOL
COMPONENT
DATA SOURCE
N-PENTANE
TWO ADSORBATE
N-HEXANE
TWO ADSORBATE
N-PENTANE
THREE ADSORBATE
N-HEXANE
THREE ADSORBATE
RELATIVE COLUMN HEIGHT - HT°/HT
10.0
2
1.0
8
6
4
2
.1
1
2
4
6
8
10
2
4
6
8
100

FIGURE A 31
SOLID PHASE DIFFUSION

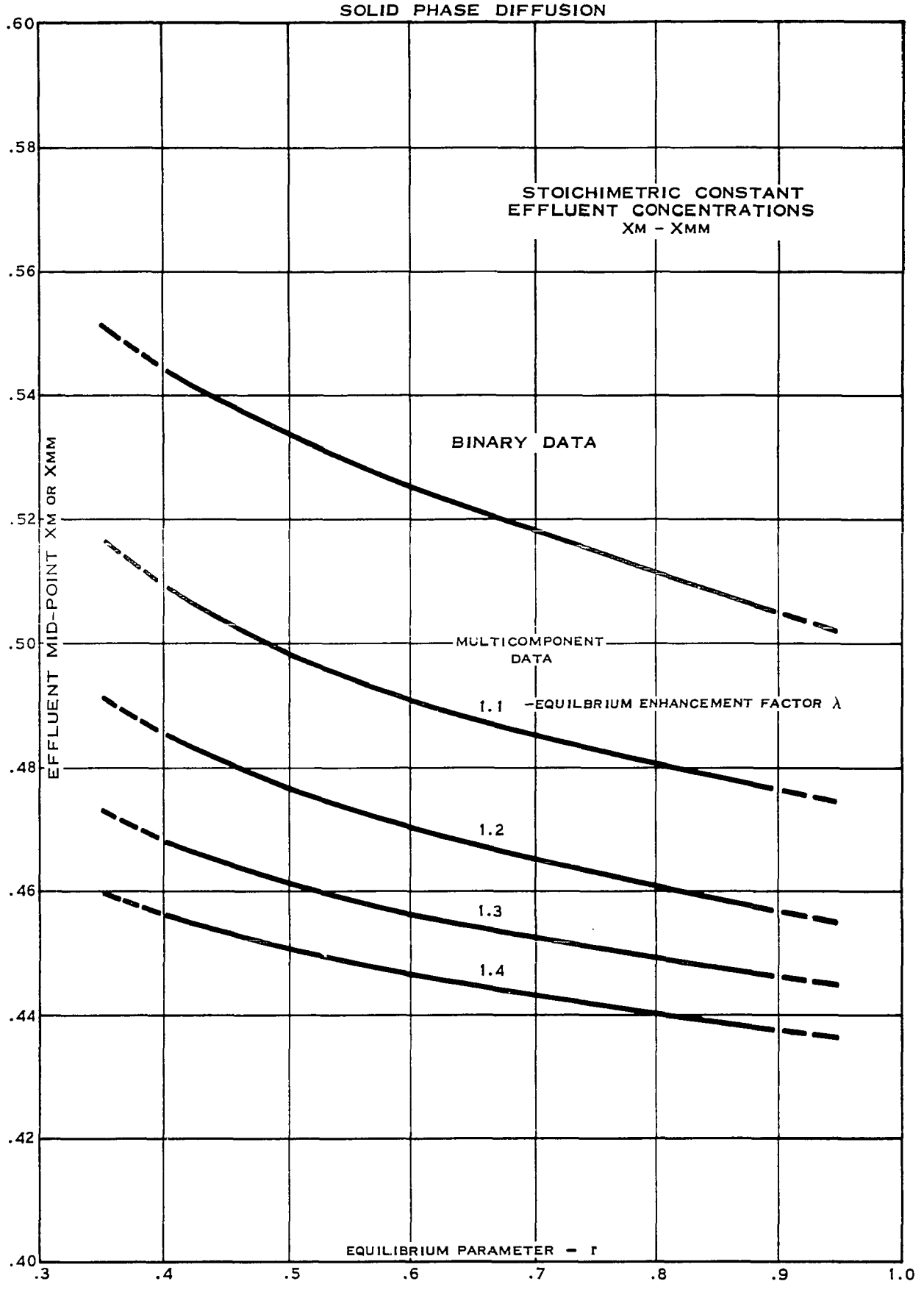

FIGURE A 32
SOLID PHASE DIFFUSION

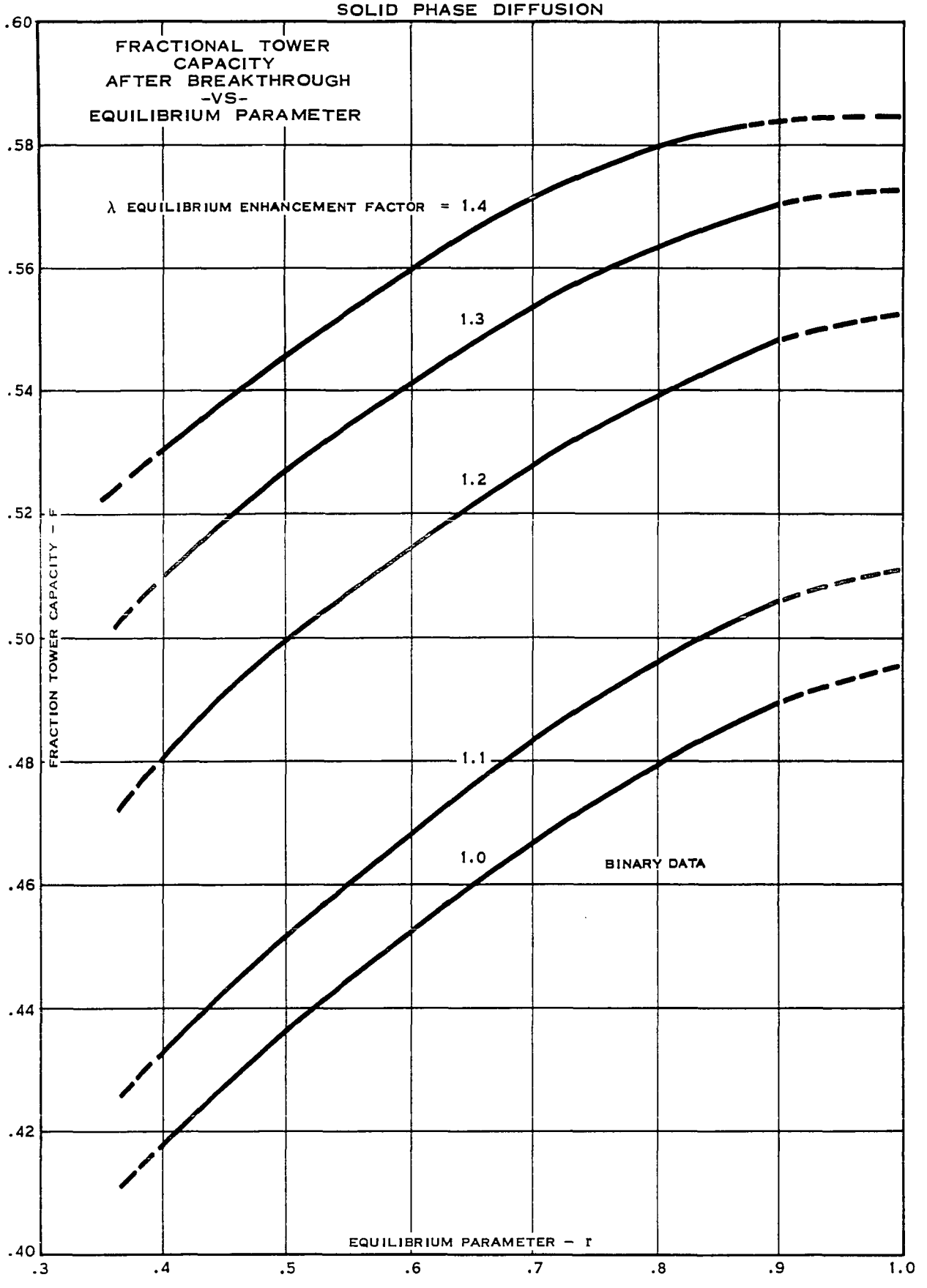

FIGURE A 33
SOLID PHASE DIFFUSION

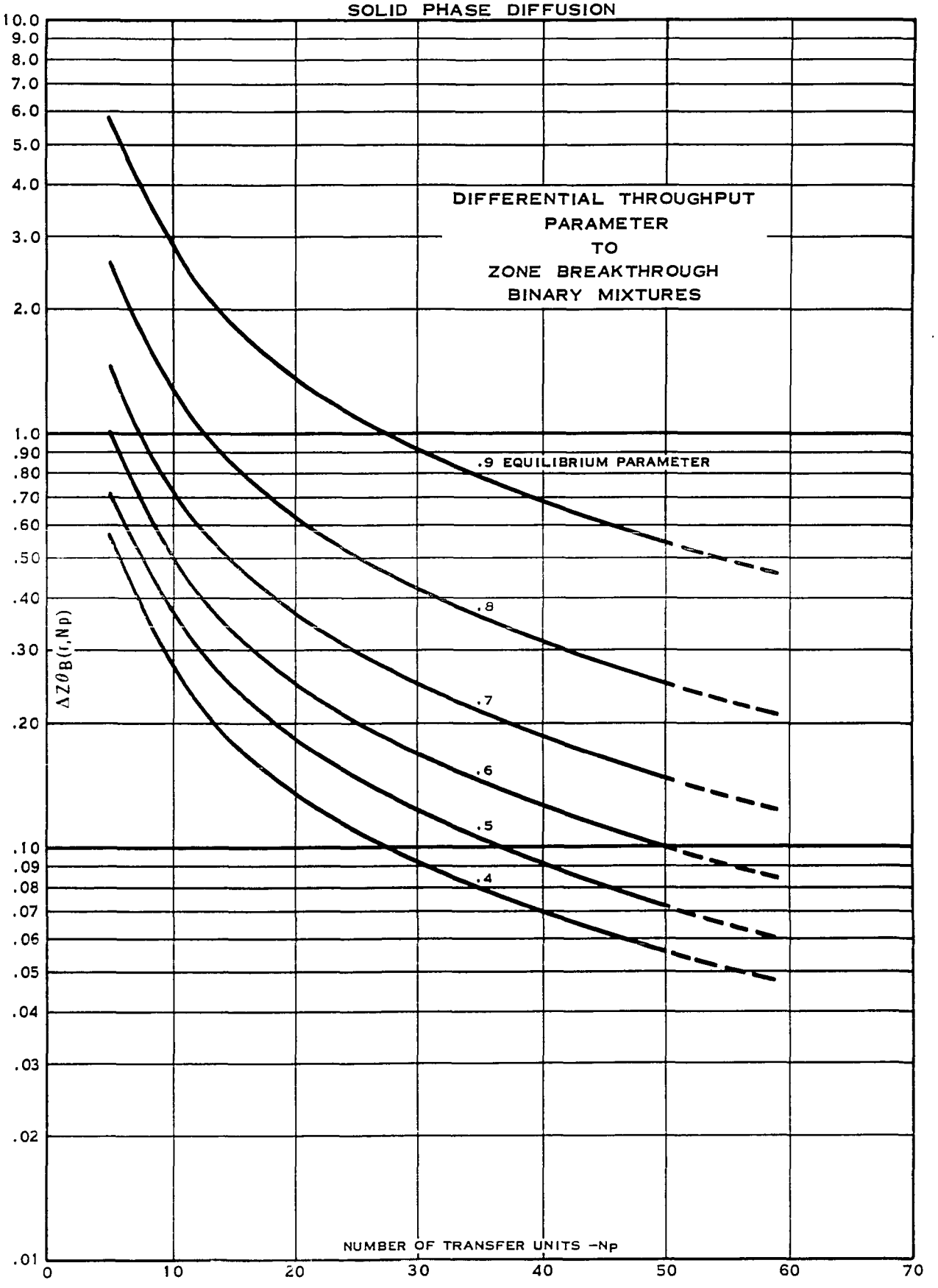

FIGURE A 34
SOLID PHASE DIFFUSION

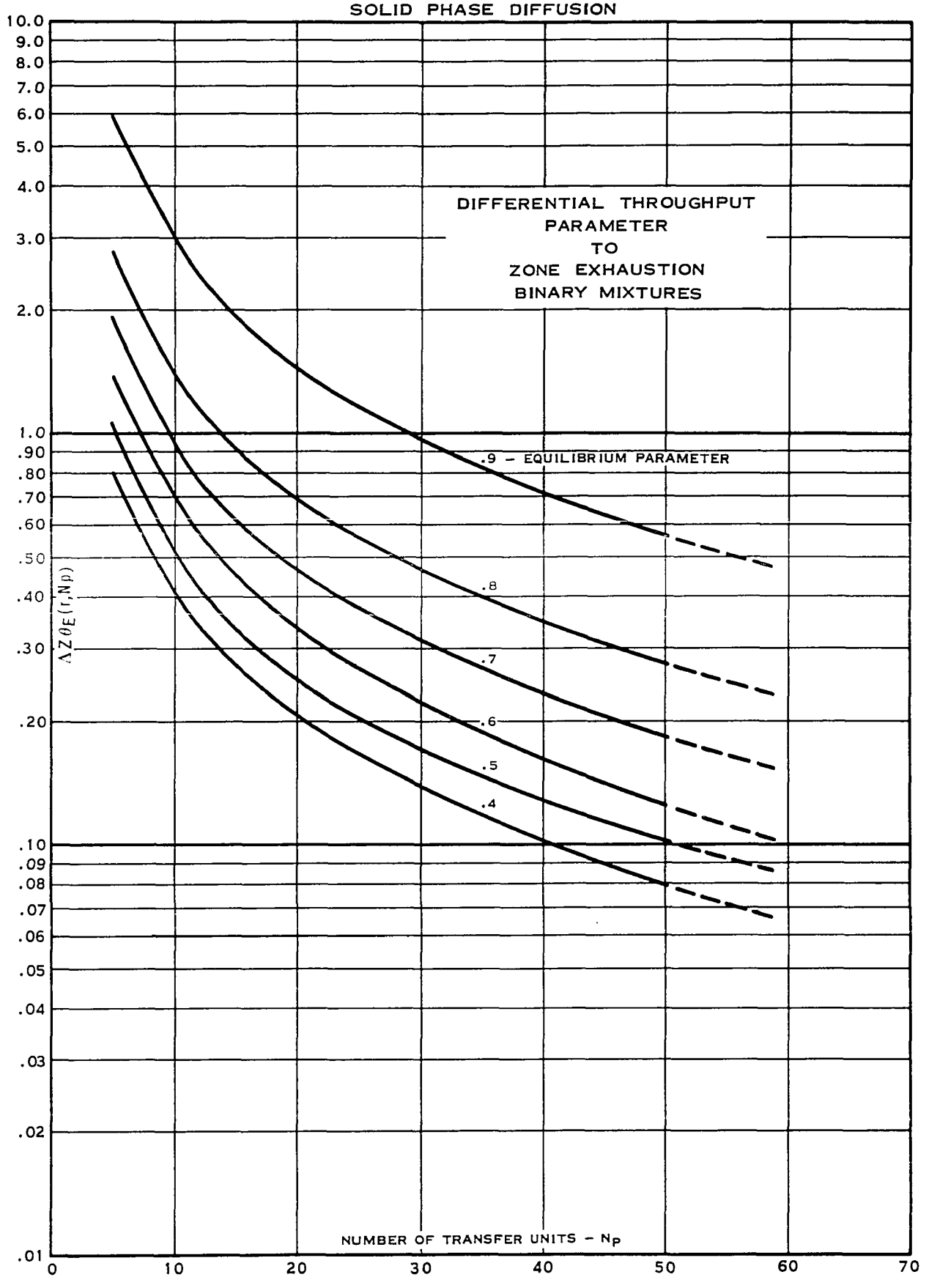

FIGURE A 35
SOLID PHASE DIFFUSION

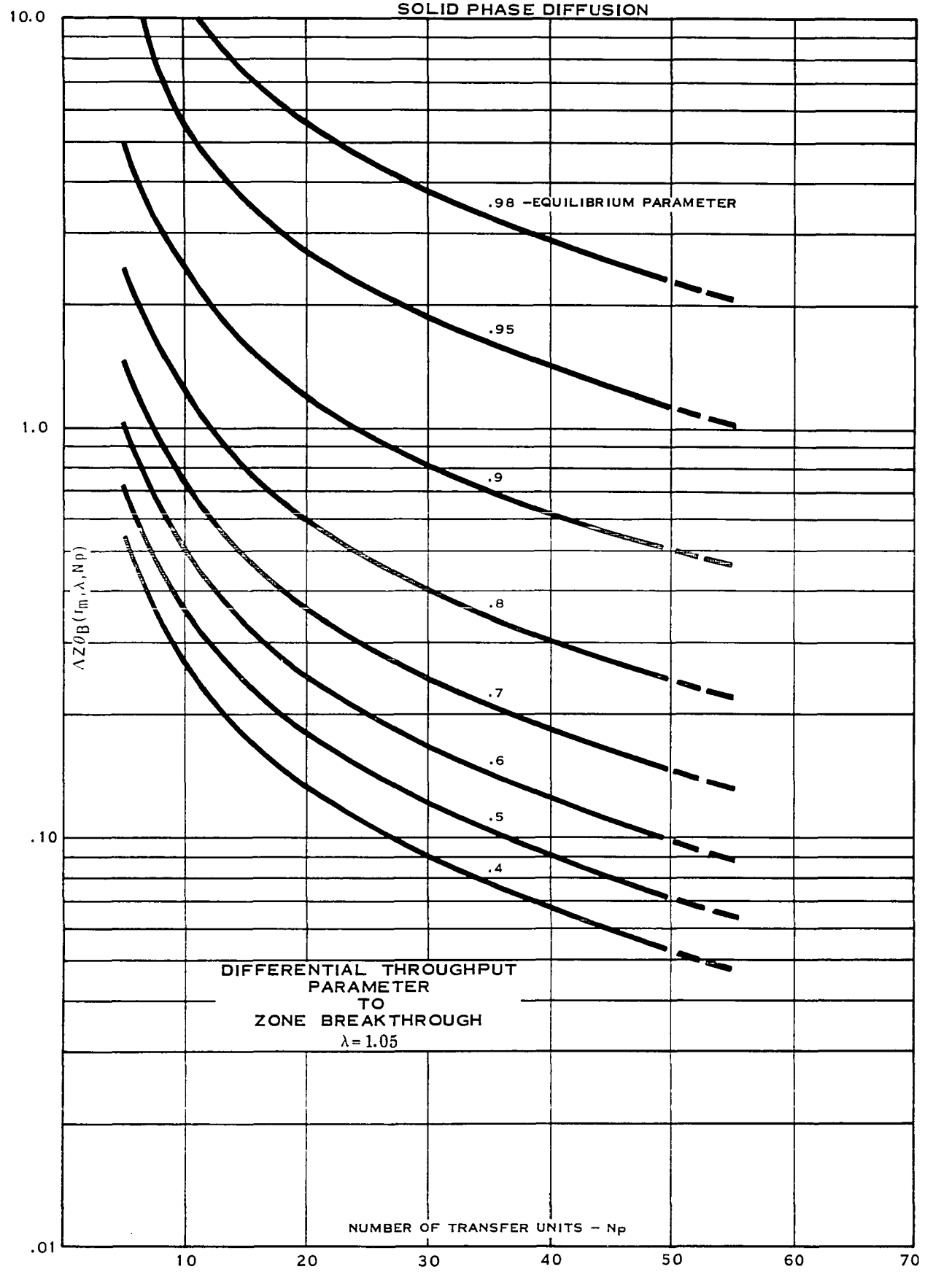

FIGURE A 36
SOLID PHASE DIFFUSION

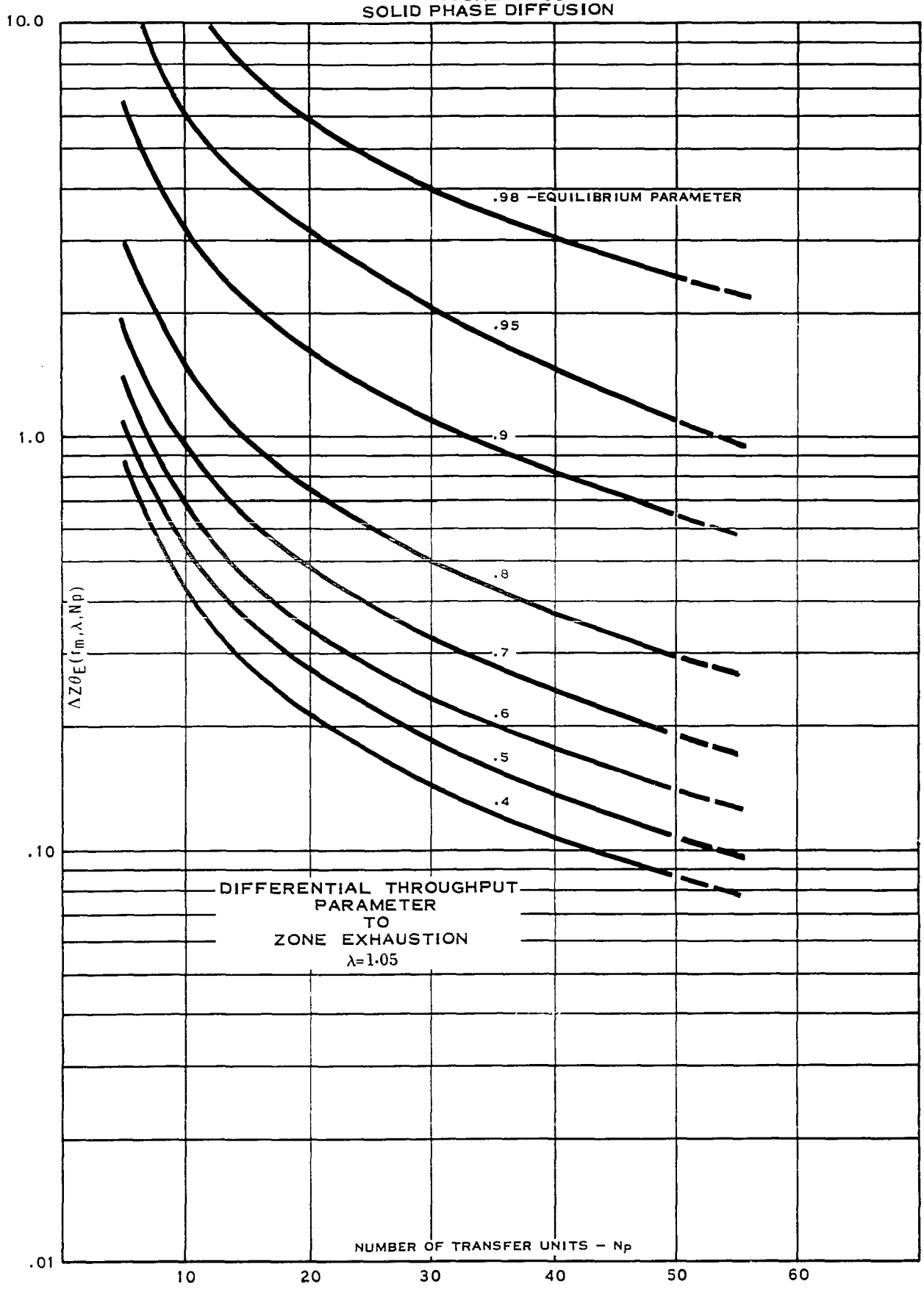

FIGURE A 37
SOLID PHASE DIFFUSION

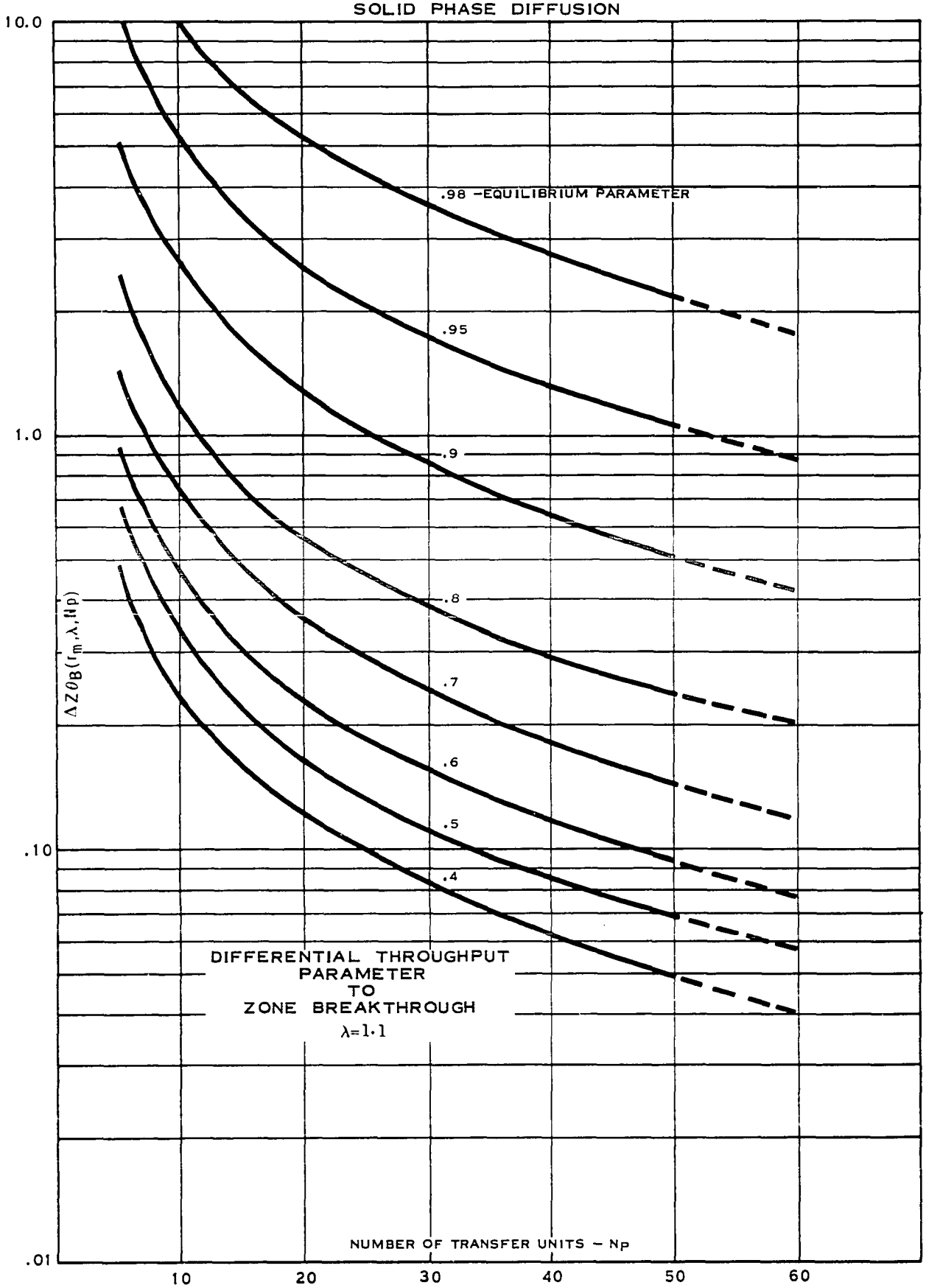

FIGURE A 38
SOLID PHASE DIFFUSION

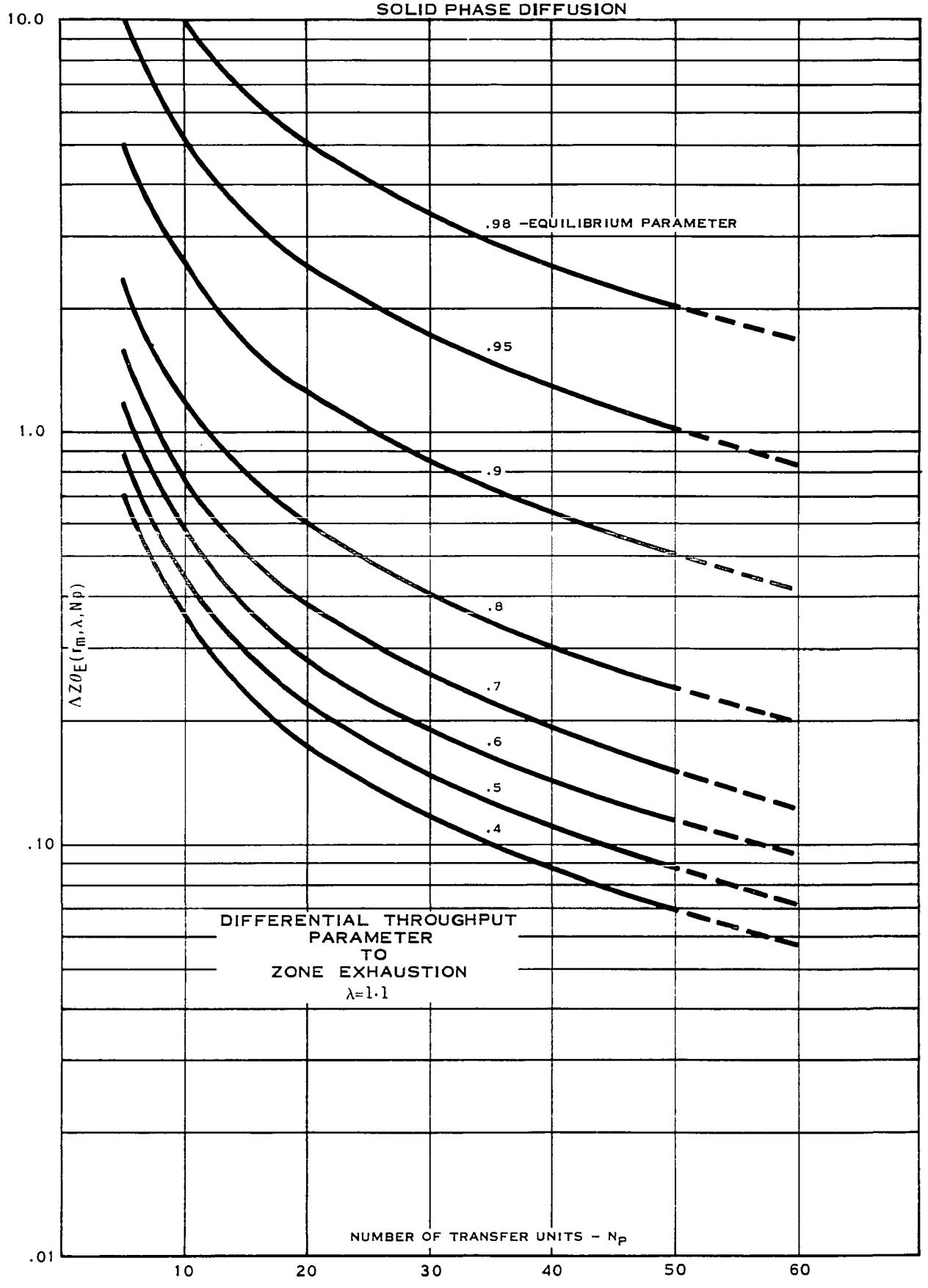

FIGURE A 39
SOLID PHASE DIFFUSION

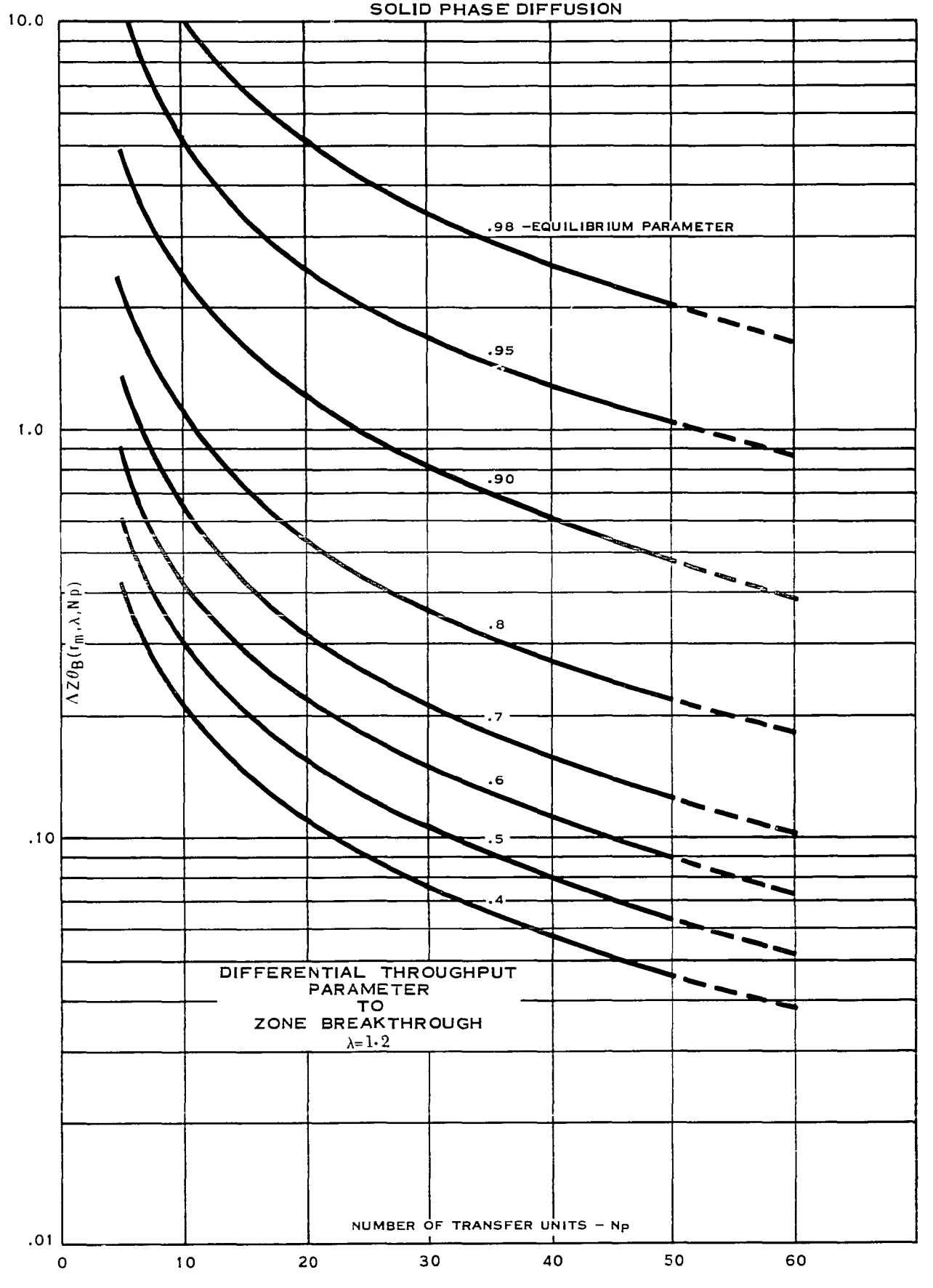

FIGURE A 40
SOLID PHASE DIFFUSION

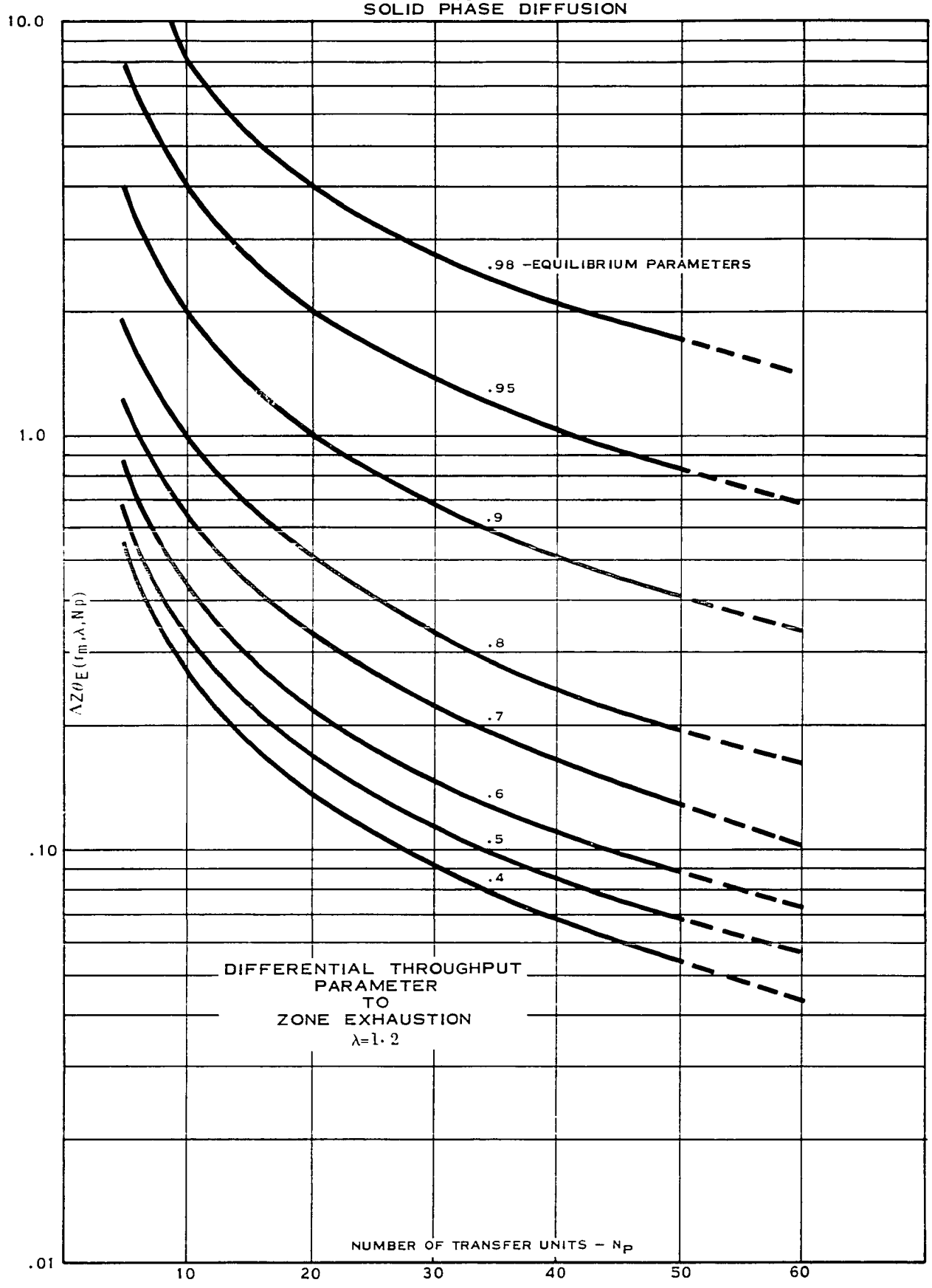

FIGURE A 41
SOLID PHASE DIFFUSION

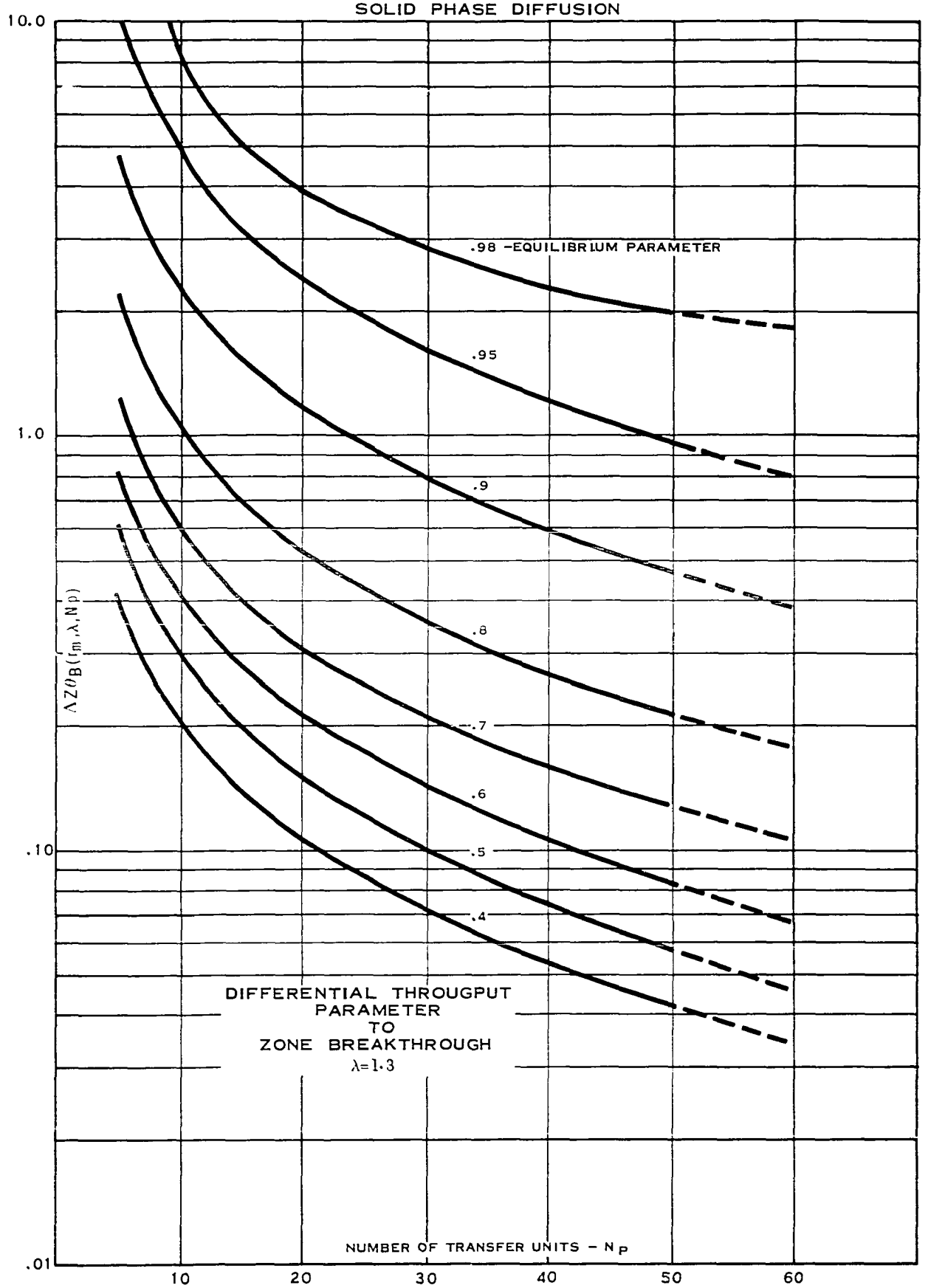

FIGURE A 42
SOLID PHASE DIFFUSION

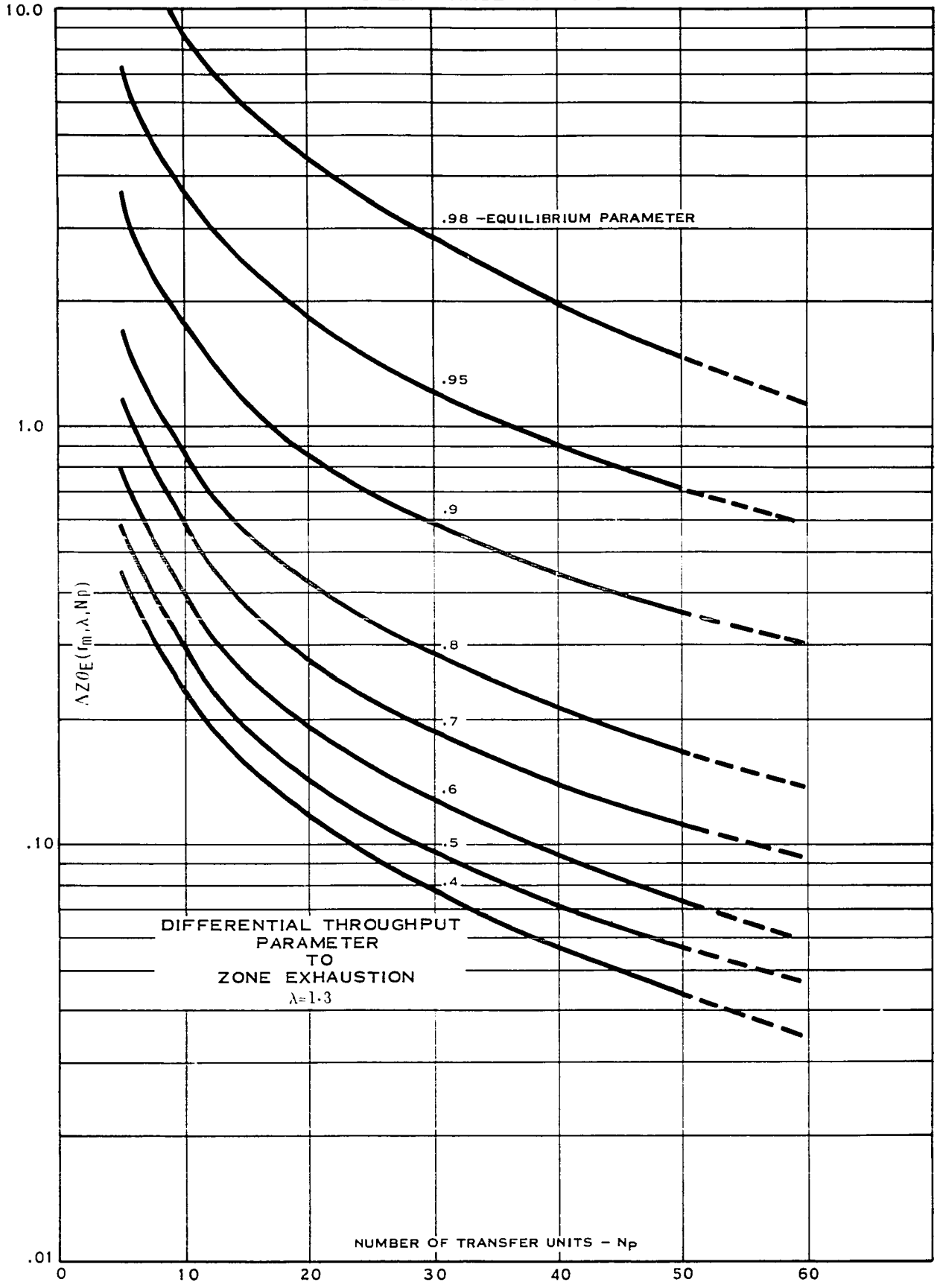

FIGURE A 43
SOLID PHASE DIFFUSION

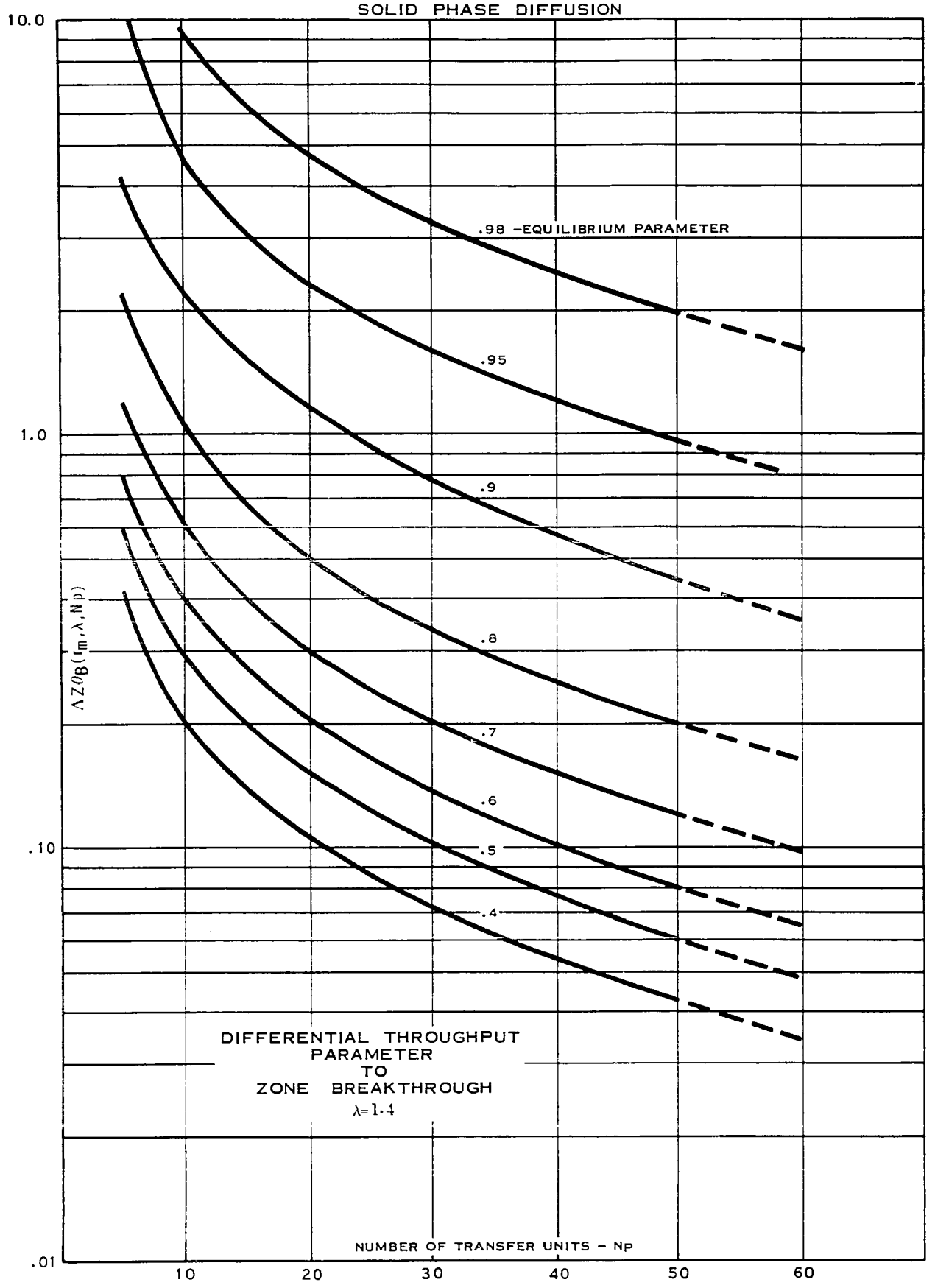

FIGURE A 44
SOLID PHASE DIFFUSION

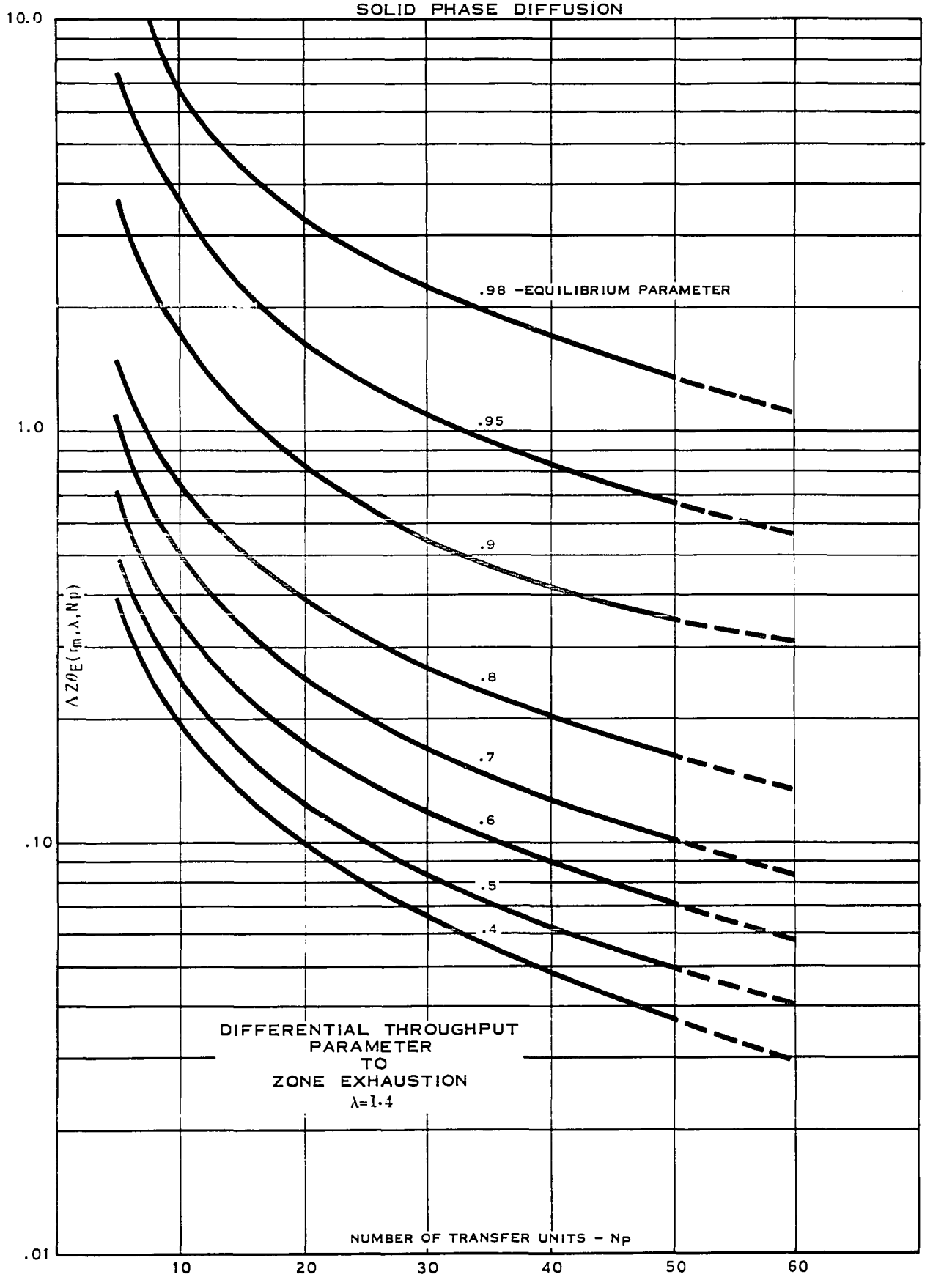

FIGURE A 45
SOLID PHASE DIFFUSION

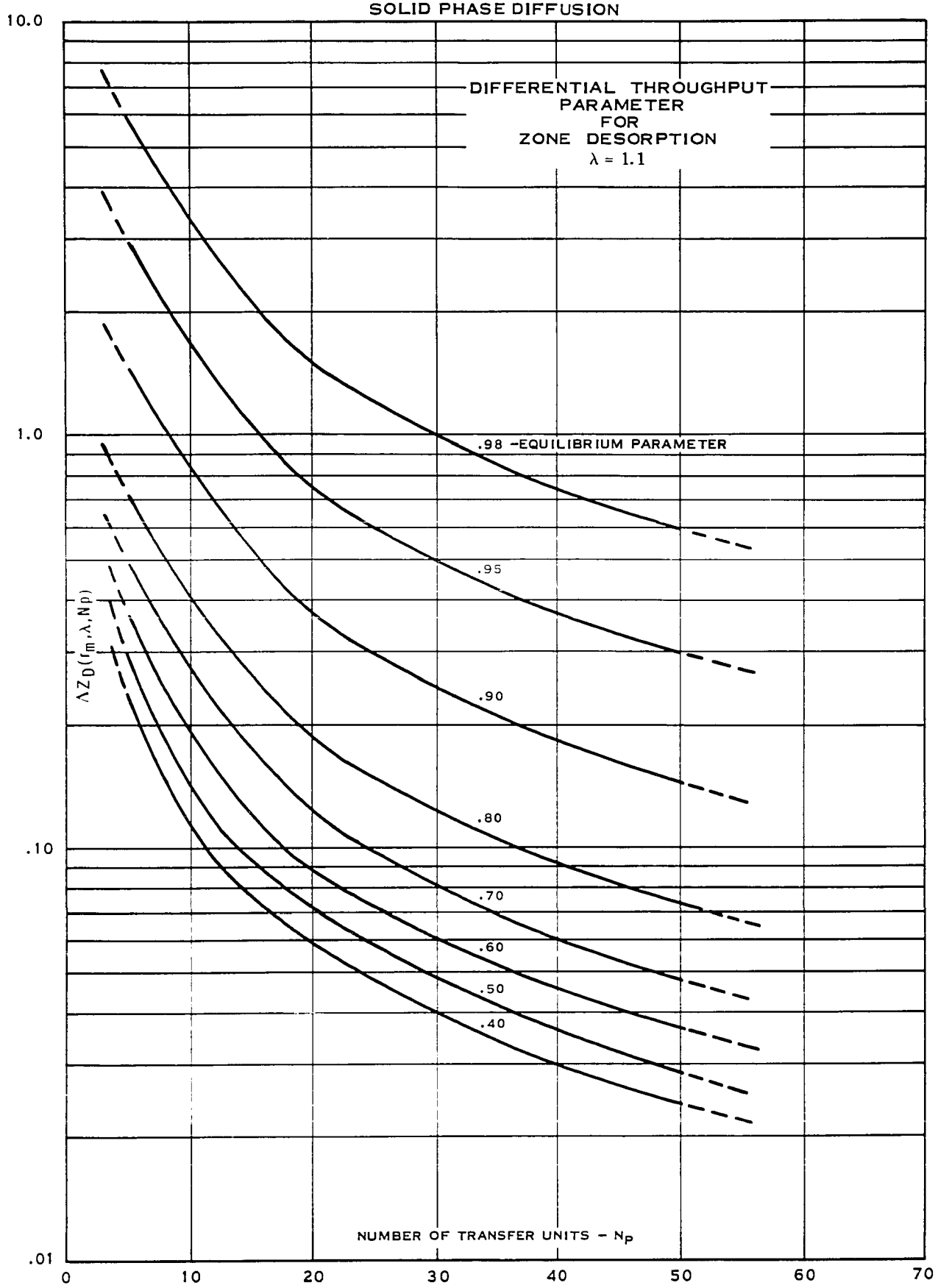

FIGURE A 46
SOLID PHASE DIFFUSION

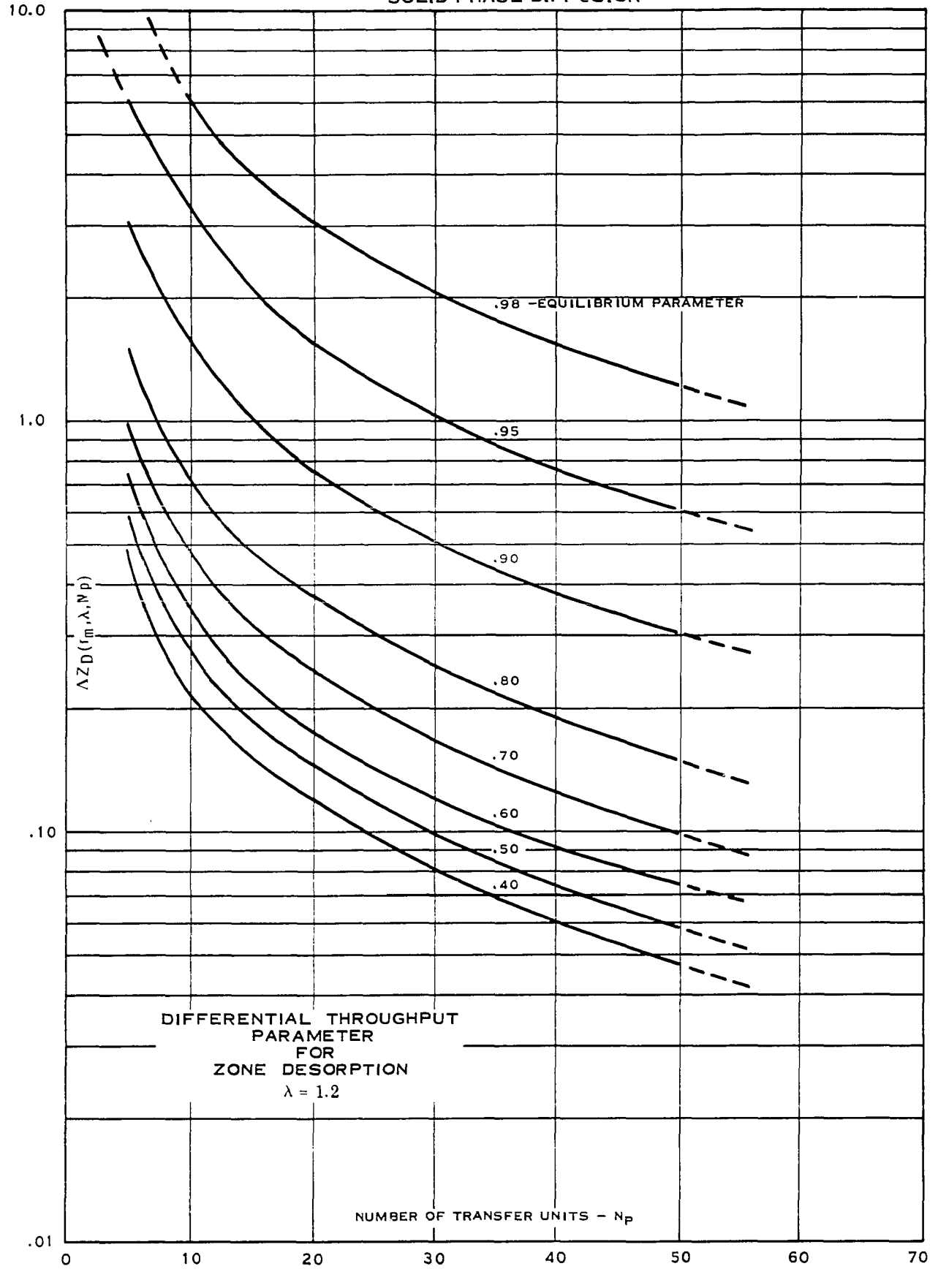

FIGURE A 47
SOLID PHASE DIFFUSION

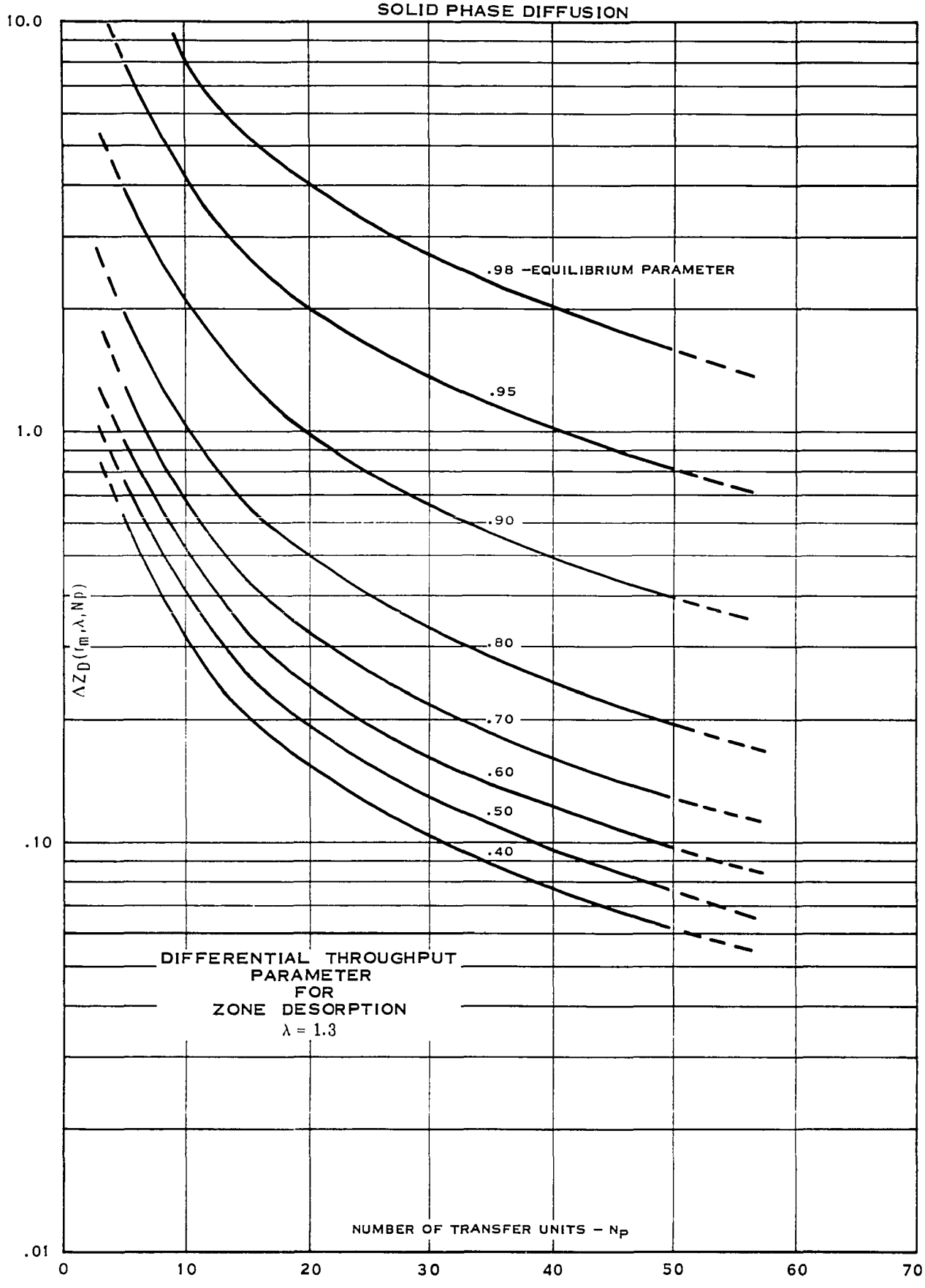

FIGURE A 48
SOLID PHASE DIFFUSION

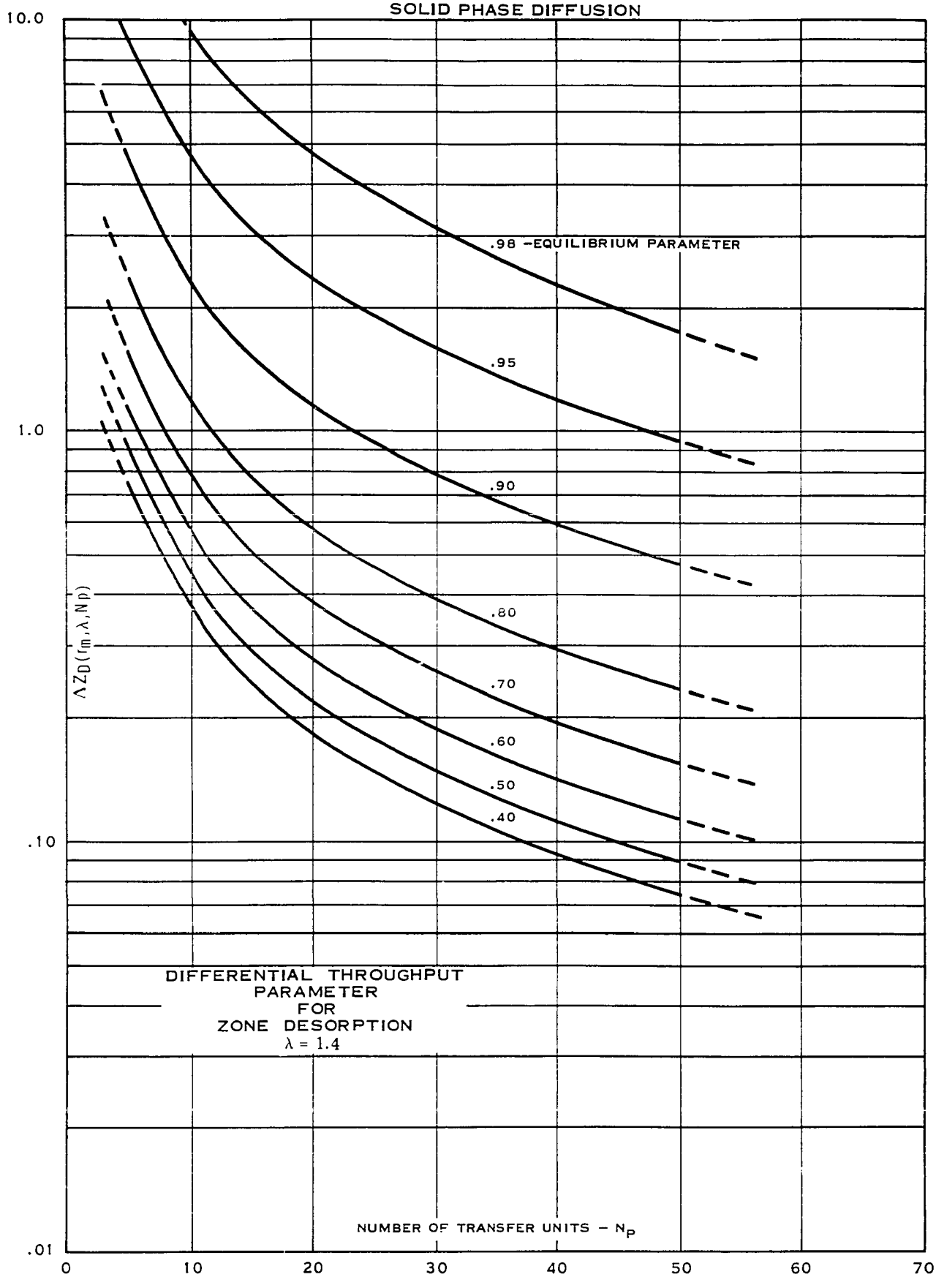

FIGURE A 49

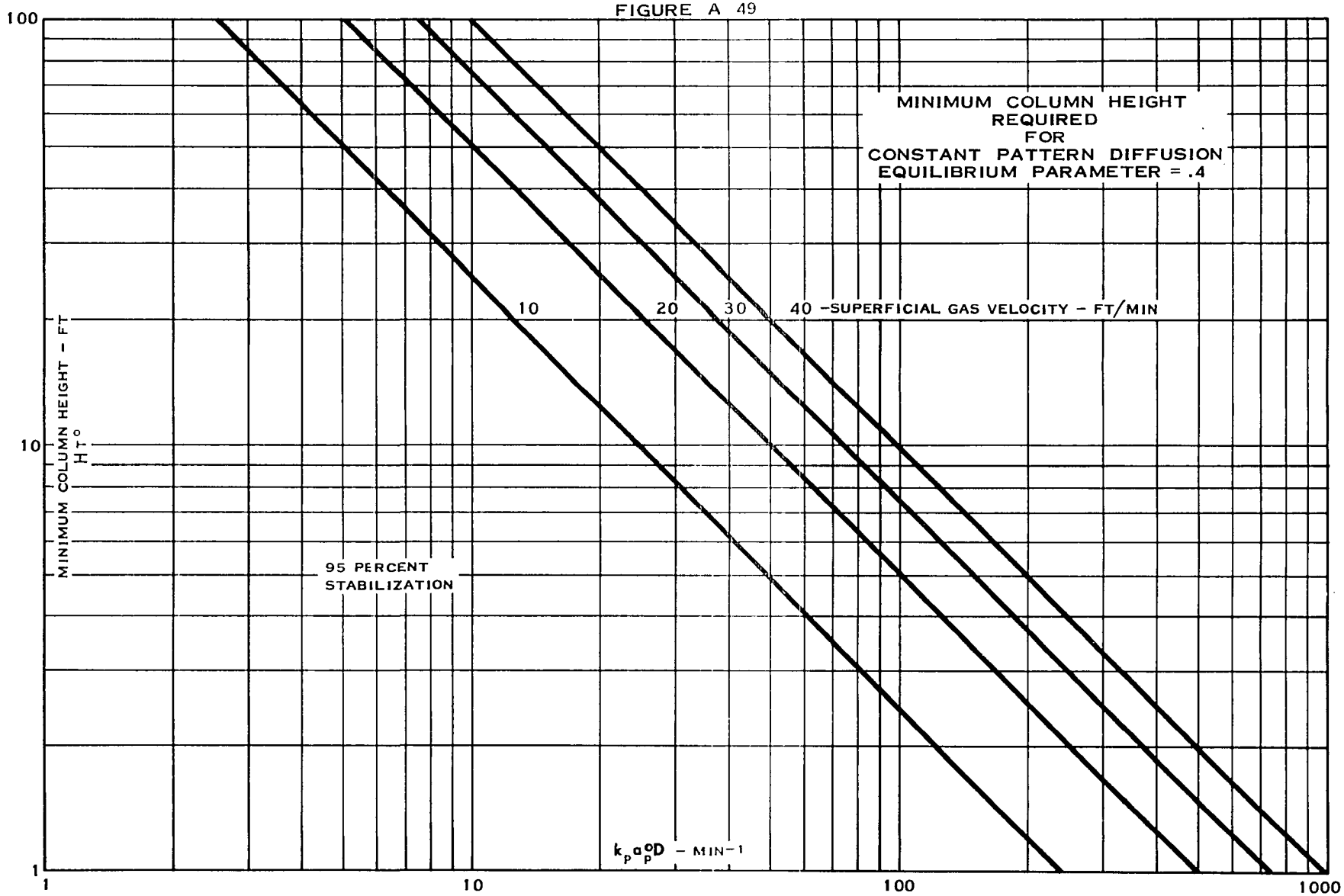
MINIMUM COLUMN HEIGHT
REQUIRED
FOR
CONSTANT PATTERN DIFFUSION
EQUILIBRIUM PARAMETER = .4
10
20
30
40 -SUPERFICIAL GAS VELOCITY - FT/MIN
MINIMUM COLUMN HEIGHT - FT
H_T°
95 PERCENT
STABILIZATION
$k_p a_p^{\circ} D$ - MIN^{-1}
100
10
1
1
10
100
1000

FIGURE A 50

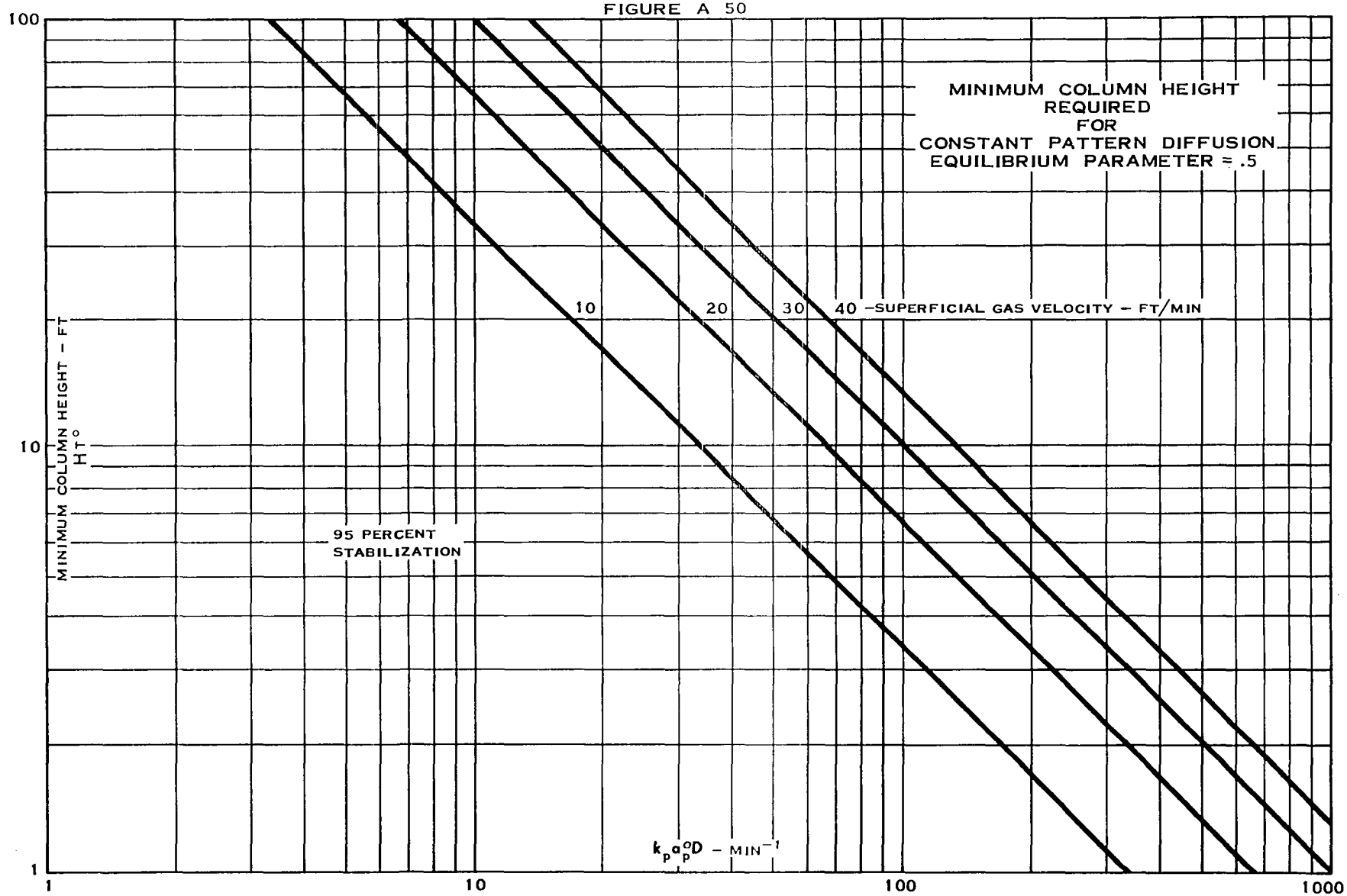
MINIMUM COLUMN HEIGHT
REQUIRED
FOR
CONSTANT PATTERN DIFFUSION
EQUILIBRIUM PARAMETER = .5
10
20
30
40 –SUPERFICIAL GAS VELOCITY – FT/MIN
95 PERCENT
STABILIZATION
MINIMUM COLUMN HEIGHT – FT
H_T°
$k_p a_p^\circ D$ – MIN^{-1}
100
10
1
1
10
100
1000

FIGURE A 51

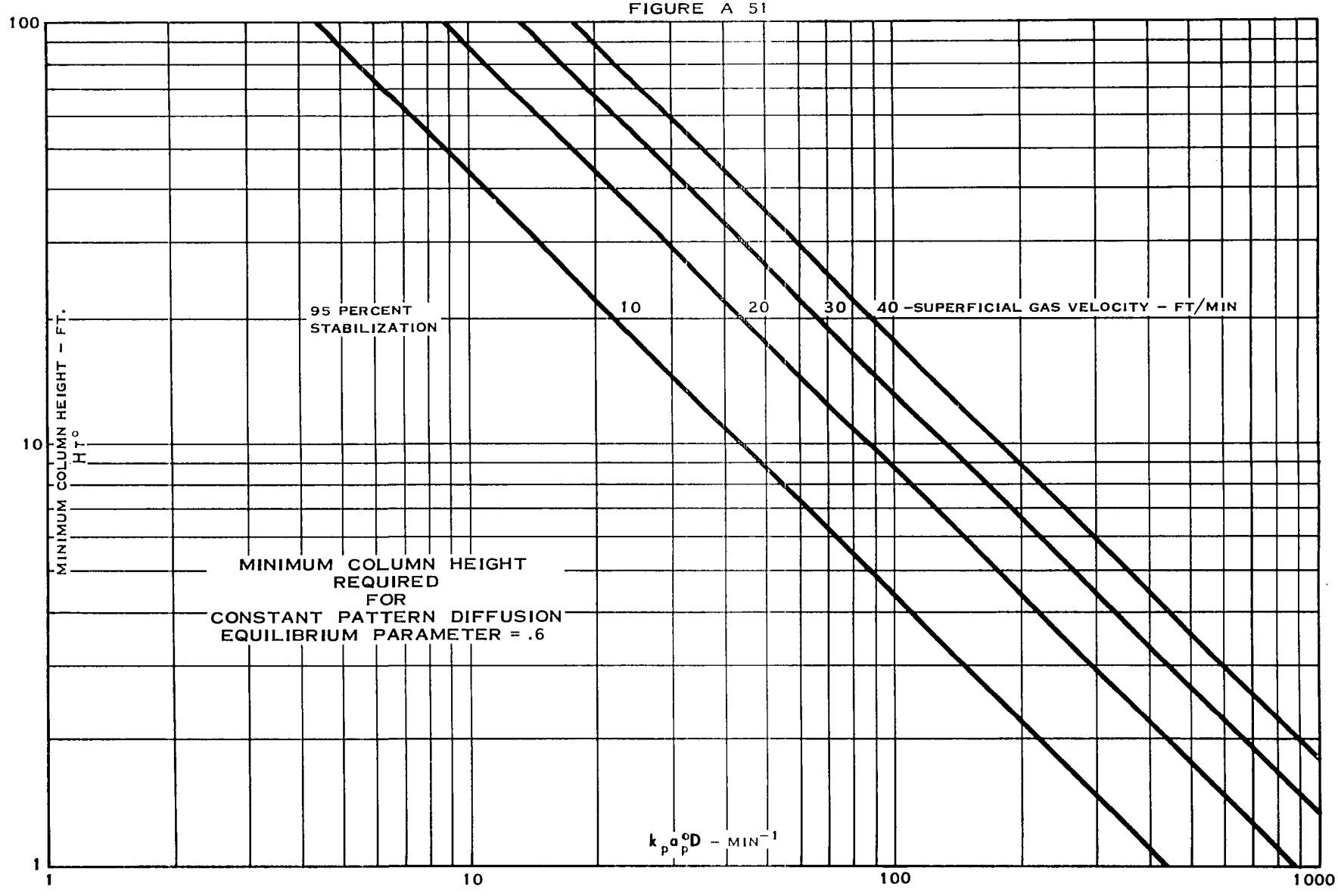
100
10
1
MINIMUM COLUMN HEIGHT - FT.
H_T°
95 PERCENT
STABILIZATION
10
20
30
40 -SUPERFICIAL GAS VELOCITY - FT/MIN
MINIMUM COLUMN HEIGHT
REQUIRED
FOR
CONSTANT PATTERN DIFFUSION
EQUILIBRIUM PARAMETER = .6
$k_p a_p^\circ D$ - MIN^{-1}
1
10
100
1000

FIGURE A 52

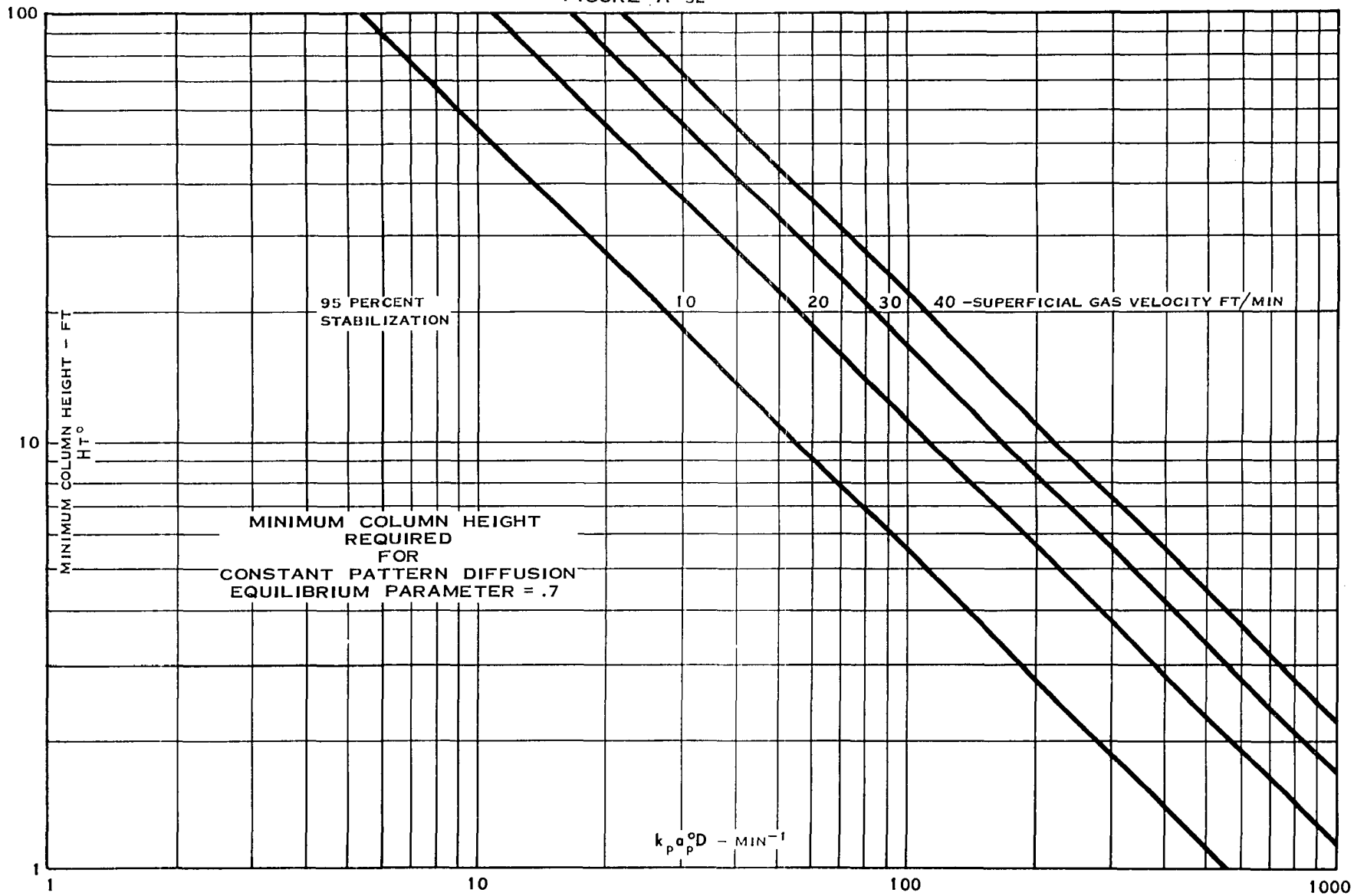
100
10
1
1
10
100
1000
MINIMUM COLUMN HEIGHT - FT
H_T°
95 PERCENT
STABILIZATION
10
20
30
40 -SUPERFICIAL GAS VELOCITY FT/MIN
MINIMUM COLUMN HEIGHT
REQUIRED
FOR
CONSTANT PATTERN DIFFUSION
EQUILIBRIUM PARAMETER = .7
$k_p a_p^\circ D$ - MIN^{-1}

FIGURE A 53

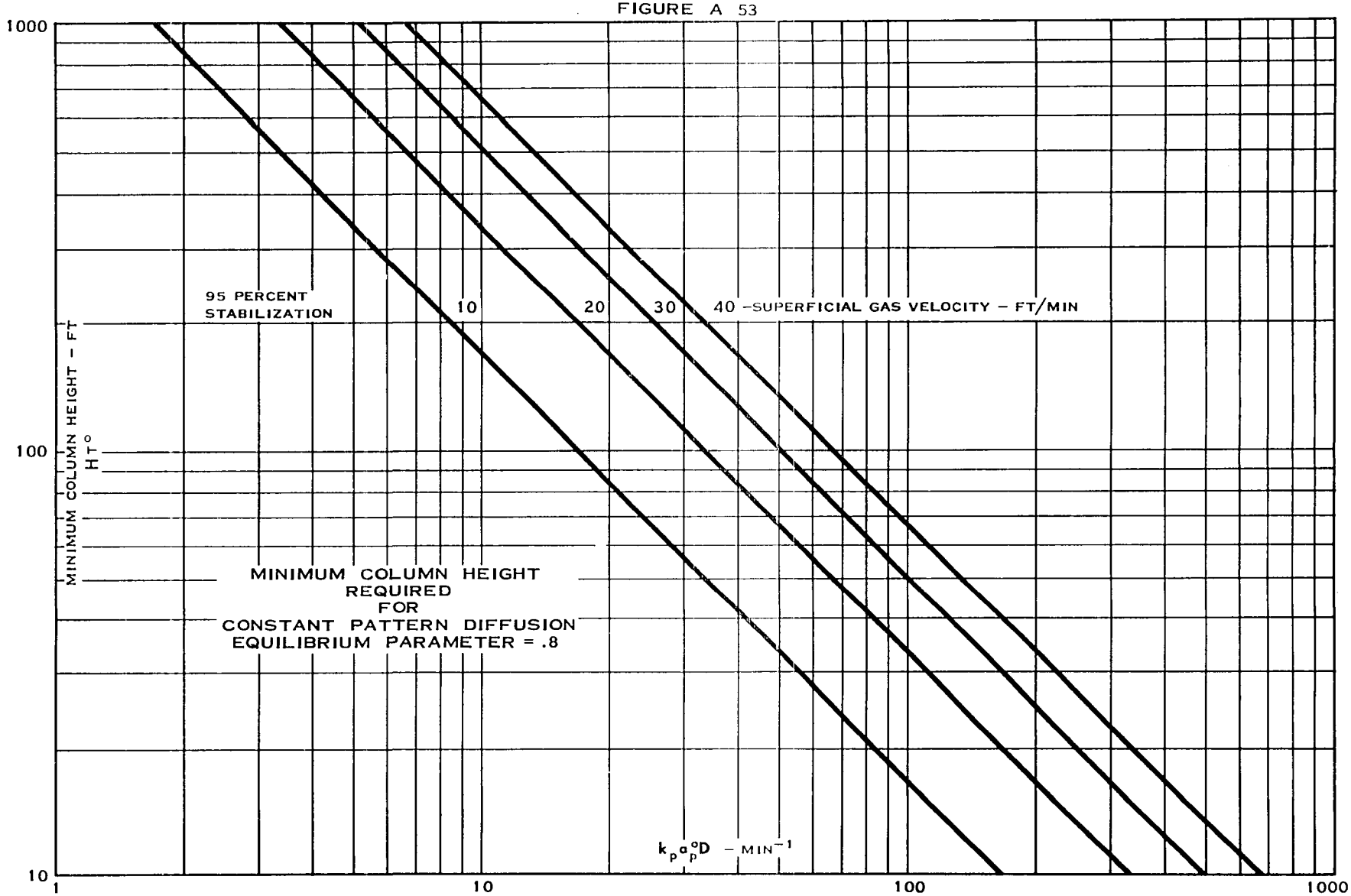
1000
100
10
1
10
100
1000
MINIMUM COLUMN HEIGHT - FT
H T°
95 PERCENT
STABILIZATION
10
20
30
40 -SUPERFICIAL GAS VELOCITY - FT/MIN
MINIMUM COLUMN HEIGHT
REQUIRED
FOR
CONSTANT PATTERN DIFFUSION
EQUILIBRIUM PARAMETER = .8
$k_p a_p^o D$ - MIN^{-1}

FIGURE A 54

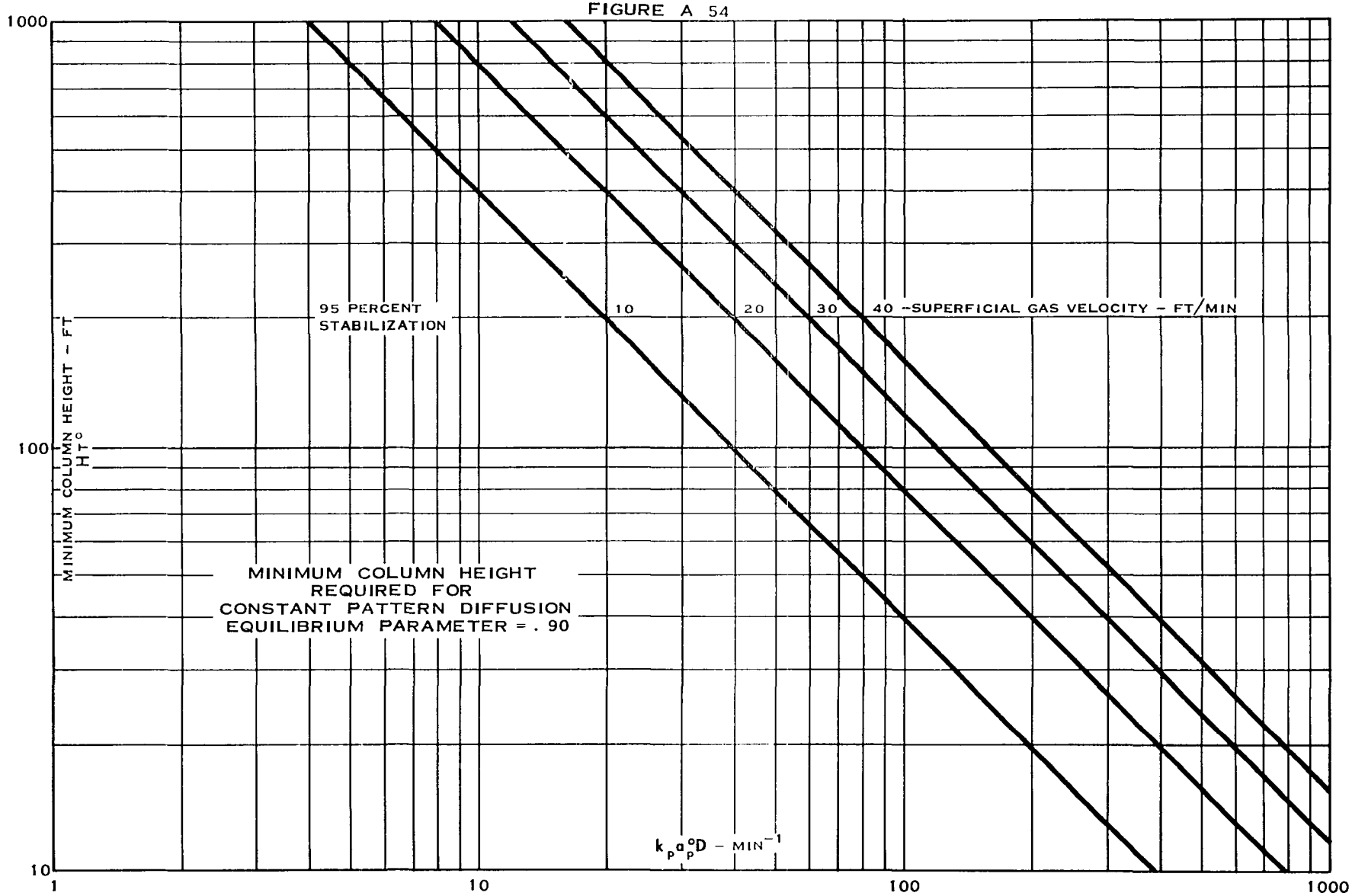
1000
100
10
1
10
100
1000
MINIMUM COLUMN HEIGHT - FT
H_T°
95 PERCENT
STABILIZATION
10
20
30
40 -SUPERFICIAL GAS VELOCITY - FT/MIN
MINIMUM COLUMN HEIGHT
REQUIRED FOR
CONSTANT PATTERN DIFFUSION
EQUILIBRIUM PARAMETER = . 90
$k_p a_p^\circ D$ - MIN^{-1}

FIGURE A 55

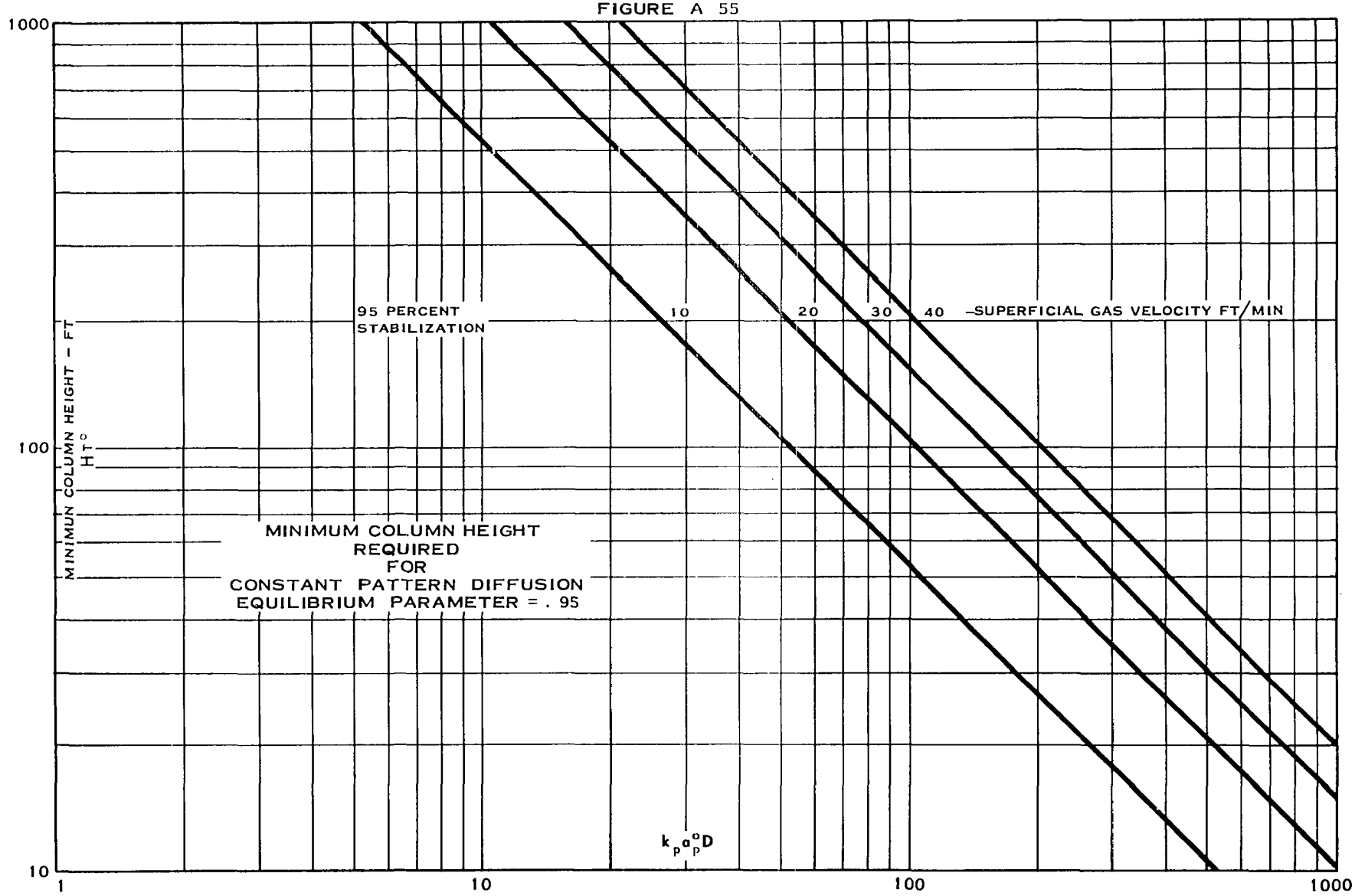
1000
100
10
1
10
100
1000
MINIMUN COLUMN HEIGHT - FT
H_T^o
95 PERCENT
STABILIZATION
10
20
30
40
-SUPERFICIAL GAS VELOCITY FT/MIN
MINIMUM COLUMN HEIGHT
REQUIRED
FOR
CONSTANT PATTERN DIFFUSION
EQUILIBRIUM PARAMETER = . 95
$k_p a_p^o D$

FIGURE A 56

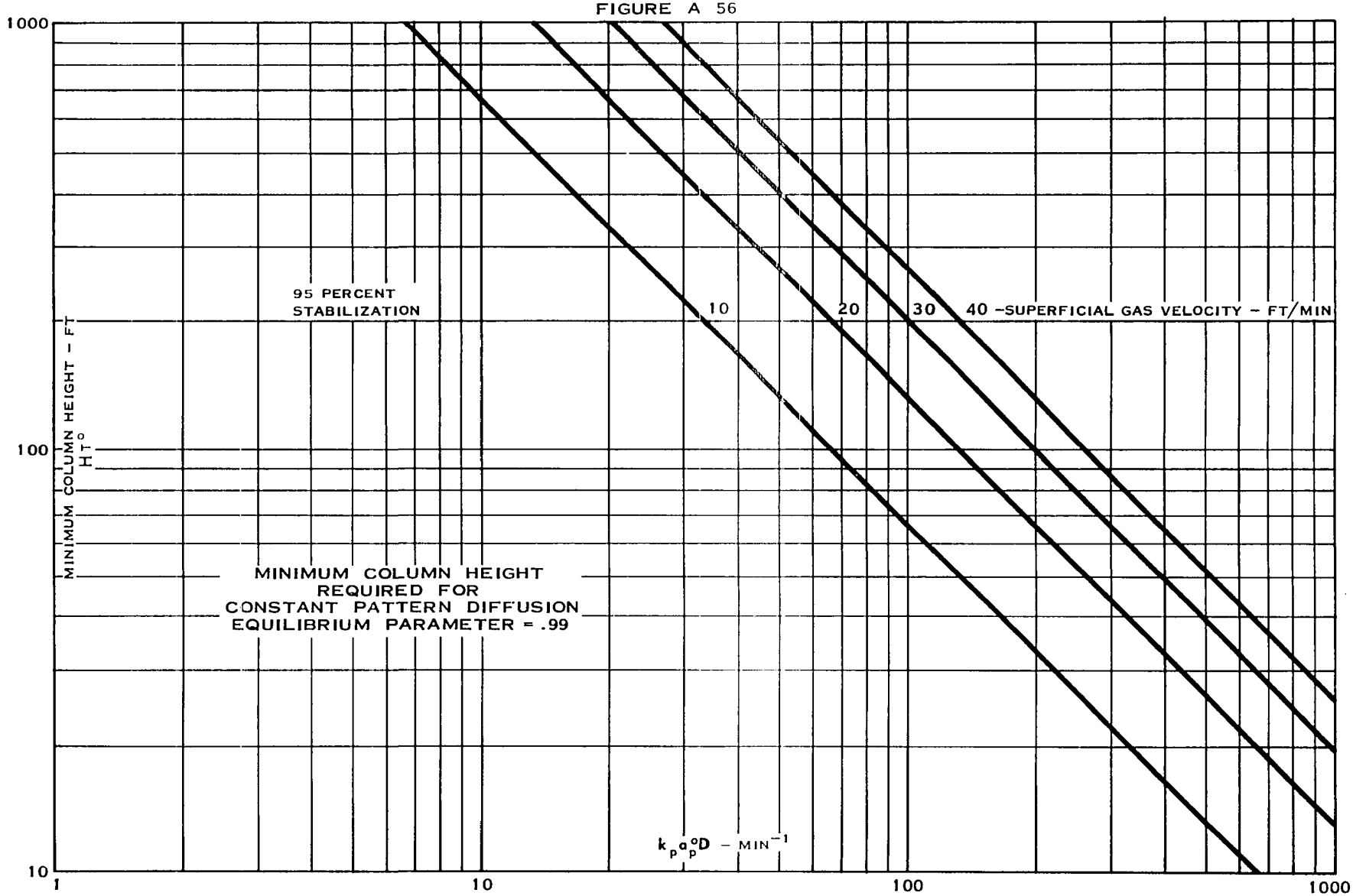
1000
100
10
1
10
100
1000
MINIMUM COLUMN HEIGHT - FT
H_T°
95 PERCENT
STABILIZATION
10
20
30
40 -SUPERFICIAL GAS VELOCITY - FT/MIN
MINIMUM COLUMN HEIGHT
REQUIRED FOR
CONSTANT PATTERN DIFFUSION
EQUILIBRIUM PARAMETER = .99
$k_p a_p^\circ D$ - MIN^{-1}

FIGURE A 57

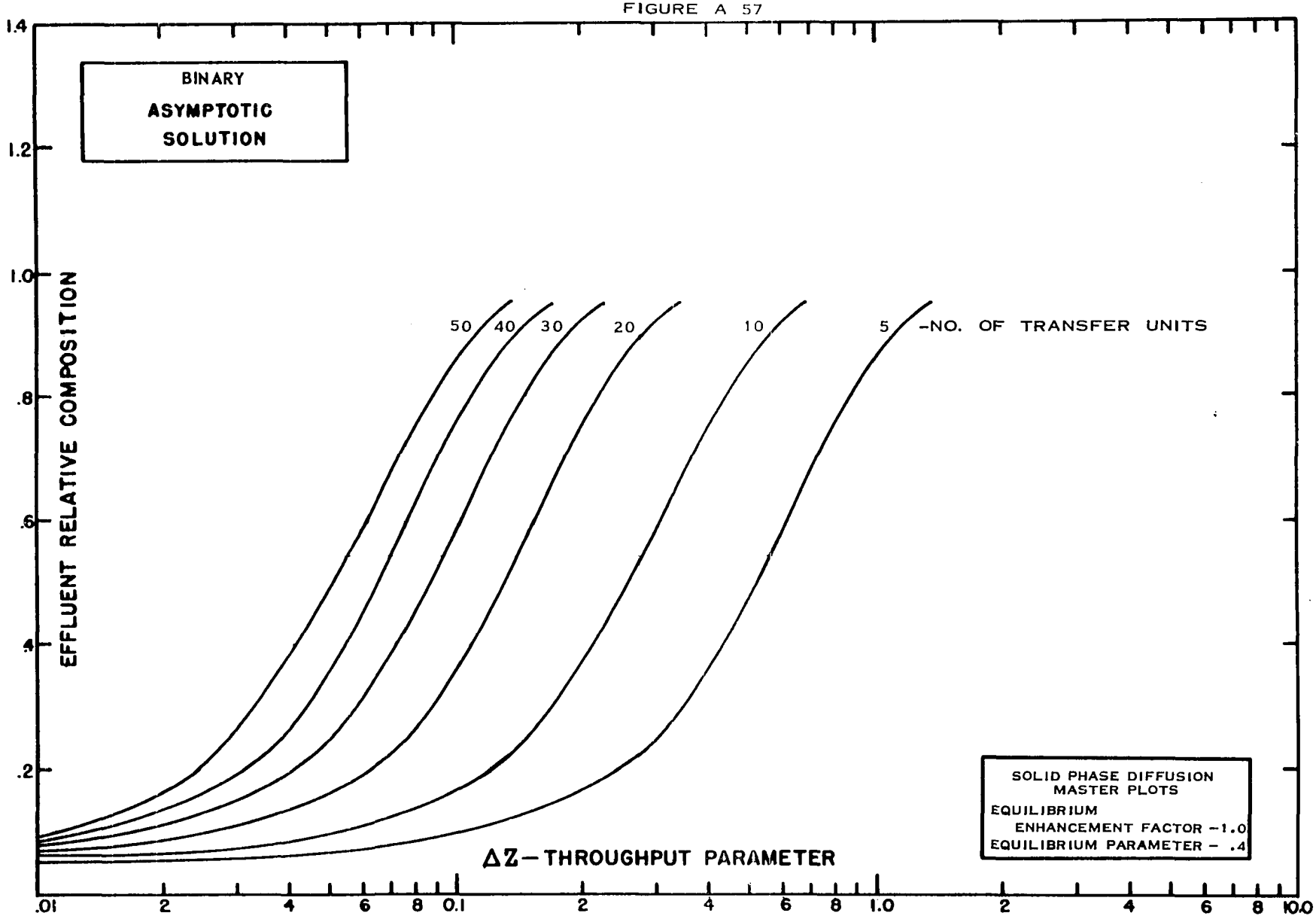
BINARY
ASYMPTOTIC
SOLUTION
EFFLUENT RELATIVE COMPOSITION
1.4
1.2
1.0
.8
.6
.4
.2
50
40
30
20
10
5
-NO. OF TRANSFER UNITS
ΔZ—THROUGHPUT PARAMETER
.01
2
4
6
8
0.1
2
4
6
8
1.0
2
4
6
8
10.0
SOLID PHASE DIFFUSION
MASTER PLOTS
EQUILIBRIUM
ENHANCEMENT FACTOR -1.0
EQUILIBRIUM PARAMETER - .4

FIGURE A 58

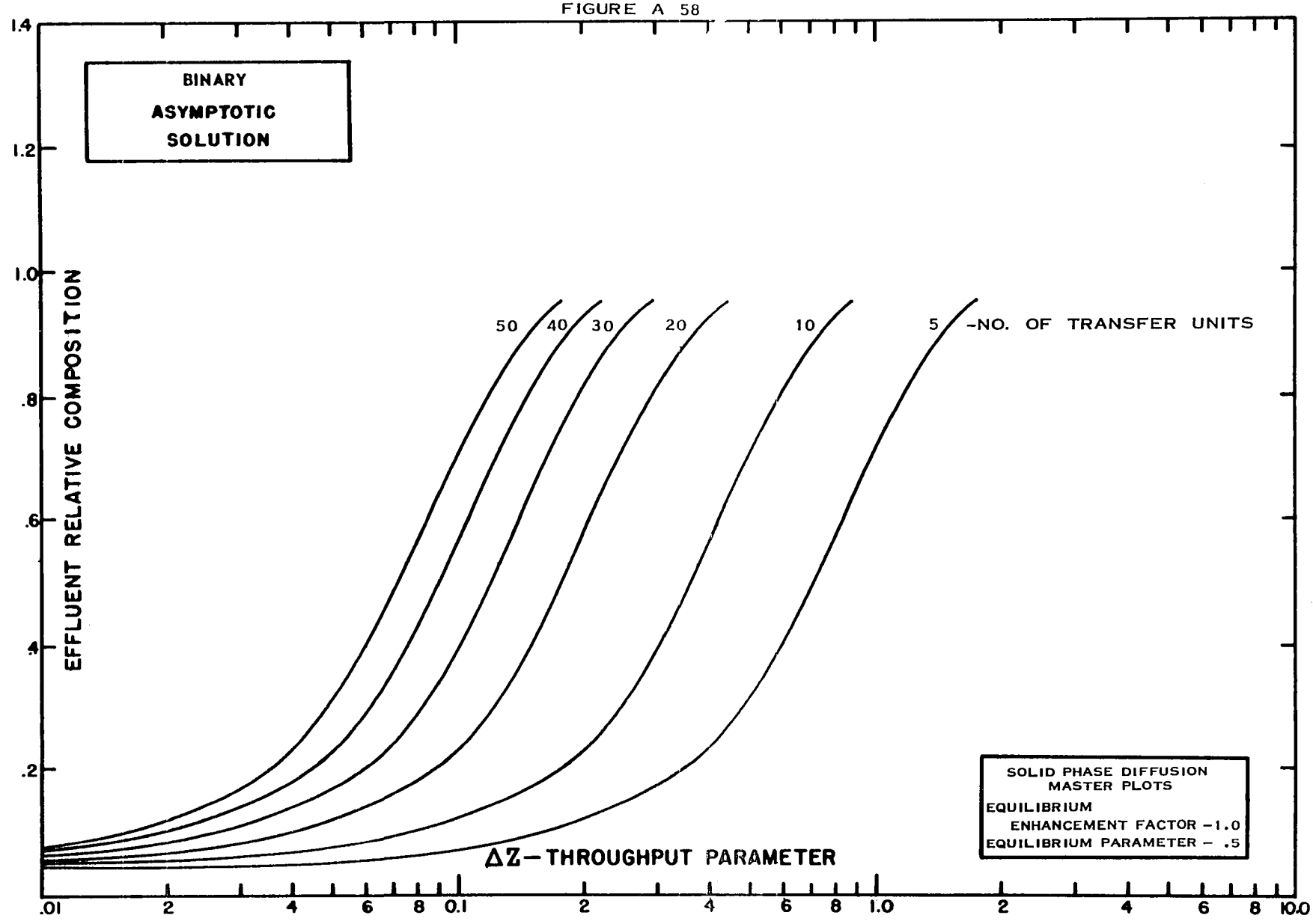
BINARY
ASYMPTOTIC
SOLUTION
EFFLUENT RELATIVE COMPOSITION
1.4
1.2
1.0
.8
.6
.4
.2
50
40
30
20
10
5
-NO. OF TRANSFER UNITS
ΔZ—THROUGHPUT PARAMETER
.01
2
4
6
8
0.1
2
4
6
8
1.0
2
4
6
8
10.0
SOLID PHASE DIFFUSION
MASTER PLOTS
EQUILIBRIUM
ENHANCEMENT FACTOR -1.0
EQUILIBRIUM PARAMETER - .5

FIGURE A 59

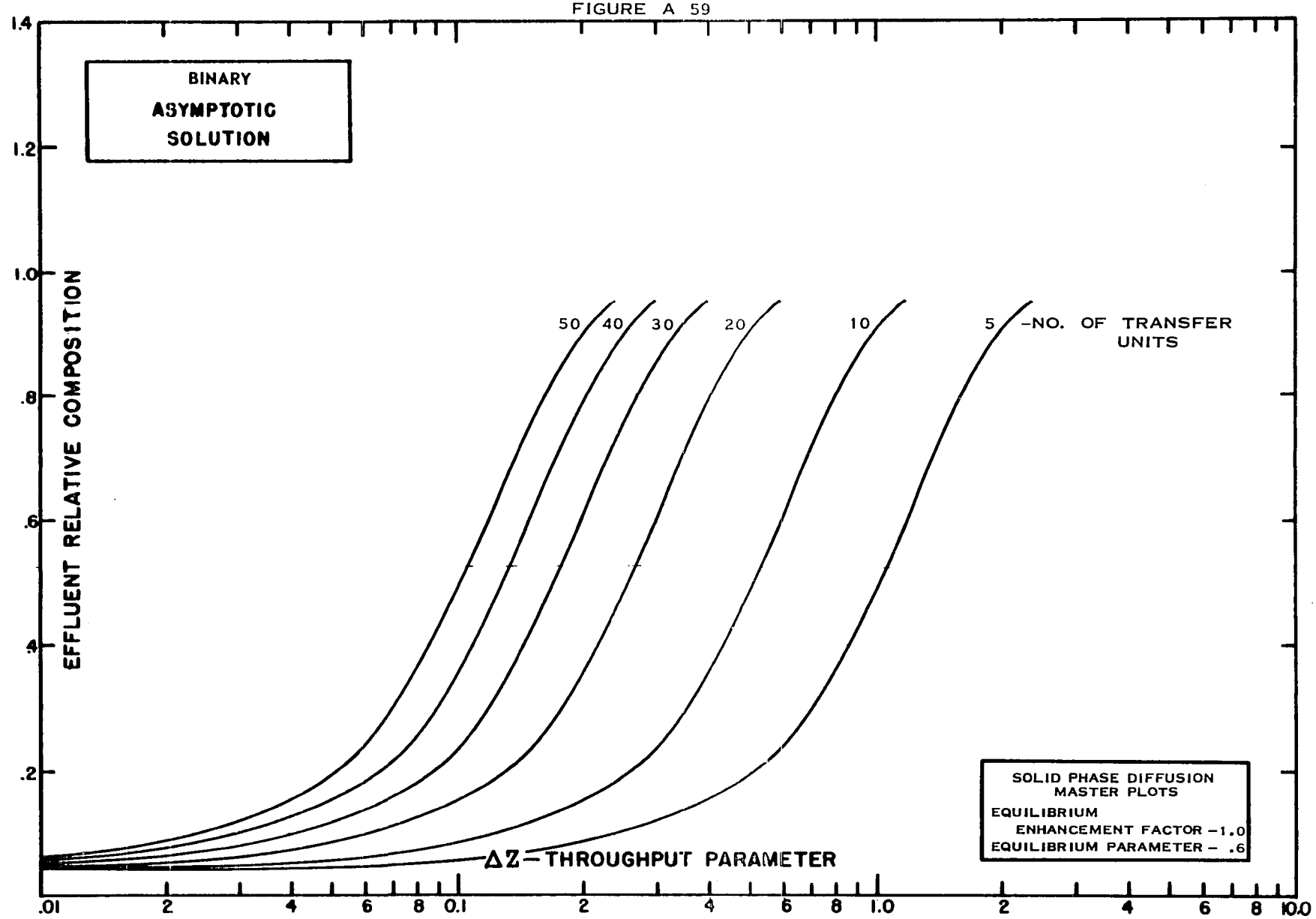
BINARY
ASYMPTOTIC
SOLUTION
EFFLUENT RELATIVE COMPOSITION
1.4
1.2
1.0
.8
.6
.4
.2
50
40
30
20
10
5
-NO. OF TRANSFER UNITS
SOLID PHASE DIFFUSION
MASTER PLOTS
EQUILIBRIUM
ENHANCEMENT FACTOR -1.0
EQUILIBRIUM PARAMETER - .6
ΔZ-THROUGHPUT PARAMETER
.01
2
4
6
8
0.1
2
4
6
8
1.0
2
4
6
8
10.0

FIGURE A 60

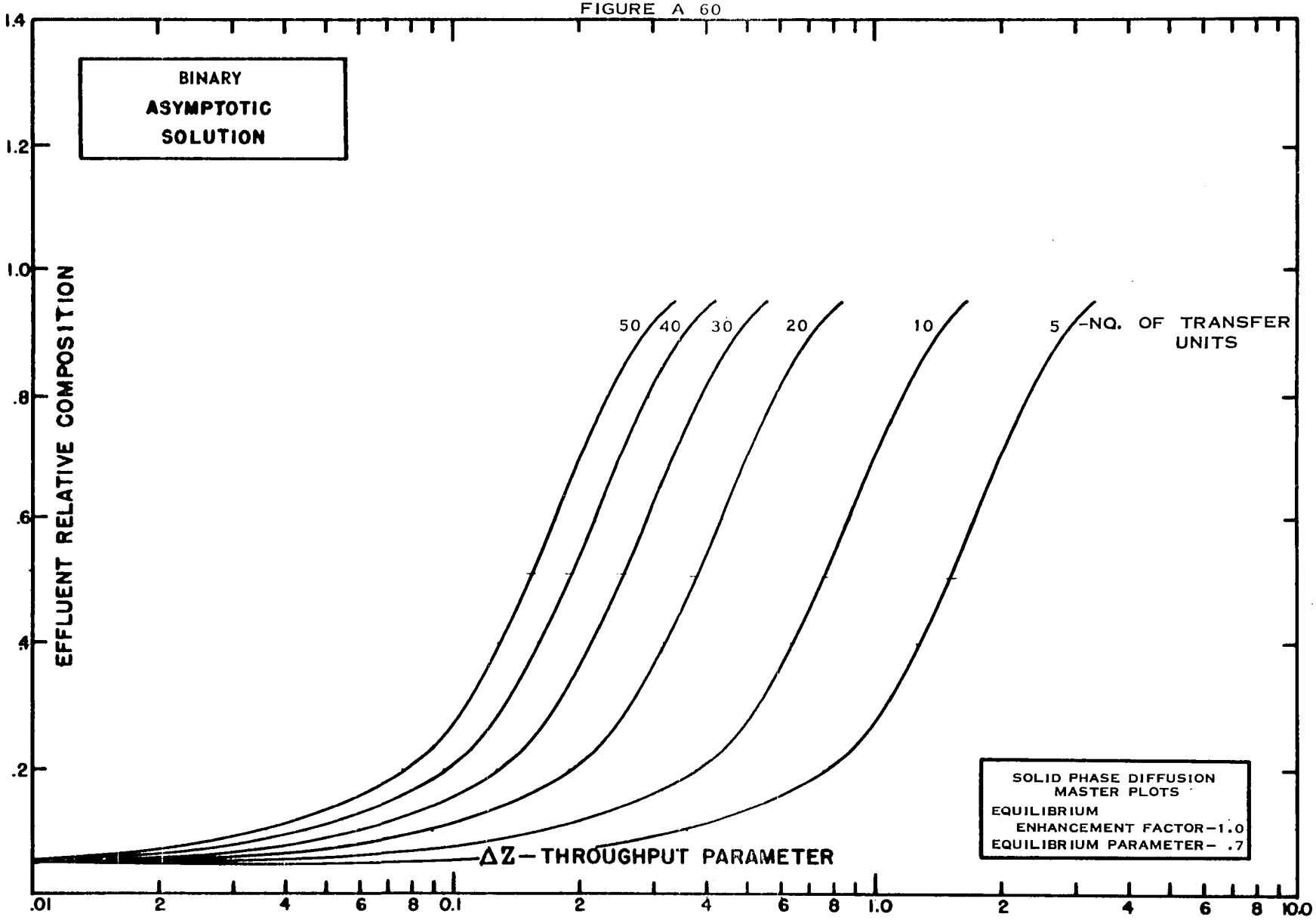
BINARY
ASYMPTOTIC
SOLUTION
EFFLUENT RELATIVE COMPOSITION
1.4
1.2
1.0
.8
.6
.4
.2
50
40
30
20
10
5
-NO. OF TRANSFER UNITS
ΔZ—THROUGHPUT PARAMETER
.01
2
4
6
8
0.1
2
4
6
8
1.0
2
4
6
8
10.0
SOLID PHASE DIFFUSION
MASTER PLOTS
EQUILIBRIUM
ENHANCEMENT FACTOR—1.0
EQUILIBRIUM PARAMETER— .7

FIGURE A 61

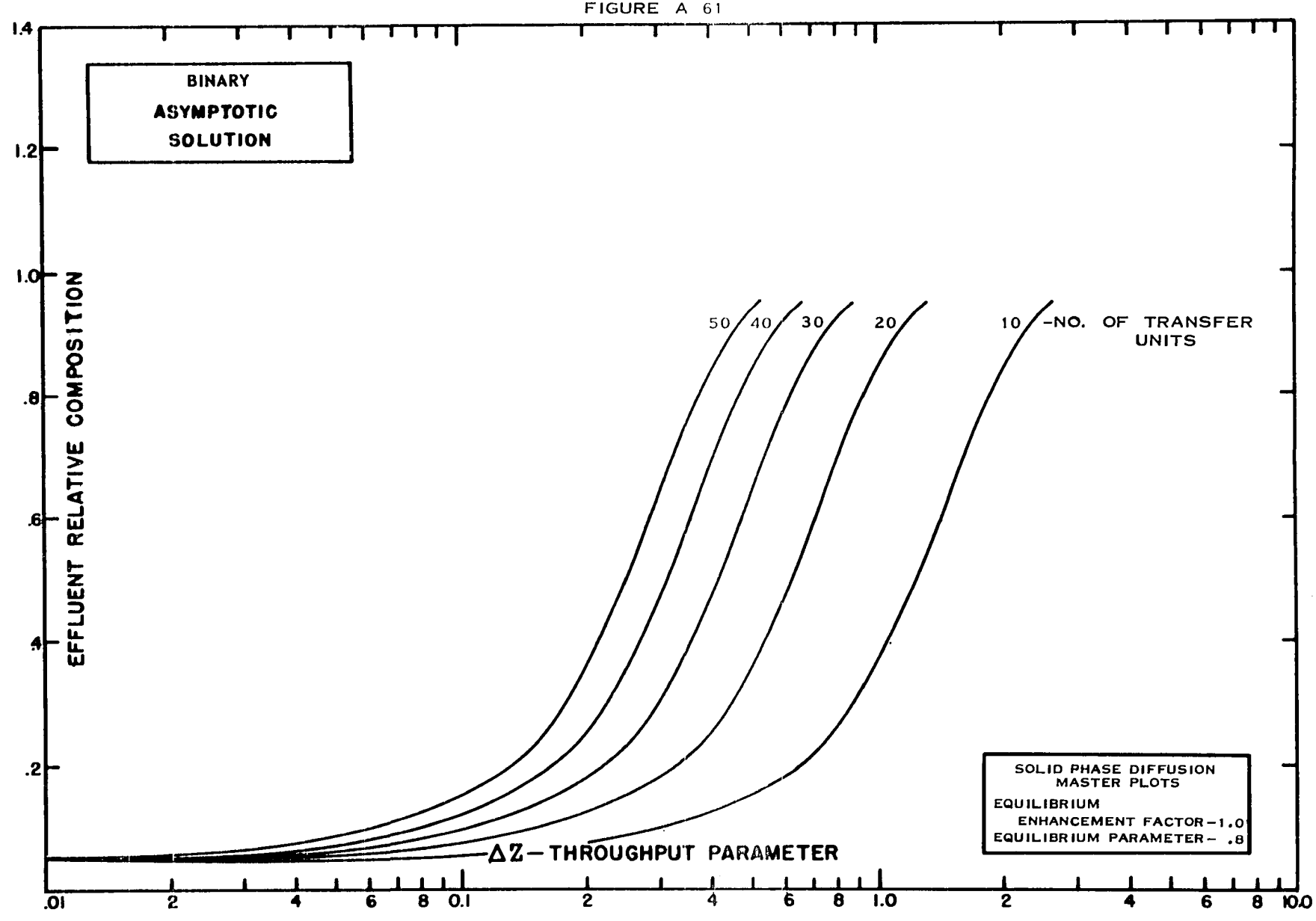
BINARY
ASYMPTOTIC
SOLUTION
EFFLUENT RELATIVE COMPOSITION
1.4
1.2
1.0
.8
.6
.4
.2
50
40
30
20
10
-NO. OF TRANSFER UNITS
SOLID PHASE DIFFUSION
MASTER PLOTS
EQUILIBRIUM
ENHANCEMENT FACTOR-1.0
EQUILIBRIUM PARAMETER- .8
ΔZ-THROUGHPUT PARAMETER
.01
2
4
6
8
0.1
2
4
6
8
1.0
2
4
6
8
10.0

FIGURE A 62

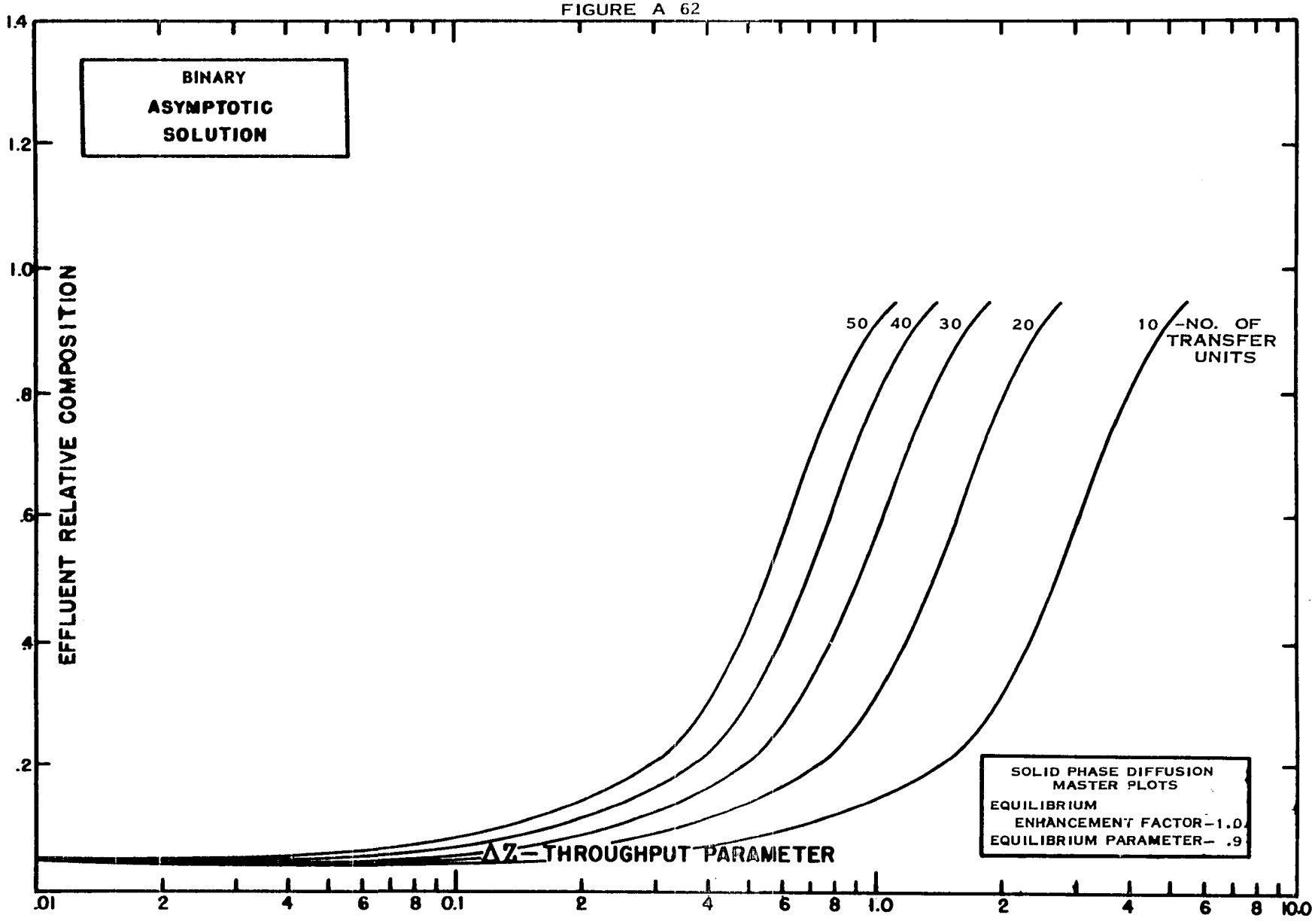
BINARY
ASYMPTOTIC
SOLUTION
EFFLUENT RELATIVE COMPOSITION
1.4
1.2
1.0
.8
.6
.4
.2
50
40
30
20
10
-NO. OF
TRANSFER
UNITS
SOLID PHASE DIFFUSION
MASTER PLOTS
EQUILIBRIUM
ENHANCEMENT FACTOR-1.0
EQUILIBRIUM PARAMETER- .9
ΔZ—THROUGHPUT PARAMETER
.01
2
4
6
8
0.1
2
4
6
8
1.0
2
4
6
8
10.0

FIGURE A 63

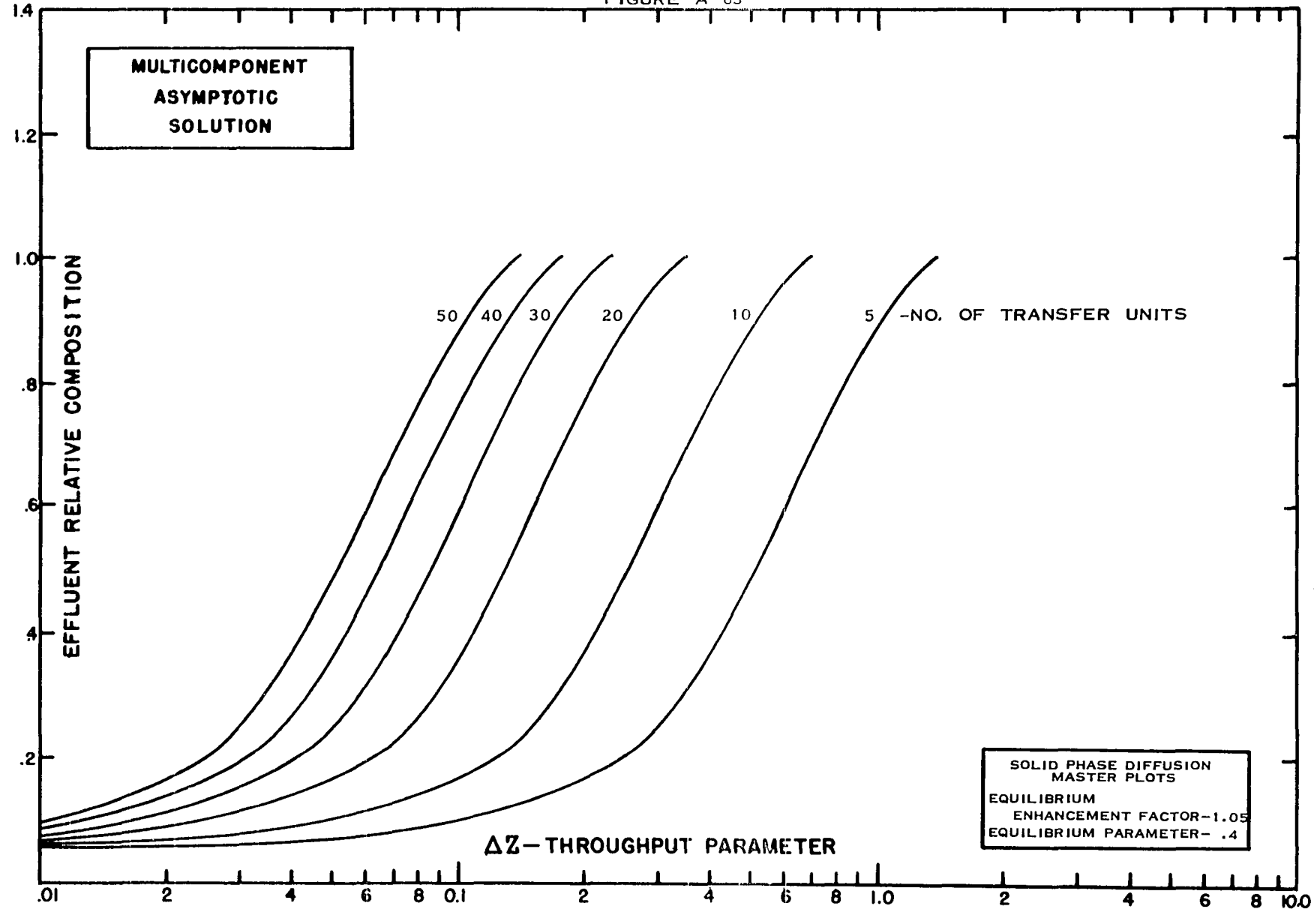
MULTICOMPONENT
ASYMPTOTIC
SOLUTION
EFFLUENT RELATIVE COMPOSITION
1.4
1.2
1.0
.8
.6
.4
.2
50
40
30
20
10
5
-NO. OF TRANSFER UNITS
ΔZ—THROUGHPUT PARAMETER
.01
2
4
6
8
0.1
2
4
6
8
1.0
2
4
6
8
10.0
SOLID PHASE DIFFUSION
MASTER PLOTS
EQUILIBRIUM
ENHANCEMENT FACTOR-1.05
EQUILIBRIUM PARAMETER- .4

FIGURE A 64

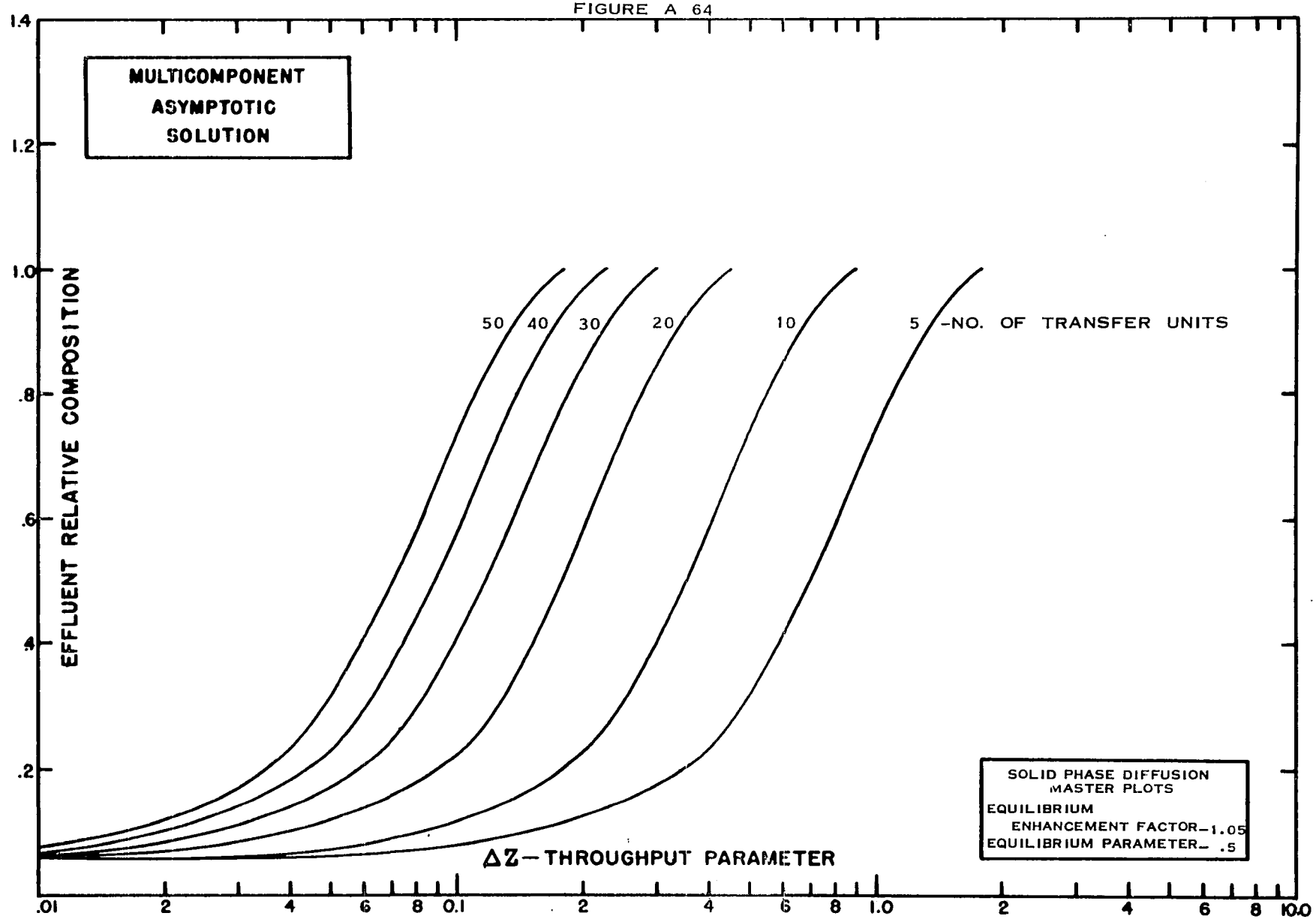
MULTICOMPONENT
ASYMPTOTIC
SOLUTION
EFFLUENT RELATIVE COMPOSITION
1.4
1.2
1.0
.8
.6
.4
.2
50
40
30
20
10
5
-NO. OF TRANSFER UNITS
SOLID PHASE DIFFUSION
MASTER PLOTS
EQUILIBRIUM
ENHANCEMENT FACTOR-1.05
EQUILIBRIUM PARAMETER- .5
ΔZ—THROUGHPUT PARAMETER
.01
2
4
6
8
0.1
2
4
6
8
1.0
2
4
6
8
10.0

FIGURE A 65

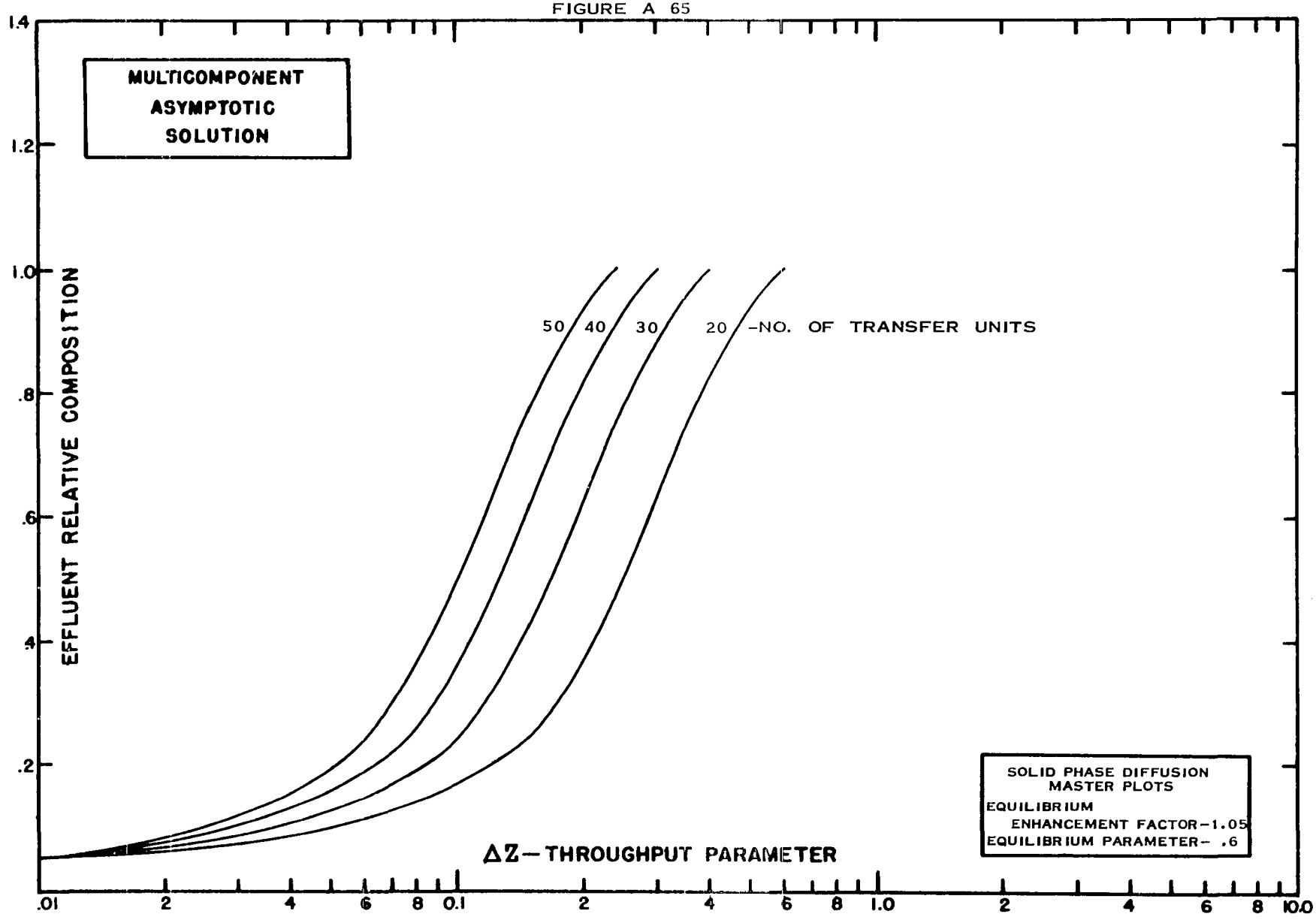
MULTICOMPONENT
ASYMPTOTIC
SOLUTION
EFFLUENT RELATIVE COMPOSITION
1.4
1.2
1.0
.8
.6
.4
.2
50
40
30
20
-NO. OF TRANSFER UNITS
ΔZ—THROUGHPUT PARAMETER
.01
2
4
6
8
0.1
2
4
6
8
1.0
2
4
6
8
10.0
SOLID PHASE DIFFUSION
MASTER PLOTS
EQUILIBRIUM
ENHANCEMENT FACTOR-1.05
EQUILIBRIUM PARAMETER- .6

FIGURE A 66

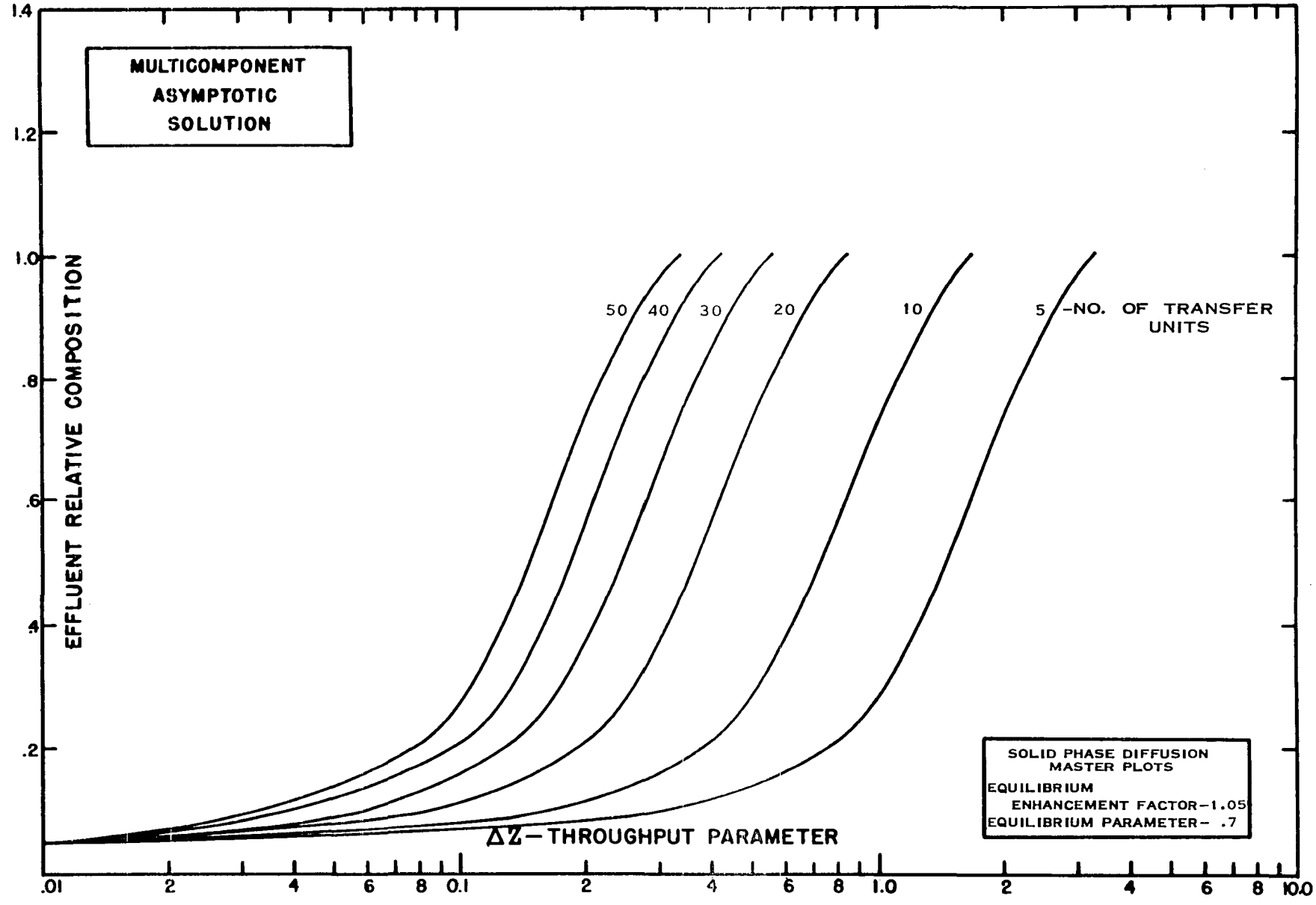
MULTICOMPONENT
ASYMPTOTIC
SOLUTION
EFFLUENT RELATIVE COMPOSITION
1.4
1.2
1.0
.8
.6
.4
.2
50
40
30
20
10
5
-NO. OF TRANSFER UNITS
ΔZ—THROUGHPUT PARAMETER
.01
2
4
6
8
0.1
2
4
6
8
1.0
2
4
6
8
10.0
SOLID PHASE DIFFUSION
MASTER PLOTS
EQUILIBRIUM
ENHANCEMENT FACTOR-1.05
EQUILIBRIUM PARAMETER- .7

FIGURE A 67

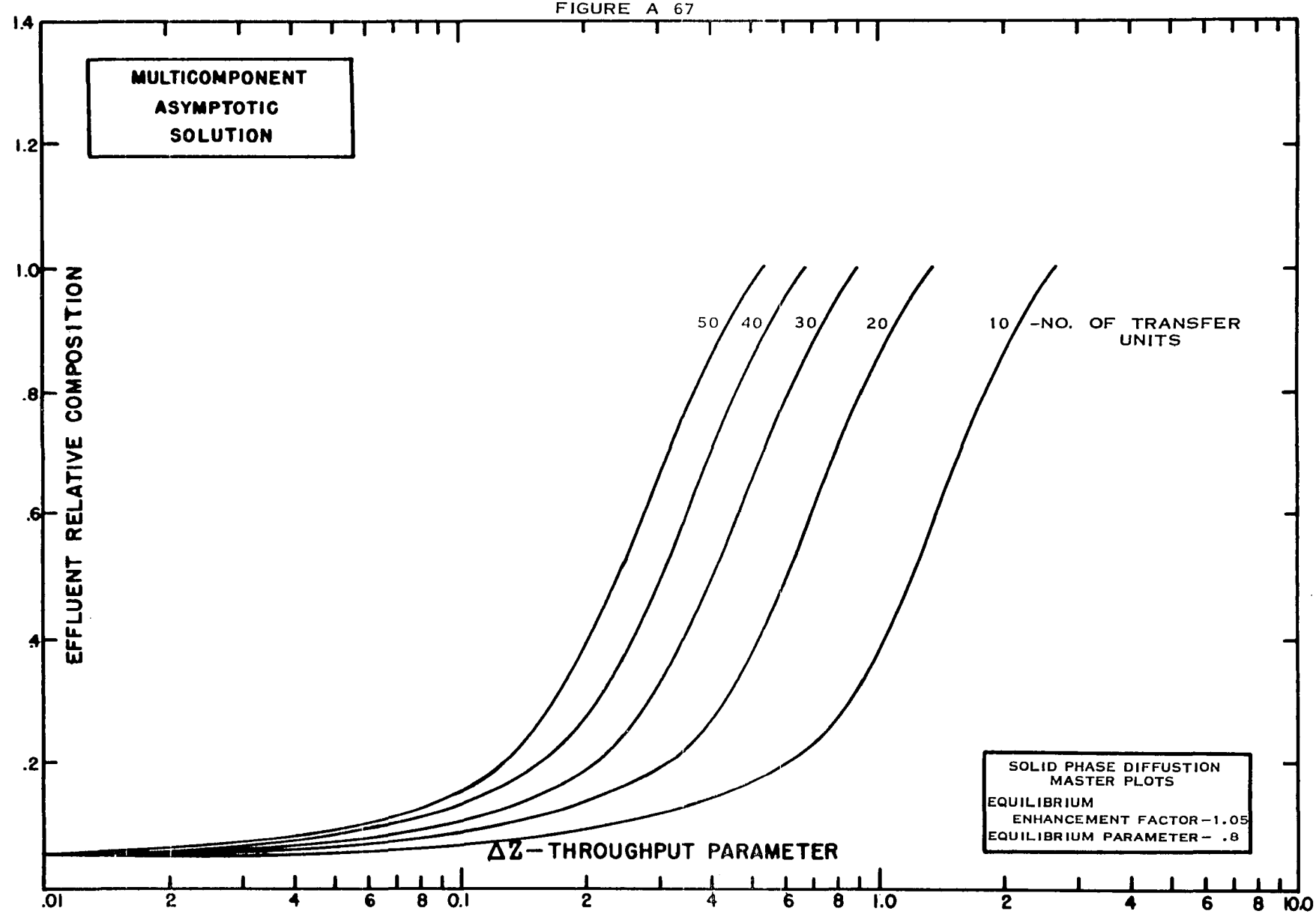
MULTICOMPONENT
ASYMPTOTIC
SOLUTION
EFFLUENT RELATIVE COMPOSITION
1.4
1.2
1.0
.8
.6
.4
.2
50
40
30
20
10
-NO. OF TRANSFER UNITS
SOLID PHASE DIFFUSTION
MASTER PLOTS
EQUILIBRIUM
ENHANCEMENT FACTOR-1.05
EQUILIBRIUM PARAMETER- .8
ΔZ-THROUGHPUT PARAMETER
.01
2
4
6
8
0.1
2
4
6
8
1.0
2
4
6
8
10.0

FIGURE A 68

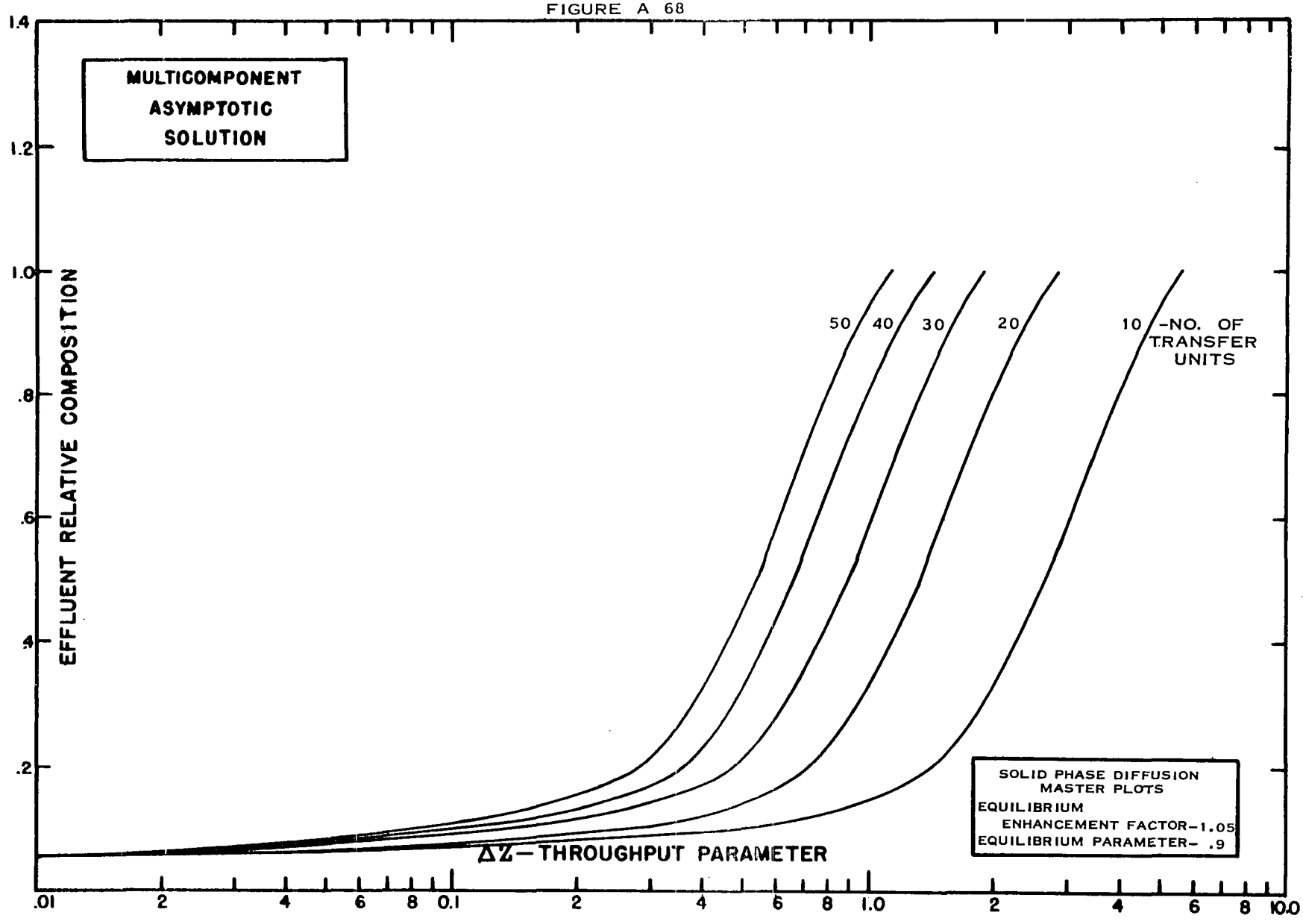
MULTICOMPONENT
ASYMPTOTIC
SOLUTION
EFFLUENT RELATIVE COMPOSITION
1.4
1.2
1.0
.8
.6
.4
.2
50
40
30
20
10
-NO. OF
TRANSFER
UNITS
SOLID PHASE DIFFUSION
MASTER PLOTS
EQUILIBRIUM
ENHANCEMENT FACTOR-1.05
EQUILIBRIUM PARAMETER- .9
ΔZ—THROUGHPUT PARAMETER
.01
2
4
6
8
0.1
2
4
6
8
1.0
2
4
6
8
10.0

FIGURE A 69

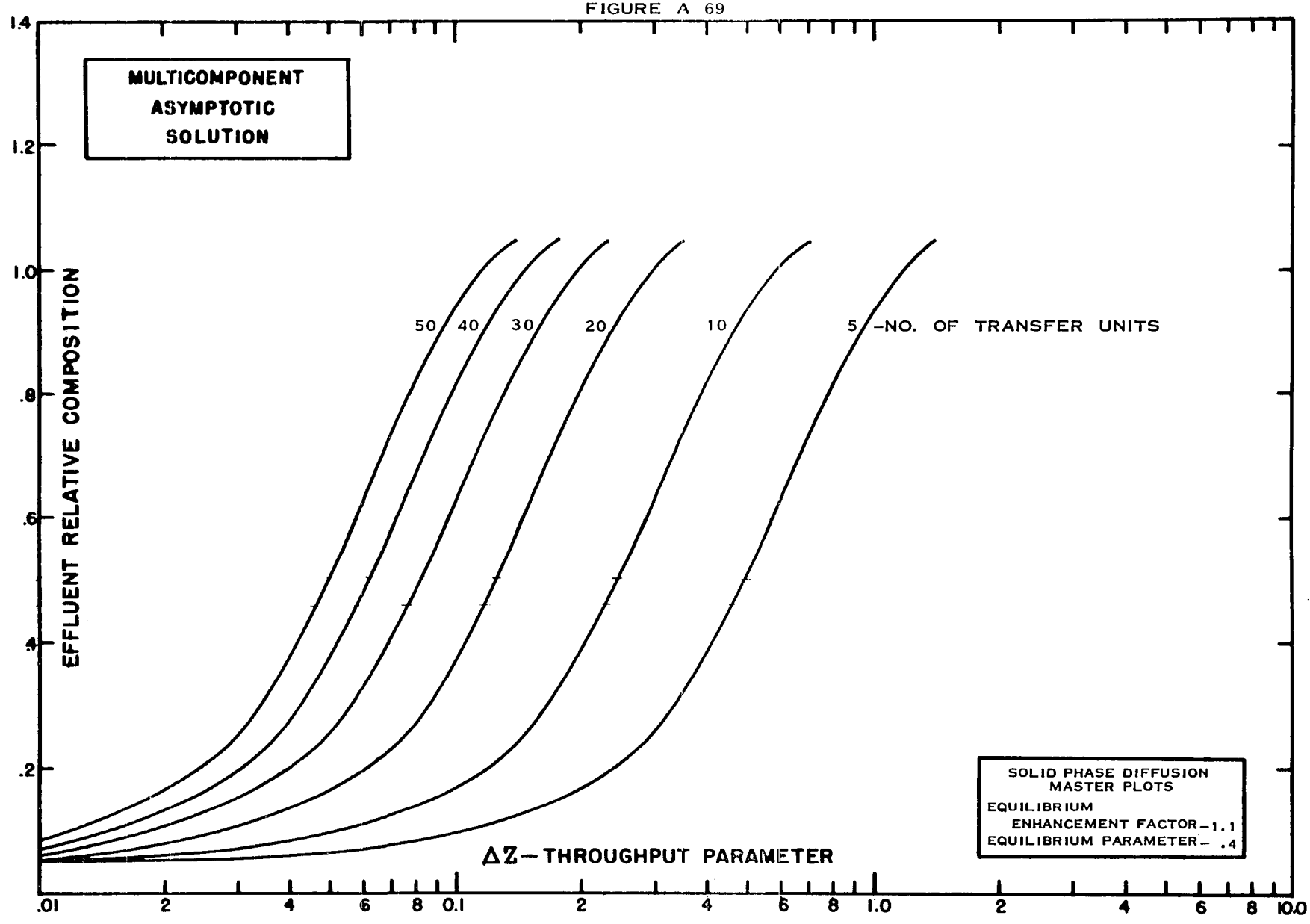
MULTICOMPONENT
ASYMPTOTIC
SOLUTION
EFFLUENT RELATIVE COMPOSITION
1.4
1.2
1.0
.8
.6
.4
.2
50
40
30
20
10
5
-NO. OF TRANSFER UNITS
ΔZ—THROUGHPUT PARAMETER
.01
2
4
6
8
0.1
2
4
6
8
1.0
2
4
6
8
10.0
SOLID PHASE DIFFUSION
MASTER PLOTS
EQUILIBRIUM
ENHANCEMENT FACTOR—1.1
EQUILIBRIUM PARAMETER— .4

FIGURE A 70

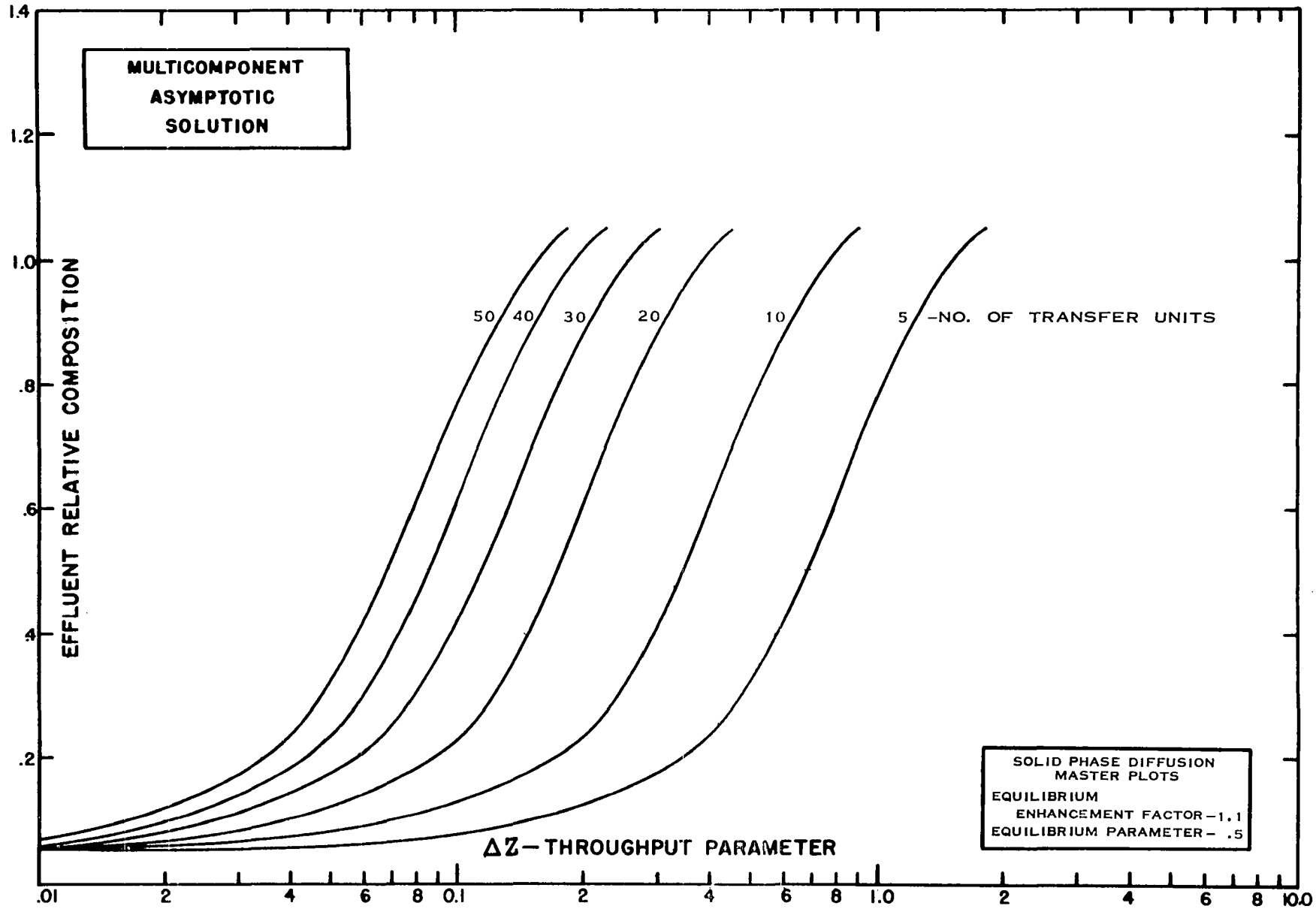
MULTICOMPONENT
ASYMPTOTIC
SOLUTION
EFFLUENT RELATIVE COMPOSITION
1.4
1.2
1.0
.8
.6
.4
.2
50
40
30
20
10
5
-NO. OF TRANSFER UNITS
SOLID PHASE DIFFUSION
MASTER PLOTS
EQUILIBRIUM
ENHANCEMENT FACTOR-1.1
EQUILIBRIUM PARAMETER- .5
ΔZ-THROUGHPUT PARAMETER
.01
2
4
6
8
0.1
2
4
6
8
1.0
2
4
6
8
10.0

FIGURE A 71

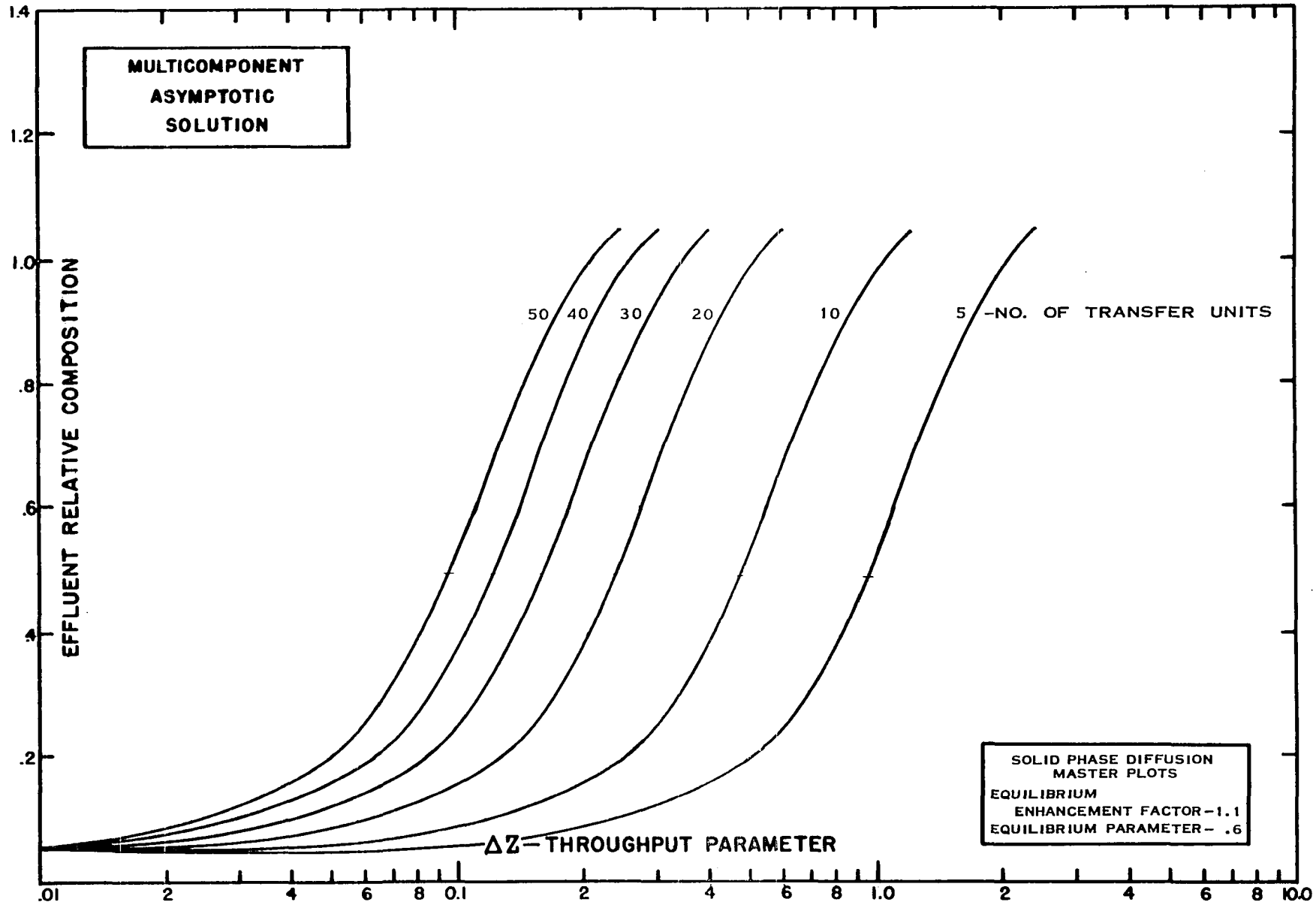
MULTICOMPONENT
ASYMPTOTIC
SOLUTION
EFFLUENT RELATIVE COMPOSITION
1.4
1.2
1.0
.8
.6
.4
.2
50
40
30
20
10
5
-NO. OF TRANSFER UNITS
SOLID PHASE DIFFUSION
MASTER PLOTS
EQUILIBRIUM
ENHANCEMENT FACTOR-1.1
EQUILIBRIUM PARAMETER- .6
ΔZ-THROUGHPUT PARAMETER
.01
2
4
6
8
0.1
2
4
6
8
1.0
2
4
6
8
10.0

FIGURE A 72

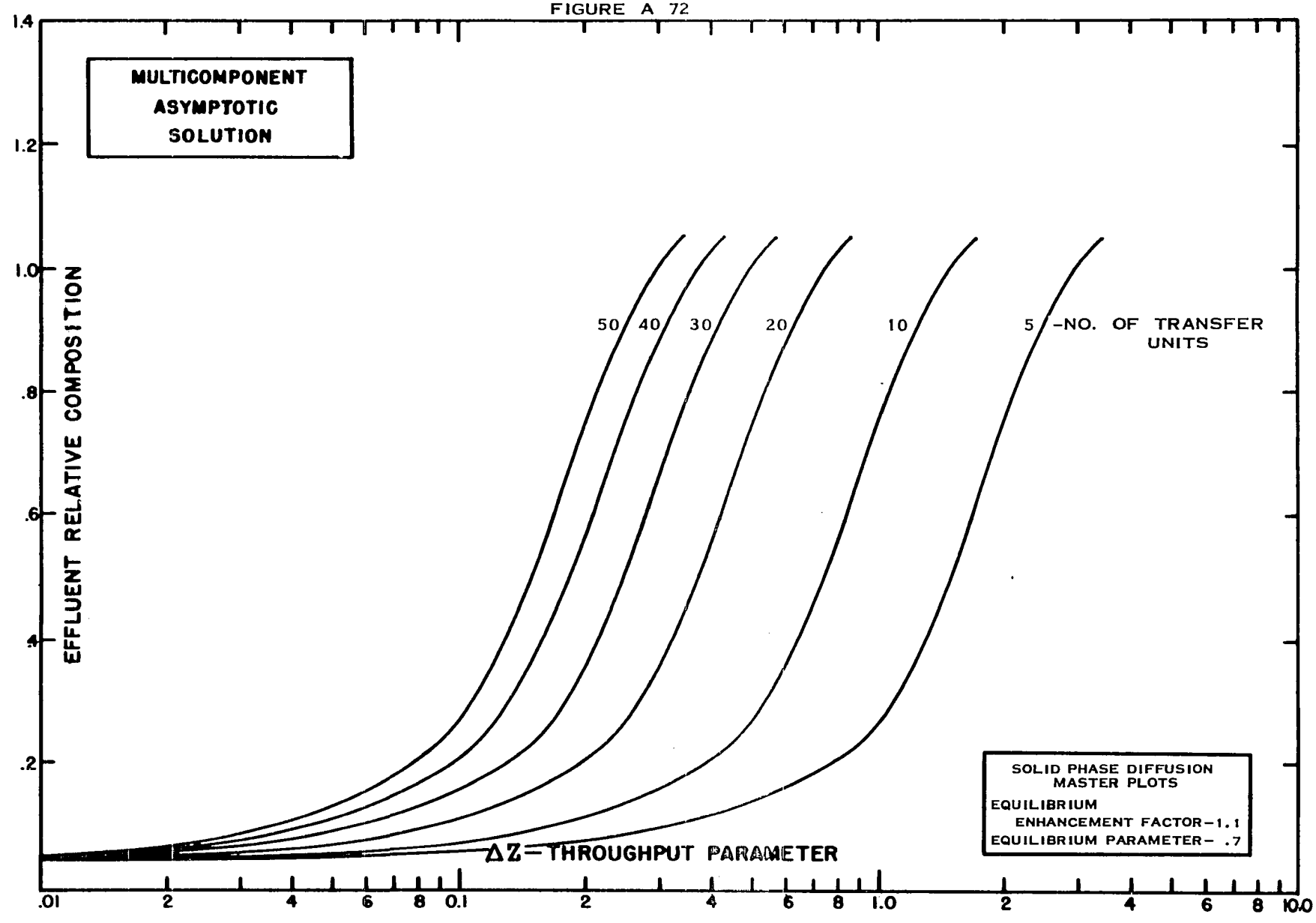
MULTICOMPONENT
ASYMPTOTIC
SOLUTION
EFFLUENT RELATIVE COMPOSITION
1.4
1.2
1.0
.8
.6
.4
.2
50
40
30
20
10
5
-NO. OF TRANSFER UNITS
SOLID PHASE DIFFUSION
MASTER PLOTS
EQUILIBRIUM
ENHANCEMENT FACTOR-1.1
EQUILIBRIUM PARAMETER- .7
ΔZ—THROUGHPUT PARAMETER
.01
2
4
6
8
0.1
2
4
6
8
1.0
2
4
6
8
10.0

FIGURE A 73

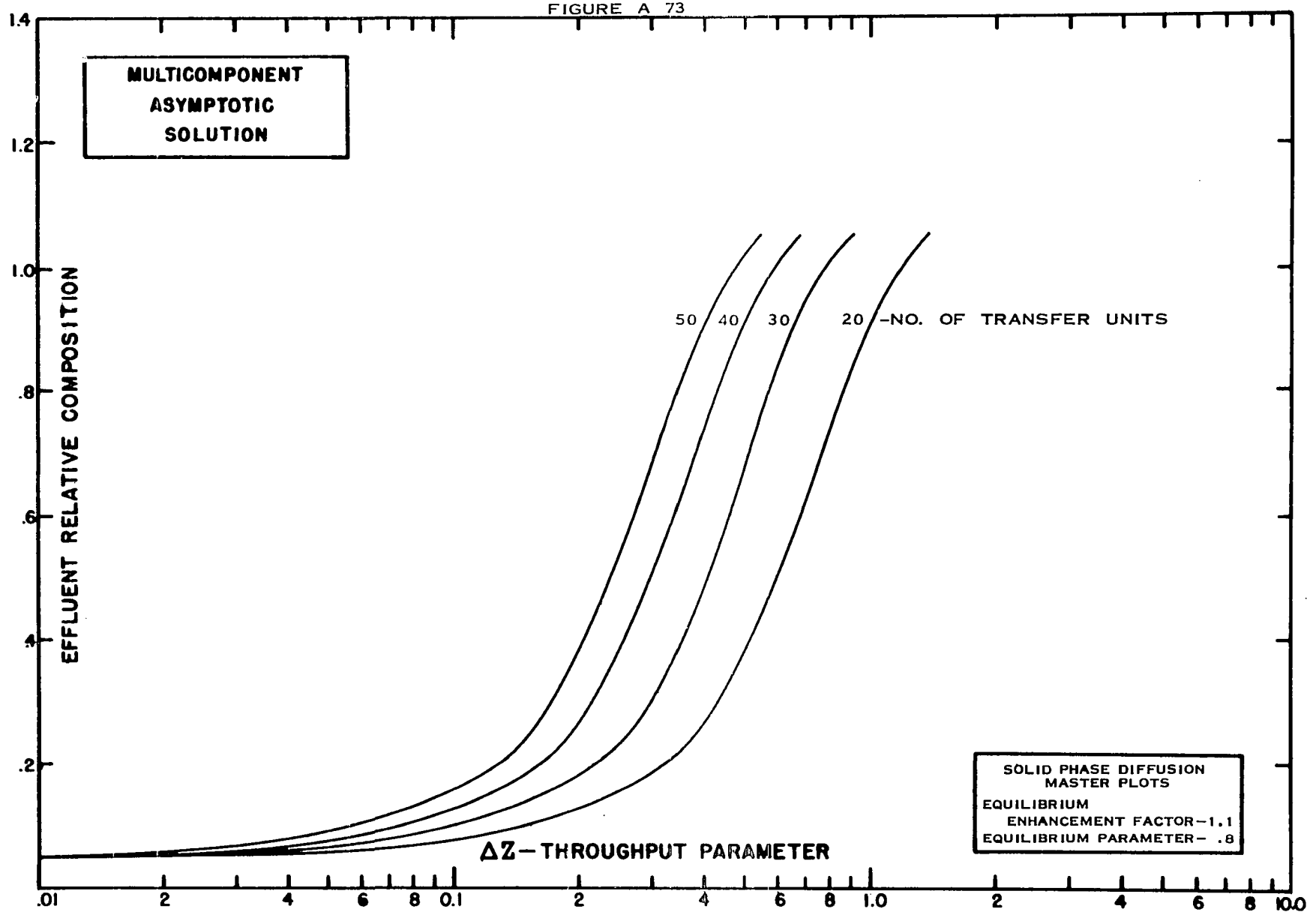
MULTICOMPONENT
ASYMPTOTIC
SOLUTION
EFFLUENT RELATIVE COMPOSITION
1.4
1.2
1.0
.8
.6
.4
.2
50
40
30
20
-NO. OF TRANSFER UNITS
SOLID PHASE DIFFUSION
MASTER PLOTS
EQUILIBRIUM
ENHANCEMENT FACTOR-1.1
EQUILIBRIUM PARAMETER- .8
ΔZ-THROUGHPUT PARAMETER
.01
2
4
6
8
0.1
2
4
6
8
1.0
2
4
6
8
10.0

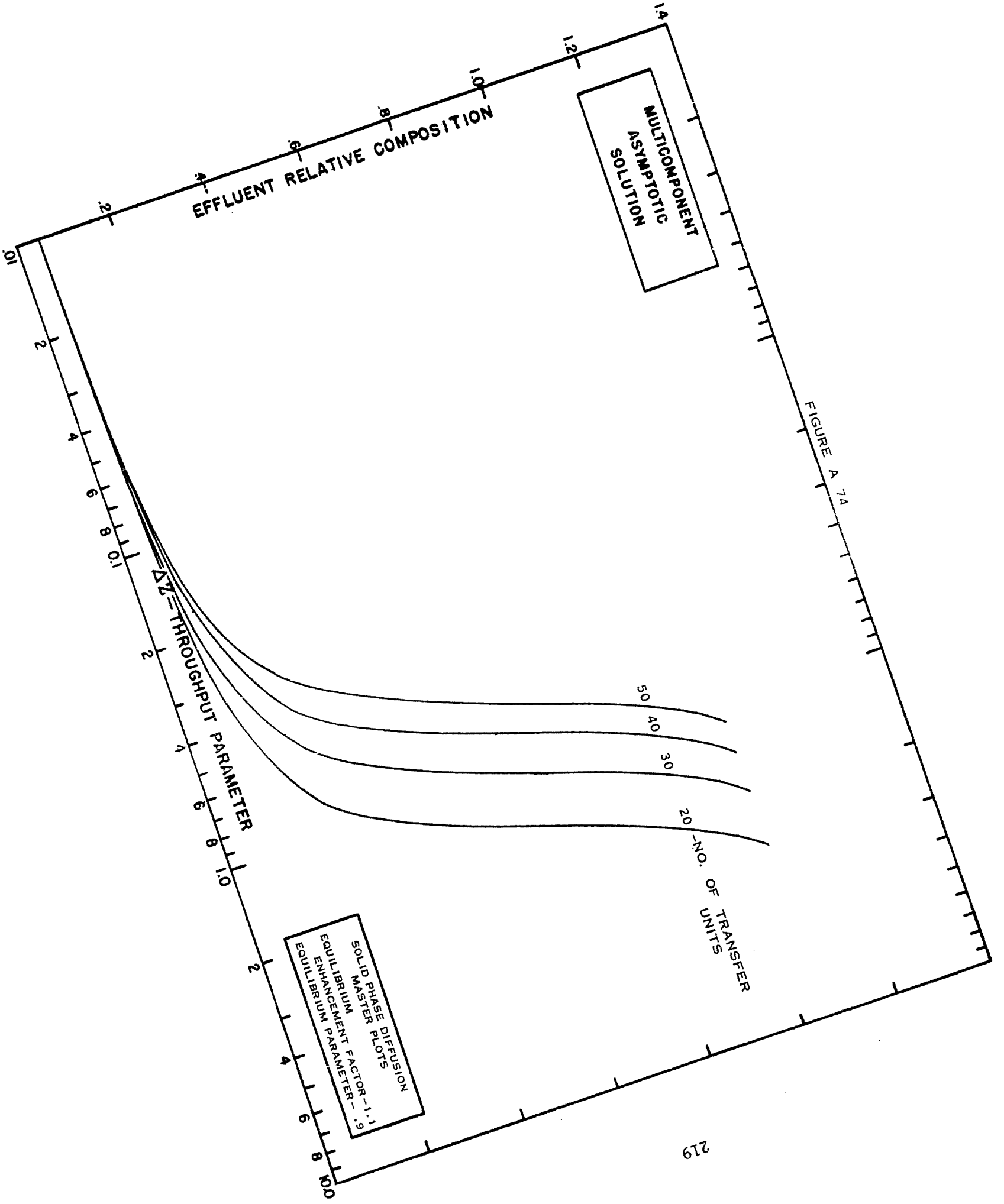
EFFLUENT RELATIVE COMPOSITION
.2
.4
.6
.8
1.0
1.2
1.4
MULTICOMPONENT ASYMPTOTIC SOLUTION
.01
2
4
6
8
0.1
2
4
6
8
1.0
2
4
6
8
10.0
ΔZ=THROUGHPUT PARAMETER
50
40
30
20
NO. OF TRANSFER UNITS
SOLID PHASE DIFFUSION MASTER PLOTS
EQUILIBRIUM ENHANCEMENT FACTOR-1.1
EQUILIBRIUM PARAMETER – .9

FIGURE A 74

FIGURE A 75

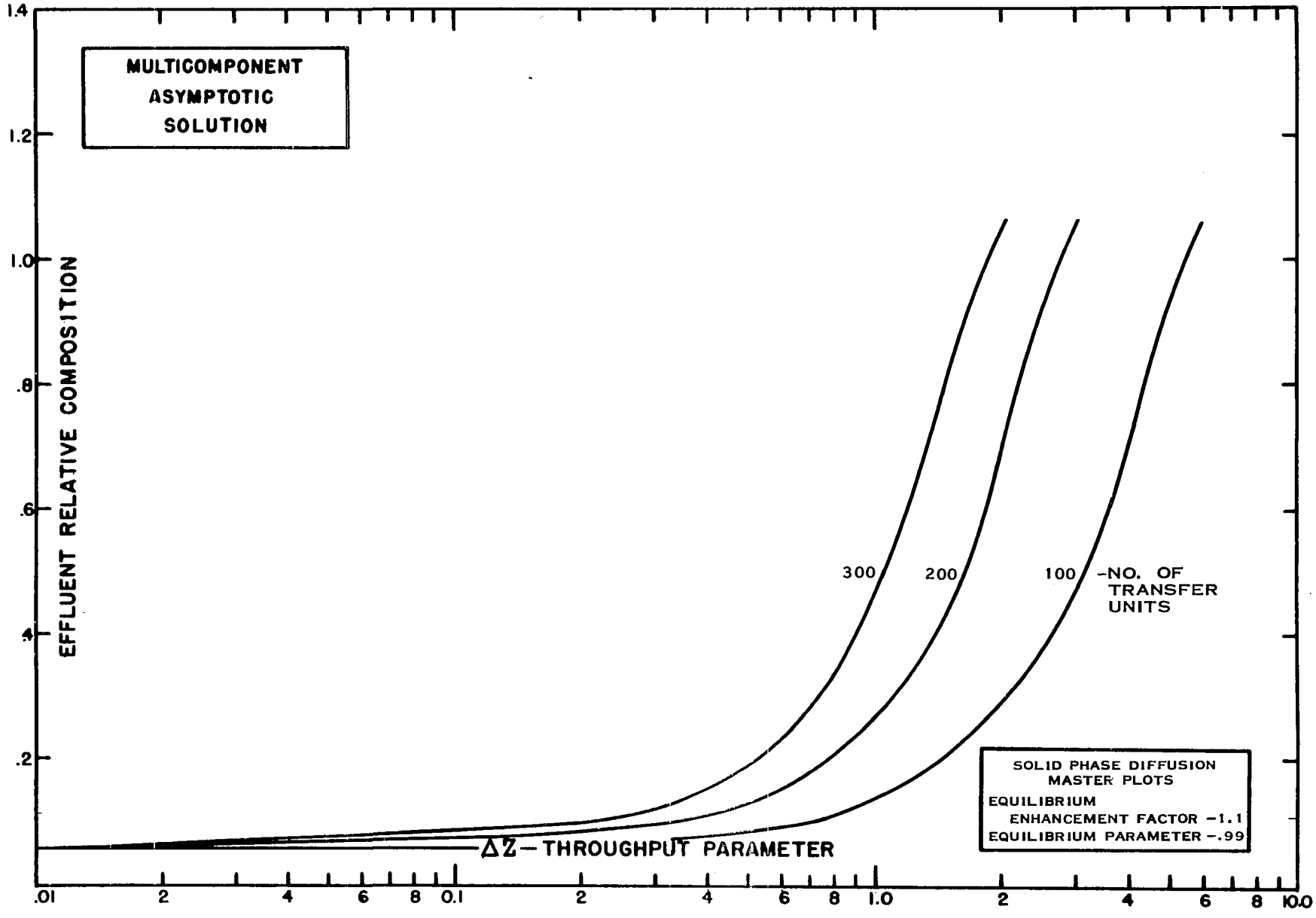
MULTICOMPONENT
ASYMPTOTIC
SOLUTION
EFFLUENT RELATIVE COMPOSITION
1.4
1.2
1.0
.8
.6
.4
.2
300
200
100
-NO. OF
TRANSFER
UNITS
SOLID PHASE DIFFUSION
MASTER PLOTS
EQUILIBRIUM
ENHANCEMENT FACTOR -1.1
EQUILIBRIUM PARAMETER -.99
ΔZ - THROUGHPUT PARAMETER
.01
2
4
6
8
0.1
2
4
6
8
1.0
2
4
6
8
10.0

FIGURE A 76

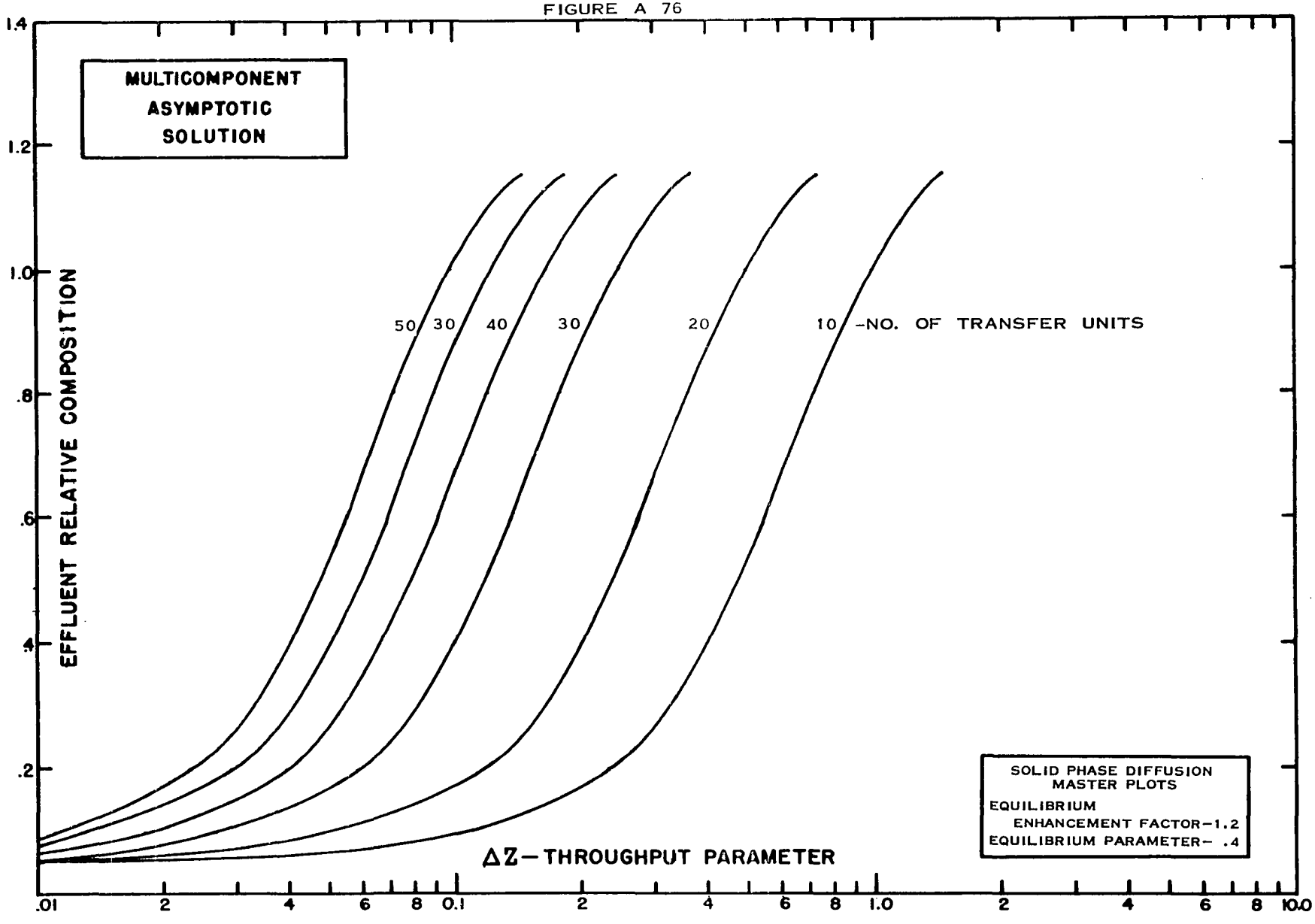
MULTICOMPONENT
ASYMPTOTIC
SOLUTION
EFFLUENT RELATIVE COMPOSITION
1.4
1.2
1.0
.8
.6
.4
.2
50
30
40
30
20
10
-NO. OF TRANSFER UNITS
SOLID PHASE DIFFUSION
MASTER PLOTS
EQUILIBRIUM
ENHANCEMENT FACTOR-1.2
EQUILIBRIUM PARAMETER- .4
ΔZ-THROUGHPUT PARAMETER
.01
2
4
6
8
0.1
2
4
6
8
1.0
2
4
6
8
10.0

FIGURE A 77

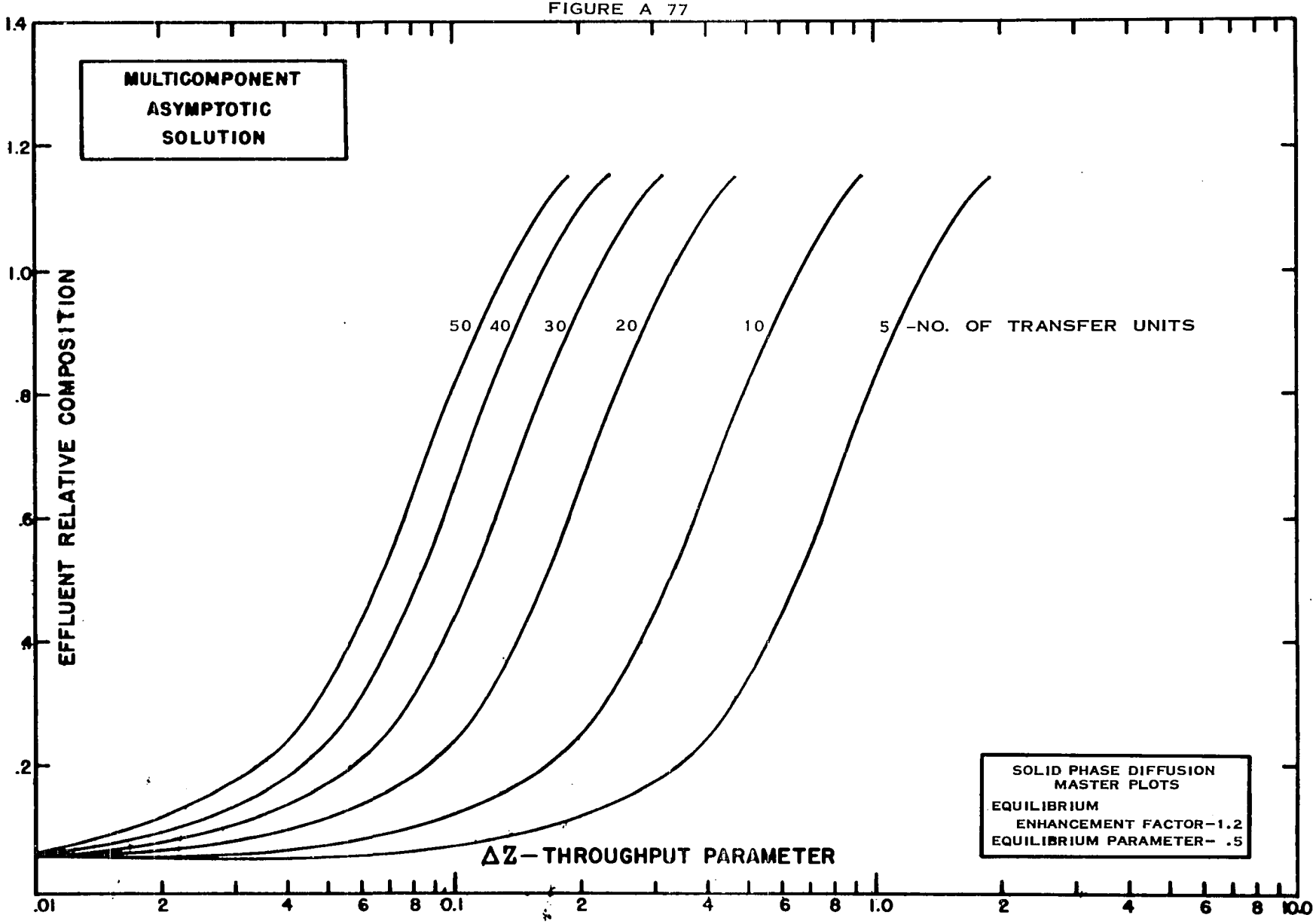
MULTICOMPONENT
ASYMPTOTIC
SOLUTION
EFFLUENT RELATIVE COMPOSITION
1.4
1.2
1.0
.8
.6
.4
.2
50
40
30
20
10
5
-NO. OF TRANSFER UNITS
ΔZ—THROUGHPUT PARAMETER
.01
2
4
6
8
0.1
2
4
6
8
1.0
2
4
6
8
10.0
SOLID PHASE DIFFUSION
MASTER PLOTS
EQUILIBRIUM
ENHANCEMENT FACTOR-1.2
EQUILIBRIUM PARAMETER- .5

FIGURE A 78

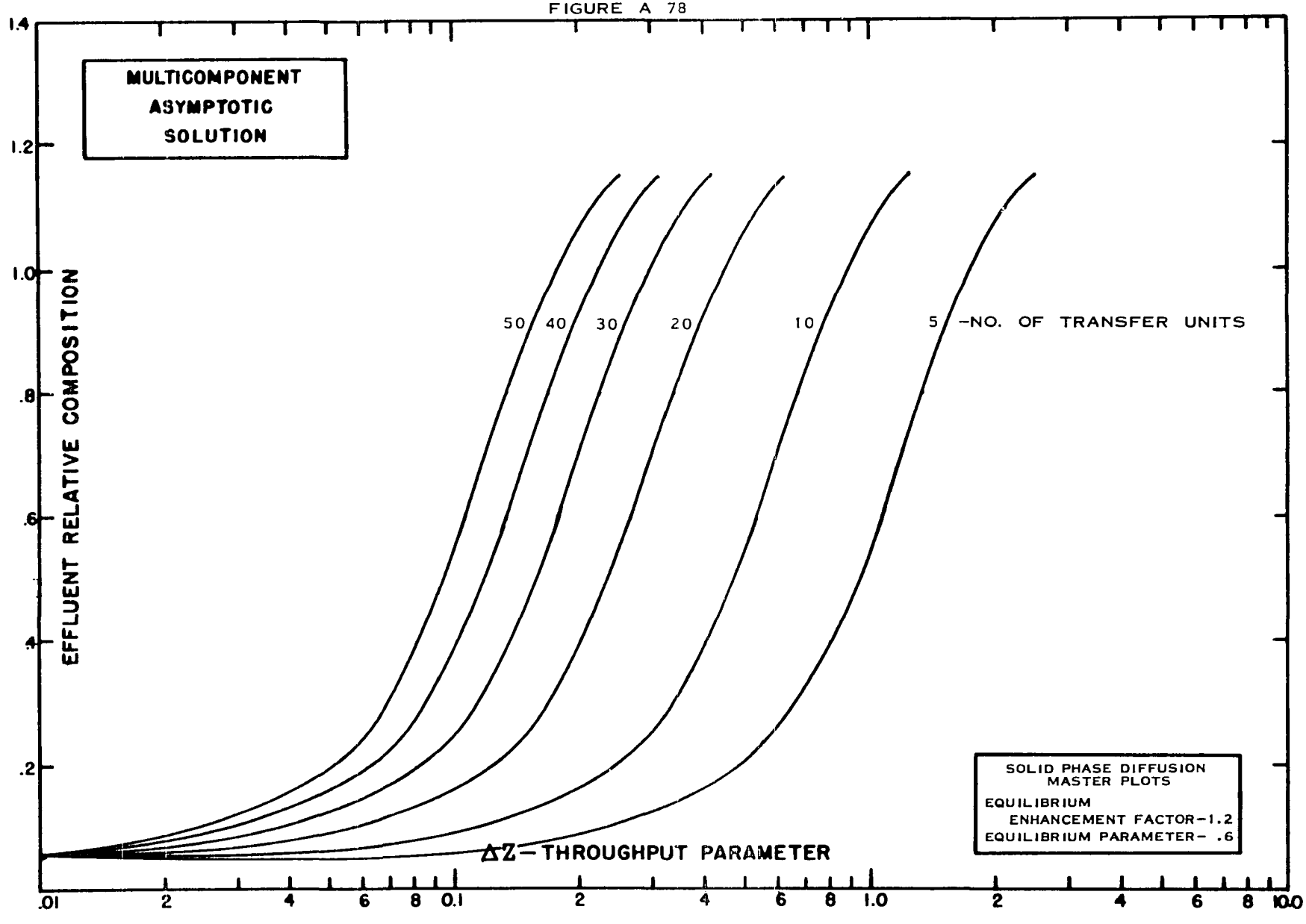
MULTICOMPONENT
ASYMPTOTIC
SOLUTION
EFFLUENT RELATIVE COMPOSITION
1.4
1.2
1.0
.8
.6
.4
.2
50
40
30
20
10
5
-NO. OF TRANSFER UNITS
ΔZ—THROUGHPUT PARAMETER
.01
2
4
6
8
0.1
2
4
6
8
1.0
2
4
6
8
10.0
SOLID PHASE DIFFUSION
MASTER PLOTS
EQUILIBRIUM
ENHANCEMENT FACTOR-1.2
EQUILIBRIUM PARAMETER- .6

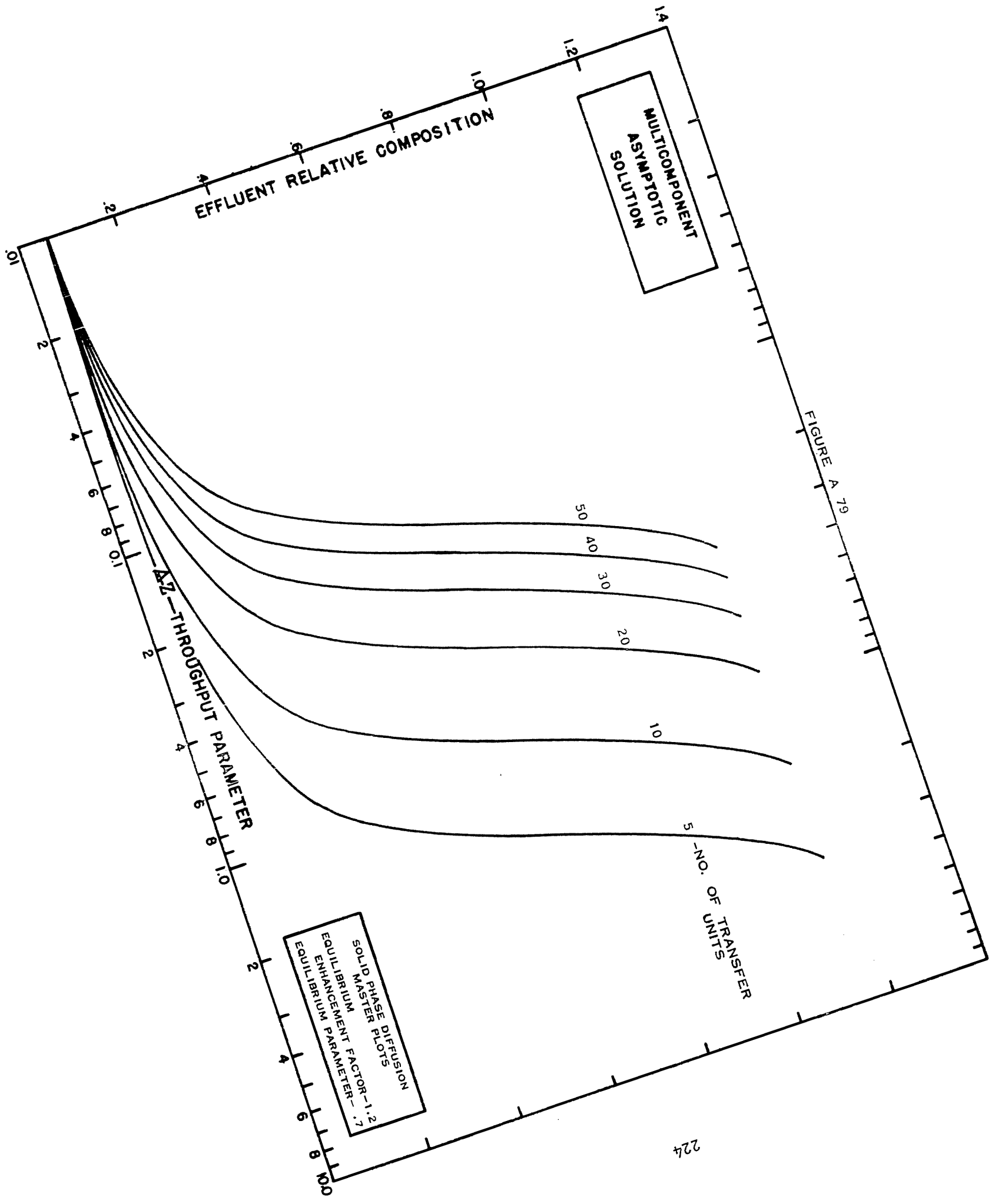
EFFLUENT RELATIVE COMPOSITION
.01
.2
.4
.6
.8
1.0
1.2
1.4
MULTICOMPONENT
ASYMPTOTIC
SOLUTION
AZ—THROUGHPUT PARAMETER
2
4
6
8
0.1
2
4
6
8
1.0
2
4
6
8
10.0
50
40
30
20
10
5
NO. OF TRANSFER
UNITS
SOLID PHASE DIFFUSION
MASTER PLOTS
EQUILIBRIUM
ENHANCEMENT FACTOR—1.2
EQUILIBRIUM PARAMETER— .7

FIGURE A 79

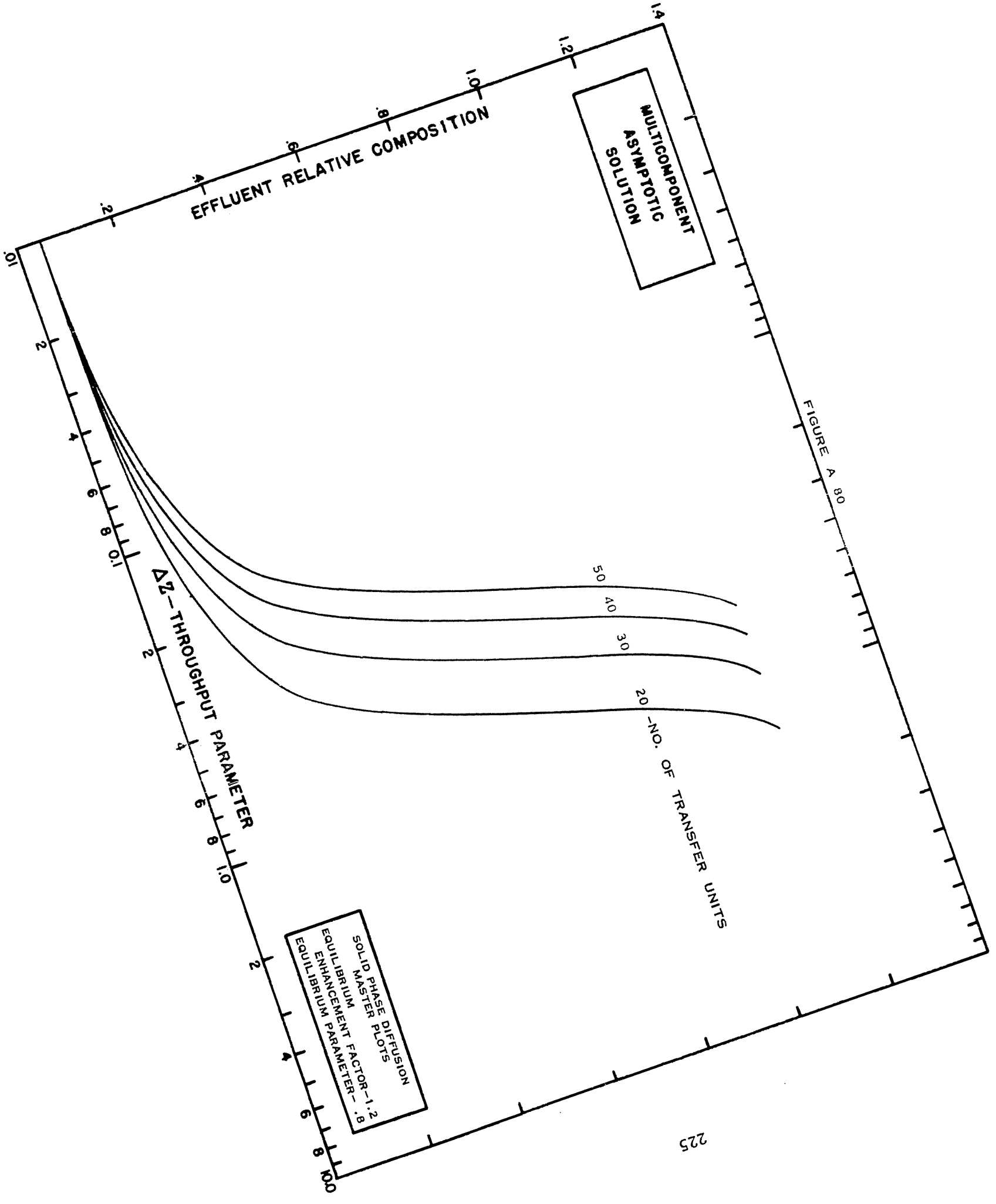
EFFLUENT RELATIVE COMPOSITION
.01
.2
.4
.6
.8
1.0
1.2
1.4
MULTICOMPONENT ASYMPTOTIC SOLUTION
ΔZ—THROUGHPUT PARAMETER
0.1
2
4
6
8
1.0
2
4
6
8
10.0
50
40
30
20
—NO. OF TRANSFER UNITS
SOLID PHASE DIFFUSION MASTER PLOTS
EQUILIBRIUM ENHANCEMENT FACTOR—1.2
EQUILIBRIUM PARAMETER— .8

FIGURE A 80

FIGURE A 81

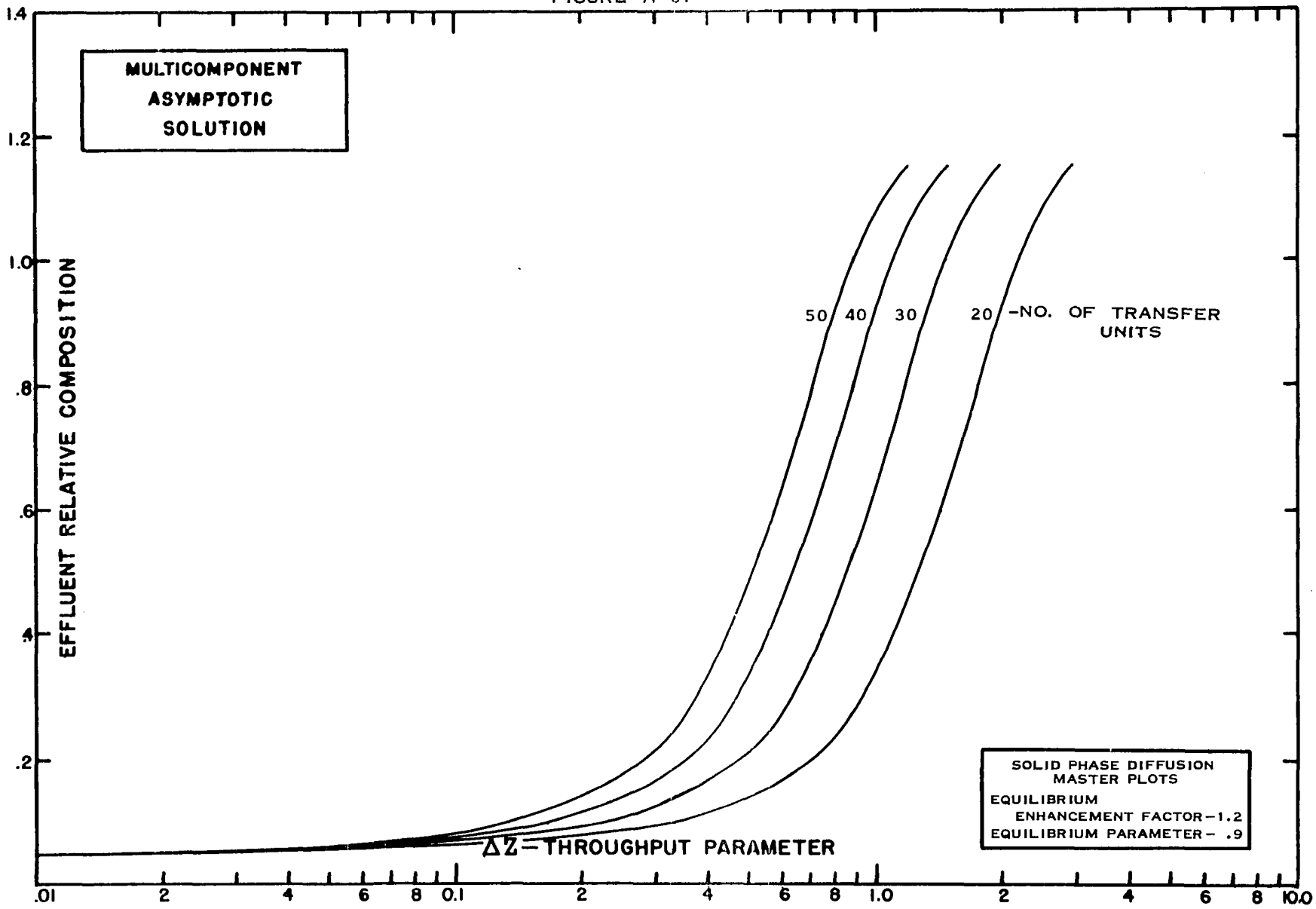
MULTICOMPONENT
ASYMPTOTIC
SOLUTION
EFFLUENT RELATIVE COMPOSITION
1.4
1.2
1.0
.8
.6
.4
.2
50
40
30
20
-NO. OF TRANSFER UNITS
SOLID PHASE DIFFUSION
MASTER PLOTS
EQUILIBRIUM
ENHANCEMENT FACTOR-1.2
EQUILIBRIUM PARAMETER- .9
ΔZ-THROUGHPUT PARAMETER
.01
2
4
6
8
0.1
2
4
6
8
1.0
2
4
6
8
10.0

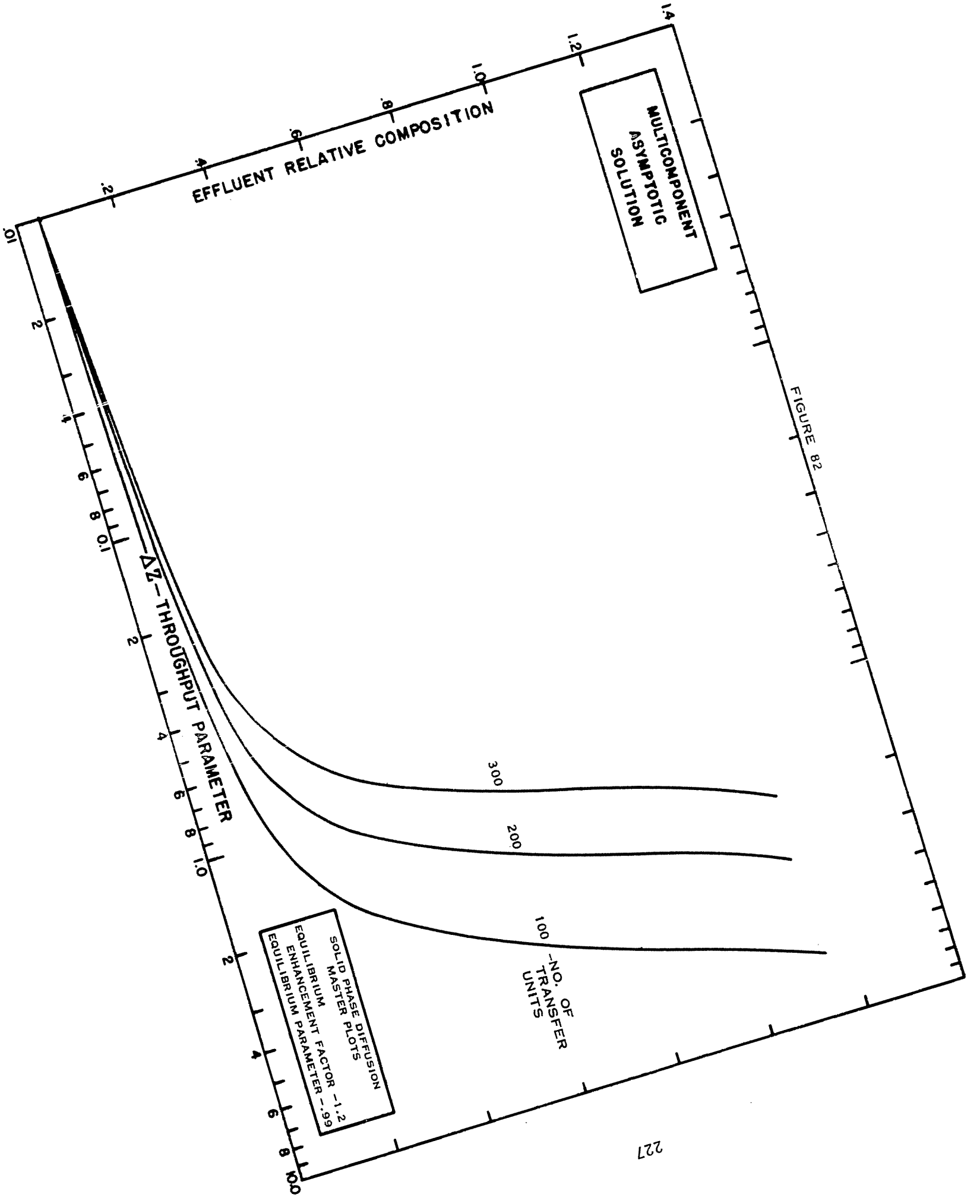
EFFLUENT RELATIVE COMPOSITION
.2
.4
.6
.8
1.0
1.2
1.4
MULTICOMPONENT ASYMPTOTIC SOLUTION
.01
.02
.04
.06
.08
.10
.2
.4
.6
.8
1.0
2
4
6
8
10.0
$-\Delta Z-$ THROUGHPUT PARAMETER
300
200
100
NO. OF TRANSFER UNITS
SOLID PHASE DIFFUSION MASTER PLOTS
EQUILIBRIUM ENHANCEMENT FACTOR -1.2
EQUILIBRIUM PARAMETER -.99

FIGURE 82

FIGURE A 83

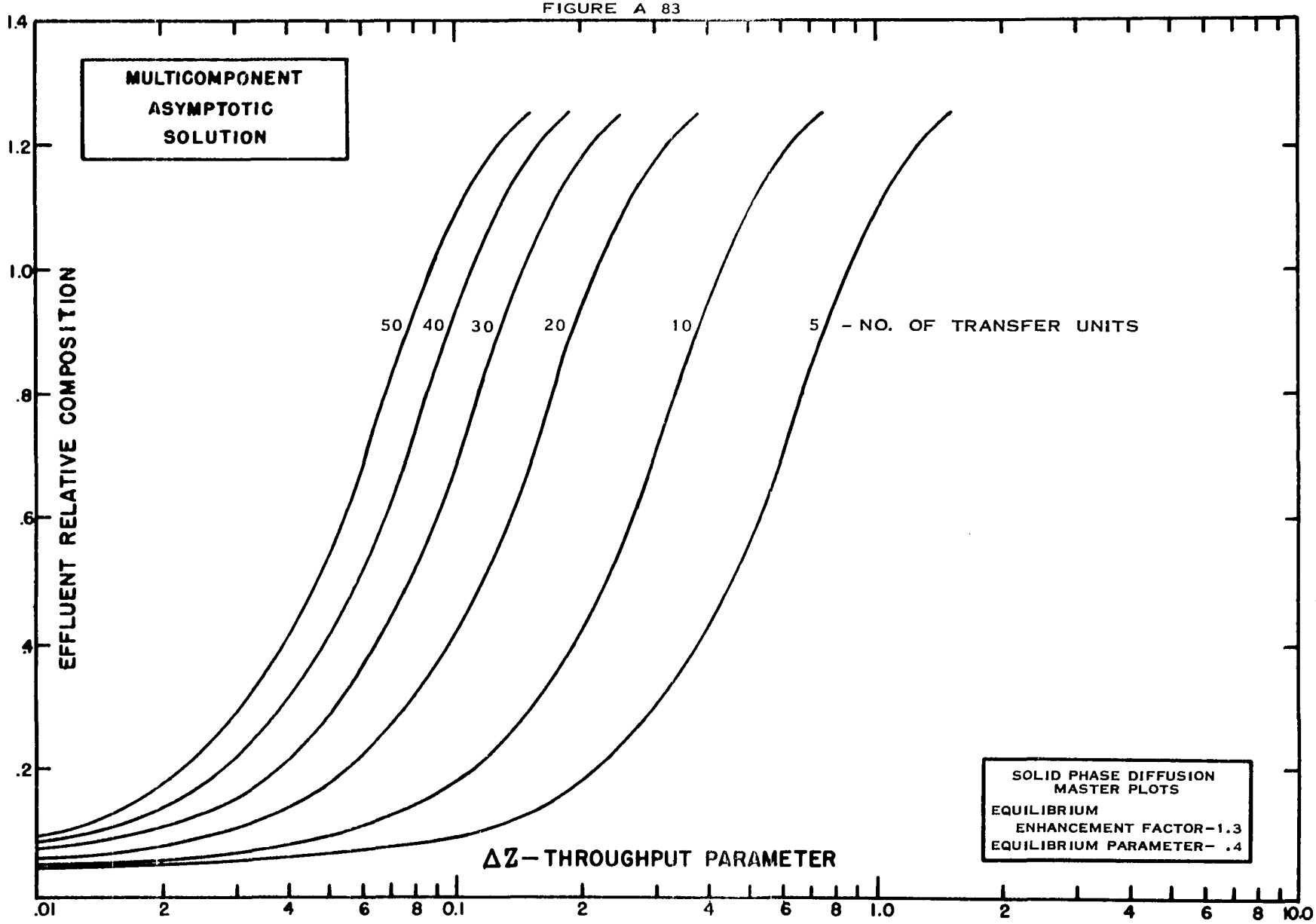
MULTICOMPONENT
ASYMPTOTIC
SOLUTION
EFFLUENT RELATIVE COMPOSITION
1.4
1.2
1.0
.8
.6
.4
.2
50
40
30
20
10
5
- NO. OF TRANSFER UNITS
ΔZ—THROUGHPUT PARAMETER
.01
2
4
6
8
0.1
2
4
6
8
1.0
2
4
6
8
10.0
SOLID PHASE DIFFUSION
MASTER PLOTS
EQUILIBRIUM
ENHANCEMENT FACTOR-1.3
EQUILIBRIUM PARAMETER- .4

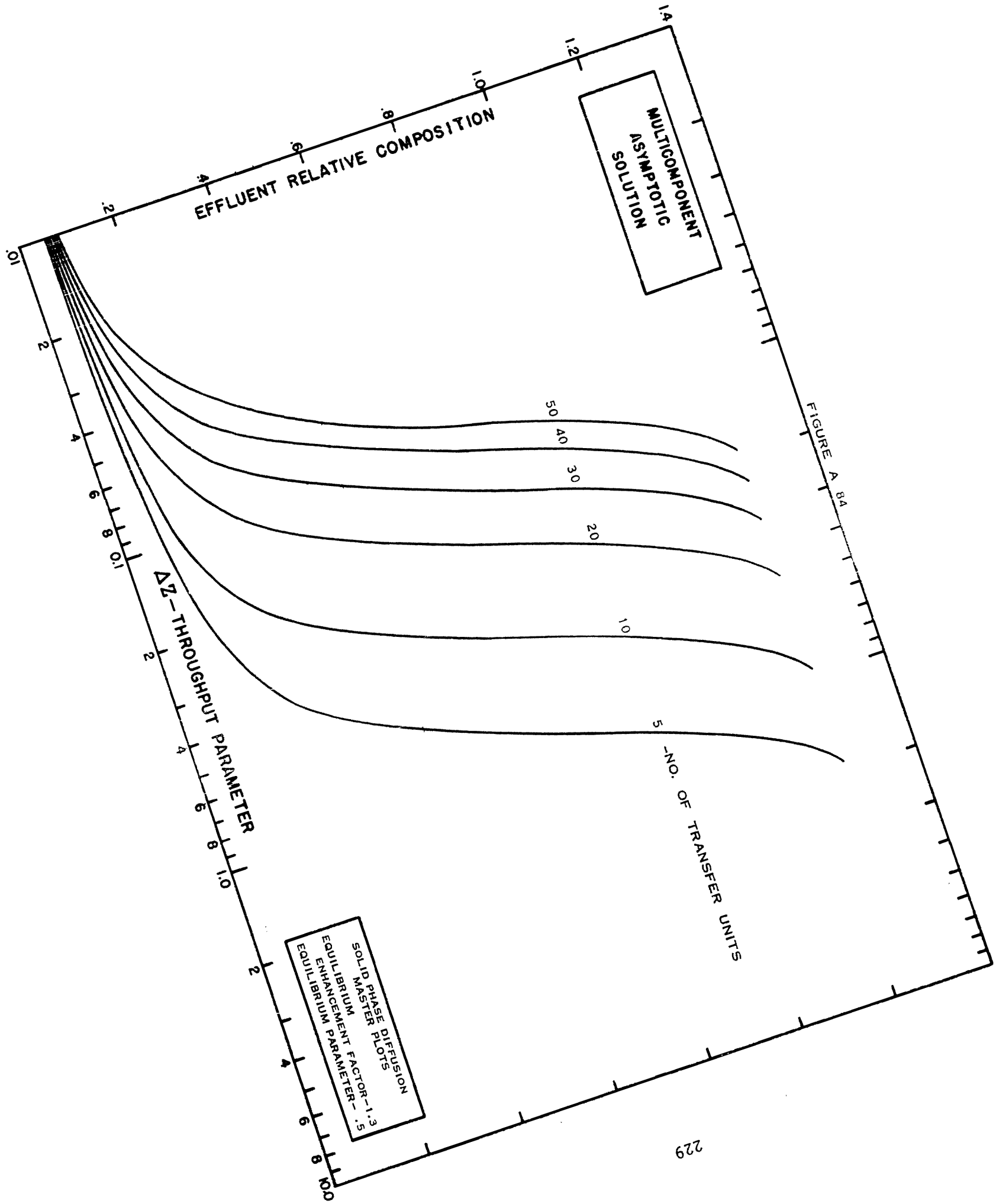
EFFLUENT RELATIVE COMPOSITION
.01
.2
.4
.6
.8
1.0
1.2
1.4
MULTICOMPONENT ASYMPTOTIC SOLUTION
50
40
30
20
10
5
NO. OF TRANSFER UNITS
ΔZ—THROUGHPUT PARAMETER
2
4
6
8
0.1
2
4
6
8
1.0
2
4
6
8
10.0
SOLID PHASE DIFFUSION MASTER PLOTS
EQUILIBRIUM ENHANCEMENT FACTOR—1.3
EQUILIBRIUM PARAMETER— .5

FIGURE A 84

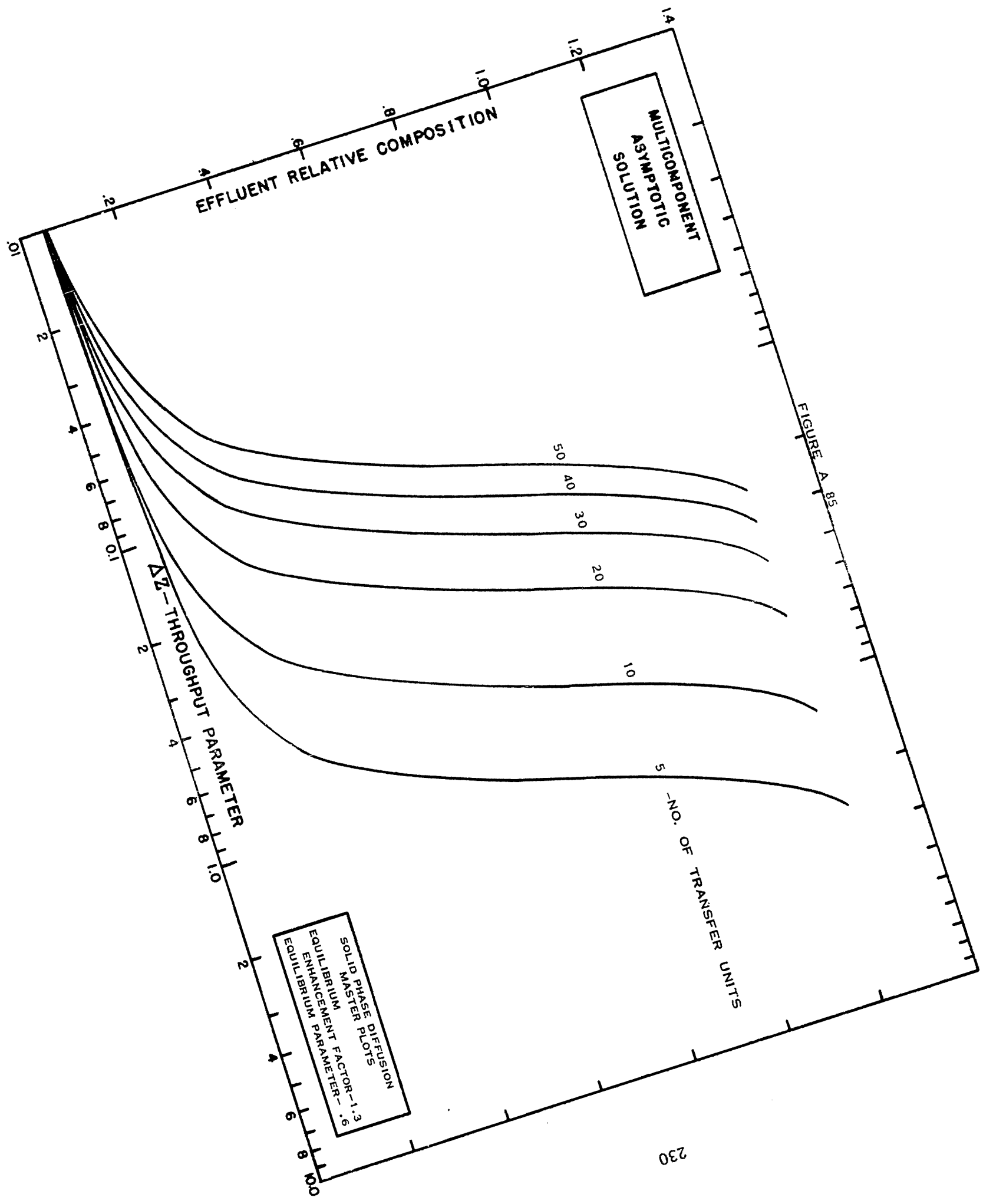
EFFLUENT RELATIVE COMPOSITION
.01
.2
.4
.6
.8
1.0
1.2
1.4
MULTICOMPONENT
ASYMPTOTIC
SOLUTION
FIGURE A 85
50
40
30
20
10
5
NO. OF TRANSFER UNITS
2
4
6
8
0.1
2
4
6
8
1.0
2
4
6
8
10.0
ΔZ—THROUGHPUT PARAMETER
SOLID PHASE DIFFUSION
MASTER PLOTS
EQUILIBRIUM
ENHANCEMENT FACTOR—1.3
EQUILIBRIUM PARAMETER— .6

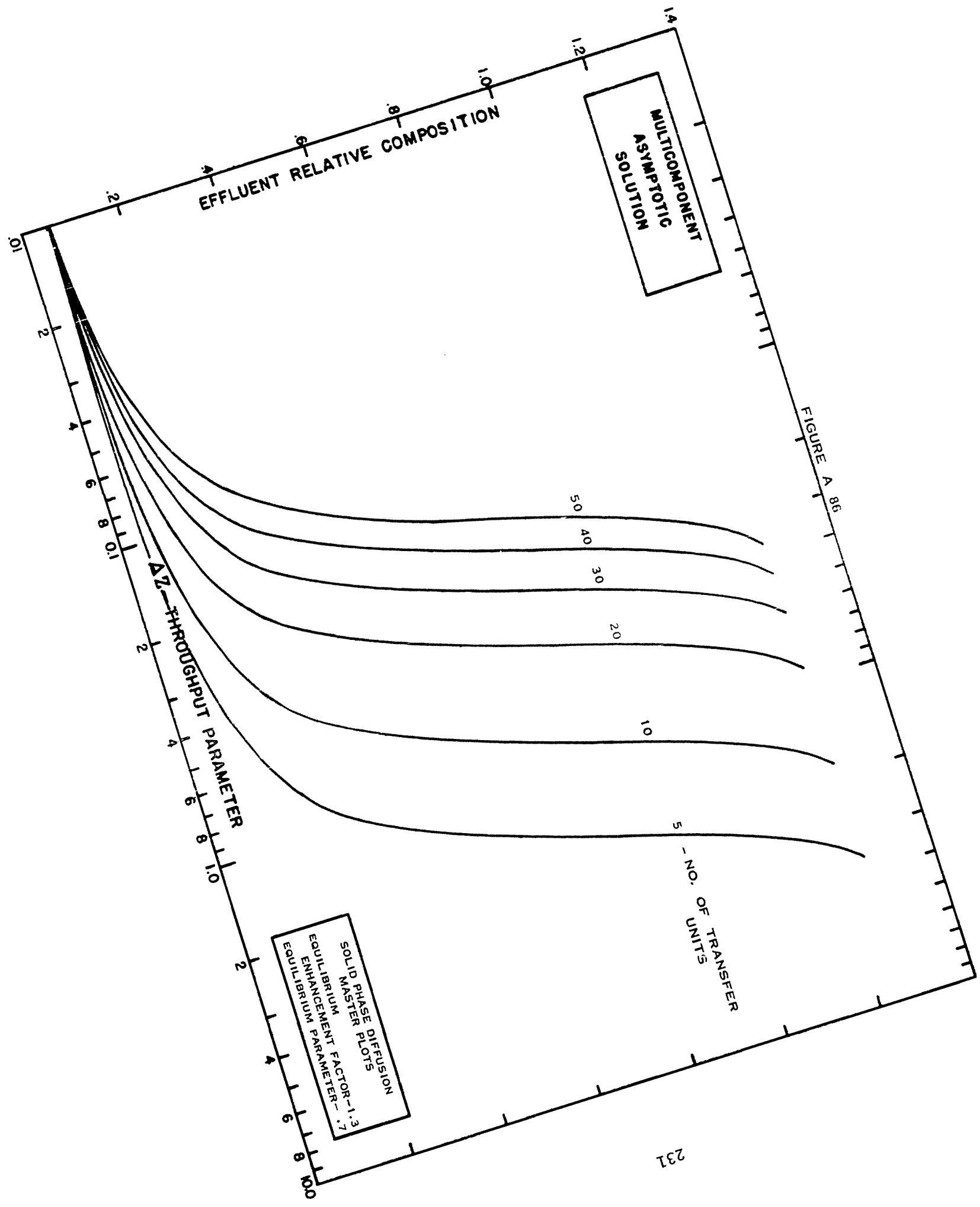
EFFLUENT RELATIVE COMPOSITION
.01
.2
.4
.6
.8
1.0
1.2
1.4
MULTICOMPONENT ASYMPTOTIC SOLUTION
50
40
30
20
10
5
NO. OF TRANSFER UNITS
ΔZ—THROUGHPUT PARAMETER
2
4
6
8
0.1
2
4
6
8
1.0
2
4
6
8
10.0
SOLID PHASE DIFFUSION MASTER PLOTS
EQUILIBRIUM ENHANCEMENT FACTOR—1.3
EQUILIBRIUM PARAMETER— .7

FIGURE A 86

FIGURE A 87

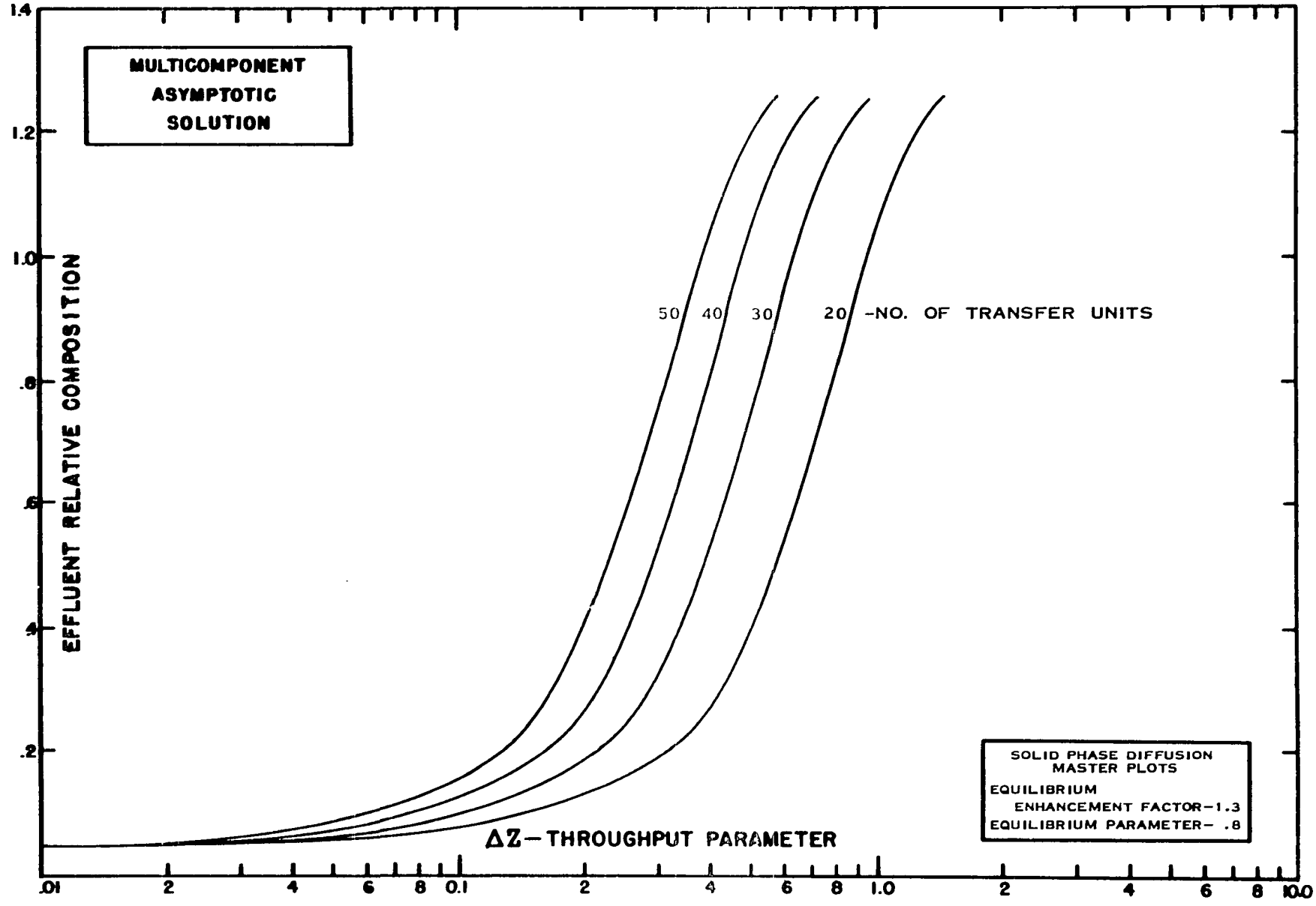
MULTICOMPONENT
ASYMPTOTIC
SOLUTION
EFFLUENT RELATIVE COMPOSITION
1.4
1.2
1.0
.8
.6
.4
.2
50
40
30
20
-NO. OF TRANSFER UNITS
SOLID PHASE DIFFUSION
MASTER PLOTS
EQUILIBRIUM
ENHANCEMENT FACTOR-1.3
EQUILIBRIUM PARAMETER- .8
ΔZ—THROUGHPUT PARAMETER
.01
2
4
6
8
0.1
2
4
6
8
1.0
2
4
6
8
10.0

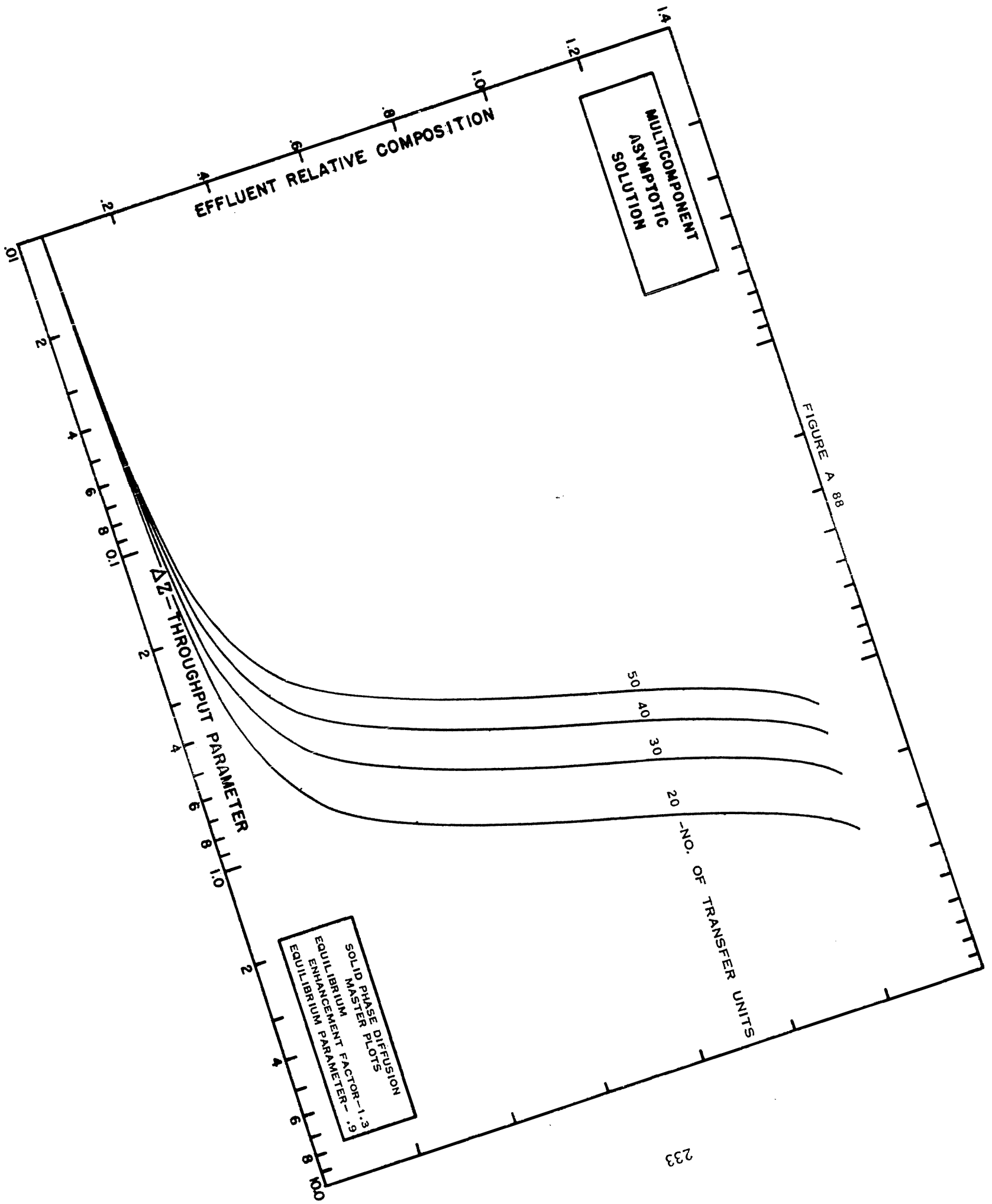
EFFLUENT RELATIVE COMPOSITION
.01
.2
.4
.6
.8
1.0
1.2
1.4
MULTICOMPONENT ASYMPTOTIC SOLUTION
Δz — THROUGHPUT PARAMETER
0.1
2
4
6
8
1.0
2
4
6
8
10.0
50
40
30
20
NO. OF TRANSFER UNITS
SOLID PHASE DIFFUSION MASTER PLOTS
EQUILIBRIUM ENHANCEMENT FACTOR—1.3
EQUILIBRIUM PARAMETER— .9

FIGURE A 88

FIGURE A 89

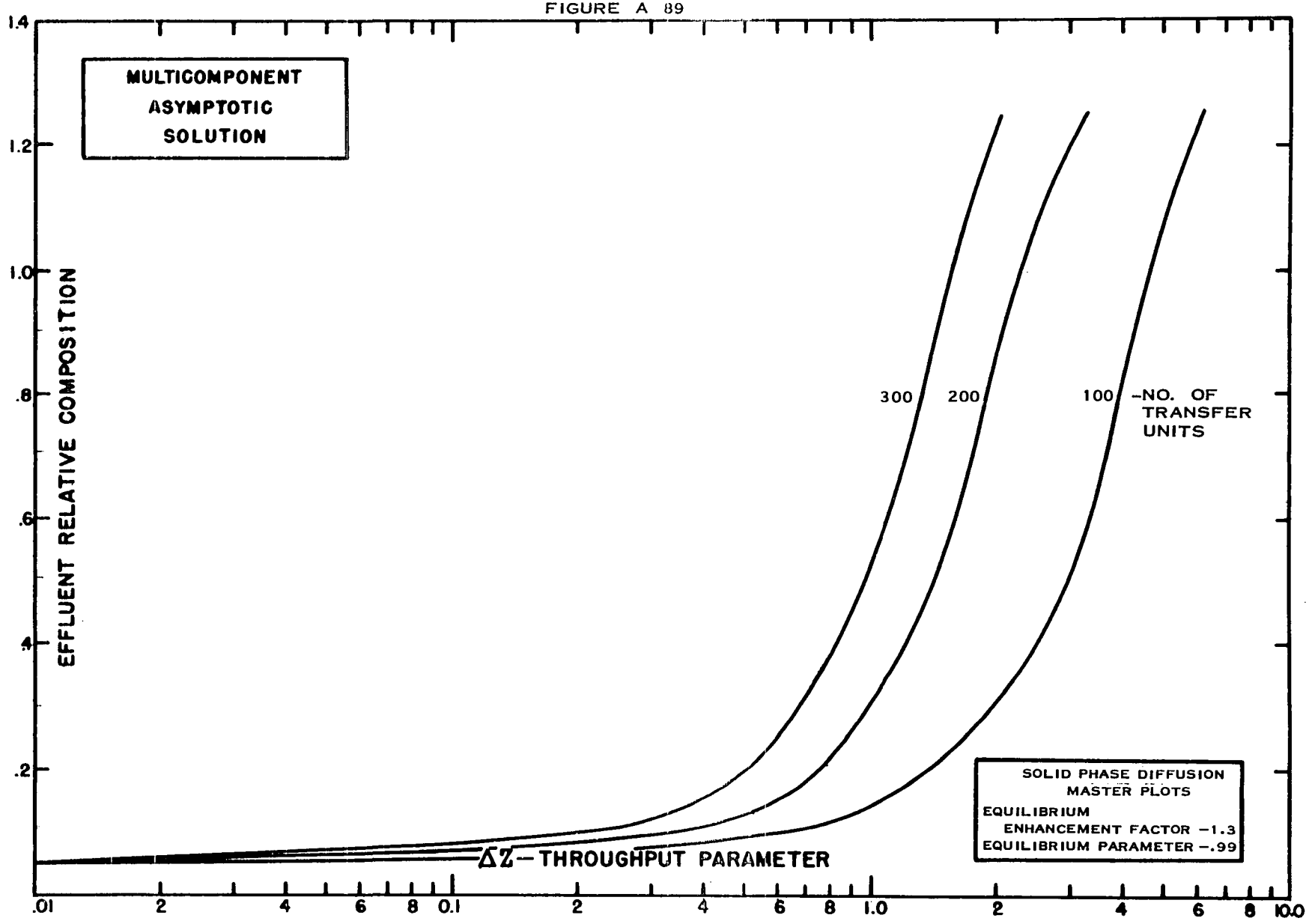
MULTICOMPONENT
ASYMPTOTIC
SOLUTION
EFFLUENT RELATIVE COMPOSITION
1.4
1.2
1.0
.8
.6
.4
.2
300
200
100
-NO. OF
TRANSFER
UNITS
SOLID PHASE DIFFUSION
MASTER PLOTS
EQUILIBRIUM
ENHANCEMENT FACTOR -1.3
EQUILIBRIUM PARAMETER -.99
ΔZ-THROUGHPUT PARAMETER
.01
2
4
6
8
0.1
2
4
6
8
1.0
2
4
6
8
10.0

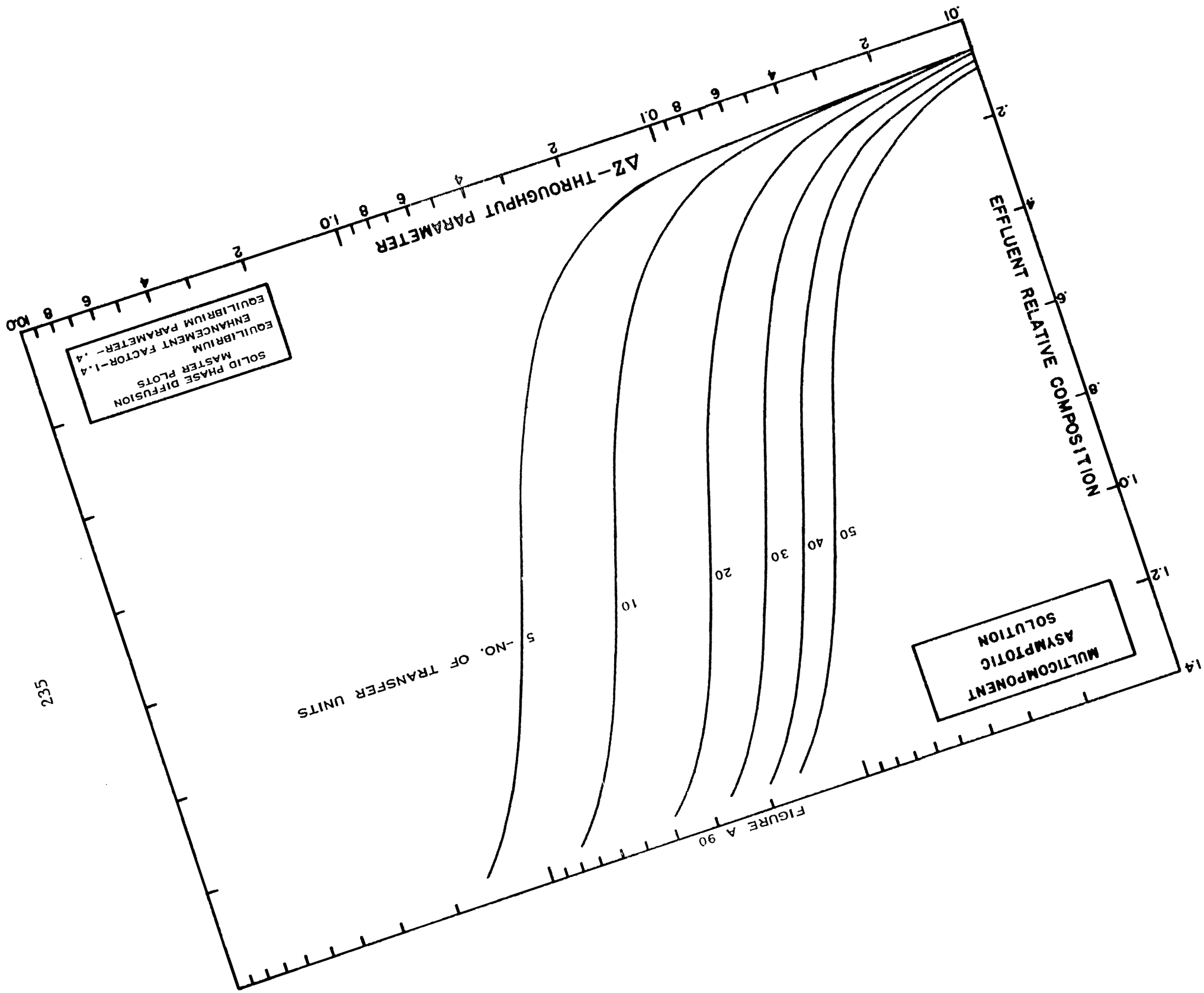
SOLID PHASE DIFFUSION
MASTER PLOTS
EQUILIBRIUM
ENHANCEMENT FACTOR-1.4
EQUILIBRIUM PARAMETER- .4
ΔZ-THROUGHPUT PARAMETER
EFFLUENT RELATIVE COMPOSITION
NO. OF TRANSFER UNITS
MULTICOMPONENT
ASYMPTOTIC
SOLUTION
FIGURE A 90
235

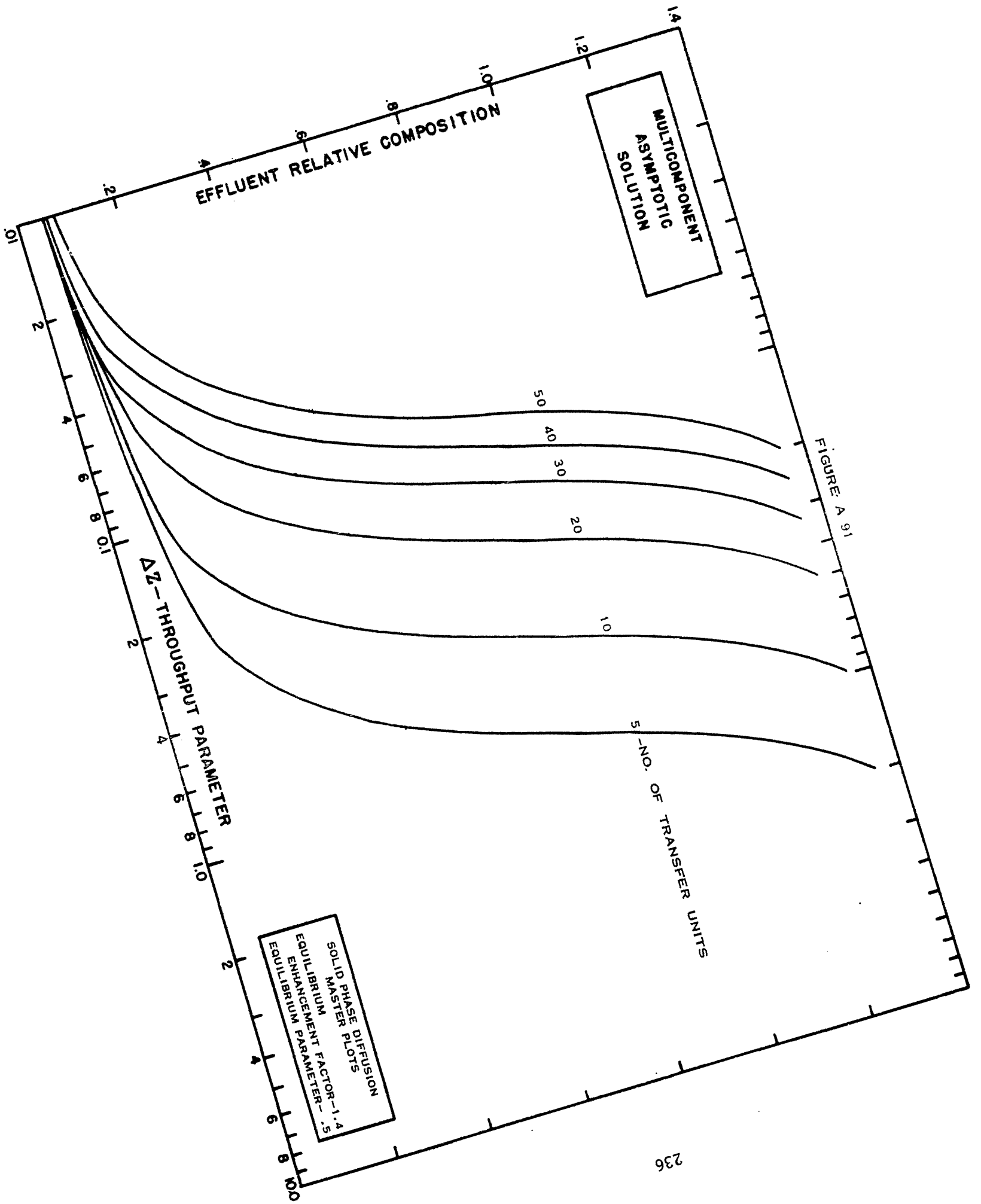
EFFLUENT RELATIVE COMPOSITION
.01
.2
.4
.6
.8
1.0
1.2
1.4
MULTICOMPONENT ASYMPTOTIC SOLUTION
50
40
30
20
10
5
NO. OF TRANSFER UNITS
ΔZ—THROUGHPUT PARAMETER
2
4
6
8
0.1
2
4
6
8
1.0
2
4
6
8
100
SOLID PHASE DIFFUSION MASTER PLOTS
EQUILIBRIUM ENHANCEMENT FACTOR—1.4
EQUILIBRIUM PARAMETER— .5

FIGURE A 91

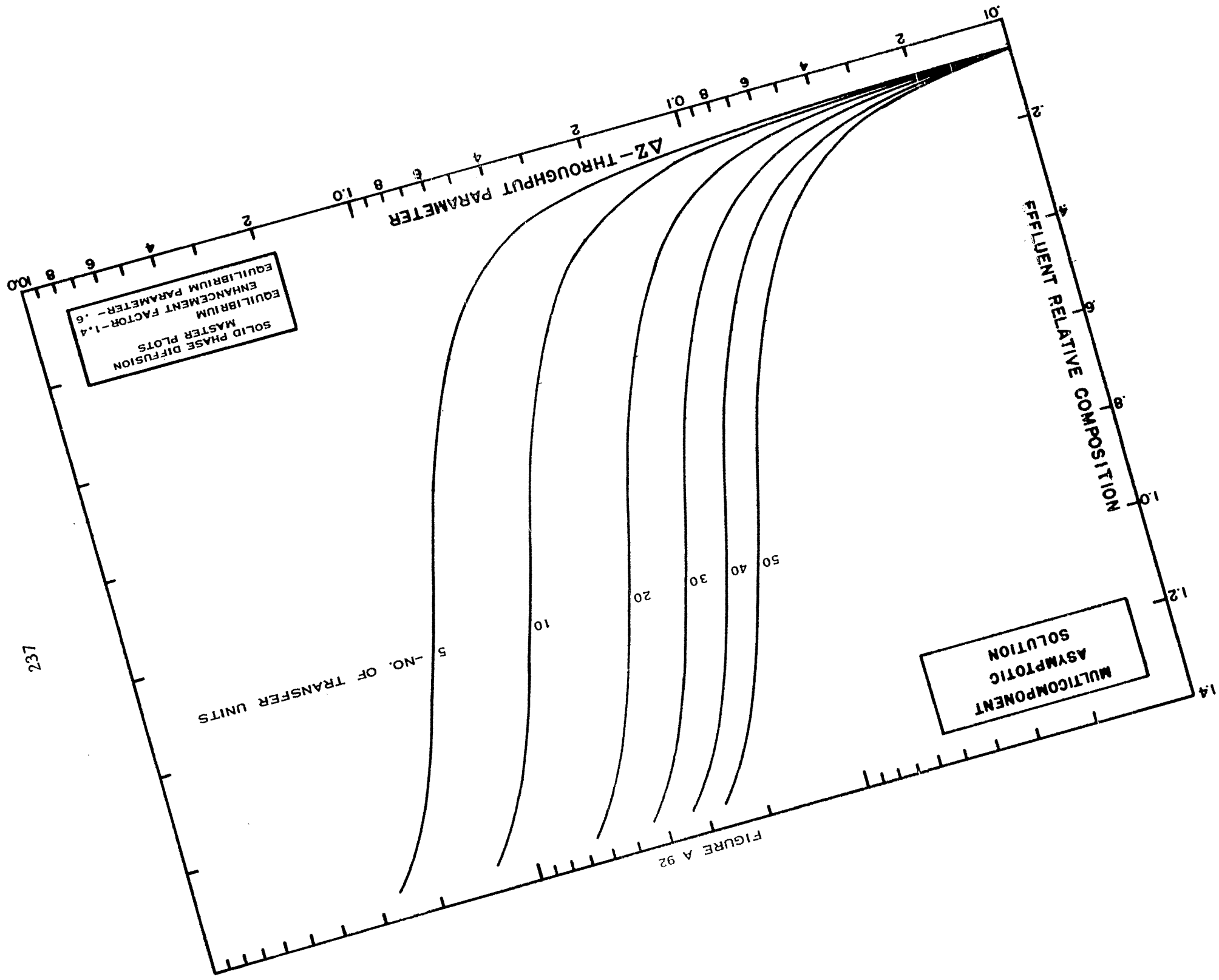
MULTICOMPONENT
ASYMPTOTIC
SOLUTION
SOLID PHASE DIFFUSION
MASTER PLOTS
EQUILIBRIUM
ENHANCEMENT FACTOR-1.4
EQUILIBRIUM PARAMETER- .6
Δ2-THROUGHPUT PARAMETER
EFFLUENT RELATIVE COMPOSITION
NO. OF TRANSFER UNITS
5
10
20
30
40
50
237

FIGURE A 92

FIGURE A 93

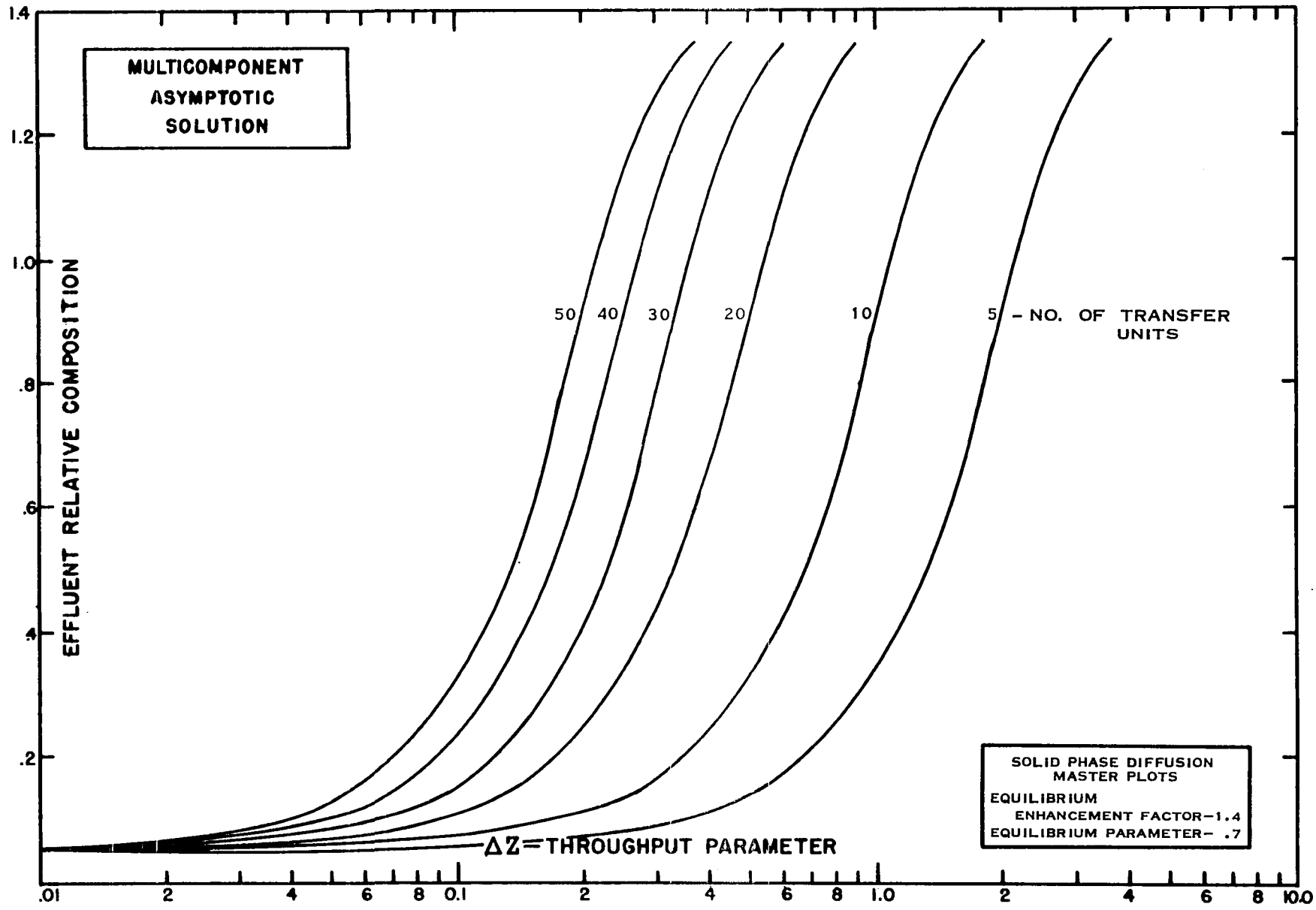
MULTICOMPONENT
ASYMPTOTIC
SOLUTION
EFFLUENT RELATIVE COMPOSITION
1.4
1.2
1.0
.8
.6
.4
.2
50
40
30
20
10
5
- NO. OF TRANSFER UNITS
SOLID PHASE DIFFUSION
MASTER PLOTS
EQUILIBRIUM
ENHANCEMENT FACTOR-1.4
EQUILIBRIUM PARAMETER- .7
ΔZ=THROUGHPUT PARAMETER
.01
2
4
6
8
0.1
2
4
6
8
1.0
2
4
6
8
10.0

FIGURE A 94

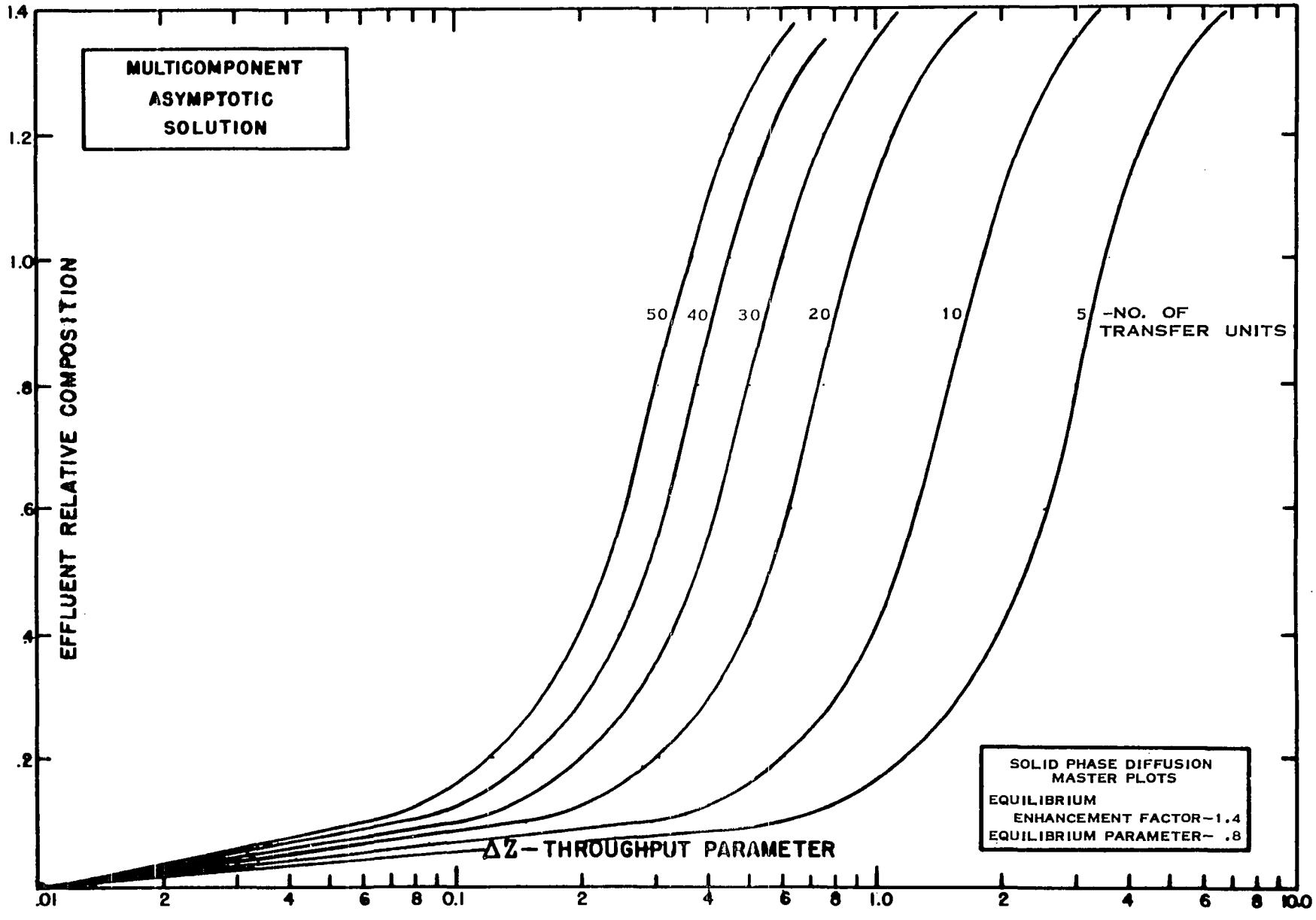
MULTICOMPONENT
ASYMPTOTIC
SOLUTION
EFFLUENT RELATIVE COMPOSITION
1.4
1.2
1.0
.8
.6
.4
.2
50
40
30
20
10
5
-NO. OF
TRANSFER UNITS
ΔZ – THROUGHPUT PARAMETER
.01
2
4
6
8
0.1
2
4
6
8
1.0
2
4
6
8
10.0
SOLID PHASE DIFFUSION
MASTER PLOTS
EQUILIBRIUM
ENHANCEMENT FACTOR–1.4
EQUILIBRIUM PARAMETER– .8

FIGURE A 95

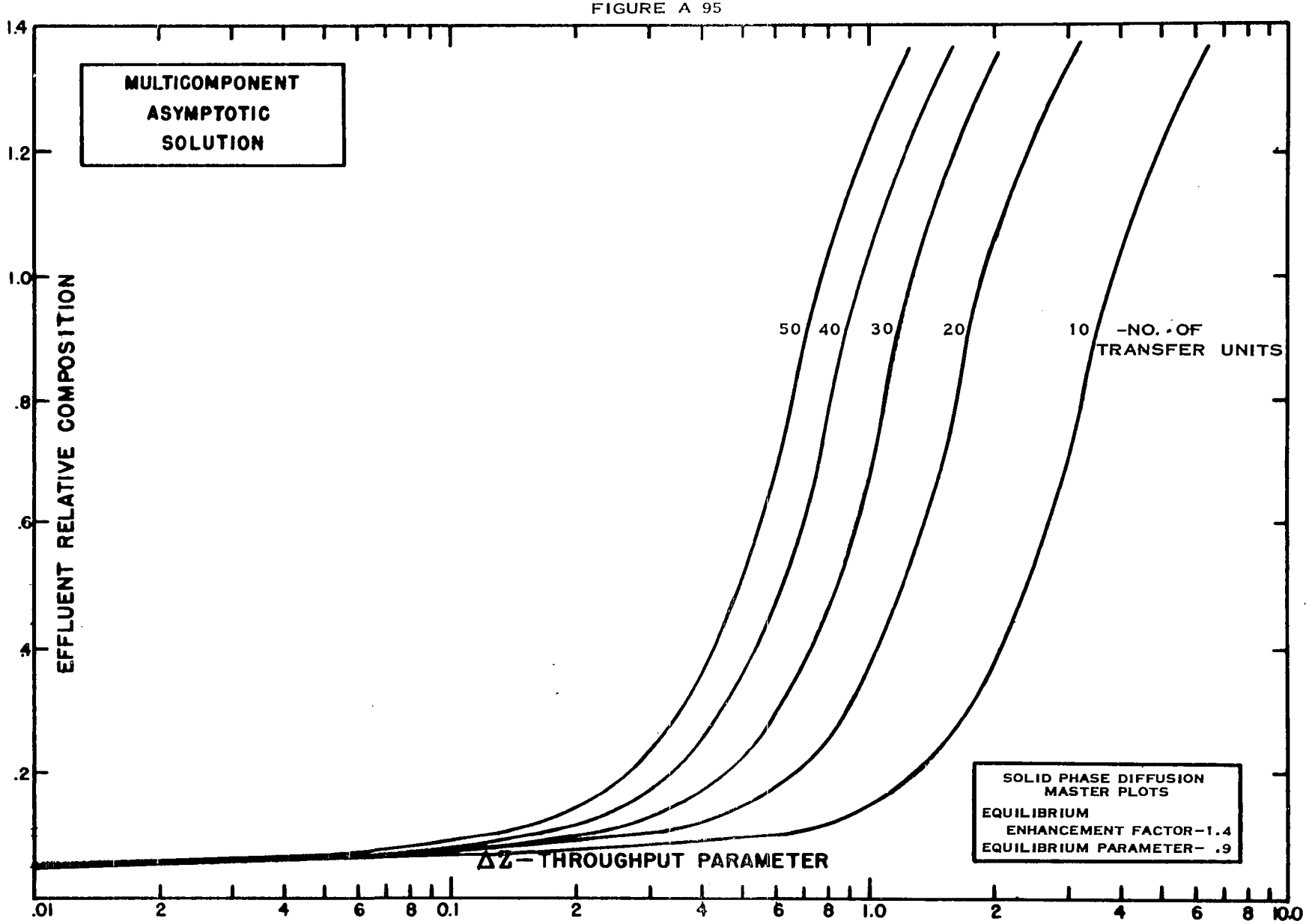
MULTICOMPONENT
ASYMPTOTIC
SOLUTION
EFFLUENT RELATIVE COMPOSITION
1.4
1.2
1.0
.8
.6
.4
.2
50
40
30
20
10
-NO. OF
TRANSFER UNITS
SOLID PHASE DIFFUSION
MASTER PLOTS
EQUILIBRIUM
ENHANCEMENT FACTOR-1.4
EQUILIBRIUM PARAMETER- .9
ΔZ-THROUGHPUT PARAMETER
.01
2
4
6
8
0.1
2
4
6
8
1.0
2
4
6
8
10.0

FIGURE A 96

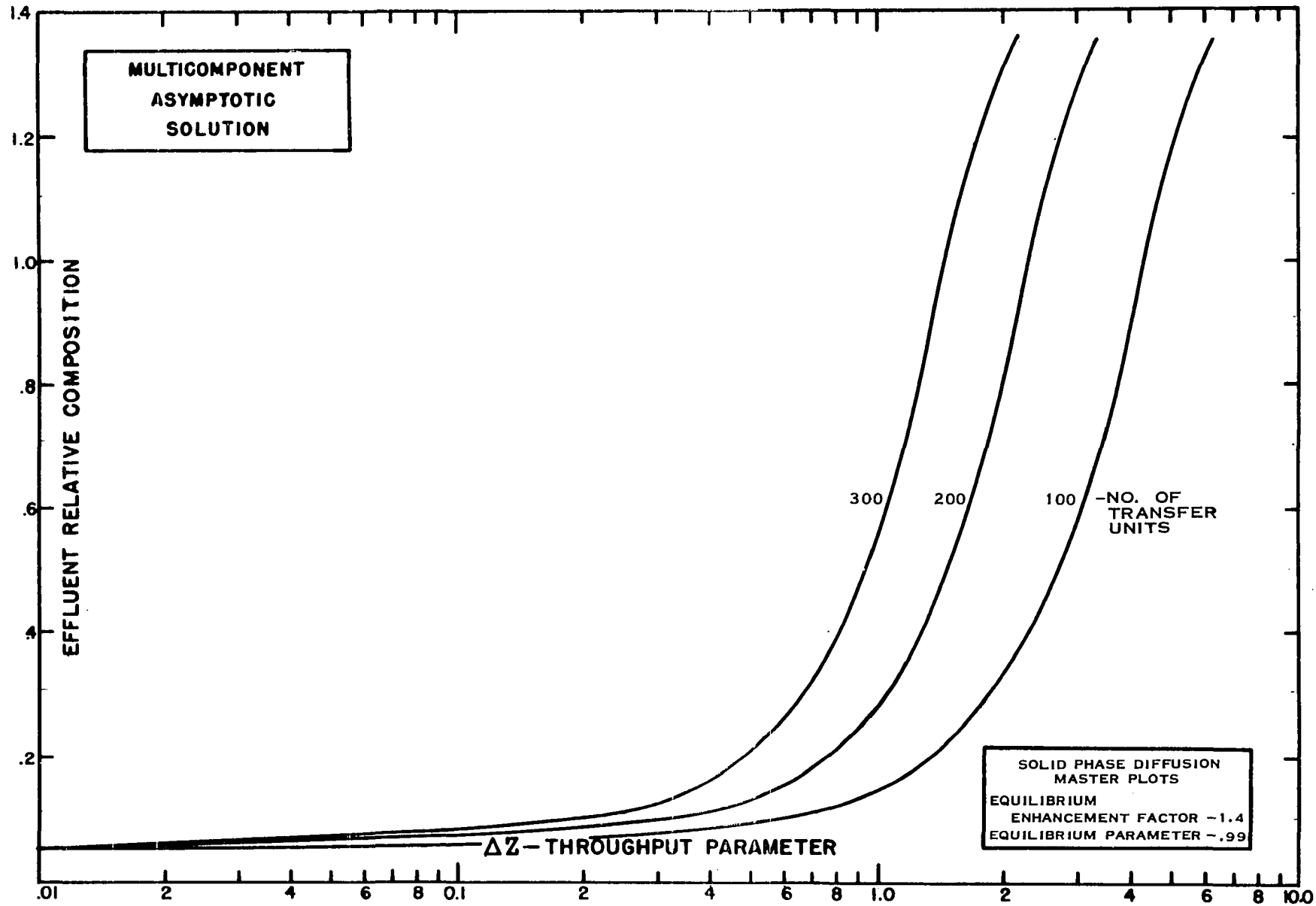
MULTICOMPONENT
ASYMPTOTIC
SOLUTION
EFFLUENT RELATIVE COMPOSITION
1.4
1.2
1.0
.8
.6
.4
.2
300
200
100
-NO. OF
TRANSFER
UNITS
SOLID PHASE DIFFUSION
MASTER PLOTS
EQUILIBRIUM
ENHANCEMENT FACTOR -1.4
EQUILIBRIUM PARAMETER -.99
ΔZ-THROUGHPUT PARAMETER
.01
2
4
6
8
0.1
2
4
6
8
1.0
2
4
6
8
10.0

RUN NO. 56 INLET TEMP. 91.5 °F INLET PRESS. 800 PSIG. TOWER I.D. 2.9 in.

TOWER LGTH. 445.5 cm. FLOW RATE 22.51 ft/min. COMPOSITION: ____%C_4 1.04 %C_5 ____%C_6 ____%C_7

DESSICANT: 03 GEL

N-PENTANE

FIGURE A 97

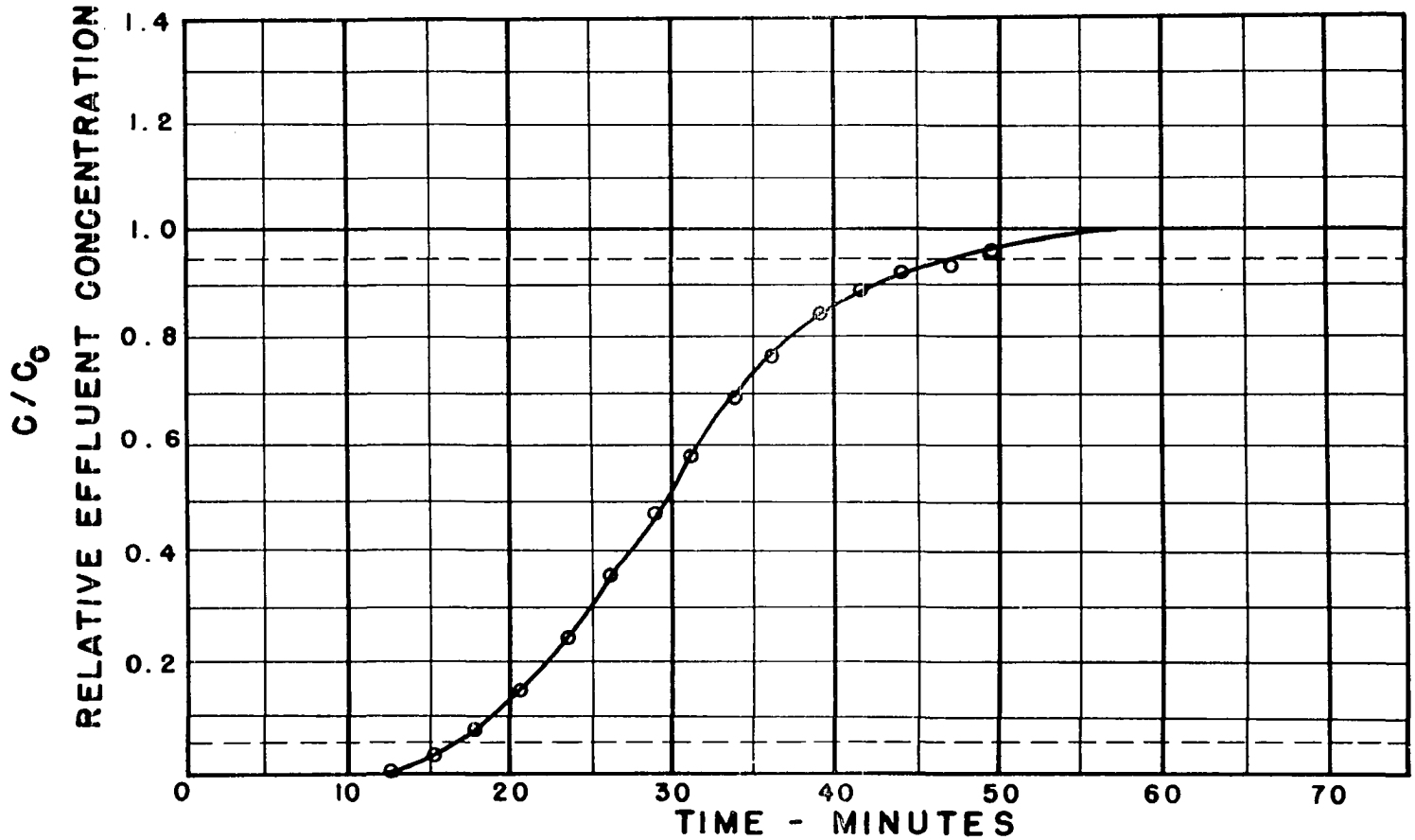

RUN NO. 57-A INLET TEMP. 89.5 °F INLET PRESS. 813 PSIG. TOWER I.D. 2.9 in.

TOWER LGTH. 445.5 cm. FLOW RATE 21.77 ft/min. COMPOSITION: ____%C_4 0.51 %C_5 ____%C_6 ____%C_7

DESSICANT: 03 GEL

N-PENTANE

FIGURE A 98

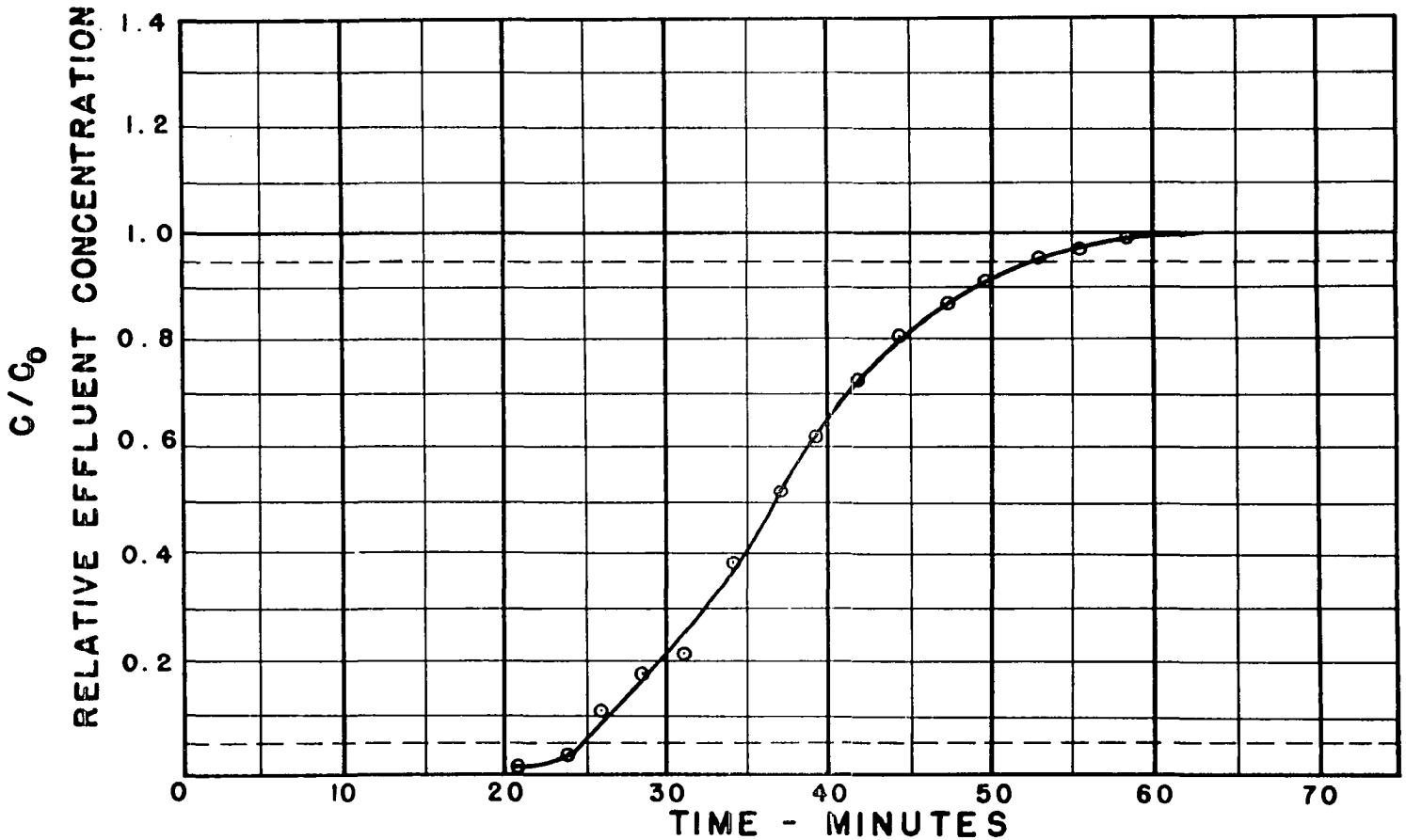

RUN NO. 58 INLET TEMP. 91.5 °F INLET PRESS. 813 PSIG. TOWER I.D. 2.9 in.

TOWER LGTH. 445.5 cm. FLOW RATE 10.86 ft/min. COMPOSITION: ____ %C_4 1.46 %C_5 ____ %C_6 ____ %C_7

DESSICANT: 03 GEL

N-PENTANE

FIGURE A 99

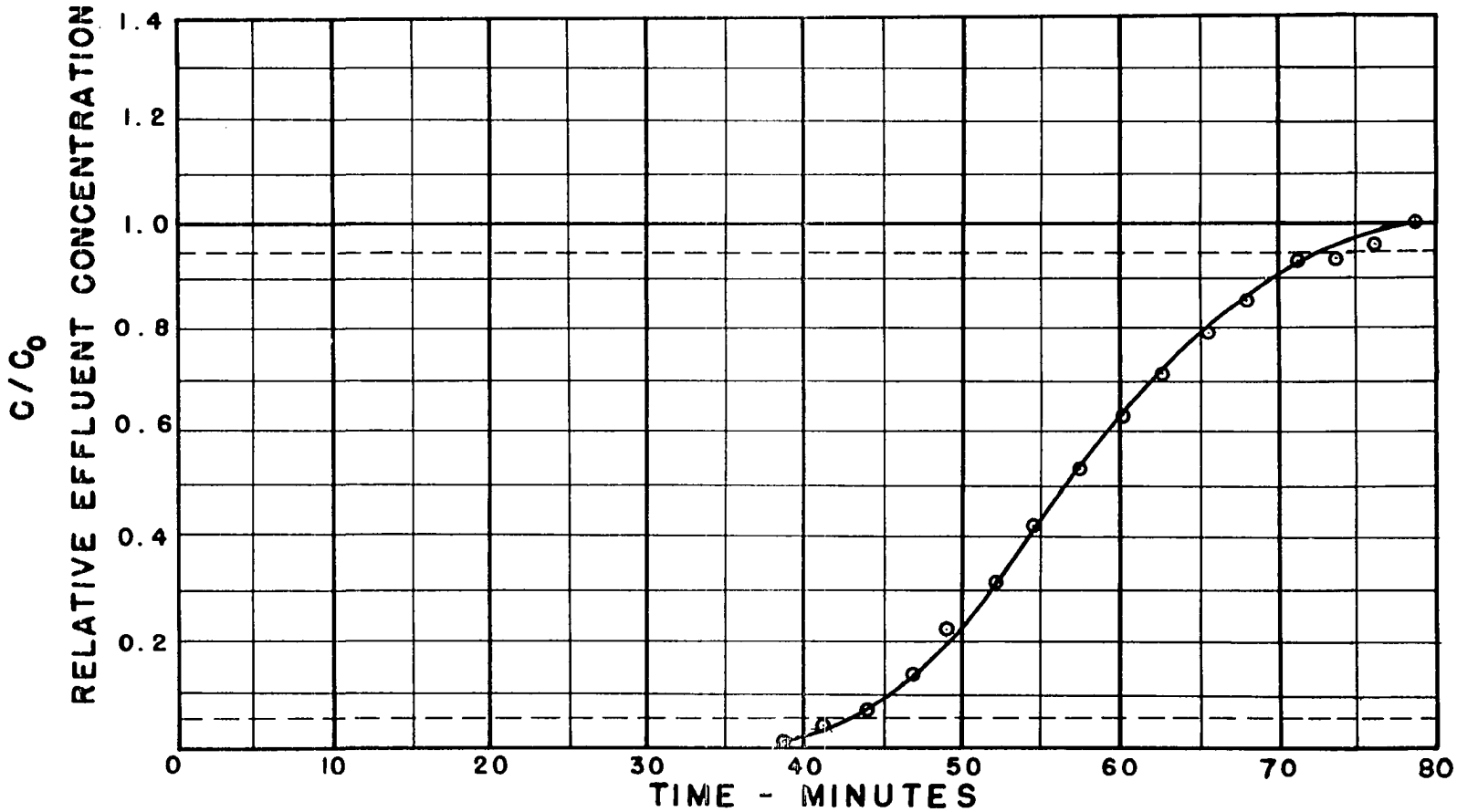

RUN NO. 59 INLET TEMP. 93 °F INLET PRESS. 800 PSIG. TOWER I. D. 2.9 in.

TOWER LGTH. 445.5 cm. FLOW RATE 11.25 ft/min. COMPOSITION: ____ %C_4 1.70 %C_5 ____ %C_6 ____ %C_7

DESSICANT: 03 GEL

N-PENTANE

FIGURE A 100

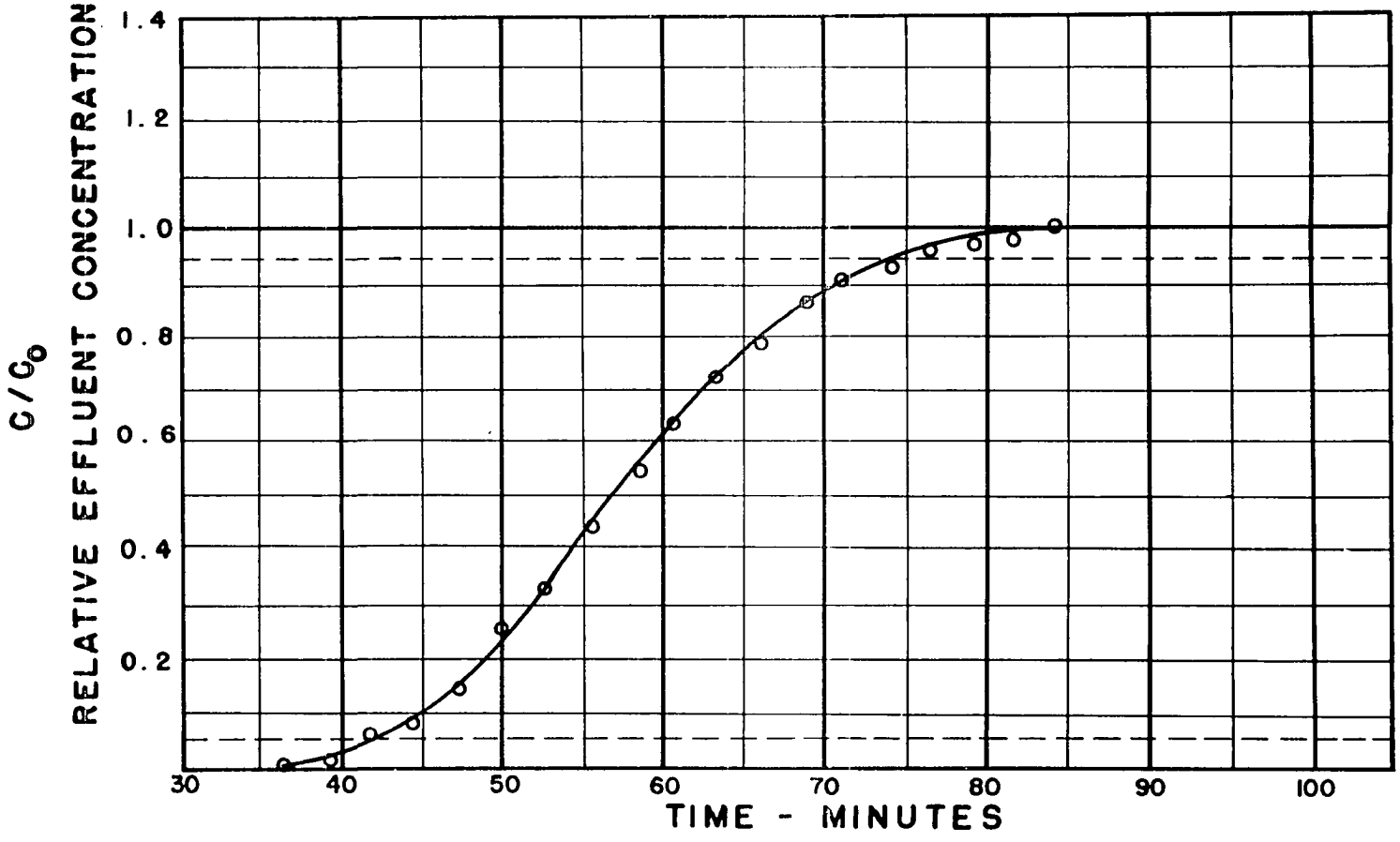

RUN NO. 60 INLET TEMP. 90.7 °F INLET PRESS. 835 PSIG. TOWER I.D. 2.9 in.

TOWER LGTH. 445.5 cm. FLOW RATE 10.55 ft/min. COMPOSITION: ____%C_4 0.66 %C_5 ____%C_6 ____%C_7

DESSICANT: 03 GEL

N-PENTANE

FIGURE A 101

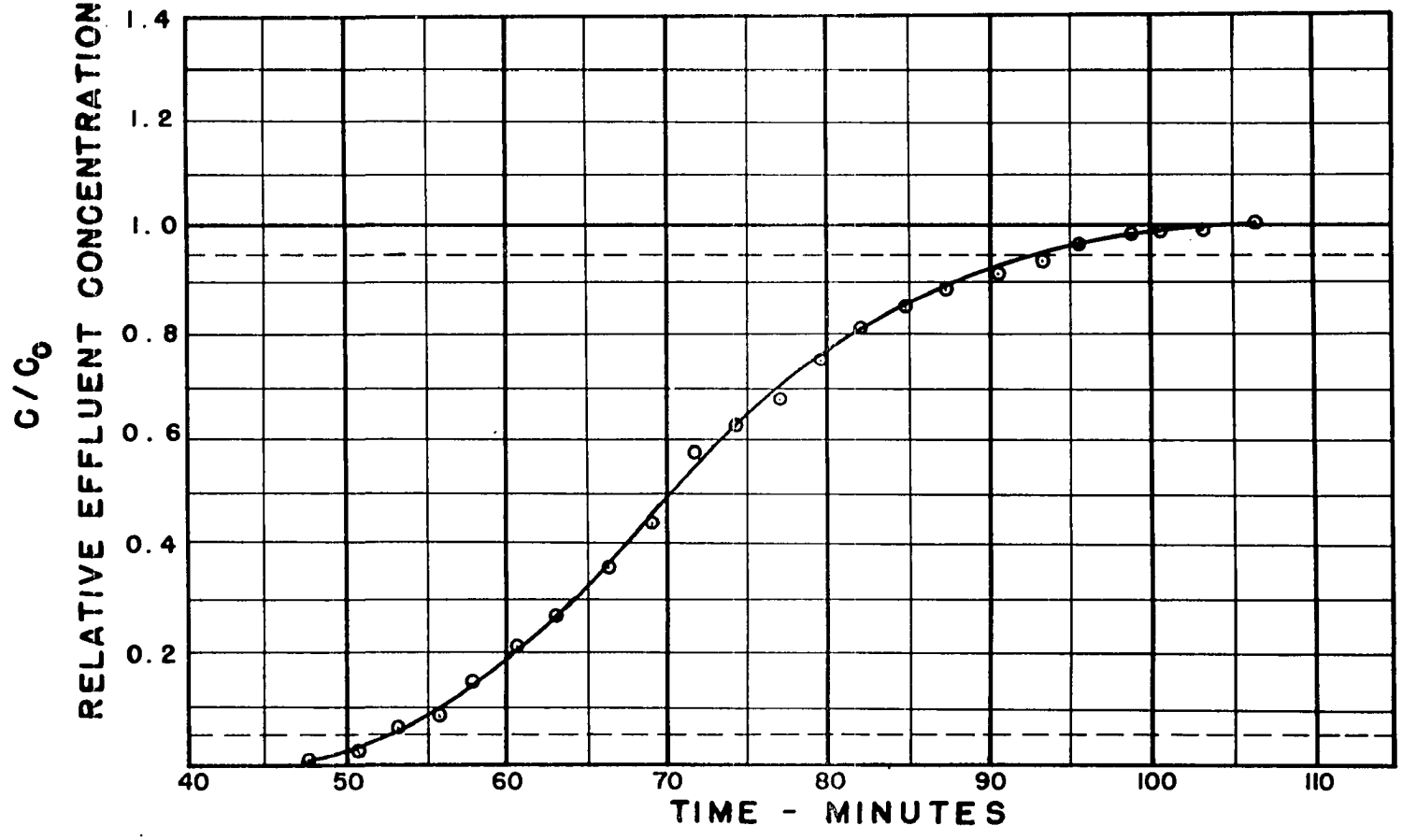

RUN NO. 61 INLET TEMP. 90.7 °F INLET PRESS. 835 PSIG. TOWER I.D. 2.9 in.

TOWER LGTH. 445.5 cm. FLOW RATE 10.55 ft/min. COMPOSITION: ____ %C_4 0.66 %C_5 ____ %C_6 ____ %C_7

DESSICANT: 03 GEL

N-PENTANE

FIGURE A 102

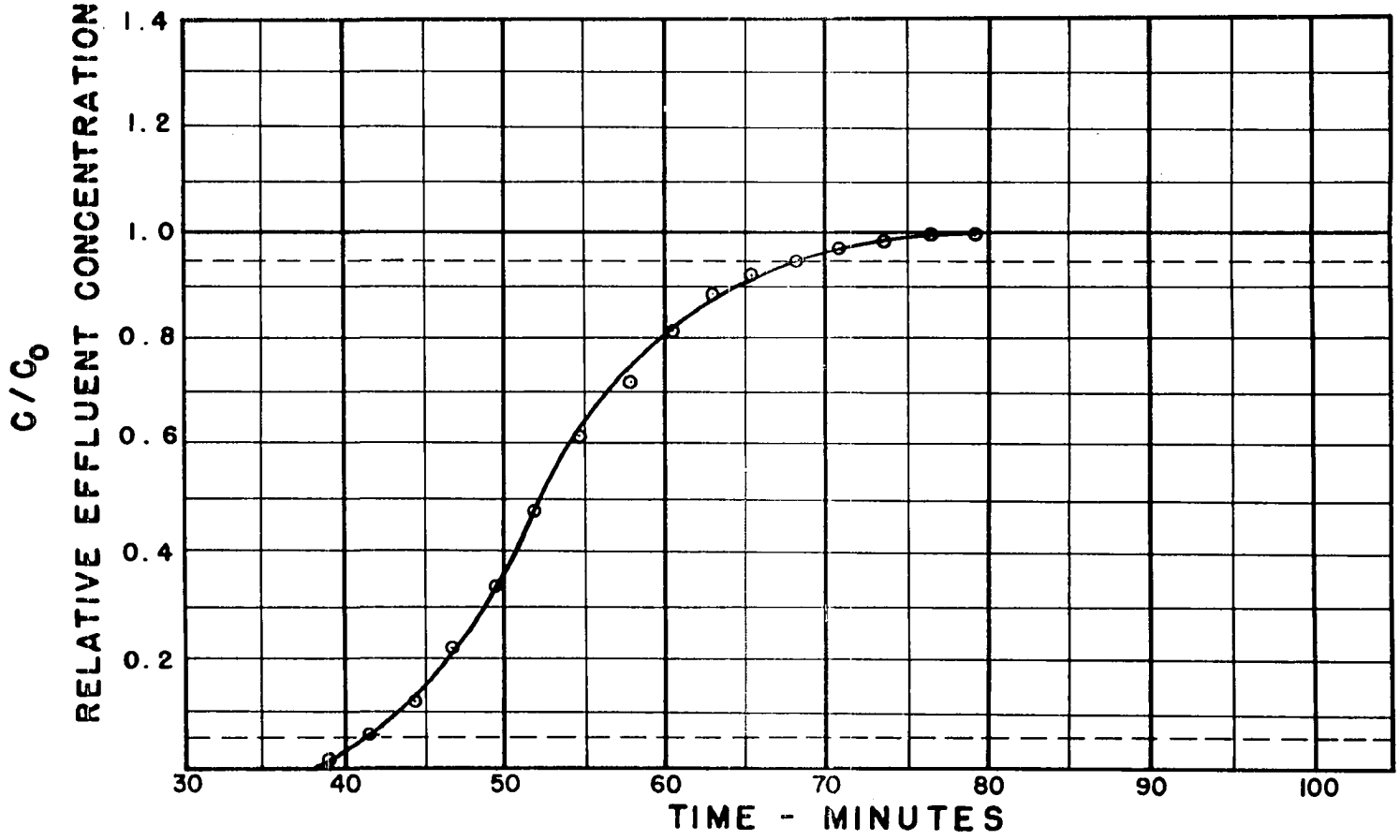

RUN NO. 62 INLET TEMP. 91 °F INLET PRESS. 810 PSIG. TOWER I.D. 2.9 in.

TOWER LGTH. 445.5 cm. FLOW RATE 10.77 ft/min. COMPOSITION: ____%C_4 1.49 %C_5 ____%C_6 ____%C_7

DESSICANT: 03 GEL

N-PENTANE

FIGURE A 103

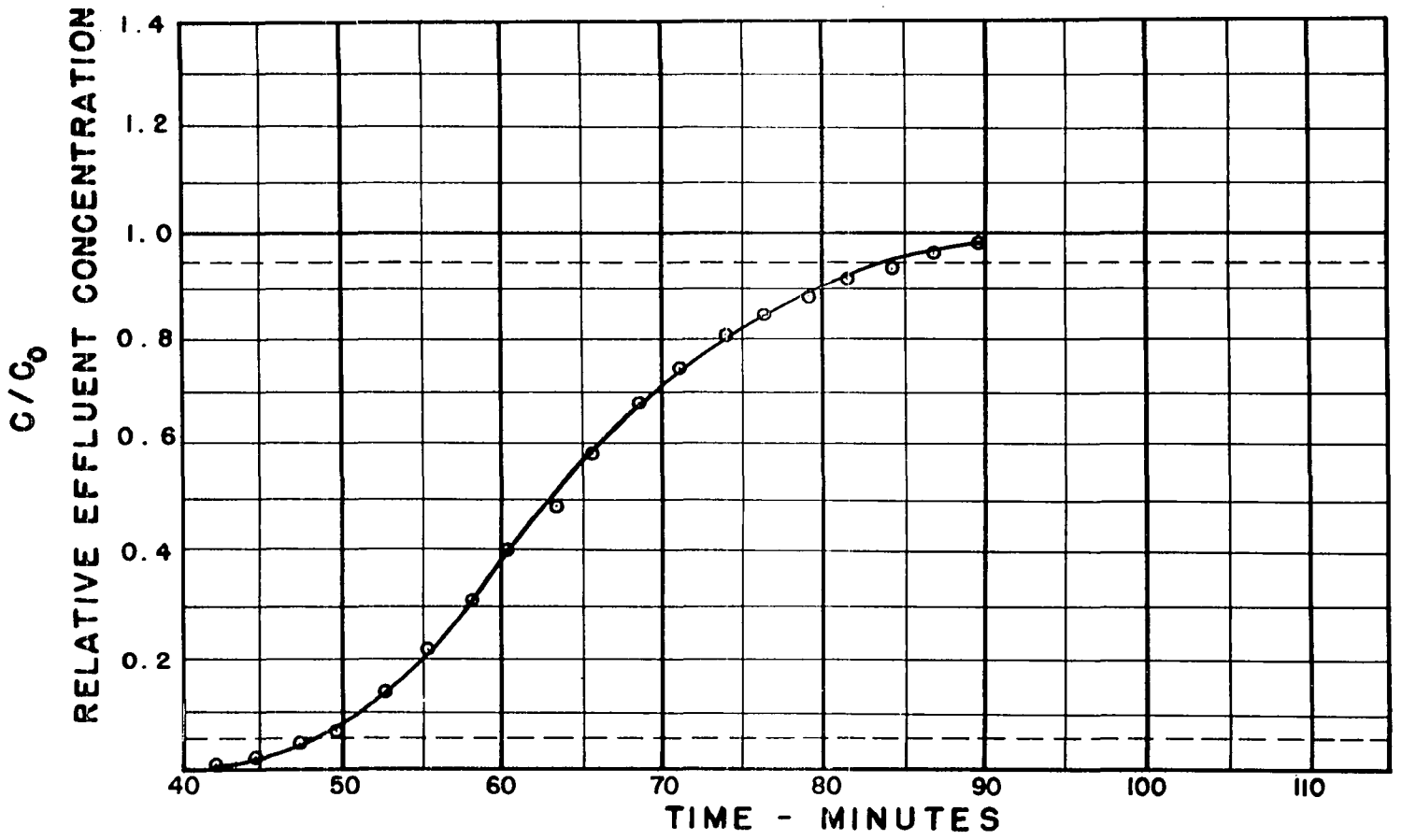

RUN NO. 63 INLET TEMP. 88.8 °F INLET PRESS. 800 PSIG. TOWER I.D. 2.9 in.

TOWER LGTH. 445.5 cm. FLOW RATE 11.10 ft/min. COMPOSITION: ____ %C_4 0.56 %C_5 ____ %C_6 ____ %C_7

DESSICANT: 03 GEL

N-PENTANE

FIGURE A 104

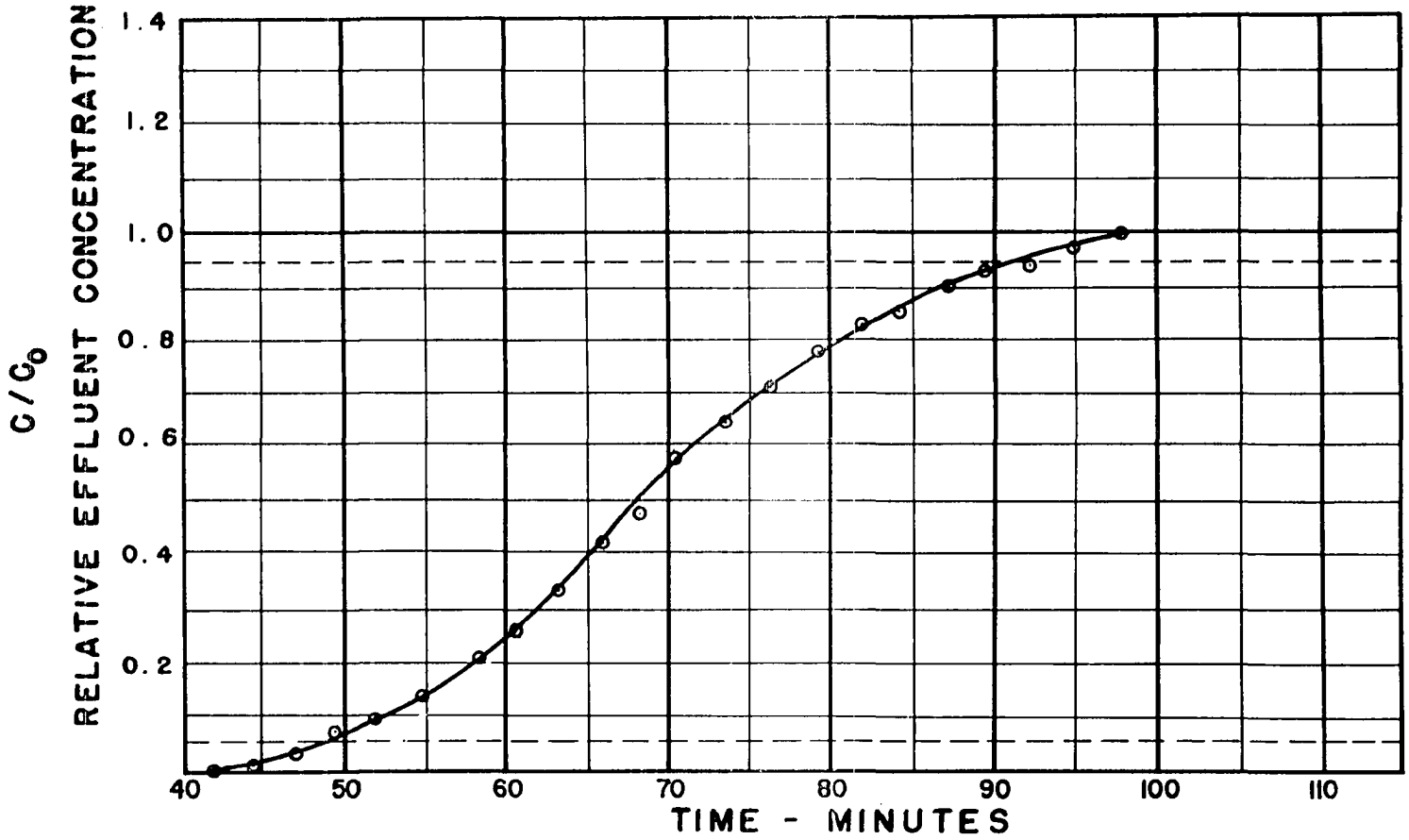

RUN NO. 64 INLET TEMP. 95.8 °F INLET PRESS. 800 PSIG. TOWER I.D. 2.9 in.

TOWER LGTH. 445.5 cm. FLOW RATE 23.04 ft/min. COMPOSITION: ____%C_4 1.52 %C_5 ____%C_6 ____%C_7

DESSICANT: 03 GEL

N-PENTANE

FIGURE A 105

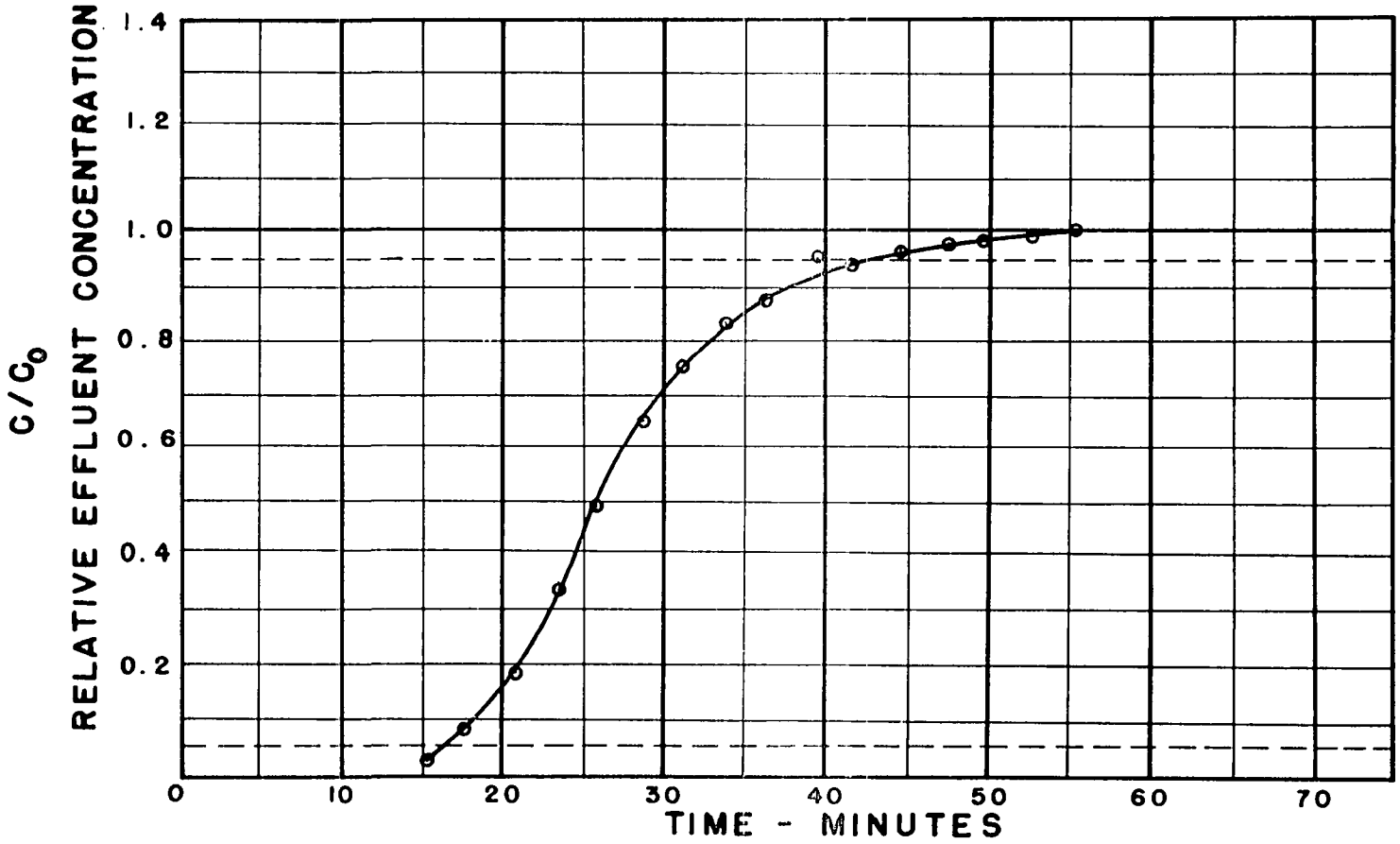

RUN NO. 65 INLET TEMP. 95.8 °F INLET PRESS. 800 PSIG. TOWER I.D. 2.9 in.

TOWER LGTH. 445.5 cm. FLOW RATE 23.04 ft/min. COMPOSITION: ____ %C_4 1.52 %C_5 ____ %C_6 ____ %C_7

DESSICANT: 03 GEL

N-PENTANE

FIGURE A 106

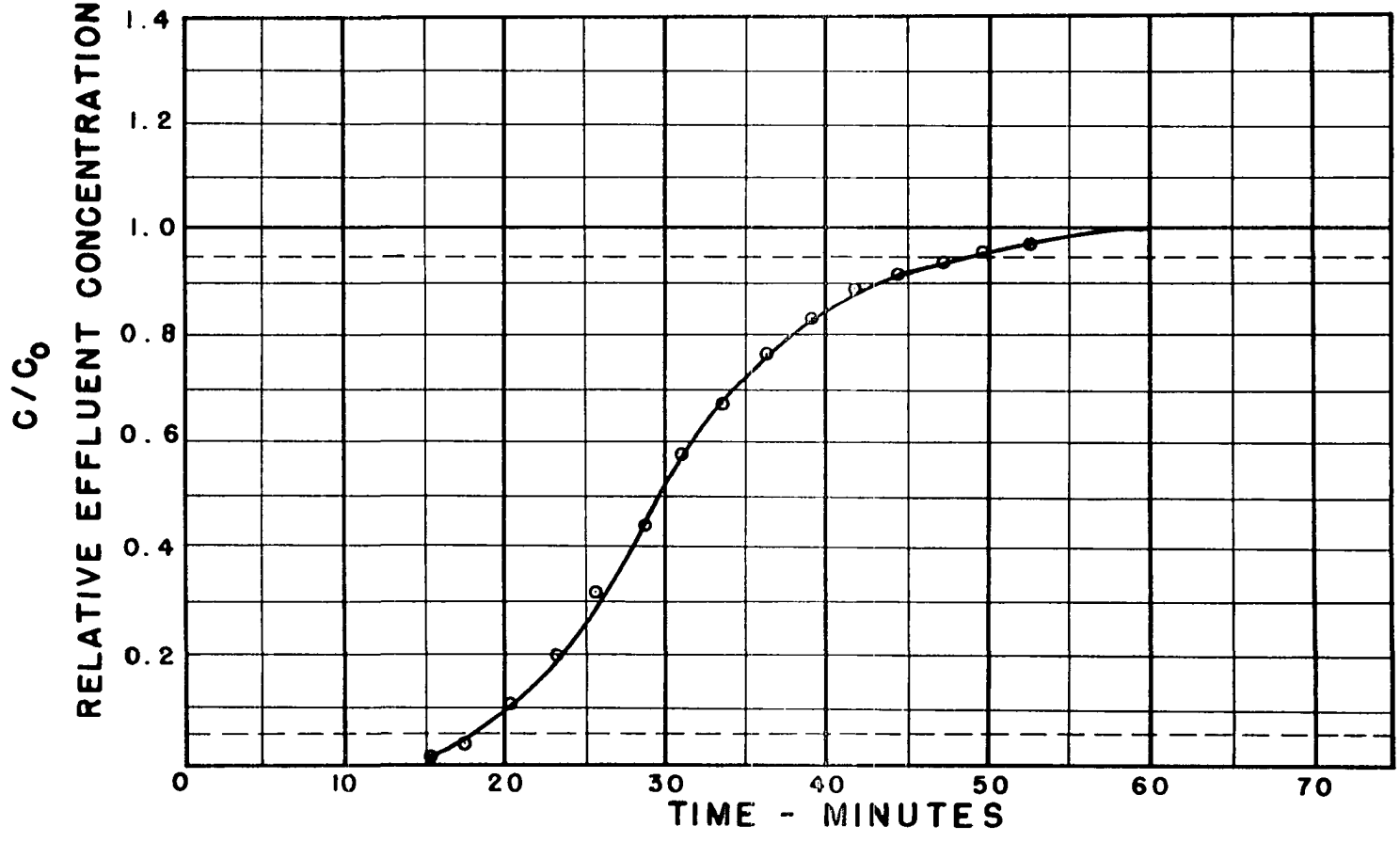

RUN NO. 66 INLET TEMP. 92 °F INLET PRESS. 810 PSIG. TOWER I.D. 2.9 in.

TOWER LGTH. 445.5 cm. FLOW RATE 23.02 ft/min. COMPOSITION: ____ %C_4 1.55 %C_5 ____ %C_6 ____ %C_7

DESSICANT: 03 GEL

N-PENTANE

FIGURE A 107

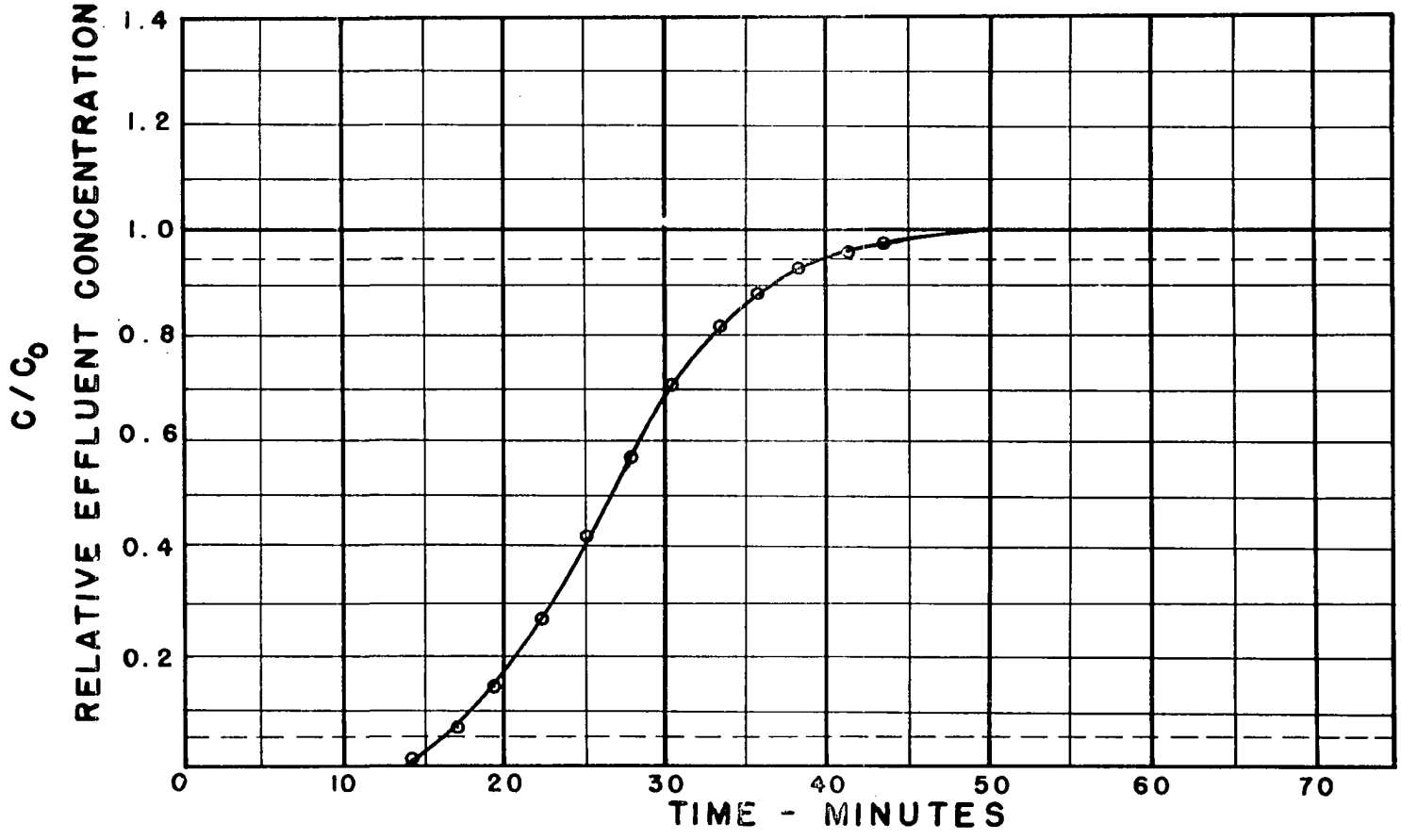

RUN NO. 68 INLET TEMP. 91 °F INLET PRESS. 805 PSIG. TOWER I. D. 2.9 in.

TOWER LGTH. 445.5 cm. FLOW RATE 23.46 ft/min. COMPOSITION: ____%C_4 0.54%C_5 ____%C_6 ____%C_7

DESSICANT: 03 GEL

N-PENTANE

FIGURE A 108

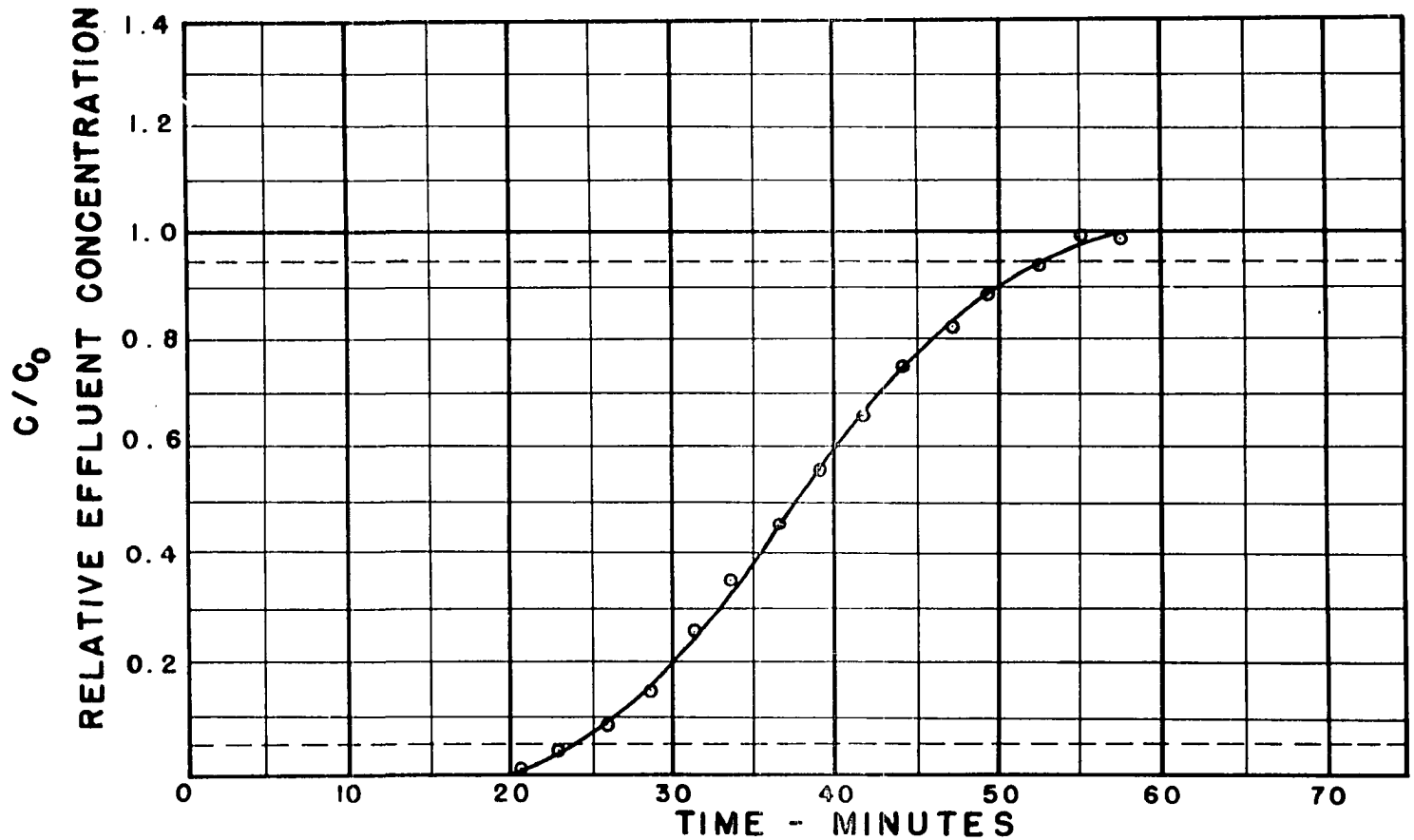

RUN NO. 84 INLET TEMP. 89.2 °F INLET PRESS. 805 PSIG. TOWER I.D. 2.9 in.

TOWER LGTH. 445.5 cm. FLOW RATE 45.81 ft/min. COMPOSITION: ____ %C_4 1.23 %C_5 ____ %C_6 ____ %C_7

DESSICANT: 03 GEL

N-PENTANE

FIGURE A 109

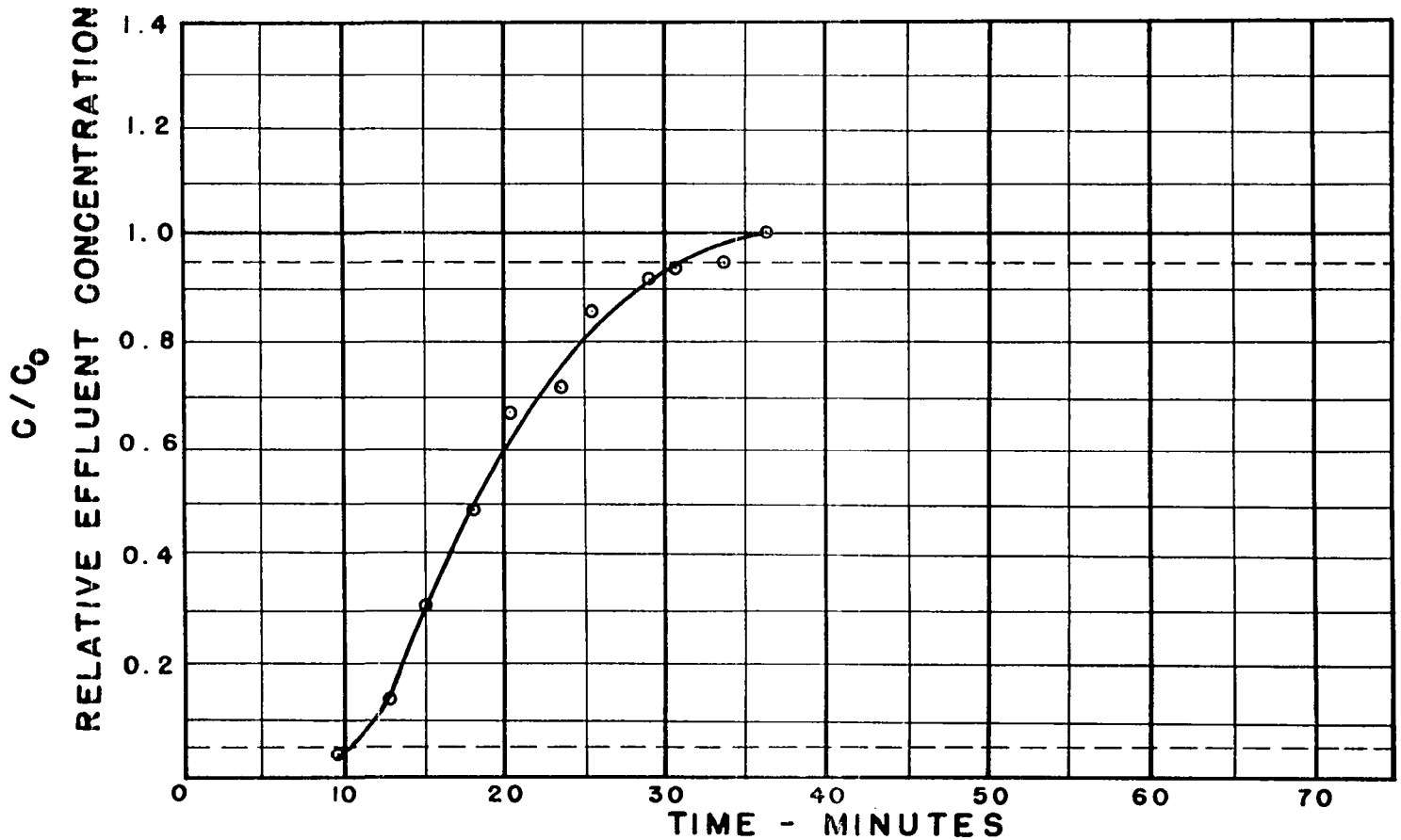

RUN NO. 86 INLET TEMP. 90 °F INLET PRESS. 808 PSIG. TOWER I.D. 2.9 in.

TOWER LGTH. 445.5 cm. FLOW RATE 45.08 ft/min. COMPOSITION: ____ %C_4 0.38 %C_5 ____ %C_6 ____ %C_7

DESSICANT: 03 GEL

N-PENTANE

FIGURE A 110

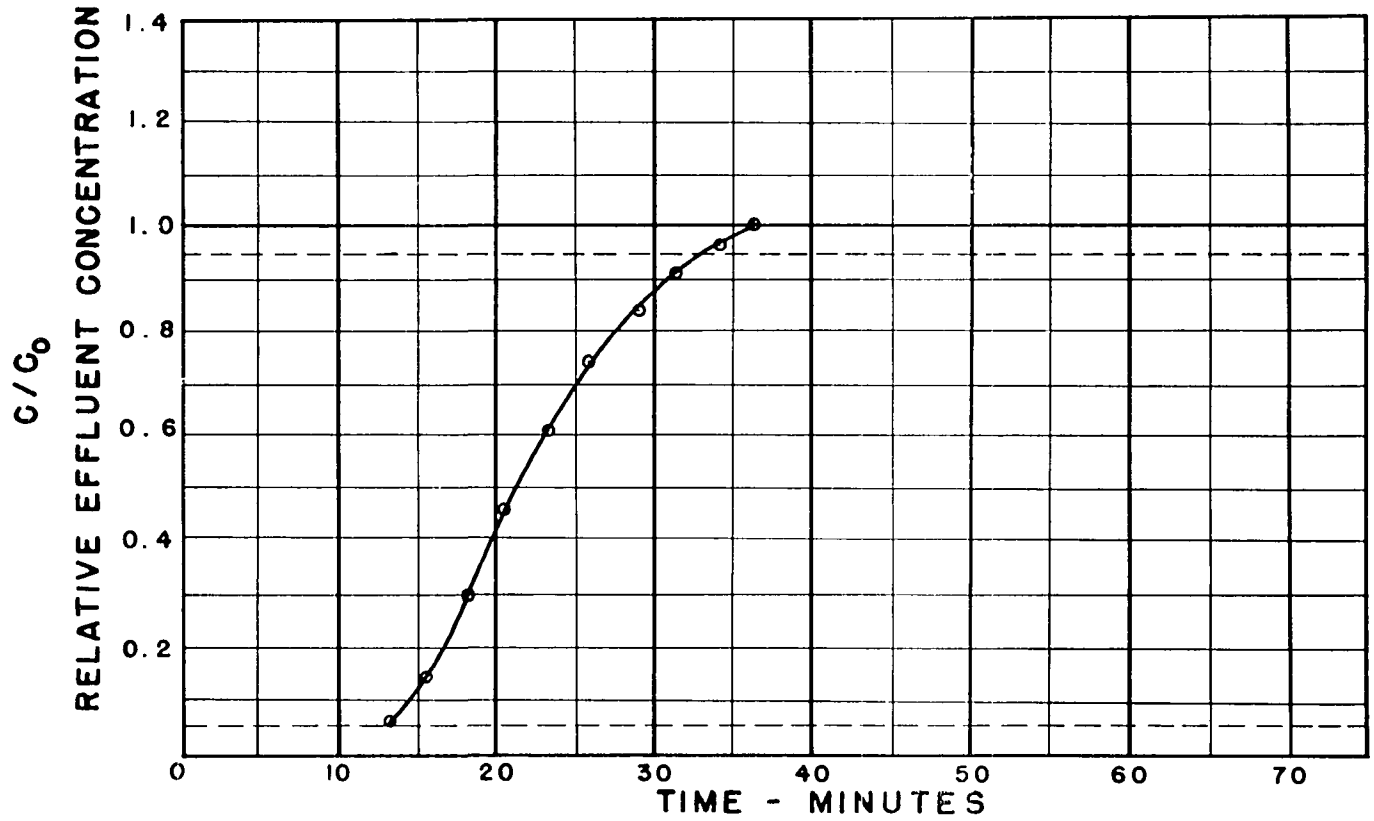

RUN NO. 87 INLET TEMP. 90.5 °F INLET PRESS. 803 PSIG. TOWER I.D. 2.9 in.

TOWER LGTH. 445.5 cm. FLOW RATE 44.57 ft/min. COMPOSITION: ____%C_4 1.62 %C_5 ____%C_6 ____%C_7

DESSICANT: 03 GEL

N-PENTANE

FIGURE A 111

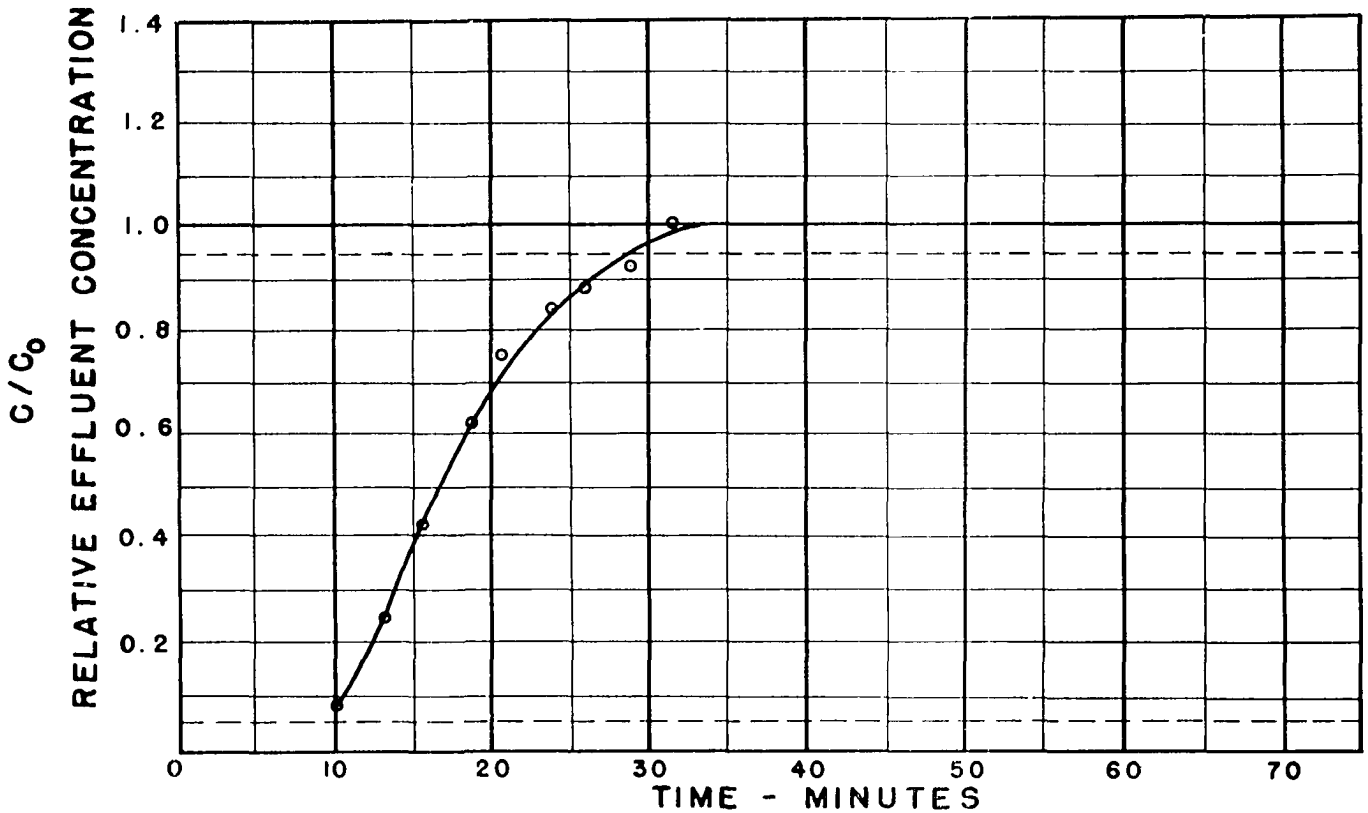

RUN NO. 88 INLET TEMP. 89 °F INLET PRESS. 810 PSIG. TOWER I.D. 2.9 in.

TOWER LGTH. 445.5 cm. FLOW RATE 45.78 ft/min. COMPOSITION: ____ %C_4 0.47 %C_5 ____ %C_6 ____ %C_7

DESSICANT: 03 GEL

N-PENTANE

FIGURE A 112

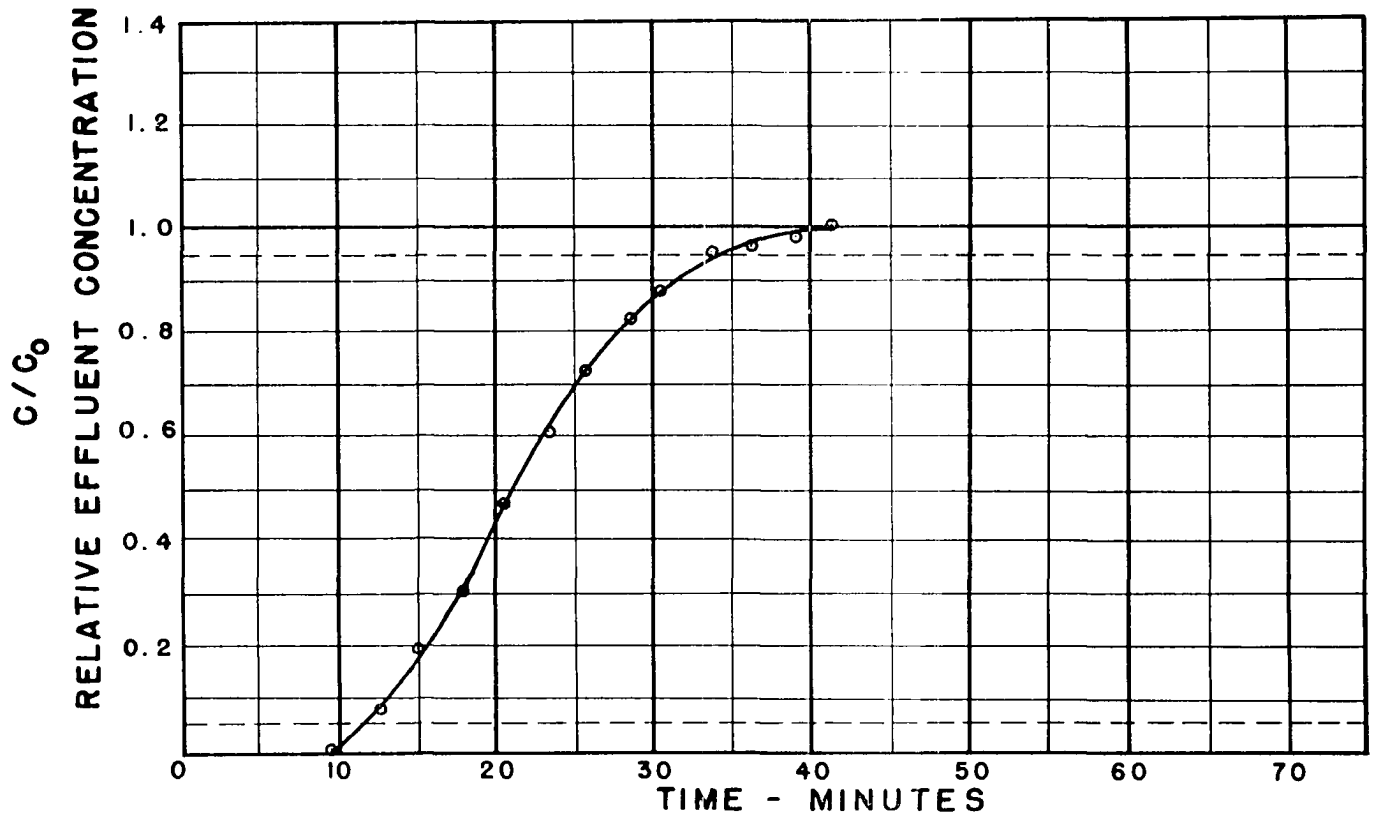

RUN NO. 89 INLET TEMP. 91 °F INLET PRESS. 800 PSIG. TOWER I.D. 2.9 in.

TOWER LGTH. 445.5 cm. FLOW RATE 44.98 ft/min. COMPOSITION: ____%C_4 .99 %C_5 ____%C_6 ____%C_7

DESSICANT: 03 GEL

N-PENTANE

FIGURE A 113

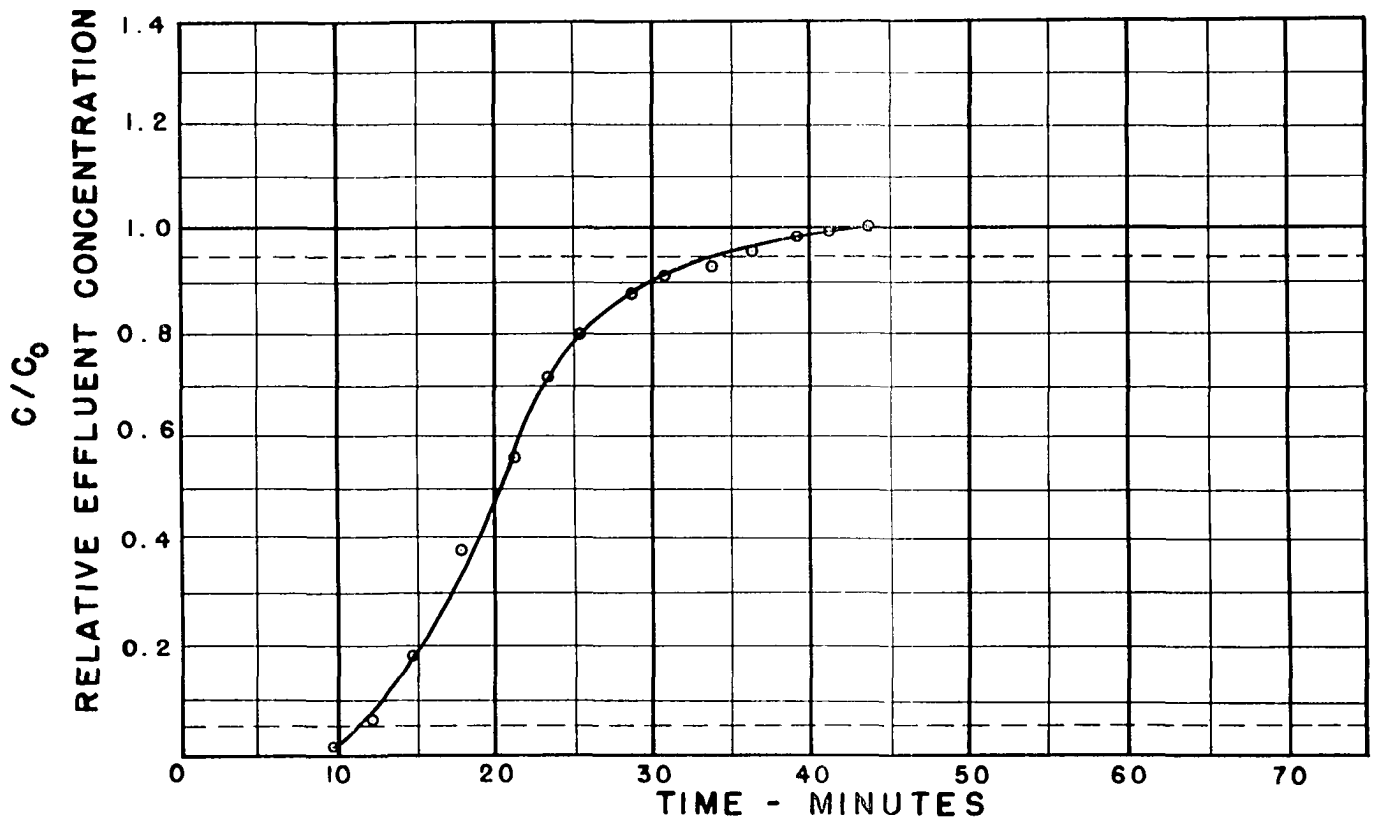

RUN NO. 90 INLET TEMP. 90 °F INLET PRESS. 795 PSIG. TOWER I.D. 2.9 in.

TOWER LGTH. 445.5 cm. FLOW RATE 46.44 ft/min. COMPOSITION: ____ %C_4 1.60 %C_5 ____ %C_6 ____ %C_7

DESSICANT: 03 GEL

N-PENTANE

FIGURE A 114

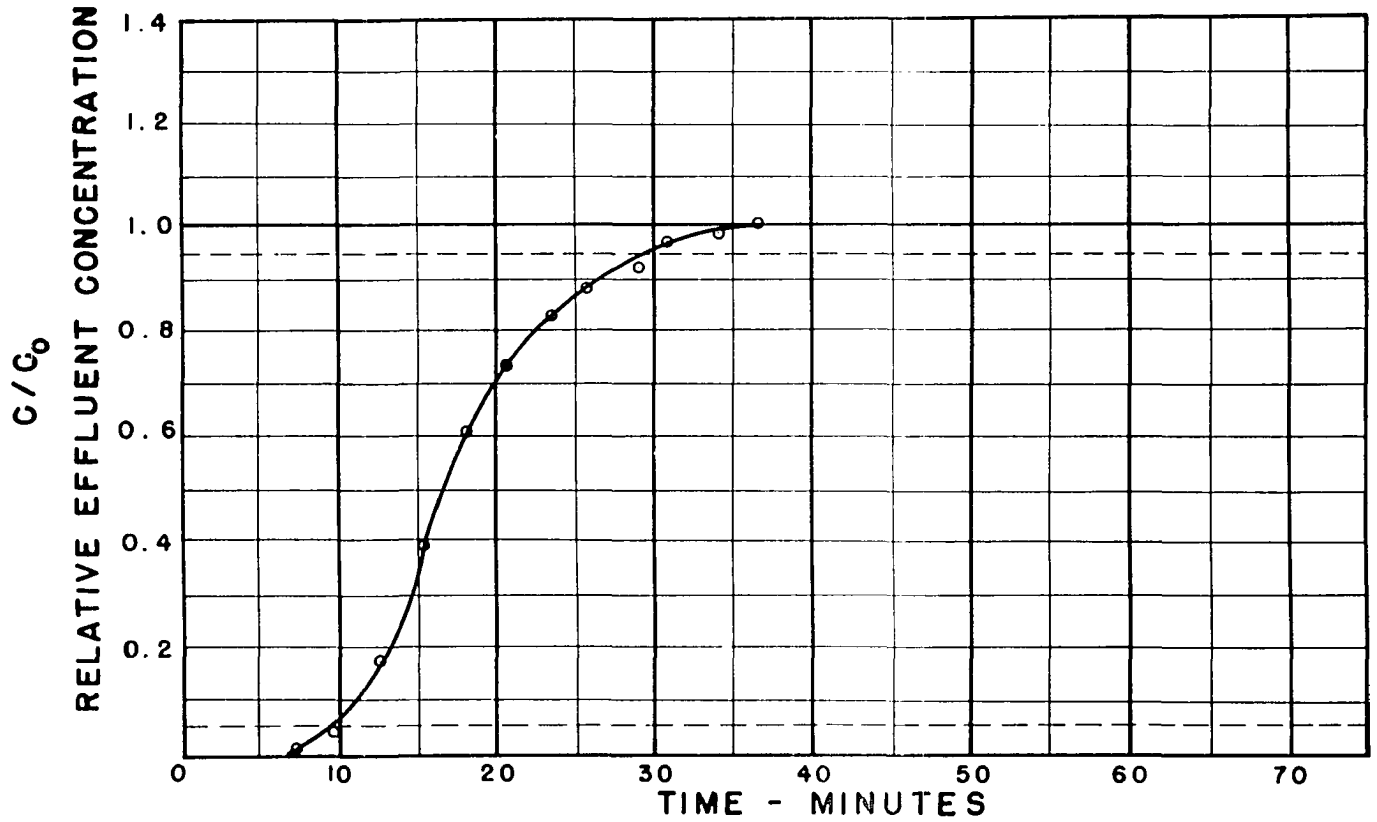

RUN NO. 119 INLET TEMP. 90.0 °F INLET PRESS. 805 PSIG. TOWER I.D. 2.9 in.

TOWER LGTH. 226 cm. FLOW RATE 10.36 ft/min. COMPOSITION: ____%C_4 1.14 %C_5 ____%C_6 ____%C_7

DESSICANT: 03 GEL

N-PENTANE

FIGURE A 115

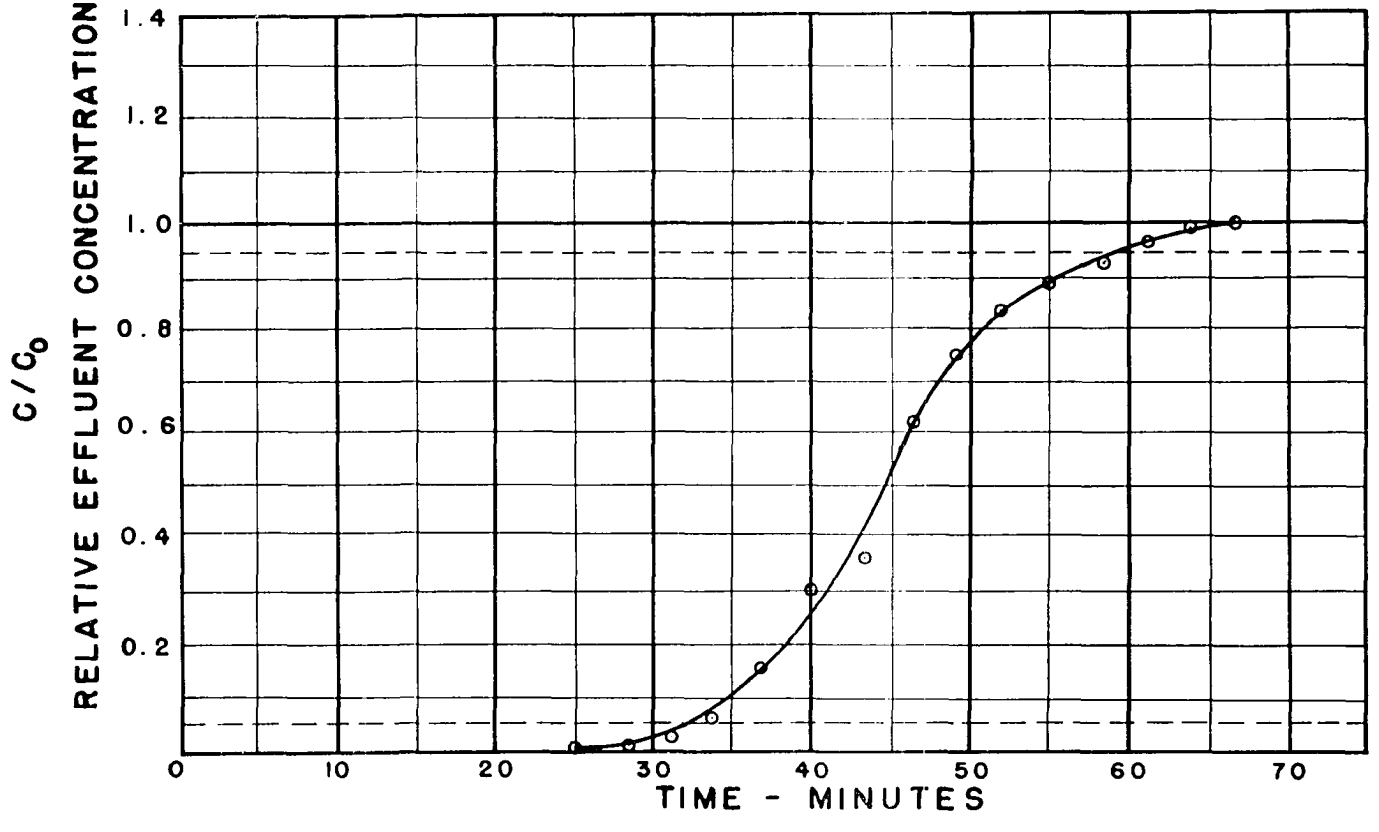

RUN NO. 120 INLET TEMP. 87 °F INLET PRESS. 800 PSIG. TOWER I.D. 2.9 in.

TOWER LGTH. 226 cm. FLOW RATE 10.45 ft/min. COMPOSITION: ____ %C_4 0.64 %C_5 ____ %C_6 ____ %C_7

DESSICANT: 03 GEL

N-PENTANE

FIGURE A 116

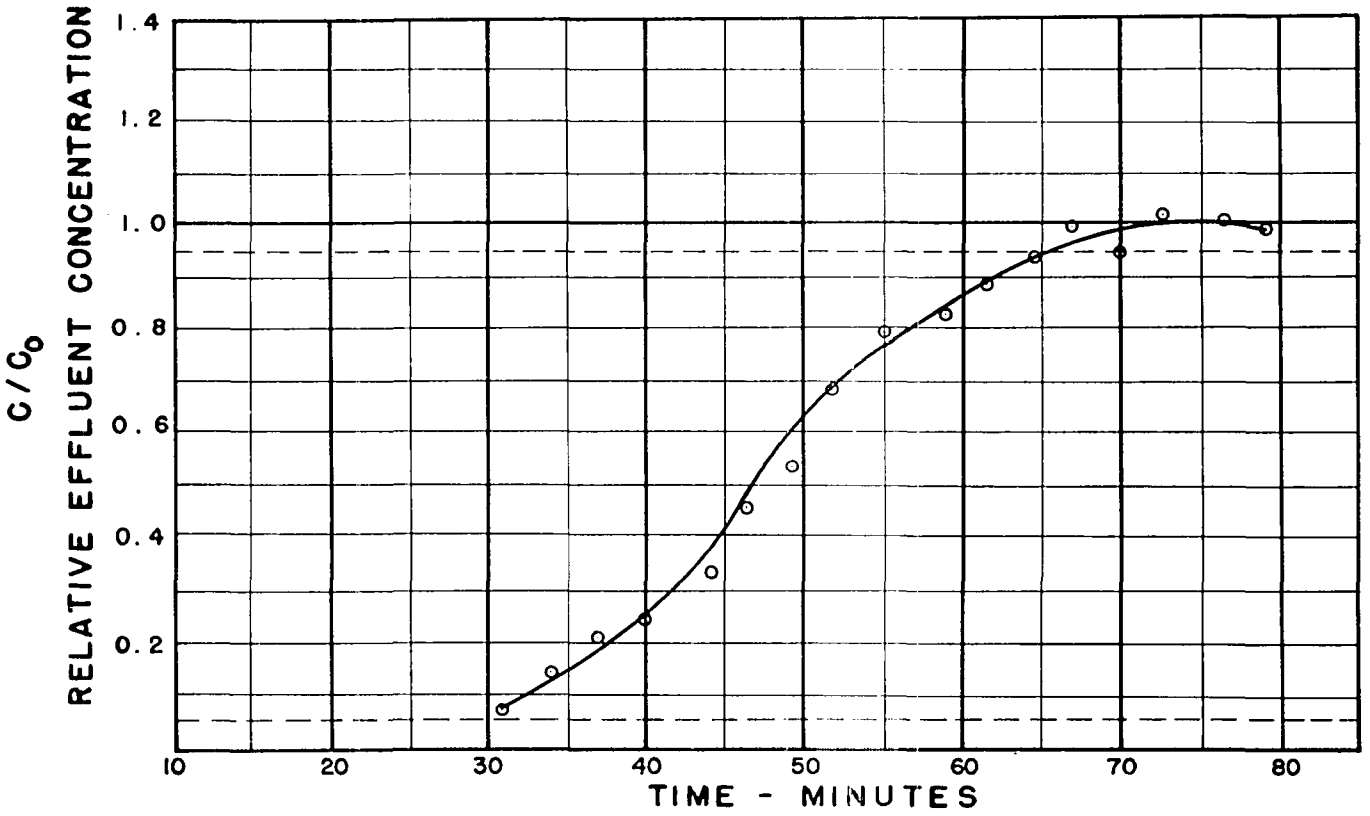

RUN NO. 121 INLET TEMP. 91.0 °F INLET PRESS. 800 PSIG. TOWER I.D. 2.9 in.

TOWER LGTH. 226 cm. FLOW RATE 10.87 ft/min. COMPOSITION: ____%C_4 0.94 %C_5 ____%C_6 ____%C_7

DESSICANT: 03 GEL

N-PENTANE

FIGURE A 117

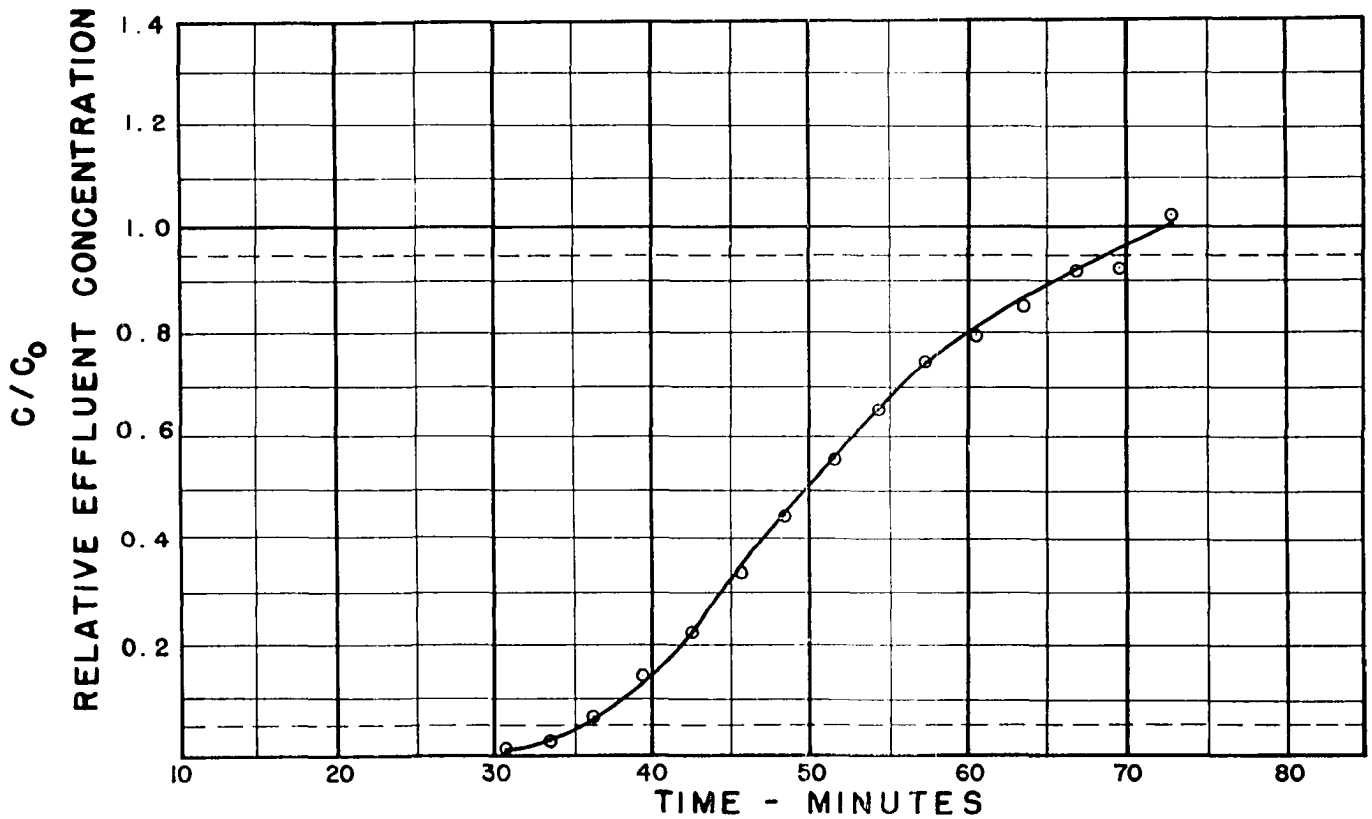

RUN NO. 122 INLET TEMP. 90 °F INLET PRESS. 800 PSIG. TOWER I.D. 2.90 in.

TOWER LGTH. 226 cm. FLOW RATE 18.98 ft/min. COMPOSITION: ____ %C_4 1.02 %C_5 ____ %C_6 ____ %C_7

DESSICANT: 03 GEL

N-PENTANE

FIGURE A 118

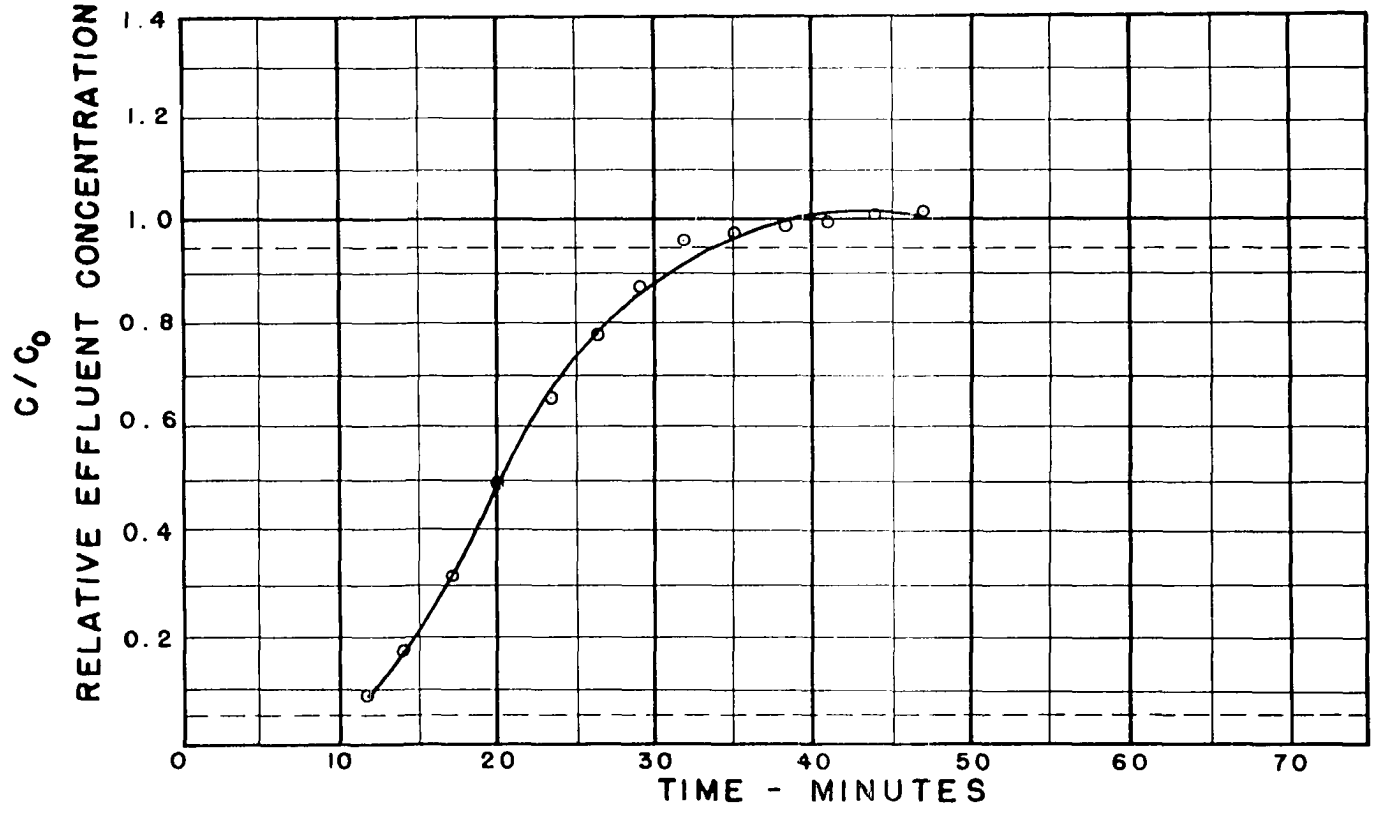

RUN NO. 125 INLET TEMP. 90.0 °F INLET PRESS. 800 PSIG. TOWER I.D. 2.9 in.

TOWER LGTH. 226 cm. FLOW RATE 41.01 ft/min. COMPOSITION: ____ %C_4 1.03 %C_5 ____ %C_6 ____ %C_7

DESSICANT: 03 GEL

N-PENTANE

FIGURE A 119

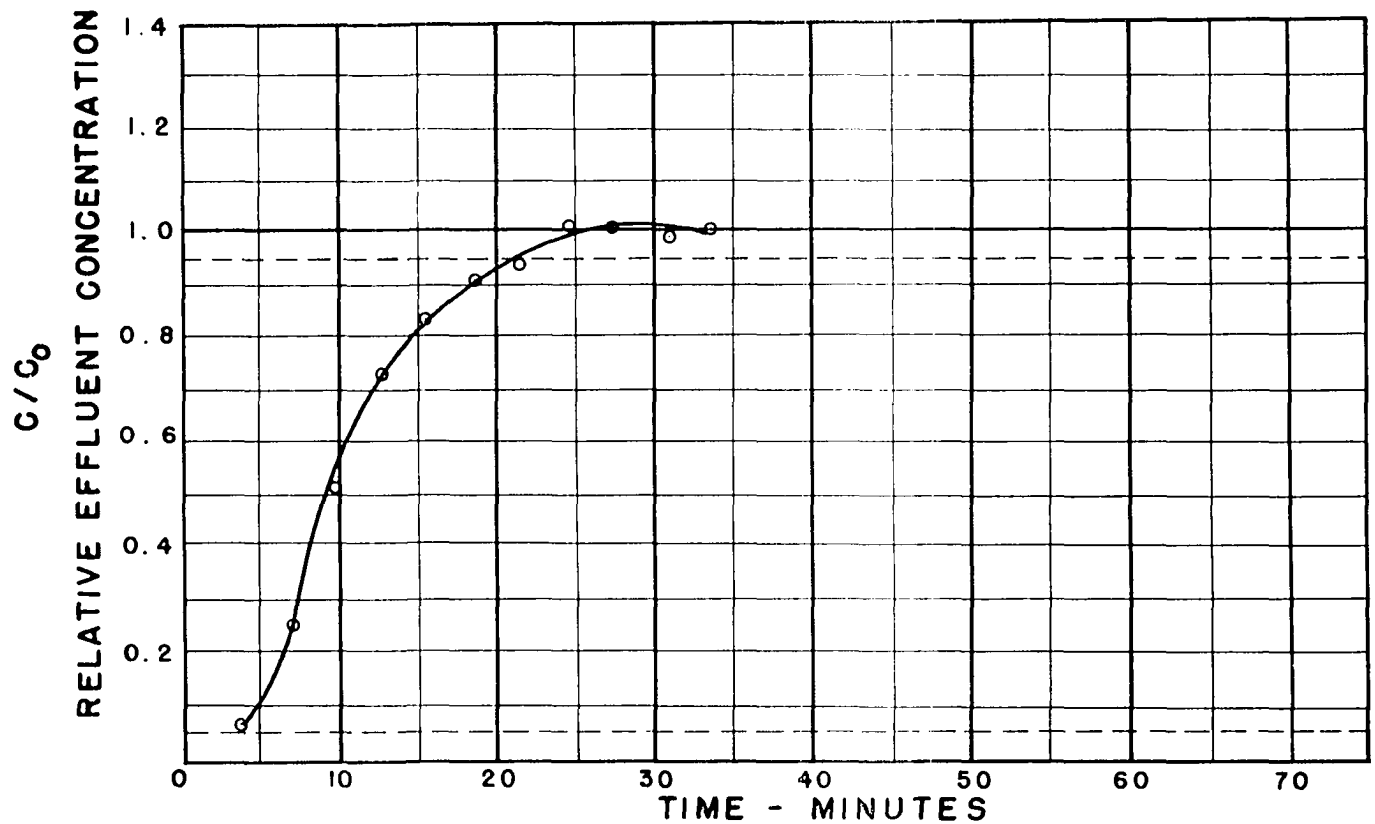

RUN NO. 126 INLET TEMP. 92.0 °F INLET PRESS. 800 PSIG. TOWER I.D. 2.9 in.

TOWER LGTH. 456 cm. FLOW RATE 35.72 ft/min. COMPOSITION: ____ %C_4 0.97 %C_5 ____ %C_6 ____ %C_7

DESSICANT: 03 GEL

N-PENTANE

FIGURE A 120

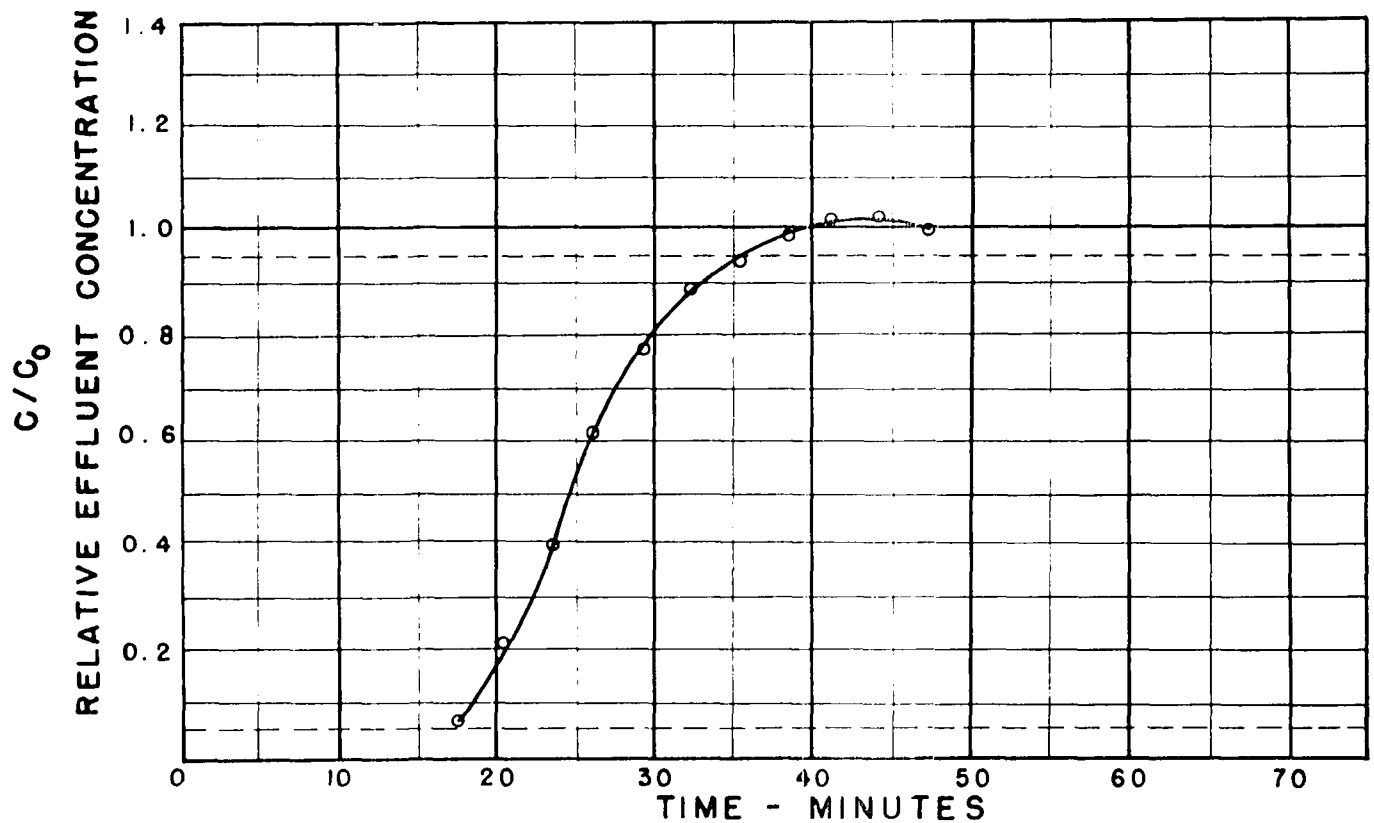

RUN NO. 132 INLET TEMP. 91.0 °F INLET PRESS. 800 PSIG. TOWER I.D. 2.9 in.

TOWER LGTH. 456 cm. FLOW RATE 20.26 ft/min. COMPOSITION: ____%C_4 0.87 %C_5 ____%C_6 ____%C_7

DESSICANT: 03 GEL

N-PENTANE

FIGURE A 121

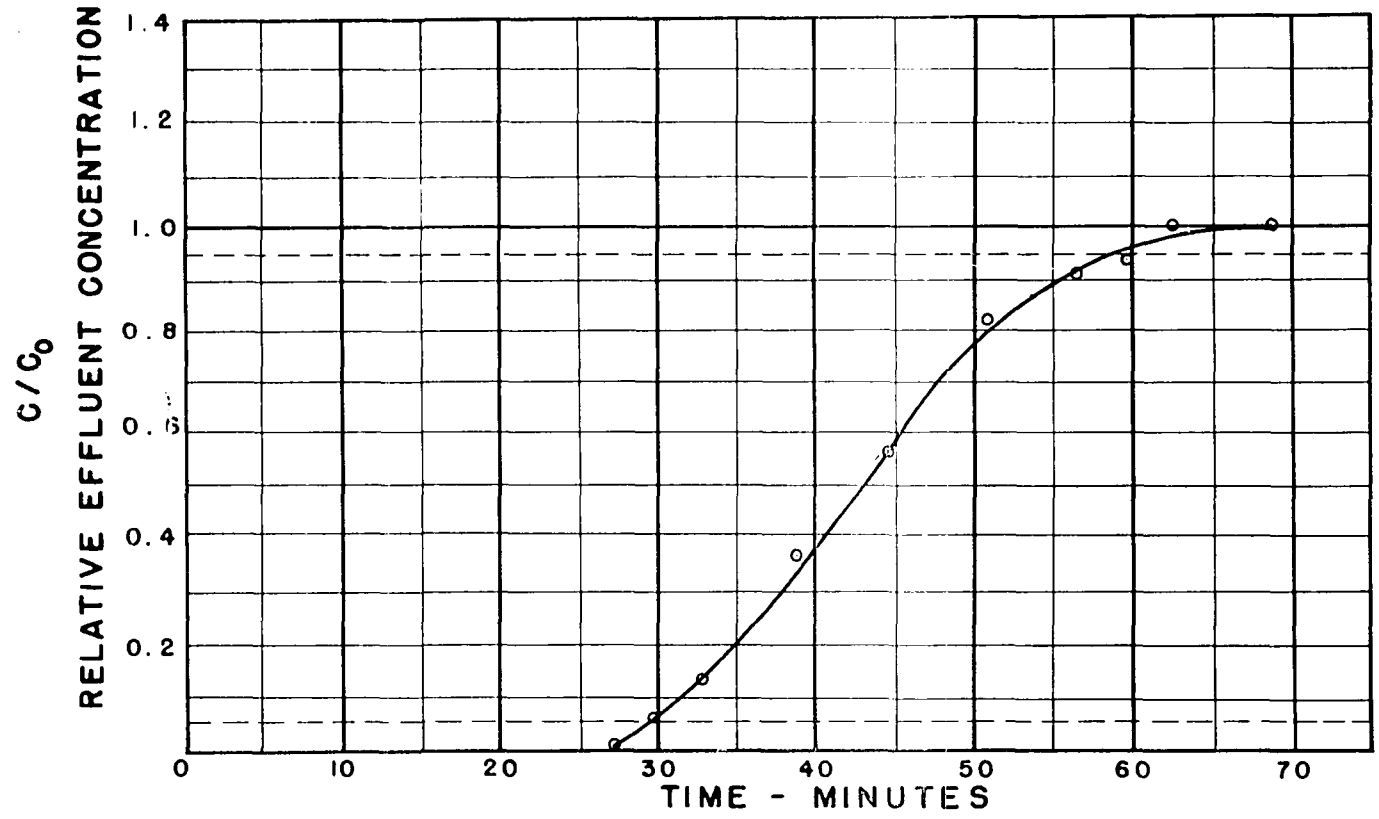

RUN NO. 135 INLET TEMP. 93.5 °F INLET PRESS. 810 PSIG. TOWER I.D. 2.9 in.

TOWER LGTH. 421 cm. FLOW RATE 10.0 ft/min. COMPOSITION: ____ %C_4 0.522 %C_5 ____ %C_6 ____ %C_7

DESSICANT: 03 GEL

N-PENTANE

FIGURE A 122

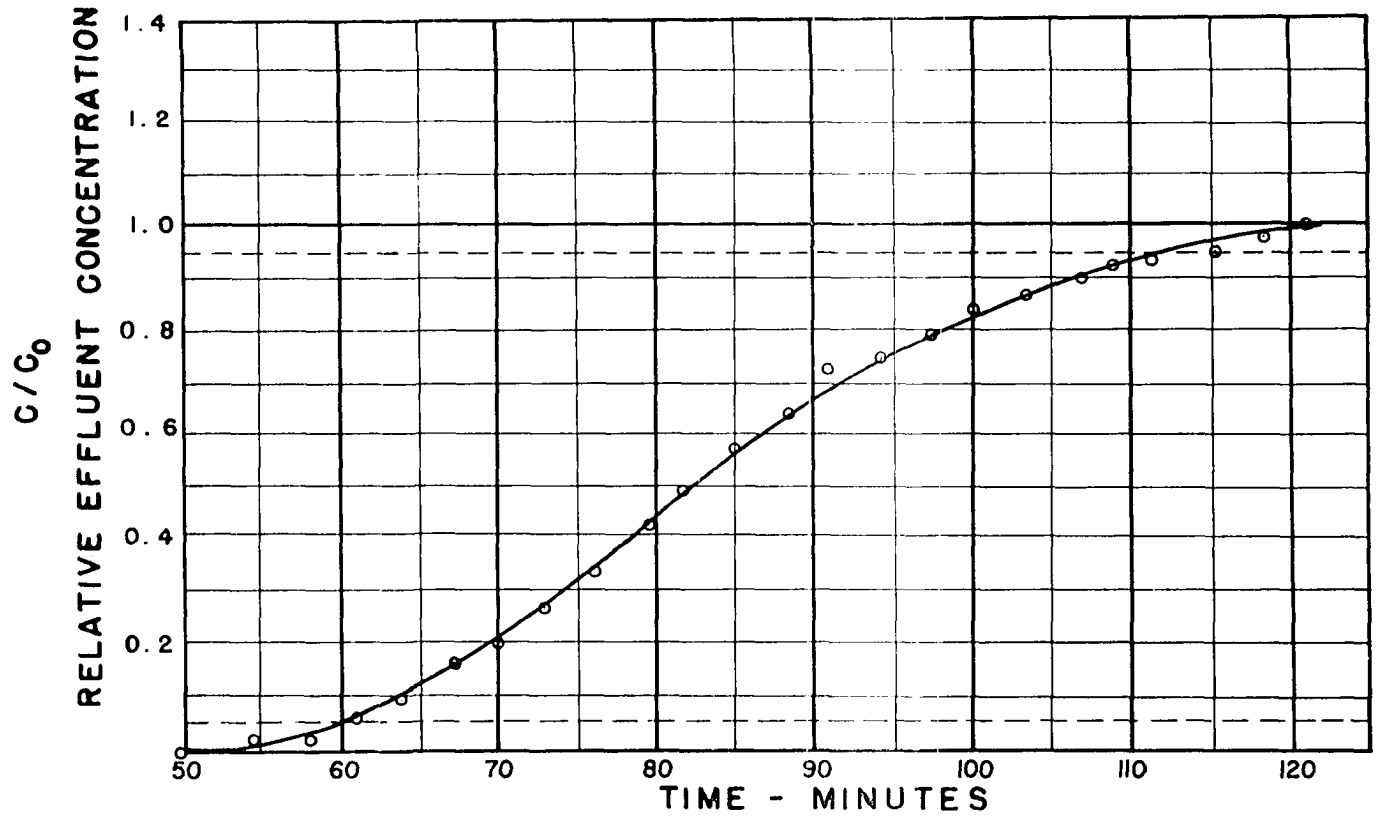

RUN NO. 52 INLET TEMP. 90.0 °F INLET PRESS. 801 PSIG. TOWER I.D. 2.067 in.

TOWER LGTH. 164 cm. FLOW RATE 24.64 ft/min. COMPOSITION: ____ %C_4 ____ %C_5 0.51 %C_6 ____ %C_7

DESSICANT: 03 GEL

N-HEXANE

FIGURE A 123

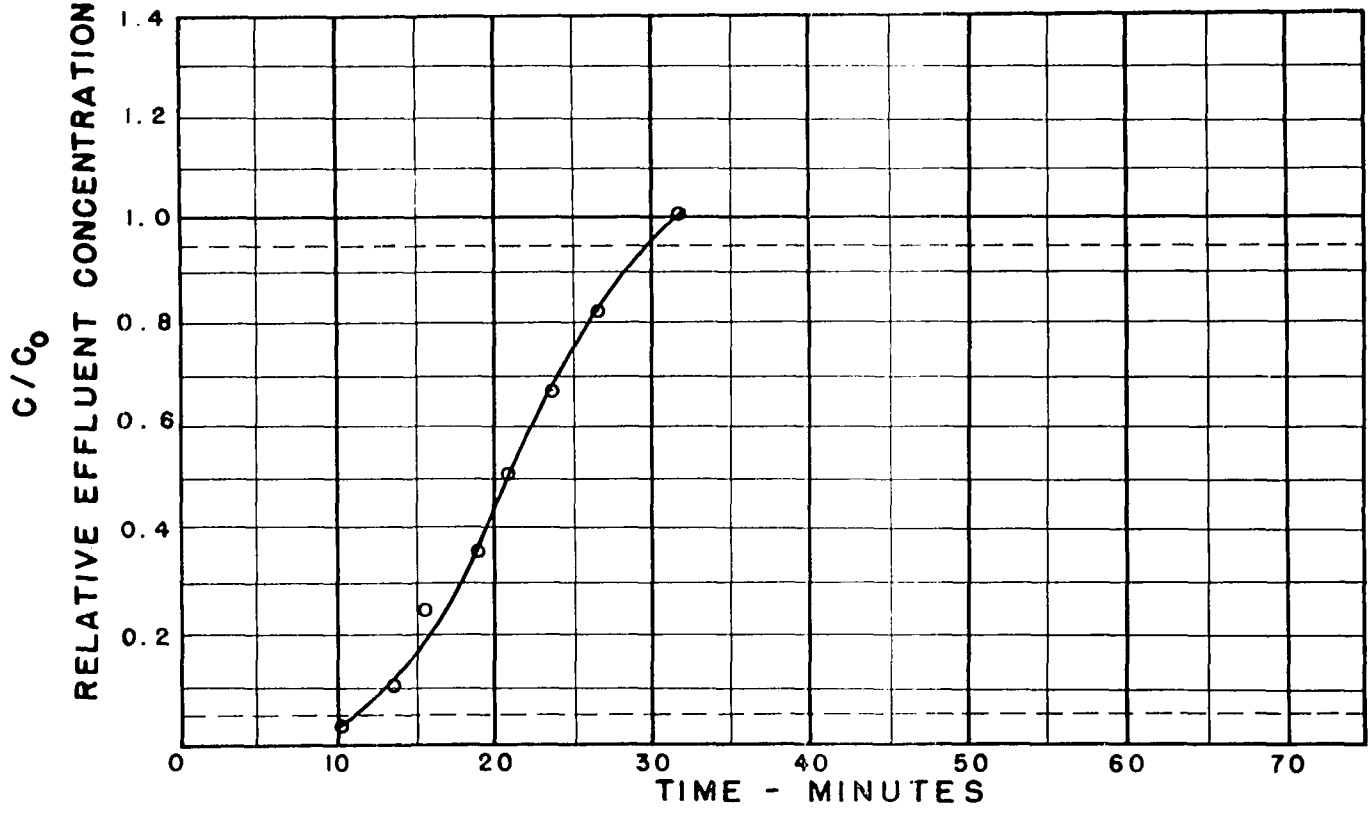

RUN NO. 55 INLET TEMP. 90.0 °F INLET PRESS. 790 PSIG. TOWER I. D. 2.067in.

TOWER LGTH. 164 cm. FLOW RATE 23.05 ft/min. COMPOSITION: ____%C_4 ____%C_5 1.16 %C_6 ____%C_7

DESSICANT: 03 GEL

N-HEXANE

FIGURE A 124

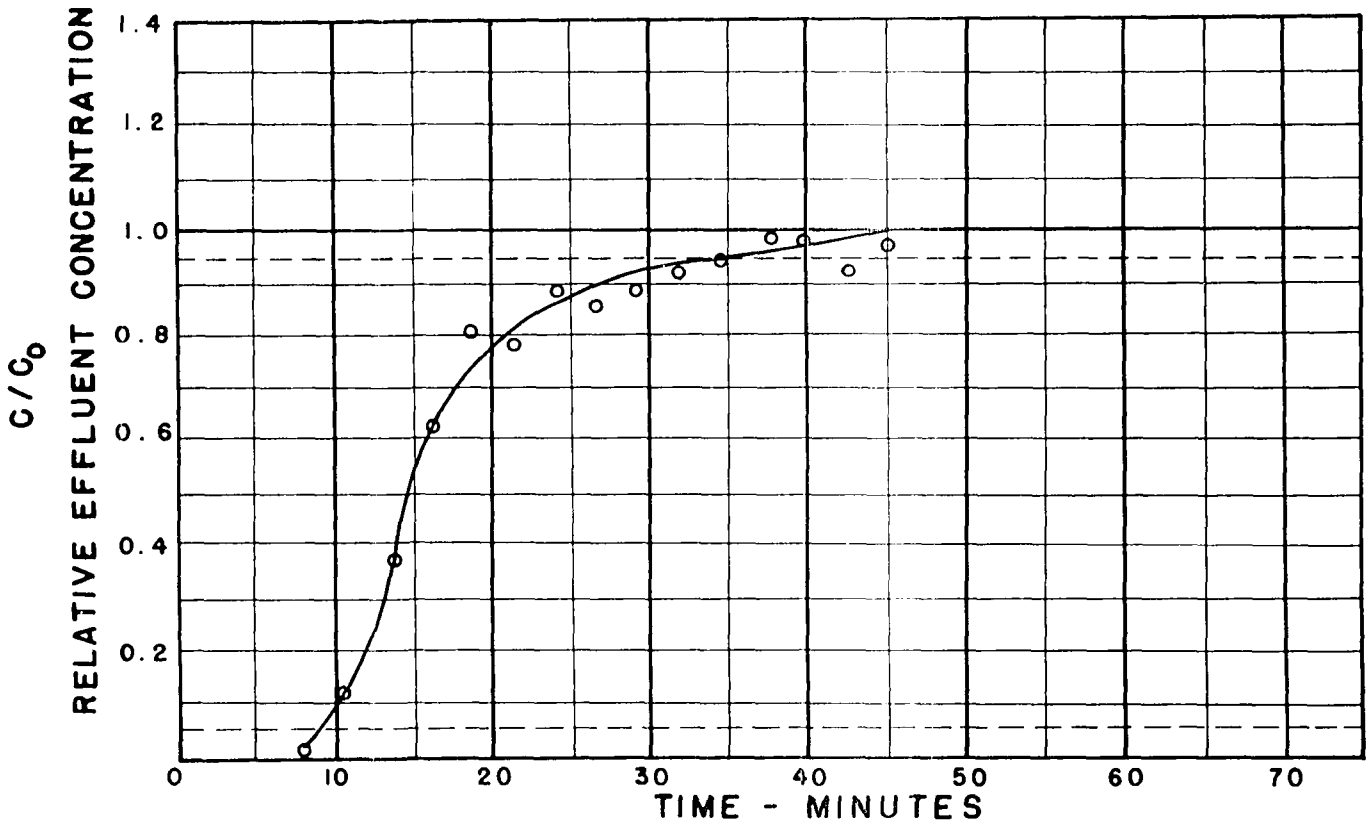

RUN NO. 69 INLET TEMP. 91.3 °F INLET PRESS. 810 PSIG. TOWER I.D. 2.9 in.

TOWER LGTH. 4.455 cm. FLOW RATE 24.37 ft/min. COMPOSITION: ____ %C_4 ____ %C_5 0.50 %C_6 ____ %C_7

DESSICANT: 03 GEL

N-HEXANE

FIGURE A 125

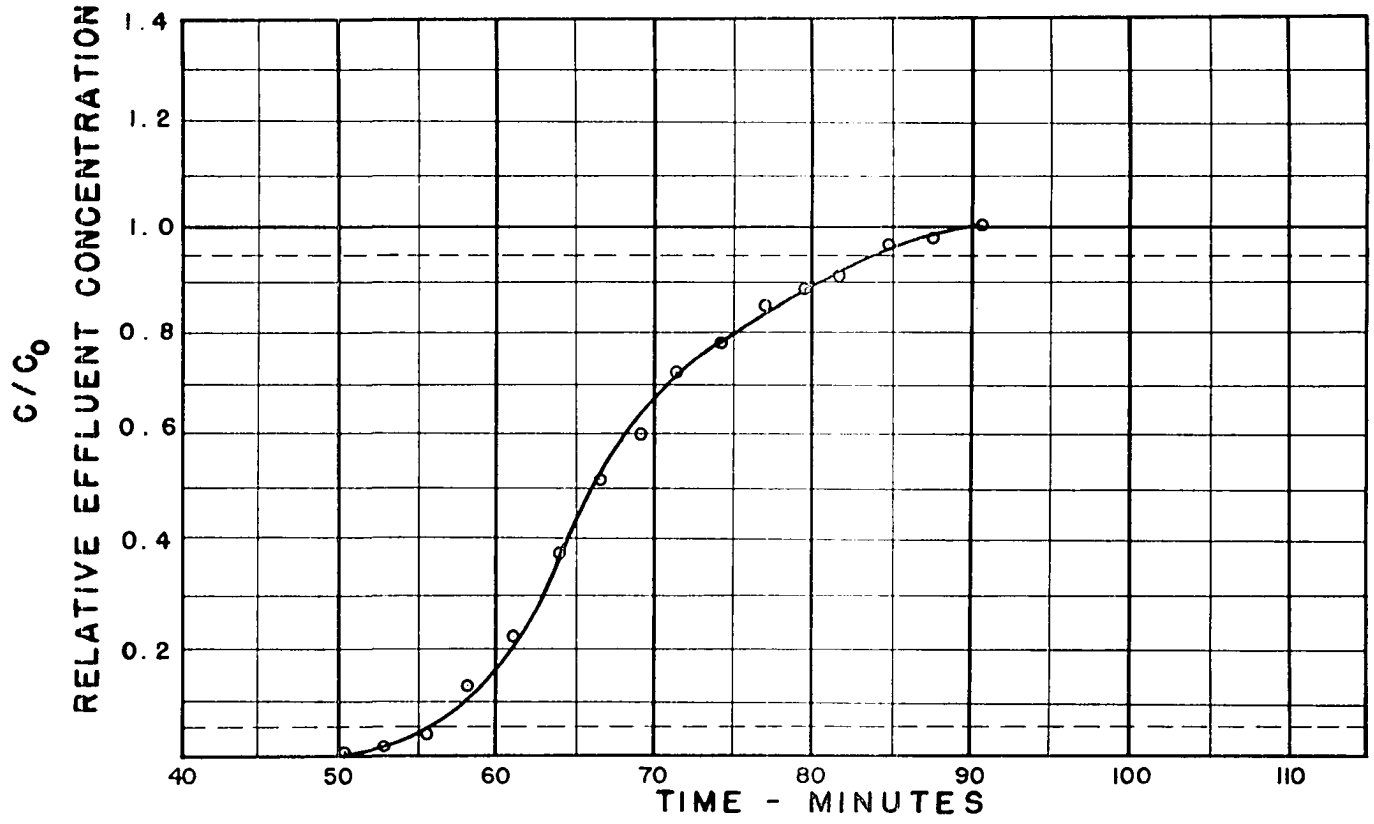

RUN NO. 70 INLET TEMP. 89 °F INLET PRESS. 808 PSIG. TOWER I.D. 2.9 in.

TOWER LGTH. 445.5 cm. FLOW RATE 24.50 ft/min. COMPOSITION: ____%C_4 ____%C_5 0.93 %C_6 ____%C_7

DESSICANT: 03 GEL

N-HEXANE

FIGURE A 126

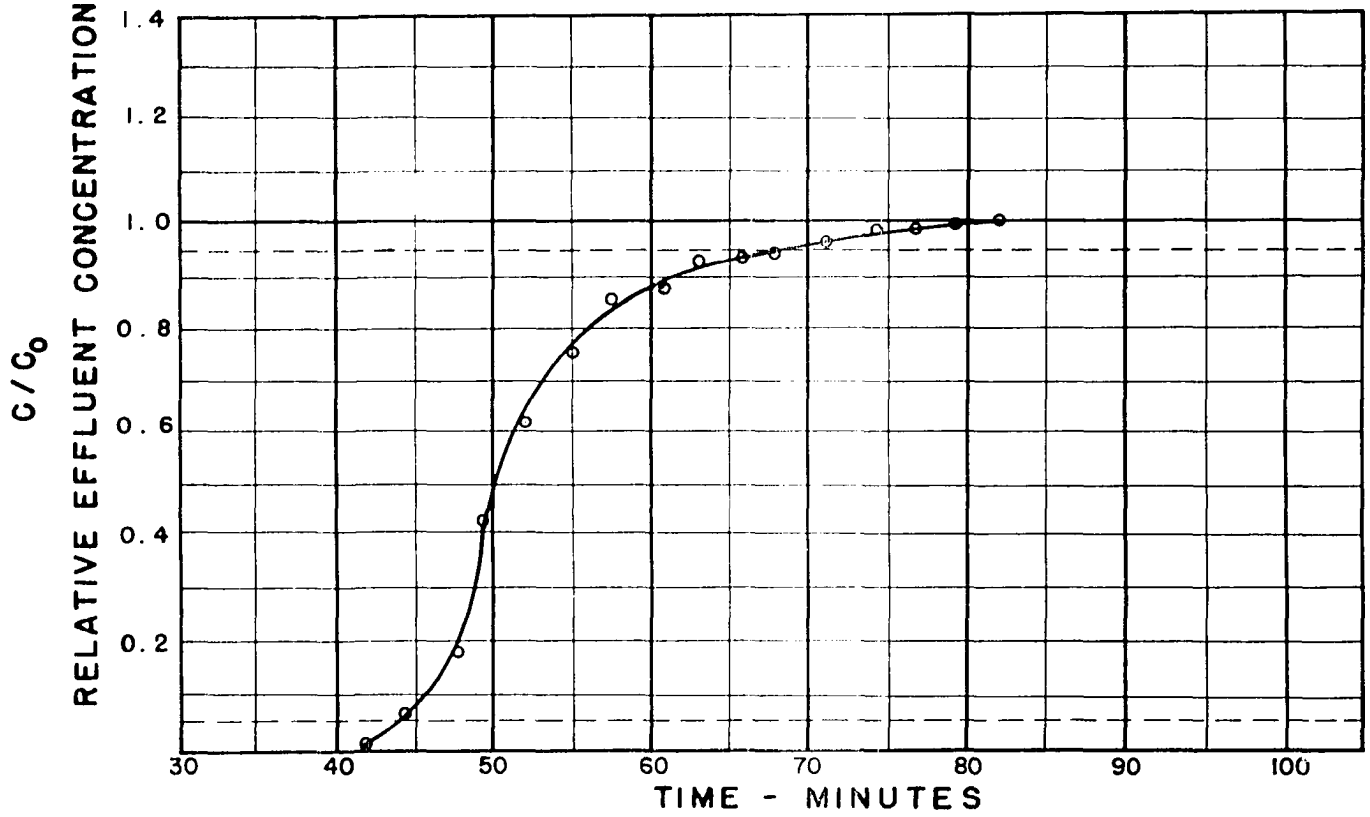

RUN NO. 71 INLET TEMP. 91 °F INLET PRESS. 806 PSIG. TOWER I.D. 2.9 in.

TOWER LGTH. 445.5 cm. FLOW RATE 10.54 ft/min. COMPOSITION: ____ %C_4 ____ %C_5 0.61 %C_6 ____ %C_7

DESSICANT: 03 GEL

N-HEXANE

FIGURE A 127

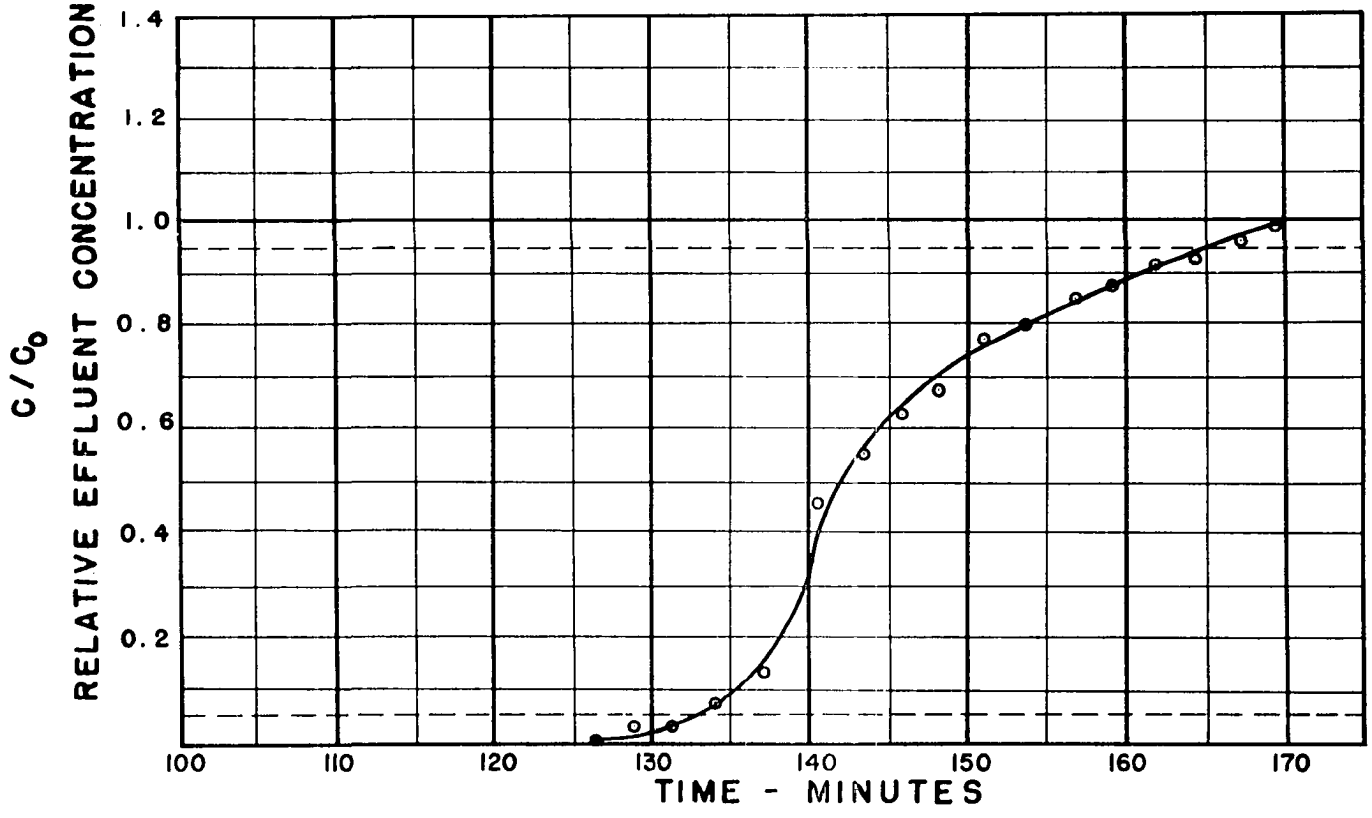

RUN NO. 72 INLET TEMP. 90.2 °F INLET PRESS. 805 PSIG. TOWER I.D. 2.9 in.

TOWER LGTH. 445.5 cm. FLOW RATE 10.71 ft/min. COMPOSITION: ____ %C_4 ____ %C_5 1.20 %C_6 ____ %C_7

DESSICANT: 03 GEL

N-HEXANE

FIGURE A 128

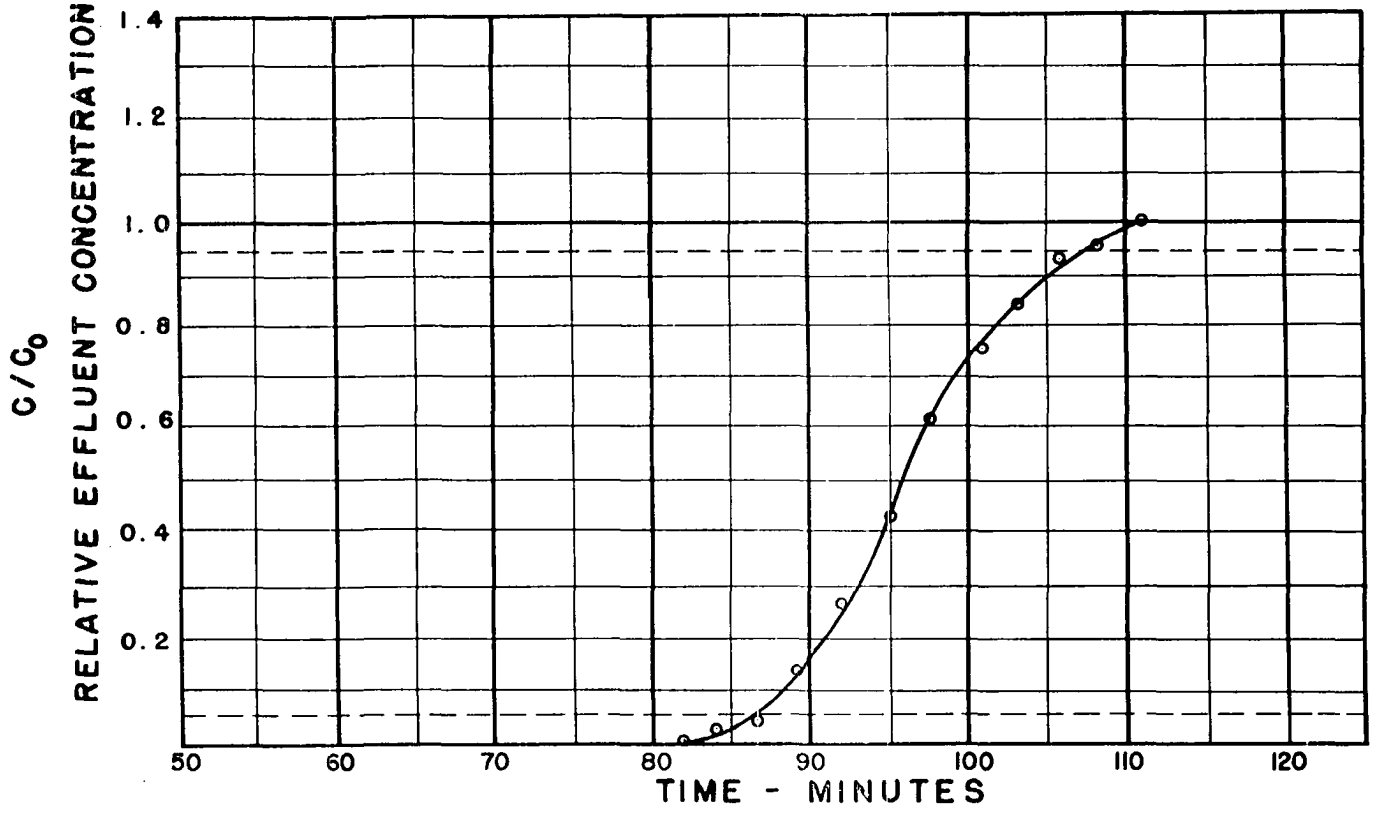

RUN NO. 73 INLET TEMP. 91 °F INLET PRESS. 802 PSIG. TOWER I. D. 2.9 in.

TOWER LGTH. 445.5 cm. FLOW RATE 11.15 ft/min. COMPOSITION: ____%C_4 ____%C_5 0.47 %C_6 ____%C_7

DESSICANT: 03 GEL

N-HEXANE

FIGURE A 129

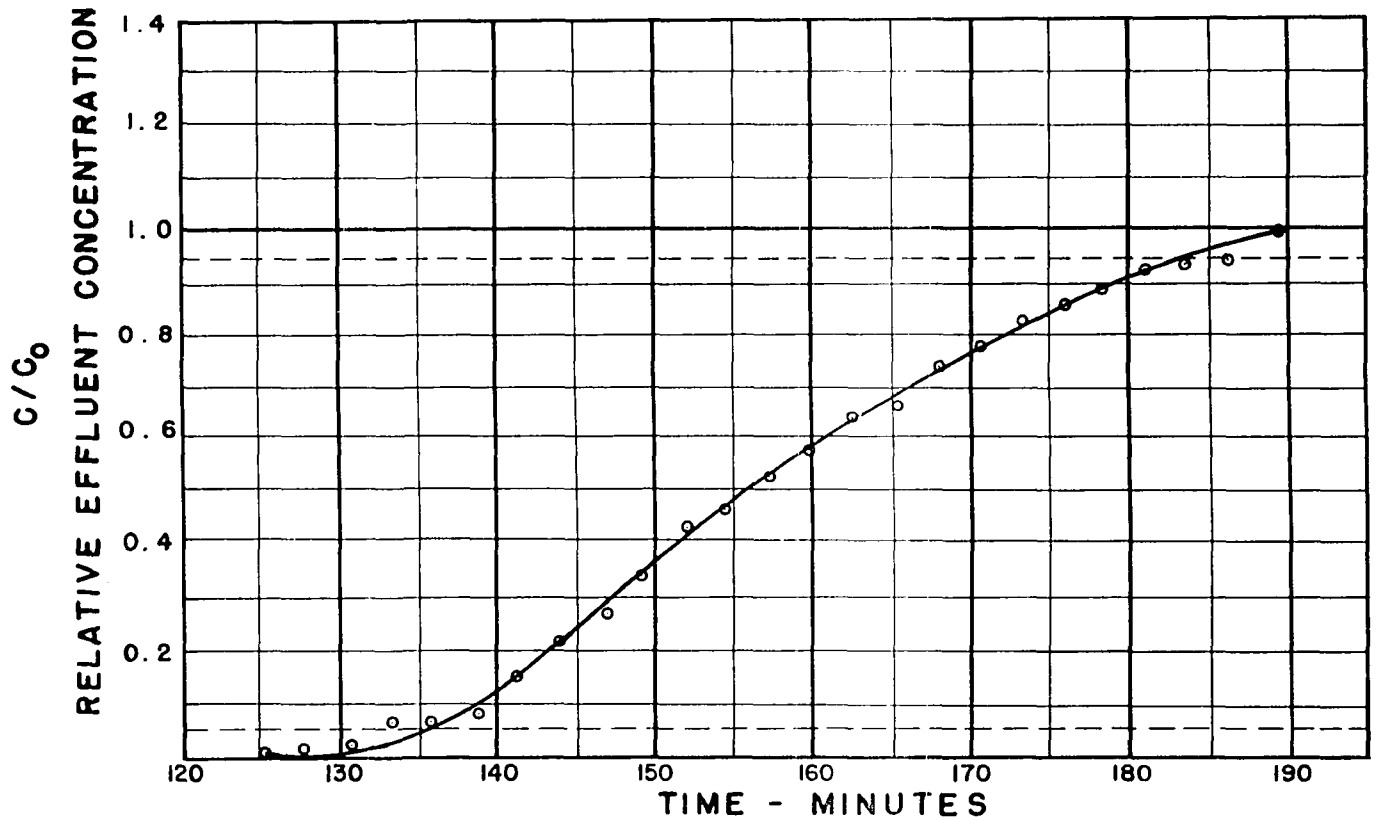

RUN NO. 74 INLET TEMP. 92 °F INLET PRESS. 785 PSIG. TOWER I.D. 2.9 in.

TOWER LGTH. 445.5 cm. FLOW RATE 11.30 ft/min. COMPOSITION: ____ %C_4 ____ %C_5 0.99 %C_6 ____ %C_7

DESSICANT: 03 GEL

N-HEXANE

FIGURE A 130

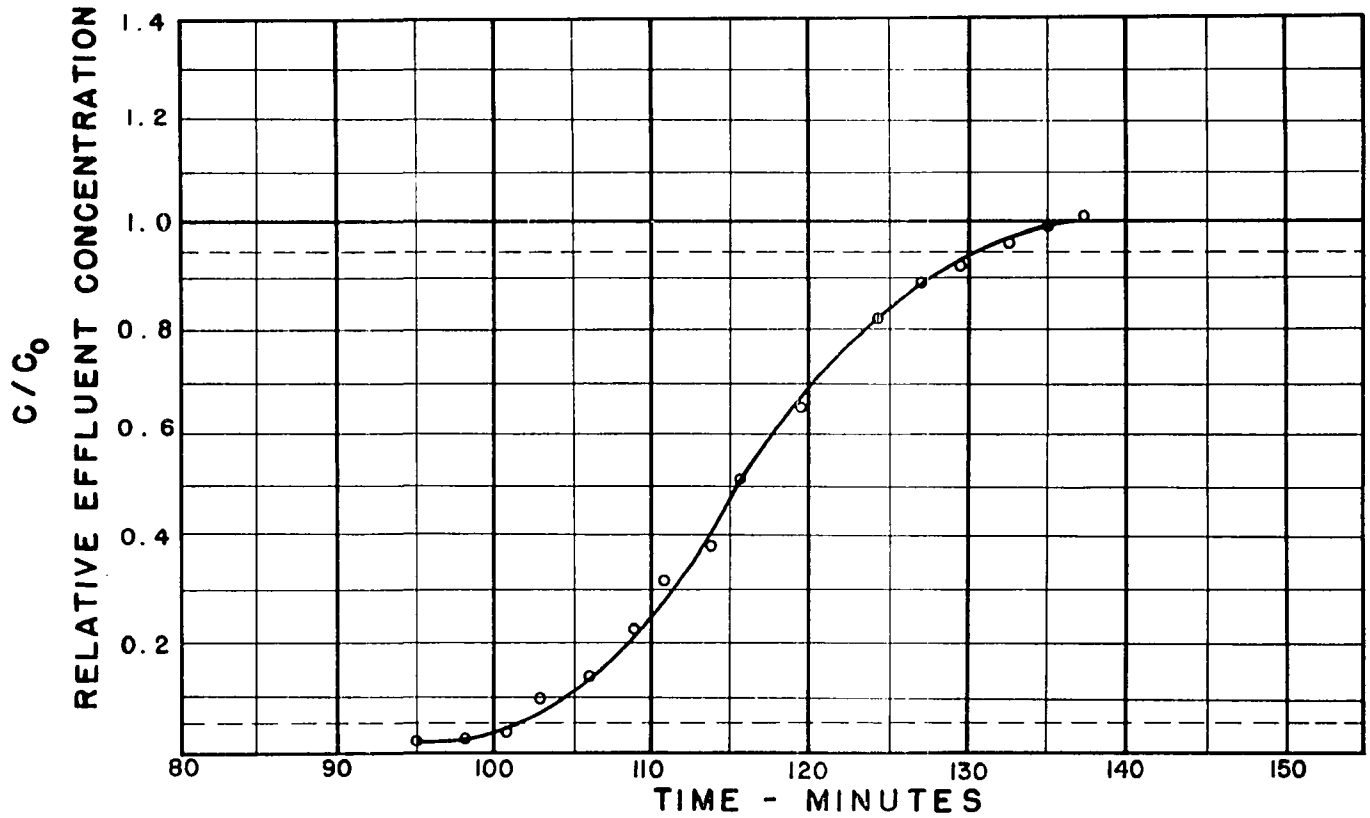

RUN NO. 76 INLET TEMP. 93 °F INLET PRESS. 815 PSIG. TOWER I.D. 2.0 in.

TOWER LGTH. 445.5 cm. FLOW RATE 21.20 ft/min. COMPOSITION: ____%C_4 ____%C_5 1.37 %C_6 ____%C_7

DESSICANT: 03 GEL

N-HEXANE

FIGURE A 131

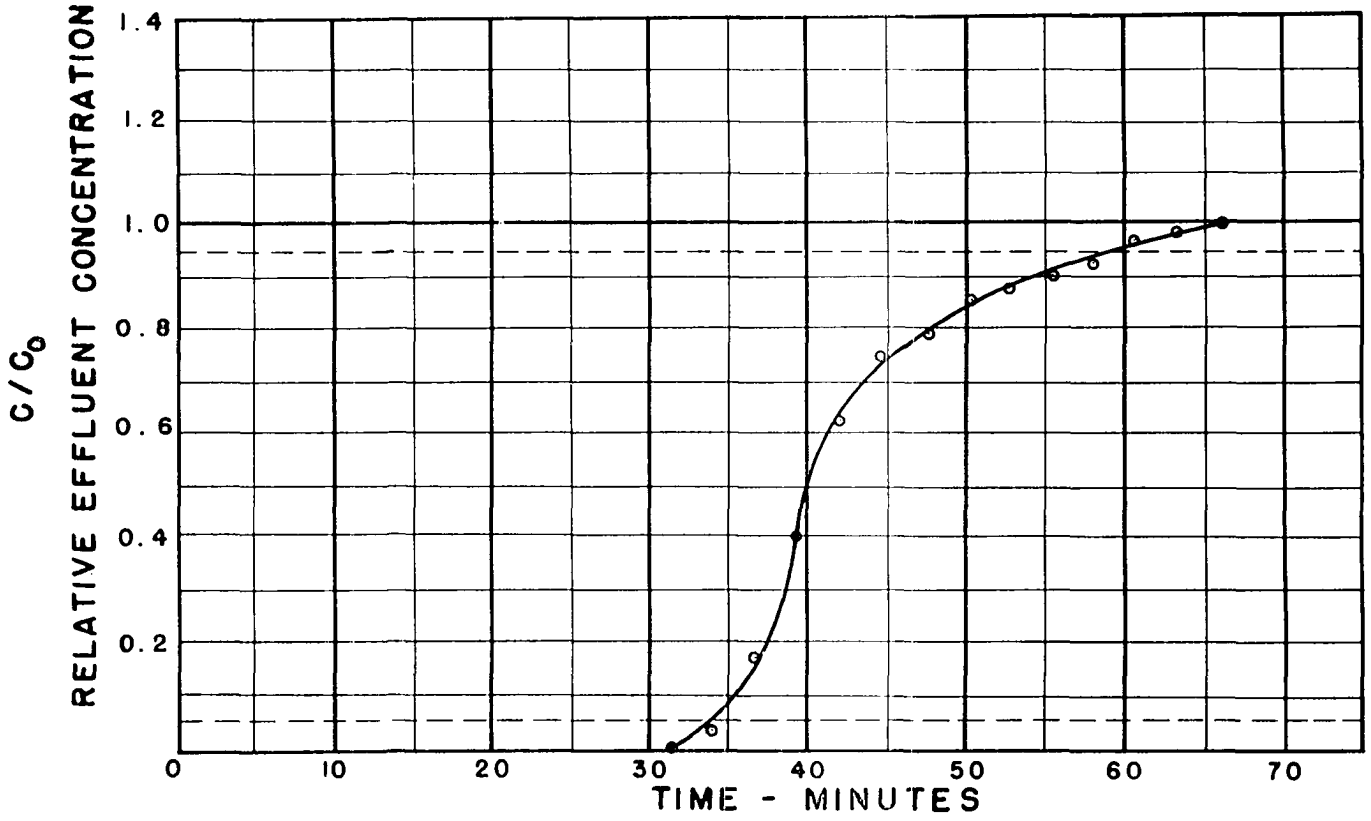

RUN NO. 77 INLET TEMP. 88 °F INLET PRESS. 820 PSIG. TOWER I.D. 2.9 in.

TOWER LGTH. 445.5 cm. FLOW RATE 19.87 ft/min. COMPOSITION: ____%C_4 ____%C_5 0.94 %C_6 ____%C_7

DESSICANT: 03 GEL

N-HEXANE

FIGURE A 132

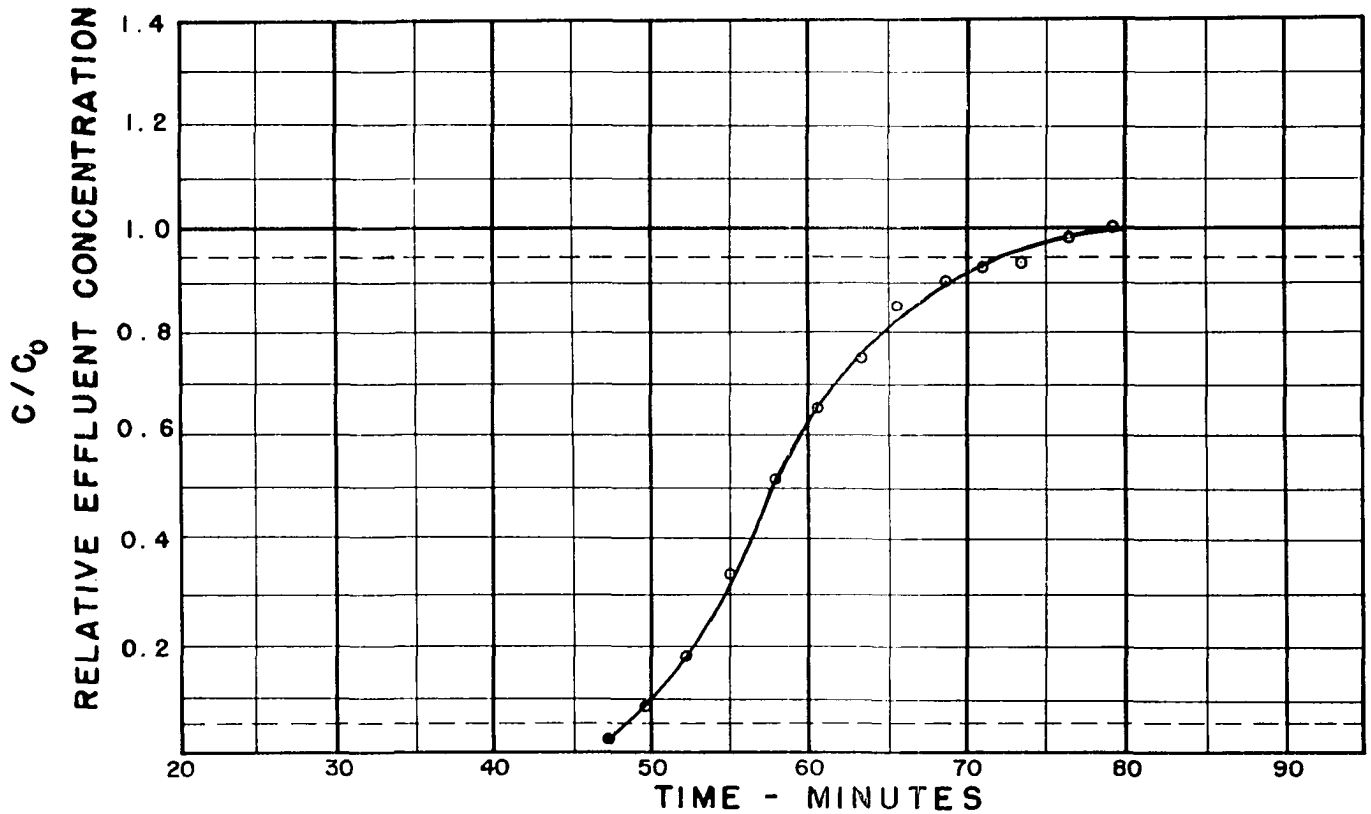

RUN NO. 78 INLET TEMP. 91 °F INLET PRESS. 800 PSIG. TOWER I.D. 2.9 in.

TOWER LGTH. 445.5 cm. FLOW RATE 19.87 ft/min. COMPOSITION: ____%C_4 ____%C_5 .48 %C_6 ____%C_7

DESSICANT: 03 GEL

N-HEXANE

FIGURE A 133

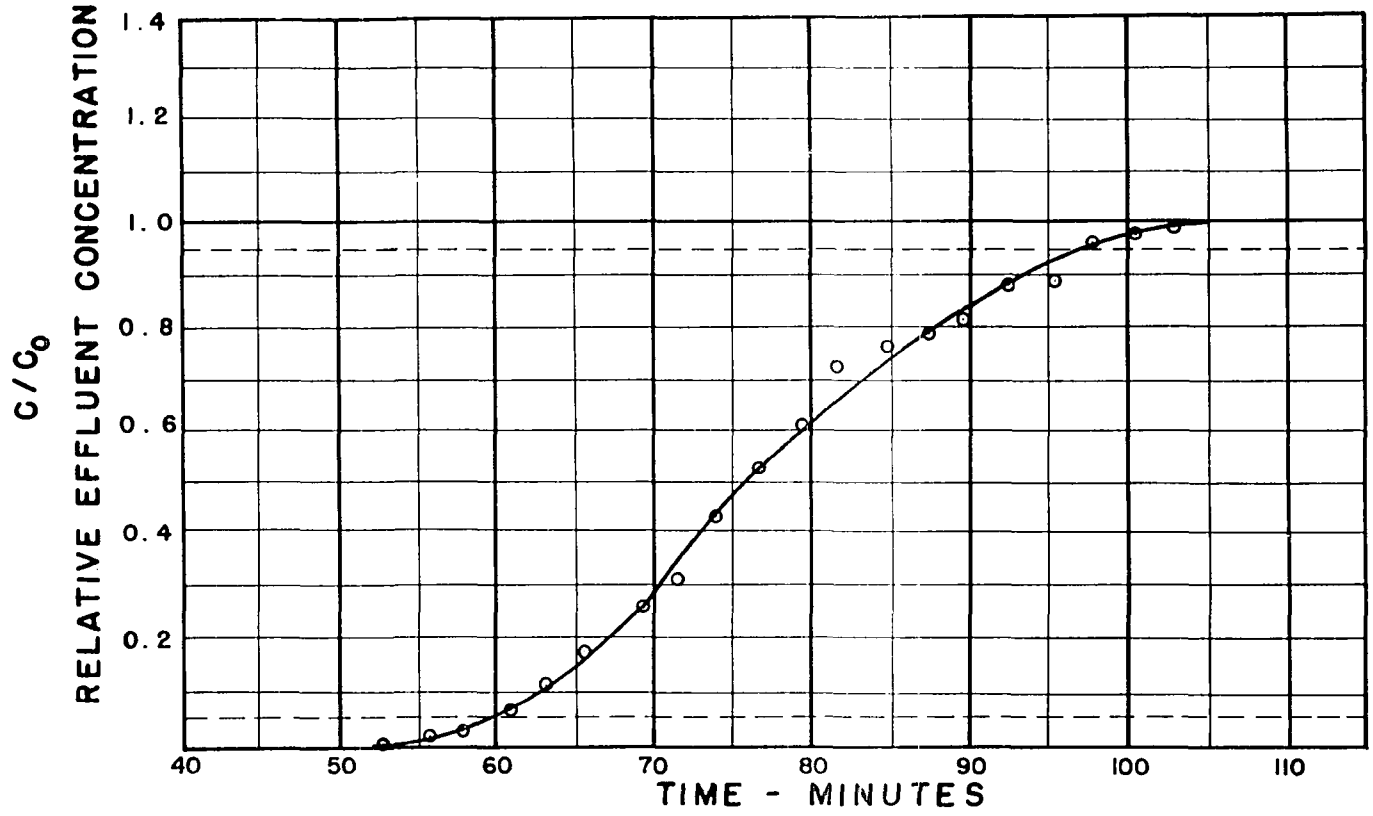

RUN NO. 79 INLET TEMP. 91 °F INLET PRESS. 800 PSIG. TOWER I.D. 2.9 in.

TOWER LGTH. 445.5 cm. FLOW RATE 42.82 ft/min. COMPOSITION: ____%C_4 ____%C_5 0.42 %C_6 ____%C_7

DESSICANT: 03 GEL

N-HEXANE

FIGURE A 134

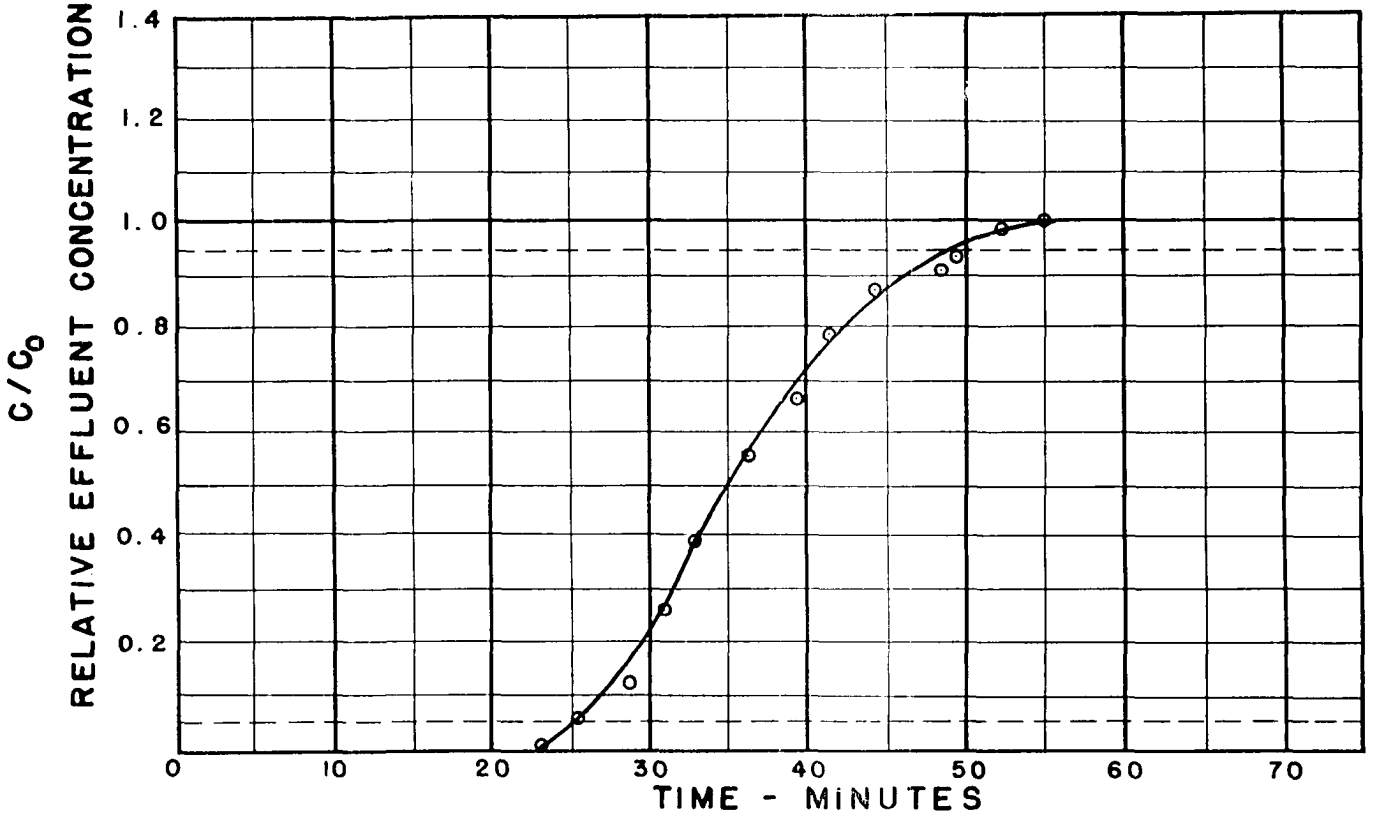

RUN NO. 80 INLET TEMP. 90 °F INLET PRESS. 808 PSIG. TOWER I.D. 2.9 in.

TOWER LGTH. 445.5 cm. FLOW RATE 44.2 ft/min. COMPOSITION: ____%C_4 ____%C_5 .37 %C_6 ____%C_7

DESSICANT: 03 GEL

N-HEXANE

FIGURE A 135

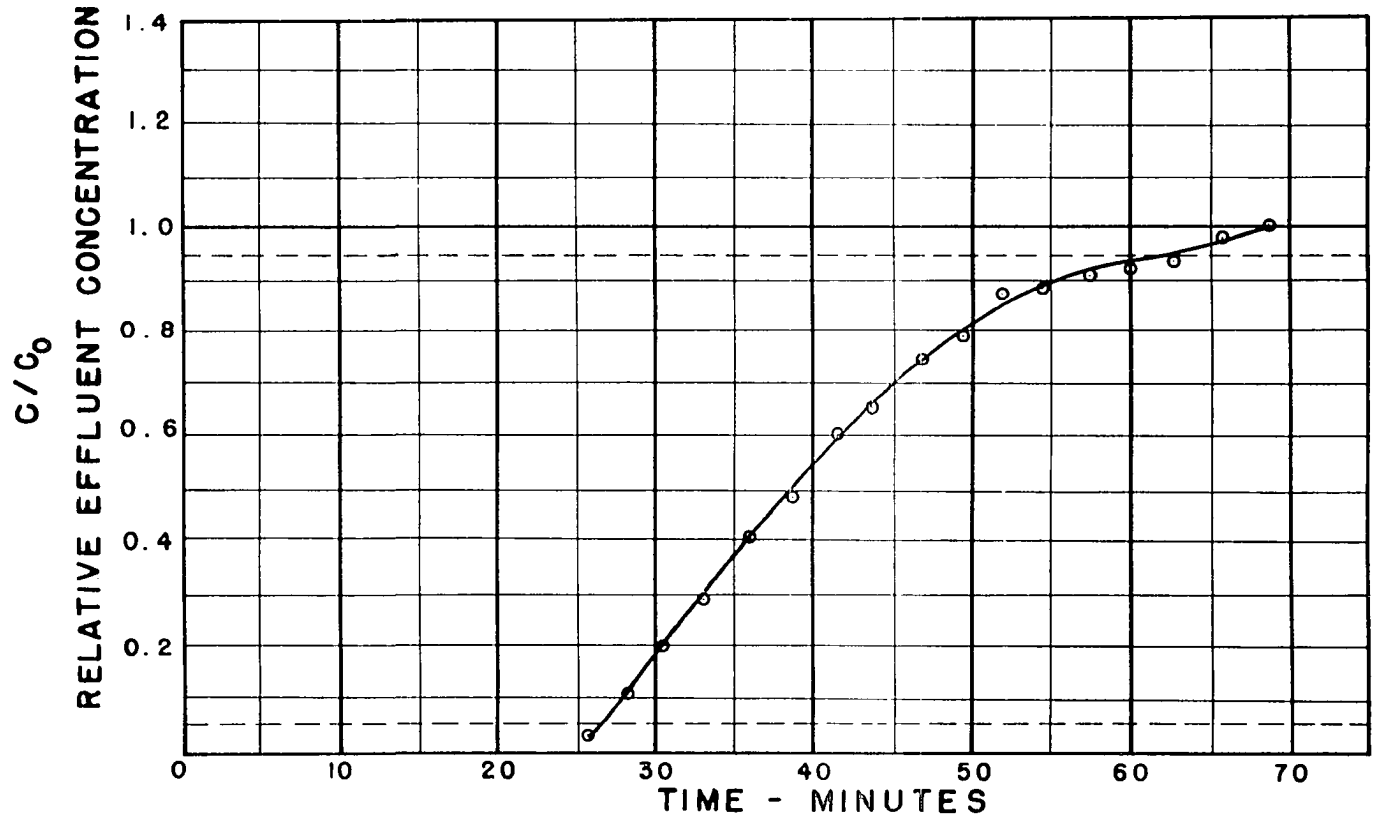

RUN NO. 81 INLET TEMP. 88 °F INLET PRESS. 800 PSIG. TOWER I.D. 2.9 in.

TOWER LGTH. 445.5 cm. FLOW RATE 39.13 ft/min. COMPOSITION: ____ %C_4 ____ %C_5 0.76 %C_6 ____ %C_7

DESSICANT: 03 GEL

N-HEXANE

FIGURE A 136

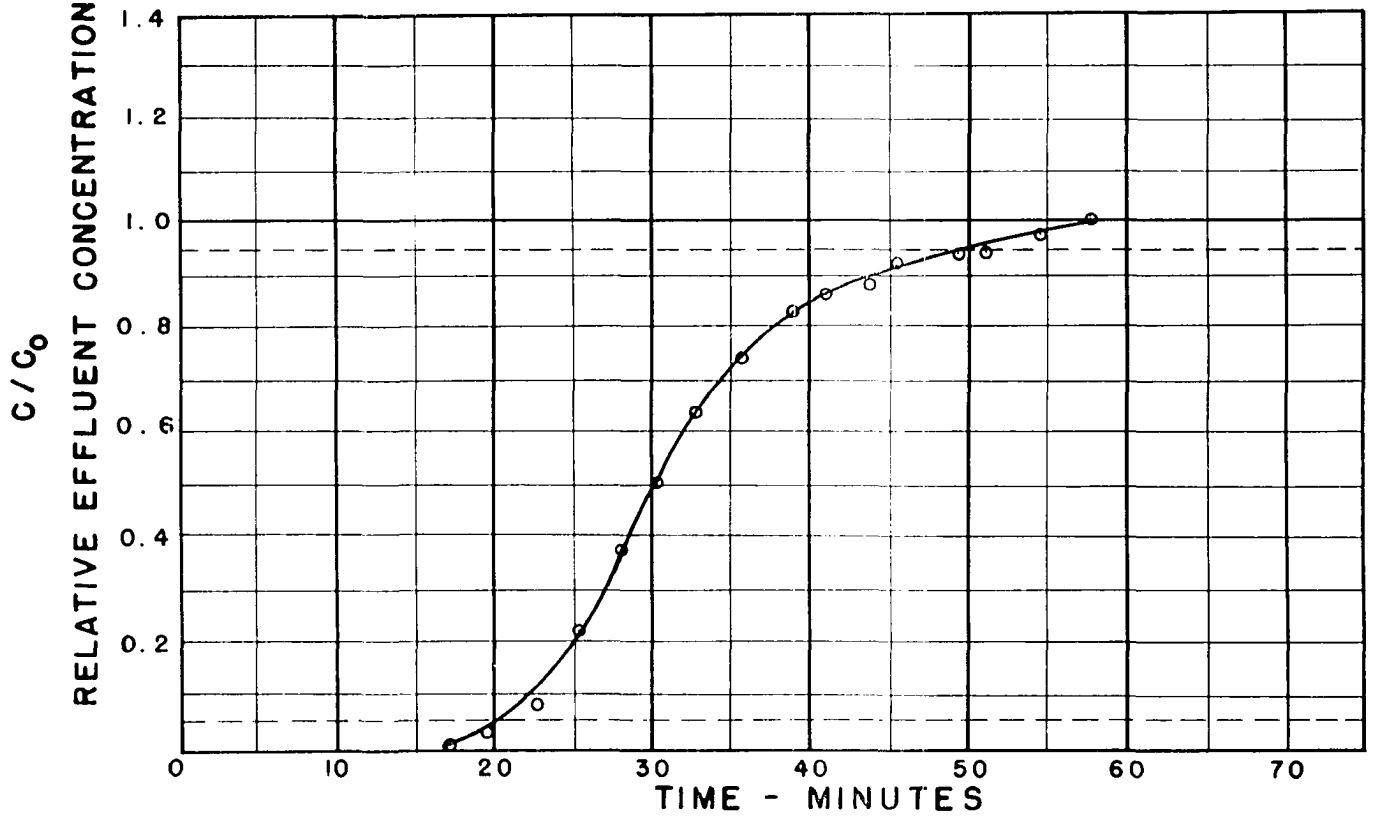

RUN NO. 83 INLET TEMP. 91.3 °F INLET PRESS. 802 PSIG. TOWER I.D. 2.9 in.

TOWER LGTH. 445.5 cm. FLOW RATE 45.77 ft/min. COMPOSITION: ____%C_4 ____%C_5 1.31 %C_6 ____%C_7

DESSICANT: 03 GEL

N-HEXANE

FIGURE A 137

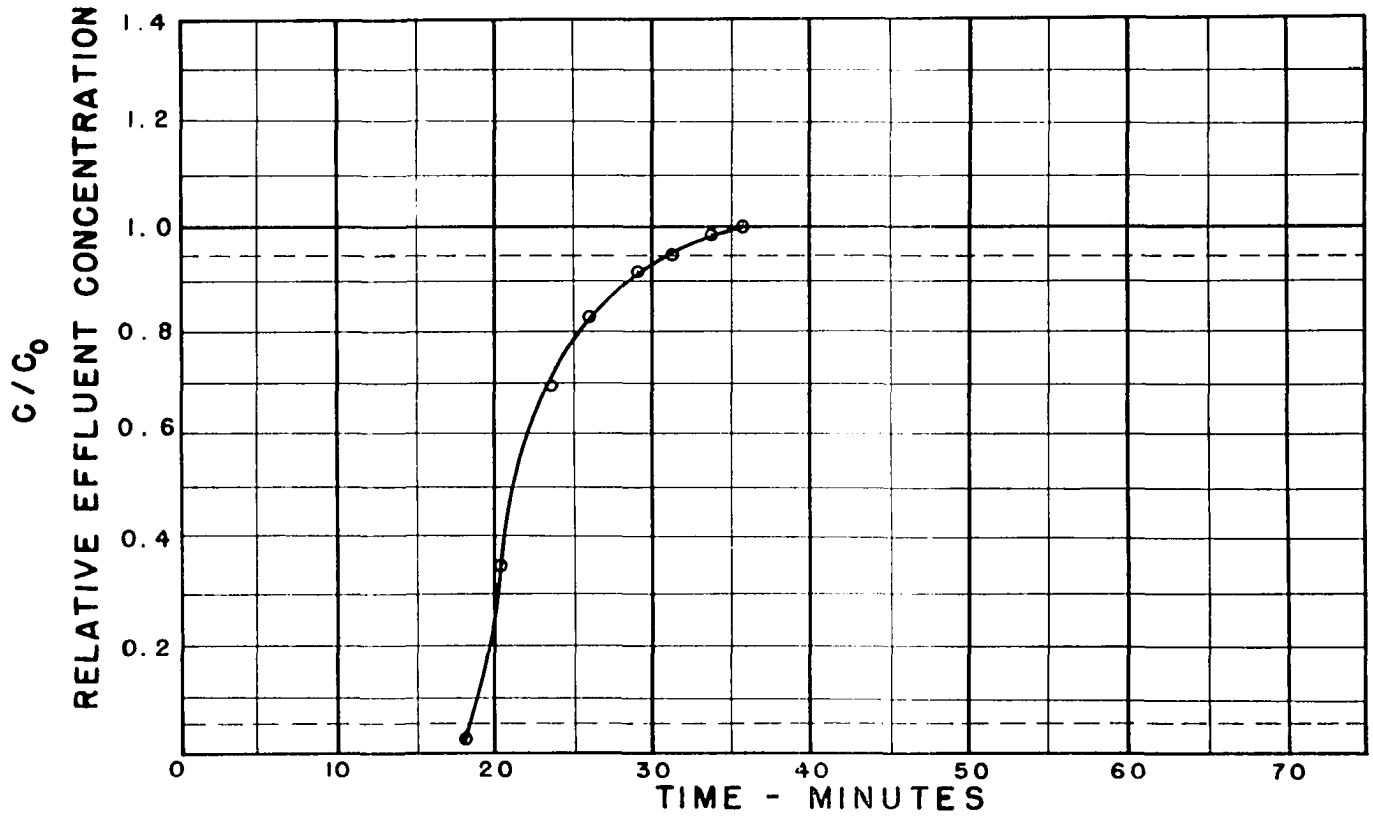

RUN NO. 117 INLET TEMP. 94.0 °F INLET PRESS. 800 PSIG. TOWER I.D. 2.90 in.

TOWER LGTH. 109.2 cm. FLOW RATE 11.48 ft/min. COMPOSITION: ____%C_4____%C_5 0.85 %C_6 ____%C_7

DESSICANT: 03 GEL

N-HEXANE

FIGURE A 138

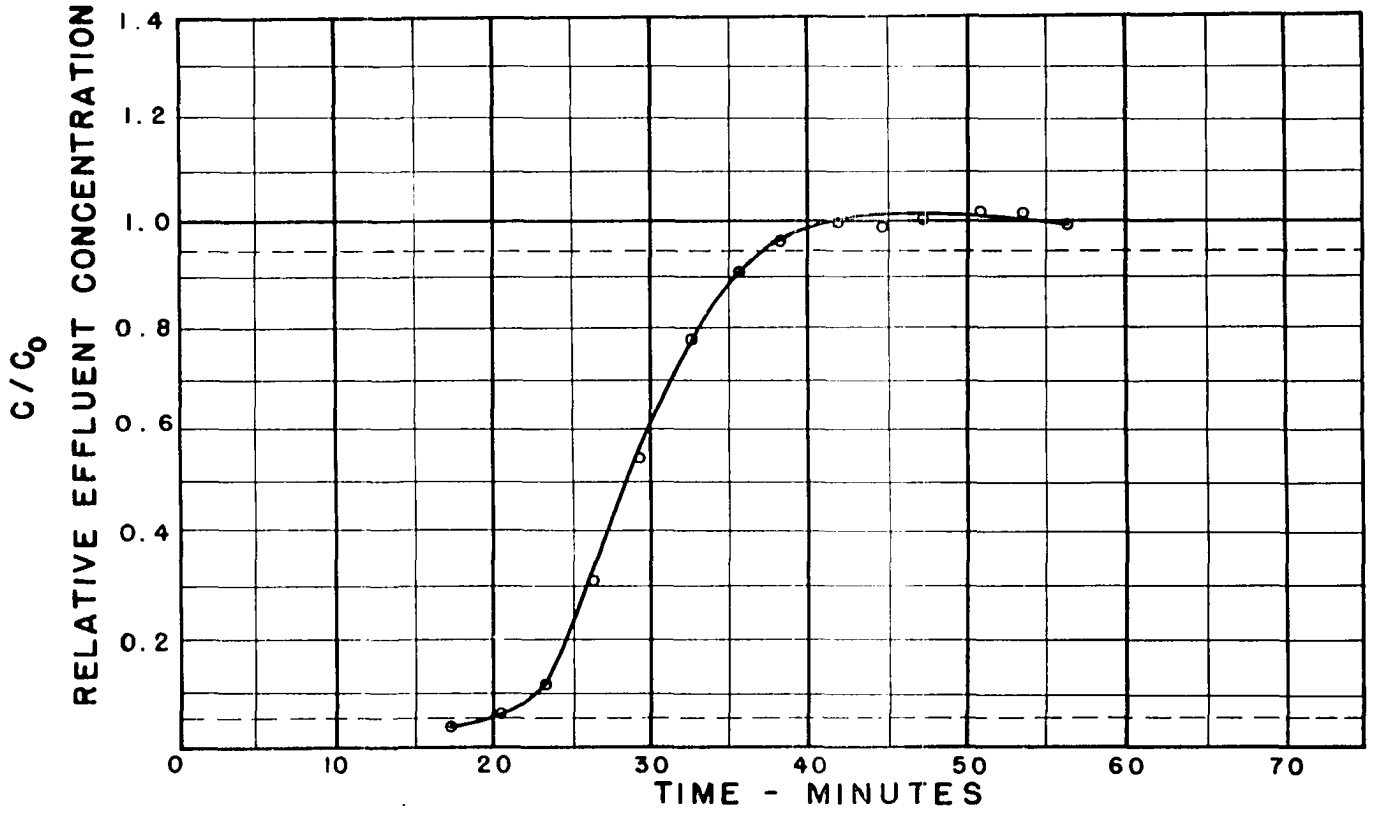

RUN NO. 118 INLET TEMP. 93.0 °F INLET PRESS. 805 PSIG. TOWER I.D. 2.90 in.

TOWER LGTH. 226 cm. FLOW RATE 10.52 ft/min. COMPOSITION: ____%C_4 ____%C_5 0.88 %C_6 ____%C_7

DESSICANT: 03 GEL

N-HEXANE

FIGURE A 139

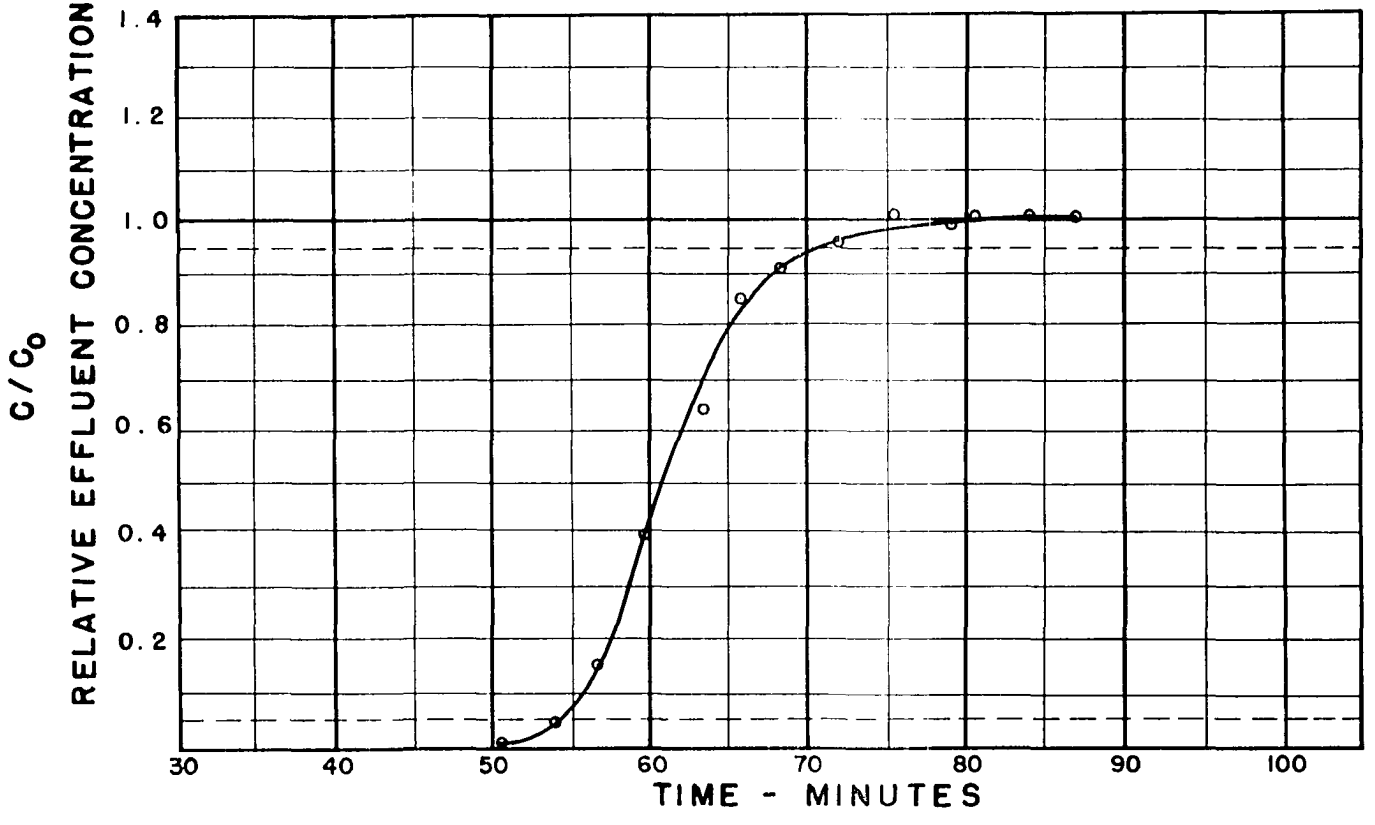

RUN NO. 121 INLET TEMP. 91 °F INLET PRESS. 800 PSIG. TOWER I.D. 2.9 in.

TOWER LGTH. 226 cm. FLOW RATE 10.87 ft/min. COMPOSITION: ____%C_4 .94 %C_5 ____%C_6 ____%C_7

DESSICANT: 03 GEL

N-PENTANE

FIGURE A 140

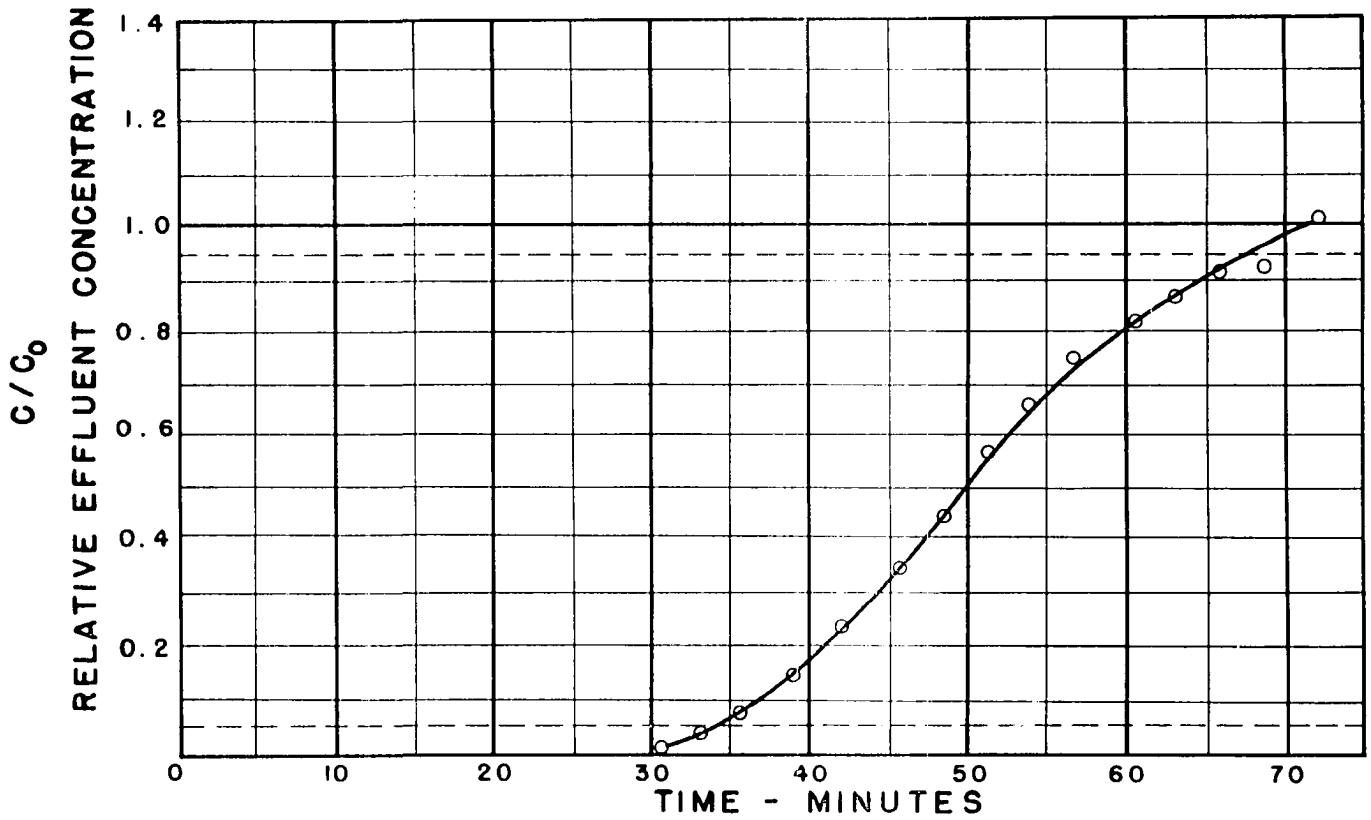

RUN NO. 123 INLET TEMP. 91.0 °F INLET PRESS. 800 PSIG. TOWER I.D. 2.9 in.

TOWER LGTH. 226 cm. FLOW RATE 19.98 ft/min. COMPOSITION: ____%C_4____%C_5 0.59 %C_6 ____%C_7

DESSICANT: 03 GEL

N-HEXANE

FIGURE A 141

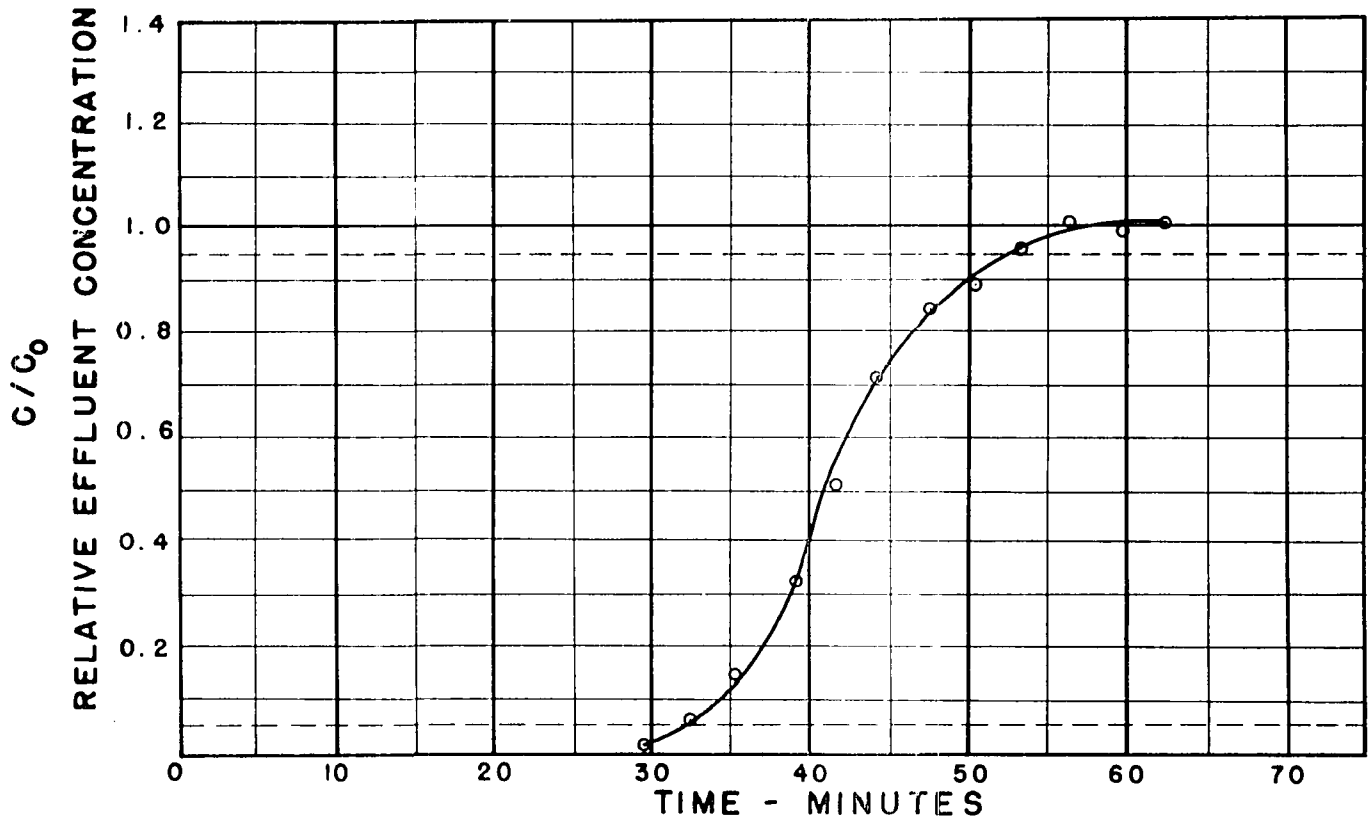

RUN NO. 124 INLET TEMP. 90 °F INLET PRESS. 805 PSIG. TOWER I.D. 2.9 in.

TOWER LGTH. 226 cm. FLOW RATE 43.73 ft/min. COMPOSITION: ____%C_4 ____%C_5 0.68 %C_6 ____%C_7

DESSICANT: 03 GEL

N-HEXANE

FIGURE A 142

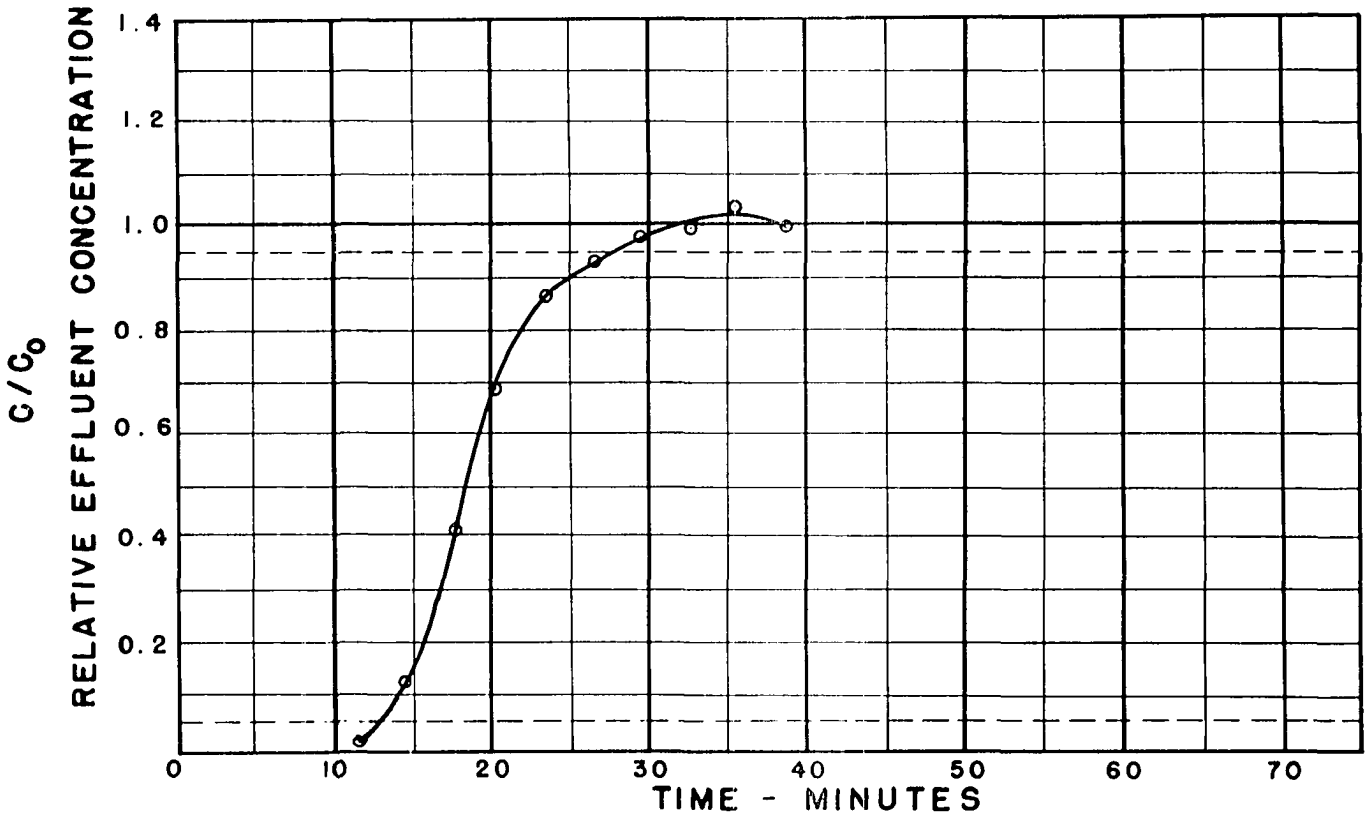

RUN NO. 129 INLET TEMP. 93.0 °F INLET PRESS. 800 PSIG. TOWER I.D. 2.9 in.

TOWER LGTH. 456 cm. FLOW RATE 41.02 ft/min. COMPOSITION: ____%C_4 ____%C_5 0.68 %C_6 ____%C_7

DESSICANT: 03 GEL

N-HEXANE

FIGURE A 143

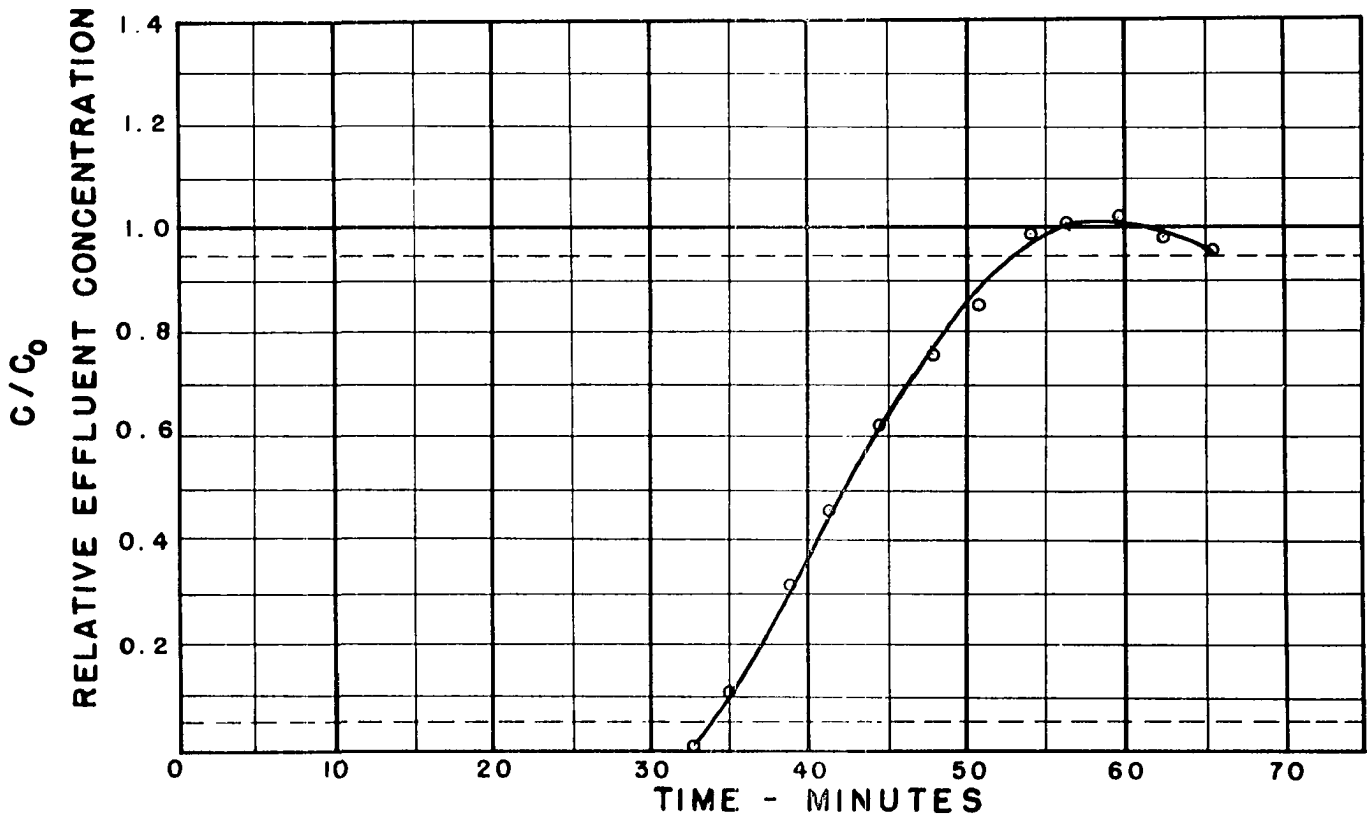

RUN NO. 130 INLET TEMP. 90.8 °F INLET PRESS. 800 PSIG. TOWER I.D. 2.9 in.

TOWER LGTH. 456 cm. FLOW RATE 10.75 ft/min. COMPOSITION: ____%C_4 ____%C_5 0.93 %C_6 ____%C_7

DESSICANT: 03 GEL

N-HEXANE

FIGURE A 144

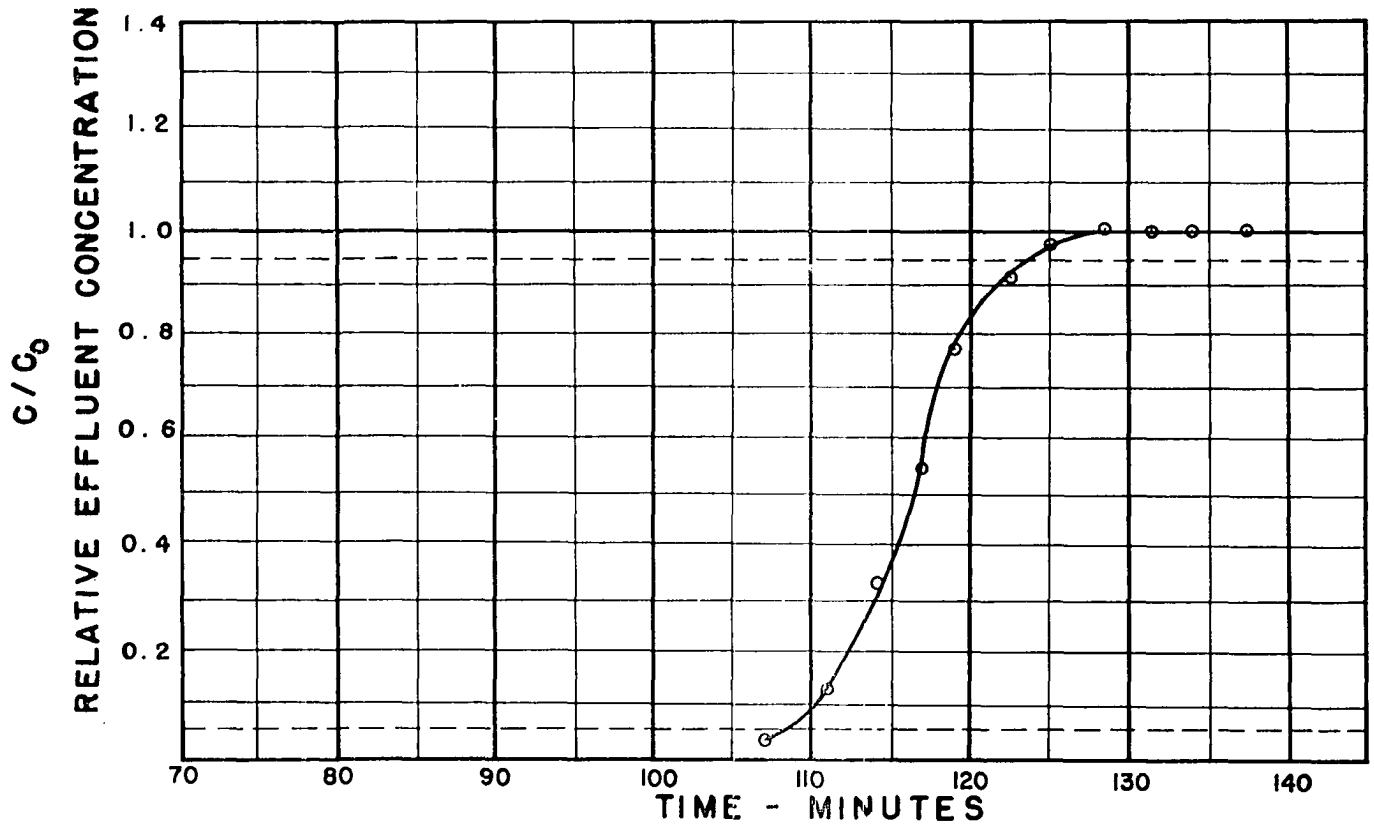

RUN NO. 143 INLET TEMP. 91.2 °F INLET PRESS. 800 PSIG. TOWER I.D. 2.9 in.

TOWER LGTH. 421 cm. FLOW RATE 40.5 ft/min. COMPOSITION: ____%C_4 ____%C_5 0.993 %C_6 ____%C_7

DESSICANT: 03 GEL

N-HEXANE

FIGURE A 145

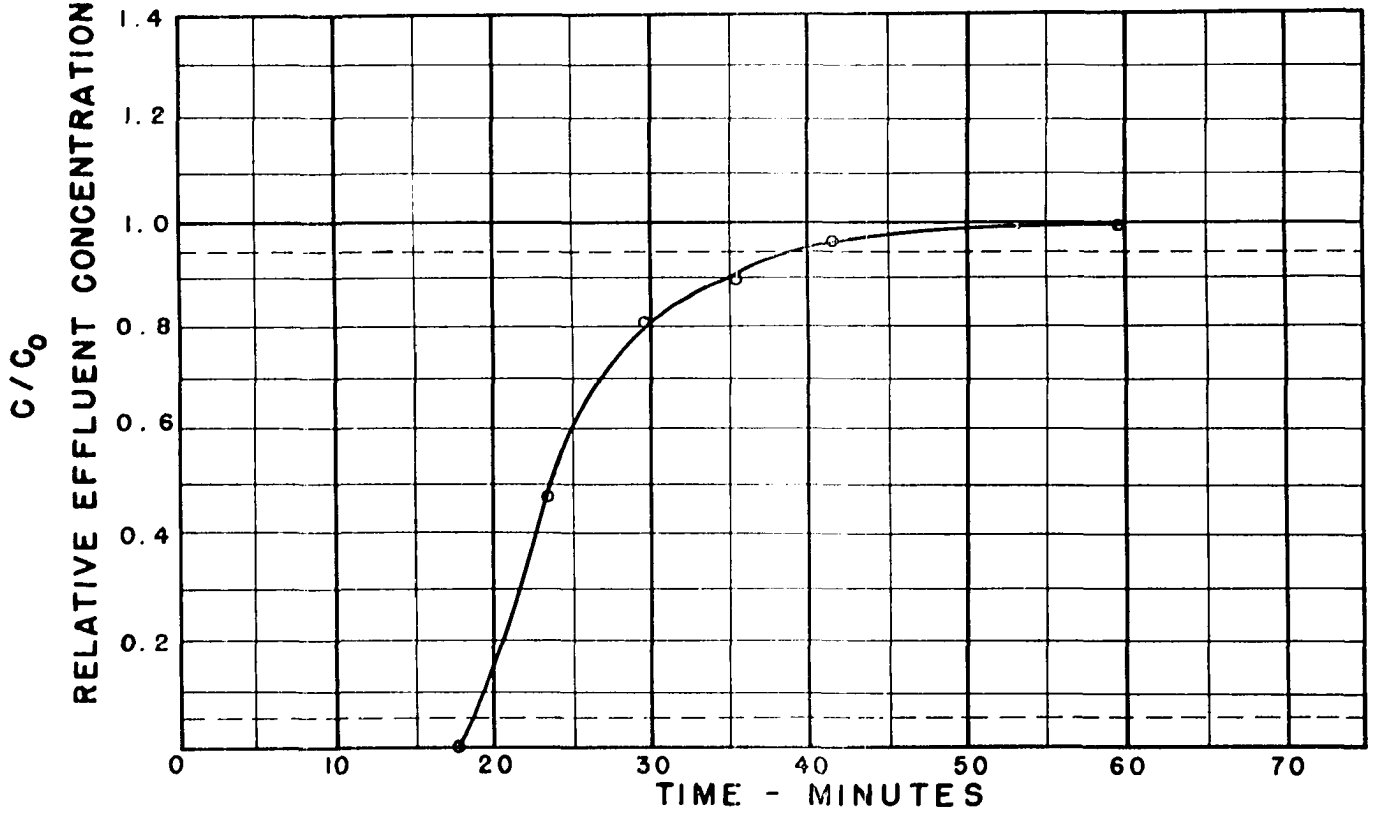

RUN NO. 1 INLET TEMP. 89.0 °F INLET PRESS. 810 PSIG. TOWER I.D. 2.067 in.

TOWER LGTH. 164 cm. FLOW RATE 35.75 ft/min. COMPOSITION: ____%C_4 0.45 %C_5 0.42 %C_6 ____%C_7

DESSICANT: 03 GEL

FIGURE A 146

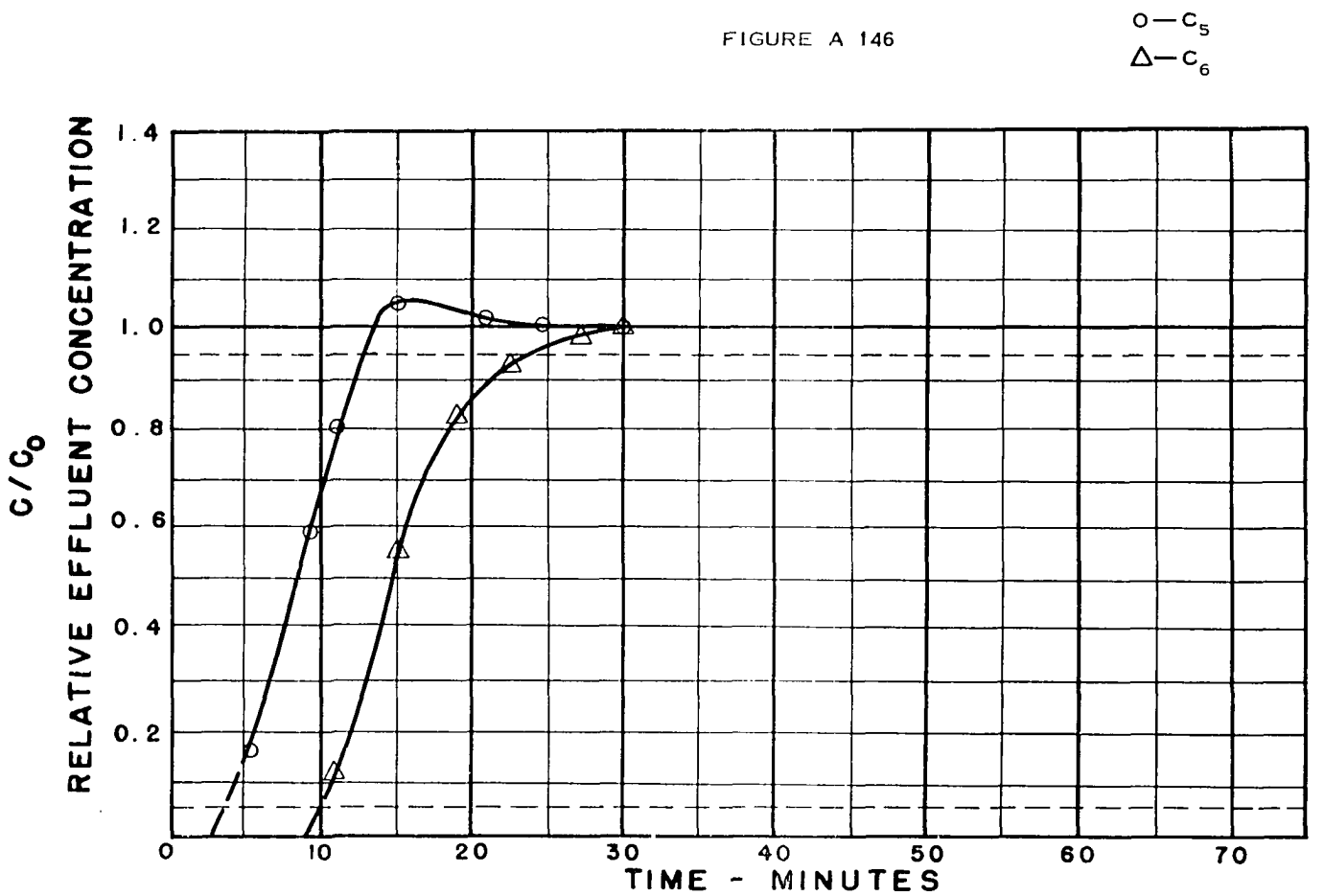

RUN NO. 4 INLET TEMP. 93.0 °F INLET PRESS. 785 PSIG. TOWER I.D. 2.067 in.

TOWER LGTH. 164 cm. FLOW RATE 34.77 ft/min. COMPOSITION: ____ %C_4 1.01 %C_5 0.45 %C_6 ____ %C_7

DESSICANT: 03 GEL

FIGURE A 147

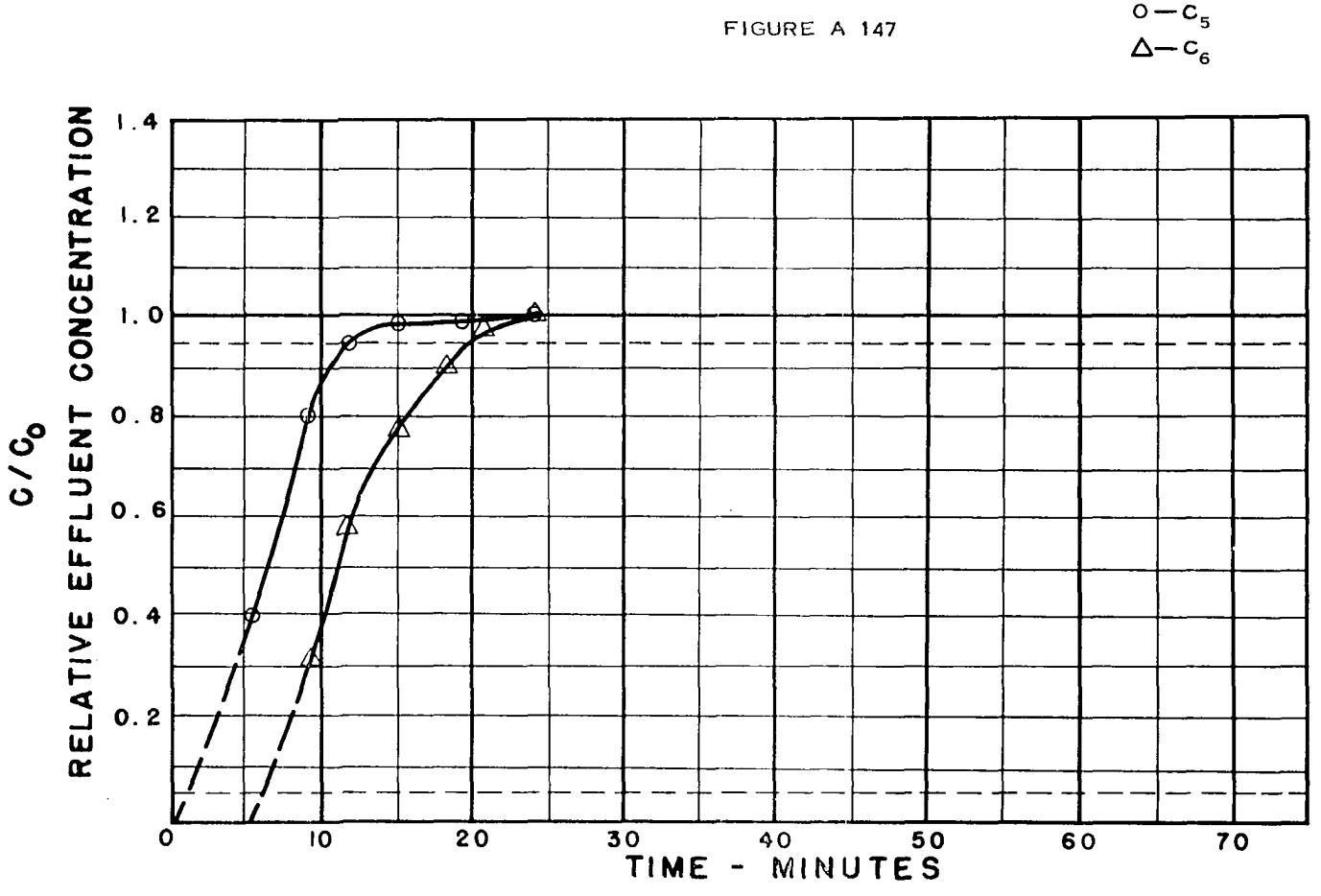

RUN NO. 46 INLET TEMP. 92.0 °F INLET PRESS. 803 PSIG. TOWER I.D. 2.067 in.

TOWER LGTH. 164 cm. FLOW RATE 24.39 ft/min. COMPOSITION: ____%C_4 0.57 %C_5 0.50 %C_6 ____%C_7

DESSICANT: 03 GEL

FIGURE A 148

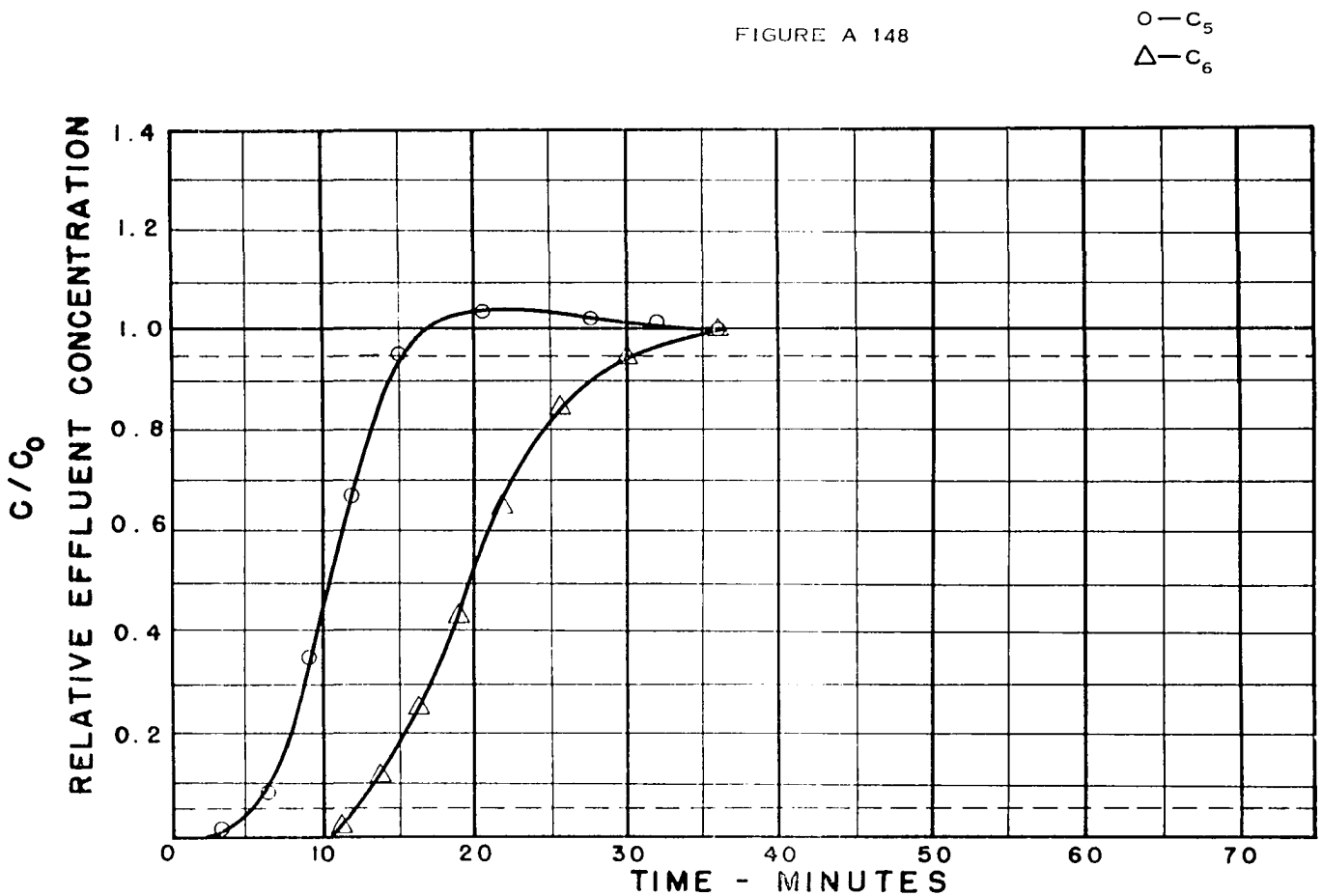

RUN NO. 49 INLET TEMP. 90.0 °F INLET PRESS. 806 PSIG. TOWER I.D. 2.067 in.

TOWER LGTH. 164 cm. FLOW RATE 24.83 ft/min. COMPOSITION: ____%C_4 1.05 %C_5 0.48 %C_6 ____%C_7

DESSICANT: 03 GEL

FIGURE A 149

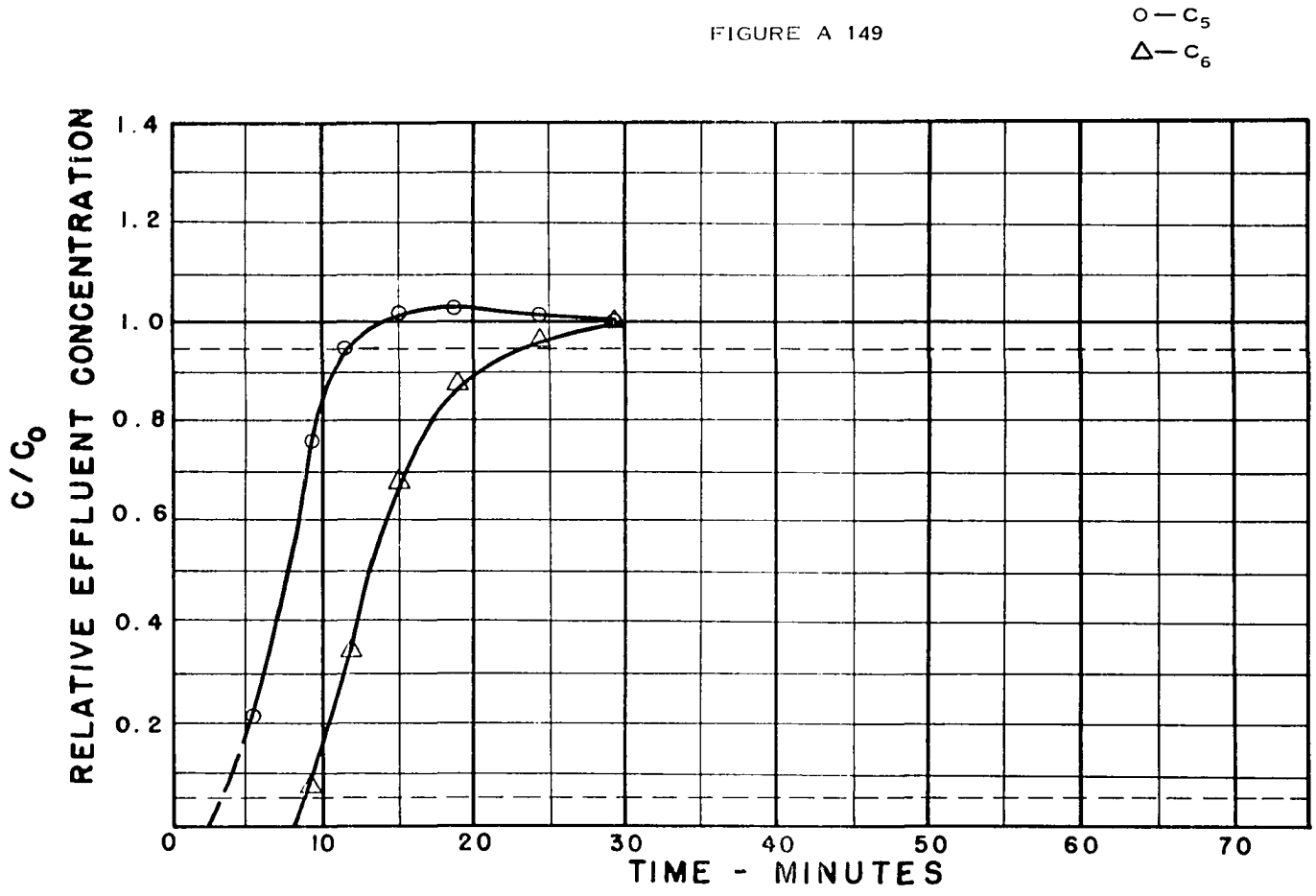

RUN NO. 51 INLET TEMP. 91.0 °F INLET PRESS. 807 PSIG. TOWER I.D. 2.067 in.

TOWER LGTH. 164 cm. FLOW RATE 24.37 ft/min. COMPOSITION: ____ %C_4 0.87 %C_5 0.40 %C_6 ____ %C_7

DESSICANT: 03 GEL

FIGURE A 150

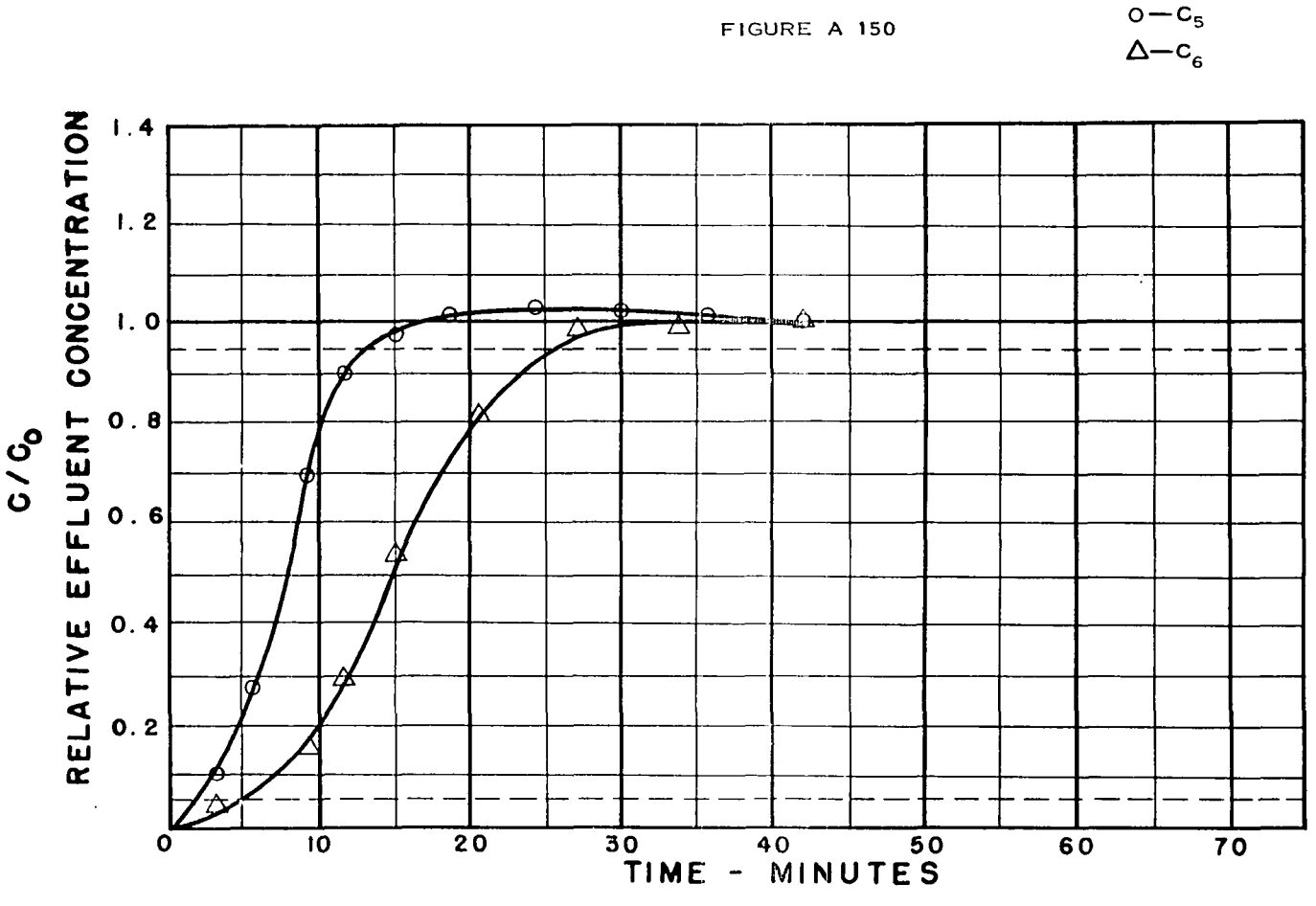

RUN NO. 103 INLET TEMP. 94.0 °F INLET PRESS. 805 PSIG. TOWER I. D. 2.9 in.

TOWER LGTH. 456 cm. FLOW RATE 11.34 ft/min. COMPOSITION: ____%C_4 .5 %C_5 0.74 %C_6 ____%C_7

DESSICANT: 03 GEL

FIGURE A 151

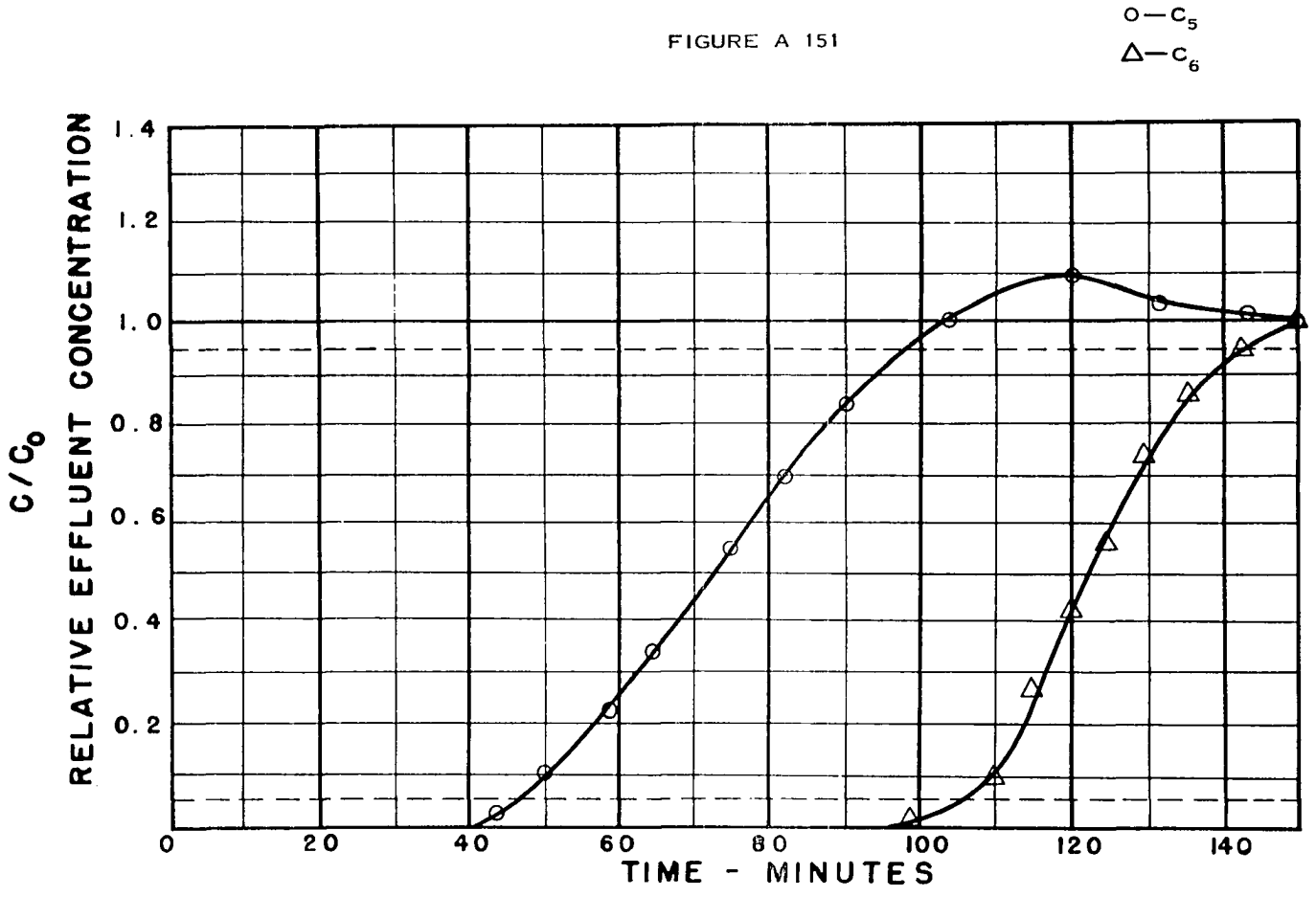

RUN NO. 105 INLET TEMP. 92.0 °F INLET PRESS. 800 PSIG. TOWER I.D. 2.9 in.

TOWER LGTH. 456 cm. FLOW RATE 11.80 ft/min. COMPOSITION: ____%C_4 1.17 %C_5 1.03 %C_6 ____%C_7

DESSICANT: 03 GEL

FIGURE A 152

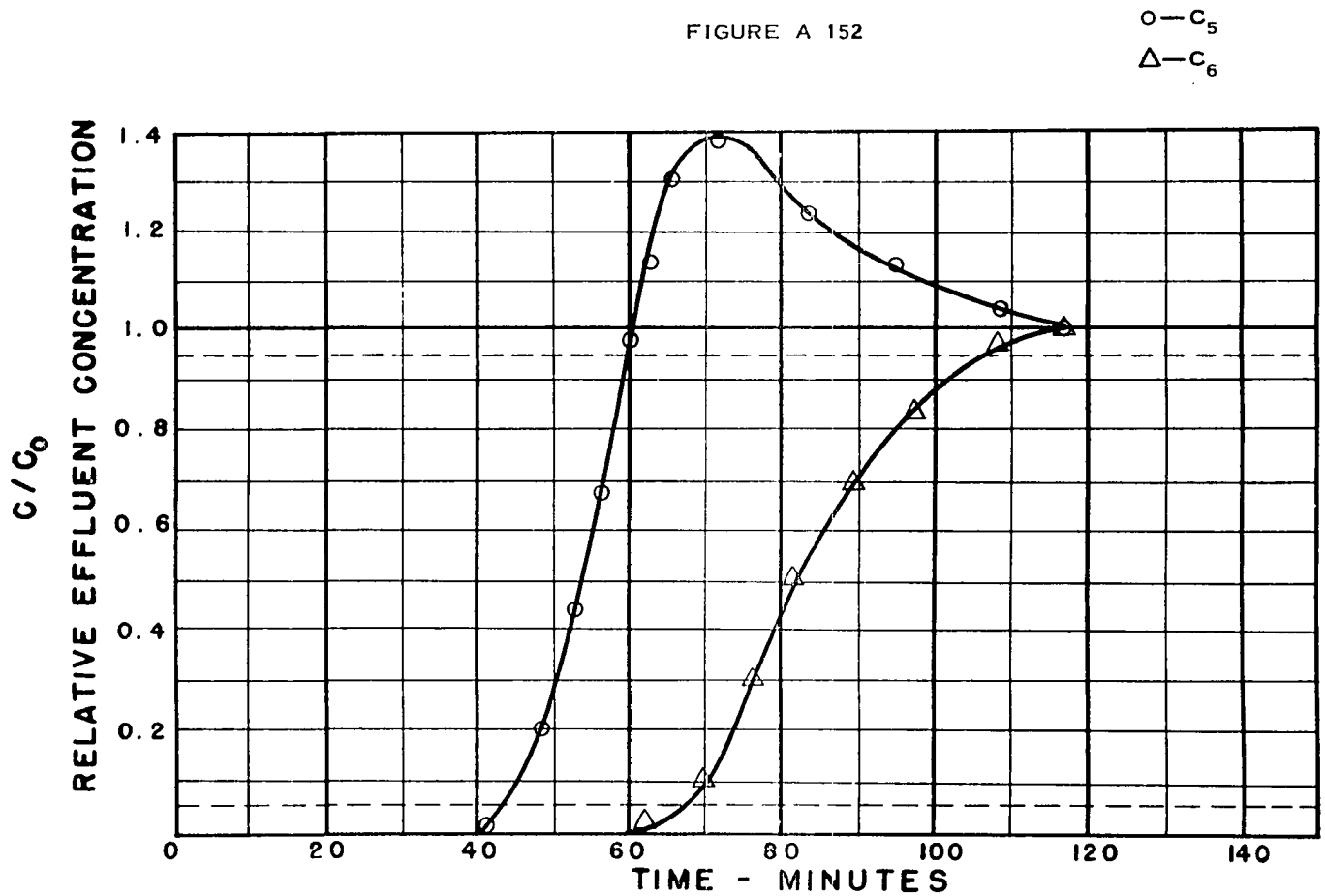

RUN NO. 106 INLET TEMP. 94.0 °F INLET PRESS. 790 PSIG. TOWER I.D. 2.9 in.

TOWER LGTH. 456 cm. FLOW RATE 22.47 ft/min. COMPOSITION: ____ %C_4 0.61 %C_5 0.54 %C_6 ____ %C_7

DESSICANT: 03 GEL

FIGURE A 153

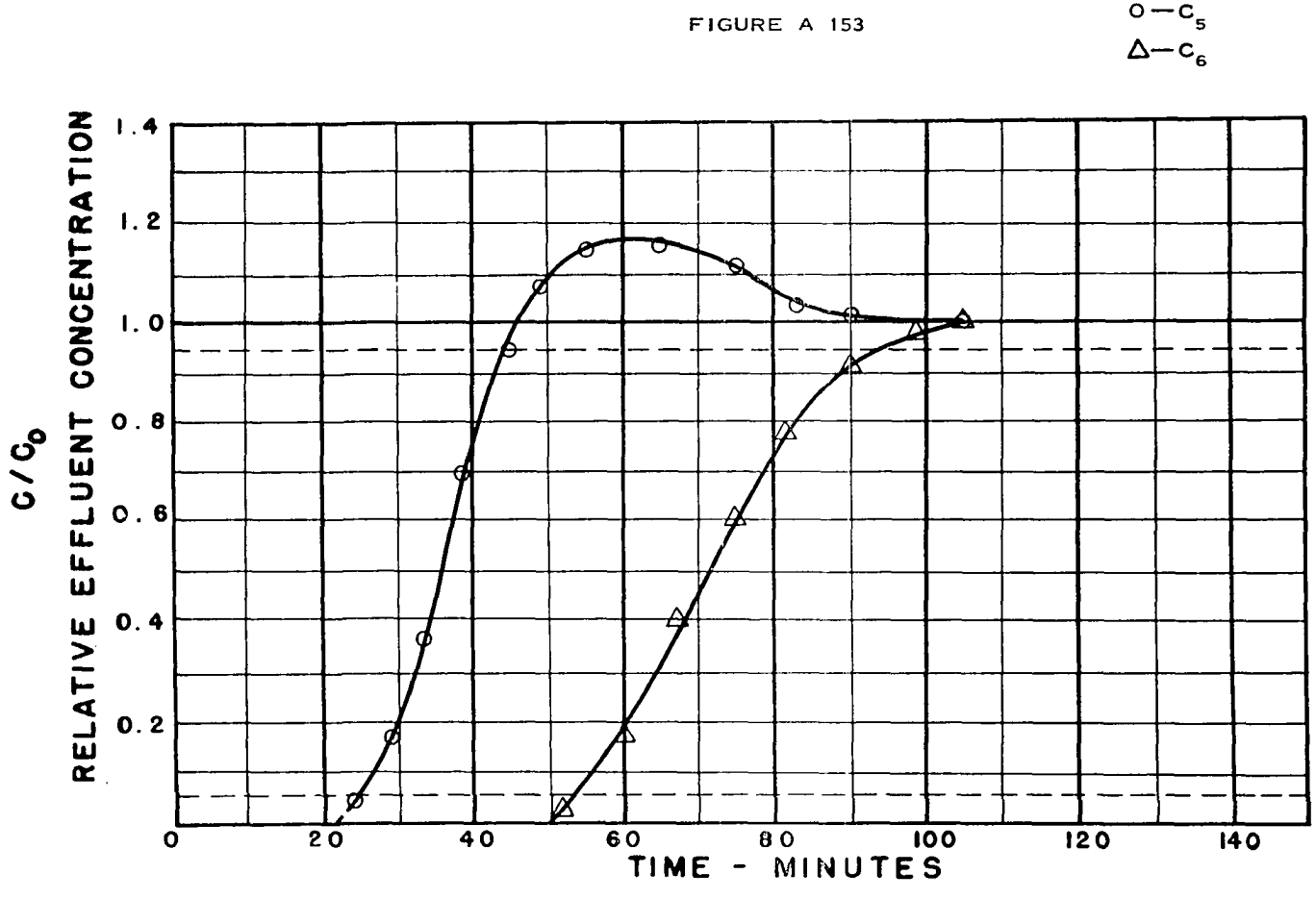

RUN NO. 108 INLET TEMP. 91.0 °F INLET PRESS. 805 PSIG. TOWER I.D. 2.90 in.

TOWER LGTH. 456 cm. FLOW RATE 21.34 ft/min. COMPOSITION: ____%C_4 0.45 %C_5 0.39 %C_6 ____%C_7

DESSICANT: 03 GEL

FIGURE A 154

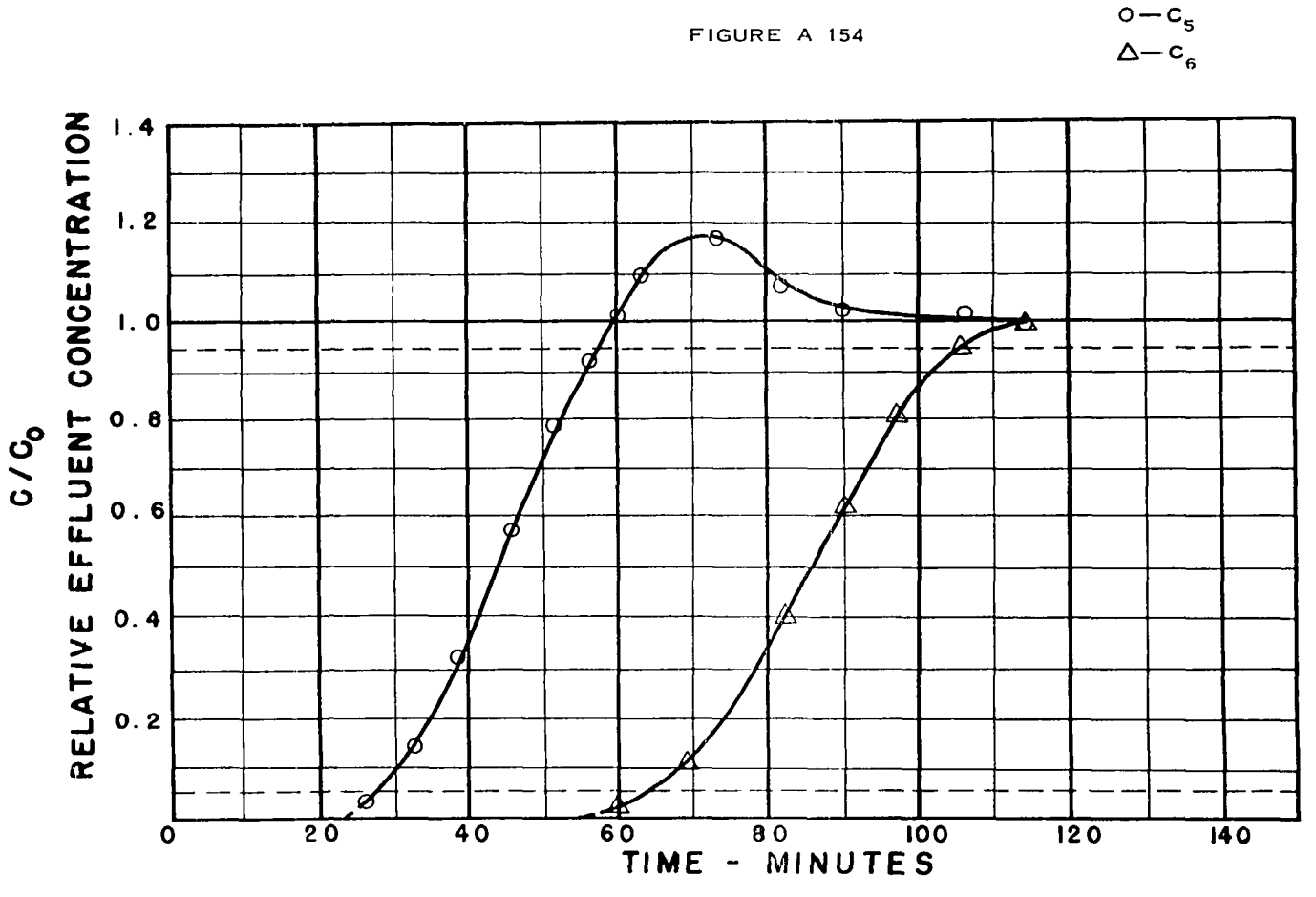

RUN NO. 110 INLET TEMP. 93.0 °F INLET PRESS. 800 PSIG. TOWER I.D. 2.9 in.

TOWER LGTH. 456 cm. FLOW RATE 44.17 ft/min. COMPOSITION: ____ %C_4 0.81 %C_5 0.80 %C_6 ____ %C_7

DESSICANT: 03 GEL

FIGURE A 155

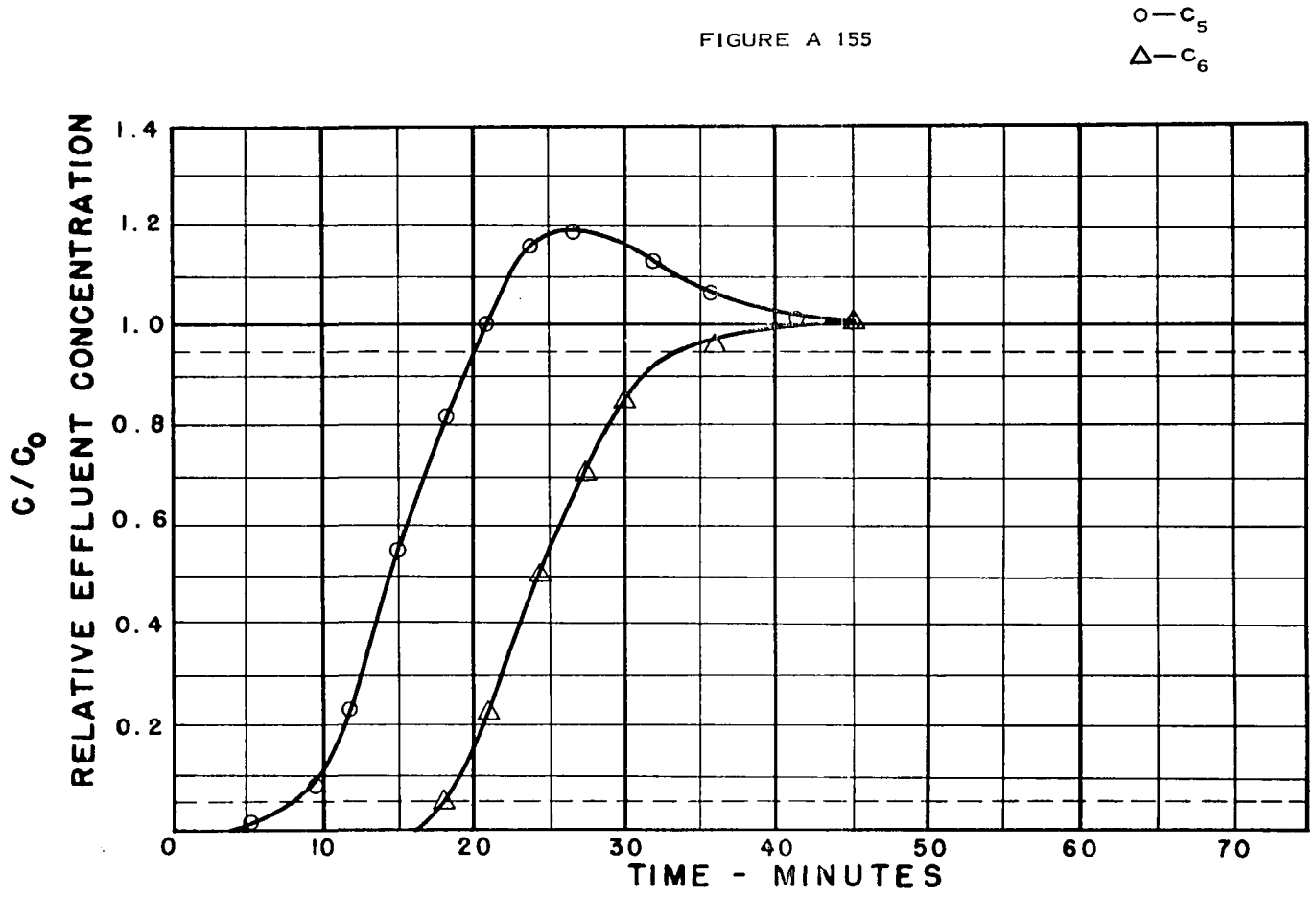

RUN NO. 112 INLET TEMP. 92.0 °F INLET PRESS. 815 PSIG. TOWER I.D. 2.9 in.

TOWER LGTH. 456 cm. FLOW RATE 23.16 ft/min. COMPOSITION: ____ %C_4 1.61 %C_5 1.42 %C_6 ____ %C_7

DESSICANT: 03 GEL

FIGURE A 156

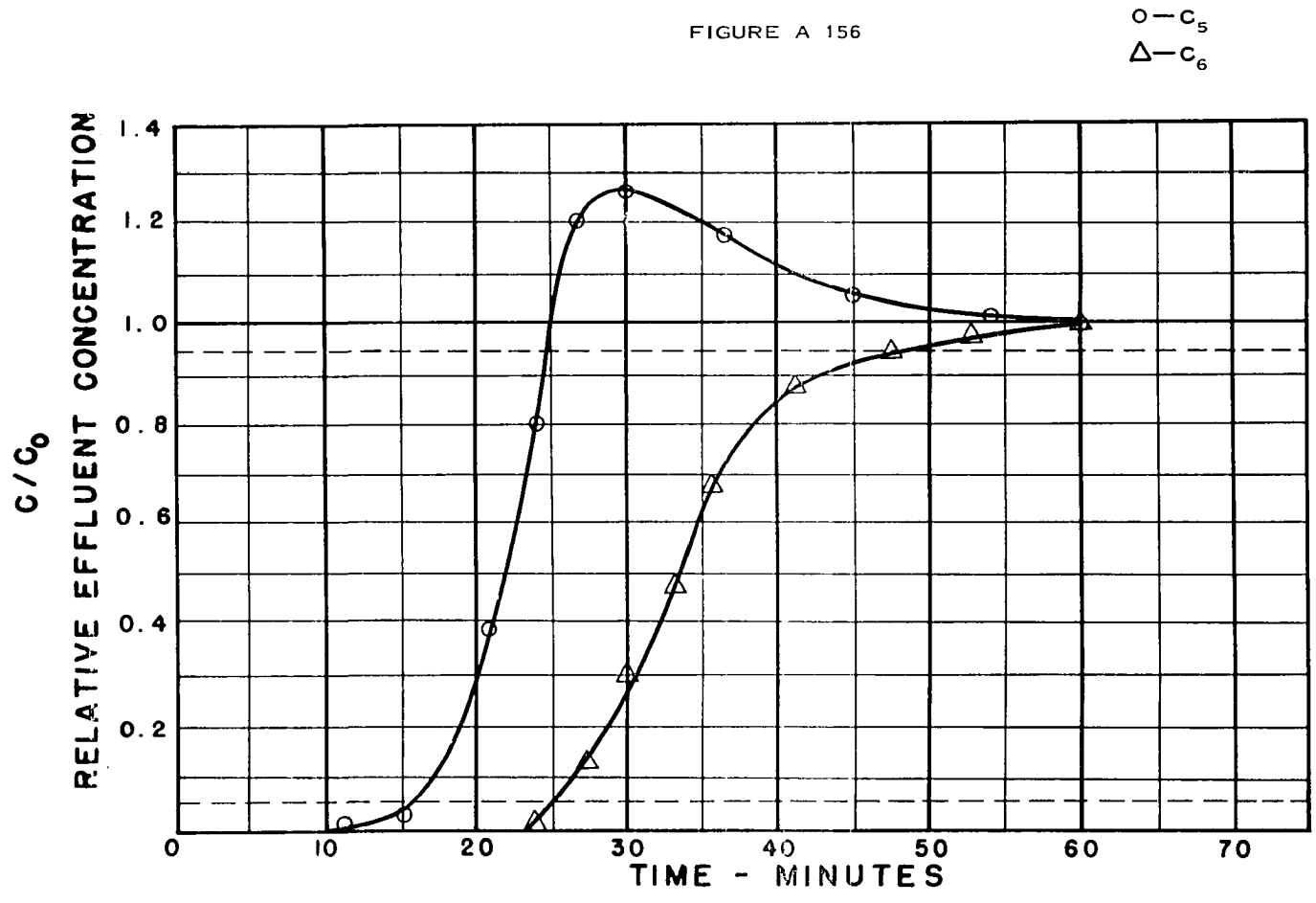

RUN NO. 113 INLET TEMP. 94.0 °F INLET PRESS. 800 PSIG. TOWER I.D. 2.9 in.

TOWER LGTH. 456 cm. FLOW RATE 45.25 ft/min. COMPOSITION: ____ %C_4 0.34 %C_5 0.30 %C_6 ____ %C_7

DESSICANT: 03 GEL

FIGURE A 157

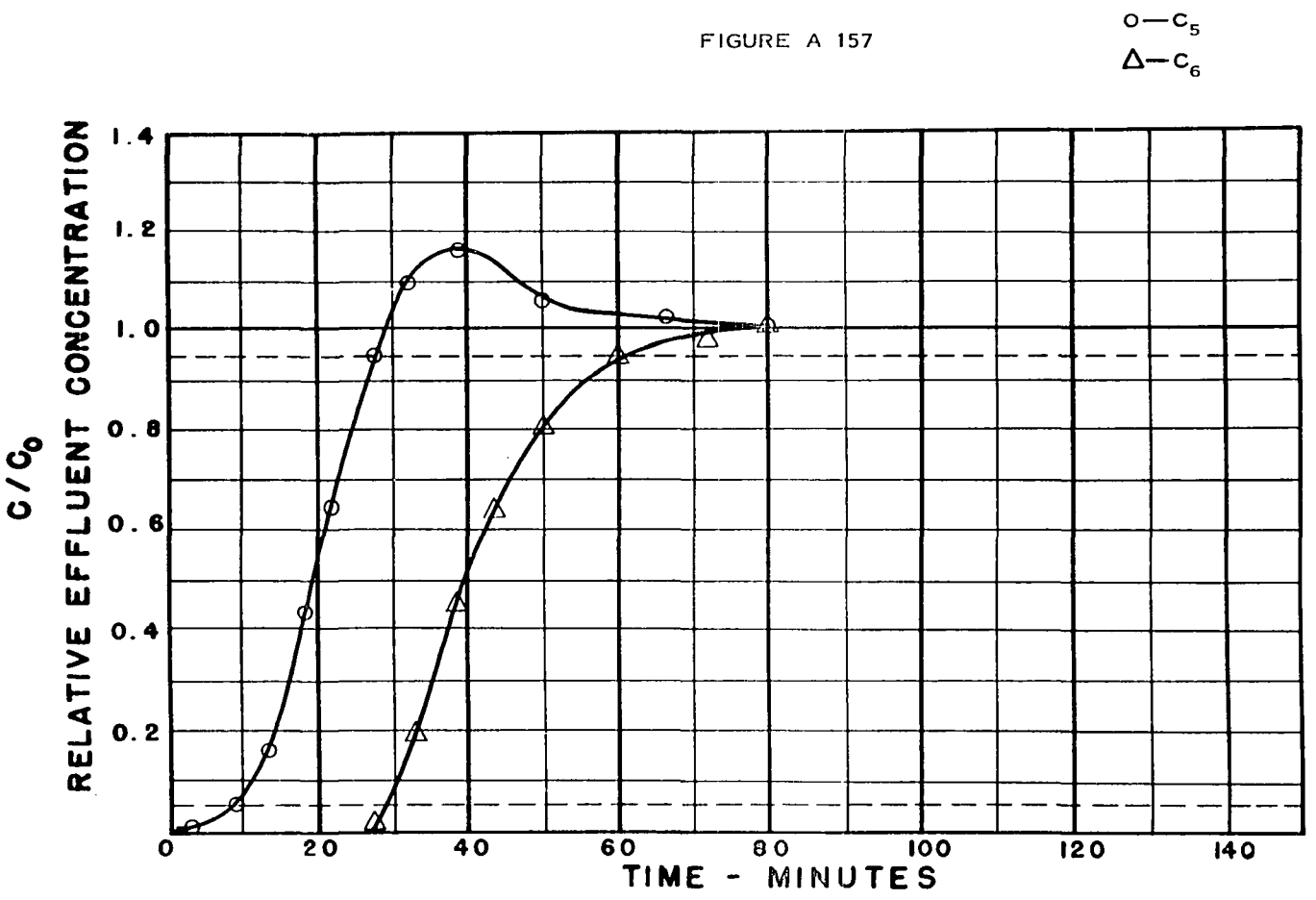

RUN NO. 201 INLET TEMP. 98.3 °F INLET PRESS. 804 PSIG. TOWER I.D. 2.9 In.

TOWER LGTH. 428.2 cm. FLOW RATE 41.0 ft/min. COMPOSITION: - %C_4 .195 %C_5 .216 %C_6 .210 %C_7

DESSICANT: 03 GEL

FIGURE A 158

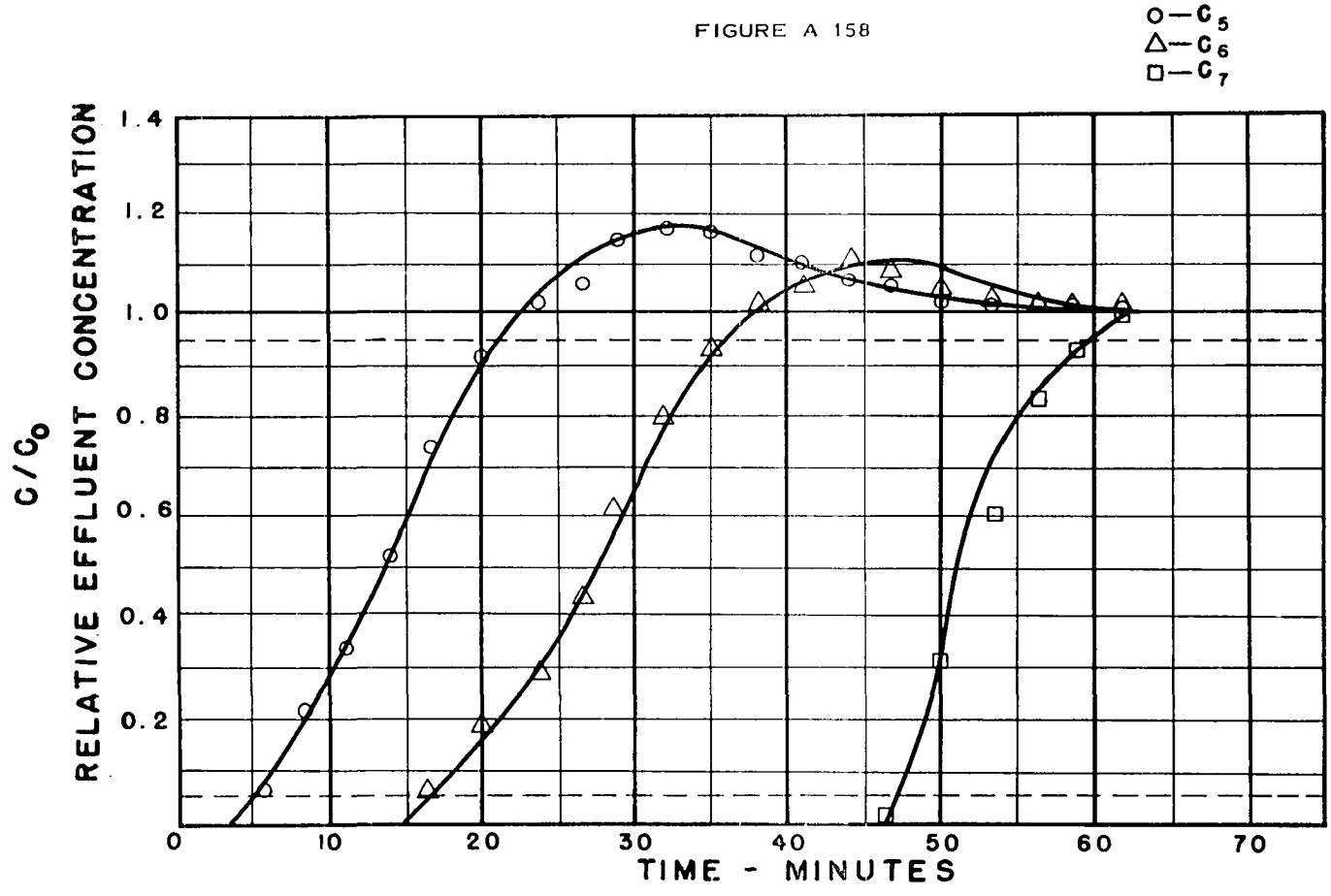

RUN NO. 217 INLET TEMP. 88 °F INLET PRESS. 800 PSIG. TOWER I.D. 2.9 in.

TOWER LGTH. 428.2 cm. FLOW RATE 27.6 ft/min. COMPOSITION: ____ %C_4 .2320 %C_5 .0618 %C_6 0.3800 %C_7

DESSICANT: 03 GEL

FIGURE A 159

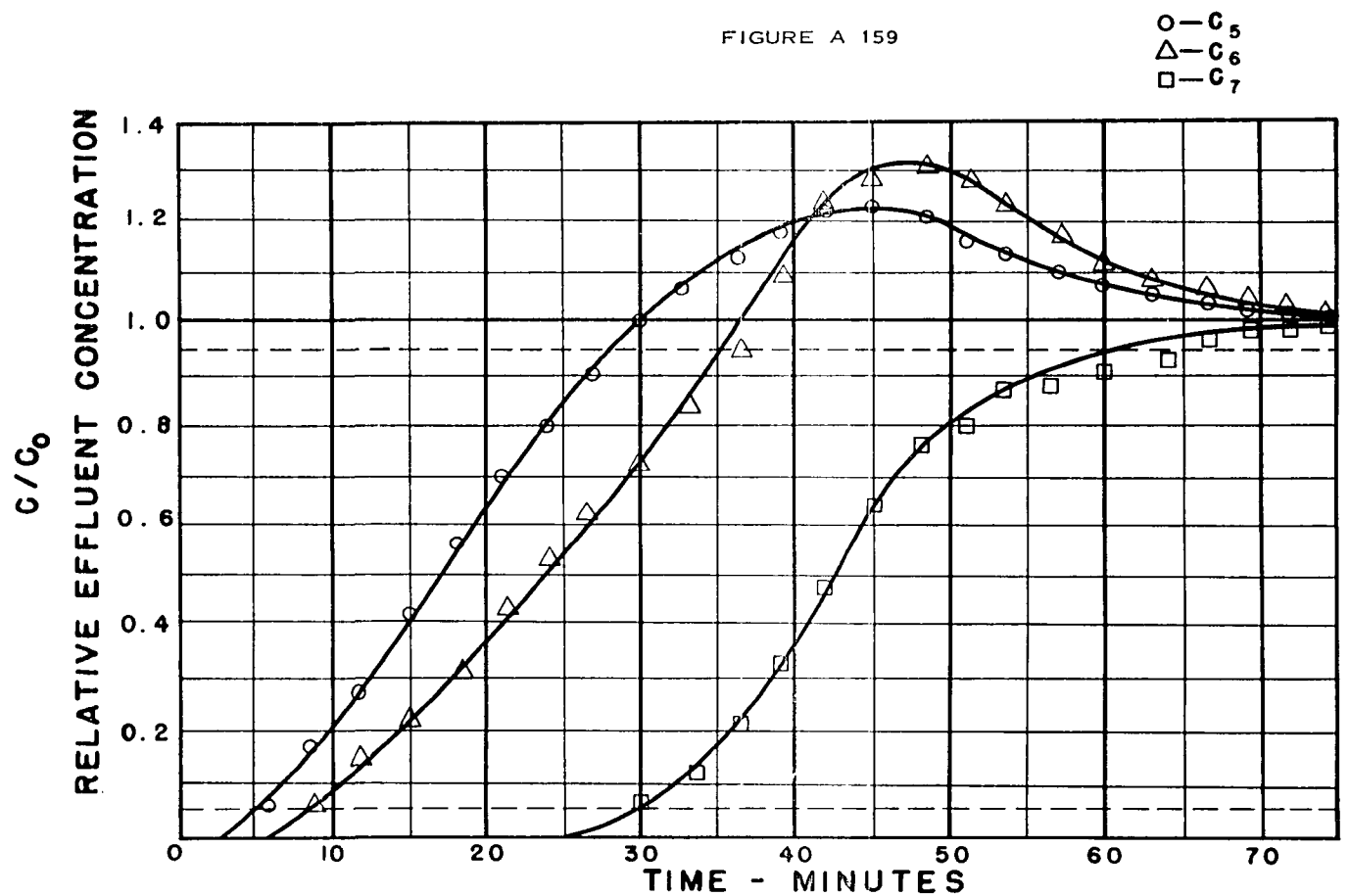

RUN NO. 220 INLET TEMP. 92.4 °F INLET PRESS. 800 PSIG. TOWER I.D. 2.9 in.

TOWER LGTH. 428.2 cm. FLOW RATE 27.2 ft/min. COMPOSITION: ____ %C_4 .1515 %C_5 .1179 %C_6 .2136 %C_7

DESSICANT: 03 GEL

FIGURE A 160

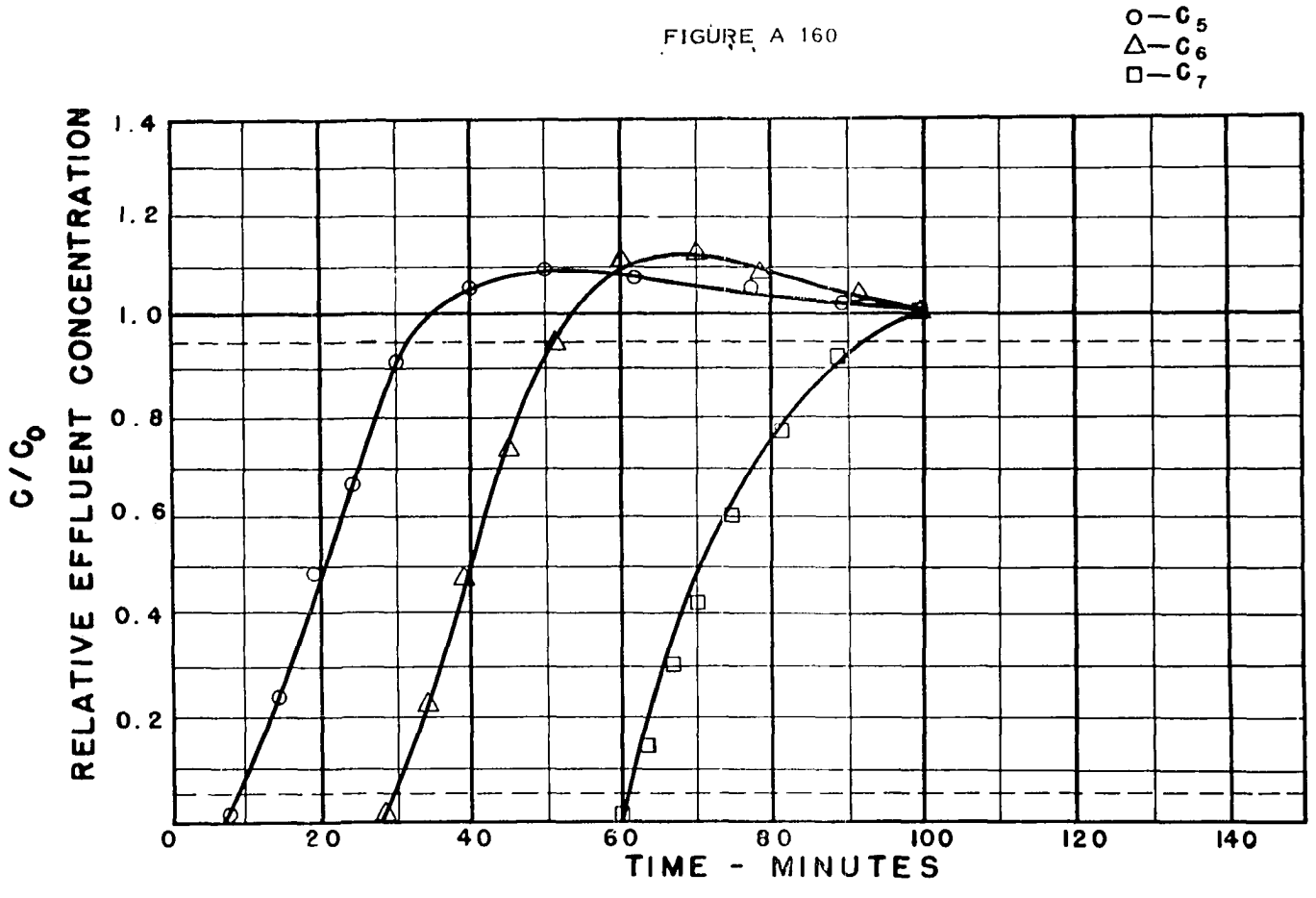

RUN NO. 221 INLET TEMP. 90 °F INLET PRESS. 800 PSIG. TOWER I.D. 2.9 in.

TOWER LGTH. 428.2 cm. FLOW RATE 27.2 ft/min. COMPOSITION: ____ %C_4 .1625 %C_5 .1248 %C_6 .285 %C_7

DESSICANT: 03 GEL

FIGURE A 161

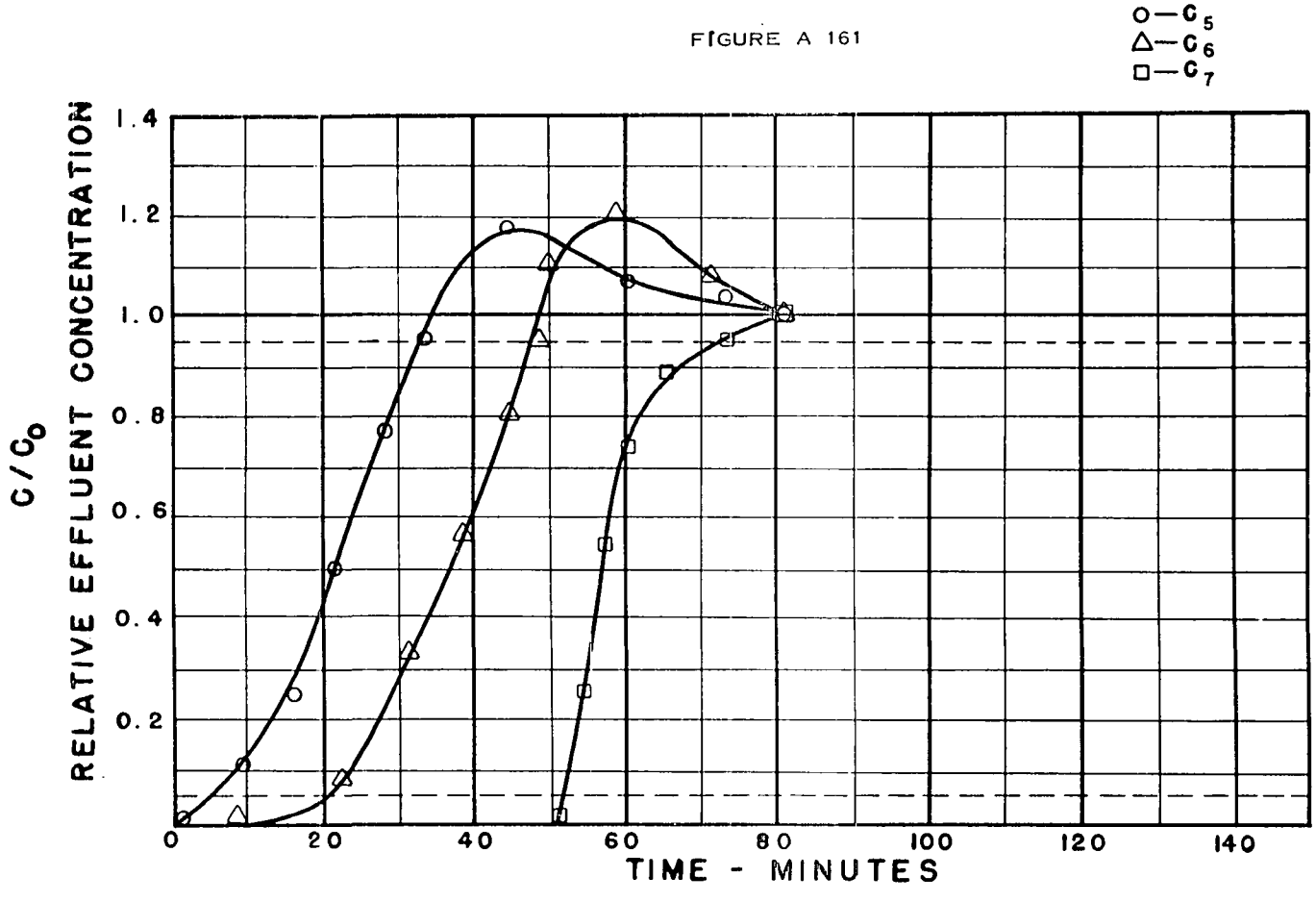

RUN NO. 222 INLET TEMP. 91.8 °F INLET PRESS. 800 PSIG. TOWER I.D. 2.9 in.

TOWER LGTH. 428.2 cm. FLOW RATE 27.4 ft/min. COMPOSITION: ____ %C_4 .1549 %C_5 .102 %C_6 .353 %C_7

DESSICANT: 03 GEL

FIGURE A 162

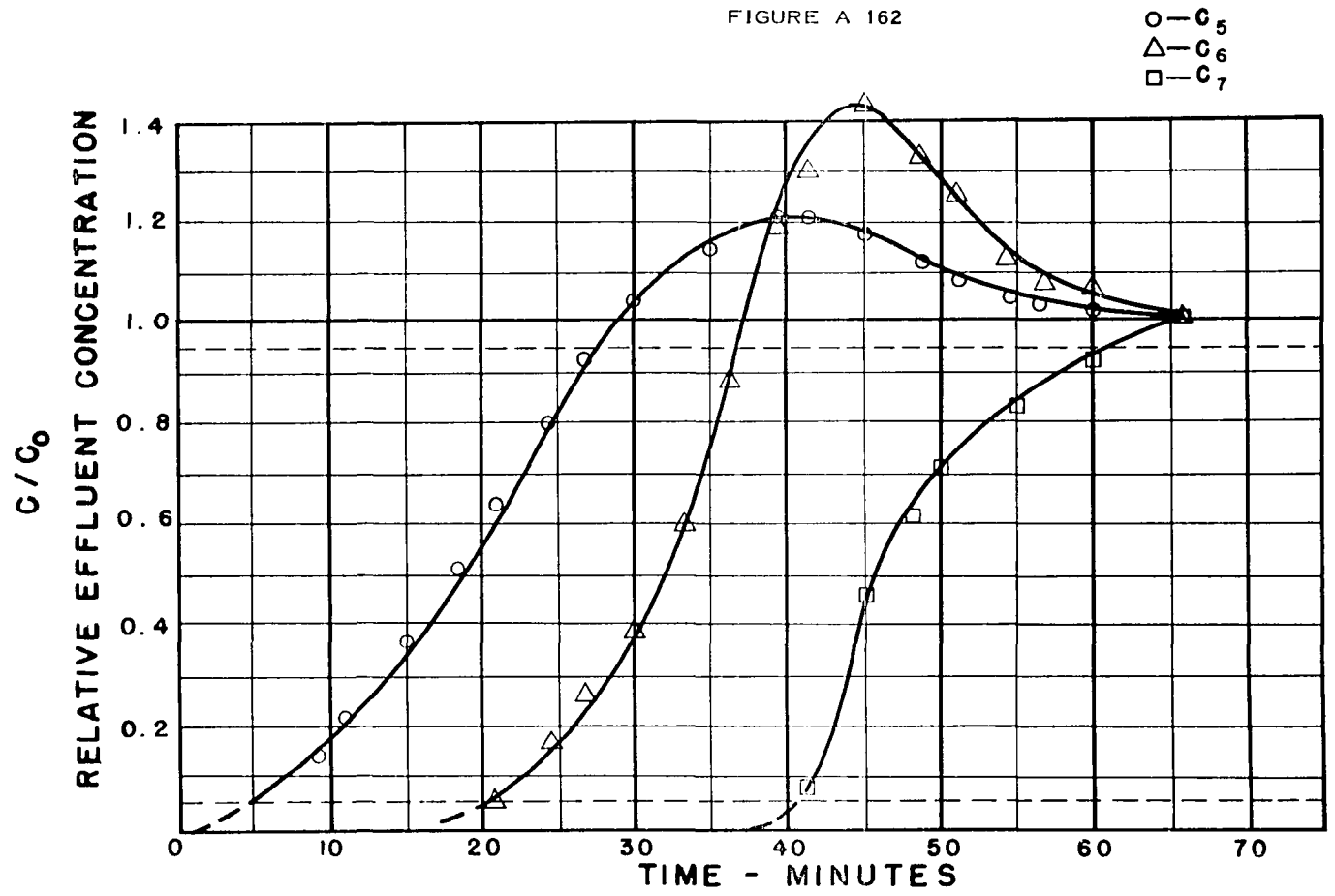

RUN NO. 225 INLET TEMP. 91.8 °F INLET PRESS. 800 PSIG. TOWER I.D. 2.9 in.

TOWER LGTH. 428.2 cm. FLOW RATE 28.6 ft/min. COMPOSITION: ____ %C_4 .0524 %C_5 .266 %C_6 0.1930 %C_7

DESSICANT: 03 GEL

FIGURE A 163

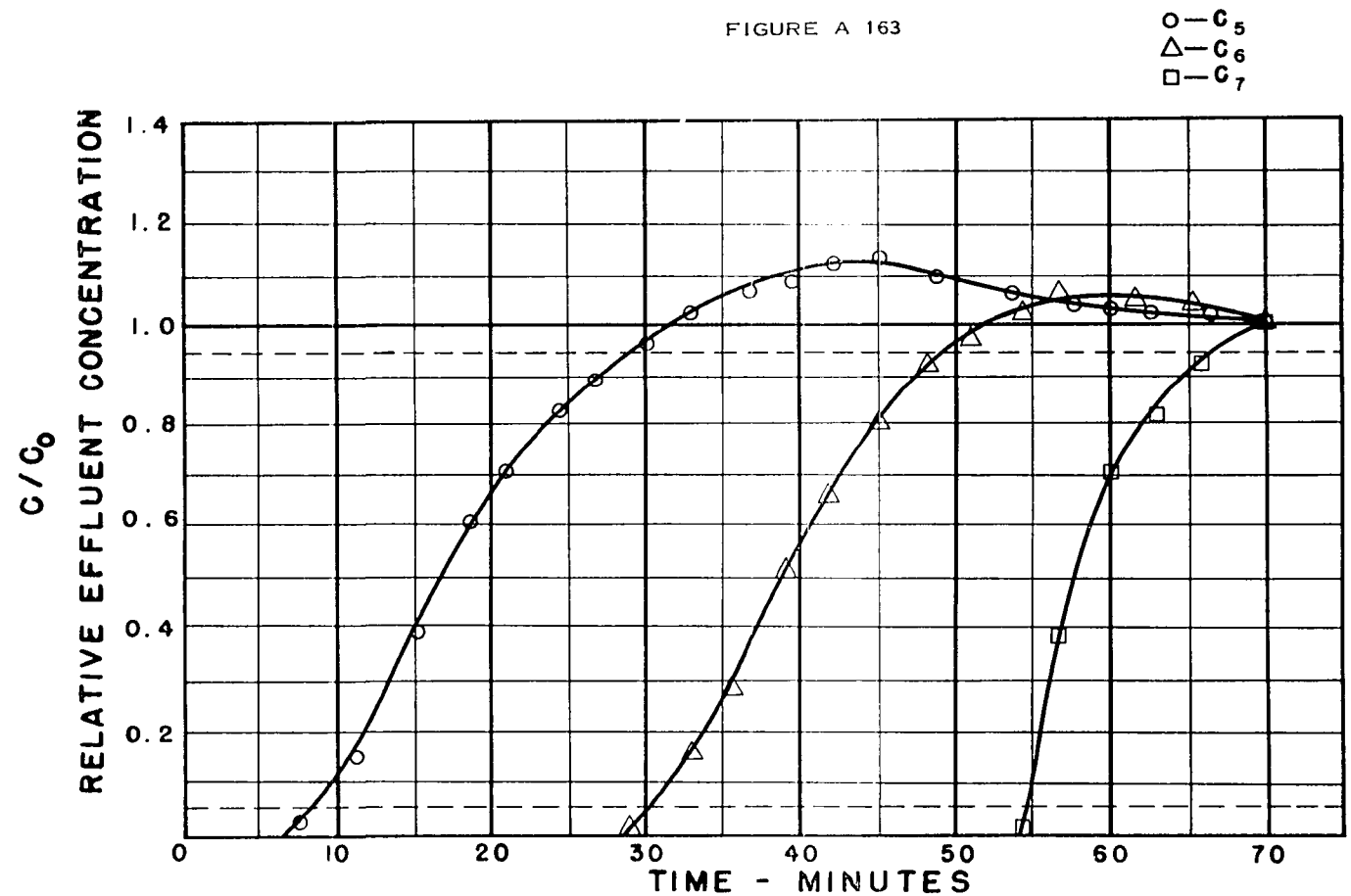

RUN NO. 226 INLET TEMP. 90.6 °F INLET PRESS. 800 PSIG. TOWER I.D. 2.9 in.

TOWER LGTH. 428.2 cm. FLOW RATE 27.8 ft/min. COMPOSITION: ____ %C_4 .0538 %C_5 .251 %C_6 .266 %C_7

DESSICANT: 03 GEL

FIGURE A 164

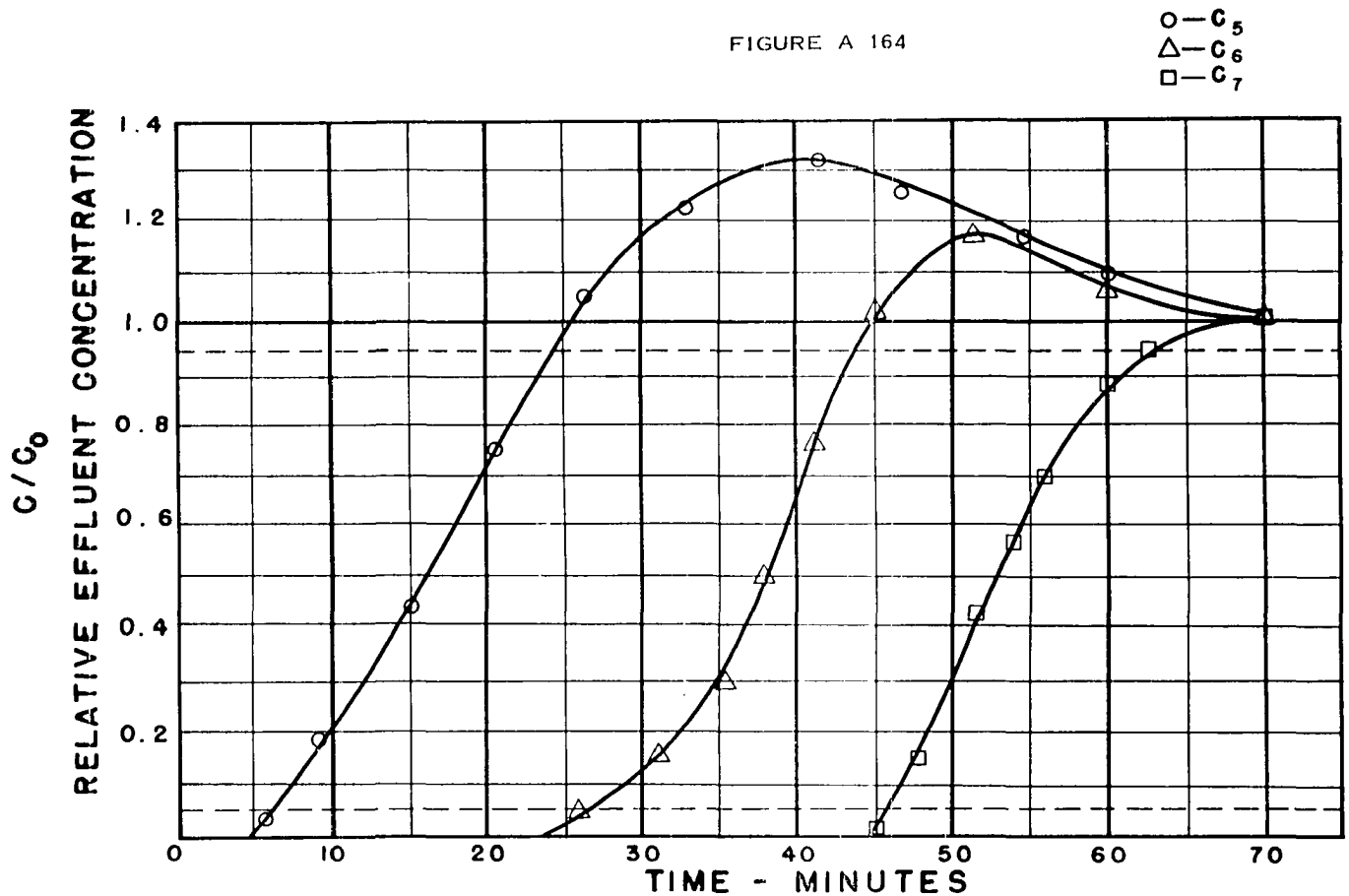

RUN NO. 227 INLET TEMP. 92.3 °F INLET PRESS. 800 PSIG. TOWER I.D. 2.9 in.

TOWER LGTH. 428.2 cm. FLOW RATE 28.1 ft/min. COMPOSITION: ____ %C_4 .0536 %C_5 .202 %C_6 0.368 %C_7

DESSICANT: 03 GEL

FIGURE A 165

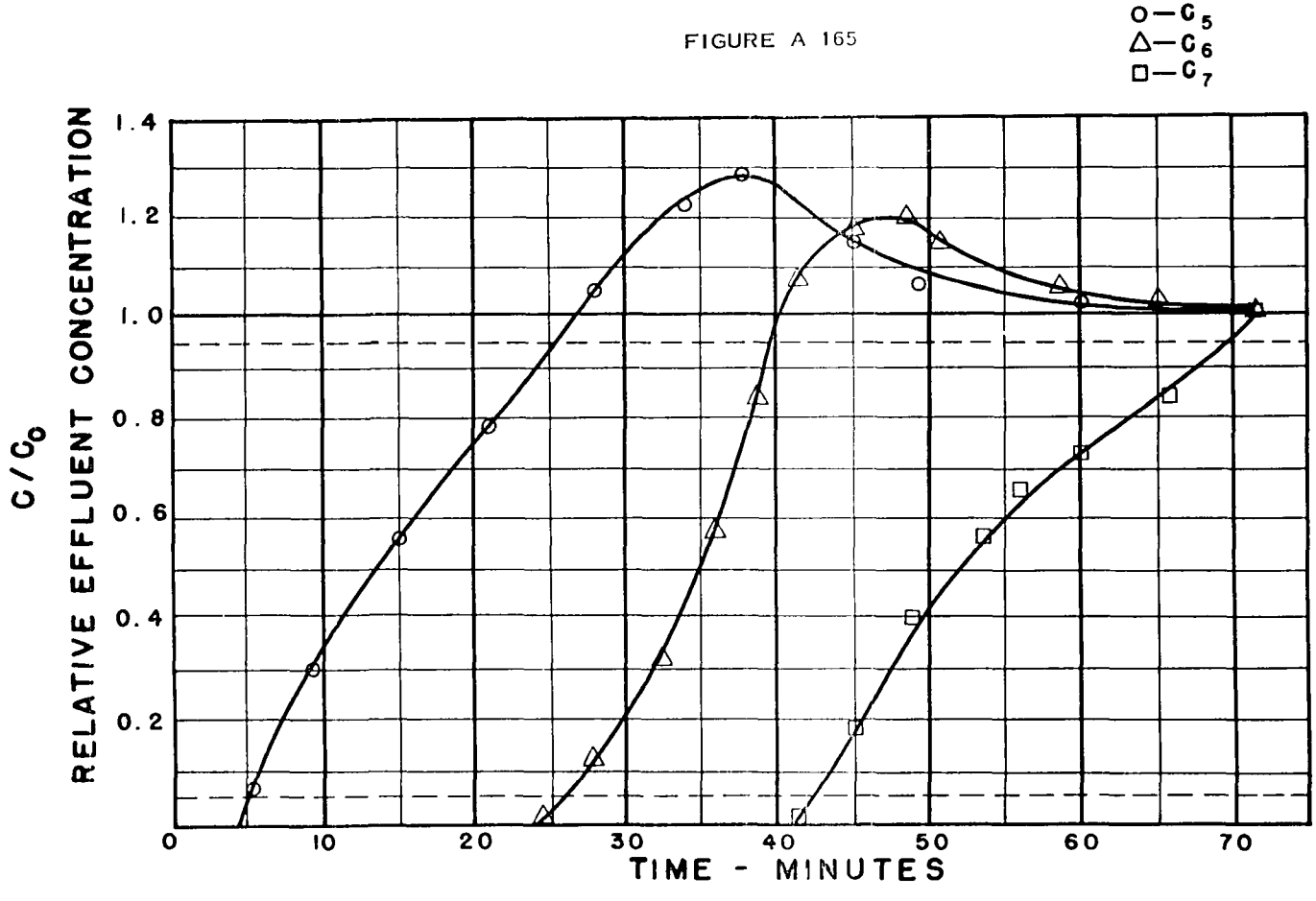

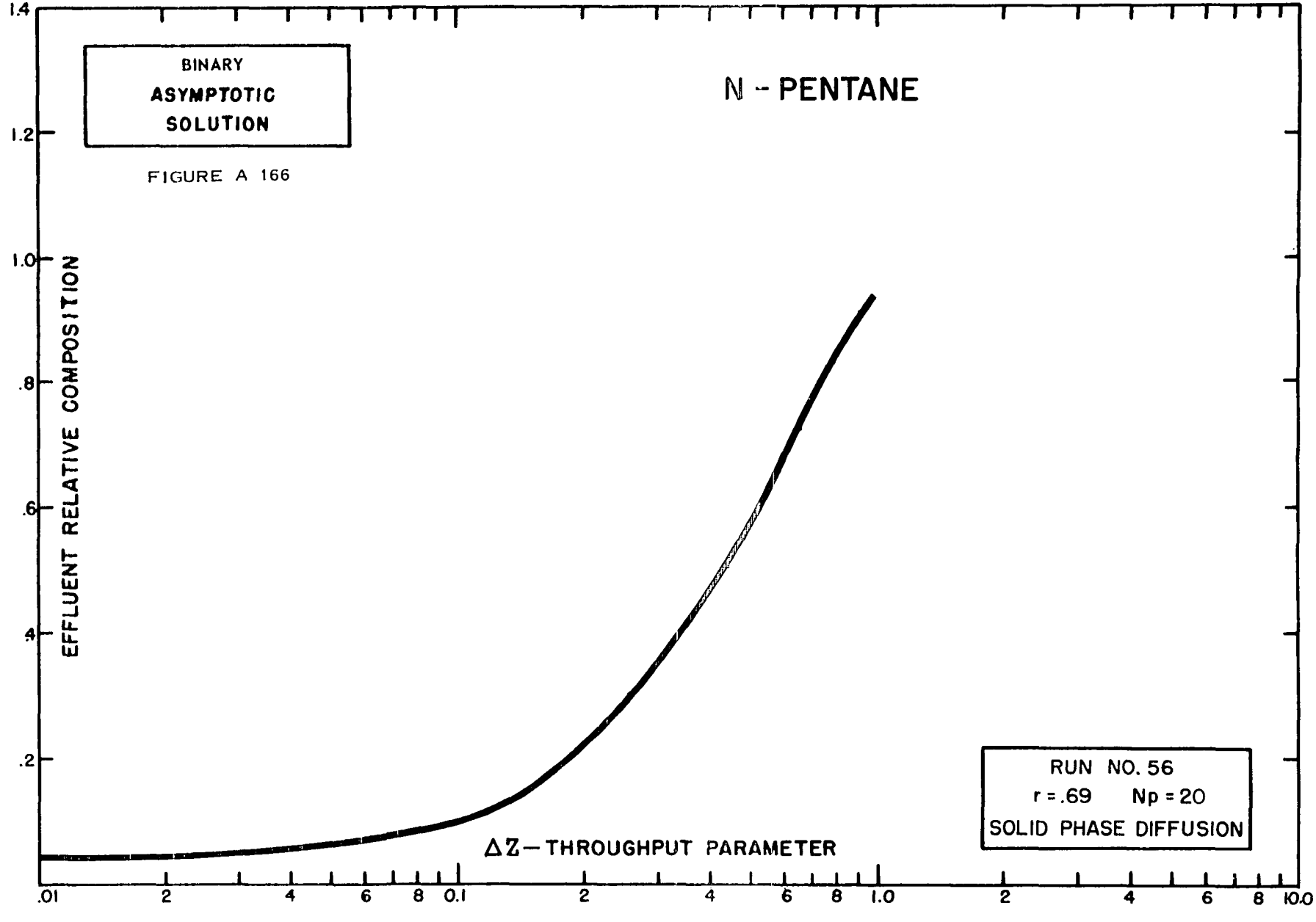
BINARY
ASYMPTOTIC
SOLUTION
N - PENTANE
EFFLUENT RELATIVE COMPOSITION
ΔZ—THROUGHPUT PARAMETER
RUN NO. 56
r = .69 Np = 20
SOLID PHASE DIFFUSION
1.4
1.2
1.0
.8
.6
.4
.2
.01
2
4
6
8
0.1
2
4
6
8
1.0
2
4
6
8
10.0

FIGURE A 166

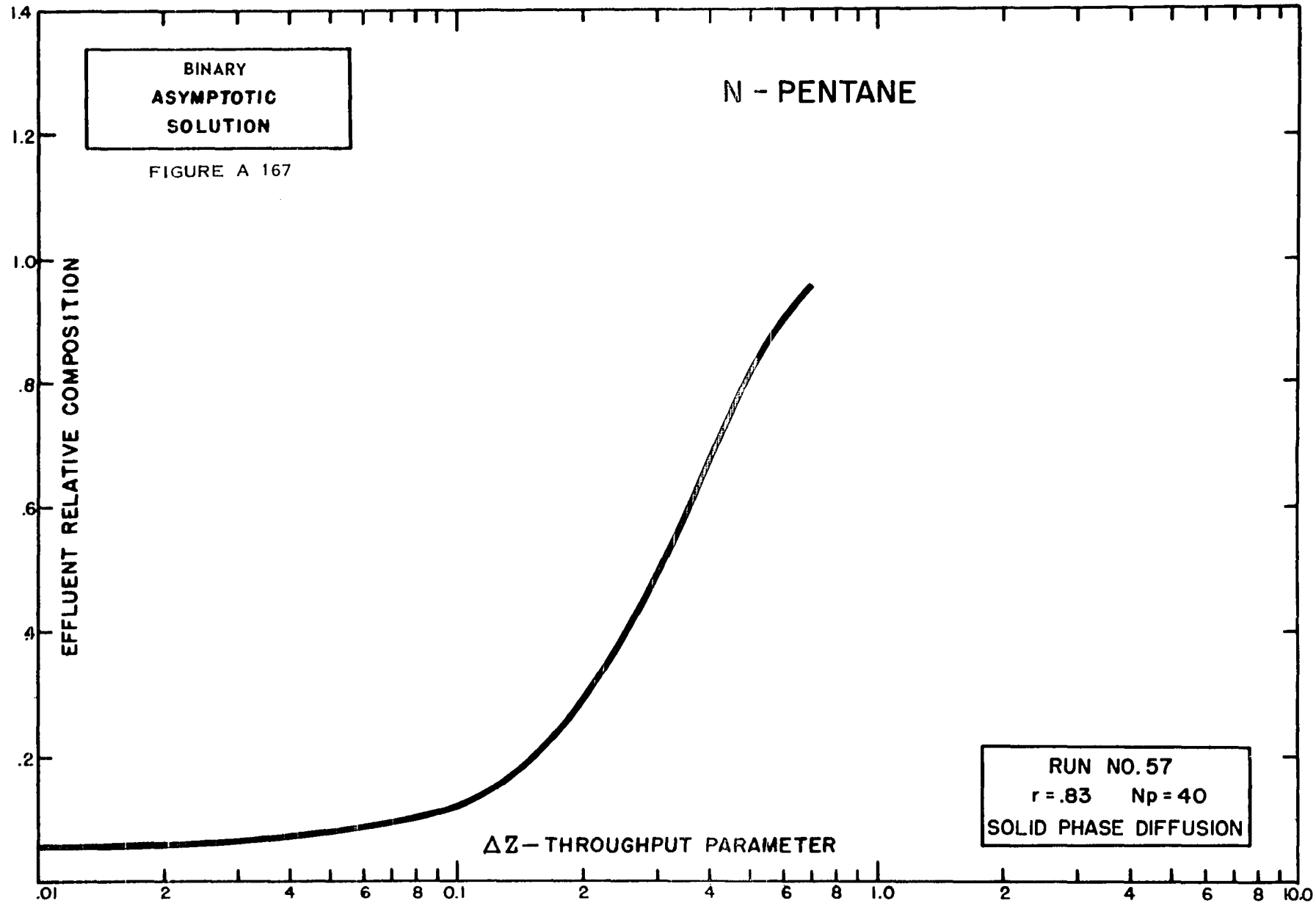
BINARY
ASYMPTOTIC
SOLUTION
N - PENTANE
EFFLUENT RELATIVE COMPOSITION
ΔZ — THROUGHPUT PARAMETER
RUN NO. 57
r = .83 Np = 40
SOLID PHASE DIFFUSION
1.4
1.2
1.0
.8
.6
.4
.2
.01
2
4
6
8
0.1
2
4
6
8
1.0
2
4
6
8
10.0

FIGURE A 167

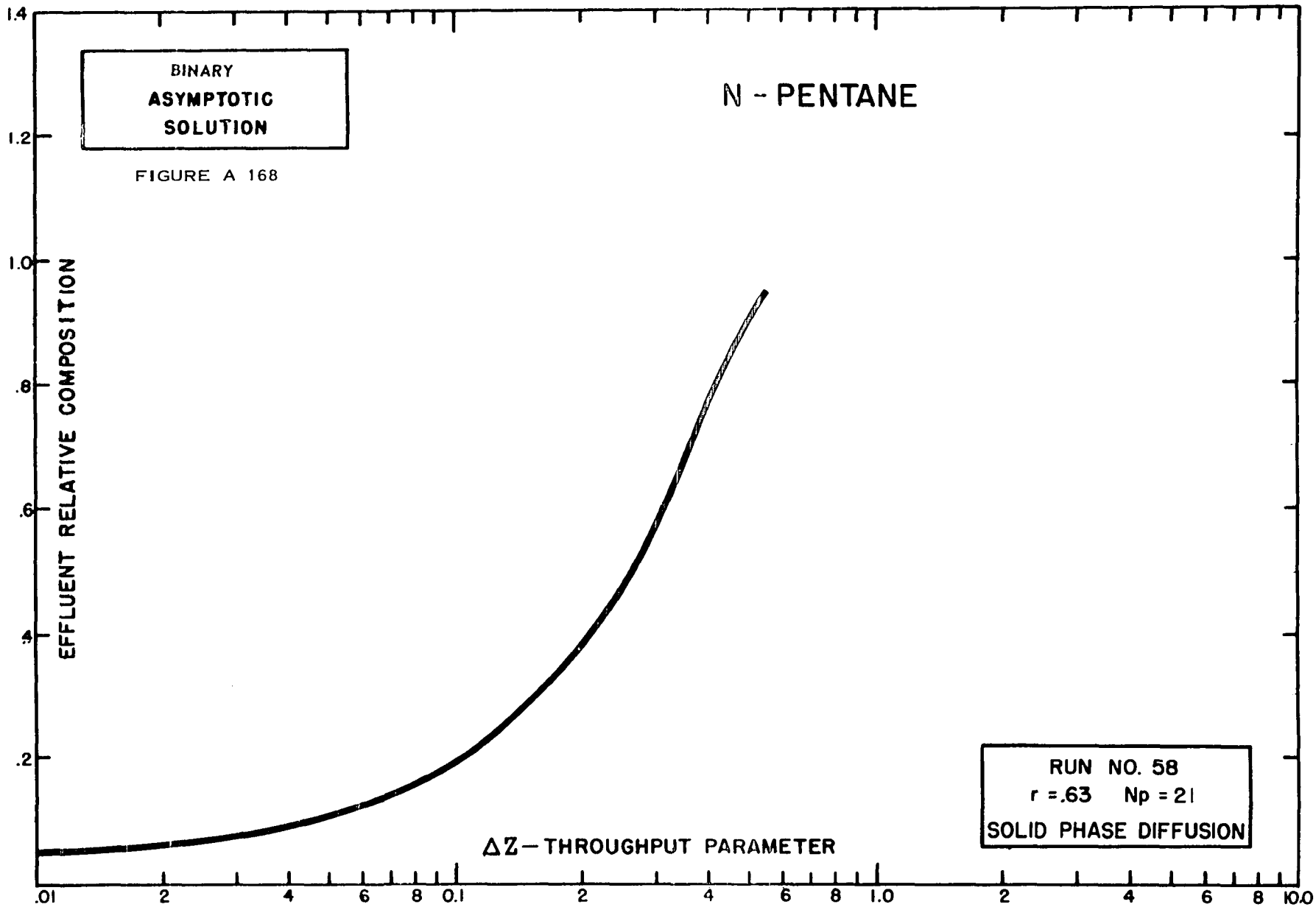
BINARY
ASYMPTOTIC
SOLUTION
N - PENTANE
EFFLUENT RELATIVE COMPOSITION
ΔZ—THROUGHPUT PARAMETER
RUN NO. 58
r = .63 Np = 21
SOLID PHASE DIFFUSION
1.4
1.2
1.0
.8
.6
.4
.2
.01
2
4
6
8
0.1
2
4
6
8
1.0
2
4
6
8
10.0

FIGURE A 168

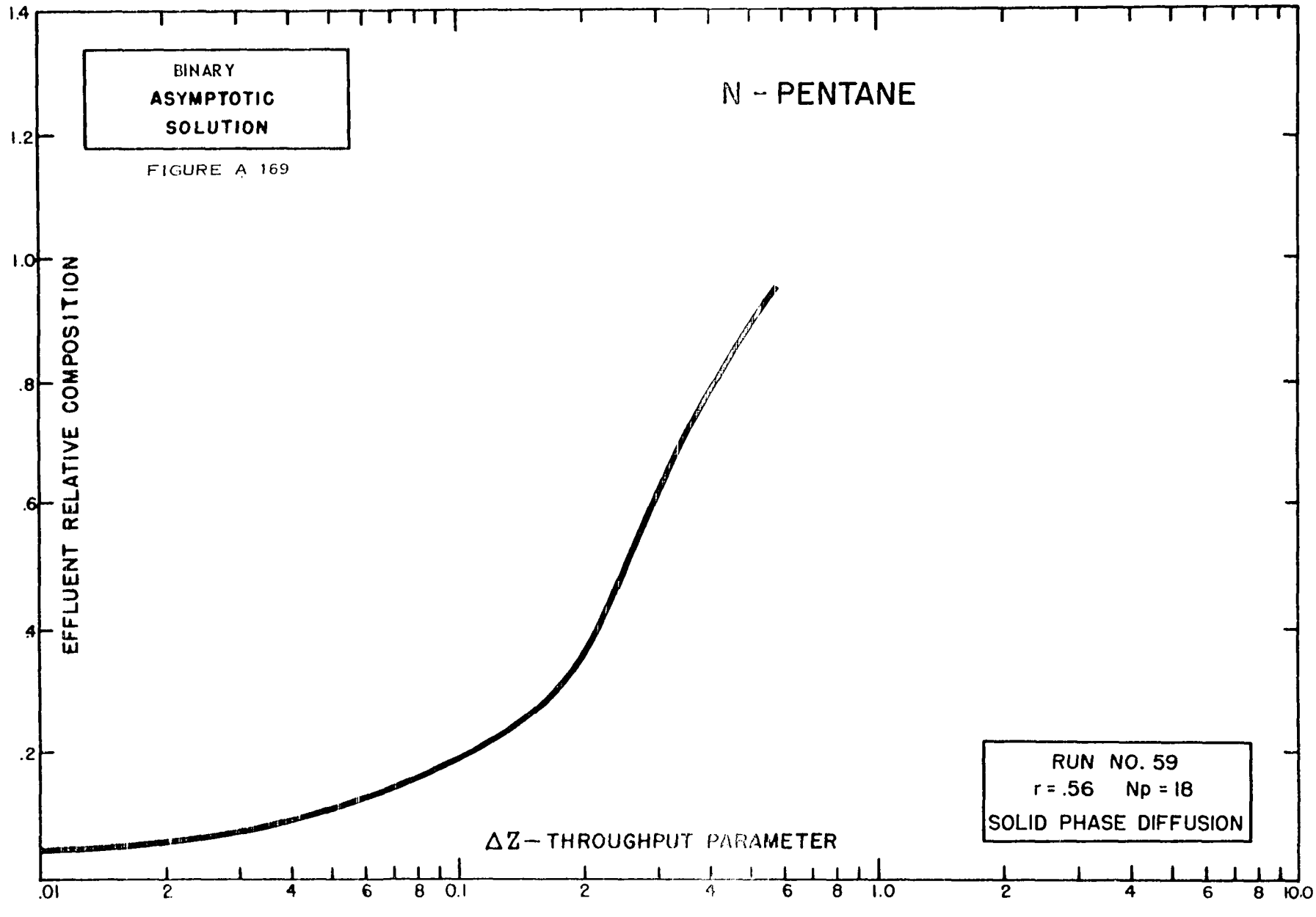
BINARY
ASYMPTOTIC
SOLUTION
N - PENTANE
EFFLUENT RELATIVE COMPOSITION
ΔZ — THROUGHPUT PARAMETER
RUN NO. 59
r = .56 Np = 18
SOLID PHASE DIFFUSION
1.4
1.2
1.0
.8
.6
.4
.2
.01
2
4
6
8
0.1
2
4
6
8
1.0
2
4
6
8
10.0

FIGURE A 169

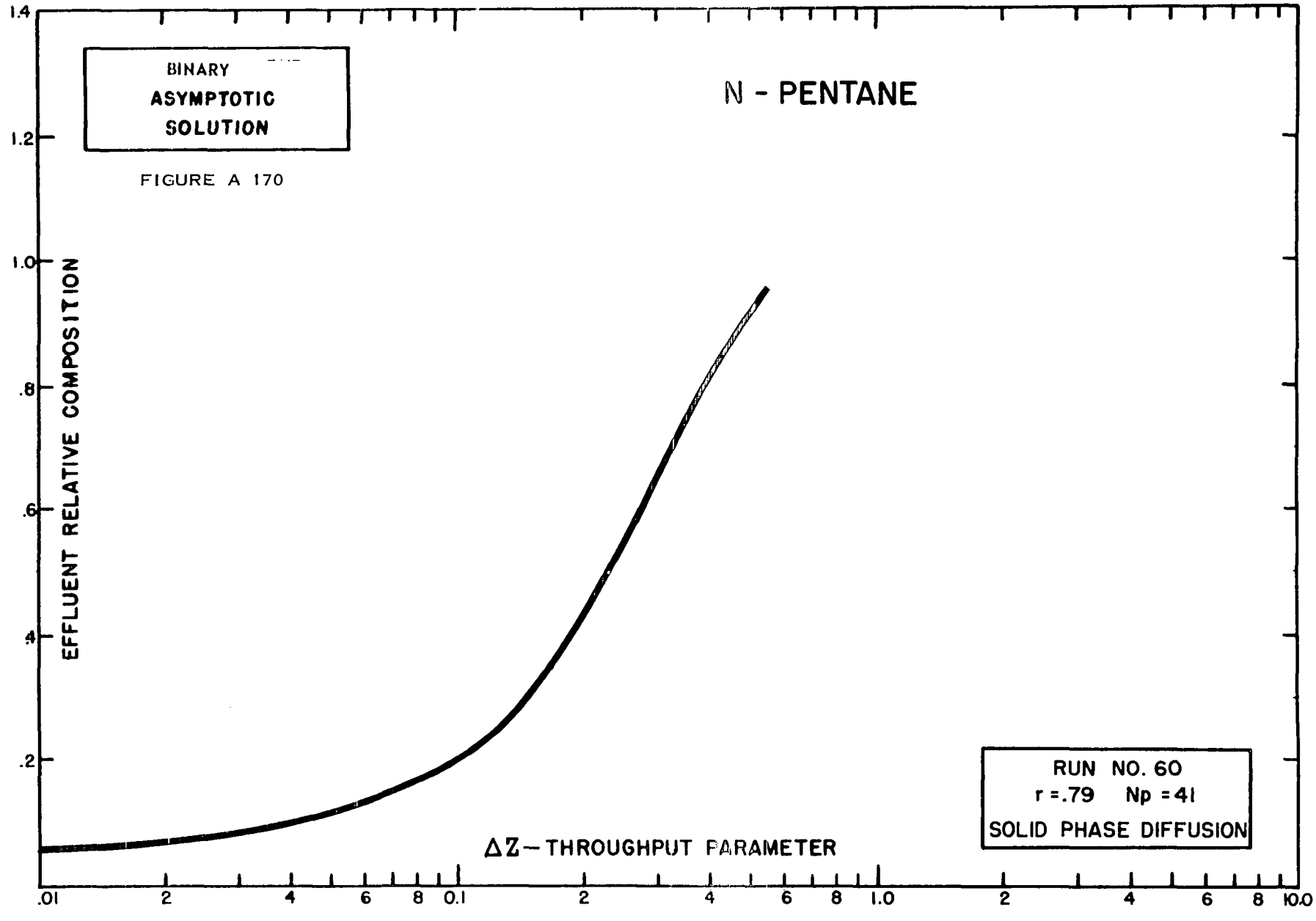
BINARY
ASYMPTOTIC
SOLUTION
N - PENTANE
EFFLUENT RELATIVE COMPOSITION
1.4
1.2
1.0
.8
.6
.4
.2
ΔZ—THROUGHPUT PARAMETER
.01
2
4
6
8
0.1
2
4
6
8
1.0
2
4
6
8
10.0
RUN NO. 60
r =.79 Np =41
SOLID PHASE DIFFUSION

FIGURE A 170

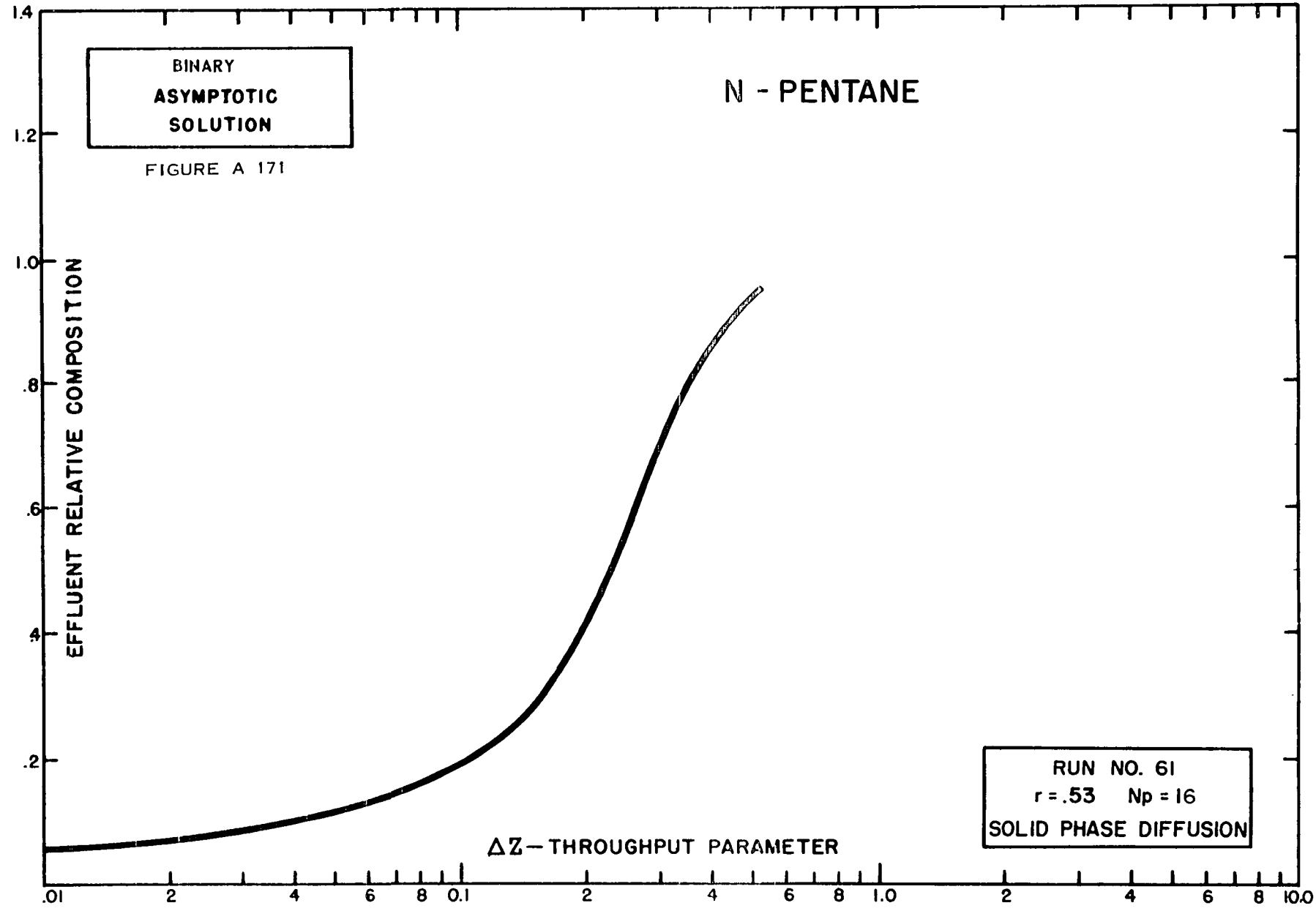
BINARY
ASYMPTOTIC
SOLUTION
FIGURE A 171
N - PENTANE
EFFLUENT RELATIVE COMPOSITION
1.4
1.2
1.0
.8
.6
.4
.2
ΔZ — THROUGHPUT PARAMETER
.01
2
4
6
8
0.1
2
4
6
8
1.0
2
4
6
8
10.0
RUN NO. 61
r = .53 Np = 16
SOLID PHASE DIFFUSION

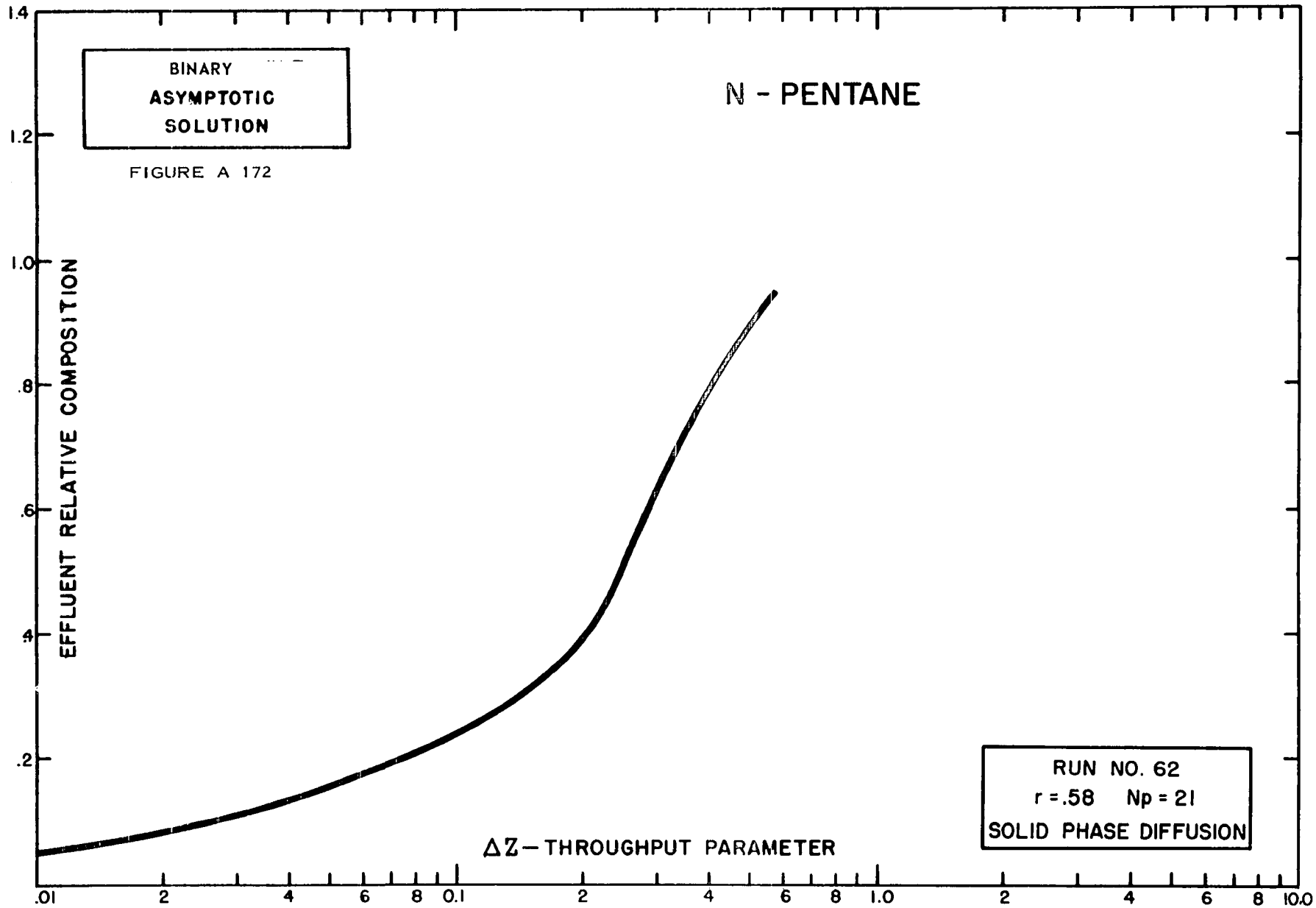
BINARY
ASYMPTOTIC
SOLUTION
N - PENTANE
EFFLUENT RELATIVE COMPOSITION
1.4
1.2
1.0
.8
.6
.4
.2
ΔZ — THROUGHPUT PARAMETER
.01
2
4
6
8
0.1
2
4
6
8
1.0
2
4
6
8
10.0
RUN NO. 62
r = .58 Np = 21
SOLID PHASE DIFFUSION

FIGURE A 172

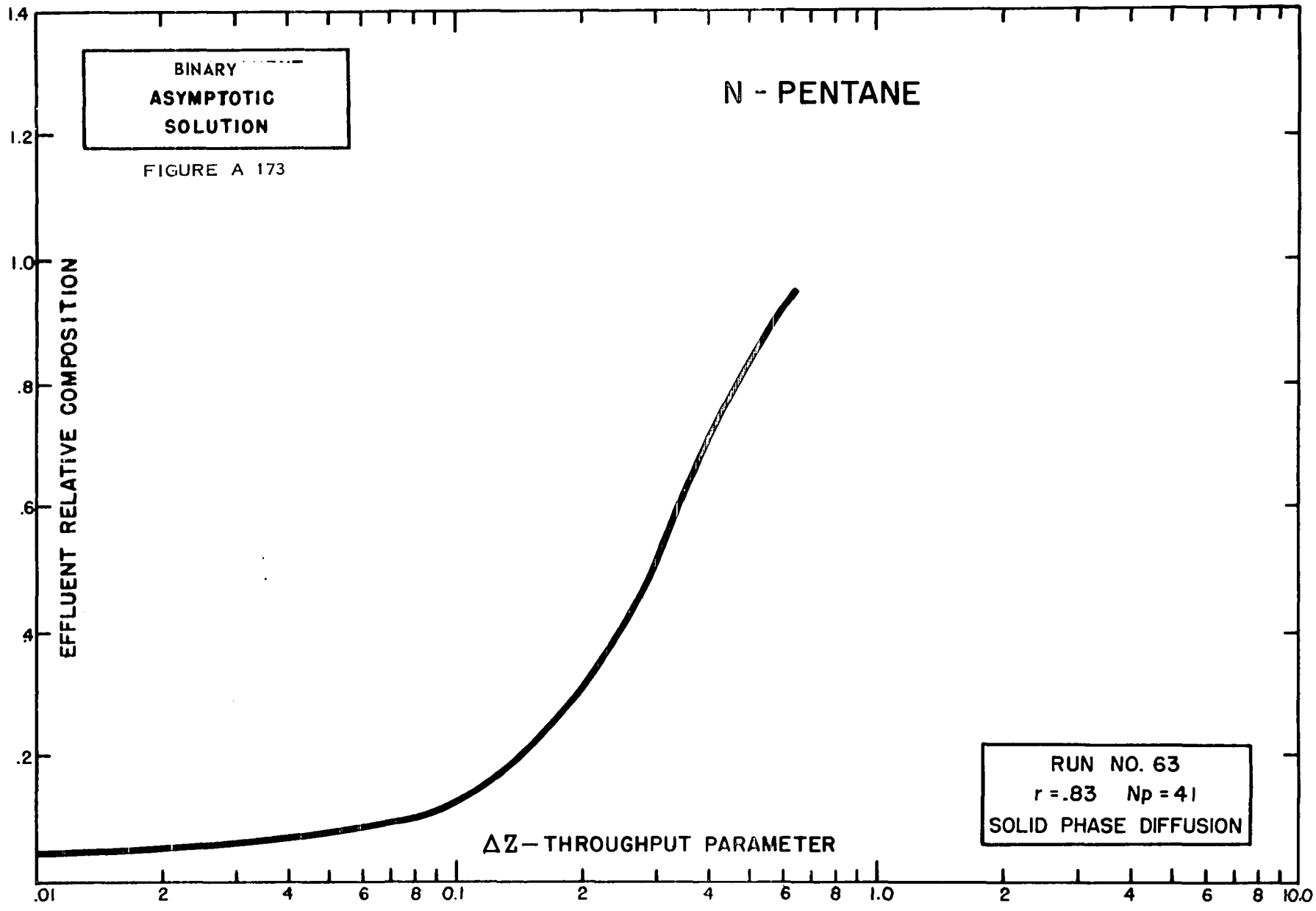
BINARY
ASYMPTOTIC
SOLUTION
N - PENTANE
EFFLUENT RELATIVE COMPOSITION
1.4
1.2
1.0
.8
.6
.4
.2
ΔZ—THROUGHPUT PARAMETER
.01
2
4
6
8
0.1
2
4
6
8
1.0
2
4
6
8
10.0
RUN NO. 63
r = .83 Np = 41
SOLID PHASE DIFFUSION

FIGURE A 173

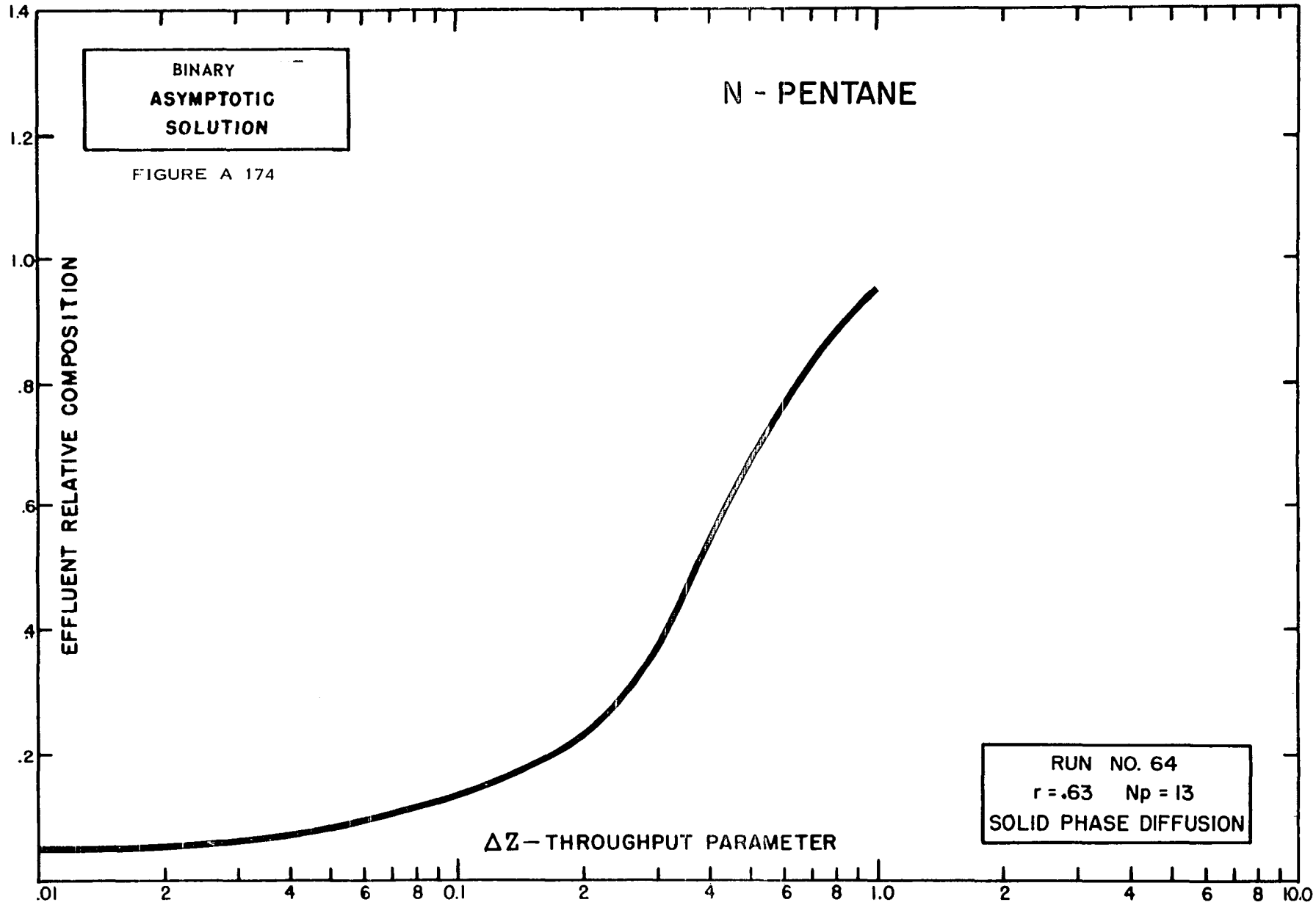
BINARY
ASYMPTOTIC
SOLUTION
N - PENTANE
EFFLUENT RELATIVE COMPOSITION
ΔZ — THROUGHPUT PARAMETER
RUN NO. 64
r = .63 Np = 13
SOLID PHASE DIFFUSION
1.4
1.2
1.0
.8
.6
.4
.2
.01
2
4
6
8
0.1
2
4
6
8
1.0
2
4
6
8
10.0

FIGURE A 174

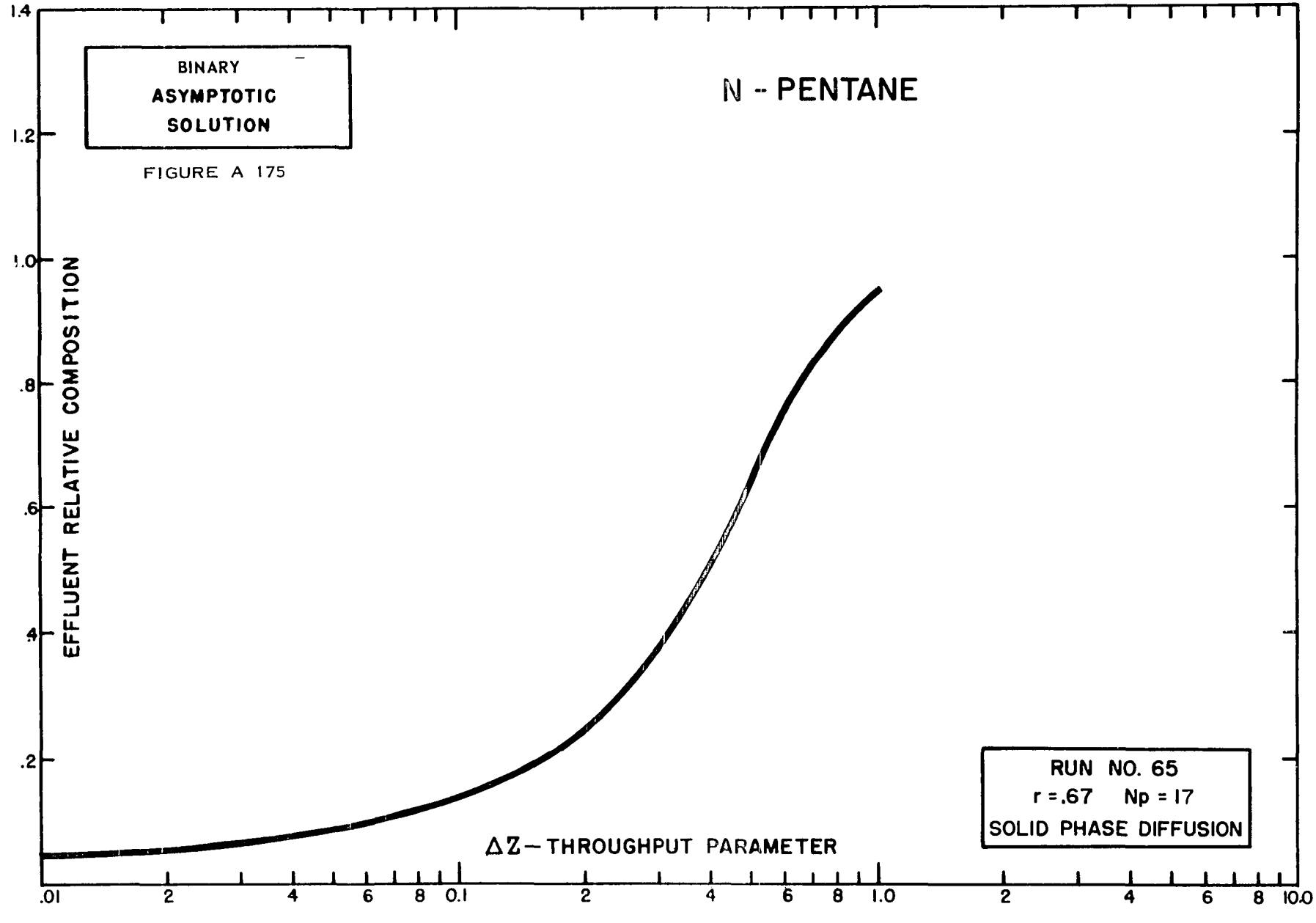
BINARY
ASYMPTOTIC
SOLUTION
N - PENTANE
EFFLUENT RELATIVE COMPOSITION
ΔZ — THROUGHPUT PARAMETER
RUN NO. 65
r = .67 Np = 17
SOLID PHASE DIFFUSION
1.4
1.2
1.0
.8
.6
.4
.2
.01
2
4
6
8
0.1
2
4
6
8
1.0
2
4
6
8
10.0

FIGURE A 175

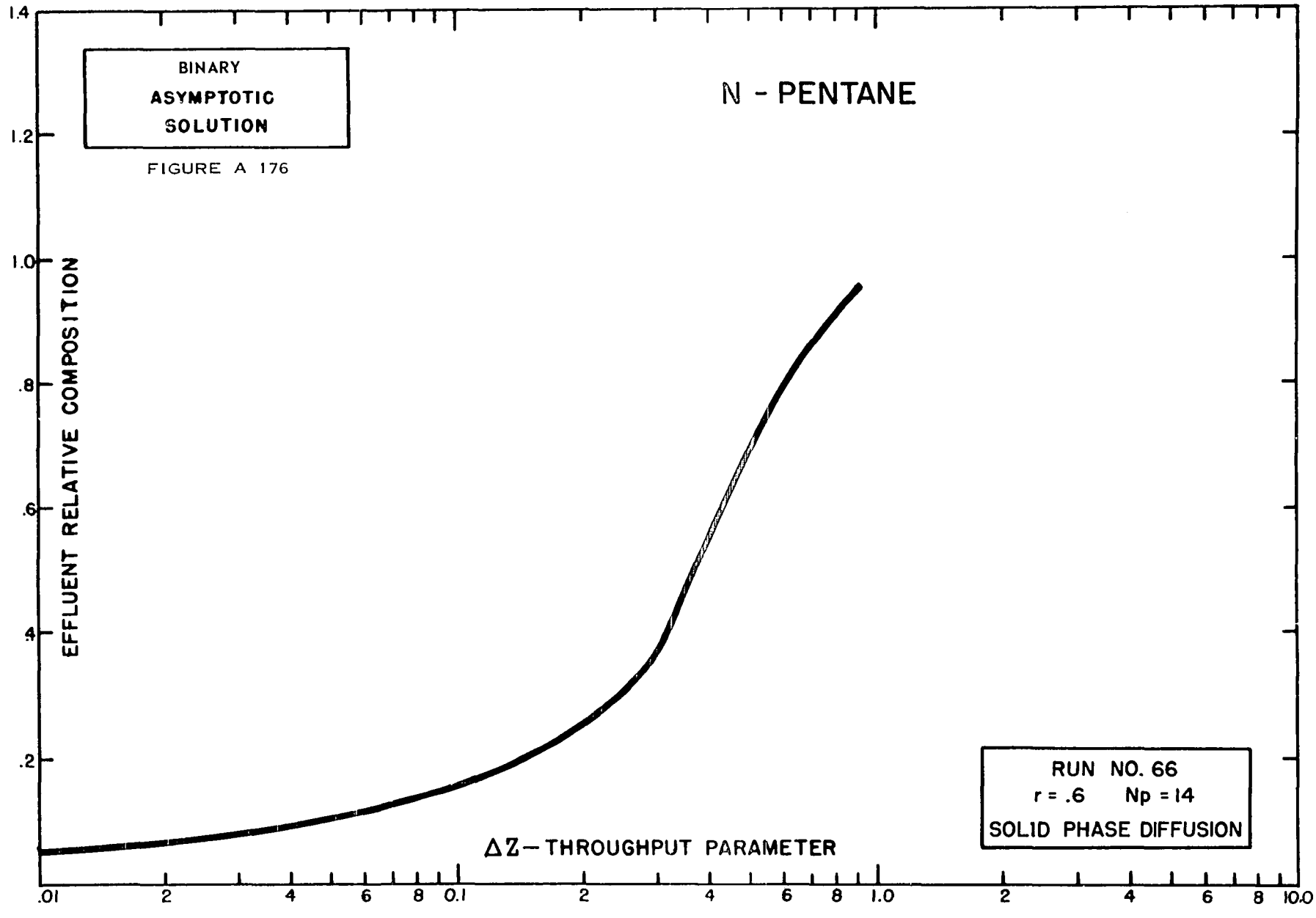
BINARY
ASYMPTOTIC
SOLUTION
N - PENTANE
EFFLUENT RELATIVE COMPOSITION
1.4
1.2
1.0
.8
.6
.4
.2
ΔZ—THROUGHPUT PARAMETER
.01
2
4
6
8
0.1
2
4
6
8
1.0
2
4
6
8
10.0
RUN NO. 66
r = .6 Np = 14
SOLID PHASE DIFFUSION

FIGURE A 176

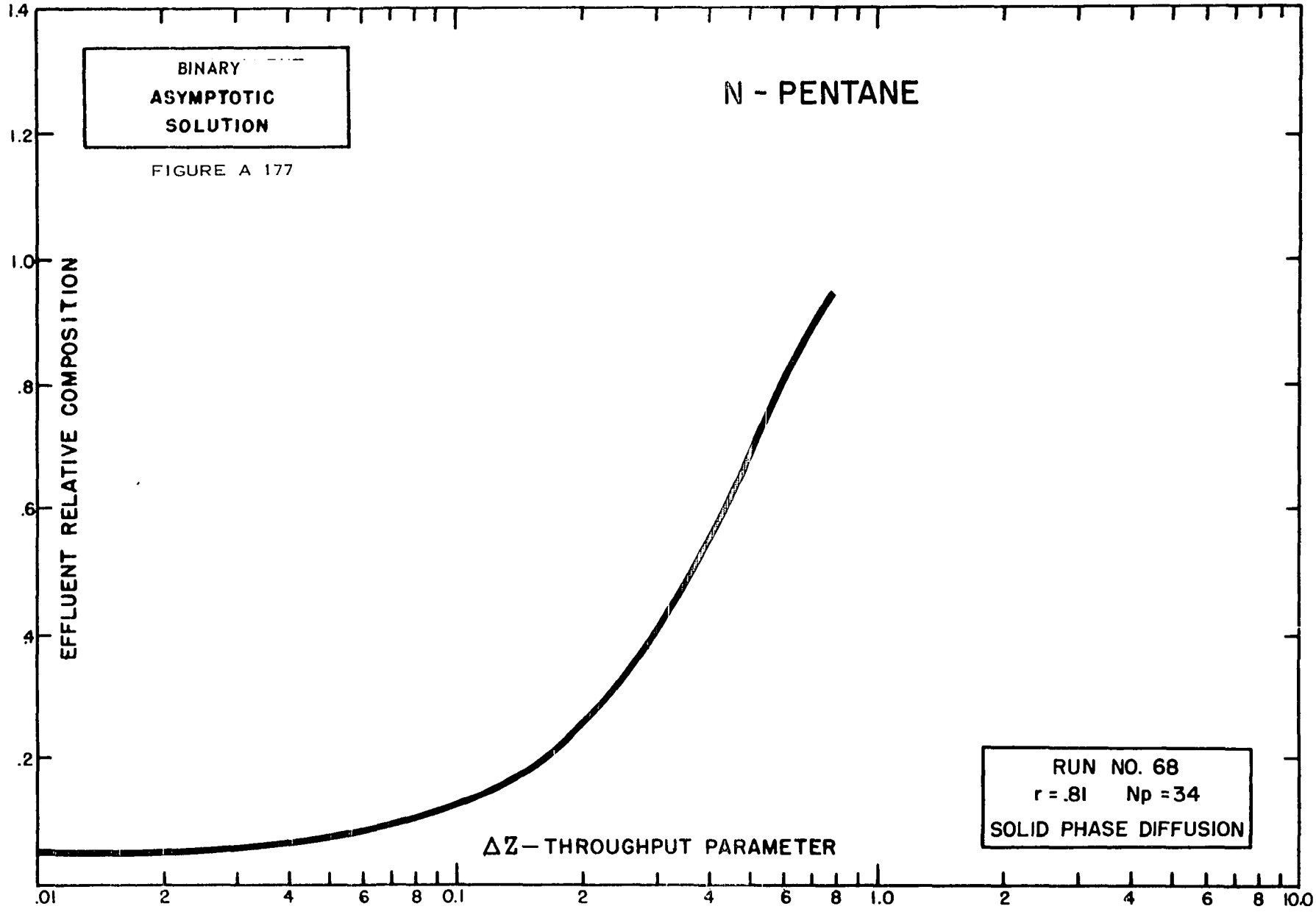
BINARY
ASYMPTOTIC
SOLUTION
N - PENTANE
EFFLUENT RELATIVE COMPOSITION
1.4
1.2
1.0
.8
.6
.4
.2
ΔZ—THROUGHPUT PARAMETER
.01
2
4
6
8
0.1
2
4
6
8
1.0
2
4
6
8
10.0
RUN NO. 68
r = .81 Np = 34
SOLID PHASE DIFFUSION

FIGURE A 177

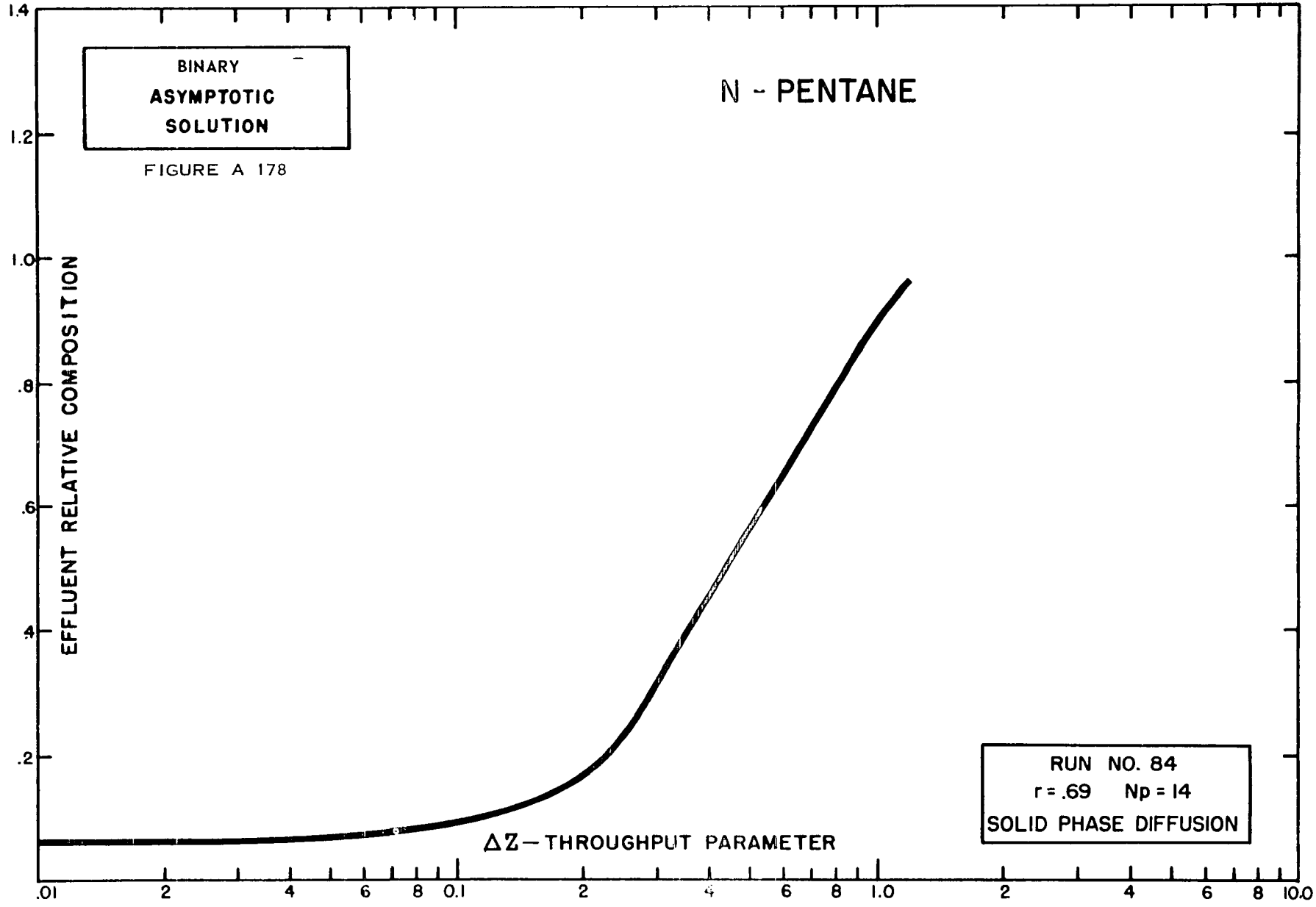
BINARY
ASYMPTOTIC
SOLUTION
N - PENTANE
EFFLUENT RELATIVE COMPOSITION
1.4
1.2
1.0
.8
.6
.4
.2
ΔZ—THROUGHPUT PARAMETER
.01
2
4
6
8
0.1
2
4
6
8
1.0
2
4
6
8
10.0
RUN NO. 84
r = .69 Np = 14
SOLID PHASE DIFFUSION

FIGURE A 178

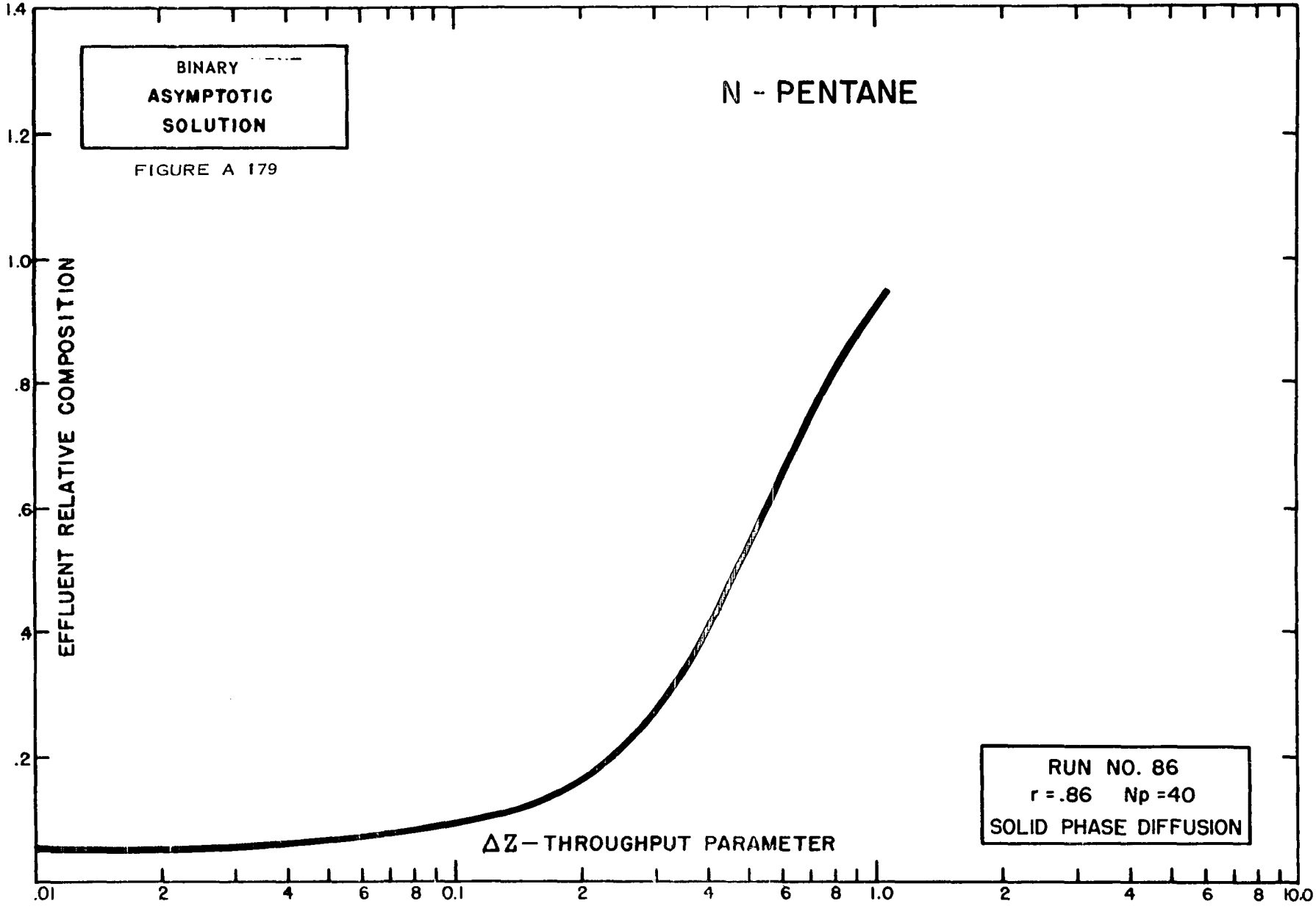
BINARY
ASYMPTOTIC
SOLUTION
N - PENTANE
EFFLUENT RELATIVE COMPOSITION
ΔZ — THROUGHPUT PARAMETER
RUN NO. 86
r = .86 Np = 40
SOLID PHASE DIFFUSION
1.4
1.2
1.0
.8
.6
.4
.2
.01
2
4
6
8
0.1
2
4
6
8
1.0
2
4
6
8
10.0

FIGURE A 179

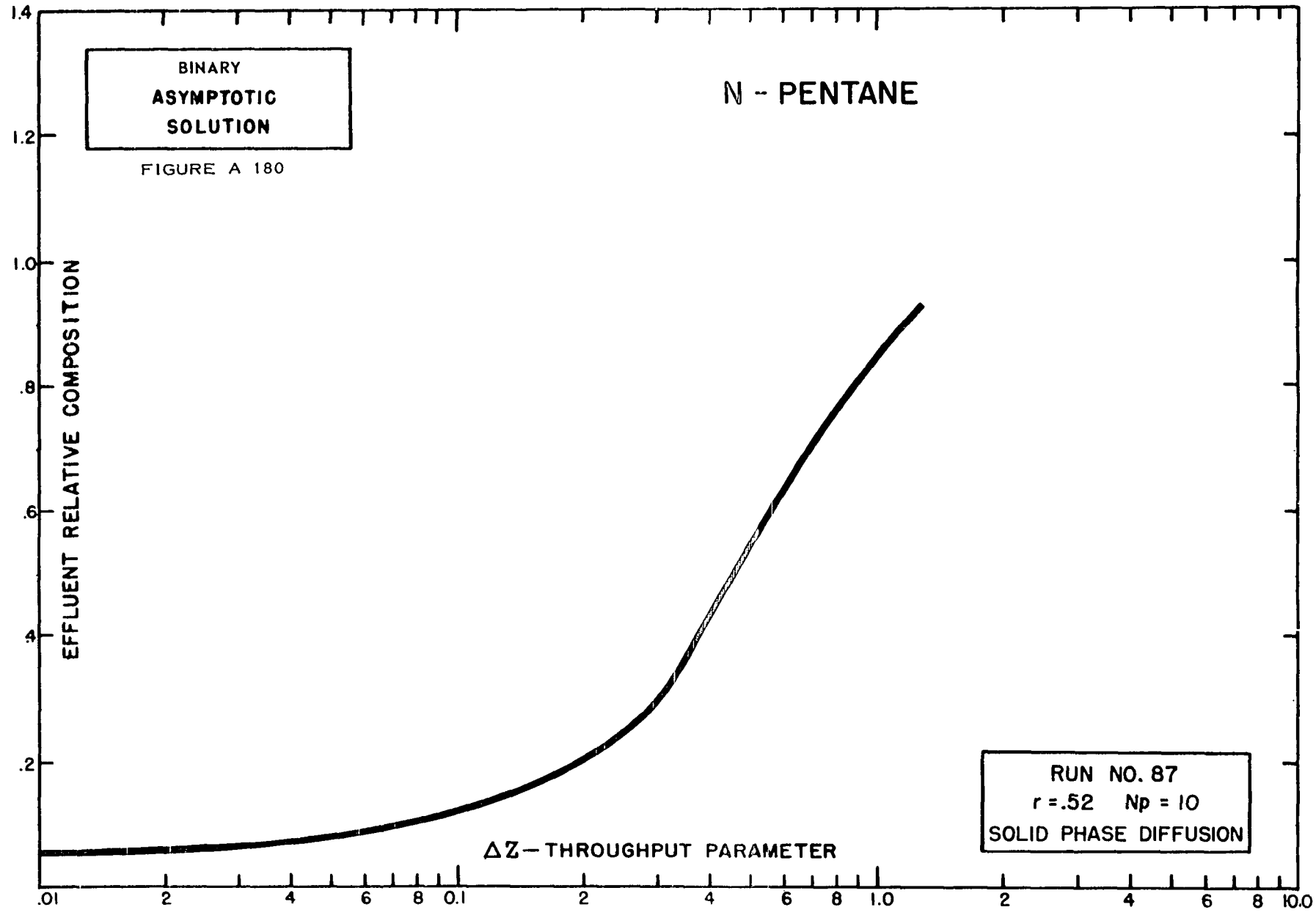
BINARY
ASYMPTOTIC
SOLUTION
FIGURE A 180
N - PENTANE
EFFLUENT RELATIVE COMPOSITION
1.4
1.2
1.0
.8
.6
.4
.2
ΔZ—THROUGHPUT PARAMETER
.01
2
4
6
8
0.1
2
4
6
8
1.0
2
4
6
8
10.0
RUN NO. 87
r = .52 Np = 10
SOLID PHASE DIFFUSION

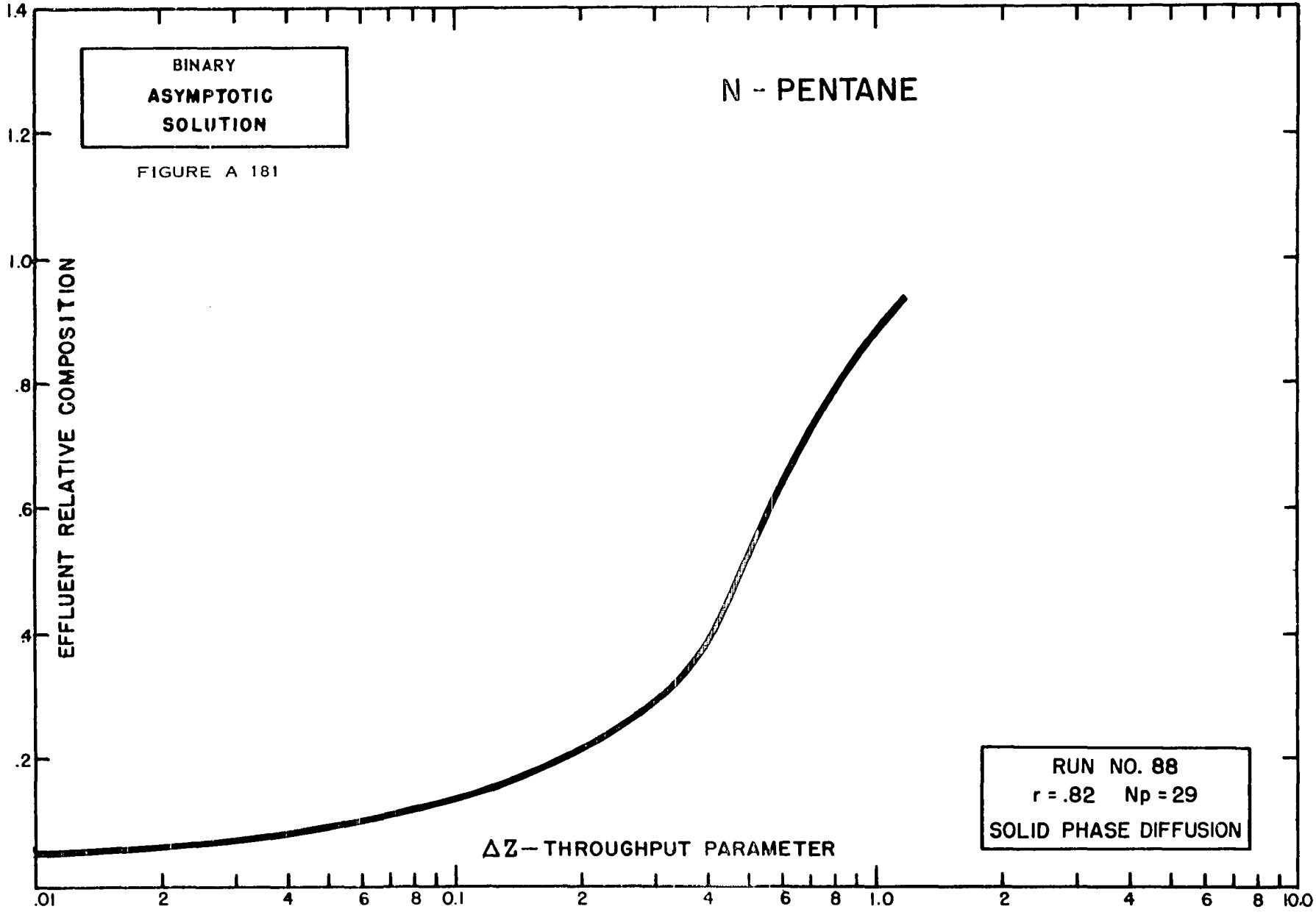
BINARY
ASYMPTOTIC
SOLUTION
N - PENTANE
EFFLUENT RELATIVE COMPOSITION
ΔZ—THROUGHPUT PARAMETER
RUN NO. 88
r = .82 Np = 29
SOLID PHASE DIFFUSION
1.4
1.2
1.0
.8
.6
.4
.2
.01
2
4
6
8
0.1
2
4
6
8
1.0
2
4
6
8
10.0

FIGURE A 181

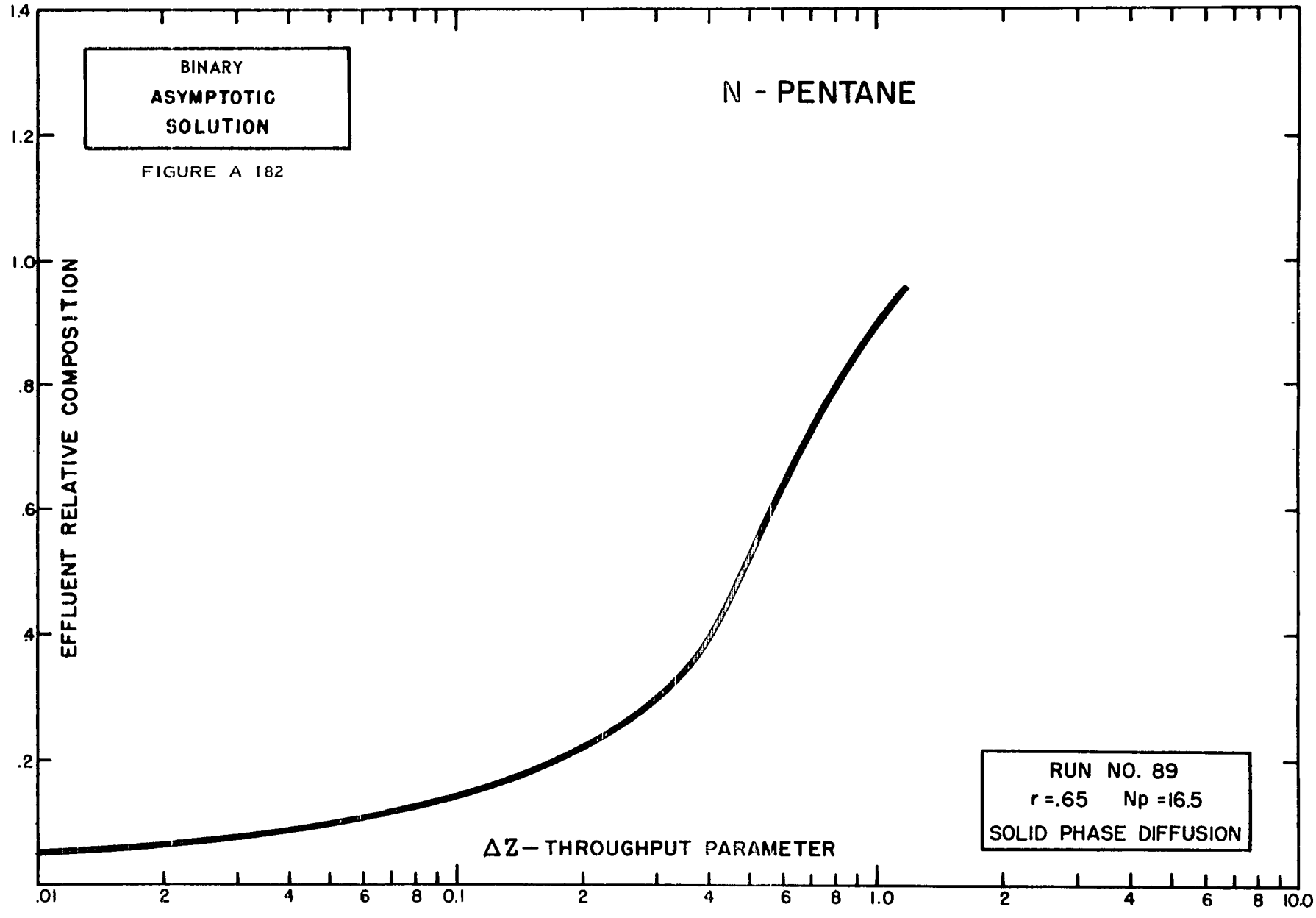
BINARY
ASYMPTOTIC
SOLUTION
N - PENTANE
EFFLUENT RELATIVE COMPOSITION
1.4
1.2
1.0
.8
.6
.4
.2
ΔZ—THROUGHPUT PARAMETER
.01
2
4
6
8
0.1
2
4
6
8
1.0
2
4
6
8
10.0
RUN NO. 89
r =.65 Np =16.5
SOLID PHASE DIFFUSION

FIGURE A 182

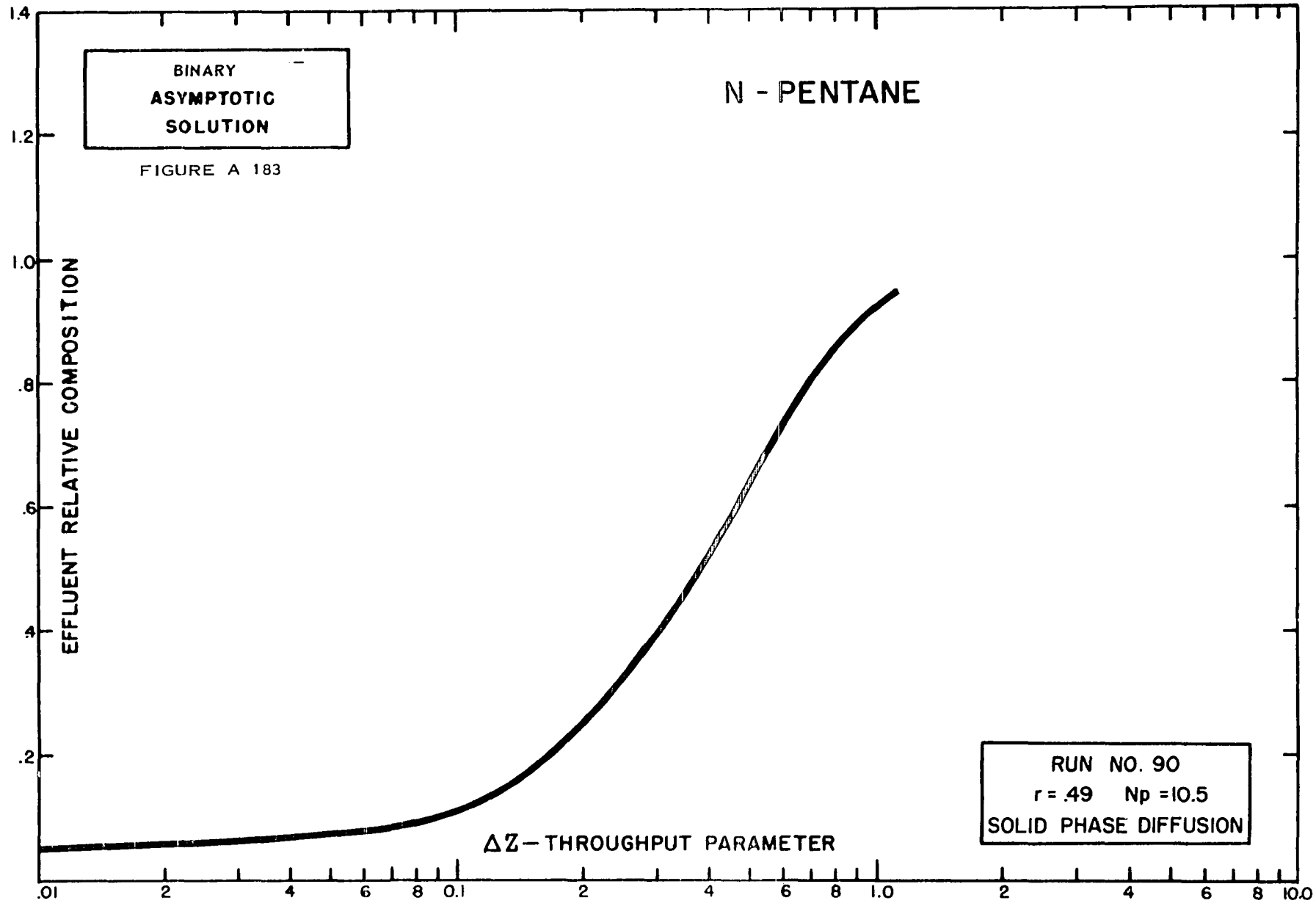
BINARY
ASYMPTOTIC
SOLUTION
N - PENTANE
EFFLUENT RELATIVE COMPOSITION
ΔZ — THROUGHPUT PARAMETER
RUN NO. 90
r = .49 Np = 10.5
SOLID PHASE DIFFUSION
1.4
1.2
1.0
.8
.6
.4
.2
.01
2
4
6
8
0.1
2
4
6
8
1.0
2
4
6
8
10.0

FIGURE A 183

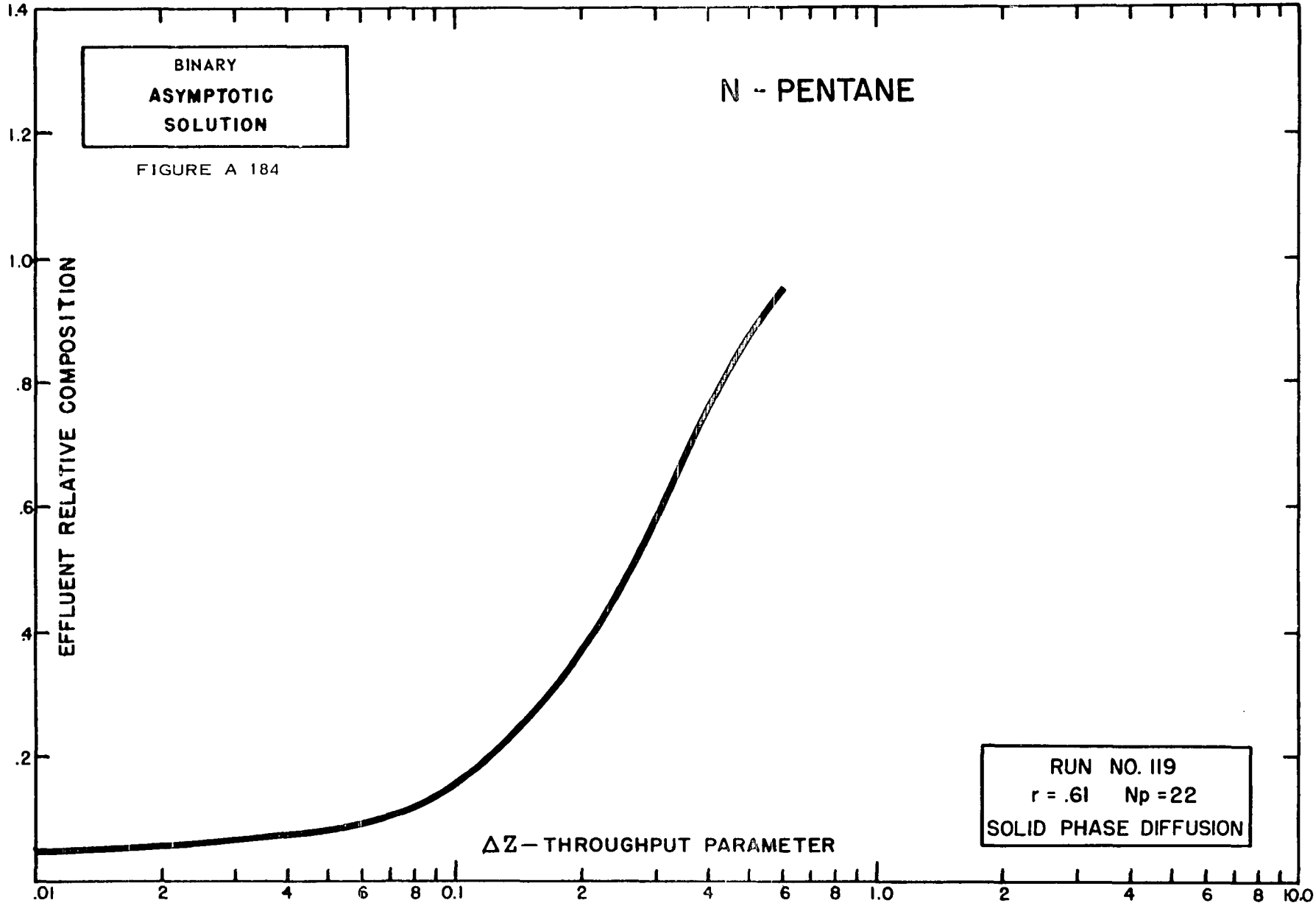
BINARY
ASYMPTOTIC
SOLUTION
N - PENTANE
EFFLUENT RELATIVE COMPOSITION
ΔZ — THROUGHPUT PARAMETER
RUN NO. 119
r = .61 Np = 22
SOLID PHASE DIFFUSION
1.4
1.2
1.0
.8
.6
.4
.2
.01
2
4
6
8
0.1
2
4
6
8
1.0
2
4
6
8
10.0

FIGURE A 184

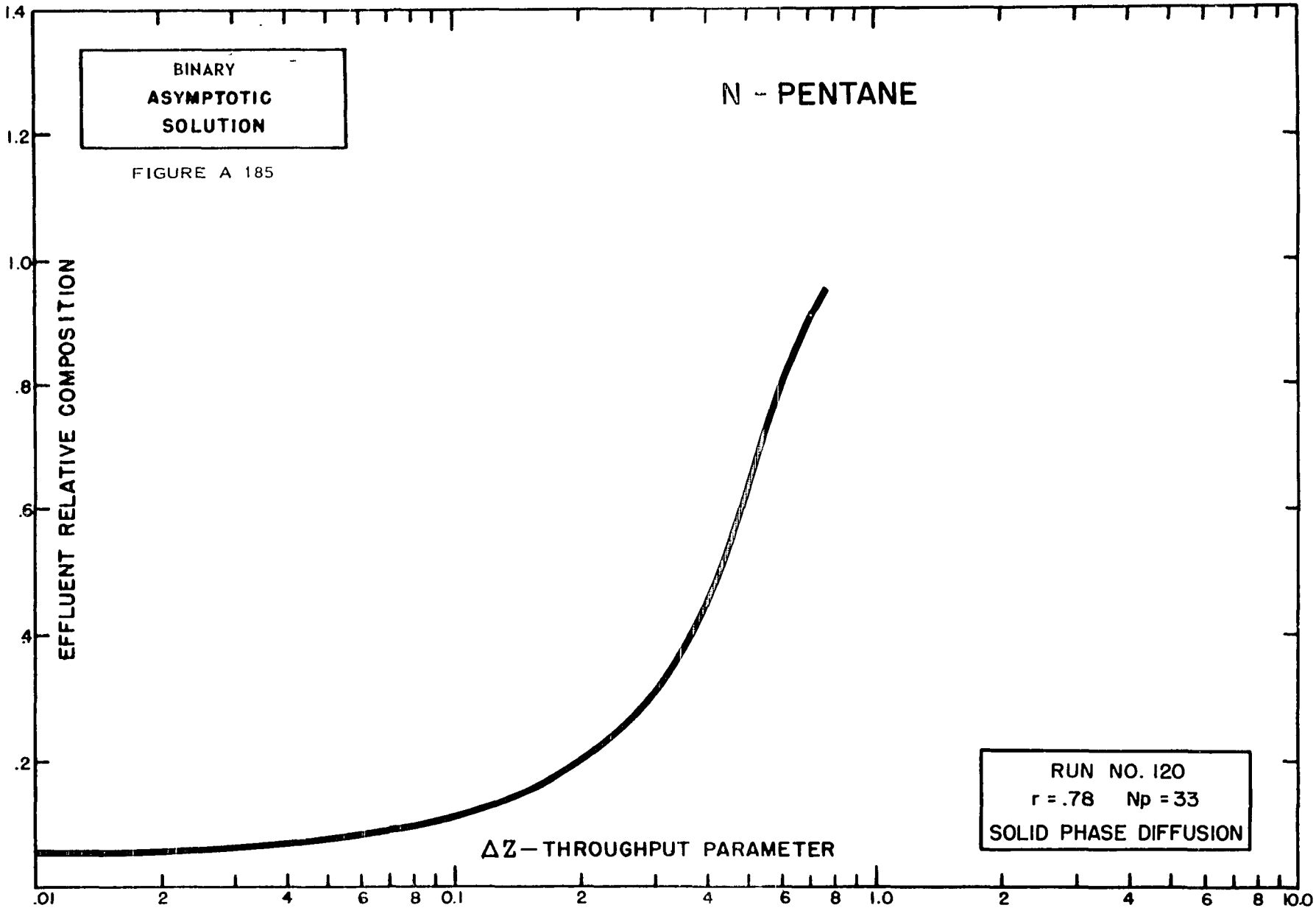
BINARY
ASYMPTOTIC
SOLUTION
N - PENTANE
EFFLUENT RELATIVE COMPOSITION
ΔZ—THROUGHPUT PARAMETER
RUN NO. 120
r = .78 Np = 33
SOLID PHASE DIFFUSION
1.4
1.2
1.0
.8
.6
.4
.2
.01
2
4
6
8
0.1
2
4
6
8
1.0
2
4
6
8
10.0

FIGURE A 185

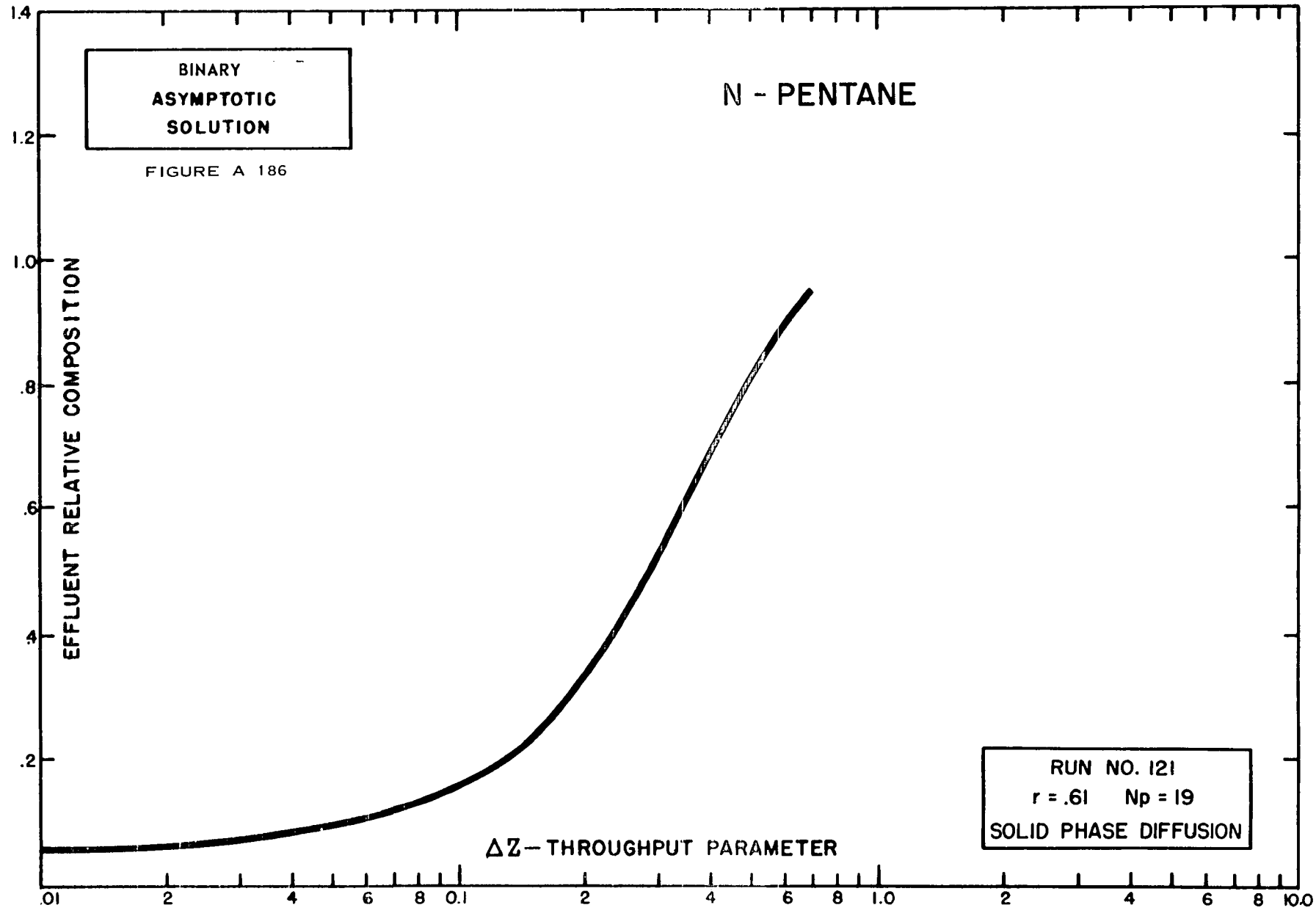
BINARY
ASYMPTOTIC
SOLUTION
N - PENTANE
EFFLUENT RELATIVE COMPOSITION
1.4
1.2
1.0
.8
.6
.4
.2
ΔZ — THROUGHPUT PARAMETER
.01
2
4
6
8
0.1
2
4
6
8
1.0
2
4
6
8
10.0
RUN NO. 121
r = .61 Np = 19
SOLID PHASE DIFFUSION

FIGURE A 186

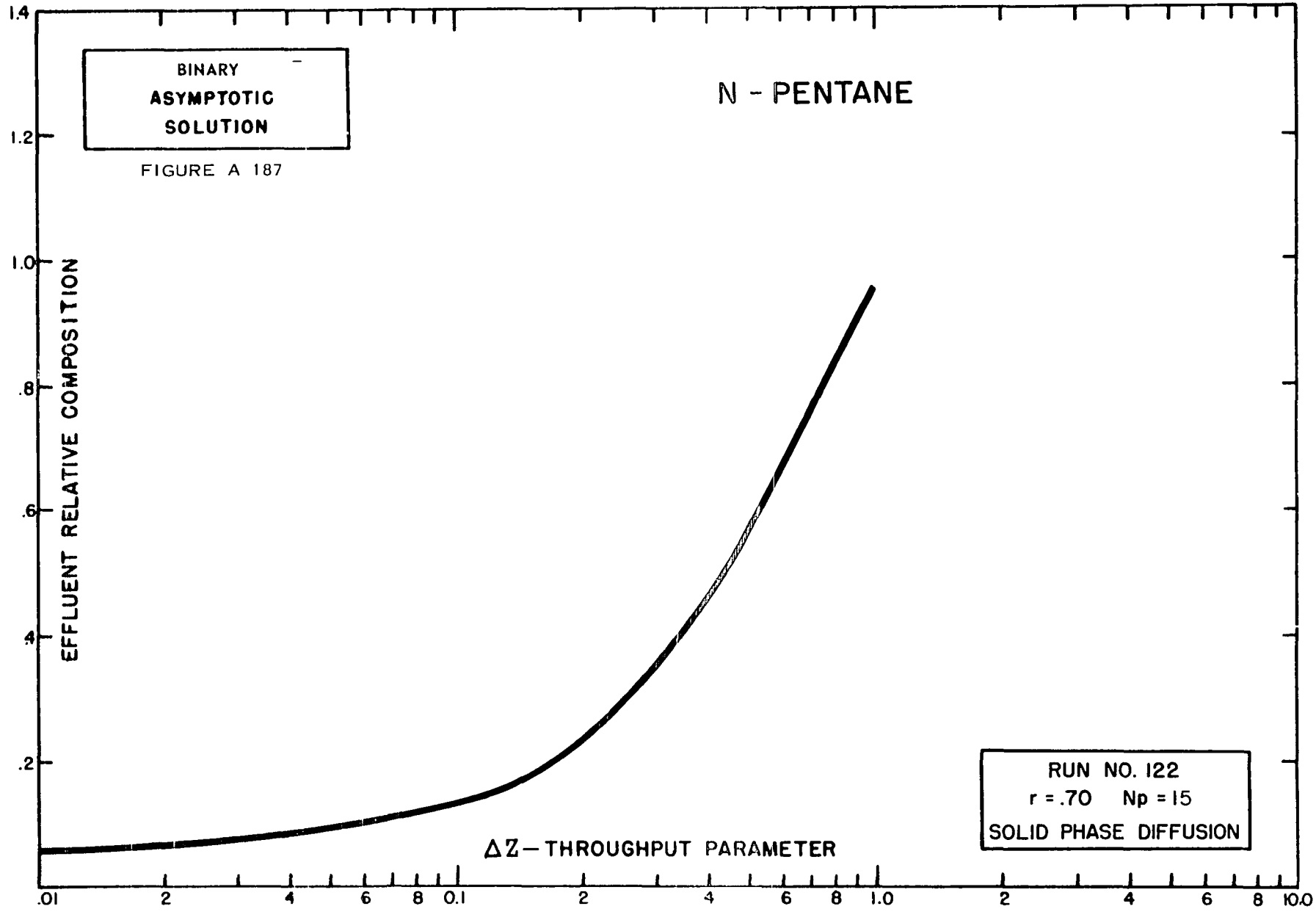
BINARY
ASYMPTOTIC
SOLUTION
N - PENTANE
EFFLUENT RELATIVE COMPOSITION
1.4
1.2
1.0
.8
.6
.4
.2
ΔZ — THROUGHPUT PARAMETER
.01
2
4
6
8
0.1
2
4
6
8
1.0
2
4
6
8
10.0
RUN NO. 122
r = .70 Np = 15
SOLID PHASE DIFFUSION

FIGURE A 187

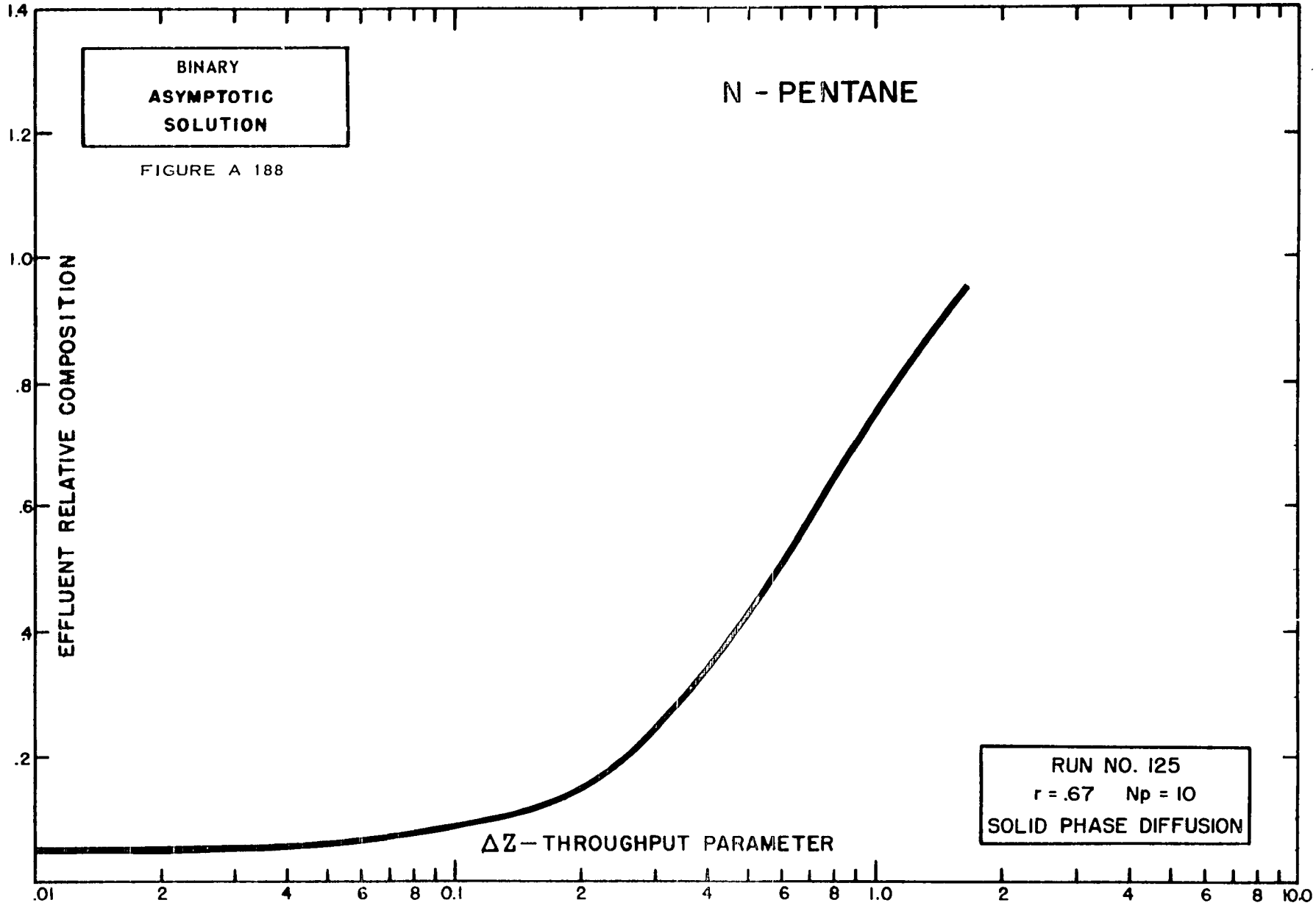
BINARY
ASYMPTOTIC
SOLUTION
N - PENTANE
EFFLUENT RELATIVE COMPOSITION
ΔZ—THROUGHPUT PARAMETER
RUN NO. 125
r = .67 Np = 10
SOLID PHASE DIFFUSION
1.4
1.2
1.0
.8
.6
.4
.2
.01
2
4
6
8
0.1
2
4
6
8
1.0
2
4
6
8
10.0

FIGURE A 188

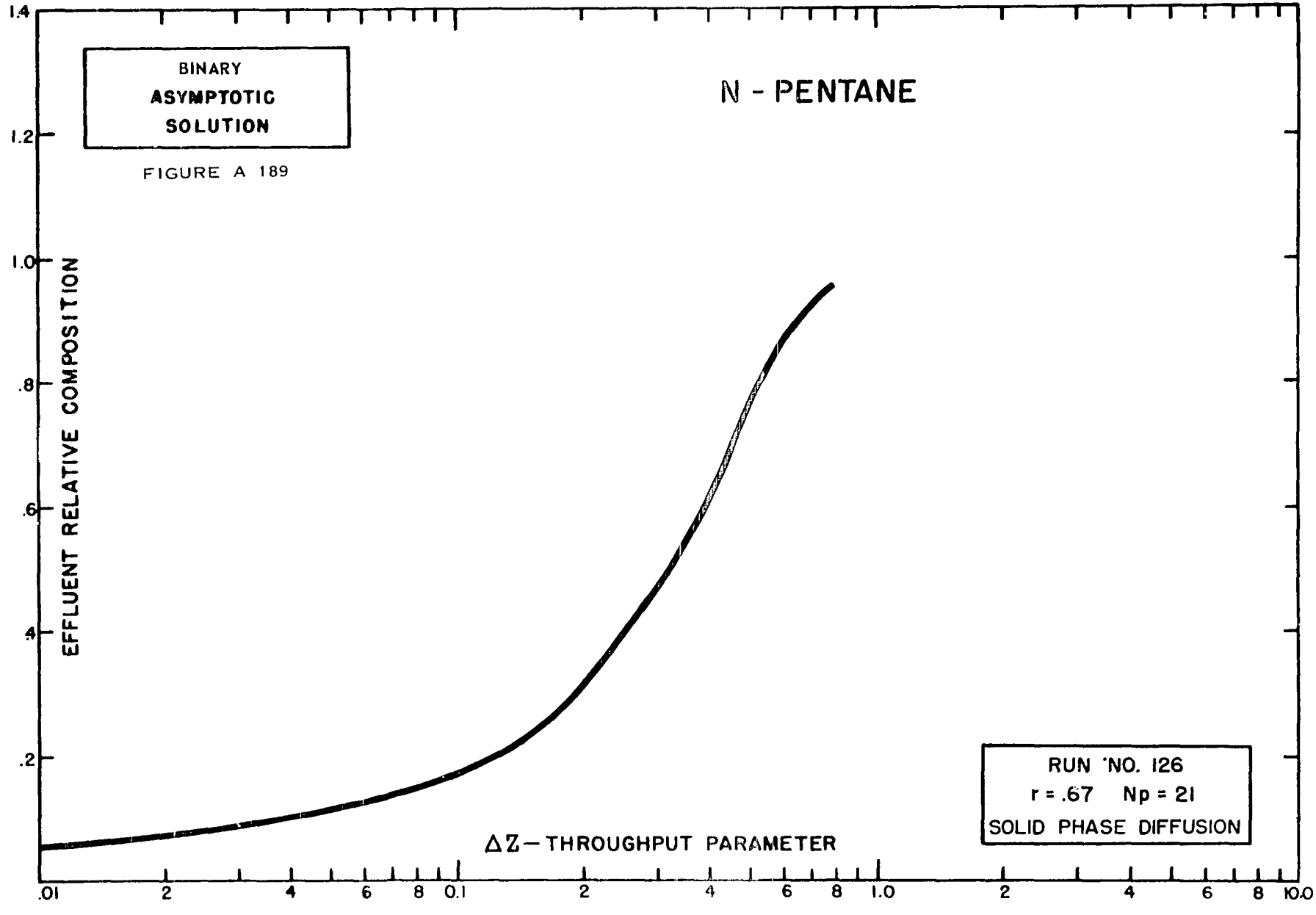
BINARY
ASYMPTOTIC
SOLUTION
N - PENTANE
EFFLUENT RELATIVE COMPOSITION
ΔZ — THROUGHPUT PARAMETER
RUN NO. 126
r = .67 Np = 21
SOLID PHASE DIFFUSION
1.4
1.2
1.0
.8
.6
.4
.2
.01
2
4
6
8
0.1
2
4
6
8
1.0
2
4
6
8
10.0

FIGURE A 189

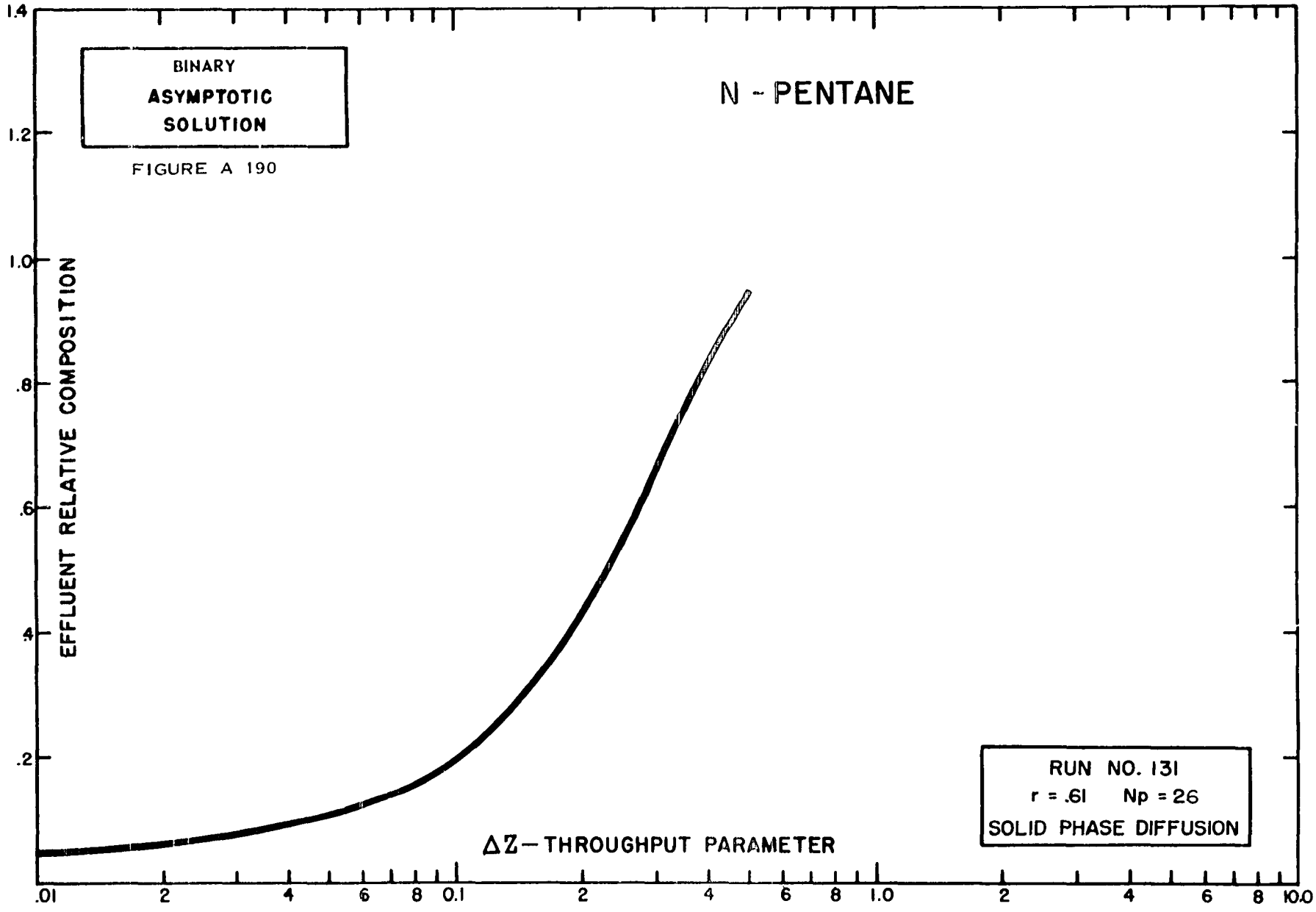
BINARY
ASYMPTOTIC
SOLUTION
N - PENTANE
EFFLUENT RELATIVE COMPOSITION
1.4
1.2
1.0
.8
.6
.4
.2
ΔZ — THROUGHPUT PARAMETER
.01
2
4
6
8
0.1
2
4
6
8
1.0
2
4
6
8
10.0
RUN NO. 131
r = .61 Np = 26
SOLID PHASE DIFFUSION

FIGURE A 190

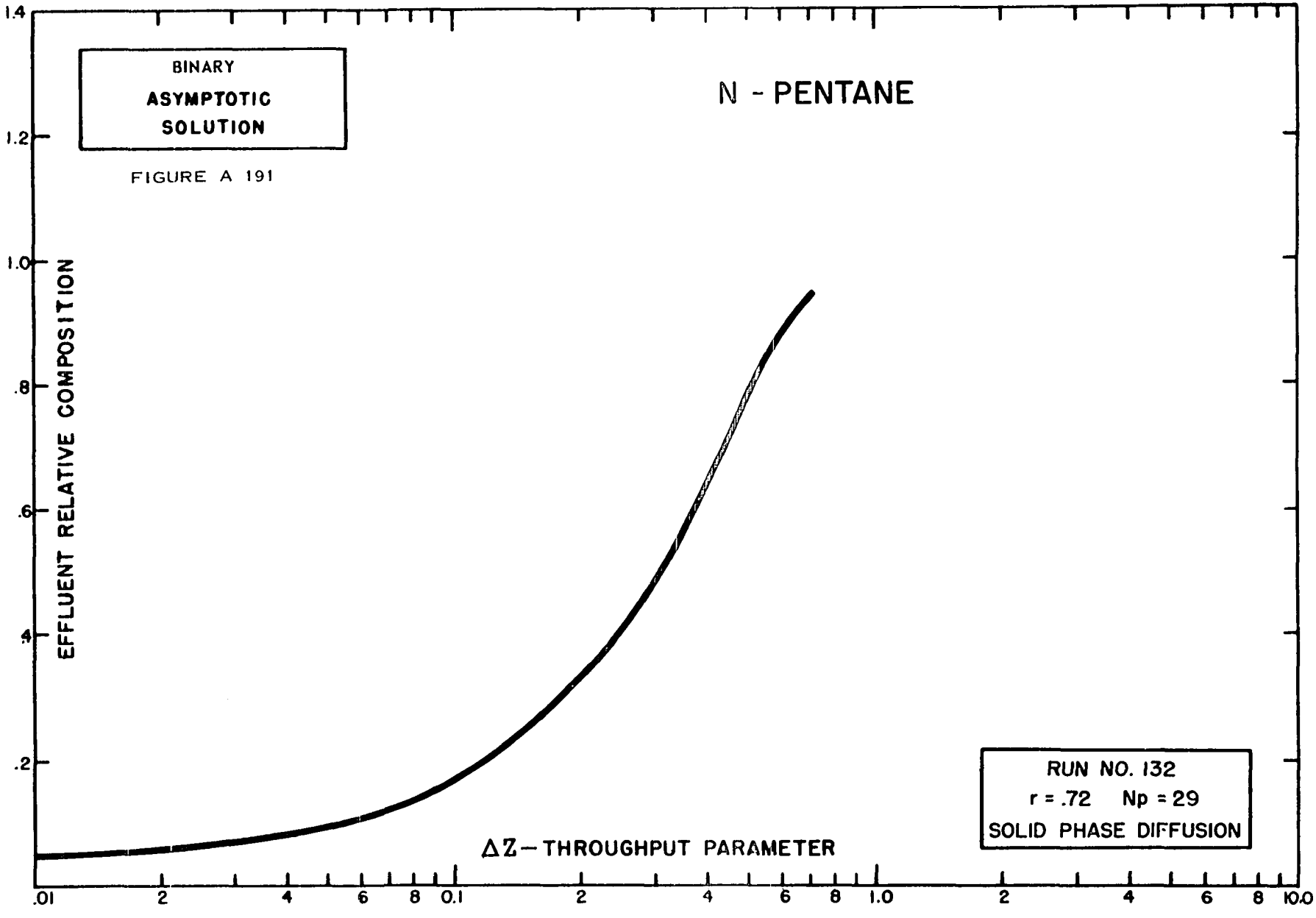
BINARY
ASYMPTOTIC
SOLUTION
N - PENTANE
EFFLUENT RELATIVE COMPOSITION
1.4
1.2
1.0
.8
.6
.4
.2
ΔZ—THROUGHPUT PARAMETER
.01
2
4
6
8
0.1
2
4
6
8
1.0
2
4
6
8
10.0
RUN NO. 132
r = .72 Np = 29
SOLID PHASE DIFFUSION

FIGURE A 191

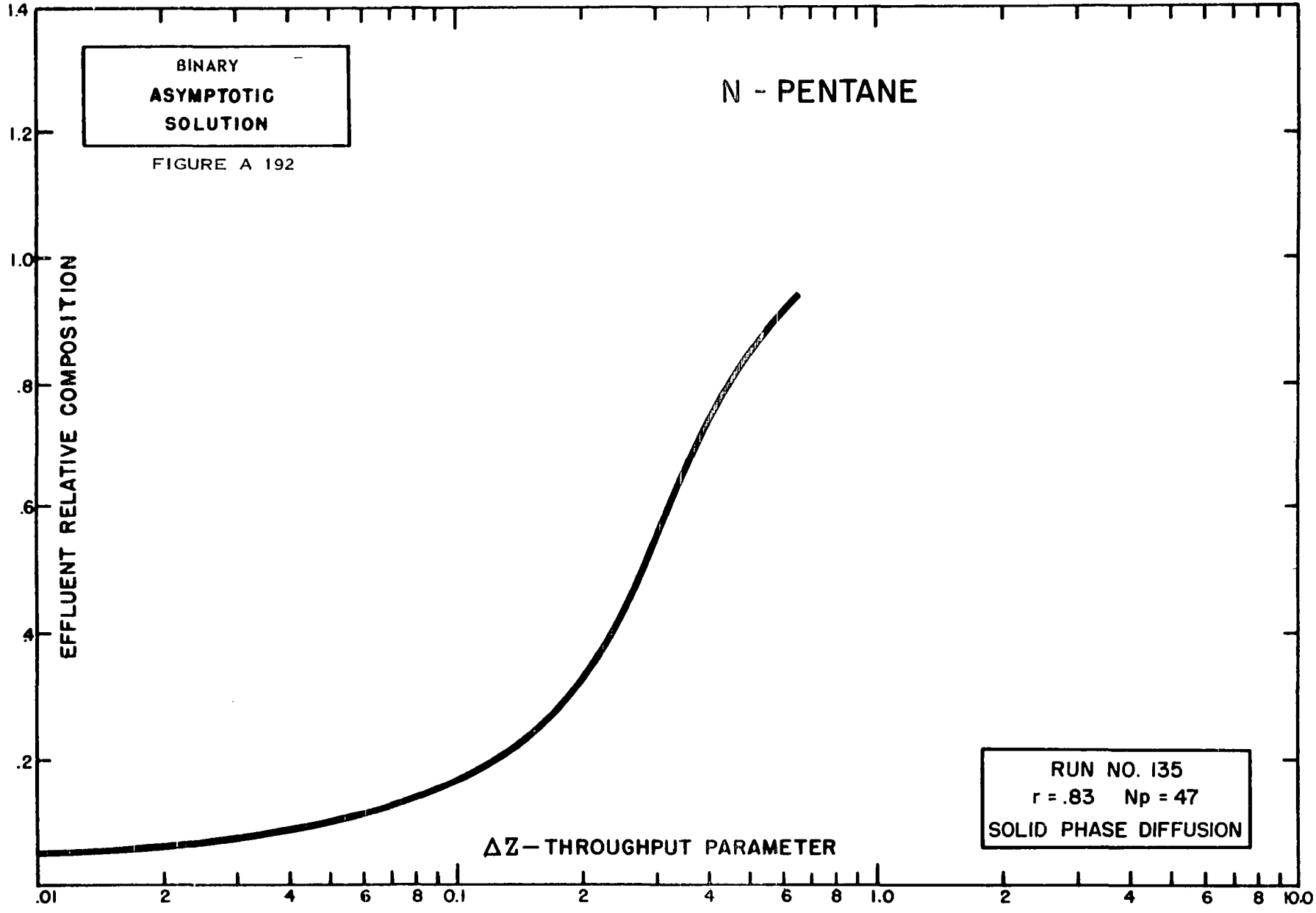
BINARY
ASYMPTOTIC
SOLUTION
N - PENTANE
EFFLUENT RELATIVE COMPOSITION
1.4
1.2
1.0
.8
.6
.4
.2
ΔZ—THROUGHPUT PARAMETER
.01
2
4
6
8
0.1
2
4
6
8
1.0
2
4
6
8
10.0
RUN NO. 135
r = .83 Np = 47
SOLID PHASE DIFFUSION

FIGURE A 192

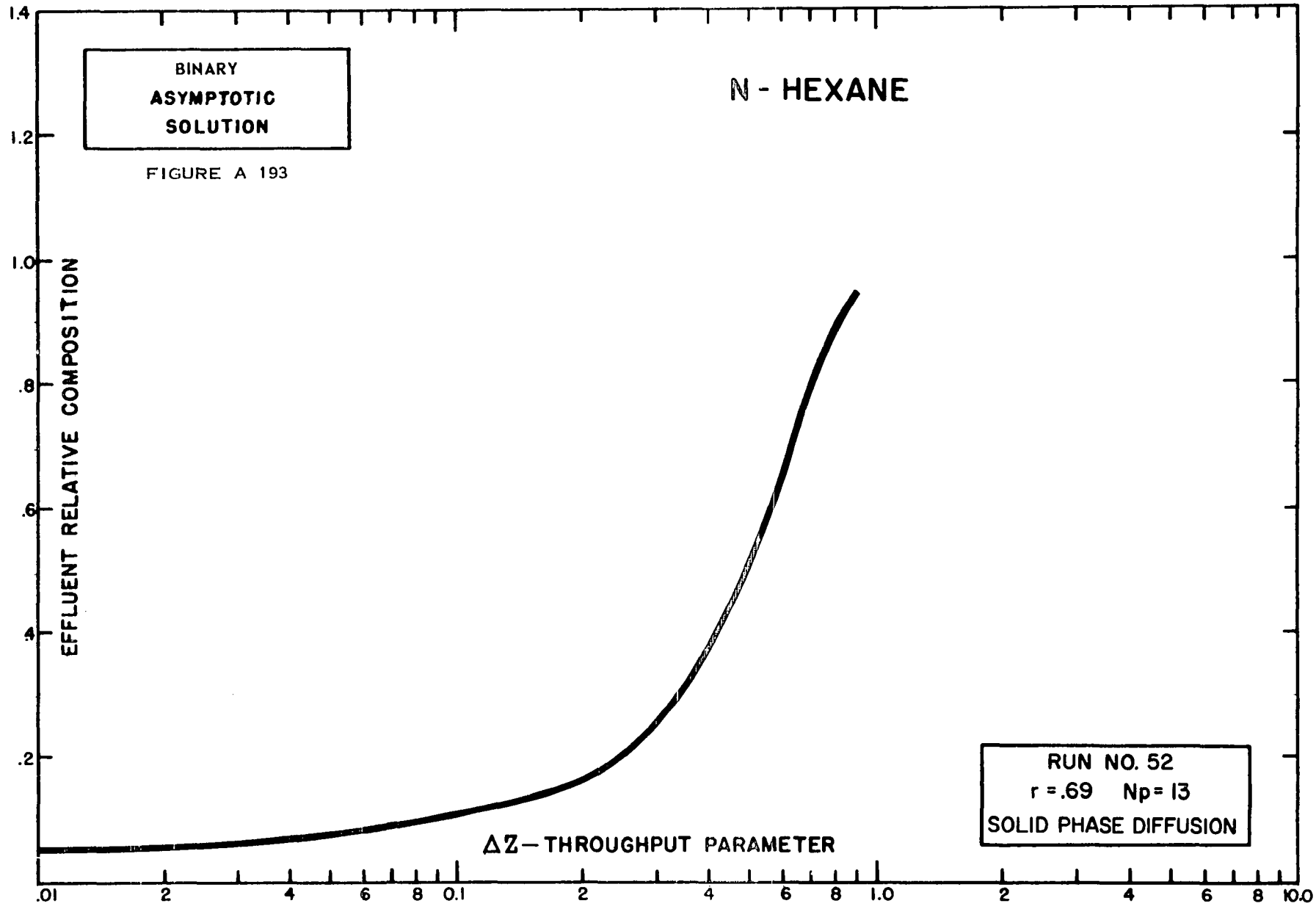
BINARY
ASYMPTOTIC
SOLUTION
N - HEXANE
EFFLUENT RELATIVE COMPOSITION
ΔZ—THROUGHPUT PARAMETER
RUN NO. 52
r = .69 Np = 13
SOLID PHASE DIFFUSION
1.4
1.2
1.0
.8
.6
.4
.2
.01
2
4
6
8
0.1
2
4
6
8
1.0
2
4
6
8
10.0

FIGURE A 193

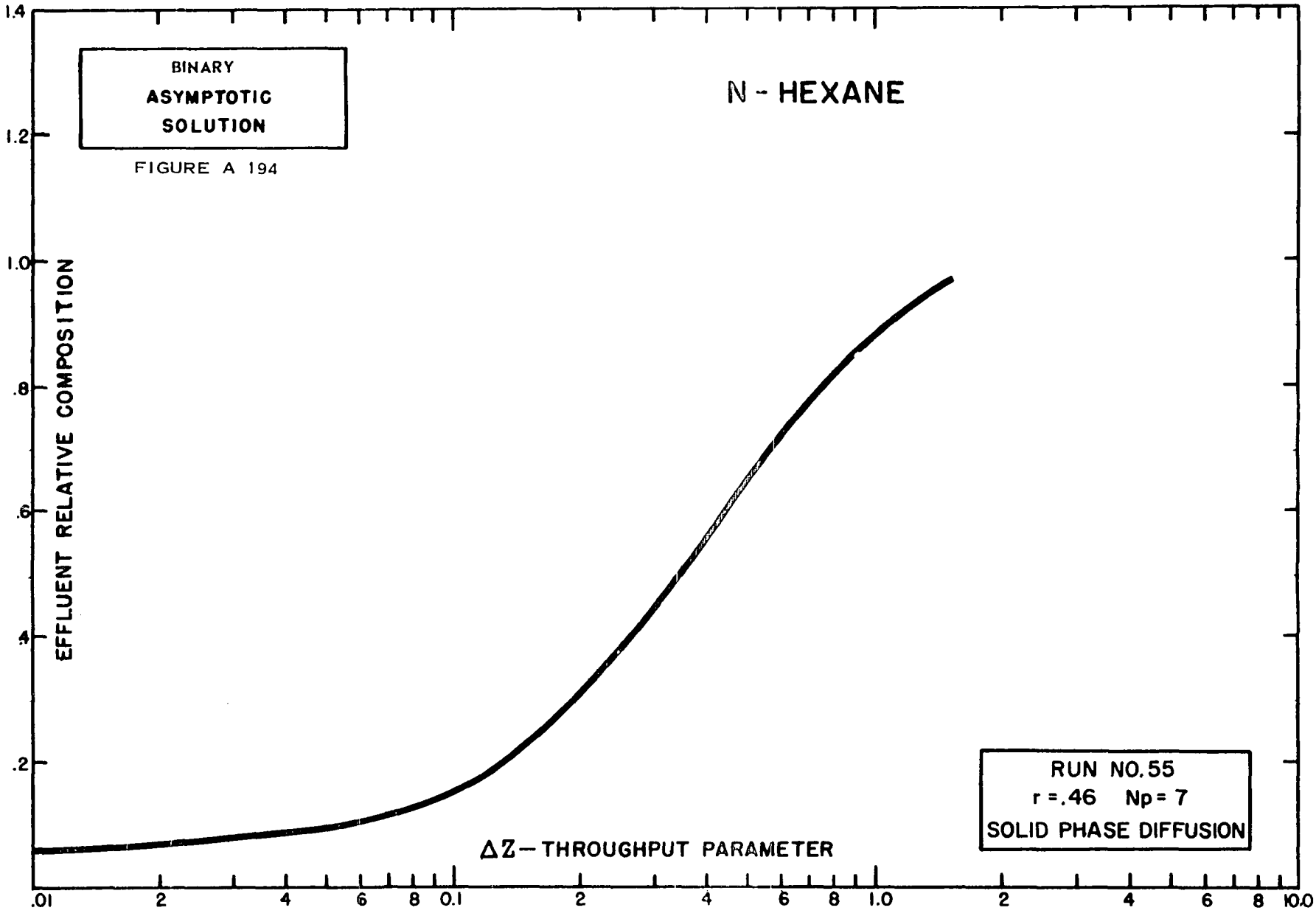
BINARY
ASYMPTOTIC
SOLUTION
N - HEXANE
EFFLUENT RELATIVE COMPOSITION
ΔZ — THROUGHPUT PARAMETER
RUN NO. 55
r = .46 Np = 7
SOLID PHASE DIFFUSION
1.4
1.2
1.0
.8
.6
.4
.2
.01
2
4
6
8
0.1
2
4
6
8
1.0
2
4
6
8
10.0

FIGURE A 194

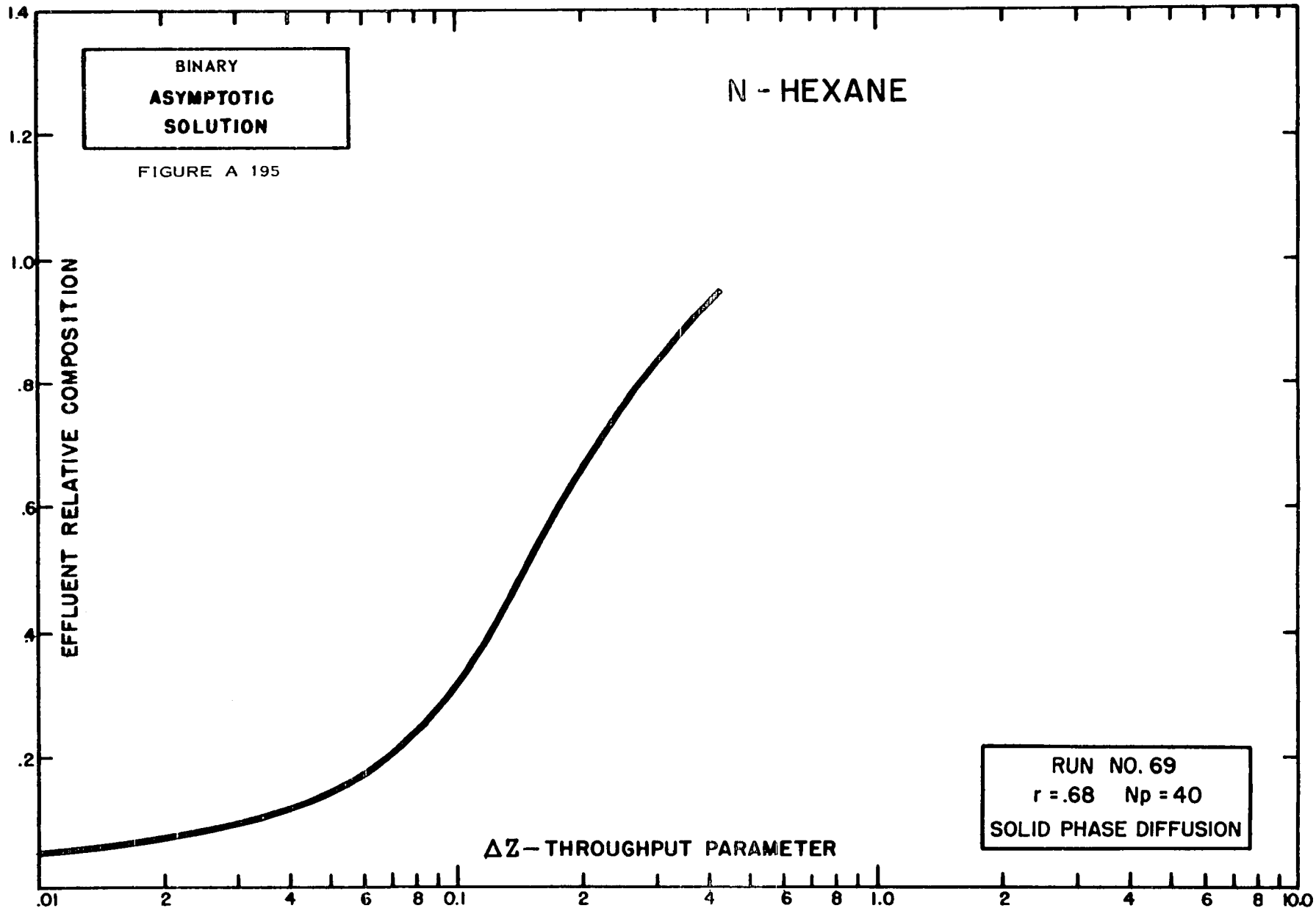
BINARY
ASYMPTOTIC
SOLUTION
N - HEXANE
EFFLUENT RELATIVE COMPOSITION
ΔZ—THROUGHPUT PARAMETER
RUN NO. 69
r = .68 Np = 40
SOLID PHASE DIFFUSION
1.4
1.2
1.0
.8
.6
.4
.2
.01
2
4
6
8
0.1
2
4
6
8
1.0
2
4
6
8
10.0

FIGURE A 195

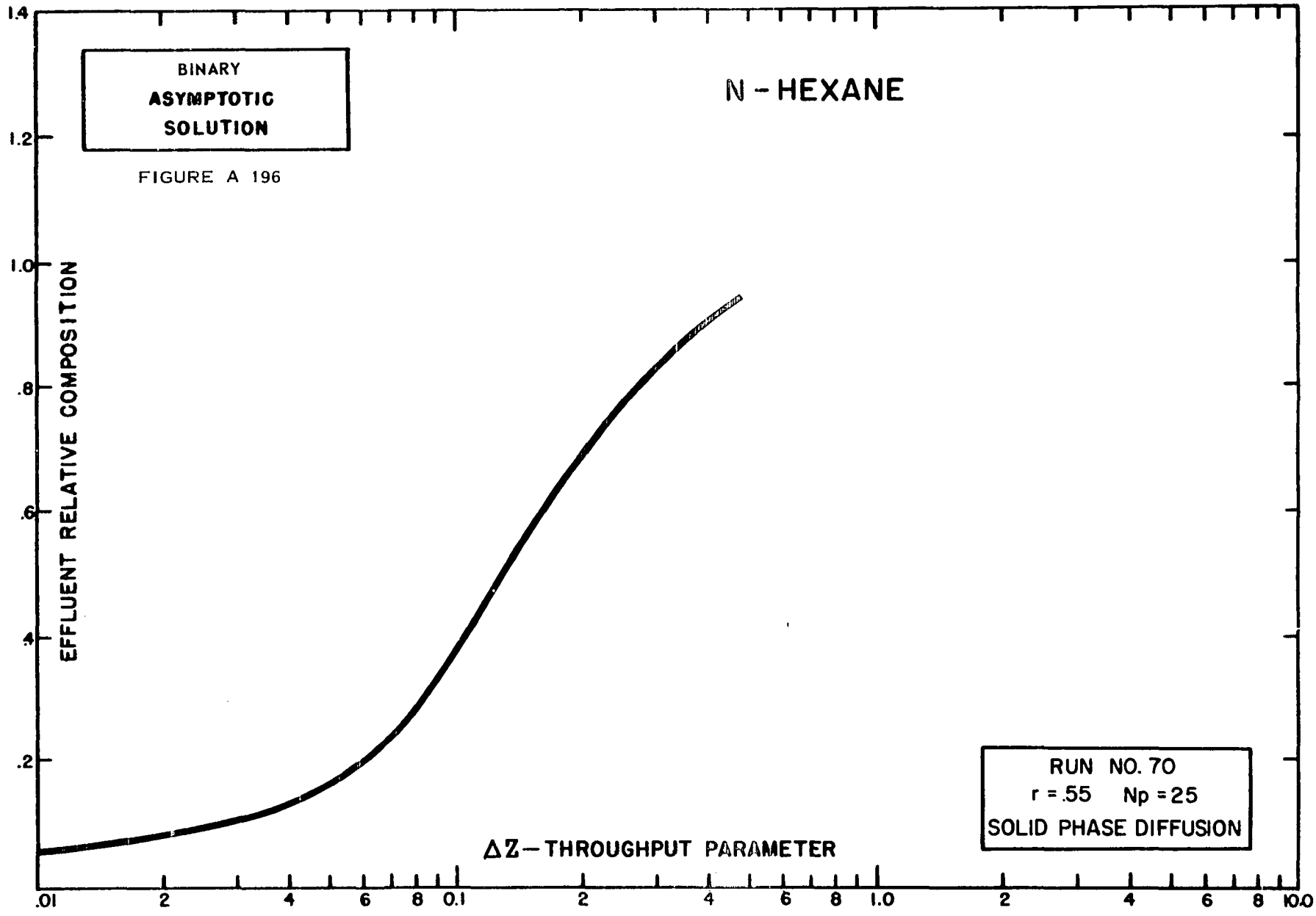
BINARY
ASYMPTOTIC
SOLUTION
N - HEXANE
EFFLUENT RELATIVE COMPOSITION
1.4
1.2
1.0
.8
.6
.4
.2
ΔZ—THROUGHPUT PARAMETER
.01
2
4
6
8
0.1
2
4
6
8
1.0
2
4
6
8
10.0
RUN NO. 70
r = .55 Np = 25
SOLID PHASE DIFFUSION

FIGURE A 196

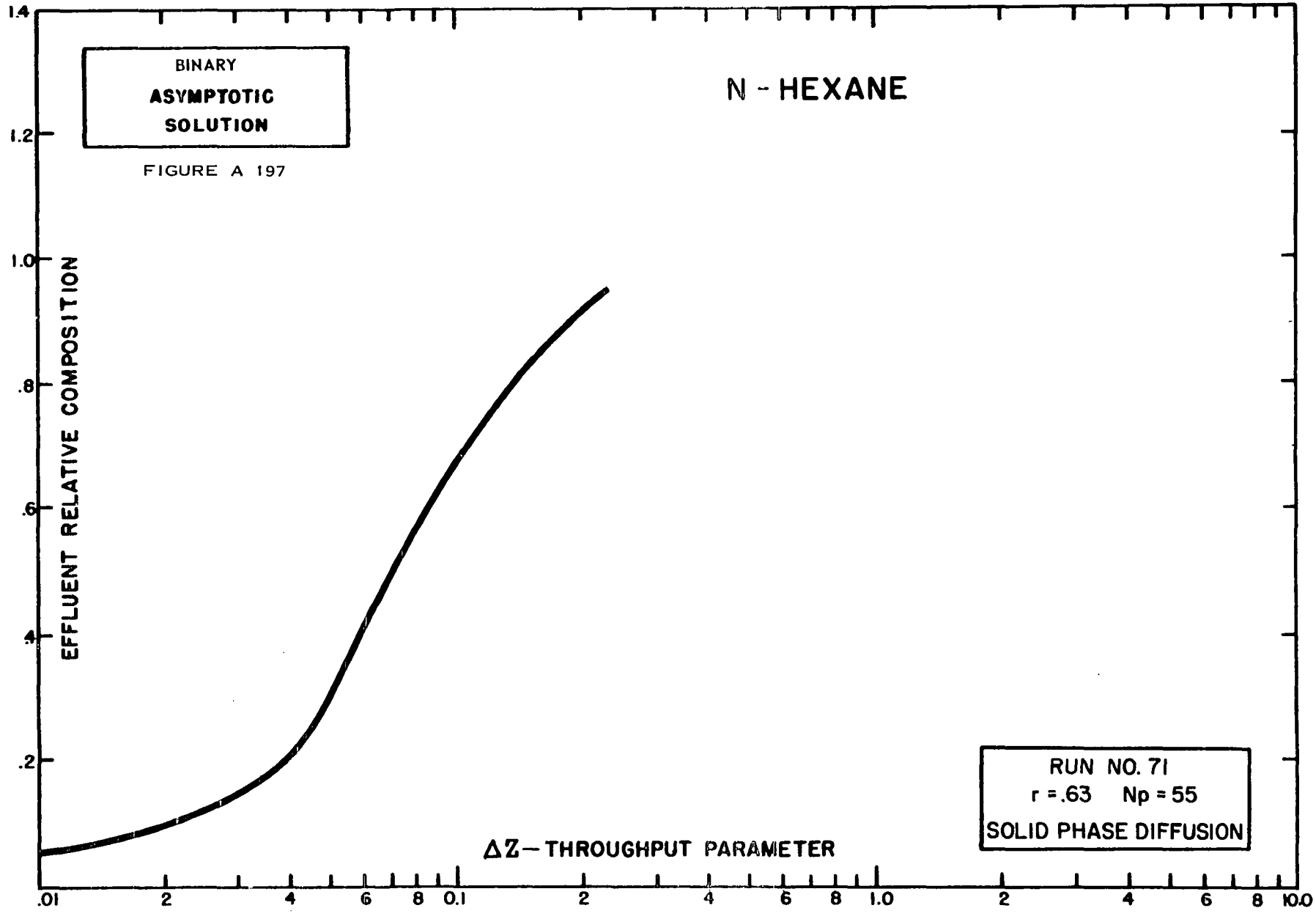
BINARY
ASYMPTOTIC
SOLUTION
N - HEXANE
EFFLUENT RELATIVE COMPOSITION
ΔZ—THROUGHPUT PARAMETER
RUN NO. 71
r = .63 Np = 55
SOLID PHASE DIFFUSION
1.4
1.2
1.0
.8
.6
.4
.2
.01
2
4
6
8
0.1
2
4
6
8
1.0
2
4
6
8
10.0

FIGURE A 197

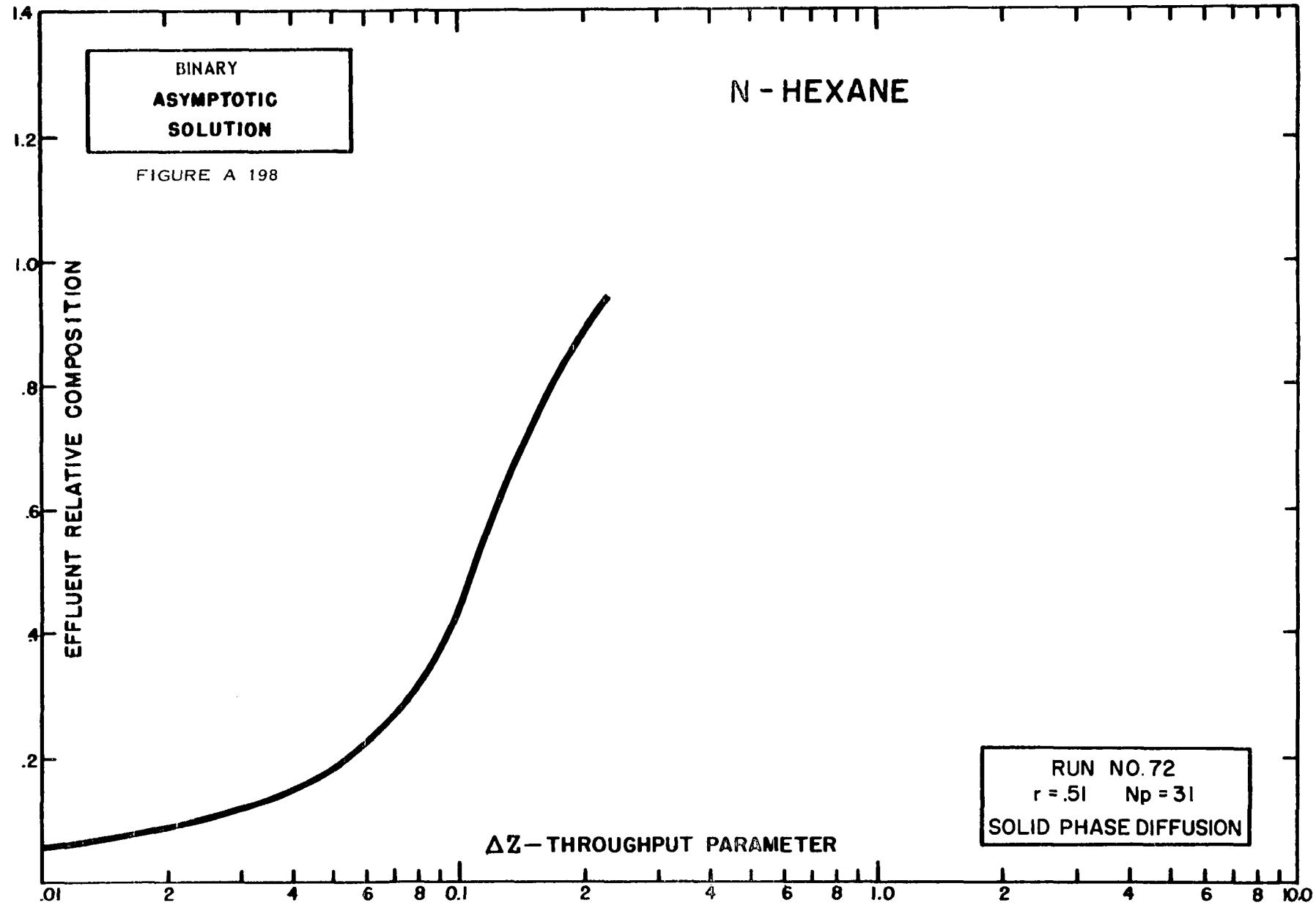
BINARY
ASYMPTOTIC
SOLUTION
N - HEXANE
EFFLUENT RELATIVE COMPOSITION
1.4
1.2
1.0
.8
.6
.4
.2
ΔZ—THROUGHPUT PARAMETER
.01
2
4
6
8
0.1
2
4
6
8
1.0
2
4
6
8
10.0
RUN NO. 72
r = .51 Np = 31
SOLID PHASE DIFFUSION

FIGURE A 198

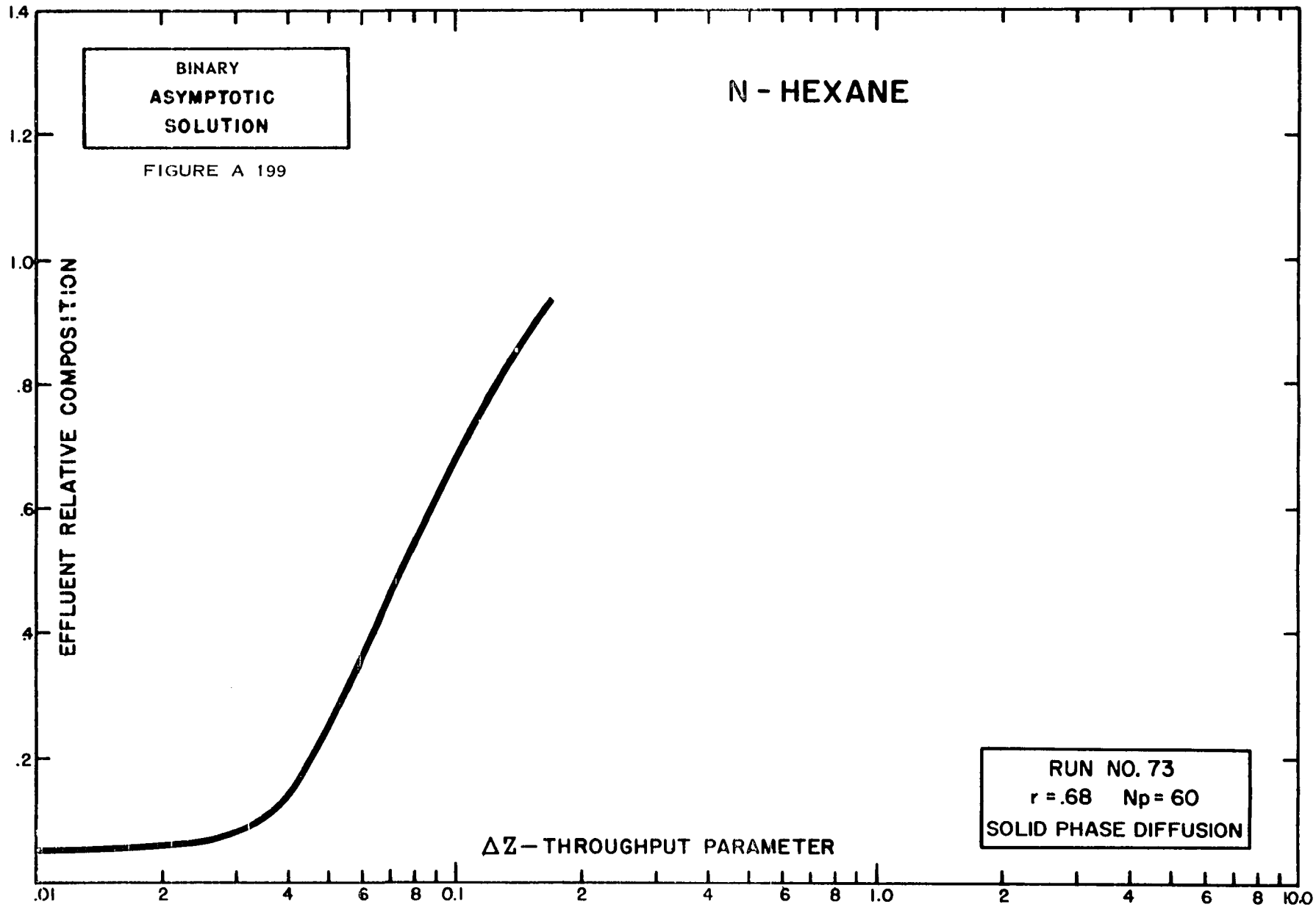
BINARY
ASYMPTOTIC
SOLUTION
N - HEXANE
EFFLUENT RELATIVE COMPOSITION
1.4
1.2
1.0
.8
.6
.4
.2
ΔZ — THROUGHPUT PARAMETER
.01
2
4
6
8
0.1
2
4
6
8
1.0
2
4
6
8
10.0
RUN NO. 73
r = .68 Np = 60
SOLID PHASE DIFFUSION

FIGURE A 199

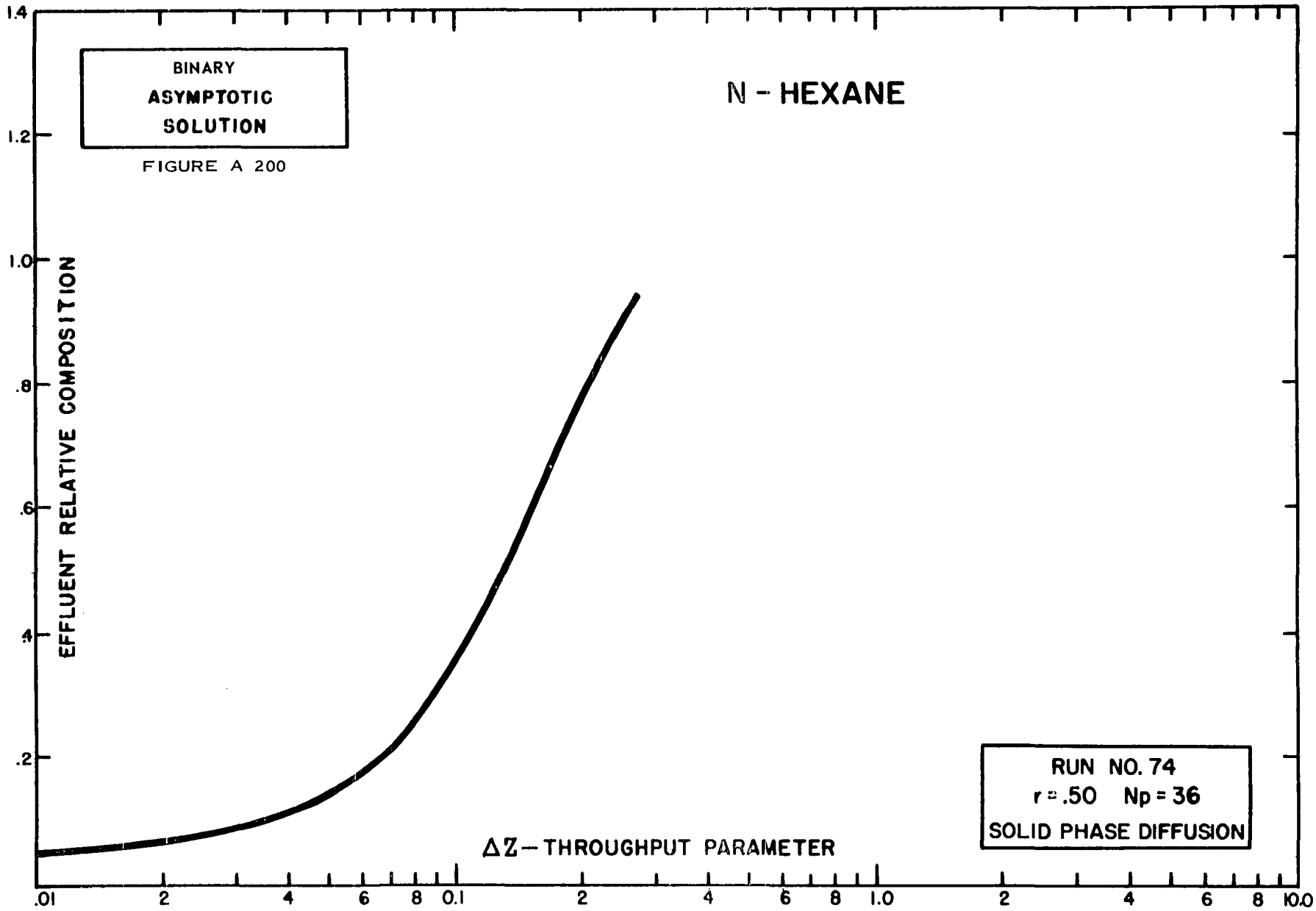
BINARY
ASYMPTOTIC
SOLUTION
N - HEXANE
EFFLUENT RELATIVE COMPOSITION
ΔZ—THROUGHPUT PARAMETER
RUN NO. 74
r = .50 Np = 36
SOLID PHASE DIFFUSION
1.4
1.2
1.0
.8
.6
.4
.2
.01
2
4
6
8
0.1
2
4
6
8
1.0
2
4
6
8
10.0

FIGURE A 200

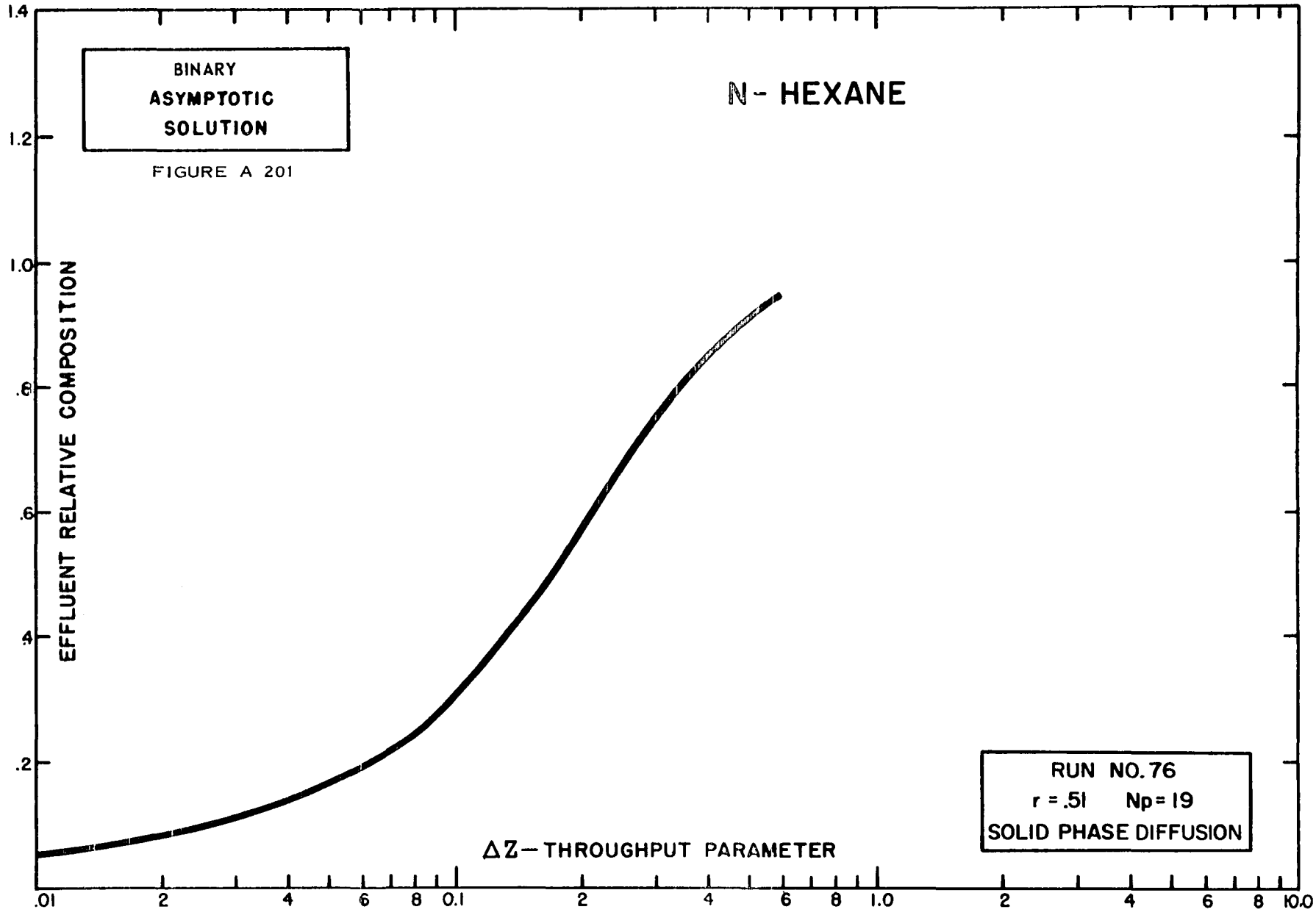
BINARY
ASYMPTOTIC
SOLUTION
N- HEXANE
EFFLUENT RELATIVE COMPOSITION
1.4
1.2
1.0
.8
.6
.4
.2
ΔZ—THROUGHPUT PARAMETER
.01
2
4
6
8
0.1
2
4
6
8
1.0
2
4
6
8
10.0
RUN NO. 76
r = .51 Np = 19
SOLID PHASE DIFFUSION

FIGURE A 201

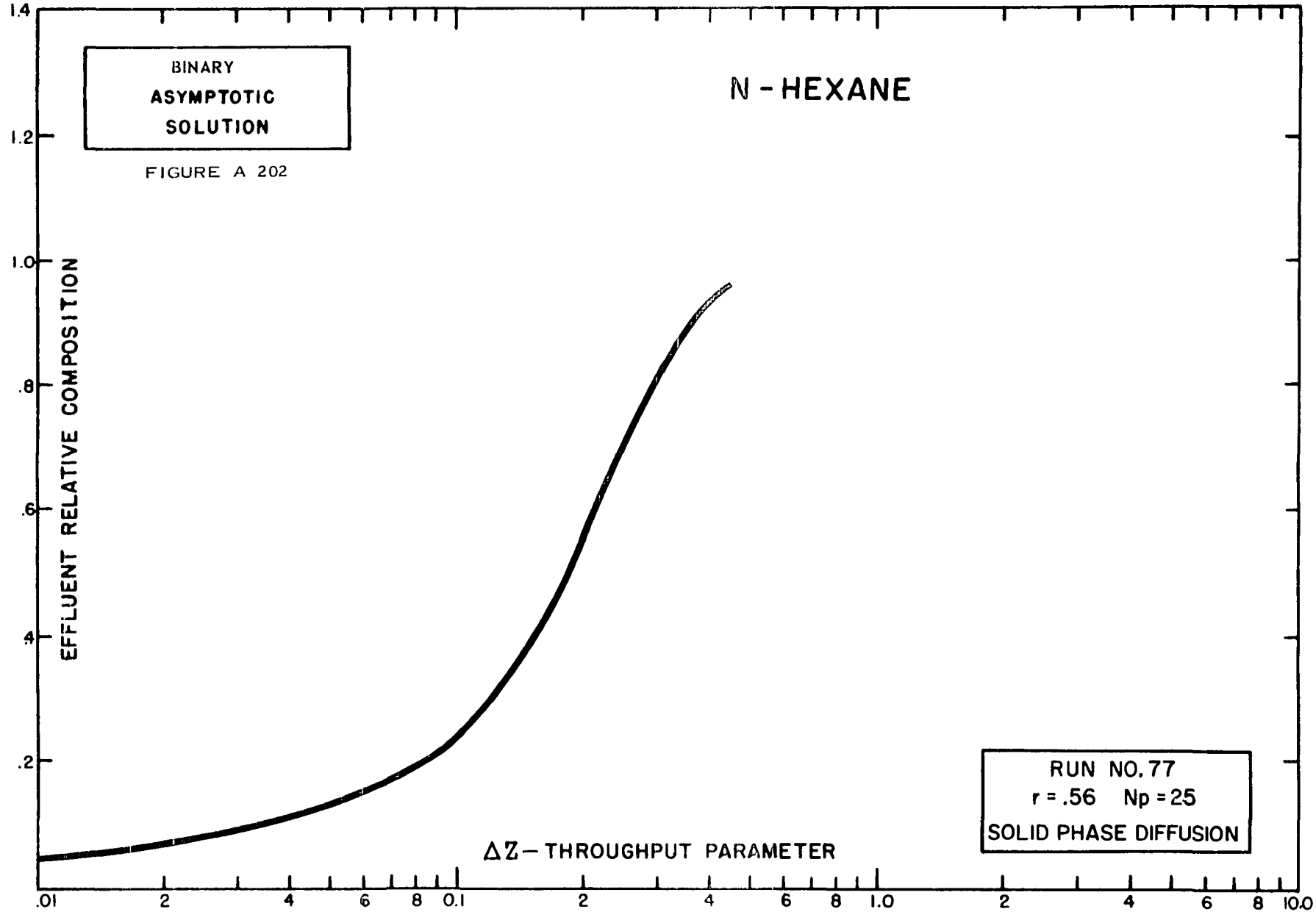
BINARY
ASYMPTOTIC
SOLUTION
N - HEXANE
EFFLUENT RELATIVE COMPOSITION
ΔZ – THROUGHPUT PARAMETER
RUN NO. 77
r = .56 Np = 25
SOLID PHASE DIFFUSION
1.4
1.2
1.0
.8
.6
.4
.2
.01
2
4
6
8
0.1
2
4
6
8
1.0
2
4
6
8
10.0

FIGURE A 202

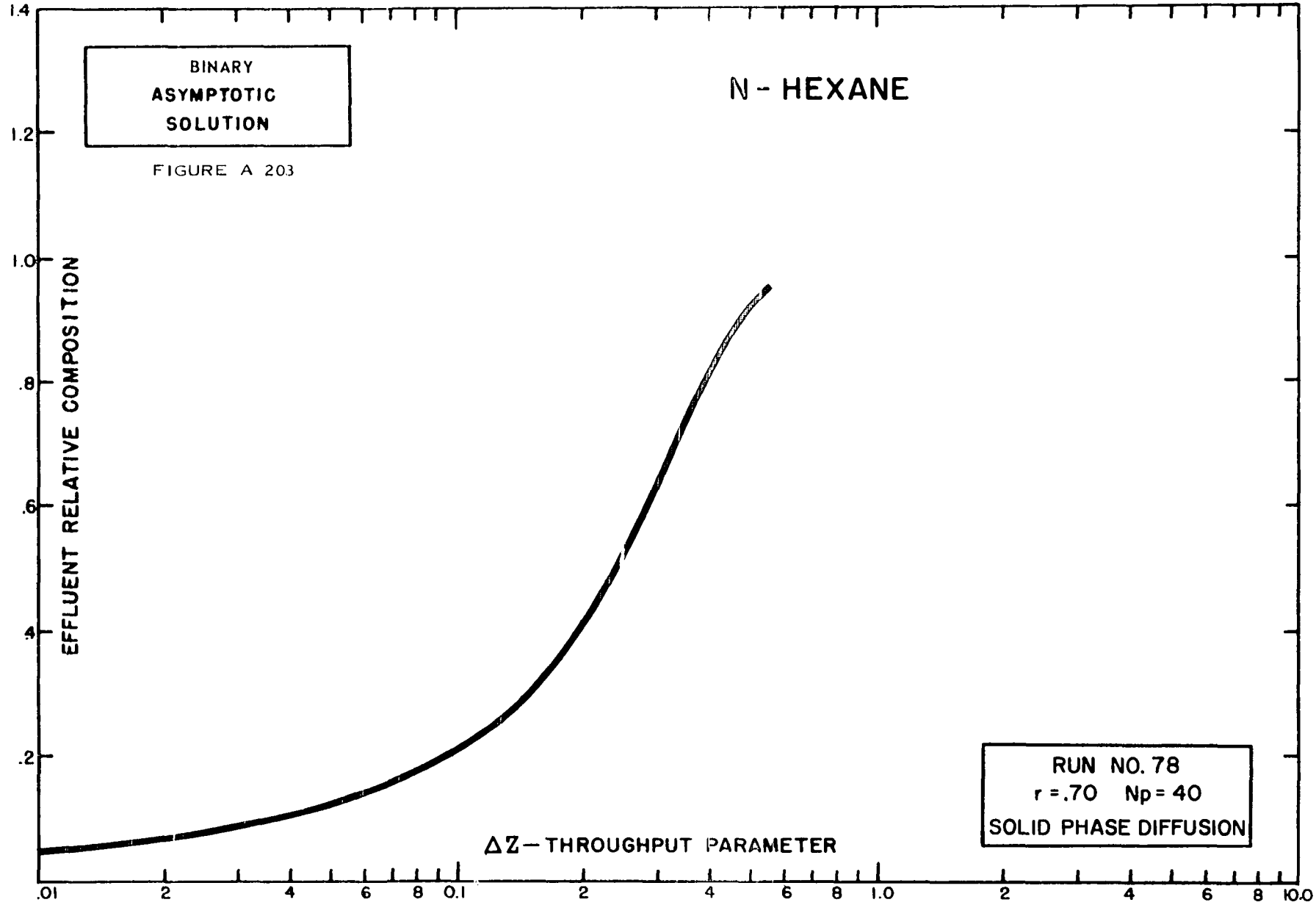
BINARY
ASYMPTOTIC
SOLUTION
N - HEXANE
EFFLUENT RELATIVE COMPOSITION
ΔZ — THROUGHPUT PARAMETER
RUN NO. 78
r = .70 Np = 40
SOLID PHASE DIFFUSION
1.4
1.2
1.0
.8
.6
.4
.2
.01
2
4
6
8
0.1
2
4
6
8
1.0
2
4
6
8
10.0

FIGURE A 203

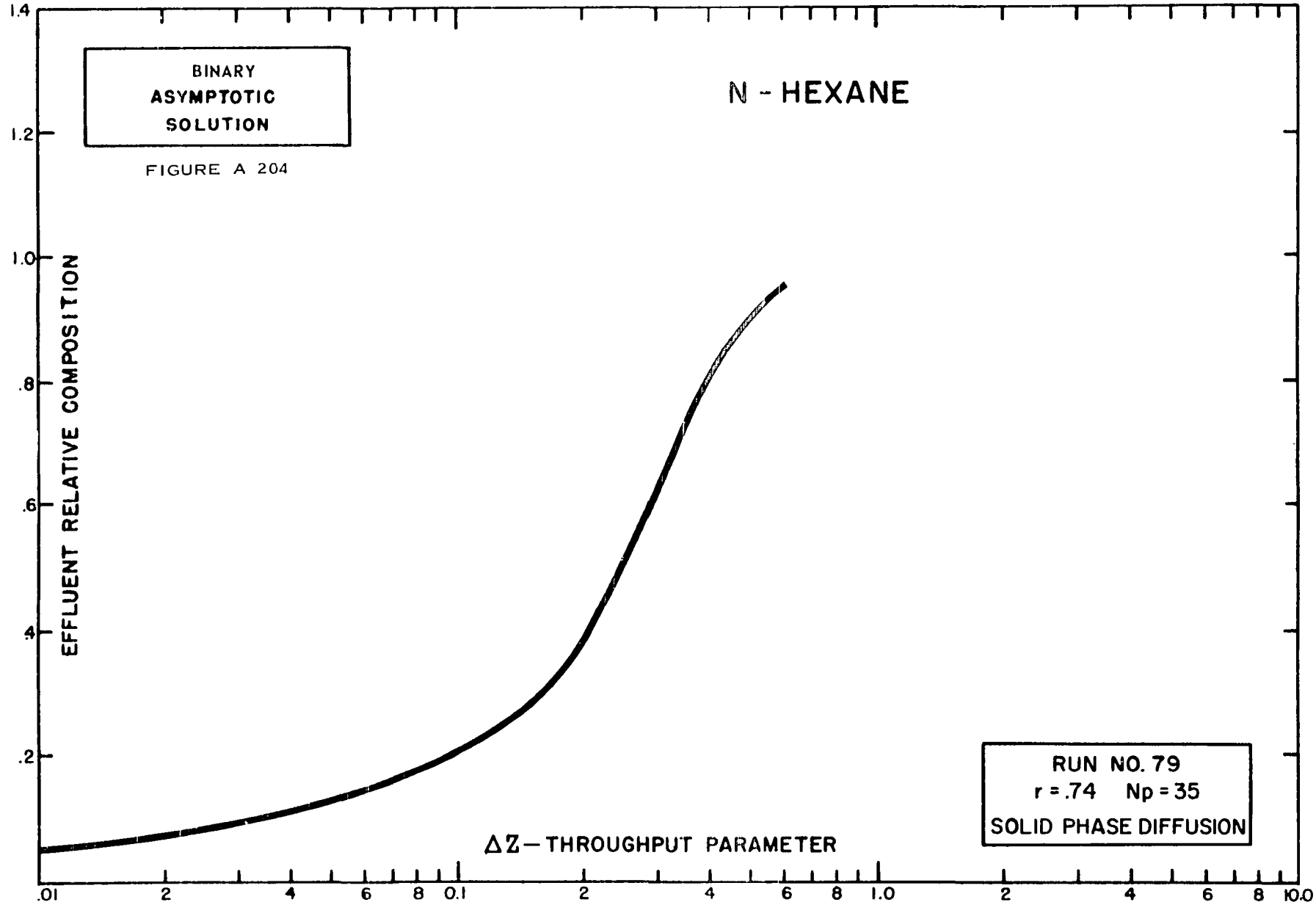
BINARY
ASYMPTOTIC
SOLUTION
N - HEXANE
EFFLUENT RELATIVE COMPOSITION
1.4
1.2
1.0
.8
.6
.4
.2
ΔZ — THROUGHPUT PARAMETER
.01
2
4
6
8
0.1
2
4
6
8
1.0
2
4
6
8
10.0
RUN NO. 79
r = .74 Np = 35
SOLID PHASE DIFFUSION

FIGURE A 204

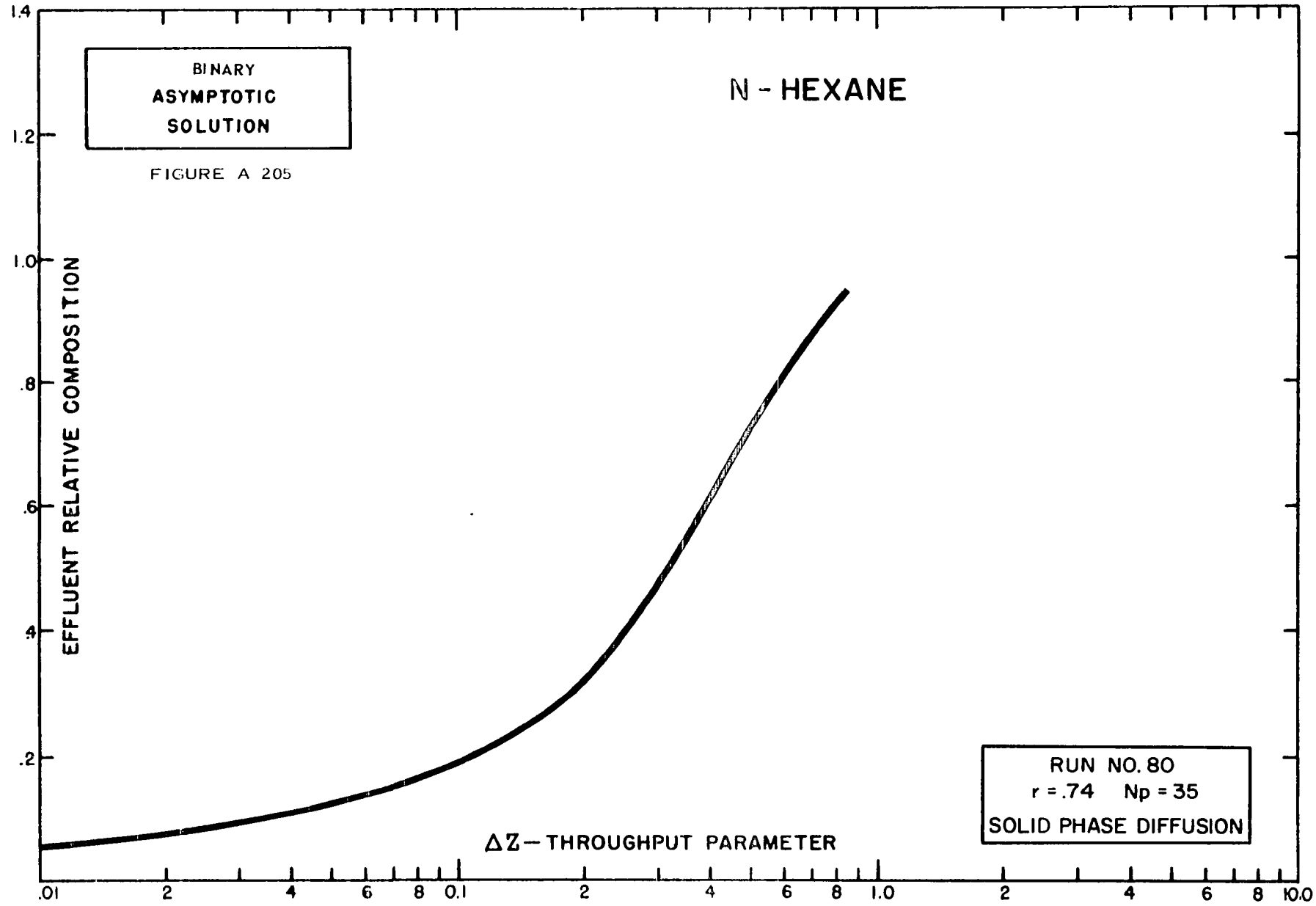
BINARY
ASYMPTOTIC
SOLUTION
N - HEXANE
EFFLUENT RELATIVE COMPOSITION
ΔZ — THROUGHPUT PARAMETER
RUN NO. 80
r = .74 Np = 35
SOLID PHASE DIFFUSION
1.4
1.2
1.0
.8
.6
.4
.2
.01
2
4
6
8
0.1
2
4
6
8
1.0
2
4
6
8
10.0

FIGURE A 205

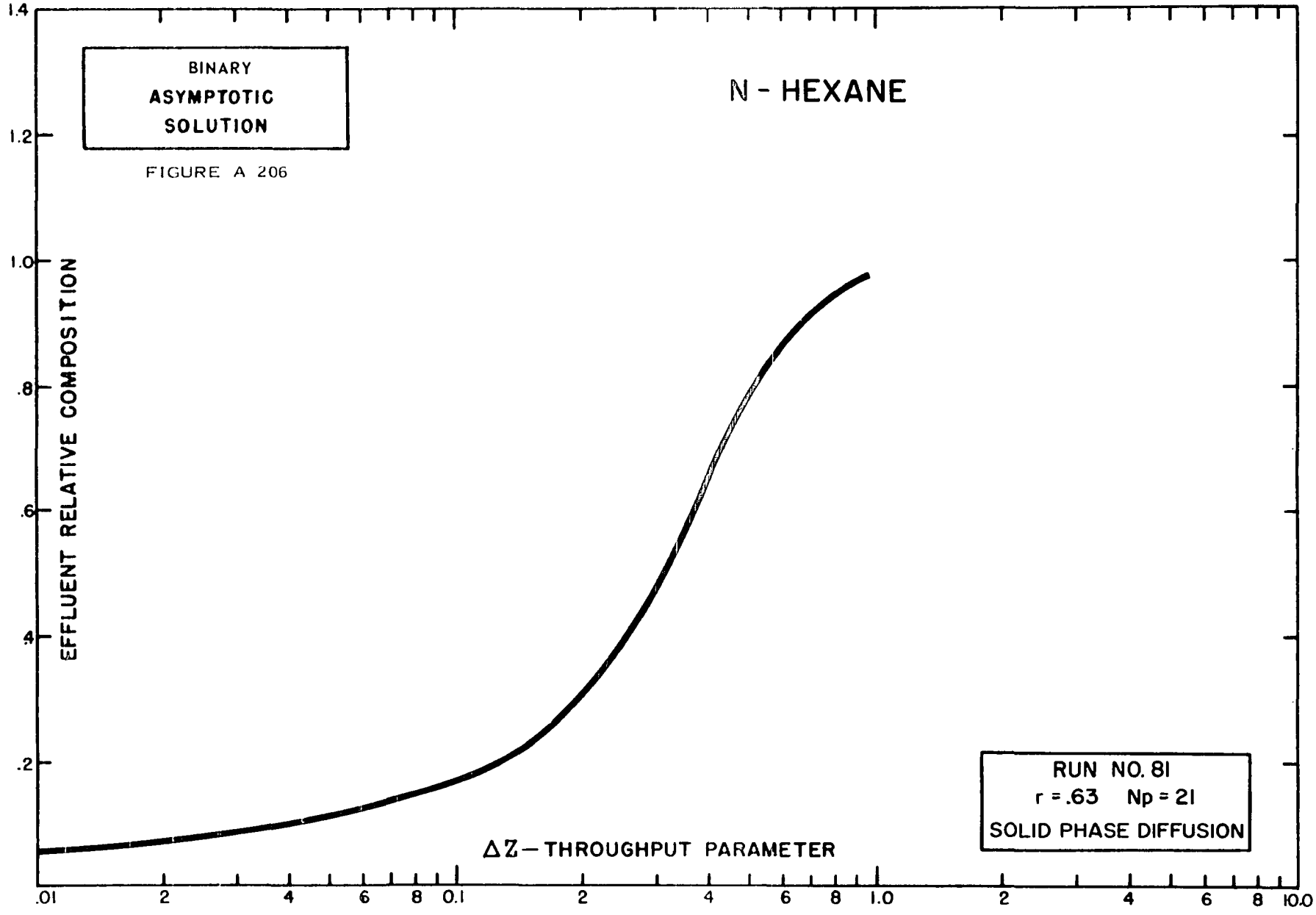
BINARY
ASYMPTOTIC
SOLUTION
N - HEXANE
EFFLUENT RELATIVE COMPOSITION
1.4
1.2
1.0
.8
.6
.4
.2
ΔZ — THROUGHPUT PARAMETER
.01
2
4
6
8
0.1
2
4
6
8
1.0
2
4
6
8
10.0
RUN NO. 81
r = .63 Np = 21
SOLID PHASE DIFFUSION

FIGURE A 206

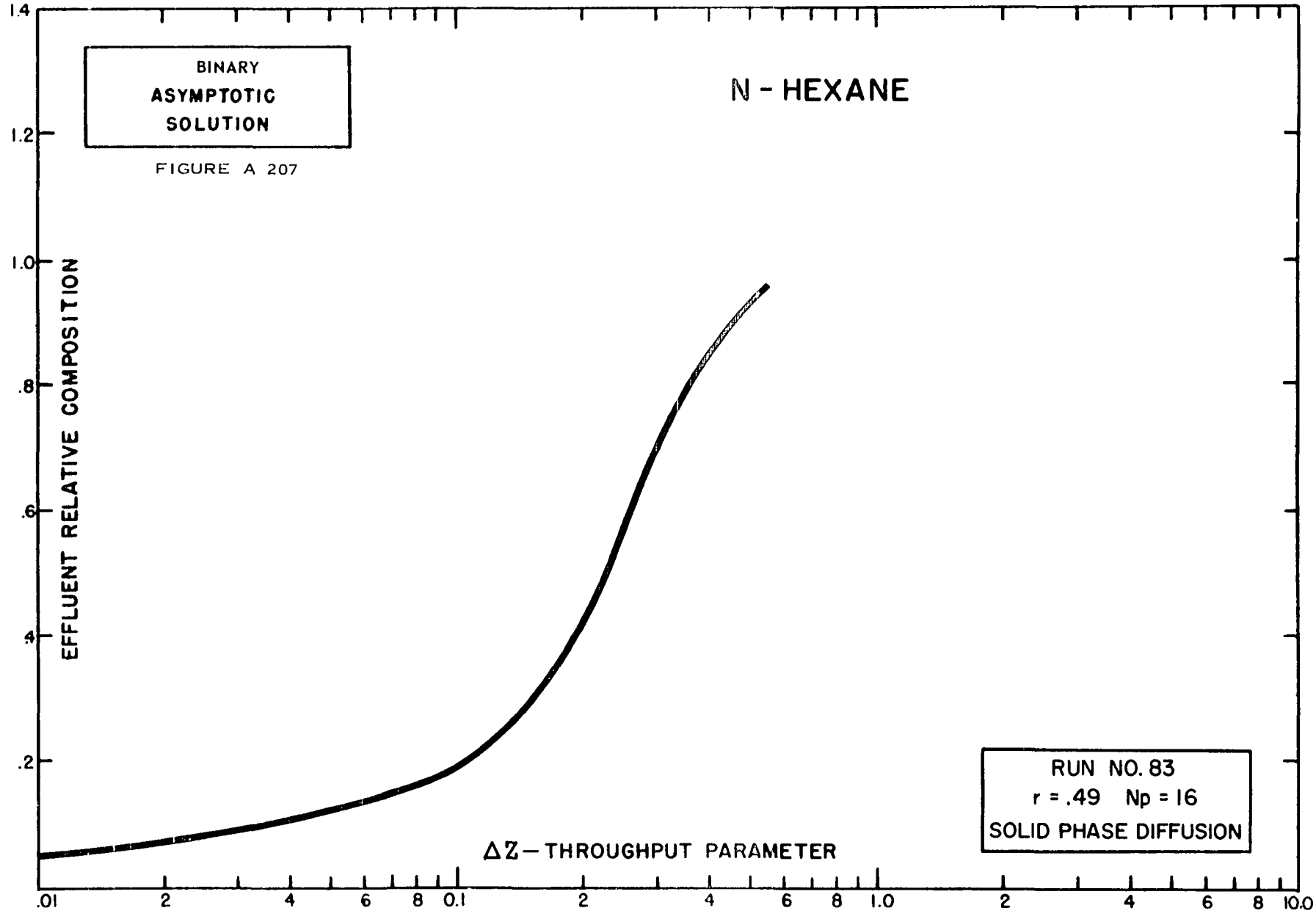
BINARY
ASYMPTOTIC
SOLUTION
N - HEXANE
EFFLUENT RELATIVE COMPOSITION
1.4
1.2
1.0
.8
.6
.4
.2
ΔZ — THROUGHPUT PARAMETER
.01
2
4
6
8
0.1
2
4
6
8
1.0
2
4
6
8
10.0
RUN NO. 83
r = .49 Np = 16
SOLID PHASE DIFFUSION

FIGURE A 207

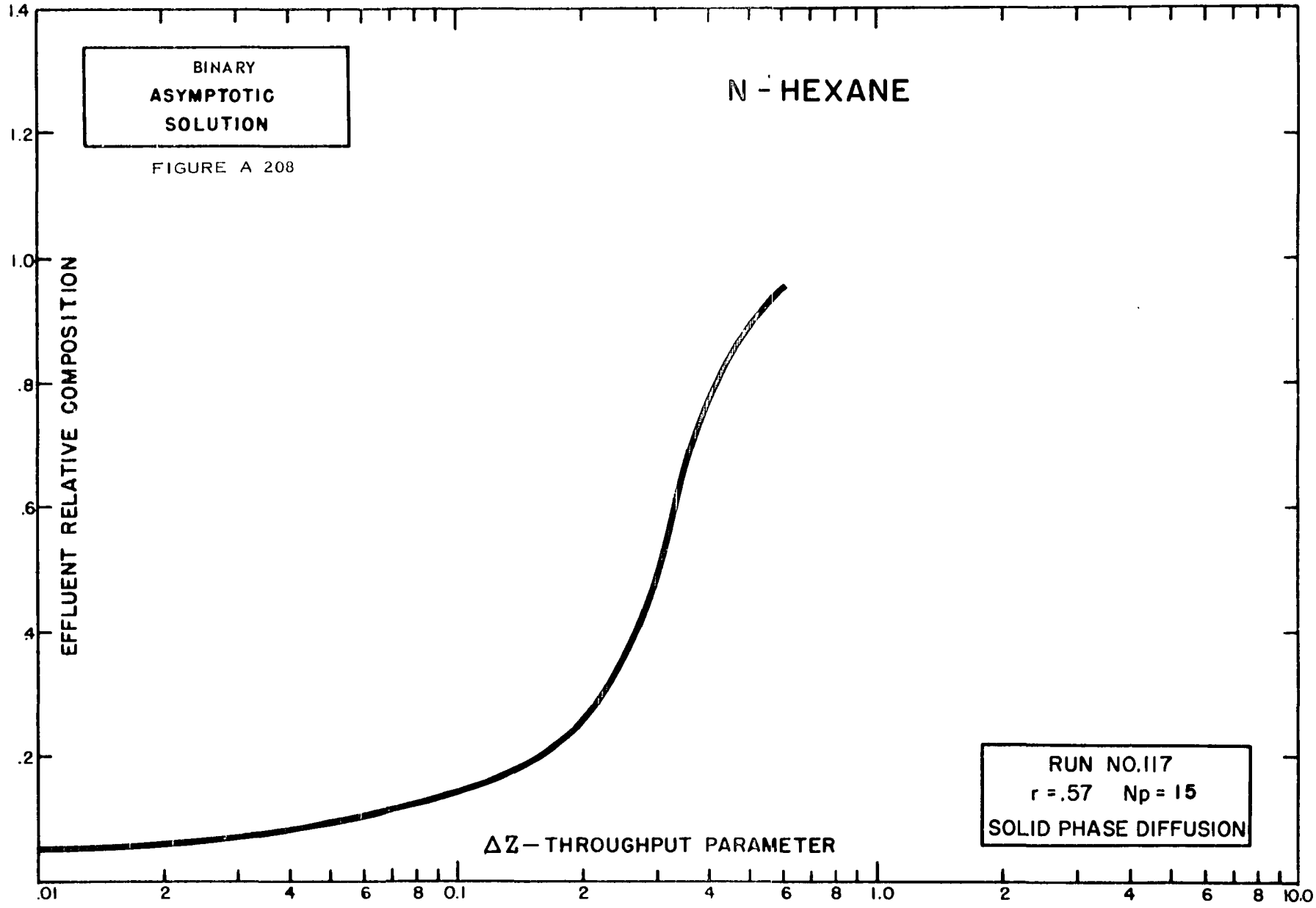
BINARY
ASYMPTOTIC
SOLUTION
N - HEXANE
EFFLUENT RELATIVE COMPOSITION
1.4
1.2
1.0
.8
.6
.4
.2
ΔZ — THROUGHPUT PARAMETER
.01
2
4
6
8
0.1
2
4
6
8
1.0
2
4
6
8
10.0
RUN NO.117
r = .57 Np = 15
SOLID PHASE DIFFUSION

FIGURE A 208

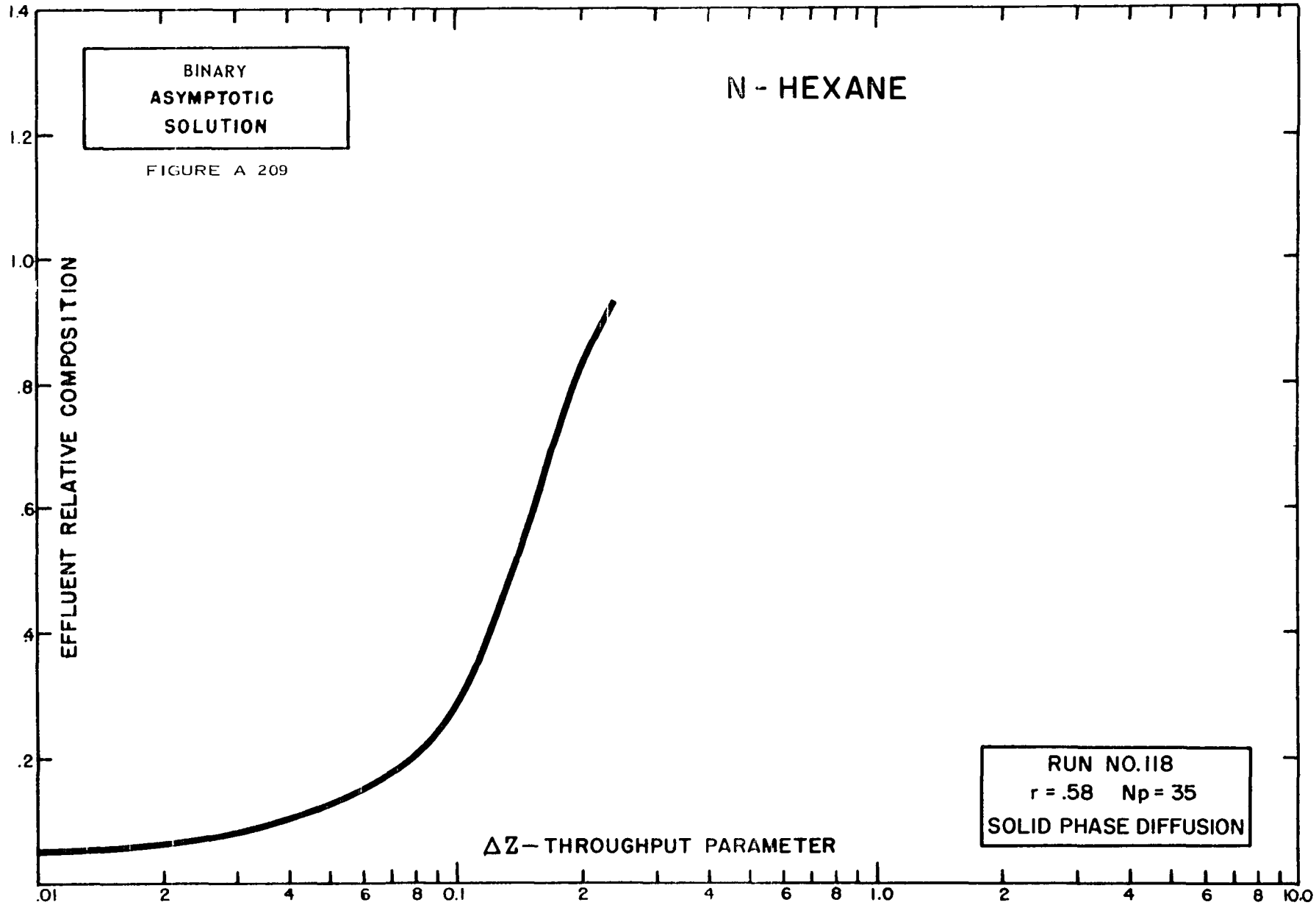
BINARY
ASYMPTOTIC
SOLUTION
N - HEXANE
EFFLUENT RELATIVE COMPOSITION
1.4
1.2
1.0
.8
.6
.4
.2
ΔZ — THROUGHPUT PARAMETER
.01
2
4
6
8
0.1
2
4
6
8
1.0
2
4
6
8
10.0
RUN NO. 118
r = .58 Np = 35
SOLID PHASE DIFFUSION

FIGURE A 209

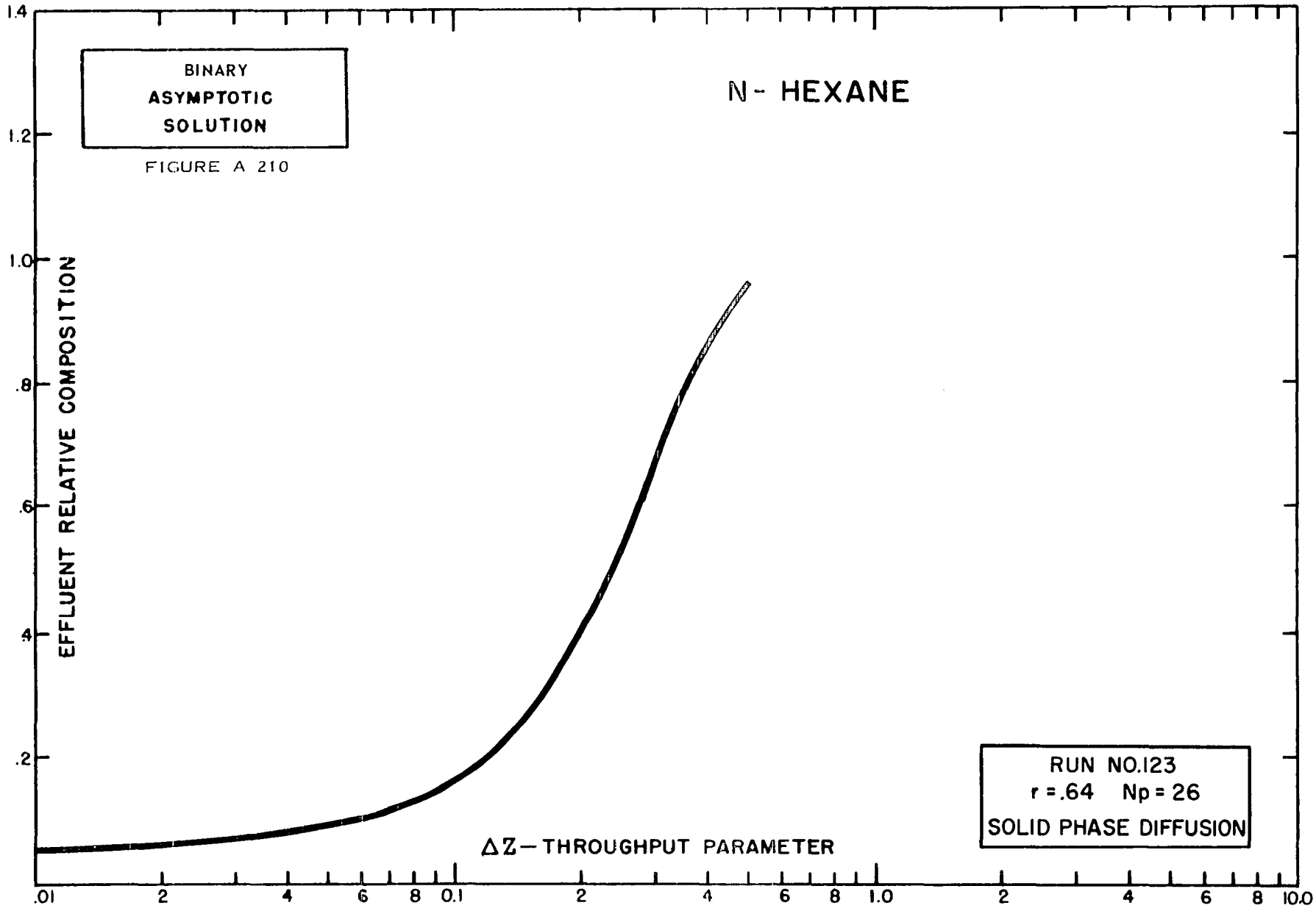
BINARY
ASYMPTOTIC
SOLUTION
N- HEXANE
EFFLUENT RELATIVE COMPOSITION
1.4
1.2
1.0
.8
.6
.4
.2
ΔZ—THROUGHPUT PARAMETER
.01
2
4
6
8
0.1
2
4
6
8
1.0
2
4
6
8
10.0
RUN NO.123
r = .64 Np = 26
SOLID PHASE DIFFUSION

FIGURE A 210

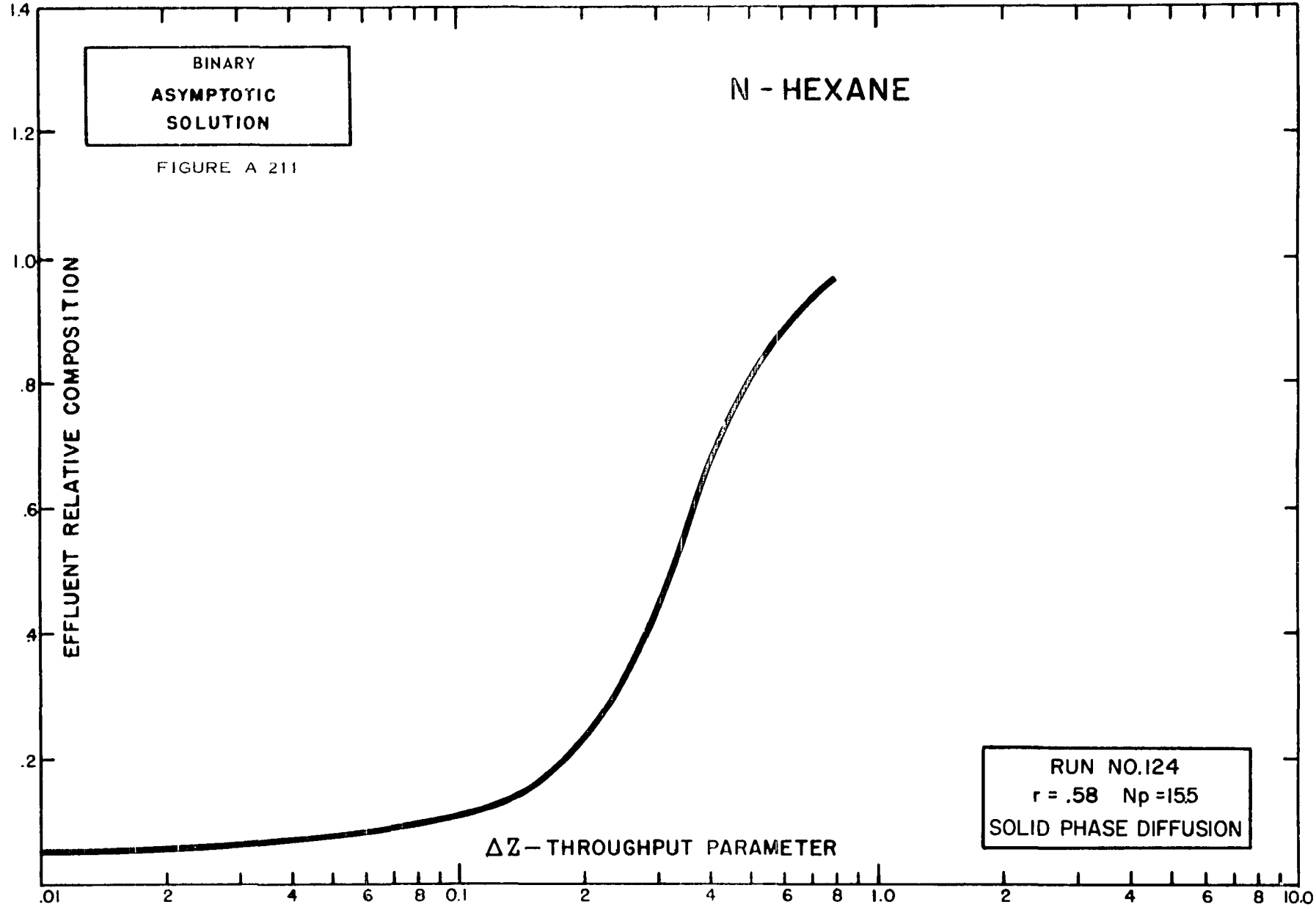
BINARY
ASYMPTOTIC
SOLUTION
N - HEXANE
EFFLUENT RELATIVE COMPOSITION
1.4
1.2
1.0
.8
.6
.4
.2
ΔZ — THROUGHPUT PARAMETER
.01
2
4
6
8
0.1
2
4
6
8
1.0
2
4
6
8
10.0
RUN NO.124
r = .58 Np =15.5
SOLID PHASE DIFFUSION

FIGURE A 211

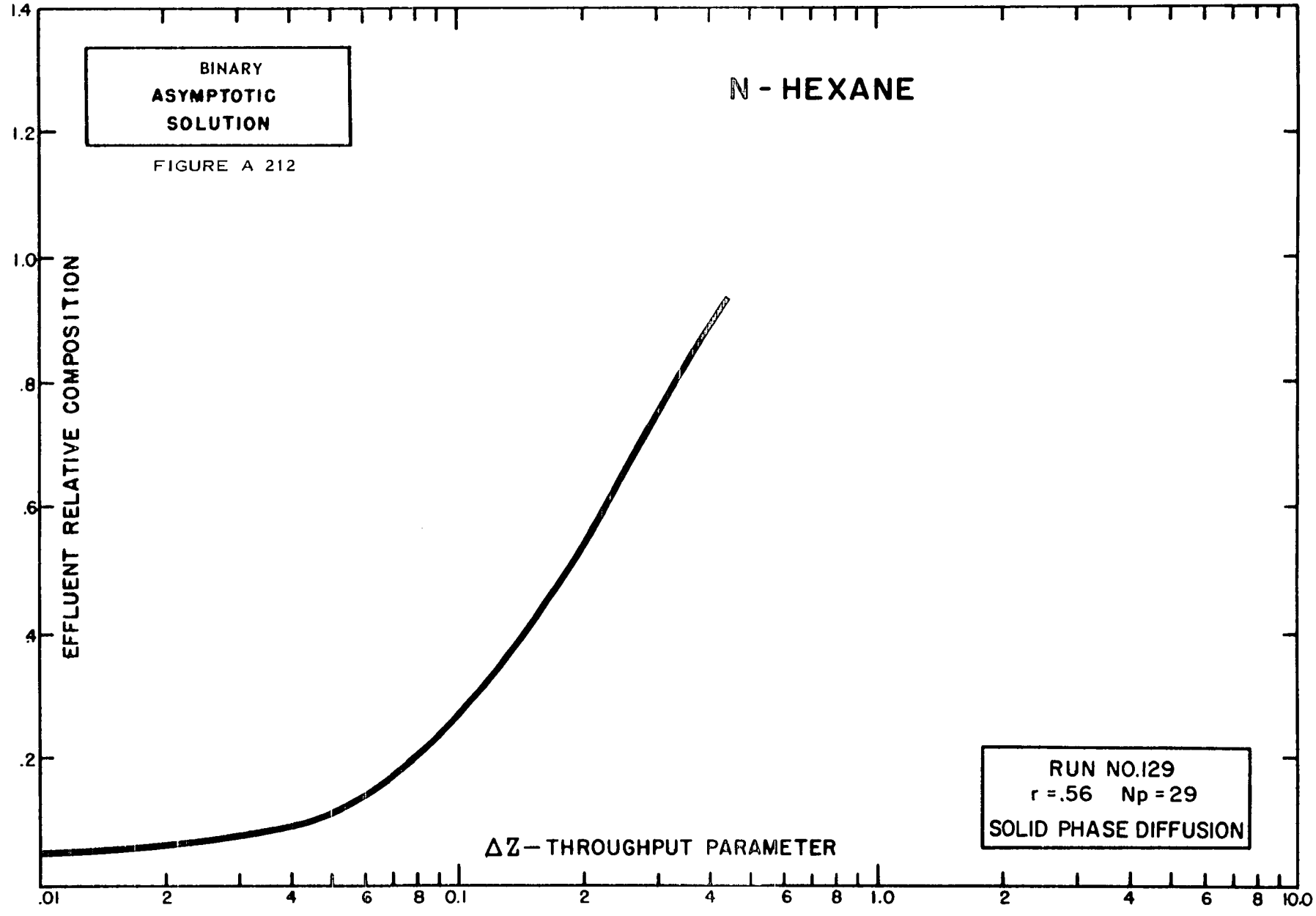
BINARY
ASYMPTOTIC
SOLUTION
N - HEXANE
EFFLUENT RELATIVE COMPOSITION
ΔZ— THROUGHPUT PARAMETER
RUN NO.129
r = .56 Np = 29
SOLID PHASE DIFFUSION
1.4
1.2
1.0
.8
.6
.4
.2
.01
2
4
6
8
0.1
2
4
6
8
1.0
2
4
6
8
10.0

FIGURE A 212

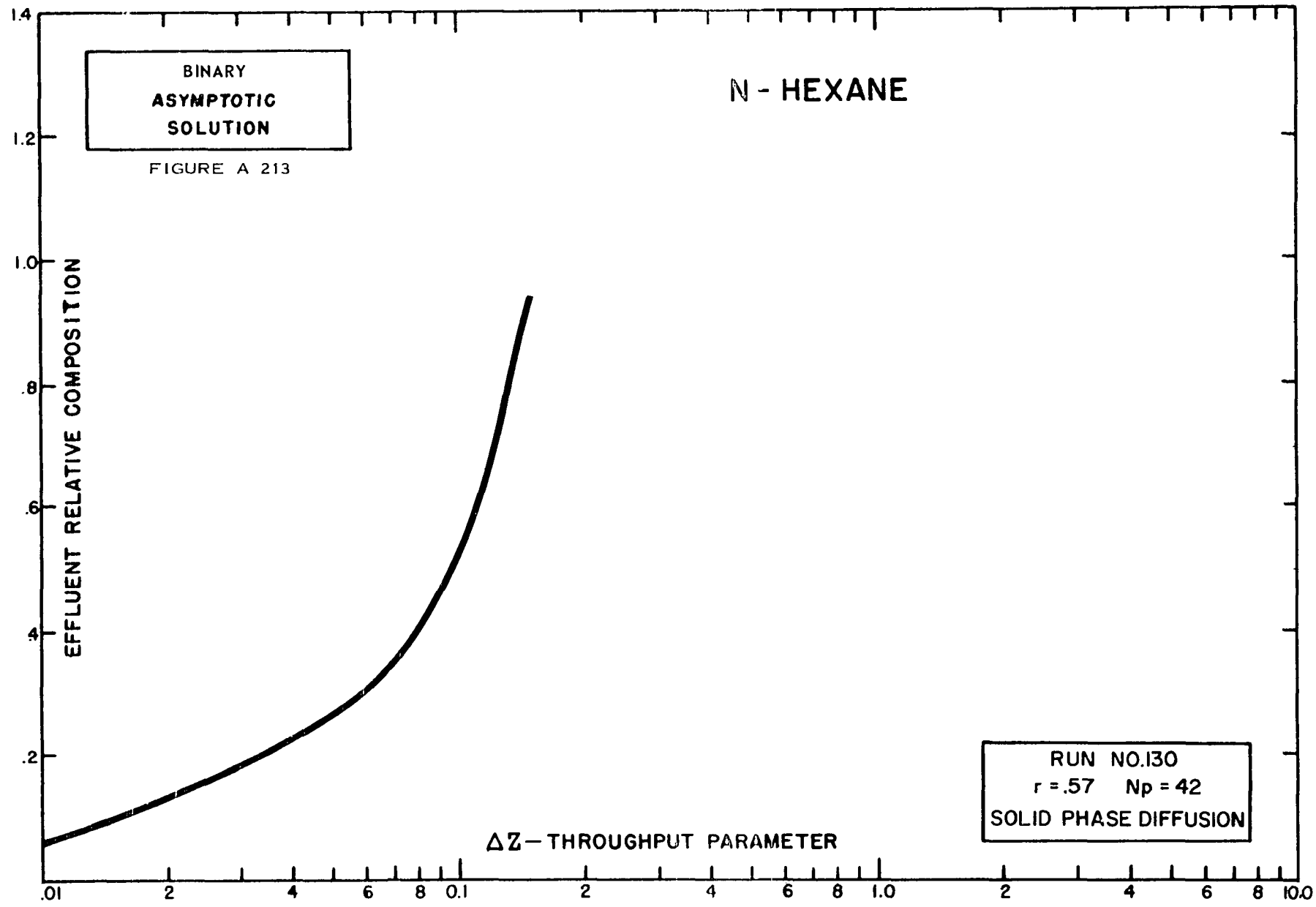
BINARY
ASYMPTOTIC
SOLUTION
N - HEXANE
EFFLUENT RELATIVE COMPOSITION
ΔZ—THROUGHPUT PARAMETER
RUN NO.130
r = .57 Np = 42
SOLID PHASE DIFFUSION
1.4
1.2
1.0
.8
.6
.4
.2
.01
2
4
6
8
0.1
2
4
6
8
1.0
2
4
6
8
10.0

FIGURE A 213

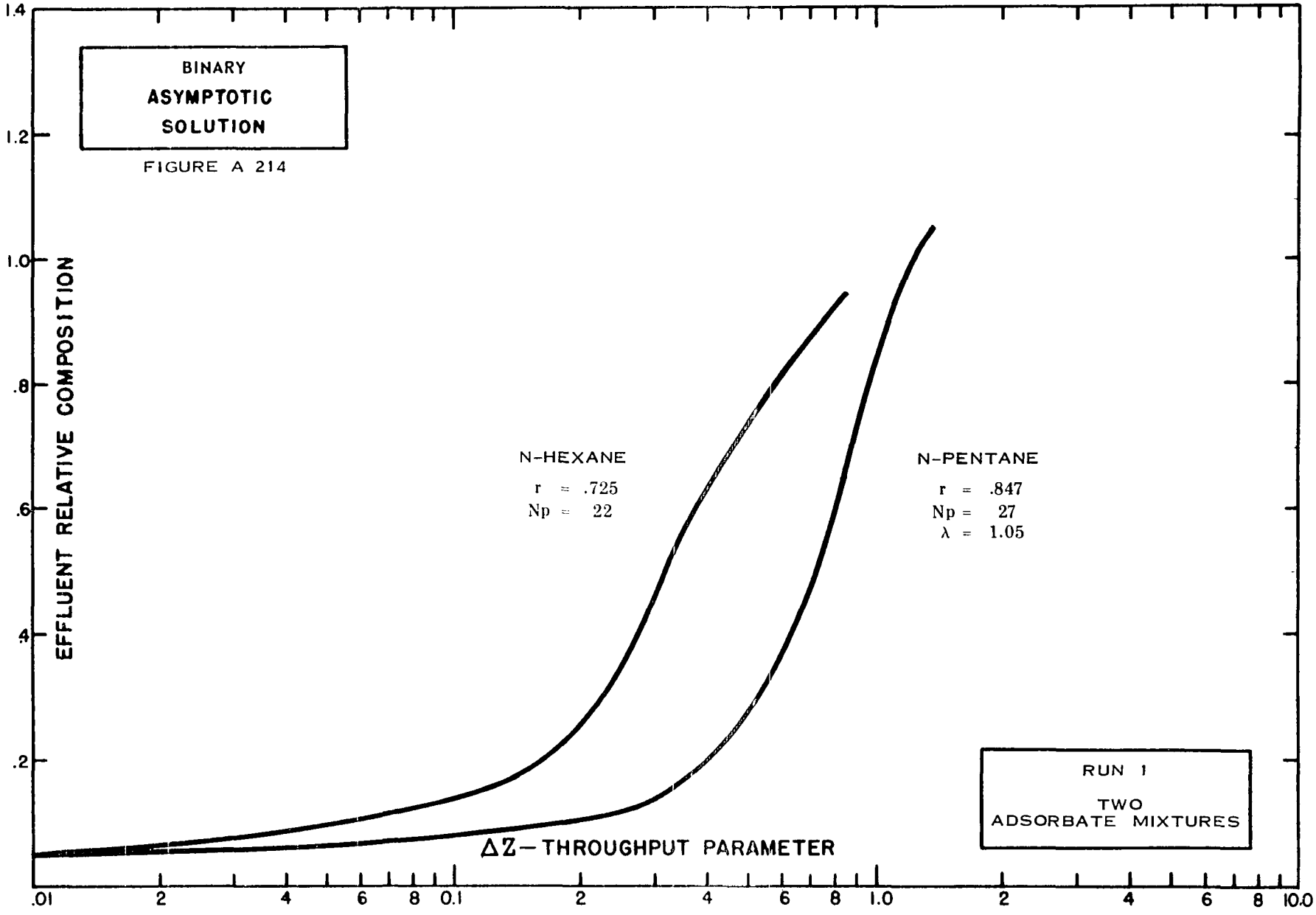
BINARY
ASYMPTOTIC
SOLUTION
FIGURE A 214
EFFLUENT RELATIVE COMPOSITION
1.4
1.2
1.0
.8
.6
.4
.2
N-HEXANE
r = .725
Np = 22
N-PENTANE
r = .847
Np = 27
λ = 1.05
RUN 1
TWO
ADSORBATE MIXTURES
ΔZ—THROUGHPUT PARAMETER
.01
2
4
6
8
0.1
2
4
6
8
1.0
2
4
6
8
10.0

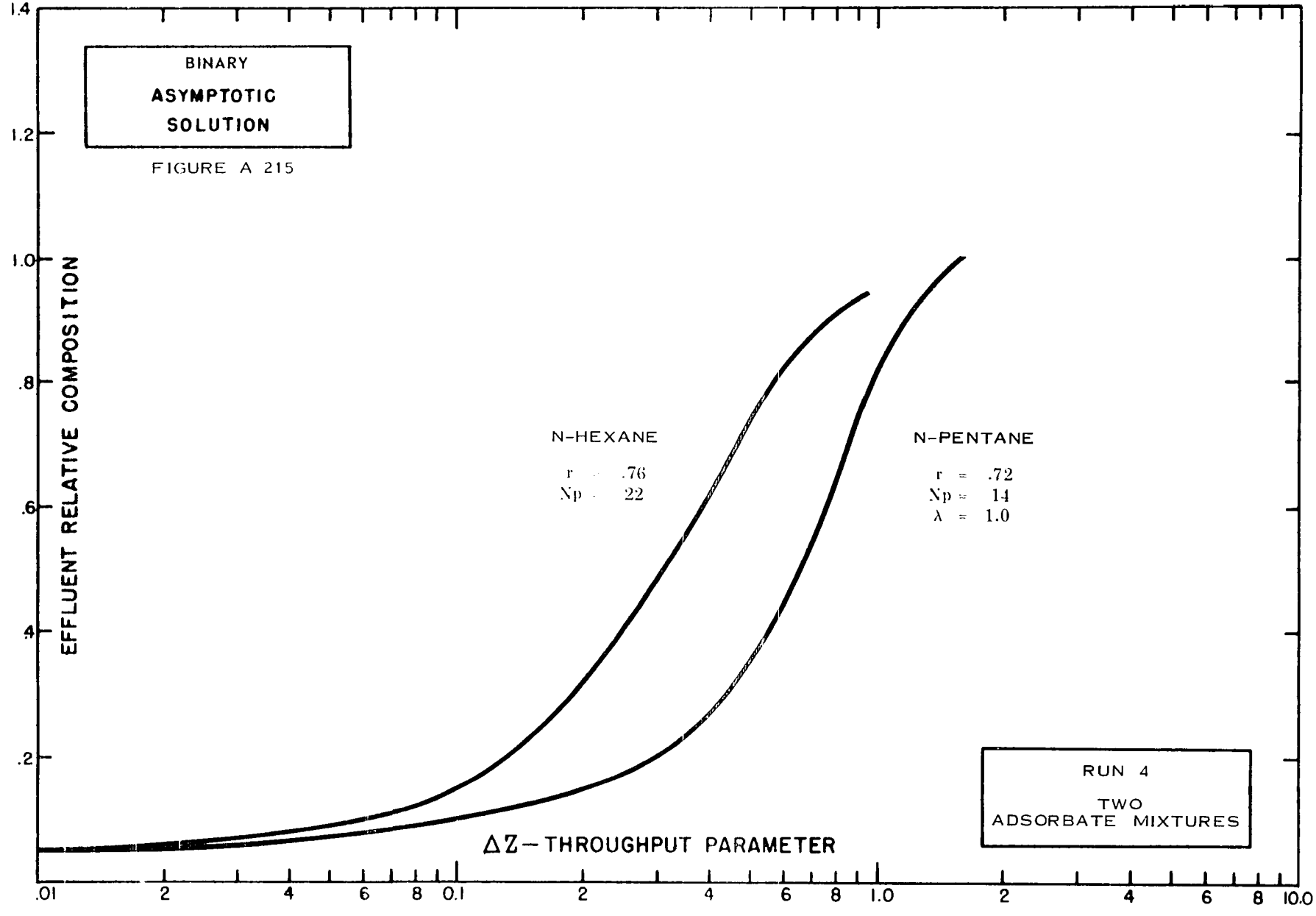
BINARY
ASYMPTOTIC
SOLUTION
FIGURE A 215
EFFLUENT RELATIVE COMPOSITION
1.4
1.2
1.0
.8
.6
.4
.2
N-HEXANE
r = .76
Np = 22
N-PENTANE
r = .72
Np = 14
λ = 1.0
RUN 4
TWO
ADSORBATE MIXTURES
ΔZ — THROUGHPUT PARAMETER
.01
2
4
6
8
0.1
2
4
6
8
1.0
2
4
6
8
10.0

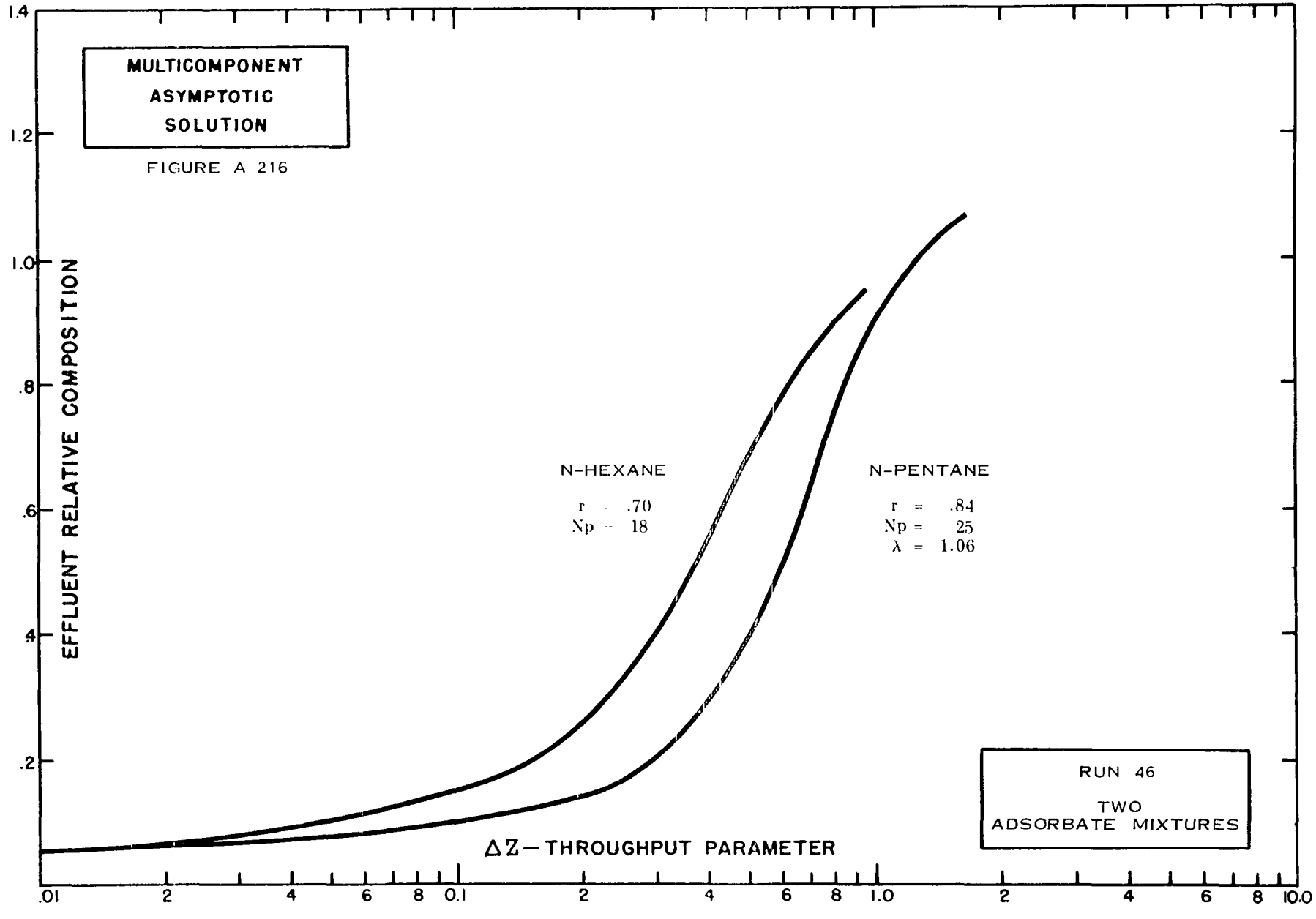
MULTICOMPONENT
ASYMPTOTIC
SOLUTION
FIGURE A 216
EFFLUENT RELATIVE COMPOSITION
1.4
1.2
1.0
.8
.6
.4
.2
N-HEXANE
r = .70
Np = 18
N-PENTANE
r = .84
Np = 25
λ = 1.06
RUN 46
TWO
ADSORBATE MIXTURES
ΔZ—THROUGHPUT PARAMETER
.01
2
4
6
8
0.1
2
4
6
8
1.0
2
4
6
8
10.0

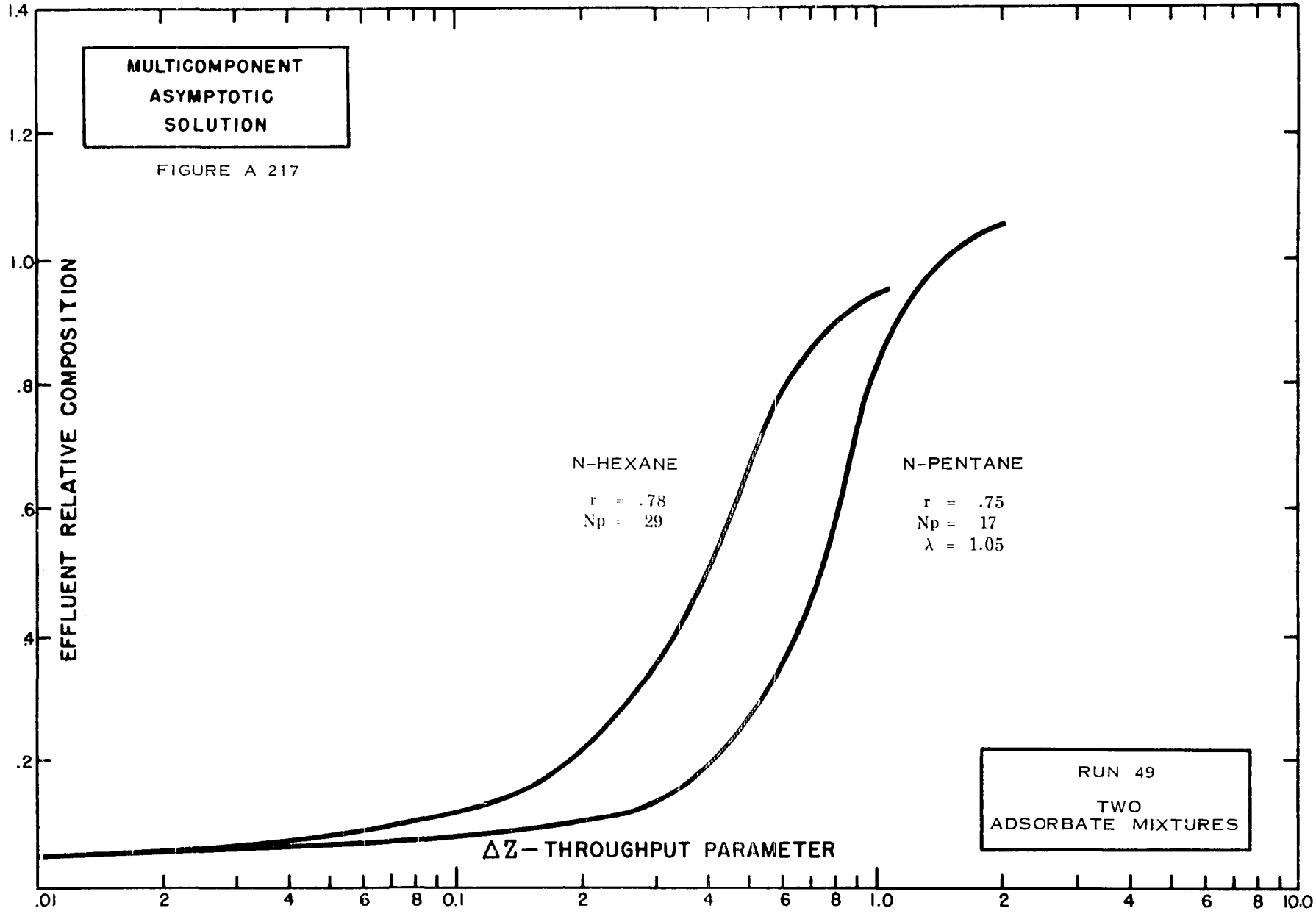
MULTICOMPONENT
ASYMPTOTIC
SOLUTION
FIGURE A 217
EFFLUENT RELATIVE COMPOSITION
1.4
1.2
1.0
.8
.6
.4
.2
N-HEXANE
r = .78
Np = 29
N-PENTANE
r = .75
Np = 17
λ = 1.05
RUN 49
TWO
ADSORBATE MIXTURES
ΔZ—THROUGHPUT PARAMETER
.01
2
4
6
8
0.1
2
4
6
8
1.0
2
4
6
8
10.0

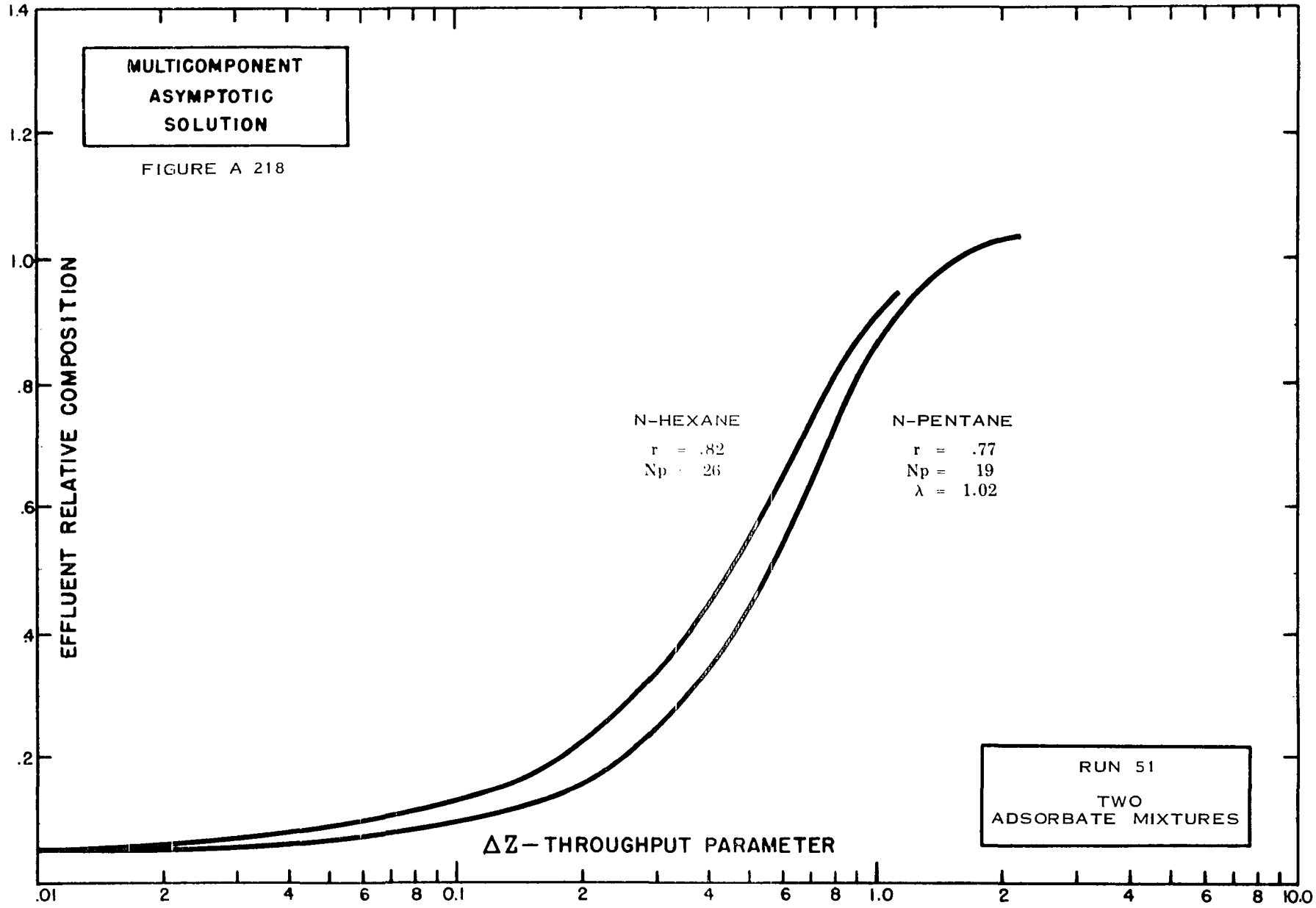
MULTICOMPONENT
ASYMPTOTIC
SOLUTION
FIGURE A 218
EFFLUENT RELATIVE COMPOSITION
1.4
1.2
1.0
.8
.6
.4
.2
N-HEXANE
r = .82
Np = 26
N-PENTANE
r = .77
Np = 19
λ = 1.02
RUN 51
TWO
ADSORBATE MIXTURES
ΔZ—THROUGHPUT PARAMETER
.01
2
4
6
8
0.1
2
4
6
8
1.0
2
4
6
8
10.0

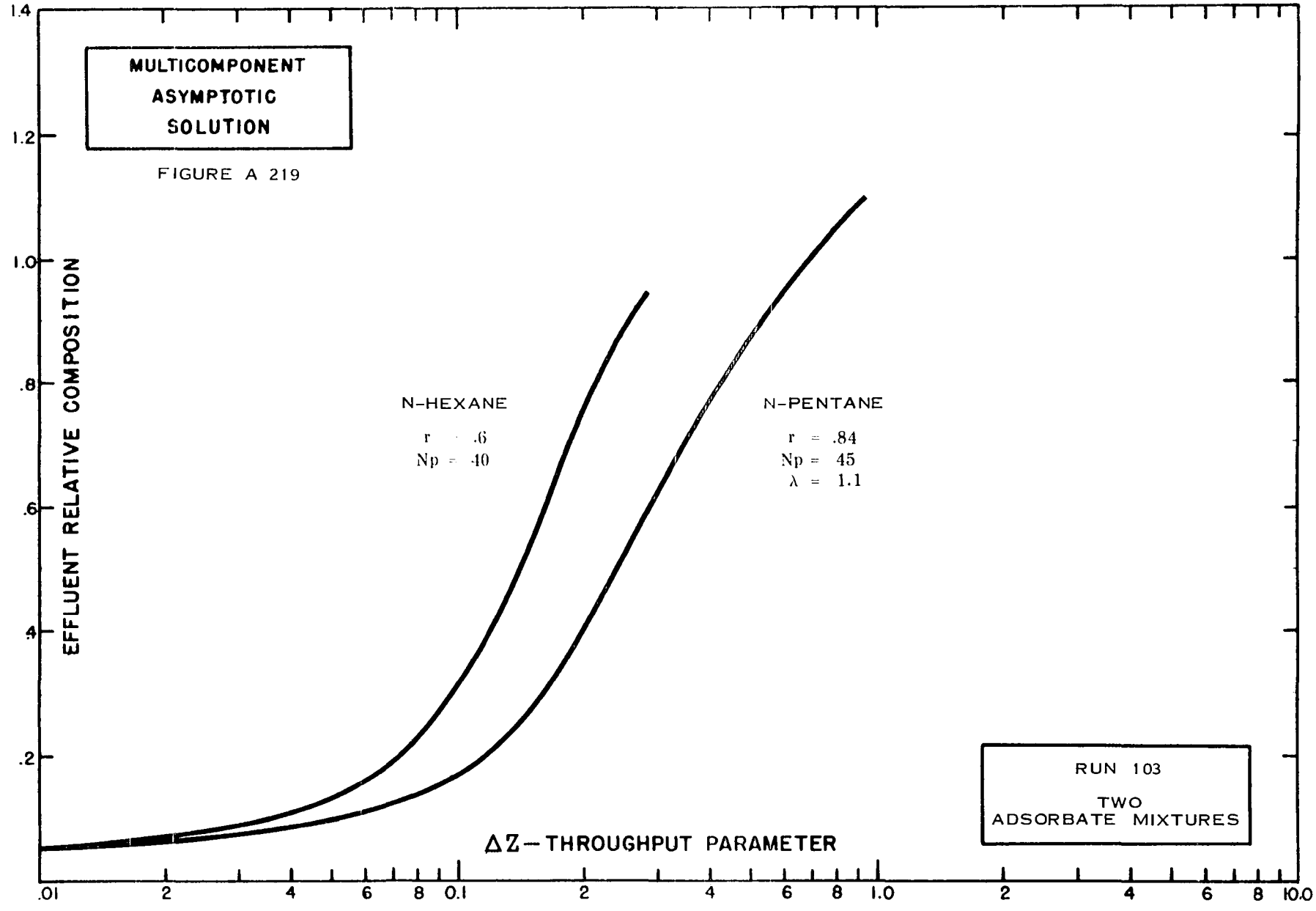
MULTICOMPONENT
ASYMPTOTIC
SOLUTION
FIGURE A 219
EFFLUENT RELATIVE COMPOSITION
1.4
1.2
1.0
.8
.6
.4
.2
N-HEXANE
r = .6
Np = 40
N-PENTANE
r = .84
Np = 45
λ = 1.1
RUN 103
TWO
ADSORBATE MIXTURES
ΔZ—THROUGHPUT PARAMETER
.01
2
4
6
8
0.1
2
4
6
8
1.0
2
4
6
8
10.0

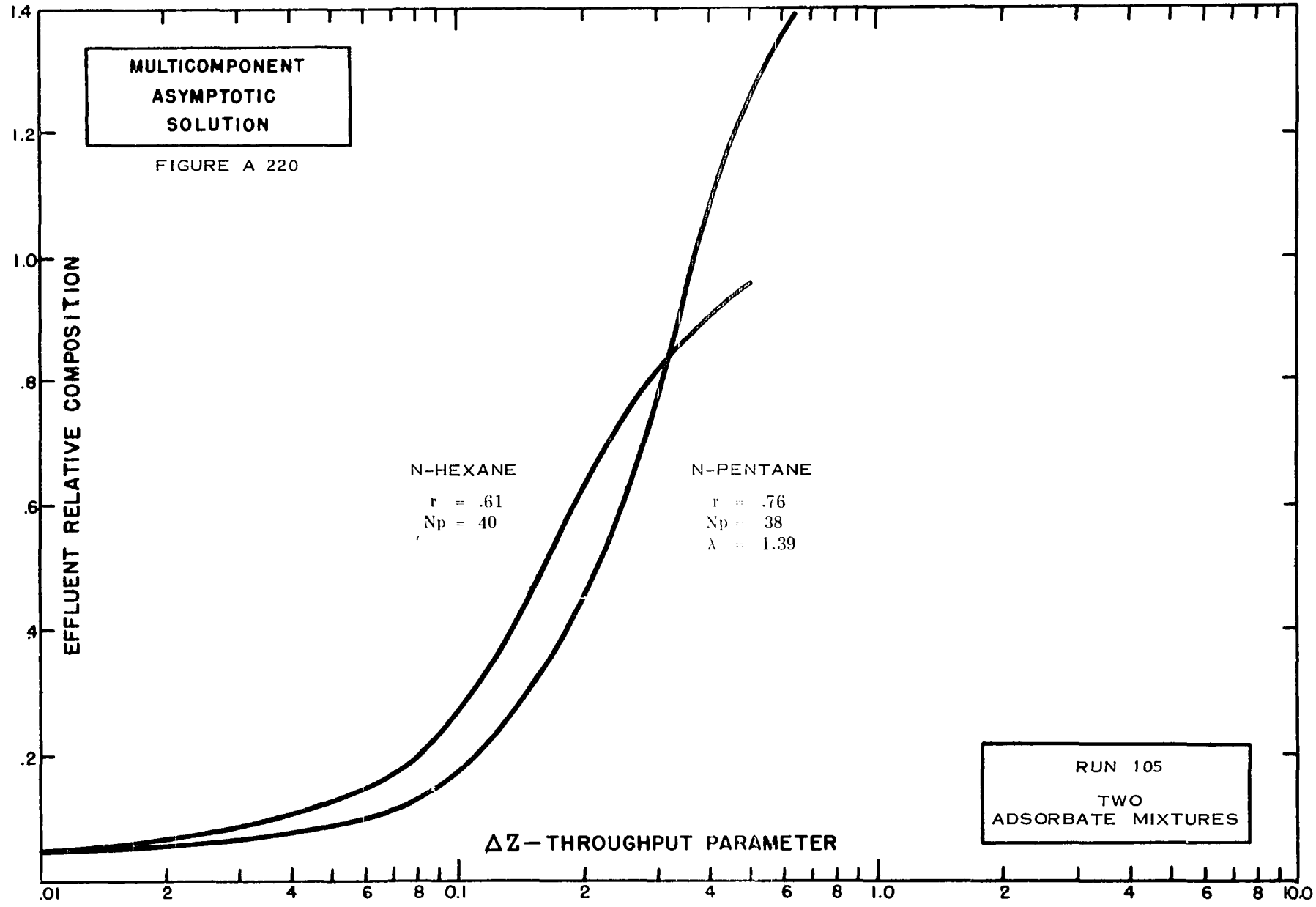
MULTICOMPONENT
ASYMPTOTIC
SOLUTION
FIGURE A 220
EFFLUENT RELATIVE COMPOSITION
1.4
1.2
1.0
.8
.6
.4
.2
N-HEXANE
r = .61
Np = 40
N-PENTANE
r = .76
Np = 38
λ = 1.39
RUN 105
TWO
ADSORBATE MIXTURES
ΔZ—THROUGHPUT PARAMETER
.01
2
4
6
8
0.1
2
4
6
8
1.0
2
4
6
8
10.0

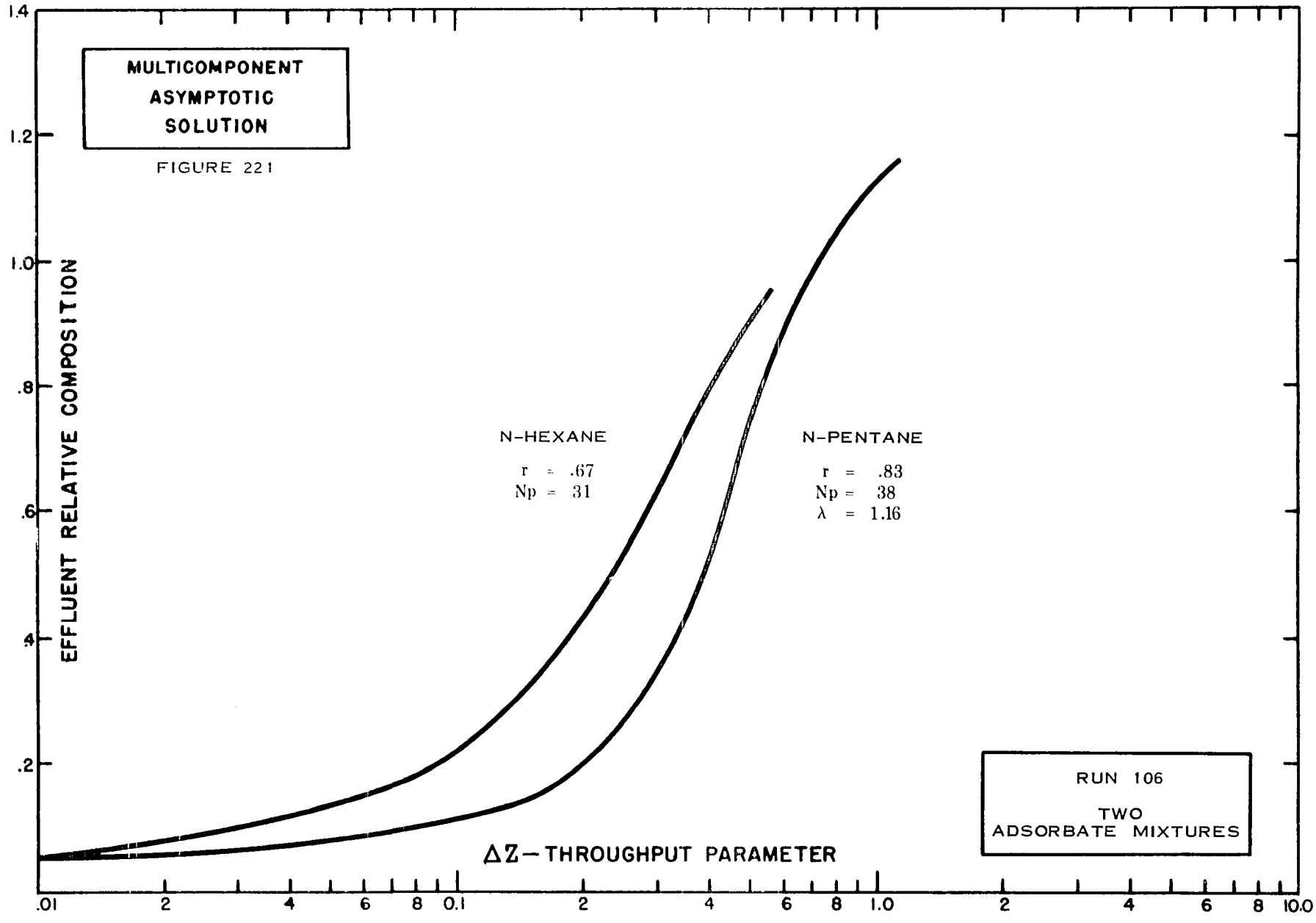
MULTICOMPONENT
ASYMPTOTIC
SOLUTION
FIGURE 221
EFFLUENT RELATIVE COMPOSITION
1.4
1.2
1.0
.8
.6
.4
.2
N-HEXANE
r = .67
Np = 31
N-PENTANE
r = .83
Np = 38
λ = 1.16
RUN 106
TWO
ADSORBATE MIXTURES
ΔZ—THROUGHPUT PARAMETER
.01
2
4
6
8
0.1
2
4
6
8
1.0
2
4
6
8
10.0

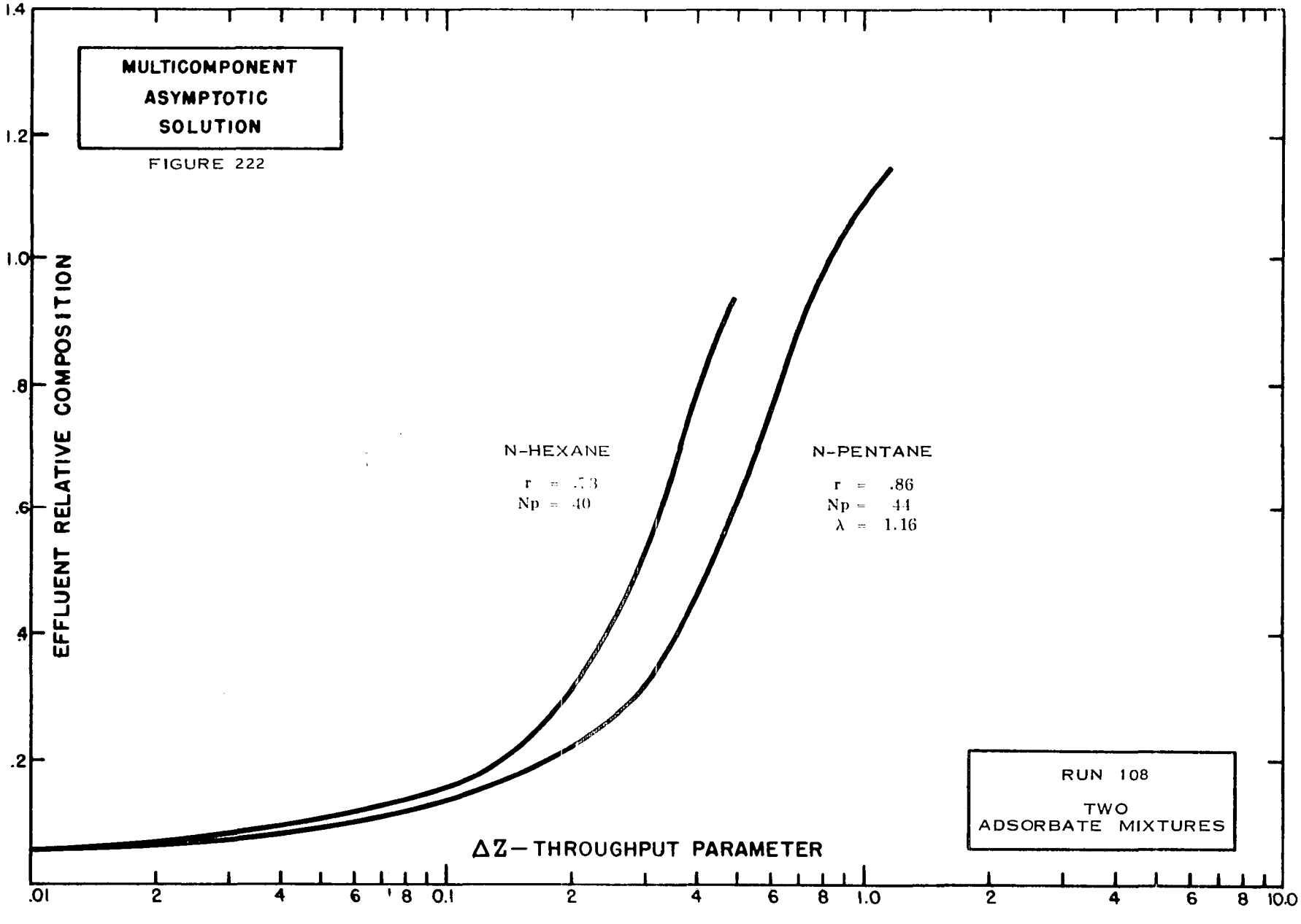
MULTICOMPONENT
ASYMPTOTIC
SOLUTION
FIGURE 222
EFFLUENT RELATIVE COMPOSITION
1.4
1.2
1.0
.8
.6
.4
.2
N-HEXANE
r = .73
Np = 40
N-PENTANE
r = .86
Np = 44
λ = 1.16
RUN 108
TWO
ADSORBATE MIXTURES
ΔZ—THROUGHPUT PARAMETER
.01
2
4
6
8
0.1
2
4
6
8
1.0
2
4
6
8
10.0

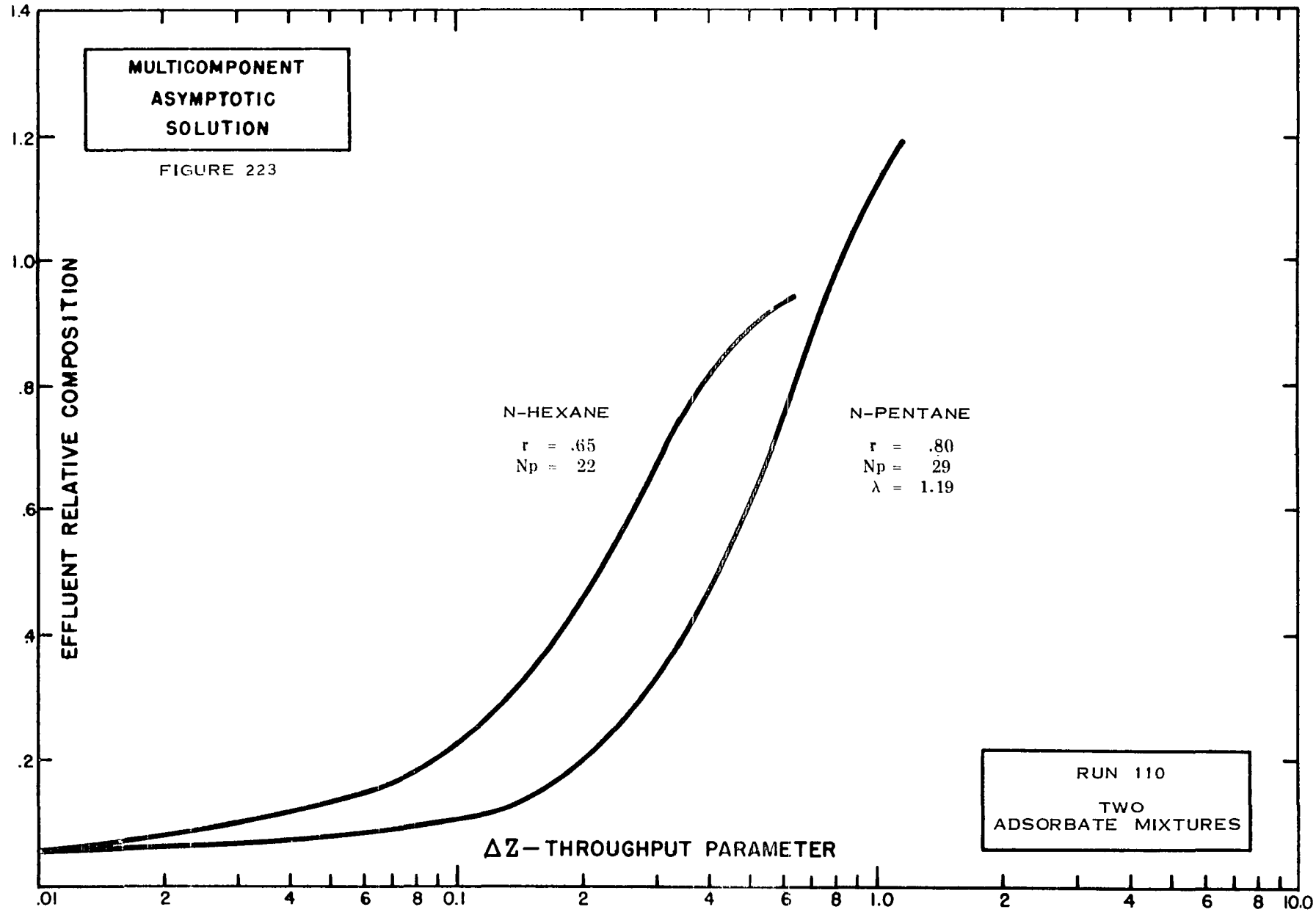
MULTICOMPONENT
ASYMPTOTIC
SOLUTION
FIGURE 223
EFFLUENT RELATIVE COMPOSITION
1.4
1.2
1.0
.8
.6
.4
.2
N-HEXANE
r = .65
Np = 22
N-PENTANE
r = .80
Np = 29
λ = 1.19
RUN 110
TWO
ADSORBATE MIXTURES
ΔZ—THROUGHPUT PARAMETER
.01
2
4
6
8
0.1
2
4
6
8
1.0
2
4
6
8
10.0

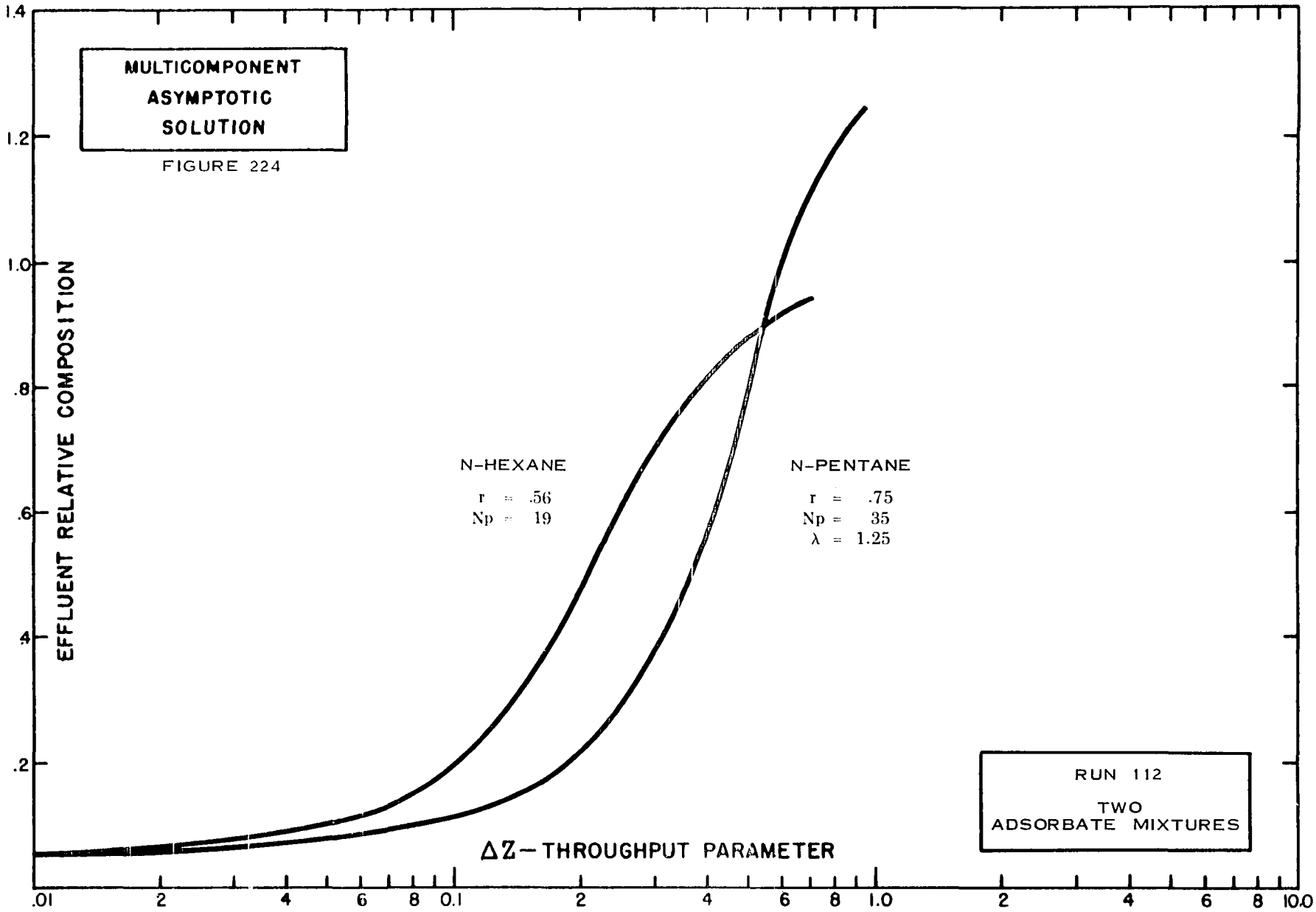
MULTICOMPONENT
ASYMPTOTIC
SOLUTION
FIGURE 224
EFFLUENT RELATIVE COMPOSITION
1.4
1.2
1.0
.8
.6
.4
.2
N-HEXANE
r = .56
Np = 19
N-PENTANE
r = .75
Np = 35
λ = 1.25
RUN 112
TWO
ADSORBATE MIXTURES
ΔZ — THROUGHPUT PARAMETER
.01
2
4
6
8
0.1
2
4
6
8
1.0
2
4
6
8
10.0

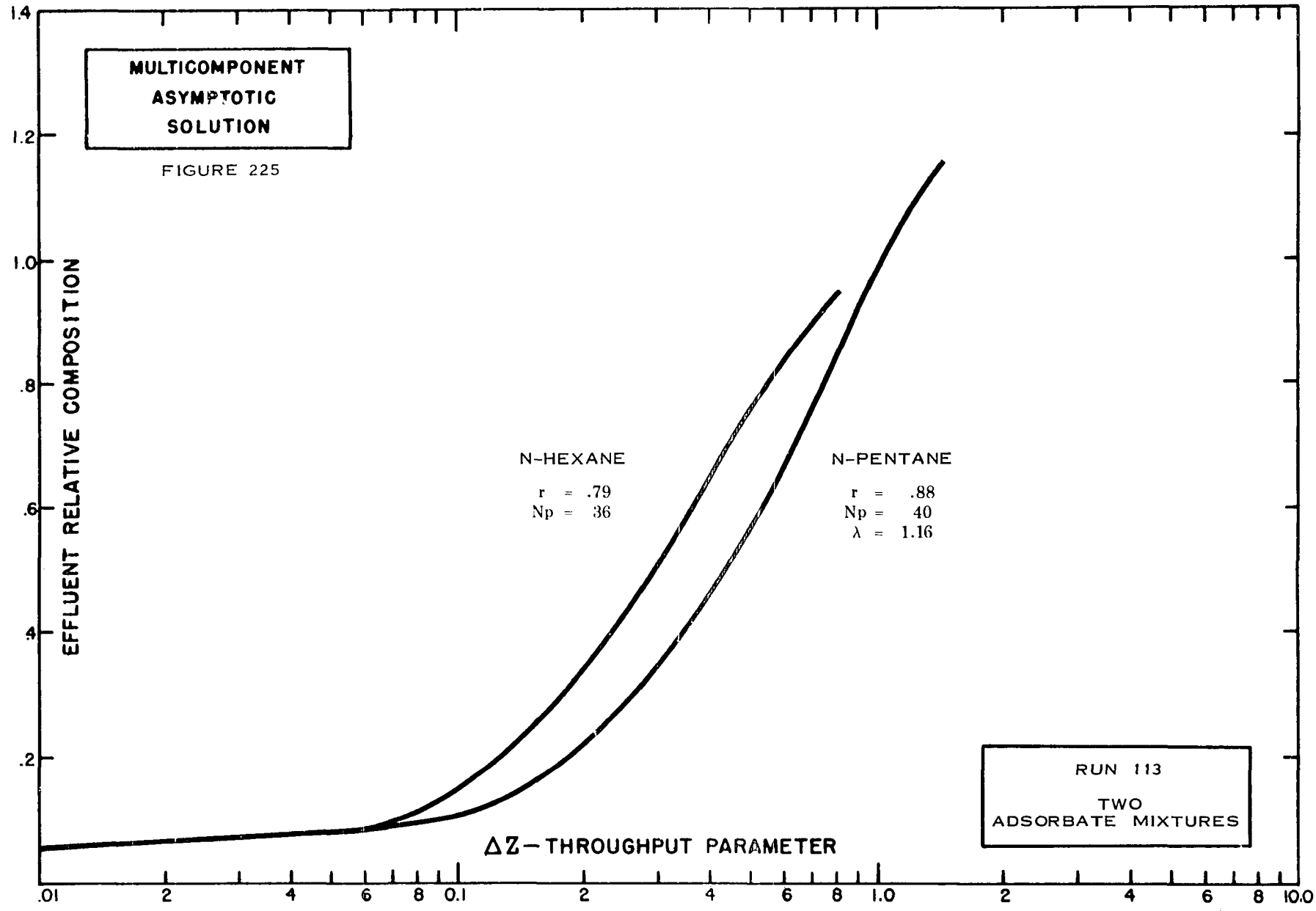
MULTICOMPONENT
ASYMPTOTIC
SOLUTION
FIGURE 225
EFFLUENT RELATIVE COMPOSITION
1.4
1.2
1.0
.8
.6
.4
.2
N-HEXANE
r = .79
Np = 36
N-PENTANE
r = .88
Np = 40
λ = 1.16
RUN 113
TWO
ADSORBATE MIXTURES
ΔZ—THROUGHPUT PARAMETER
.01
2
4
6
8
0.1
2
4
6
8
1.0
2
4
6
8
10.0

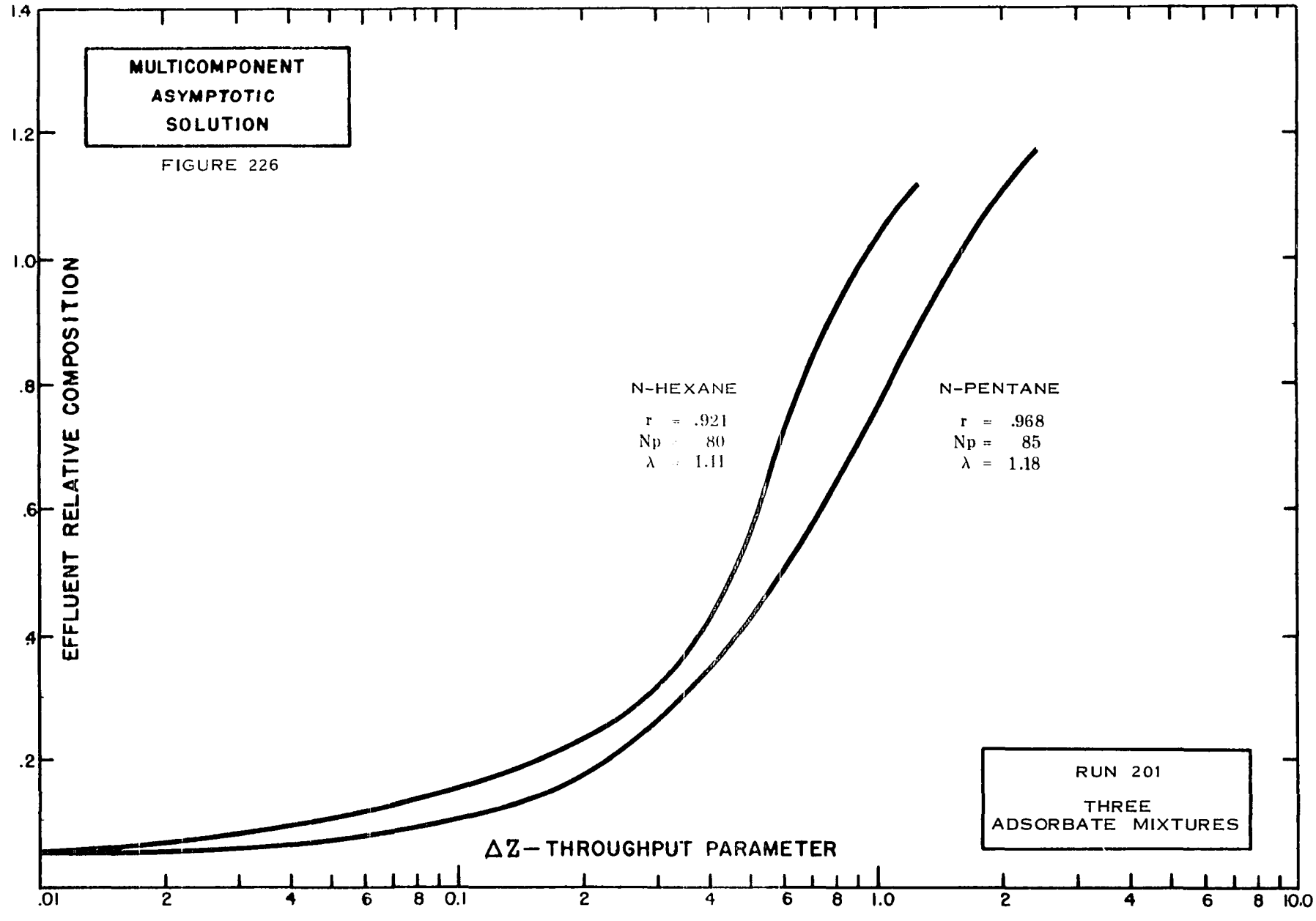
MULTICOMPONENT
ASYMPTOTIC
SOLUTION
FIGURE 226
EFFLUENT RELATIVE COMPOSITION
1.4
1.2
1.0
.8
.6
.4
.2
N-HEXANE
r = .921
Np = 80
λ = 1.11
N-PENTANE
r = .968
Np = 85
λ = 1.18
RUN 201
THREE
ADSORBATE MIXTURES
ΔZ—THROUGHPUT PARAMETER
.01
2
4
6
8
0.1
2
4
6
8
1.0
2
4
6
8
10.0

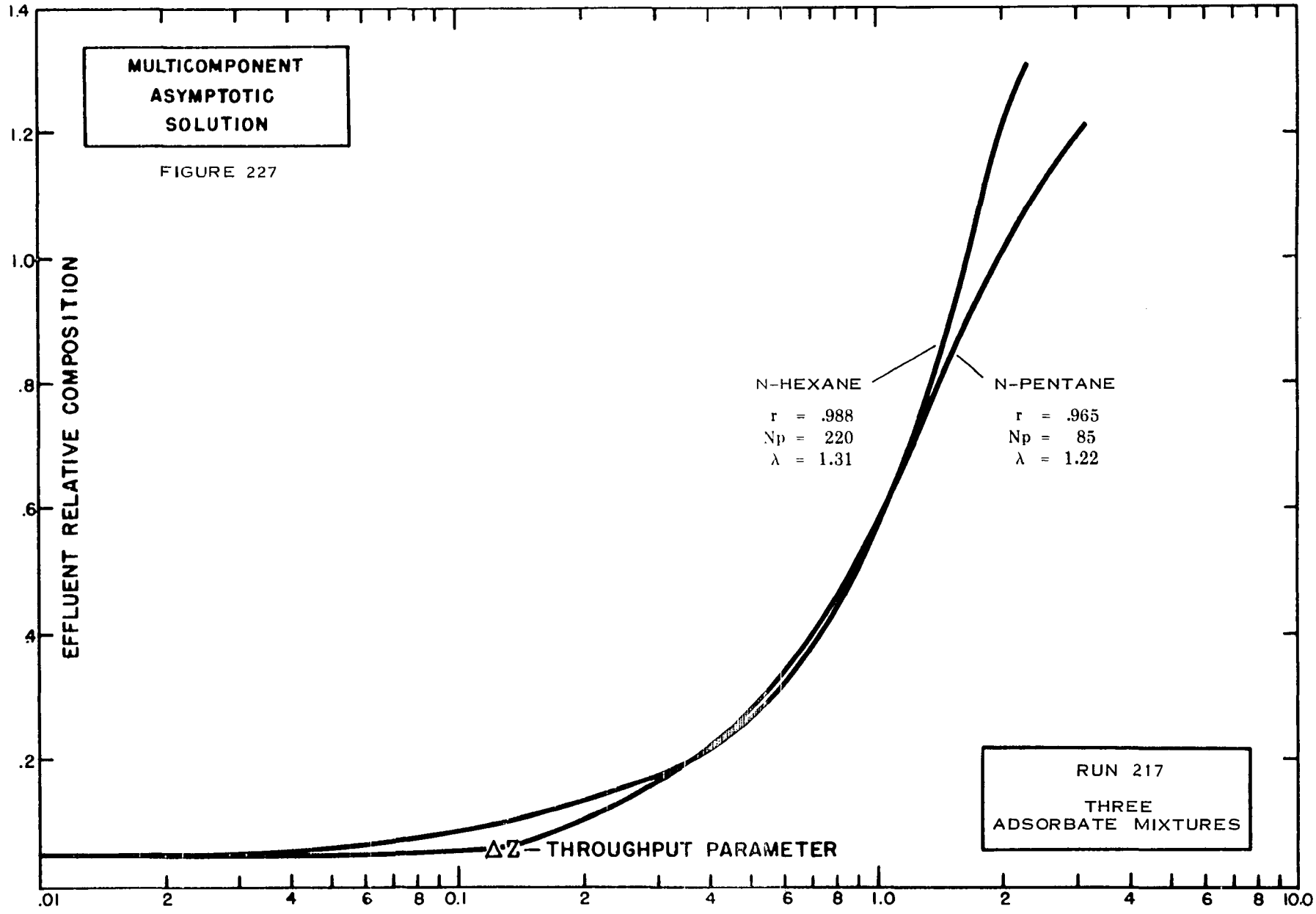
MULTICOMPONENT
ASYMPTOTIC
SOLUTION
FIGURE 227
EFFLUENT RELATIVE COMPOSITION
1.4
1.2
1.0
.8
.6
.4
.2
N-HEXANE
r = .988
Np = 220
λ = 1.31
N-PENTANE
r = .965
Np = 85
λ = 1.22
RUN 217
THREE
ADSORBATE MIXTURES
ΔΣ — THROUGHPUT PARAMETER
.01
2
4
6
8
0.1
2
4
6
8
1.0
2
4
6
8
10.0

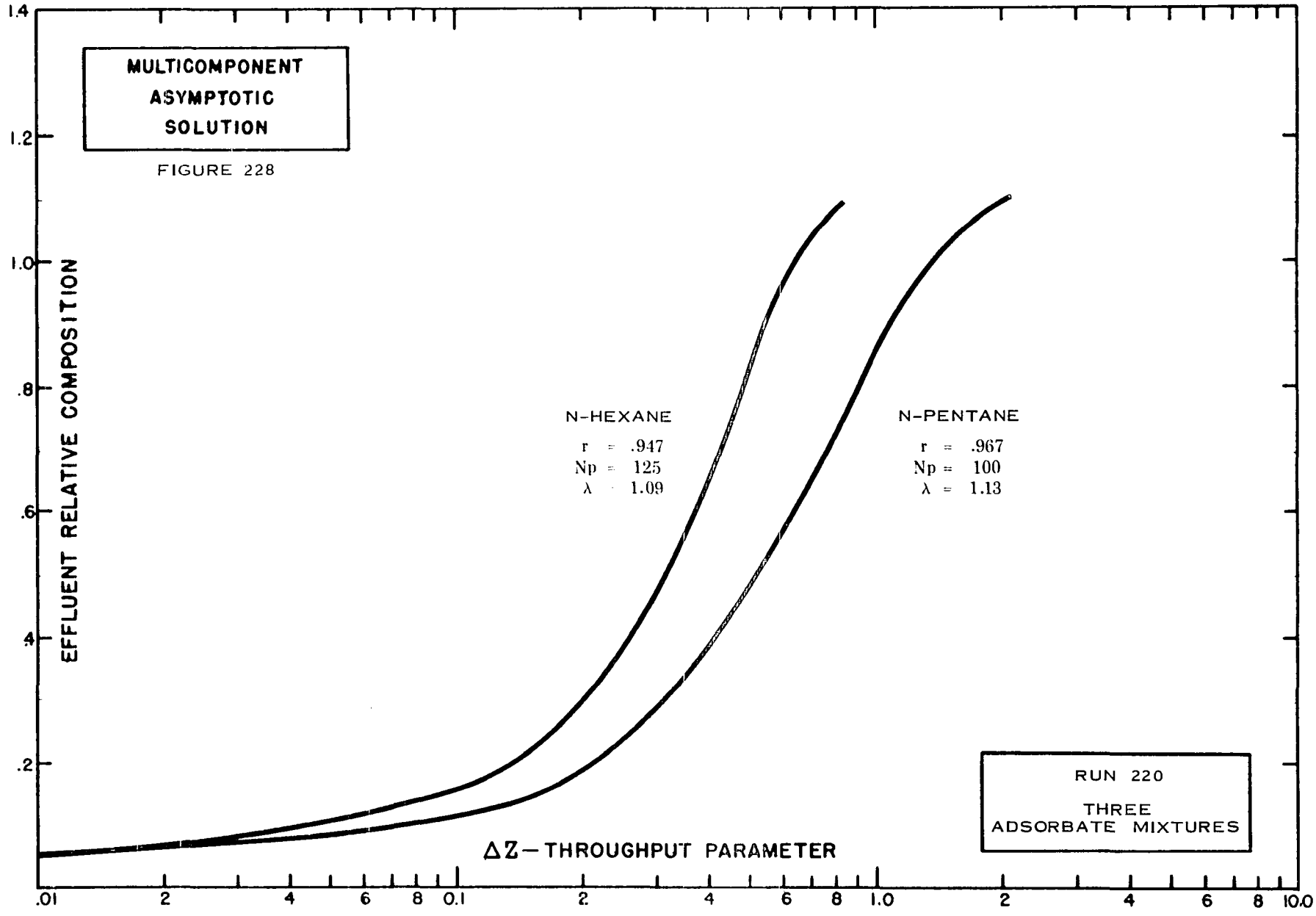
MULTICOMPONENT
ASYMPTOTIC
SOLUTION
FIGURE 228
EFFLUENT RELATIVE COMPOSITION
1.4
1.2
1.0
.8
.6
.4
.2
N-HEXANE
r = .947
Np = 125
λ = 1.09
N-PENTANE
r = .967
Np = 100
λ = 1.13
RUN 220
THREE
ADSORBATE MIXTURES
ΔZ—THROUGHPUT PARAMETER
.01
2
4
6
8
0.1
2
4
6
8
1.0
2
4
6
8
10.0

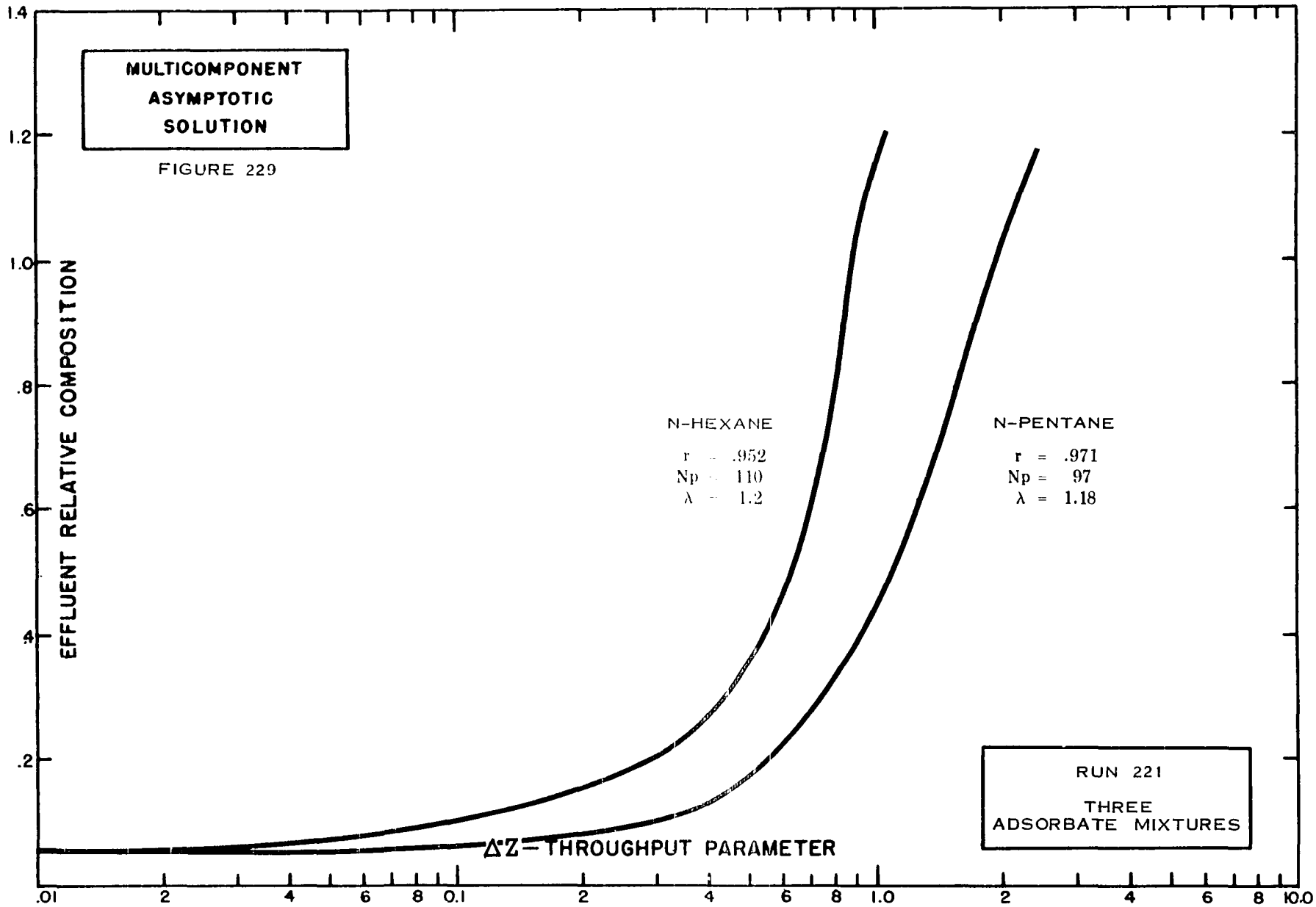
MULTICOMPONENT
ASYMPTOTIC
SOLUTION
FIGURE 229
EFFLUENT RELATIVE COMPOSITION
1.4
1.2
1.0
.8
.6
.4
.2
N-HEXANE
r = .952
Np = 110
λ = 1.2
N-PENTANE
r = .971
Np = 97
λ = 1.18
RUN 221
THREE
ADSORBATE MIXTURES
Δ'Z—THROUGHPUT PARAMETER
.01
2
4
6
8
0.1
2
4
6
8
1.0
2
4
6
8
10.0

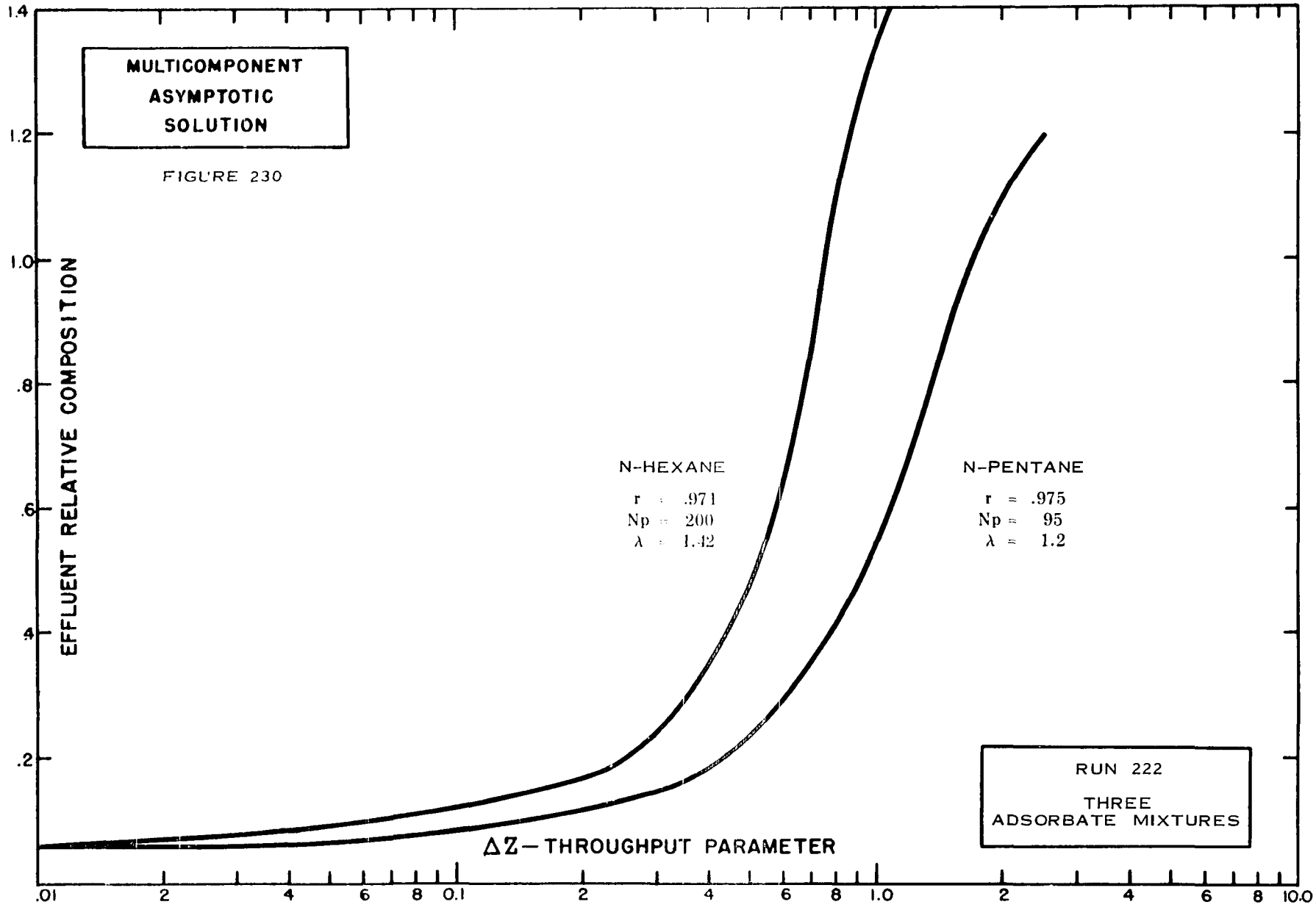
MULTICOMPONENT
ASYMPTOTIC
SOLUTION
FIGURE 230
EFFLUENT RELATIVE COMPOSITION
1.4
1.2
1.0
.8
.6
.4
.2
N-HEXANE
r = .971
Np = 200
λ = 1.42
N-PENTANE
r = .975
Np = 95
λ = 1.2
RUN 222
THREE
ADSORBATE MIXTURES
ΔZ — THROUGHPUT PARAMETER
.01
2
4
6
8
0.1
2
4
6
8
1.0
2
4
6
8
10.0

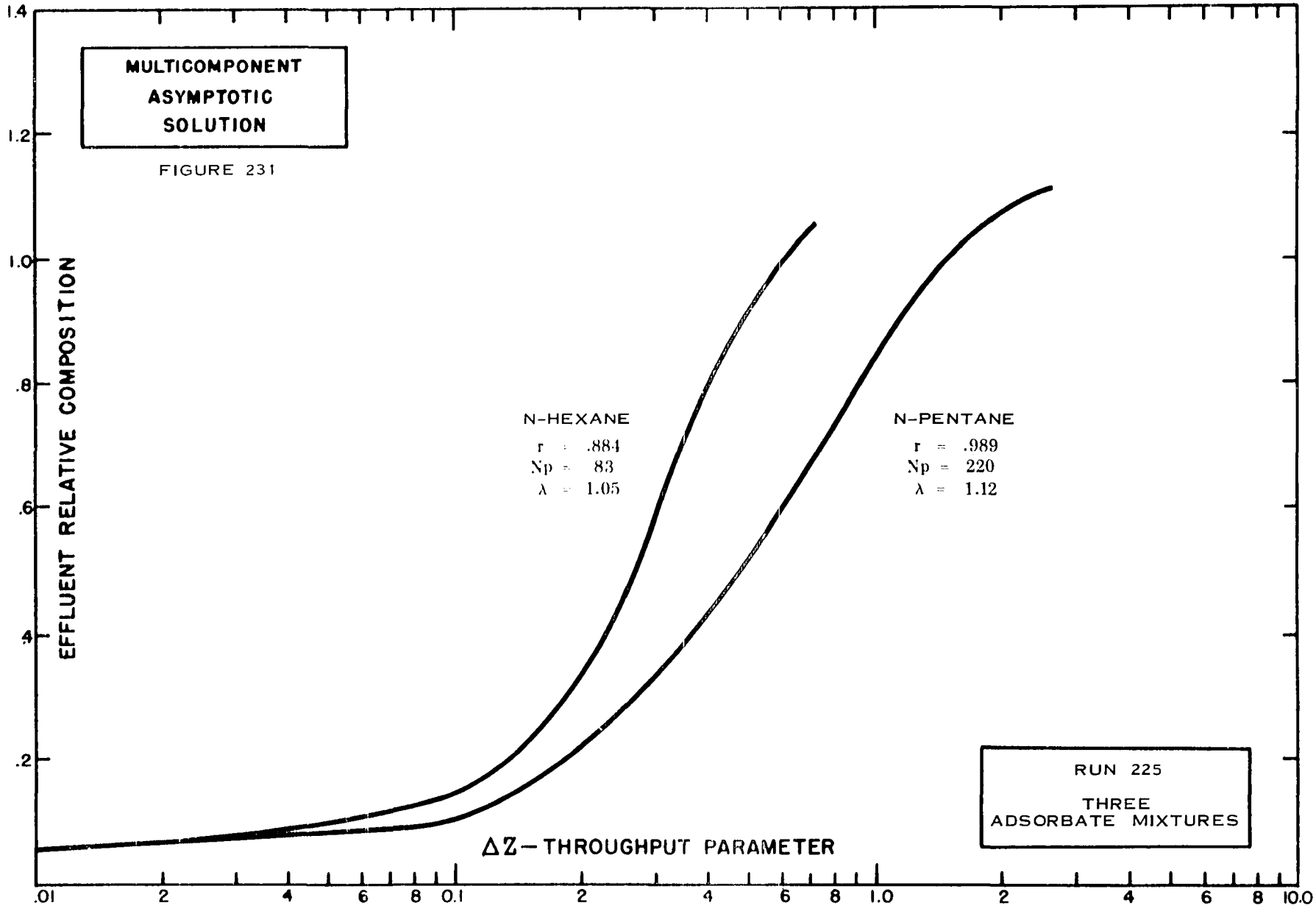
MULTICOMPONENT
ASYMPTOTIC
SOLUTION
FIGURE 231
EFFLUENT RELATIVE COMPOSITION
1.4
1.2
1.0
.8
.6
.4
.2
N-HEXANE
r = .884
Np = 83
λ = 1.05
N-PENTANE
r = .989
Np = 220
λ = 1.12
RUN 225
THREE
ADSORBATE MIXTURES
ΔZ—THROUGHPUT PARAMETER
.01
2
4
6
8
0.1
2
4
6
8
1.0
2
4
6
8
10.0

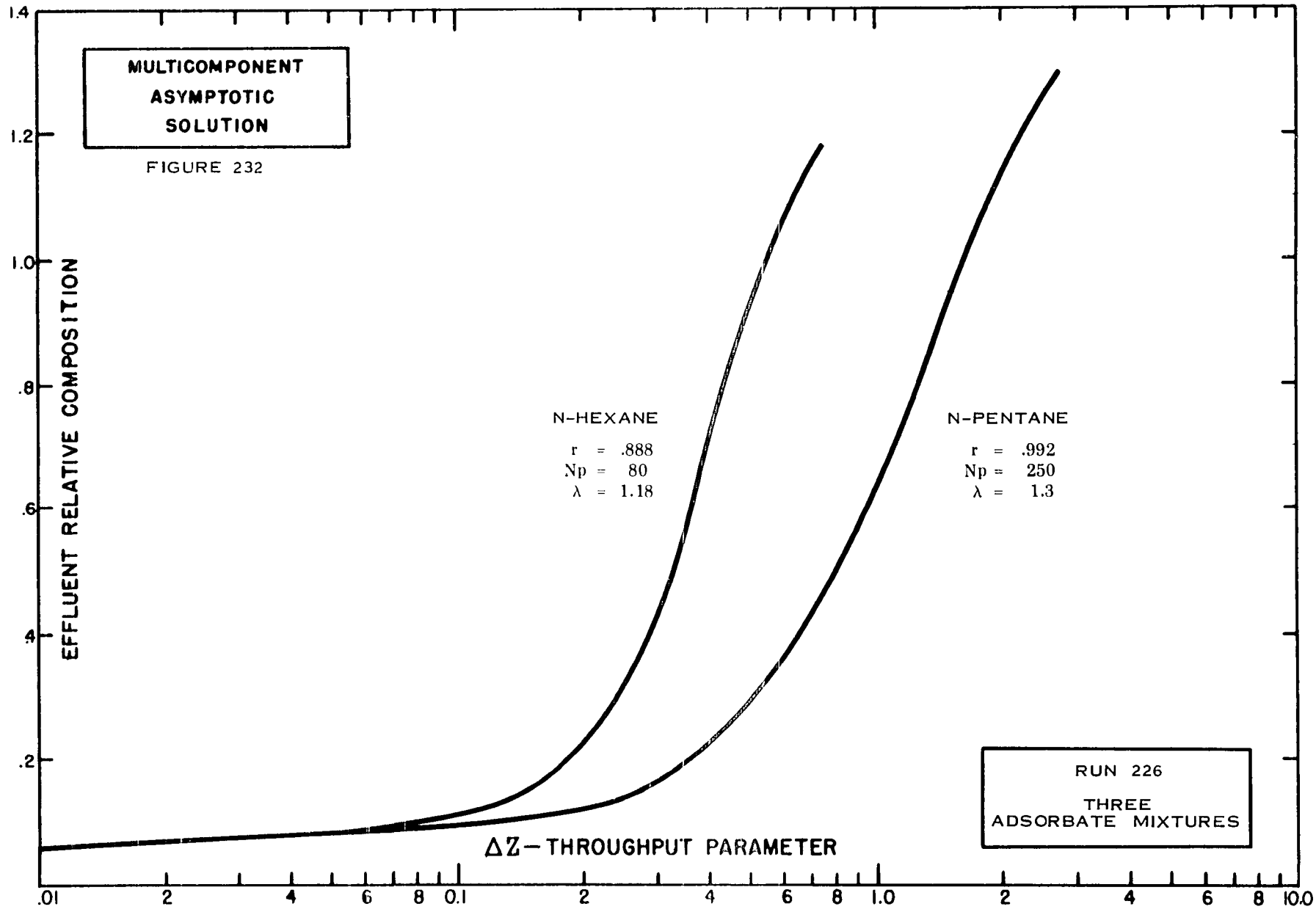
MULTICOMPONENT
ASYMPTOTIC
SOLUTION
FIGURE 232
EFFLUENT RELATIVE COMPOSITION
1.4
1.2
1.0
.8
.6
.4
.2
N-HEXANE
r = .888
Np = 80
λ = 1.18
N-PENTANE
r = .992
Np = 250
λ = 1.3
RUN 226
THREE
ADSORBATE MIXTURES
ΔZ—THROUGHPUT PARAMETER
.01
2
4
6
8
0.1
2
4
6
8
1.0
2
4
6
8
10.0

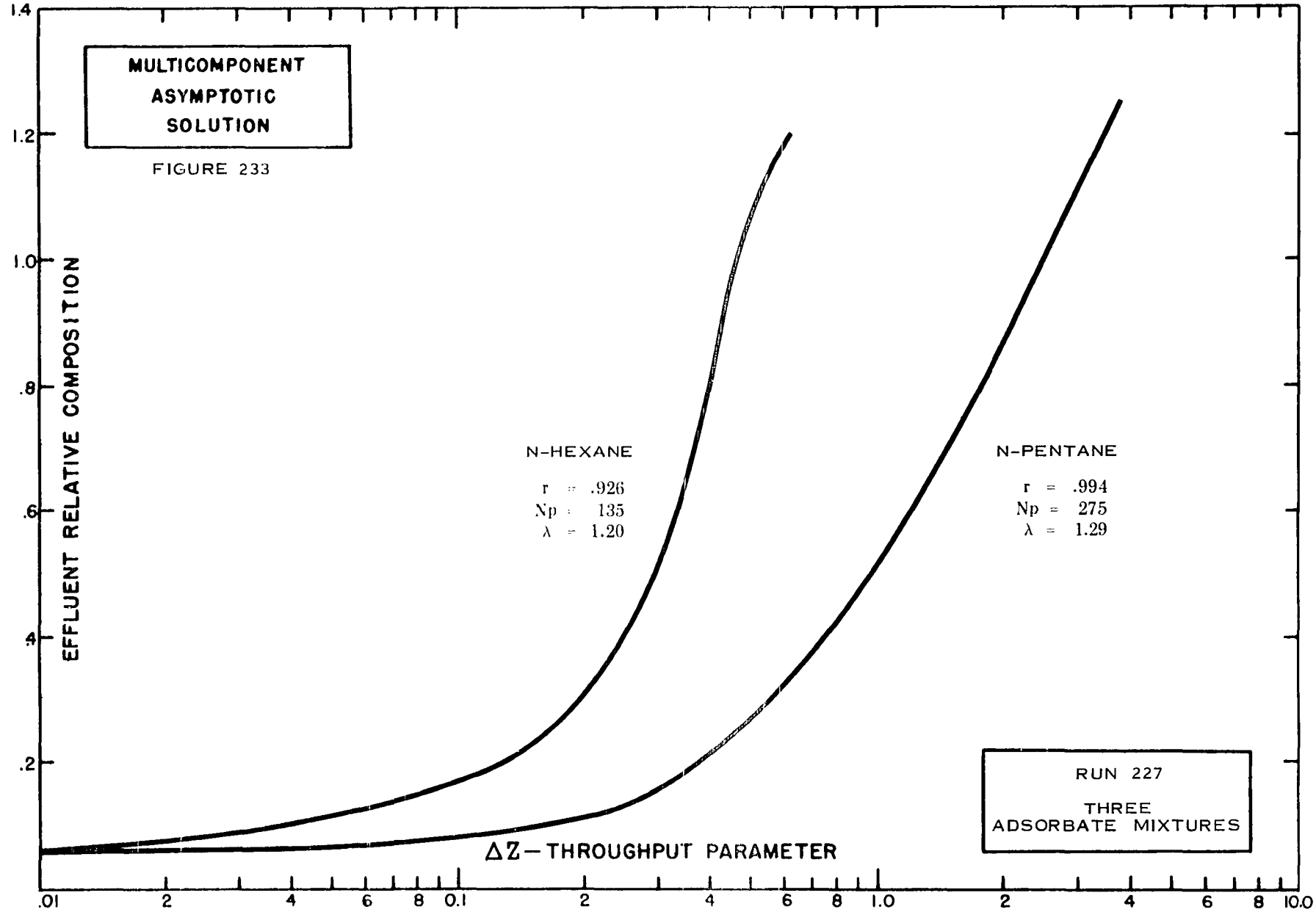
MULTICOMPONENT
ASYMPTOTIC
SOLUTION
FIGURE 233
EFFLUENT RELATIVE COMPOSITION
1.4
1.2
1.0
.8
.6
.4
.2
N-HEXANE
r = .926
Np = 135
λ = 1.20
N-PENTANE
r = .994
Np = 275
λ = 1.29
RUN 227
THREE
ADSORBATE MIXTURES
ΔZ—THROUGHPUT PARAMETER
.01
2
4
6
8
0.1
2
4
6
8
1.0
2
4
6
8
10.0

APPENDIX B

DEFINITIONS AND DERIVATIONS

OF

GENERAL ADSORPTION DIMENSIONLESS PARAMETERS

APPENDIX B

DEFINITIONS AND DERIVATIONS OF GENERAL ADSORPTION DIMENSIONLESS PARAMETERS

Surface Reaction Kinetics

As shown in an earlier chapter, the general adsorption rate equation written according to the Langmuir theory can be summarized as:

$$\frac{dq_a}{d\theta} = k_{kin}\left[c_a\left[q_\infty^{\,o} - q_a\right] - \frac{q_a}{k_{AD}^{\,o}}\right] \qquad \text{B-1}$$

at $dq_a/d\theta = 0$:

$$c_o(q_\infty^{\,o} - q_\infty) = \frac{q_\infty}{k_{AD}^{\,o}}\,. \qquad \text{B-2}$$

This equation is the general dynamic adsorption isotherm applied to the adsorption analysis. Solving for $q_\infty^{\,o}$ from B-2 and combining with B-1 gives:

$$\frac{dq_a}{d\theta} = k_{kin}\left[c_a\left[\frac{(1 + k_{AD}^{\,o}\, c_o)}{k_{AD}^{\,o}\, c_o}\, q_\infty - q_a\right] - \frac{q_a}{k_{AD}^{\,o}}\right]. \qquad \text{B-3}$$

Rearrangement of the equation can be seen to give:

$$\frac{d(q_a/q_\infty)}{d\left\{\frac{(1 + k_{AD}^{\,o}\, c_o)}{k_{AD}^{\,c}}\, k_{kin}\theta\right\}} = \frac{c_a}{c_o} - \left[\frac{c_o k_{AD}^{\,o}}{1+k_{AD}^{\,o} c_o}\right]\frac{q_a c_a}{q_\infty c_o} - \left[\frac{1}{1+k_{AD}^{\,o} c_o}\right]\frac{q_a}{q_\infty} \qquad \text{B-4}$$

Defining a dimensionless time, t, as:

$$t = \frac{k_{kin}\ \theta\ (1 + k_{AD}^{o}\ c_o)}{k_{AD}^{o}} \qquad \text{B-5}$$

with an effective adsorption time, θ', as:

$$\theta' = \theta - \frac{h\Phi}{v_g} \qquad \text{B-6}$$

yields:

$$k_{kin}\ \theta' \frac{(1 + k_{AD}^{o}\ c_o)}{k_{AD}^{o}} = t. \qquad \text{B-7}$$

Now, noting that $r = \frac{1}{1 + k_{AD}^{o}\ c_o}$, as described in an earlier chapter,

Equation B-2 yields:

$$c_o q_\infty^{o} = c_o q_\infty [1 + \frac{1}{k_{AD}^{o}\ c_o}] \qquad \text{B-8}$$

$$= c_o q_\infty [\frac{k_{AD}^{o}\ c_o + 1}{k_{AD}^{o}\ c_o}] \qquad \text{B-9}$$

$$c_o q_\infty^{o} = \frac{c_o\ q_\infty}{r\ k_{AD}^{o}\ c_o}. \qquad \text{B-10}$$

Thus:

$$r = 1 - \frac{q_\infty}{q_\infty^{o}}, \qquad \text{B-11}$$

is an alternate expression for r that can be applied as well as $r = \frac{1}{1 + k_{AD}^{o}\ c_o}$.

$$t = \frac{k_{kin}\, c_o\, q_\infty^{\,o}}{q_\infty} \left[\theta - \frac{h\Phi}{v_g}\right] \qquad \text{B-12}$$

In defining a further relationship for t, use is made of a parameter, D, such that:

$$t = \frac{k_{ms}}{D} \left[\theta - \frac{h\Phi}{v_g}\right]. \qquad \text{B-13}$$

Where D is the Column Distribution Coefficient defined by:

$$D = \frac{q_\infty \rho_B}{c_o \Phi} : (c_o \text{ is in the proper units}) \qquad \text{B-14}$$

k_{ms} is the surface reaction mechanism proportionality factor that will allow other rate equations to be compared to Equation B-1.

$$k_{kin} = k_{ms} \frac{\Phi}{q_\infty^{\,o} \rho_B} \qquad \text{B-15}$$

Returning to B-4 gives:

$$\frac{d(q_a/q_\infty)}{dt} = \frac{c_a}{c_o} - \frac{q_a c_a}{c_o q_\infty} (1-r) - r \frac{q_a}{q_\infty}. \qquad \text{B-16}$$

Or,

$$\frac{dy}{dt} = x[1-y] - ry[1-x]. \qquad \text{B-17}$$

Equation B-17 is the generalized rate equation that applies directly to the adsorption theory along with the material balance equation.

APPENDIX C

GENERAL DERIVATIONS

OF

DYNAMIC ADSORPTION RELATIONSHIPS

APPENDIX C

GENERAL DERIVATIONS OF DYNAMIC ADSORPTION RELATIONSHIPS

Differential Material Balance

The generalized dynamic adsorption material follows in an analagous form to the energy balance in conduction heat transfer in a linear system. The following derivation closely follows the heat transfer solution derived by Schuman (S1), and Furnas (F1). It's application to the dynamic mass transfer process occurs only at an equilibrium parameter equal to unity as will be shown:

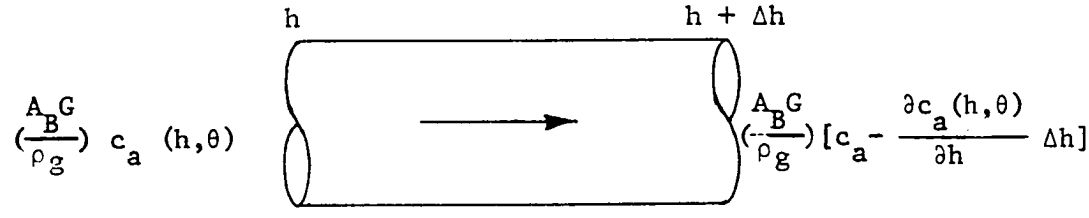

Illustration C-1

The above illustration shows a differential tower element of volume, V, with an adsorbate laden carrier flowing through at mass flow rate, G. All terms have been defined previously. For this analysis, c_a will have the units - m/ft^3.

The general material balance can be summarized as:

Adsorbate lost by gas = Adsorbate gained by solid + Adsorbate remaining in voids.

Expressed symbolically: C-1

$$\Delta\theta \frac{A_B G}{\rho_g}\{c_a(h,\theta) - c_a(h + \Delta h, \theta)\} = \rho_B\{q_a(h, \theta + \Delta\theta) - q_a(h, \theta)\} A_B \Delta h + \Phi\{c_a(h, \theta + \Delta\theta) - c_a(h, \theta)\}A_B\Delta h$$

Thus:

$$- v_g\left(\frac{\partial c_a}{\partial h}\right)_\theta = \rho_B \left(\frac{\partial q_a}{\partial \theta}\right)_h + \Phi \left(\frac{\partial c_a}{\partial \theta}\right)_h. \quad \text{C-2}$$

Simplifying C-2 gives:

$$-v_g\left(\frac{\partial c_a}{\partial h}\right)_\theta = \rho_B \left(\frac{\partial q_a}{\partial \theta}\right)_h + \Phi\left(\frac{\partial c_a}{\partial \theta}\right)_h. \quad \text{C-3}$$

As before, the net time of adsorption at any volume corresponding to h, is given by:

$$\theta' = \theta - \frac{h\Phi}{v_g}. \quad \text{C-4}$$

Thus:

$$\left(\frac{\partial c_a}{\partial h}\right) = \left(\frac{\partial c_a}{\partial \theta'}\right)\left(\frac{\partial \theta'}{\partial h}\right) + \frac{\partial c_a}{\partial h} \quad \text{C-5}$$

$$= -\left(\frac{\partial c_a}{\partial \theta'}\right)\frac{\Phi}{v_g} + \frac{\partial c_a}{\partial h}. \quad \text{C-6}$$

Replacing C-6 into C-3:

$$\Phi\left(\frac{\partial c_a}{\partial \theta'}\right)_h - \left(\frac{\partial c_a}{\partial h}\right)_\theta v_g = \rho_B \left(\frac{\partial q_a}{\partial \theta'}\right)_h + \Phi\left(\frac{\partial c_a}{\partial \theta}\right)_h. \quad \text{C-7}$$

Thus:

$$-\left(\frac{\partial c_a}{\partial h}\right)_\theta v_g = \rho_B \left(\frac{\partial q_a}{\partial \theta'}\right)_h. \quad \text{C-8}$$

Dividing C-8 by c_o, q_∞, and noting that:

$$t = \frac{k_m}{D}\left[\theta - \frac{h\Phi}{v_g}\right] \quad \text{C-8A}$$

$$s = k_m \frac{h\Phi}{v_g} \qquad \text{C-8B}$$

$$- v_g \left(\frac{\partial x}{\partial s}\right) \frac{k_m \Phi}{q_\infty v_g} = \frac{\rho_B}{c_o} \frac{k_m \Phi c_o}{q_\infty \rho_B} \left(\frac{\partial y}{\partial t}\right) \qquad \text{C-8C}$$

$$-\left(\frac{\partial x}{\partial s}\right) = \left(\frac{\partial y}{\partial t}\right). \qquad \text{C-9}$$

Equation C-9 is the material balance equation written in differential form with the dimensionless parameters, t and s.

Solution for the Adsorption Case When r = 1

The general rate equation given in Appendix C is:

$$\left(\frac{\partial y}{\partial t}\right)_s = x(1-y) - ry(1-x). \qquad \text{C-10}$$

At r = 1, which corresponds to the trace chromatogram case,

$$\left(\frac{\partial y}{\partial t}\right)_s = x - y. \qquad \text{C-11}$$

The stipulation made by C-9 is such that a function, U, is assured to exist such that:

$$dU = \left(\frac{\partial U}{\partial s}\right) ds + \left(\frac{\partial U}{\partial t}\right) dt = 0. \qquad \text{C-12}$$

And:

$$\frac{\partial^2 U}{\partial t \partial s} = \left(\frac{\partial x}{\partial s}\right)_t \qquad \text{C-13}$$

$$\frac{\partial^2 U}{\partial s \partial t} = \left(\frac{\partial y}{\partial t}\right)_s. \qquad \text{C-14}$$

Thus the partial derivatives of the theoretical function with respect to s and t are defined at any point by y and x.

Schuman (S1) suggests the assumption of a solution for x and y such that:

$$y = \{U(t,s) - V(t,s)\} \exp[-(t + s)] \qquad \text{C-15}$$

$$x = \{U(t,s) + V(t,s)\} \exp[-(t + s)] . \qquad \text{C-16}$$

Thus:

$$-\frac{\partial x}{\partial s} = +\{U(t,s) + V(t,s)\} \exp[-(t + s)] - \qquad \text{C-17}$$

$$\exp[-(t + s)] \left\{\frac{\partial U(t,s)}{\partial s} + \frac{\partial V(t,s)}{\partial s}\right\} .$$

And:

$$\frac{\partial y}{\partial t} = - \{U(t,s) - V(t,s)\} \exp[-(t + s)] +$$

$$\exp[-(t + s)] \left\{\frac{\partial U(t,s)}{\partial t} - \frac{\partial V(t,s)}{\partial t}\right\} . \qquad \text{C-18}$$

Rewriting C-18 and C-17 with C-11 and C-9 (with U = U(t,s): V= V(t,s)),

$$-2V \exp[-(t + s)] = -(U + V) \exp[-(t + s)] + \qquad \text{C-19}$$

$$\left(\frac{\partial U}{\partial s} + \frac{\partial V}{\partial s}\right) \exp[-(t + s)]$$

$$2V \exp[-(t + s)] = -(U - V) \exp[-(t + s)] +$$

$$\left(\frac{\partial U}{\partial t} - \frac{\partial V}{\partial t}\right) \exp[-(t + s) . \qquad \text{C-20}$$

Thus:

$$-2V = -(U + V) + \left(\frac{\partial U}{\partial s} + \frac{\partial V}{\partial s}\right) \qquad \text{C-21}$$

$$2V = -(U - V) + \left(\frac{\partial U}{\partial t} - \frac{\partial V}{\partial t}\right) . \qquad \text{C-22}$$

Solving these relationships for U and V gives:

$$\left(\frac{\partial U}{\partial s} + \frac{\partial V}{\partial s}\right) = U - V . \qquad \text{C-23}$$

$$\left(\frac{\partial U}{\partial t} - \frac{\partial V}{\partial t}\right) = U + V \qquad \text{C-24}$$

In order to reduce this equation to an expression involving only one dependent variable, say, V in terms of s and t, the expressions are differentiated again:

$$\frac{\partial^2 U}{\partial s \partial t} + \frac{\partial^2 V}{\partial s \partial t} = \frac{\partial U}{\partial t} - \frac{\partial V}{\partial t} \qquad \text{C-25}$$

$$\frac{\partial^2 U}{\partial t \partial s} - \frac{\partial^2 V}{\partial t \partial s} = \frac{\partial U}{\partial s} + \frac{\partial V}{\partial s}. \qquad \text{C-26}$$

Thus, combining C-26 and C-25 gives:

$$2\,\frac{\partial^2 V}{\partial t \partial s} = U + V - U + V \qquad \text{C-27}$$

$$\frac{\partial^2 V}{\partial t \partial s} - V = 0\,. \qquad \text{C-28}$$

Equation C-28 is a general hyperbolic partial differential equation reduced to its canonical form.

In order to evaluate the boundary conditions for U and V, use is made of the general rate equation:

$$\frac{\partial y}{\partial t} = x - y\,.$$

Evaluating this equation at s = 0

$$dy = (x - y)\,dt\,. \qquad \text{C-29}$$

Demanding that:

$$x(0,t) = 1 \qquad \text{C-30}$$

$$\frac{dy}{1-y} = dt\,. \qquad \text{C-31}$$

Or:

$$-\ln\,(1-y) = t + \eta_1\,. \qquad \text{C-32}$$

At $t = 0$, $y = y^o$, thus:

$$\eta_1 = -\ln (1-y^o) . \qquad \text{C-33}$$

Finally

$$\ln[\frac{1-y^o}{1-y}] = t . \qquad \text{C-34}$$

Solving this equation for y:

$$y = 1 - (1-y^o)\, e^{-t} . \qquad \text{C-35}$$

For $y^o = 0$ or assuming an initially adsorbate free adsorbent:

$$y = 1 - e^{-t} . \qquad \text{C-36}$$

Equation C-36 is the solution to the material balance and general rate equation at h = 0 (s=0). This expression will be used to evaluate the boundary conditions on V and U. In order to find a solution for x, a moving boundary is assumed for h, i.e., $h = v_g\theta$. At this variable dimensionless time, t, y = 0 since the adsorption front is defined only for positive values of:

$$\theta - \frac{h\Phi}{v_g}$$

Thus:

$$\frac{dx}{dt} = -x \qquad \text{C-37}$$

and:

$$\ln x = -t \qquad \text{C-38}$$

$$x = \exp (-t) . \qquad \text{C-39}$$

Now at s = 0, from C-15

$$y = (U - V) \exp (-t)$$

but:

$$y = 1 - \exp (-t) .$$

So that combination of C-36 and C-15 gives:

$$1 - \exp(-t) = (U - V)\exp(-t). \qquad \text{C-40}$$

In addition the stipulations for x from C-16 give:

$$x = (U + V)\exp(-t).$$

At s = 0, however, x = 1.0 so that:

$$U + V = \exp(t). \qquad \text{C-41}$$

Solving C-41 and C-40 simultaneously yields:

$$\begin{aligned} V &= 1/2 \\ &\qquad (s = 0) \qquad \text{C-42} \\ U &= \exp(t) - 1/2. \end{aligned}$$

Equations C-42 are the boundary conditions for the unknown functions U(s,t) and V(s,t) at s = h = 0.

Likewise at t = 0, C-15 and C-36 yield:

$$y = (U - V)\exp(-s).$$

But y = 0 since the adsorbate is assumed virgin, so:

$$U - V = 0 \qquad \text{C-43}$$

C-16 and C-39 yield:

$$x = (U + V) \qquad \text{C-44}$$

$$x = \exp(-t) = 1.0.$$

Solving C-44 and C-43 together, yield:

$$\begin{aligned} U &= 1/2 \\ &\qquad (t = 0) \qquad \text{C-45} \\ V &= 1/2. \end{aligned}$$

Equations C-45 complete the evaluation for the boundary conditions on U(s,t) and V(s,t) for both end points.

As is the case with the hyperbolic equation, C-14 the following substitution reduces the equation to an ordinary homogeneous differential equation:

$$\psi^2 = -4st. \qquad \text{C-46}$$

Thus:

$$\frac{\partial \psi}{\partial s} = \frac{\psi}{2s}$$

$$\frac{\partial \psi}{\partial t} = \frac{\psi}{2t} \qquad \text{C-47}$$

$$\frac{\partial^2 \psi}{\partial s \partial t} = \frac{1}{2s} \ .$$

And:

$$\frac{\partial^2 V}{\partial t \partial s} = \frac{\partial}{\partial \psi} \left[\frac{\partial V}{\partial \psi} \frac{\partial \psi}{\partial s}\right] \frac{\partial \psi}{\partial t}$$

$$= \frac{d^2 V}{d\psi^2} - \frac{1}{\psi} \frac{dV}{d\psi} \ . \qquad \text{C-48}$$

Finally, Equation C-48 becomes:

$$\frac{d^2 V}{d\psi^2} - \frac{1}{\psi} \frac{dV}{d\psi} - V = 0 \ . \qquad \text{C-49}$$

This equation can be immediately recognized as the Bessel Equation of order zero. The general solution for V(s,t) is therefore:

$$V(t,s) = A\ J_o(\psi) + B\ Y_o(\psi) \ . \qquad \text{C-50}$$

Where:

$J_o(\psi)$ = Bessel function of the first kind order zero.

$Y_o(\psi)$ = Bessel function of the second kind order zero.

At $\psi = 0$, implied by s or t = 0, yields V = 1/2 from C-42 and C-45. In addition, the Bessel function of the second kind approaches infinitely large negative values for an increasingly small argument, ψ, while $J_o(0)$ equals unity.

Thus:

$B = 0$ and $A = 1/2$.

And:

$$V(t,s) = 1/2\ J_o(2i\sqrt{st}). \qquad \text{C-51}$$

Now, C-15 and C-16 indicate that

$$x - y = 2\ V(t,s)\ \exp[-(t + s)]. \qquad \text{C-52}$$

Thus C-52 and C-51 become with C-11 and C-9:

$$-\left(\frac{\partial x}{\partial s}\right)_t = J_o(2i\sqrt{st})\ \exp[-(t + s)]. \qquad \text{C-53}$$

Integrating C-53 for constant s:

$$x = -\int_0^s J_o(2i\sqrt{\xi\ t})\ \exp[-(t + \xi)]\ d\xi + \eta(t). \qquad \text{C-54}$$

Where:

$\eta(t)$ = a function of t alone

The integral, $J_o(2i\sqrt{st})$ is the Bessel function with an imaginary argument, $I_o(2\sqrt{st})$. Also, the following values are noted for the parameters:

$$@\ \xi = 0,\ x = 1,\ -\exp[-(\xi + t)] \int_0^s I_o(2\sqrt{\xi t})\ d\xi = 0.$$

Thus:

$$\eta(t) = 1.0.$$

Incorporating these results into C-54 gives:

$$x = 1 - \exp[-(t + \xi)] \int_0^s I_o(2\sqrt{\xi t})\ d\xi. \qquad \text{C-55}$$

Likewise, the expression for y yields:

$$\left(\frac{\partial y}{\partial t}\right)_s = I_o(2\sqrt{st})\ \exp[-(t + s)] \qquad \text{C-56}$$

$$y = \exp[-(s + \alpha)] \int_0^t I_o(2\sqrt{s\alpha})\ d\alpha + \gamma(s). \qquad \text{C-57}$$

At $t = 0$, $y = 0$ so that $\gamma(s) = 0$

Thus:

$$y = \exp[-(s + \alpha)] \int_0^t I_o(2\sqrt{s\alpha})\, d\alpha . \qquad \text{C-58}$$

C-58 and C-56 are the required solutions for x and y under the stipulations of the assumed rate equations, as well as r = 1.

Proportionate Pattern Mechanics

For this particular application, a constant equilibrium parameter is assumed, such that the derivative: dy/dx is a function of x alone. From the relationship between x, y, and r:

$$\frac{dy}{dx} = \frac{r}{((1-r)\, x + r)^2} . \qquad \text{C-59}$$

From the material balance:

$$-\left(\frac{\partial x}{\partial s}\right)_t = \left(\frac{\partial y}{\partial t}\right)_s \qquad \text{C-60}$$

$$= -\left(\frac{\partial y}{\partial x}\right)_s \left(\frac{\partial x}{\partial t}\right)_s , \qquad \text{C-61}$$

with the stipulation that (dy/dx) is constant, then:

$$\frac{dy}{dx} = \left(\frac{dt}{ds}\right)_x . \qquad \text{C-62}$$

Expressing t in terms of Z:

$$Z = \frac{V - v\Phi}{Dv\Phi} = \frac{t}{s} \qquad \text{C-63}$$

$$s = k_m \frac{v\Phi}{Q} \qquad \text{C-63A}$$

$$\frac{dy}{dx} = \frac{d(Zs)}{ds} = Z + s\frac{dZ}{ds} \qquad \text{C-64}$$

$$\frac{1}{s}\frac{dy}{dx} = \frac{Z}{s} + \frac{dZ}{ds} . \qquad \text{C-65}$$

At constant t, the solution to C-65 is:

$$(Zs) = s\frac{dy}{dx} + A \qquad \text{C-66}$$

from C-59, and noting that A = 0

$$Z = \frac{r}{((1-r)\ x + r)^2}\ , \qquad \text{C-67}$$

solving for x gives:

$$x = \frac{(r/Z)^{1/2} - r}{1 - r}\ . \qquad \text{C-68}$$

This equation holds only for the following stipulations:

(1) $s >> 1.0$

(2) $r = \text{const.}$

Constant Pattern Mechanics - Solid Phase Diffusion

Binary Equations

For this case, the basic rate equation is:

$$\frac{dq_a}{d\theta} = k_p a_p^{\,o}(q_a^{\,*} - q_a). \qquad \text{C-69}$$

In addition, the constant pattern diffusion theory states that:

$$\left(\frac{\partial s}{\partial t}\right)_x = 1, \qquad \text{C-70}$$

This expression written in conjunction with the material balance yields:

$$x = y.$$

For binary mechanics, the instantaneous adsorbate concentration on the adsorbate is given by the Langmuir theory.

$$\frac{q_a^{\,*}}{q_\infty} = \frac{c_a/c_o}{r + (1-r)\ c_a/c_o}\ . \qquad \text{C-71}$$

Replacing C-71 in C-69 gives:

$$\frac{dq_a}{d\theta} = k_p a_p^{\,o} \left[\frac{xq_\infty}{r + (1-r)\,x} - q_a\right]. \qquad \text{C-72}$$

Further simplification leads to:

$$\frac{dy}{d\theta} = \frac{k_p a_p^{\,o}}{r + (1-r)\,x} \left[x - y\,(r + (1-r)\,x)\right]. \qquad \text{C-73}$$

Or:

$$\frac{dy}{d\theta} = \frac{k_p a_p^{\,o}}{r + (1-r)\,x} \left[x\,(1-y) - ry\,(1-x)\right]. \qquad \text{C-74}$$

This equation is similar to Equation B-17 (Appendix B). If the condition is met that:

$$\frac{k_{int}}{D} = \frac{k_p a_p^{\,o}}{r + (1-r)\,x}. \qquad \text{C-75}$$

Where:

k_{int} = The solid phase mechanism proportionality factor corresponding to k_{ms} for the surface reaction case.

Then the rate Equation C-74 may be used in the general solution to the material balance. The dimensionless variables, s and t are thus written:

$$t = \frac{k_p a_p^{\,o}}{(r + (1-r)\,x)} \left(\frac{v - v\Phi}{Q}\right)$$
$$s = \frac{k_p a_p^{\,o} D}{(r + (1-r)\,x)} \frac{v\Phi}{Q}. \qquad \text{C-76}$$

Further, a Column Capacity Parameter, Σ (or N), and Column Throughput Parameter, Θ, are defined such that:

$$\Theta = k_p a_p^{o} \left(\frac{v - v\Phi}{Q}\right)$$

$$\Sigma = k_p a_p^{o} D \frac{v\Phi}{Q} \quad . \qquad \text{C-77}$$

Where:

$$\Theta = t(r + (1-r)\ x)$$

$$\Sigma = s(r + (1-r)\ x)\ . \qquad \text{C-78}$$

By the fundamental laws of differentiation:

$$\frac{dy}{d\Theta}\frac{d\Theta}{dt}\frac{dt}{d\theta} = \frac{dy}{d\theta}\ , \qquad \text{C-79}$$

Writing C-79 with C-74:

$$\frac{dy}{d\Theta}\frac{(r + (1-r)\ x)}{(r + (1-r)\ x)} k_p a_p^{o} = \frac{k_p a_p^{o}}{r + (1-r)\ x}\ [x\ (1-x) - rx(1-x)]. \qquad \text{C-80}$$

Thus:

$$\frac{dx}{d\Theta} = \frac{x\ (1-x)\ (1-r)}{r + (1-r)\ x}\ , \qquad \text{C-81}$$

Rearrangement of this equation into a reasonable expression for subsequent integration, gives:

$$\left(\frac{1}{1-r}\right)\left\{\int \frac{r\,dx}{x(1-x)} + (1-r)\int \frac{dx}{(1-x)}\right\} = \Delta\Theta. \qquad \text{C-82}$$

Equation C-77 can be integrated by partial fractions by writing:

$$\frac{A_1}{x} + \frac{B_1}{1-x} = \frac{r}{x(1-x)}\ .$$

And: $\qquad \text{C-83}$

$$\frac{A_2}{1} + \frac{B_2}{1-x} = \frac{1 - r}{(1-x)}\ .$$

For $A_1 = r$, $B_1 = r$. Likewise, at $A_2 = \frac{+r}{1-x}$, $B_2 = 1$. Thus C-82 becomes:

$$\left(\frac{1}{1-r}\right)\left\{r\left[\int_{x_1}^{x_2}\frac{dx}{x}+\int_{x_1}^{x_2}\frac{dx}{1-x}\right]+\right.$$

$$\left.\left[\int_{x_1}^{x_2}\frac{-r\ dx}{1-x}+\int_{x_1}^{x_2}\frac{dx}{1-x}\right]\right\}=\Delta\Theta. \qquad \text{C-84}$$

Integration and simplification of C-84 gives the final binary solid phase asymptotic solution:

$$\left(\frac{r}{1-r}\right)\ln\left[\frac{x_2(1-x_1)}{x_1(1-x_2)}\right]-\ln\left(\frac{1-x_2}{1-x_1}\right)=\Delta\Theta. \qquad \text{C-85}$$

Where $\Delta\Theta = N_p\Delta Z$.

Multicomponent Equations

The multicomponent case is defined by the condition:

$$\lambda > 1.0. \qquad \text{C-86}$$

Thus, the Langmuir relationship for q_a^* yields:

$$\frac{q_a^*}{q_{\infty m}}=\frac{c_a/c_{om}}{r_m+(1-r_m)\ c_a/c_{om}}. \qquad \text{C-87}$$

Introducing this equation into the rate equation:

$$\frac{dq_a}{d\theta}=k_p a_p'\left[\frac{c_a/c_{om}\ q_{\infty m}}{r_m+(1-r_m)\ c_a/c_{om}}-q_a\right]. \qquad \text{C-88}$$

Thus:

$$\frac{dq_a}{d\theta}=\frac{k_p a_p'}{r_m+(1-r_m)\ c_a/c_{om}}\left[\frac{c_a}{c_{om}}q_{\infty m}-q_a\left(r_m+(1-r_m)\ \frac{c_a}{c_{om}}\right)\right] \qquad \text{C-89}$$

Since the stipulations for the multicomponent case are that:

$$c_{om}=\lambda\ c_o$$

$$q_{\infty m}=\lambda\ q_\infty \qquad \text{C-90}$$

Then, C-89 can be further simplified to read:

$$\frac{dq_a}{d\theta} = \frac{k_p a_p'}{r_m + (1-r_m)\frac{c_a}{c_o\lambda}} \left[\frac{c_a}{c_o} q_\infty - q_a\left(r_m + (1-r_m)\frac{c_a}{c_o\lambda}\right)\right]. \qquad \text{C-91}$$

Simplification and division by q_∞ gives:

$$\frac{dy}{d\theta} = \frac{k_p a_p'}{\lambda r_m + (1-r_m)\, x} \left[\lambda x - \lambda y\left(r_m + (1-r_m)\frac{x}{\lambda}\right)\right]. \qquad \text{C-92}$$

Or, with $y = x$:

$$\frac{dx}{d\theta} = k_p a_p' \frac{x(\lambda-x)\,(1-r_m)}{\lambda r_m + (1-r_m)\, x}. \qquad \text{C-93}$$

As before, in terms of the dimensionless variables:

$$\left(\frac{1}{1-r_m}\right)\left\{r_m \int_{x_1}^{x_2} \frac{\lambda dx}{x(\lambda-x)} + (1-r_m)\int_{x_1}^{x_2} \frac{dx}{(\lambda-x)}\right\} = \Delta\Theta. \qquad \text{C-94}$$

Integration of expression C-94 yields the required multicomponent solution:

$$\left(\frac{r_m}{1-r_m}\right) \ln\left[\frac{x_2(\lambda-x_1)}{x_1(\lambda-x_2)}\right] - \ln\left(\frac{\lambda-x_2}{\lambda-x_1}\right) = N_p \Delta Z. \qquad \text{C-95}$$

This equation is only applicable so long as the original assumptions are valid. The fact, however, that instantaneous equilibrium values increase beyond the binary level for both gaseous and solid phases lends support to the original contention for $\lambda > 1.0$. The most important aspect in C-95 is that of determining a valid Σ value for multicomponent mixtures where "steady-state" mass exchange has not been initiated. For these cases, however, a 'pseudo-steady state' value of Σ may be computed as a function of adsorption parameters. This procedure has been outlined in Chapter VII, and allows use of Equation C-95 for transient dynamic cases.

The practicality of this relationship, as opposed to more precise yet more complex equations, lends it a useful tool in predicting multicomponent adsorption phenomenon.

Combined Phases Reaction

When the overall resistance for the solid - gas interface is considered to be a combination of the external phase diffusion and internal phase diffusion cases, the resulting expression can be equated to the generalized surface reaction case, i.e.:

$$\left[\frac{c_a - c_a^*}{c_o} + \frac{q_a^* - q_a}{q_\infty}\right] = \frac{dq_a}{d\theta}\left[\frac{1}{k_p a_p^o q_\infty} + \frac{D}{k_f a_p^o q_\infty}\right]. \qquad \text{C-96}$$

Solving for $\frac{dq_a}{d\theta}$:

$$\frac{dq_a}{d\theta} = \frac{(q_a^* - q_a) + \frac{q_\infty}{c_o}(c_a - c_a^*)}{\frac{1}{k_p a_p^o} + \frac{D}{k_f a_p^o}}. \qquad \text{C-97}$$

This expression may now be equated to the surface reaction equation:

$$\frac{q_\infty^o c_o k_{kin}}{q_\infty}\left[c_a(q_\infty - q_a) - rq_a(c_o - c_a)\right] = \frac{(q_a^* - q_a) + \frac{q_\infty}{c_o}(c_a - c_a^*)}{\frac{1}{k_p a_p^o} + \frac{D}{k_f a_p^o}}. \qquad \text{C-98}$$

Therefore:

$$\frac{c_a(q_\infty - q_a) - rq_a(c_o - c_a)}{\frac{q_\infty}{q_\infty^o c_o k_{kin}}} = \frac{(q_a^* - q_a) + \frac{q_\infty}{c_o}(c_a - c_a^*)}{\frac{1}{k_p a_p^o} + \frac{D}{k_f a_p^o}}. \qquad \text{C-99}$$

Rearrangement gives:

$$\frac{1}{k_p a_p{}^o} + \frac{D}{k_f a_p{}^o} = \frac{q_\infty}{q_\infty{}^o c_o k_{kin}} \left[\frac{(q_a{}^* - q_a) + \frac{q_\infty}{c_o}(c_a - c_a{}^*)}{c_a(q_\infty - q_a) - rq_a(c_o - c_a)}\right]. \qquad \text{C-100}$$

By defining a parameter, b, that is a function only of the transient adsorption phenomenon:

$$b = \frac{q_a{}^* - q_a + \frac{q_\infty}{c_o}(c_a - c_a{}^*)}{c_a(q_\infty - q_a) - rq_a(c_o - c_a)} .$$

Thus:

$$\frac{1}{k_p a_p{}^o D} + \frac{1}{k_f a_p{}^o} = \frac{b\Phi}{\rho_B q_\infty{}^o k_{kin}} . \qquad \text{C-101}$$

Vermeulen (V2) outlines a procedure for the determination of b for any r at an average elution value of .5 for x. By Equation C-101, values of $k_f a_p{}^o$ or $k_p a_p{}^o$ can be determined as a function of the surface reaction group, $b\Phi/\rho_B q_\infty{}^o k_{kin}$.

From C-101 it is further evident that:

$$\frac{1}{N_p} + \frac{1}{N_E} = \frac{b}{N_R}. \qquad \text{C-102}$$

This equation is useful in design cases where either N_E or N_p is desired from a previous knowledge of b and N_R.

APPENDIX D

DERIVATION

OF THE

ZONE VELOCITY EQUATIONS

APPENDIX D

DERIVATION OF THE ZONE VELOCITY EQUATIONS

Constant Pattern Equations

The original stipulation for constant pattern adsorption, is that:

$$\left(\frac{\partial s}{\partial t}\right)_x = 1.0 \quad . \qquad \text{D-1}$$

From the solid phase diffusion definitions for s and t:

$$t = \frac{k_p a_p}{r + (1-r)\,x}\left(\theta - \frac{h\Phi}{v_g}\right) \qquad \text{D-2}$$

$$s = \frac{k_p a_p D}{r + (1-r)\,x}\left(\frac{h\Phi}{v_g}\right) \quad . \qquad \text{D-3}$$

Thus:

$$s = \left(\frac{h\Phi}{v_g}\right)\left(\frac{tD}{\theta - \frac{h\Phi}{v_g}}\right) \quad . \qquad \text{D-4}$$

And:

$$1 = \left(\frac{h\Phi}{v_g}\right)\left(\frac{v_g D}{\theta v_g - h\Phi}\right) \text{ (for } \partial s/\partial t = 1). \qquad \text{D-5}$$

Since the distance, h, divided by the time, θ, represents the velocity of the adsorption wave, V_Z, (in order to satisfy x = const.):

$$1 = \frac{\Phi D}{\frac{v_g}{V_Z} - \Phi} \quad . \qquad \text{D-6}$$

Solving for V_Z:

$$V_Z = \frac{v_g/\Phi}{1 + D} \cdot \qquad \text{D-7}$$

This equation is the basic constant pattern zone velocity equation used in this work.

Zone Velocity Equations From the Material Balance

Written in terms of h and θ, the material balance is:

$$-v_g \rho_g \left(\frac{\partial c_a}{\partial h}\right)_\theta = \rho_B \left(\frac{\partial q_a}{\partial \theta}\right)_h + \rho_g \Phi \left(\frac{\partial c_a}{\partial \theta}\right)_h . \qquad \text{D-8}$$

Assuming that c_a is a function of x and θ, the criteria of interest (i.e. constant x) is denoted by:

$$dc_a = 0 = \left(\frac{\partial c_a}{\partial h}\right)_\theta dh + \left(\frac{\partial c_a}{\partial \theta}\right)_h d\theta . \qquad \text{D-9}$$

Rearrangement gives:

$$V_Z = - \left(\frac{\partial c_a}{\partial \theta}\right)_h / \left(\frac{\partial c_a}{\partial h}\right)_\theta . \qquad \text{D-10}$$

By replacement of C-10 into D-8:

$$\left(\frac{\partial c_a}{\partial \theta}\right)_h \frac{v_g \rho_g}{V_Z} = \rho_B \left(\frac{\partial q_a}{\partial \theta}\right)_h + \rho_g \Phi \left(\frac{\partial c_a}{\partial \theta}\right)_h . \qquad \text{D-11}$$

Differentiation of the Langmuir expression for the adsorbate yields:

$$\left(\frac{\partial q_a}{\partial \theta}\right)_h = \frac{(q_\infty/c_o) r}{(r + (1-r)\, x)^2} \left(\frac{\partial c_a}{\partial \theta}\right)_h . \qquad \text{D-12}$$

Equation D-12 may be evaluated at x = .5, in order to represent average mass transfer conditions. Thus:

$$\left(\frac{\partial q_a}{d\theta}\right)_h = \frac{4(q_\infty/c_o) r}{(1+r)^2} \left(\frac{\partial c_a}{\partial \theta}\right)_h . \qquad \text{D-13}$$

Replacement of D-13 into D-11 gives:

$$\frac{v_g}{V_Z} = \frac{4\rho_B (q_\infty/c_o)}{(1+r)^2 \rho_g} + \Phi \cdot \qquad \text{D-14}$$

Simplification of this equation with $r = 1 - \frac{q_\infty}{q_\infty^o}$ yields the desired expression for V_Z:

$$\frac{1}{V_Z} = \frac{\Phi}{v_g} + \frac{400\ \rho_B\ MW_g}{v_g\ \rho_g\ MW_i} \frac{q_\infty q_\infty^o}{c_o} \left[\frac{q_\infty^o - q_\infty}{(2q_\infty^o - q_\infty)^2}\right]. \qquad \text{D-15}$$

This equation is identical with D-7 when the former is written as:

$$\frac{1}{V_Z} = \frac{\Phi}{v_g} + \frac{\Phi}{v_g} D. \qquad \text{D-16}$$

The equations represent a linear plot when represented on a co-ordinate scale with the following parameters:

	INTERCEPT	SLOPE
Constant Pattern (D-16)	Φ/v_g	Φ/v_g
Zone Velocity (D-15)	Φ/v_g	$\frac{400\rho_B MW_g}{v_g \rho_g MW_i}$

These equations have been proven valid in the laboratory as described previously.

APPENDIX E

STEADY STATE ADSORPTION EQUATIONS

THE MICHAELS APPROACH

APPENDIX E

STEADY STATE ADSORPTION EQUATIONS - THE MICHAELS APPROACH

Adsorption Capacity Equations

The amount of the adsorbate contained within the adsorbent bed at $\theta = \theta_B$ can be written as:

$$Q_B = (H_T - H_Z)\ A_B \rho_B\ q_\infty + H_Z A_B \rho_B\ (1-F)\ q_\infty . \qquad \text{E-1}$$

Or:

$$Q_B = (H_T - FH_Z)\ A_B \rho_B\ q_\infty . \qquad \text{E-2}$$

Likewise, at $\theta = \theta_E$, or the zone exhaustion time, the total amount adsorbed on the bed is:

$$Q_T = H_T A_B \rho_B\ q_\infty . \qquad \text{E-3}$$

E-3 and E-2 result in an interesting relationship that is useful in the evaluation of F:

$$\frac{Q_B}{Q_T} = 1 - F\,\frac{H_Z}{H_T} . \qquad \text{E-4}$$

The efficiency of a tower can be determined by noting that the fractional adsorption of the bed to zone breakthrough is denoted by:

$$E_B = \frac{Q_B}{Q_T + (1-F)\ A_B \rho_B\ q_\infty H_Z} \qquad \text{E-5}$$

$$E_B = \frac{H_T - FH_Z}{H_T + (1-F)\ H_Z} .$$

At zone exhaustion:

$$E_E = \frac{Q_T}{Q_T + (1-F)\, A_B \rho_B\, H_Z}$$

$$E_E = \frac{H_T}{H_T + (1-F)\, H_Z} \cdot \qquad \text{E-6}$$

Adsorption Time Equations

Michaels (M3) has shown that the ion-exchange theory yields important times that can be classified as:

TIME	OCCURRENCE
θ_B	Zone Breakthrough
θ_E	Zone Exhaustion
θ_F	Zone Formation

These times have analagous adsorption counterparts that can be related to other adsorption variables.

From E-1 it can be seen that:

$$\theta_B = \frac{A_B \rho_B\, q_\infty}{I.R_o} [H_T - FH_Z]. \qquad \text{E-7}$$

Where: $I.R_o$ = injection rate of any adsorbate into the tower.

Likewise:

$$\theta_E = \frac{A_B \rho_B\, q_\infty}{I.R.} H_T. \qquad \text{E-8}$$

From these equations, it can be seen that the zone velocity is equivalent to:

$$V_Z = \frac{I.R.}{A_B \rho_B q_\infty}, \qquad \text{E-9}$$

which may be useful in design once q_∞ is determined. In addition, I.R. can be expressed as:

$$\text{I.R.} = .0183\ Q\ c_o\ MW_i \text{ lb/min.} \qquad \text{E-10}$$

Where: All terms have been previously defined.

Further relationships involving the time parameters are herein presented:

$$\frac{H_T}{\theta_E - \theta_F} = \frac{H_Z}{\theta_Z} = V_Z . \qquad \text{E-11}$$

Thus:

$$H_Z = \frac{H_T \theta_Z}{\theta_E - \theta_F} . \qquad \text{E-12}$$

θ_F is equivalent to:

$$\theta_F = (1-F)\ \theta_Z . \qquad \text{E-13}$$

Therefore:

$$H_Z = \frac{H_T \theta_Z}{\theta_B + F\theta_Z} . \qquad \text{E-14}$$

Values of the Michaels zone velocity V_Z can be calculated by E-14 from measure laboratory parameters, i.e.: H_T, θ_B, F, θ_Z. Likewise, H_Z, the mass transfer zone height is:

$$H_Z = V_Z\ \theta_Z . \qquad \text{E-15}$$

These equations are defined for a steady state zone advance, a condition that may not necessarily be met during a dynamic process.

APPENDIX F

EXAMPLE CALCULATIONS FOR BINARY AND MULTICOMPONENT MIXTURES

APPENDIX F

EXAMPLE CALCULATIONS FOR BINARY AND MULTICOMPONENT MIXTURES

Let it be desired to calculate the dynamic behavior of independent binary mixtures of methane - n-pentane and methane - n-hexane in a silica gel adsorber for the following adsorbate concentrations:

Component	Mole - %
n-pentane	1.0
n-hexane	.75

In addition, the theoretical incoming gas is flowing at 10 MMCFD. The cycle time is to be set at 20 minutes. Hardware specifications, and adsorption behavior demand a velocity of 30 ft./min. Adsorption pressure and temperature are 800 psig and 90°F. The packed gel density is 50 $lb/ft.^3$.

Binary Calculations

Step 1 - Adsorbate Equilibrium Concentrations

Figures A-1 and A-2 give the n-pentane and n-hexane adsorbent concentrations:

$$\left(\frac{1}{q_\infty}\right)_p \text{ @ } 1.0 \ (1/c_o) = 9.8 \qquad \text{F-1}$$

$$q_{\infty p} = \underline{0.102}$$

$$\left(\frac{1}{q_\infty}\right)_{hx} @ 1.333(1/c_o)_{hx} = 5.9 \qquad \text{F-2}$$

$$q_{\infty hx} = \underline{.1695} \ .$$

Step 2 - Column Distribution Coefficients

The general expression for the column distribution coefficient is given as: (with the c_o's as mole fractions)

$$D = \frac{q_\infty \rho_B \ (T + 460) \ 10.72}{c_o MW_i \ (P + 14.7)\Phi} \qquad \text{F-3}$$

$$D_p = \frac{.102 \times 50 \times 550 \times 10.72}{.010 \times 72 \times 814.7 \times .4} = \underline{128}$$

$$D_{hx} = \frac{.1695 \times 50 \times 550 \times 10.72}{.0075 \times 86 \times 814.7 \times .4} = \underline{238} \ .$$

Step 3 - Column Area and Diameter

For a given gas flow rate and a stipulated gas velocity the tower cross section must be fixed. This macroscopic bed area, A_B, can be expressed as:

$$A_B = 19.65 \frac{Q}{v_g} \left(\frac{T + 460}{P + 14.7}\right) . \qquad \text{F-4}$$

Where:

Q = MMCFD

v_g = ft/min.

T = °F

P = psig

The subsequent bed diameter is:

$$D_T = \left[25 \frac{Q}{v_g} \left(\frac{T + 460}{P + 14.7}\right)\right]^{1/2} . \qquad \text{F-5}$$

Thus:

$$A_B = 19.65 \times \frac{10}{30} \times \frac{550}{814.7}$$

$$= \underline{4.42 \text{ ft}^2}$$

$$D_T = [\frac{4.42}{.785}]^{1/2} = \underline{2.374 \text{ ft.}}$$

Step 4 - Calculation of r, the Equilibrium Parameter

$$r = 1 - \frac{q_\infty}{q_\infty^o}, \text{ or} \qquad \text{F-6}$$

$$r = \frac{1}{1 + k_{AD}{}^o c_o} \qquad \text{F-6A}$$

$$r_p = 1 - \frac{.102}{.333} = \underline{.694}$$

$$r_p = \frac{1}{1 + .444 \times 1.0} = \frac{1}{1.444} = \underline{.694}$$

$$r_{hx} = 1 - \frac{.1695}{.408} = \underline{.586}$$

$$r_{hx} = \frac{1}{1 + .959 \times .75} = \frac{1}{1.716} = \underline{.583} .$$

Step 5 - Determination of the Mass Transfer Coefficients, $k_p a_p{}^o$

Assuming constant pattern results, Figures A-17 and A-18 give the corresponding values of $k_p a_{p_p}{}^o$ and $k_p a_{p_{hx}}{}^o$.

$$k_p a_{p_p}{}^o = .80$$

$$k_p a_{p_{hx}}{}^o = .52 .$$

Step 6 - Column Throughput Parameter Determinations - Real Time Equations

For either n-pentane or n-hexane the value of N_p (or Σ)

$$N_p = k_p a_p^{\circ} D \frac{v\Phi}{Q} . \qquad \text{F-7}$$

Corresponding real times have been derived as:

$$\theta_B = \frac{Dv\Phi}{Q} [1 - \Delta Z_{\theta B} (r, N_p) + \frac{1}{D}] \qquad \text{F-8}$$

$$\theta_M = \frac{v\Phi}{Q} [D + 1] \qquad \text{F-8A}$$

$$\theta_E = \frac{v\Phi}{Q} [D [1+ \Delta Z_{\theta E}(r, N_p)] + 1] . \qquad \text{F-8B}$$

Expressing these equations in terms of field units, i.e., Q = MMCFD, $v = A_B H_T$ ft^3, $\Phi = .4$, gives:

$$\theta_B = .02039(\frac{P + 14.7}{T + 460}) \frac{A_B H_T D}{Q} [1 - \Delta Z_{\theta B}(r,N_p) + \frac{1}{D}] \qquad \text{F-9}$$

$$\theta_M = .02039(\frac{P + 14.7}{T + 460}) \frac{A_B H_T}{Q} [D + 1] \qquad \text{F-9A}$$

$$\theta_E = .02039(\frac{P + 14.7}{T + 460}) \frac{A_B H_T}{Q} [D [1 + \Delta Z_{\theta E}(r,N_p)] + 1] \qquad \text{F-9B}$$

Noting the equation steady state mass transfer unit height:

$$HTU_p^{\circ} = \frac{v_g/\Phi}{k_p a_p {}^{\circ}D} = \frac{75}{102.5} \qquad \text{F-10}$$

$$= \underline{.731} \qquad \text{(n-pentane).}$$

For $r_p = .694$, $v_g = 30$, Figure A-27 shows $HTU_p^{\circ} = .73$

$$HTU_{hx}^{\circ} = \frac{75}{131} = \underline{.572} \qquad \text{(n-hexane).} \qquad \text{F-10A}$$

Again, Figure A-27 shows $HTU^{\circ} = .6$ for $r_{hx} = .586$, $v_g = 30$.

Step 7 - Tower Length Calculations

The unknowns in the time dependent equations for $\theta_B(r,N_p)$ and $\theta_E(r,N_p)$ are $\Delta Z_{\theta B}(r,N_p)$, $\Delta Z_{\theta E}(r,N_p)$, and H_T respectively. As both the

differential throughput parameters are functions of H_T the procedure involved is a trial and error solution for H_T. As θ_B was 'set' at 20 minutes, the $H_T(1 - \Delta Z)$ product is:

$$H_T[1-\Delta Z(.694,N_p) + \frac{1}{D}] = \frac{49.1 \times 550 \times 10 \times 20}{814.7 \times 4.42 \times 128} \qquad \text{F-11}$$

$$= \underline{11.8} \qquad \text{(n-pentane)} .$$

And,

$$H_T[1-\Delta Z(.586,N_p) + \frac{1}{D}] = \frac{49.1 \times 550 \times 10 \times 20}{814.7 \times 4.42 \times 208} \qquad \text{F-12}$$

$$= \underline{6.4} \qquad \text{(n-hexane)} .$$

Assuming for n-pentane, $H_T = 15'$, the value of N_p is:

$$N_{p_p} = \frac{15}{.731} = 20.5$$

The binary value of $\Delta Z_{\theta B}$ (.694, 20.5) from Figure A-33 gives:

$$\Delta Z_{\theta B}(.694,\ 20.5) = .35 .$$

Recalculation of Equation F-11 gives:

$$15 \times .658 = 9.85 \ (\neq 11.8).$$

Repeating the procedure for $H_T = 17$

$$N_p = \frac{17}{.731} = 23.2$$

$$\Delta Z_{\theta B}(.694,\ 23.2) = .31$$

$$17 \times .698 = 11.87 \simeq 11.8 .$$

The second iteration establishes the tower height for n-pentane in methane at 17' (approximately).

For n-hexane the procedure yields: ($H_T = 10'$)

$$\Delta Z_{\theta B}(.586,\ 17.5) = .28$$

$$10 \times .72 = 7.2 \; (\neq 6.4)$$

Repeating for $H_T = 9'$

$$\Delta Z_{\theta B}(.586,\ 15.75) = .3$$

$$9 \times .7 = 6.3 \simeq 6.4.$$

Thus, the n-hexane tower length is approximately 9'.

Figure A-22 indicates that for $N_p = 23.2$ for $r = .694$, and $N_p = 15.75$ for $r = .586$ the zones should be stabilized.

Step 8 - Real Time Effluent Concentration Calculations

Determination of the tower heights, now, allows evaluation of the adsorption times:

$$\theta_B = \frac{.02039 \times 128 \times 4.42 \times 814.7 \times 17}{550 \times 10}\,[1 - .31 + .0078] \qquad \text{F-13}$$

$$= 28.9 \times .698 = \underline{20 \text{ min.}}$$

$$\theta_M = \frac{28.9}{128} \times [129] = \underline{29.2 \text{ min.}} \qquad \text{F-13A}$$

$$\theta_E = \frac{28.9}{128} \times [128\,[1 + .39] + 1]$$

$$= .226 \times 179 = \underline{40.4 \text{ min.}} \qquad \text{F-13B}$$

Where .39 is $\Delta Z_{\theta E}(.694,\ 23.2)$ from Figure A-34

For n-hexane, the time evaluations are:

$$\theta_B = \frac{.02039 \times 238 \times 4.42 \times 814.7 \times 9}{550 \times 10}[1 - .30 + .0042] \qquad \text{F-14}$$

$$\theta_B = 28.5 \times .724 = \underline{20.0 \text{ min.}}$$

$$\theta_M = \frac{28.5}{238}\,[239] = \underline{28.6 \text{ min.}} \qquad \text{F-14A}$$

$$\theta_E = \frac{28.5}{238}\,[238\,[1 + .40] + 1] \qquad \text{F-14B}$$

$$= .12 \times 334 = \underline{40.2 \text{ min.}}$$

Again .40 is $\Delta Z_{\theta E}$(.586, 15.75) from Figure A-34.

The corresponding values of x for both adsorbates are:

	TIME-min.		RELATIVE EFFLUENTS-x	
θ	n-pentane	n-hexane	n-pentane	n-hexane
θ_B	20.0	20.0	.05	.05
θ_M	29.2	28.6	.52	.527
θ_E	40.4	40.2	.95	.95

Where .52 and .527 are the x_m values for n-pentane and n-hexane as given by Figure A-31.

Step 9 - Overall Theoretical Adsorption Calculations

The zone velocity for n-pentane is given by:

$$V_{Zcp}^{\circ} = \frac{v_g/\phi}{D_p + 1} = \frac{75}{129} = .581 \text{ ft/min.} \qquad \text{F-15}$$

As shown by Equation V-4B in Chapter V, the total tower adsorption is defined as:

$$Q_T = \text{I.R.}\left(\frac{H_T - FH_Z}{V_Z^{\circ}}\right) + \text{I.R. } F\frac{H_Z}{V_Z^{\circ}} \qquad \text{F-16}$$

$$Q_T = \text{I.R.}\frac{H_T}{V_Z^{\circ}} \quad \text{(Equation V-54).} \qquad \text{F-16A}$$

Where:

$$\text{I.R.} = .0183\ Q\ c_o MW_i \text{ lb/min.}$$

= Injection rate of the component into the tower

Thus:

$$Q_T = .0183 \times 10 \times 1 \times 72 \times \frac{17}{.581} = 385 \text{ lbs. n-pentane/cycle (40 min.)}$$

The tower bed density was taken as 50, so that the gel requirements for the n-pentane design are:

$$\rho_B A_B H_T = 50 \times 4.42 \times 17 = \underline{3750 \text{ lbs. gel}}$$

Thus:

$$\frac{385}{3750} = .1025 = q_{\infty p}, \text{ the equilibrium capacity.}$$

The calculated value of $q_{\infty p}$, agrees precisely with the original value, .102, establishing coordination between all parameters.

For n-hexane, the zone velocity is:

$$V_{Zhx}^{o} = \frac{v_g/\Phi}{D_{hx}+1} = \frac{75}{239} = \underline{.314 \text{ ft/min.}} \qquad \text{F-18}$$

Likewise, the total theoretical adsorption for this case:

$$Q_T = (\text{I. R.}) \frac{H_T}{V_{Z_{hx}}^{o}} \qquad \text{F-19}$$

$$= .0183 \times 10 \times .75 \times 86 \times \frac{9}{.314}$$

$$= \underline{338 \text{ lbs. n-hexane/cycle}} \text{ (40 min.)}$$

For a 9' tower the amount of gel is:

$$4.42 \times 9 \times 50 = \underline{1990 \text{ lbs. gel}} .$$

Thus, the calculated equilibrium capacity:

$$q_{\infty_{hx}} = \frac{338}{1990} = \underline{.1698} .$$

This value again agrees well with the value given by the isotherm, .1695.

In summary, the calculated results for the hypothetical cases are as follows:

N-PENTANE/METHANE

Gas flow rate	- 10 MMCFD
Gas velocity	- 30 ft/min (superficial)
Adsorption conditions	- 90°F 800 psig
Tower diameter	- 2.374 ft.
Tower area	- 4.42 ft.^{2}

N-PENTANE/METHANE (Con't.)

Tower length	- 17 ft.
Cycle time	- 20 min.
Zone mid-point time	- 29 min. (c_a/c_o = .52)
Zone exhaustion time	- 40 min.
Tower adsorption	- 264 lbs. n-pentane/20 minutes
Gel requirements	- 3750 lbs. 03 grade silica gel

N-HEXANE/METHANE

Gas Flow Rate	- 10 MMCFD
Gas velocity	- 30- ft/min.
Adsorption conditions	- 90°F; 800 psig
Tower diameter	- 2.374 ft.
Tower area	- 4.42 $ft.^2$
Tower length	- 9 ft.
Cycle time	- 20 minutes
Zone mid-point time	- 29 minutes (c_a/c_o= .527)
Zone exhaustion time	- 40 minutes
Tower adsorption	- 236 lbs. n-hexane/20 minutes
Gel requirements	- 1990 lbs. 03 grade silica gel

It should be noted that, generally, an even tower diameter will be used as close as possible to the calculated value of D_T. For this reason the adsorption calculations must be repeated to account for the altered tower conditions.

Also, the calculations could have proceeded in a slightly different form, if the tower height were known and the breakthrough time was the desired variable. For this case, the calculations are more direct, since the overall column capacity parameter can be directly calculated. This facilitates the evaluation of the 'ΔZ' parameters, and allows direct computation of all real times.

Binary Data Reproduction

For the purpose of illustrating the binary correlations of adsorption data presented by McLeod, and herein revised, the conditions of Run No. 122 for n-pentane will be assumed valid. The unknowns are the breakthrough and exhaustion times.

Run 122

c_o (n-pentane)	= 1.022 mole %	ρ_B	= 54 lb/ft.^{3}
v_g	= 18.93 ft/min.	A_B	= .0458 ft.^{2}
Q	= .890 ft^3/min.	T	= 90°F
H_T	= 7.5 ft.	P	= 800 psig

Step 1 - Adsorbate Equilibrium Concentration.

$1/c_{op}$ = .978, thus from Figure A-1

$1/q_{\infty p}$ = 9.9, and:

$q_{\infty p}$ = .101 .

Step 2 - Column Distribution Coefficient.

$$D_p = \frac{q_{\infty p}\, \rho_B (T + 460)\ 10.72}{c_{op} MW_i (P + 14.7).4}$$

$$D_p = \frac{.101 \times 54 \times 550 \times 10.72}{.0102 \times 72 \times 814.7 \times .4}$$

D_p = 134.3 .

Step 3 - Column Flow Rate. Since in this example the flow rate as well as the column area are set, the corresponding flow rate in field units will be:

$$Q = .05089\ A_B\ v_g \left(\frac{P + 14.7}{T + 460}\right)$$

$$Q = .05089 \times .0458 \times 18.93 \times \frac{814.7}{550}$$

Q = .0654 MMCFD .

Step 4 - Calculation of the Equilibrium Parameter, r.

$$r = 1 - \frac{q_\infty}{q_\infty^{\,o}}$$

$$r = 1 - \frac{.101}{.333}$$

$$r = \underline{.70} \quad .$$

Step 5 - Determination of the Mass Transfer Coefficient, $k_p a_p^o$.

From : $k_p a_p^o$ for n-pentane at $\pm$ 20 ft/min. is: .685

$$k_p a_p^o = .685 \, .$$

Step 6 - Determination of the Number of Transfer Units. Since the height of the column is a given condition, the number of transfer units for n-pentane can be directly calculated:

$$N_p = k_p a_p^o \, D \, \frac{v\Phi}{Q}$$

$$N_p = \frac{.685 \times 134.3 \times 7.5 \times .0458 \times .4}{.890}$$

$$N_p = .685 \times 20.7 = \underline{14.2} \, .$$

Step 7 - Real Time Calculations. From Figures A-33 and A-34, the values of $\Delta Z_{\theta B}(.7, 14.2)$ and $\Delta Z_{\theta E}(.7, 14.2)$ are:

$$\Delta Z_{\theta B}(.7, 14.2) = .49$$

$$\Delta Z_{\theta E}(.7, 14.2) = .68 \, .$$

Thus:

$$\theta_B = \frac{Dv\Phi}{Q} [1 - \Delta Z_{\theta B}(r, N_p) + \frac{1}{D_p}]$$

$$= 20.7 \times .503 = \underline{10.35 \text{ min.}}$$

$$\theta_M = \frac{v\Phi}{Q} [D_p + 1]$$

$$= .154[135.3]$$

$$= \underline{20.83 \text{ min.}}$$

$$\theta_E = \frac{v\Phi}{Q}[D_p[1 + \Delta Z_{\theta E}(r, N_p)] + 1]$$

$$= .154[134.3\ [1.68] + 1]$$

$$= .154 \times 226.5 = \underline{34.96 \text{ min.}}$$

Figure A-31 indicates that x_m @ r = .7 is:

$$x_m = .519 .$$

Comparison with the measured values of Run 122 indicate the following results:

(Run 122)

Time - min. θ	Relative Effluent Concentration
10.35	.05
20.83	.51
34.96	.96

The agreement of the calculated and measured data indicate a good applicability of the procedure to binary data.

It is of interest to note that the entire effluent curve can be constructed by referring to Figure A-60 of the binary master curves for r = .7, N_p = 14.2. Values of ΔZ for a given x multiplied by:

$$\frac{Dv\Phi}{Q} ,$$

will give the corresponding value of the time, $\Delta\theta$, associated with the ΔZ and x. The calculated points on Illustration F-1 indicate a close agreement for the entire effluent curve.

The following table illustrates the results obtained by solving the solid phase equation for r = .7 and N_p = 14.2.

x	ΔZ	$\Delta\theta$	θ
.05	0.00	0.000	10.35 (θ_B)
.10	0.13	2.690	13.04
.20	0.27	5.589	15.94

x	ΔZ	Δθ	θ
.30	0.37	7.659	18.01
.40	0.46	9.522	19.87
.50	0.54	11.178	21.53
.60	0.62	12.834	23.19
.70	0.71	14.697	25.05
.80	0.83	17.181	27.53
.90	1.02	21.114	31.46
.95	1.19	24.633	34.98 (θ_E)

In most practical applications, however, the times θ_B, θ_m, and θ_E, should serve to sufficiently define the effluent curve.

Multicomponent Calculations

The same general data as in the previous calculation will apply, with the exception that the n-pentane, and n-hexane are both in the incoming gas stream. In addition, n-heptane is present as n-heptanes+ at .28 mole %. The entering gas analysis is taken as:

Component	Mole - %
n-pentane	.16
n-hexane	.12
n-heptanes+	.28

Bed density = .876 x 62.4 = 54.6 lb/ft.^{3} (Run 221)

For this case, the bed length will be established as 15 ft., in order to demonstrate the alternate calculation of the real times. The data follow closely with the three adsorbate Run No. 221 for comparison of the results.

Step 1 - Adsorbate Equilibrium Concentrations

N-pentane is experiencing an alternate 'pseudo-binary' concentration of:

$$c_{o_{hx}} + c_{o_{hp}} = .12 + .28 = .40 \text{ mole \%} .$$

Likewise n-hexane is present with an alternate total component of:

$$c_{o_p} + c_{o_{hp}} = .16 + .28 = .44 \text{ mole \%} .$$

Figures A-9 and A-10 indicate n-pentane and n-hexane multicomponent equilibrium constants of:

$$k_{AD_p}'' = .20$$

$$k_{AD_{hx}}'' = .36.$$

From the multicomponent isotherms, the single point values for the equilibrium concentrations are:

$$q_{\infty_p}'' = \frac{q_{\infty_p}^{o} c_{o_p} k_{AD_p}''}{1 + k_{AD_p}'' c_{o_p}} \qquad \text{F-21}$$

$$= \frac{.333 \times .16 \times .20}{1 + .16 \times .20} = \frac{.01065}{1.032}$$

$$= \underline{.0103 \text{ (n-pentane)}}$$

$$q_{\infty_{hx}}'' = \frac{q_{\infty_{hx}}^{o} c_{o_{hx}} k_{AD_{hx}}''}{1 + k_{AD_{hx}}'' c_{o_{hx}}} \qquad \text{F-22}$$

$$= \frac{.408 \times .12 \times .36}{1 + .12 \times .36} = \frac{.01765}{1.0431}$$

$$= \underline{.01690 \text{ (n-hexane)}}.$$

The binary levels of q_{∞_p} and $q_{\infty_{hx}}$ are:

$$q_{\infty p} = .022 \text{ (n-pentane)}$$

$$q_{\infty hx} = .0421 \text{ (n-hexane).}$$

Step 2 - Column Distribution Coefficients

For both adsorbates, the multicomponent as well as binary column distribution coefficients are needed.

Thus:

$$D_p'' = \frac{q_\infty'' \rho_B (T + 460)\ 10.72}{c_{oi} MW_i (P + 14.7) \Phi} \qquad \text{F-23}$$

$$D_p'' = \frac{.0103 \times 54.6 \times 550 \times 10.72}{.0016 \times 72 \times 814.1 \times .4}$$

$$= \underline{88.5}$$

$$D_p^o = 88.5 \times \frac{.022}{.0103} = \underline{189.0} \qquad \text{F-24}$$

$$D_{hx}'' = \frac{.0169 \times 54.6 \times 550 \times 10.72}{.0012 \times 86 \times 814.7 \times .4} \qquad \text{F-25}$$

$$= \underline{162}$$

$$D_{hx}^o = 162 \times \frac{.0421}{.01690} = \underline{404}.$$

Step 3 - Calculation of the Multicomponent Equilibrium Parameters r_m

$$r_{mp} = 1 - \frac{.0103}{.333} = \underline{.969} \qquad \text{F-26}$$

$$r_{mp} = \frac{1}{1 + .16 \times .2} = .969 \qquad \text{F-26A}$$

$$r_{mhx} = 1 - \frac{.01690}{.408} = \underline{.960} \qquad \text{F-27}$$

$$r_{mhx} = \frac{1}{1 + .12 \times 35} = .960. \qquad \text{F-27A}$$

Step 4 - Evaluation of the Desorption Equilibrium Concentrations - $\Delta q_{\infty iD}$

The governing equation, presented in Chapter V for the $\Delta q''_{\infty iD}$ parameter is:

$$\Delta q''_{\infty Di} = \frac{1}{q_{\infty i}'' \rho_B A_B H_T}\{(q_{\infty i} - q_{\infty i}'')A_B \rho_B H_T - .0183\, Q\, MW_i\, c_{oi}[\frac{H_T}{V_Z^o} - \frac{H_T}{V_Z''}]\} \qquad \text{F-28}$$

The steady state zone velocities will apply only if the mass transfer unit has been fairly well established. For this criteria to be met the parameters:

$$k_p a_p{}^o{}_p D_p'', \quad k_p a_p{}^o{}_{hx} D_{hx}'',$$

are used with Figures A-55 and A-56 to determine the minimum bed length requirements.

The binary mass transfer coefficients are:

$$k_p a_p{}^o{}_p = 2.0 \text{ (Figure A-17)}$$

$$k_p a_p{}^o{}_{hx} = .82 \text{ (Figure A-18).}$$

Thus:

$$k_p a_p{}^o D_p'' = 88.5 \times 2 = 177$$

$$k_p a_p{}^o D_p'' = 162 \times .82 = 133.$$

Figures A-55 and A-56, for r = .95 and r = .99, are used to determine the minimum column height required to achieve steady state conditions:

H_{Tp}^{o} (min) = 110' (n-pentane

H_{Thx}^{o}(min) = 115' (n-pentane).

Thus:

H_T^{o}/H_T = 110/15 = 7.34 (n-pentane

H_T^{o}/H_T = 115/15 = 7.67 (n-hexane).

Figure A-30 indicates that at these relative column heights the ratios of the constant pattern velocity to the Michaels velocity are 1.10 and 1.05 for n-pentane and n-hexane respectively. Thus, the Michael's zone velocities applicable to this calculation are:

$$nC_5\ V_{Zpm}'' = \frac{75}{81.5 \times 1.1} = .761 \text{ ft/min.}$$

$$nC_5\ V_{Zpm}^{o} = \frac{75}{190} = .395 \text{ ft/min. (binary)}$$

$$nC_6 V_{Zhxm}'' = \frac{75}{163 \times 1.05} = .439 \text{ ft/min.}$$

$$nC_6 V_{Zhxm}^{o} = \frac{75}{405} = .185 \text{ ft/min. (binary)}$$

Returning to F-28:

$$\Delta q_{\infty Dp}'' = \frac{1}{.0103 \times 3620} \{.0117 \times 3620 - .0183 \times 10 \times 72 \times .16 \times 15[2.53 - 1.31]\}$$

$$= .0268\ [42.4 - 38.50]$$

$$= .0268 \times 3.9 = \underline{.1045} \text{ (n-pentane)}$$

$$\Delta q_{\infty Dhx}'' = \frac{1}{.01645 \times 3620} \{.02565 \times 3620 - .0183 \times 10 \times 86 \times .12 \times 15[5.40 - 2.28]\}$$

$$= .01682\ [92.6 - 88.4] = \underline{.0706} \quad \text{(n-hexane)}.$$

Step 5 - Evaluation of the Equilibrium Enhancement Factor - λ

Equation V-54 is the defining equation for λ:

$$\lambda_i = \left(\frac{2}{I.R.}\right)\left(\frac{\Delta Q_D(\lambda)}{\Delta Z_D(r, \lambda, N_p)}\right)\left(\frac{k_p a_p'}{N_p}\right) + 1 \qquad \text{F-29}$$

Where: $\dfrac{k_p a_p'}{N_p} = \dfrac{Q}{D v \Phi}$ and $\Delta Q_D(\lambda) = \dfrac{\Delta Q_D}{2}$

For n-pentane and n-hexane, values of D vΦ/Q are:

$$\frac{D''_p v\Phi}{Q} = \frac{.02039 \times 814.7 \times 4.42 \times 15 \times 88.5}{550 \times 10} \qquad \text{F-30}$$

$$= \underline{17.65} \quad \text{(n-pentane)}$$

$$\frac{D''_{hx}\, v\Phi}{Q} = \frac{.02039 \times 814.7 \times 4.42 \times 15 \times 162}{550 \times 10} \qquad \text{F-31}$$

$$= \underline{32.4} \quad \text{(n-hexane)}$$

Values calculated previously for each adsorbate are reviewed.

	I. R. (lb/min)	$\Delta Z_D(\lambda)$(lb)	H_T°/H_T
n-pentane	2.105	1.95	7.34
n-hexane	1.889	2.10	7.67

The factor that still must be calculated is the individual HTU' for each adsorbate, in order to determine the total transfer units 15 feet of tower represents to the components.

Figures A-28 and A-29 present the Transient Column Parameter as:

$$\frac{v_g c_o H_T}{\Phi D H_T^{\circ}} = X_T \,. \qquad \text{F-32}$$

Thus, the Transient Parameters for the adsorbates are:

$$\frac{75 \times .16}{88.5 \times 7.34} = \underline{.0185} \quad \text{(n-pentane)}$$

$$\frac{75 \times .12}{162 \times 7.67} = \underline{.00725} \quad \text{(n-hexane)}.$$

The transient mass transfer unit heights from Figures A-28 and A-29 are seen to be

Component	HTU'
n-pentane	.130
n-hexane	.100

From these values the transfer units are calculated:

$$N_{pp} = \frac{15}{.13} = 115.1 \quad \text{(n-pentane)} \qquad \text{F-33}$$

$$N_{phx} = \frac{15}{.1} = 150. \quad \text{(n-hexane)}. \qquad \text{F-34}$$

Assuming, initially, that $\lambda_p = 1.2$ for n-pentane, Figure A-46 indicates a $\Delta Z_D(.969, 1.2, 115.1)$ value of:

$$\Delta Z_D(.969, 1.2, 115.1) = .42 \quad (\lambda_p = 1.2).$$

Recalculating λ_p from F-29 gives:

$$\lambda_p = \left(\frac{2}{2.105}\right) \times \left(\frac{1.95}{.42}\right) \left(\frac{1}{17.65}\right) + 1.0$$

$$\lambda_p = 1.249 \quad (\neq 1.2).$$

Thus, for $\lambda_p = 1.3$, $\Delta Z_D(.969, 1.3, 115.1) = .58$ (Figure A-47)

$$\lambda_p = \left(\frac{2}{2.105}\right) \times \left(\frac{1.95}{.58}\right) \left(\frac{1}{17.65}\right) + 1.0$$

$$\lambda_p = 1.181 \quad (\neq 1.3)$$

The following plot illustrates an approximate way in which λ_p can be found from the iterations:

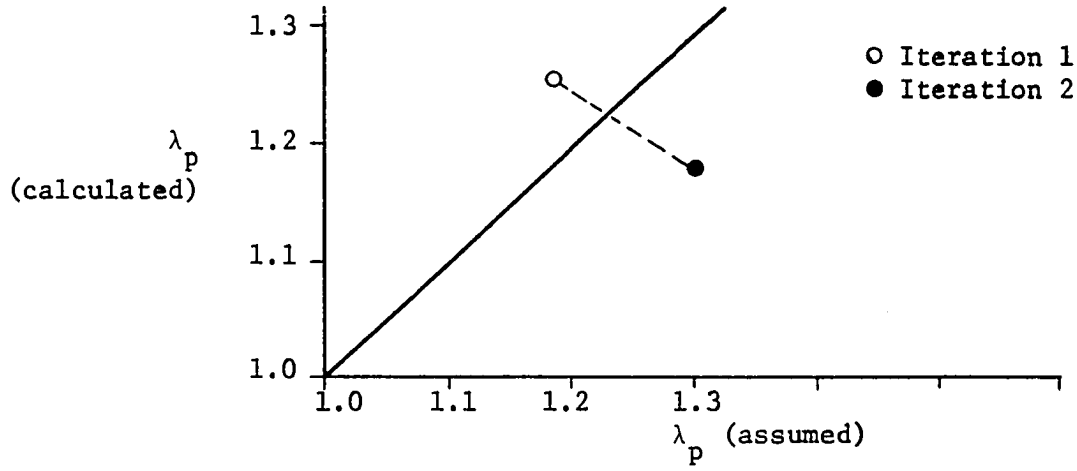

Illustration F-1

$\lambda_p = 1.21$; from the intersection of the dashed line and the 45° line. This value of λ_p gives the equivalence between calculated and assumed equilibrium enhancement factors.

For n-hexane λ_{hx} is also taken initially as 1.2, thus:

$$\Delta Z_D\ (.96,\ 12.,\ 150) = .27$$

$$\lambda_{hx} = \left(\frac{2}{1.889}\right)\left(\frac{2.1}{.27}\right)\ \left(\frac{1}{32.4}\right) + 1$$

$$\lambda_{hx} = 1.255 \neq (1.2).$$

Redefining λ_{hx} as 1.3, $\Delta Z_D(.96,\ 1.3,\ 150) = .36$ Figure A-47.

Re-evaluation of λ_{hx} gives:

$$\lambda_{hx} = \left(\frac{2}{1.889}\right)\ \left(\frac{2.1}{.36}\right)\ \left(\frac{1}{32.4}\right) + 1.0$$

$$\lambda_{hx} = 1.19\ (\neq 1.3).$$

The acceptable value of λ_{hx} can therefore be expected to fall between 1.2 and 1.1. Illustration F-2 indicates the graphical results:

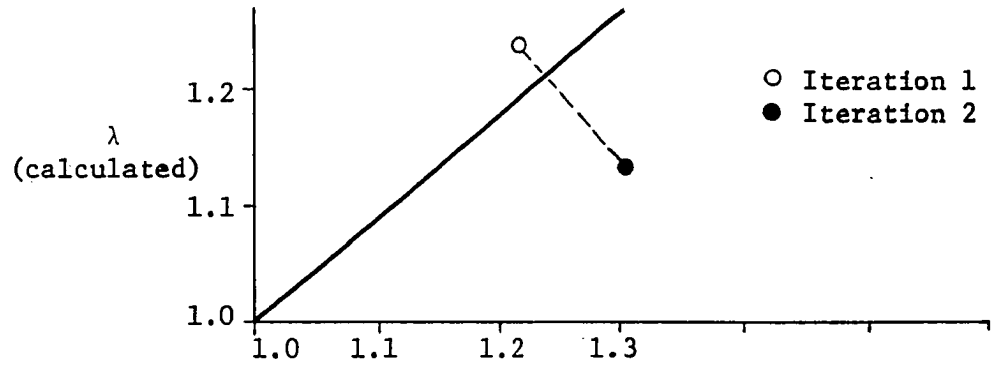

Illustration F-2

The results are summarized, and compared with the measured data from Run 221.

Component	λ(Calculated	λ(Measured) (Run 221)
n-pentane	1.21	1.28
n-hexane	1.21	1.20

Step 6 - Real Time Evaluations

Determinations of the values for $\Delta q''_{\infty Dp}$, $\Delta q''_{\infty Dhx}$, as well as λ_p and λ_{hx} allows the selection of the proper master curves from which to determine values of the ΔZ terms.

For n-pentane, the correct throughput parameter values are:

$$\Delta Z_{\theta B}(.969, 1.21, 115.1) = .69 \text{ (Figure A-39)}$$

$$\Delta Z_{\theta E}(.969, 1.21, 115.1) = .61 \text{ (Figure A-40)}$$

For n-hexane the corresponding values are:

$$\Delta Z_{\theta B}(.96, 1.21, 150) = .42 \text{ (Figure A-39)}$$

$$\Delta Z_{\theta E}(.96, 1.21, 150) = .37 \text{ (Figure A-40)}$$

Subsequent adsorption times are therefore: (Following the equations from Chapter V)

$$\theta_{Bm} = .02039 \frac{(P + 14.7)}{(T + 460)} \frac{A_B \times H_T \times D''}{Q} [1 + \Delta q_\infty D_p'' - \Delta Z_{\theta B}(r_m, \lambda, N_p) + \frac{1}{D}]$$

F-35

$$\theta_{Mm} = .02039 \frac{(P + 14.7)}{(T + 460)} \frac{A_B \times H_T}{Q} [D'' [1 + \Delta q_\infty D_p''] + 1] \qquad \text{F-36}$$

$$\theta_{Em} = .02039 \frac{(P + 14.7)}{(T + 460)} \frac{A_B \times H_T}{Q} [D''[1 + \Delta q_\infty D_p'' + \Delta Z_{\theta E}(r_m, \lambda, N_p)] + 1]$$

F-37

$$\theta_{Bm} = \frac{.02039 \times 814.7 \times 4.42 \times 15 \times 88.5}{550 \times 10}[1 + .1045 - .68]$$

$$= 17.56 [.4275] = \underline{7.48 \text{ minutes}} \quad \text{(n-pentane)}$$

$$\theta_{Mm} = \frac{17.56}{88.5} [88.5 [1.1045] + 1]$$

$$= .1985 \times 98.6 = \underline{19.6 \text{ minutes}} \quad \text{(n-pentane)}$$

$$\theta_{Em} = .1985 \times [88.5 [1 + .1045 + .61] + 1]$$

$$= .1985 [154.5] = \underline{30.3 \text{ minutes}} \quad \text{(n-pentane)}$$

The value of $\Delta\theta_{Em}(r_m, \lambda, N_p)$ for this case is: (From Chapter V, Equation V-73)

$$\Delta\theta_{Em} = .02039 \frac{(P + 14.7)}{(T + 460)} \frac{A_B H_T D''}{Q} \Delta Z_{Em}(r, \lambda, N_p)$$

Where:

$$\Delta Z_{Em}(r_m, \lambda, N_p) = \frac{.05}{115.1}[\frac{r_m + .95 (1 - r_m)}{.0475 (1 - r_m)}]$$

$$= \frac{.05}{115.1} [\frac{.969 + .95 \times .031}{.0475 \times .031}]$$

$$= \frac{.05 \times .999}{115.1 \times .0475 \times .031} = .294 .$$

The differential time at which the n-pentane effluent reaches a value of unity is then:

$$\Delta\theta_{Em} = 17.56 \times .294 = \underline{5.16 \text{ min.}} \quad \text{(n-pentane).}$$

Thus:

$$\theta_{Em} + \Delta Q_{Em} \simeq \underline{35.46 \text{ minutes}} .$$

The throughput parameter for zone desorption is given as

$$\Delta Z_D(.969,\ 1.21,\ 115.1) = .43 .$$

Thus, the <u>total</u> time at which the n-pentane effluent has reached a value of λ_p is:

$$\theta_E(\lambda)_p = \theta_{Em} + \Delta\theta_{Em} + .02039 \times \frac{(P + 14.7)}{(T + 460)} \frac{A_B\ H_T\ D''}{Q} \times$$

$$\Delta Z_D\ (.969,\ 1.21,\ 115.1)$$

$$= 35.46 + \frac{.02039 \times 814.7 \times 4.42 \times 15 \times 88.5 \times .43}{550 \times 10}$$

$$= 35.46 + 7.56$$

$$= \underline{43.02 \text{ min.}} \quad \text{(n-pentane).}$$

Figure A-31 indicates that for $\lambda_p = 1.21$, $x_{mm} = .458$, thus the times and effluent concentrations for n-pentane are summarized

Time-θ(min)	x	(x meas.) Run 221
7.48 (θ_{Bm})	.05	.05
19.6 (θ_{Mm})	.458	.40
30.3 (θ_{Em})	.95	.91

(con't.)

Time-θ(min)	x	(x meas.) Run 221
35.46 (θ_{Em} + $\Delta\theta_{Em}$)	1.00	1.00
43.02 ($\theta_E(\lambda)$)	1.21	1.18

The analagous n-hexane values follow in the same manner:

$$\theta_{Bm} = 17.56 \times \frac{162}{88.5} \times [1 + .0706 - .40 + .00618] \qquad \text{F-39}$$

$$= 32.2 \times .6768 = \underline{21.69 \text{ minutes}} \quad \text{(n-hexane)}$$

$$\theta_{Mm} = \frac{32.2}{162} [162 [1.0706] + 1] \qquad \text{F-40}$$

$$= .1986 \times 174.8 = \underline{34.7 \text{ minutes}} \quad \text{(n-hexane)}$$

$$\theta_{Em} = .1986 [162 [1.0706 + .37] + 1] \qquad \text{F-41}$$

$$= .1986 \times 235.0$$

$$= \underline{46.7 \text{ minutes}} \quad \text{(n-hexane)}.$$

The value of $\Delta Z_{Em}(r, \lambda, N_p)$ for n-hexane from F-38

$$\Delta Z_{Em}(.96, 1.21, 150) = \frac{.05}{150} \times [\frac{.96 + .95 \times .05}{.0475 \times .05}] \qquad \text{F-42}$$

$$= \frac{.05 \times 1.0075}{150 \times .0475 \times .05}$$

$$= .141 .$$

The time, $\Delta\theta_{Em}$, is:

$$\Delta\theta_{Em} = 32.2 \times .141 = 4.4 \text{ minutes (n-hexane)}.$$

Thus:

$\theta_E(\lambda) = 46.7 + 4.4 + 32.2 \times .28$, where: $\Delta Z_D(.96, 1.21, 150) = .28$

$= \underline{59.8 \text{ minutes}}$ (n-hexane).

The n-hexane data is summarized as:

Time-θ(min)	x	x(meas.) Run 221
21.7 (θ_{Bm})	.05	.075
34.7 (θ_{Mm})	.459	.34
46.7 (θ_{Em})	.95	.90
51.1 ($\theta_{Em} + \Delta\theta_{Em}$)	1.00	1.08
59.8 ($\theta_E(\lambda)$)	1.21	1.20

Step 7 - Overall Theoretical Adosrption Calculations

As with the binary calculations, the total adsorption to $\theta = \theta_{Em}$ for n-pentane is:

$$Q_T = (I.R.) \frac{H_T}{V_{Zpm}''} \qquad \text{F-43}$$

$$= 2.105 \times \frac{15}{.761} = 41.4 \text{ lbs. n-pentane/cycle .}$$

The equilibrium capacity of the silica gel for the n-pentane is therefore (with the desorbed amount of 3.9 lbs.)

$$q_{\infty p}'' = \frac{41.4 - 3.9}{3620} = \frac{37.5}{3620} = .01035 . \qquad \text{F-44}$$

This number agrees exactly with the original isotherm value of .0103 lb (n-pane)/lb gel.

Likewise for n-hexane:

$$Q_T = 1.889 \times \frac{15}{.439} = 72 \text{ lbs. n-hexane/cycle.}$$

For the same bed weight, the equilibrium capacity for the n-hexane is:

$$q''_{\infty hx} = \frac{64.4 - 4.2}{3620}$$

$$= \frac{60.2}{3620}$$

$$= \underline{.01661}\ .$$

Again .01661 agrees very closely with the original isotherm value of .01690.

The calculations herein presented could very well have solved for a tower length, if the cycle time were stipulated. In such a case, an iterative procedure for H_T will yield the required parameter. The multicomponent simultaneous adsorption calculations are nevertheless well suited to solve for any unknown parameter, with the minimum input data as presented here. No attempt is made in this work to describe the n-heptane component behavior as an effluent, since the adsorption cycle is usually never allowed to proceed much beyond the n-hexane exhaustion time in practice.

RUN NO. 122 INLET TEMP. 90 °F INLET PRESS. 800 PSIG. TOWER I.D. 2.9 in.

TOWER LGTH. 226 cm. FLOW RATE 18.98 ft/min. COMPOSITION: - %C_4 1.02 %C_5 - %C_6 - %C_7

DESSICANT: 03 GEL

MEASURED VS. CALCULATED BINARY DATA

● — C_5 CALCULATED
○ — C_5 MEASURED

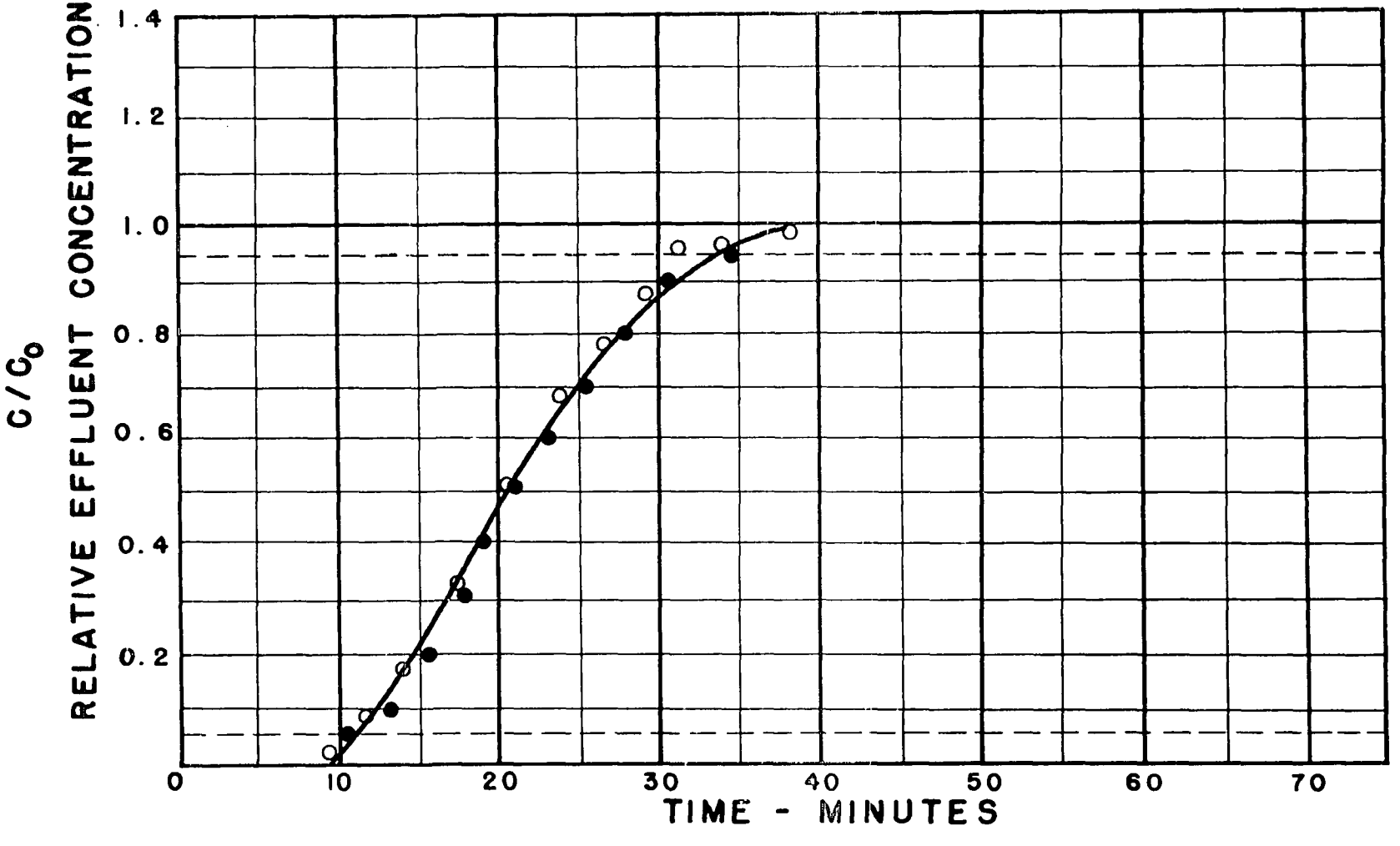

RUN NO. 221 INLET TEMP. 90 °F INLET PRESS. 800 PSIG. TOWER I.D. 2.9 in.

TOWER LGTH. 428.2 cm. FLOW RATE 30.6 ft/min. COMPOSITION: - %C_4 .1625%C_5 .1248 %C_6 .285 %C_7

DESSICANT: 03 GEL

MEASURED VS. CALCULATED RESULTS